

Application of modified xantphos ligands in homogeneous catalysis and photochemistry

Paola Andrea Forero Cortés



University
of
St Andrews

This thesis is submitted in partial fulfilment for the degree of

Doctor of Philosophy (PhD)

at the

University of St Andrews

School of Chemistry

Professor Paul C. J. Kamer Research Group

December 11, 2018

Candidate's declaration

I, Paola Andrea Forero Cortés, hereby certify that this thesis, which is approximately 59830 words in length, has been written by me, and that it is the record of work carried out by me, or principally by myself in collaboration with others as acknowledged, and that it has not been submitted in any previous application for a higher degree.

I was admitted as a research student in September, 2014 and as a candidate for the degree of Doctor of Philosophy in August 2015; the higher study for which this is a record was carried out in the University of St Andrews between 2014 and 2018.

Date: December 11, 2018

Signature of the candidate:

(Paola Andrea Forero Cortés)

Funding

I received funding from an organisation or institution and have acknowledged the funder(s) in the full text of my thesis. This work was supported by the Marie Curie Initial Training Network: Sustainable Biomass Conversions by highly Efficient Catalytic Processes - SuBiCat [PITN-GA-2013-607044] for a period of three years; and Leibniz-Institut für Katalyse e. V. (LIKAT, Rostock) for the final year.

Date: December 11, 2018

Signature of the candidate:

(Paola Andrea Forero Cortés)

General considerations

All compounds synthesised are numbered and ordered by chapter in order of their appearance in this work (e.g. 1, 2, 3... etc.). In cases where a compound features in multiple chapters, it is given a new number for that chapter, to prevent tiresome cross referencing throughout the thesis. Where a compound has two or more numbers, all numbers used to refer to it are given in the corresponding experimental section.

Date: December 11, 2018

Signature of the candidate:

(Paola Andrea Forero Cortés)

Research data/Digital outputs access statement

Research data underpinning this thesis are available at [<https://doi.org/10.17630/4dc98a72-4ffe-4f96-813f-fae5b089f768>] “*Application of modified xantphos ligands in homogeneous catalysis and photochemistry (thesis data)*”, ID 25637206.

Date: December 11, 2018

Signature of the candidate:

(Paola Andrea Forero Cortés)

Collaboration statement

I, Paola Andrea Forero Cortés, acknowledge this thesis contains work carried out under academic collaborations with the following contributions:

Mass spectrometry was performed either by the EPSRC National Mass Spectrometry Service in Swansea and by Leibniz-Institut für Katalyse e. V. (LIKAT, Rostock). NMR analysis was carried out in St. Andrews on machines maintained and run by Dr. Tomas Lebl and Melanja Smith at University of St Andrews and Dr. Wolfgang Baumann, Dipl.-Ing. Andreas Koch and Mrs. Susann Buchholz at Leibniz-Institut für Katalyse e. V. (LIKAT, Rostock). Elemental analysis was carried out at London Metropolitan University and Leibniz-Institut für Katalyse e. V. (LIKAT, Rostock).

Scientific collaborators divided by institutions are listed below:

University of St Andrews, United Kingdom

Chenfei Li (Dr. Eli Zysman-Colman group): Electrochemical and photophysical characterization of heteroleptic copper complexes (Chapter II).

Dr. David B. Cordes and Professor. Alexandra M. Z. Slawin: Single crystal X-ray structure determinations, by collecting, solving and analyzing the data (Chapters II and III).

Professor. David Cole-Hamilton: Scientific advice for the synthesis of imidazolium-tagged ligands and catalysis in ionic liquids.

Robert Dickson (Professor. Michael Büehl group): DFT calculations (Chapter II).

Universiteit Utrecht, The Netherlands

Dr. Christopher Lancefield (Professor. Peter C.A. Bruijninx/Professor. Bert Weckhuysen Inorganic Chemistry and Catalysis Group): Synthesis of more elaborated lignin model compounds and synthetic polymer. Supervision in catalysis in ionic liquids (Chapter III).

Leibniz-Institut für Katalyse e. V. (LIKAT, Rostock), Germany

Dr. Esteban Mejía: Supervision for the application of heteroleptic copper complexes in photocatalysis (Chapter II and IV), manuscript preparation (Chapter II).

Collaboration statement

Maximilian Marx (Professor. Matthias Beller/Dr. Henrick Junge group): Joint photocatalytic experiments (Chapter IV).

Dr. Nils Rockstroh (Dr. Ursula Bentrup group): Assistance in emission quenching experiments (Chapter II).

Dr. Anke Spannenberg: Single crystal X-ray structure determinations, by collecting, solving and analyzing the data (Chapters II).

Dr. Nikolaos Moustakas and Dr. Tim Peppel (Dr. Jennifer Strunk): High purity experiments and ionic liquids discussion, respectively (Chapter IV).

University of Basel, Switzerland

Fabian Brunner (Professors Catherine Housecroft and Edwin Constable group): Electrochemical and photophysical characterization of heteroleptic copper complexes (Chapter IV).

Date: December 11, 2018

Signature of the candidate:

(Paola Andrea Forero Cortés)

Date: December 11, 2018

Signature of the supervisor:

(Professor. Paul C. J. Kamer)

Date: December 11, 2018

Signature of the supervisor:

(Professor. Andrew Smith)

Supervisor's declaration

I, Paul C. J. Kamer, hereby certify that the candidate has fulfilled the conditions of the Resolution and Regulations appropriate for the degree of PhD in the University of St Andrews and that the candidate is qualified to submit this thesis in application for that degree.

I, Andrew Smith, hereby certify that the candidate has fulfilled the conditions of the Resolution and Regulations appropriate for the degree of PhD in the University of St Andrews and that the candidate is qualified to submit this thesis in application for that degree.

Date: December 11, 2018

Signature of the supervisor:

(Professor. Paul C. J. Kamer)

Signature of the supervisor:

(Professor. Andrew Smith)

Permission for publication

In submitting this thesis to the University of St Andrews we understand that we are giving permission for it to be made available for use in accordance with the regulations of the University Library for the time being in force, subject to any copyright vested in the work not being affected thereby. We also understand, unless exempt by an award of an embargo as requested below, that the title and the abstract will be published, and that a copy of the work may be made and supplied to any bona fide library or research worker, that this thesis will be electronically accessible for personal or research use and that the library has the right to migrate this thesis into new electronic forms as required to ensure continued access to the thesis.

I, Paola Andrea Forero Cortes, confirm that my thesis does not contain any third-party material that requires copyright clearance.

The following is an agreed request by candidate and supervisors regarding the publication of this thesis:

Printed copy

Embargo on all of print copy for a period of 2 years on the following ground(s):

- Publication would preclude future publication

Supporting statement for printed embargo request

I have publications pending

Electronic copy

Embargo on all of electronic copy for a period of 2 years on the following ground(s):

- Publication would preclude future publication

Supporting statement for electronic embargo request

Permission for publication

I have publications pending

Title and Abstract

- I require an embargo on the title and abstract but I understand that the title will be used in the graduation booklet.

Date: December 11, 2018

Signature of the candidate:

(Paola Andrea Forero Cortés)

Date: December 11, 2018

Signature of the supervisor:

(Professor. Paul C. J. Kamer)

Date: December 11, 2018

Signature of the supervisor:

(Professor. Andrew Smith)

Underpinning research data or digital outputs

Candidate's declaration

I, Paola Andrea Forero Cortes, understand that by declaring that I have original research data or digital outputs, I should make every effort in meeting the University's and research funders' requirements on the deposit and sharing of research data or research digital outputs.

Date: December 11, 2018

Signature of the candidate:

(Paola Andrea Forero Cortés)

Permission for publication of underpinning research data or digital outputs

We understand that for any original research data or digital outputs which are deposited, we are giving permission for them to be made available for use in accordance with the requirements of the University and research funders, for the time being in force.

We also understand that the title and the description will be published, and that the underpinning research data or digital outputs will be electronically accessible for use in accordance with the license specified at the point of deposit, unless exempt by award of an embargo as requested below.

The following is an agreed request by candidate and supervisor regarding the publication of underpinning research data or digital outputs:

Embargo on all of electronic files for a period of 2 years on the following ground(s):

- Publication would preclude future publication

Supporting statement for embargo request

I have publications pending

Title and Description

- I require an embargo on the title and description

Date: December 11, 2018

Signature of the candidate:

(Paola Andrea Forero Cortés)

Date: December 11, 2018

Signature of the supervisor:

(Professor. Paul C. J. Kamer)

Date: December 11, 2018

Signature of the supervisor:

(Professor. Andrew Smith)

Acknowledgements

I would like to thank the following people, groups and institutions who actively helped for the realization of this work:

My PhD Supervisor, Professor Paul. C. J. Kamer not only for giving me the opportunity of conducting my doctoral studies in your group but also for teaching me to be a critical, more focused person and leave excuses behind to find solutions. I also would like to thank you for the advices when I was blind by stress and frustration. I am very thankful for the massive amount of opportunities I had to travel and network during my PhD, it was really impressive and helped me so much to develop my career. I am also grateful for giving me the opportunity to join you in Germany, it was indeed an adventure. Thank you very much for the xantphos discussions and the very productive writing. I am glad we wrote this thesis despite the difficulties that appeared on the way. Something I am trying to learn from my PhD is: "No seas siempre riguroso, ni siempre blando, y escoge el medio entre estos dos extremos; que en esto está el punto de la discreción" *Don Quijote de la Mancha*. ***Ontzettend bedankt voor alles!.***

Professor Matthias Beller for hosting me in LIKAT and funding the last year of my PhD. Thank you very much for the access to all facilities, the conservancy of a team work environment and in general for the nice opportunity to work there.

My second PhD Supervisor, Professor Andrew Smith for your administrative support after we left for Rostock. To my previous supervisors: Professors Ricardo Fierro (UN, Colombia), Iván Castillo (UNAM, Mexico) and Klaus Poerschke (MPI – Muelheim, Germany) for supporting me during my career.

Professor David Cole-Hamilton for your support since we discussed the synthesis of the ligand until now. Thank you very much for helping me to see the big picture when I could not do it. Thank you very much for your scientific advices, patience and for taking the time to talk to me when needed.

Acknowledgements

Dr. Esteban Mejía for your patience, for hosting me in your lab, for helping me to understand photochemistry. I am glad we coincided in LIKAT and I could be guided in a topic which was not familiar for any of the people involved in the project. Thank you so much for saving the project and helping me to apply our complexes successfully. I hope we get our paper out and we can celebrate it one day. Thank you very much for dealing with it all.

Maximilian Marx for your priceless help with the carbon dioxide project. I am very glad you believed in this idea and we carried out many experiments together. Thank you very much for supporting me, even more during the last weeks when I was moving back to St Andrews. I really like working with you, it has been a very nice experience. Please never forget about the “Kanulka” catalyst (Spanish pronunciation) and the power of xantphos!. I wish you the best for your PhD and cannot wait to see one day you become a professor!.

Professors Peter C.A. Bruijninx and Bert Weckhuysen for hosting me in your group during my doctoral internship in Utrecht. Thanks to Dr. Christopher Lancefield for your help with the lignin project.

Professors Catherine Housecroft and Edwin Constable for supporting me with the corresponding characterization for the last chapter of my thesis. Thank you very much for giving me the opportunity of joining your group as a postdoctoral fellow in the very near future. Many thanks to Fabian Brunner for performing the experiments, the updates, the nice reports, the corrections, the favors and the positive attitude, you helped me so much. I cannot wait to join your group in Basel!.

Herr. Dr. Alexander Haydl for your great help and support since we met. I think you are a very inspiring person and a nice model to follow. Thank you very much for being honest and direct and for helping me to evolve in life. Keep your nice attitude and charisma and never forget about... Snacks!.

All members of the Kamer Group St Andrews, specially Giulia Buccolini who was always helpful, friendly and supportive. Thank you very much for doing Large-scale of precursors

Acknowledgements

with me and for helping me when my eyes were in a very bad stage. Thank you very much for the nice meals and also for dancing with me in the lab. There is no better labmate than you. Special thanks go also to Dr. Amanda Jarvis for your great help with the writing during my first year and all the efforts to help me to have more organized schedules. Dr. Upulani Somisara for bringing a positive atmosphere and nice times to the group, also for the amazing Sri Lankan food and the lipstick jokes. To Luke Shaw (Lucky Ciao) for the fun times in 336 and the glove box, dancing and singing Shakira, for all the selfies and the chats about crazy topics #phosphoruschemistry #ligninteam #iambatman. To Dr. Ciaran Lahive for your support when I was in St Andrews. I would like to thank Bob Cathcart for the tremendous help during my PhD with technical issues in the lab and also for all the jokes and good times!.

Kamer Group fusion in Rostock. Thanks to everyone. Special thanks to future Dr. Robert Konrath for making my time over there less lonely and helping me to continue with the lab set up. Thank you for your patience. Million thanks for saving my phosphine after two years of work when I could not access the lab. Thank you for your understanding and help with the language and endnote!. To Dr. Jens Deutsch for your guidance and company when I was setting the new lab in LIKAT. It was good to talk to someone by the end of the day after my arrival in Germany.

Dr. Henrick Junge and Dr. Jennifer Strunk for supporting me in the CO₂ project. Dr. Ursula Bentrup for the help in the first photocatalytic project. I really enjoyed working in your teams!. To Dr. Nills Rockstroh for having the patience to explain to me some photocatalysis. Thank you for helping me to prepare the talks for the conferences. To Dr. Nikolaos Moustakas for the high purity experiments for CO production.

Analytical departments at St Andrews and LIKAT for collecting the data for this thesis. It was a very supportive service from both institutions. To Mr. Fraser Kirk for helping me to set up my new PC to finish my thesis, it was/is a very intense moment.

Acknowledgements

My friends, who supported me during this great adventure: Dr. Martha Lucía Borrás Guevara, Sonia Chabbra, Laura Lopez, Lina Restrepo, Dr. Talia Marroquín, Dr. Daniel O'Donovan, Dr. Claudia de Fusco, Marielle Ponticiello, Dr. Desislava Petkova and Dr. Melissa Lee.

My best friend Dr. Bertrand Schweitzer (After all these years and still... I cannot pronounce your name, so... Bertie!) for your immense help and support during all these years. For being always there when I needed to talk. For supporting me when everything got together and I was not able to keep going. Thanks for your help also with the chemistry, I never imagined to end up doing photochemistry and you made my journey much less painful (Still, it was very painful!). You are one of the best people I know on earth, please keep it up!. Thank you very much for believing in me when perhaps no one else did, not even myself. Thank you very much for the sleepless nights talking about chemistry. I honestly, can't wait to see you managing a research team, you deserve it. I hope we can meet up soon!.

Dr. Michael Trose for your great support during my PhD time, for taking care of many important issues, it helped me to concentrate on my studies. Many thanks for helping me to overcome panic and to define my plan for the writing, it saved a lot of tears. Many thanks for proofreading my thesis. Thanks for the delicious food and the supportive company. I wish life brings you where you want to be and clarity and direction take over your pathway in this intense journey called life. Many, many thanks for standing all this, it was not an easy period and you were always there to cheer me up.

Last but not least, I would like to thank my parents for their unconditional support, for coming to visit me during those amazing two weeks this year and for believing in myself and in all my crazy projects. Thank you for educating me for life. *Los amo!*.

To my parents, Martha Luisa Cortés Rojas and Efrain Forero Ulloa who have always encouraged me to pursue my dreams and true passion.

“Success is not final, failure is not fatal: it is the courage to continue that counts.”

— Winston L. S. Churchill

This PhD work has been presented at:

- Jahrestagung der Fachgruppe Nachhaltige Chemie, Aachen, Germany, 17-19 September, 2018. Oral presentation
- BASF 135th International Summer Course, Ludwischafen, Germany, 19-25 August, 2018. Flash oral presentation and poster
- 28th International Conference on Organometallic Chemistry, Florence, Italy, 15-20 July, 2018. Flash oral presentation
- 51. Jahrestreffen Deutscher Katalytiker, Weimar, Germany, 14-16 March, 2018. Poster
- 11th Carla Winter School, Heidelberg, Germany, 18-23 February, 2018. Flash oral presentation and poster
- SuBiCat Final Annual Workshop, Eindhoven, the Netherlands, 4-6 September, 2017. Oral presentation
- SuBiCat Annual Workshop, Helsinki, Finland, 31 August-2 September, 2016. Oral presentation
- SuBiCat Mid-Term Meeting and Annual Workshop, Utrecht, the Netherlands, 24-26 August, 2015. Oral presentation
- Catalysis Fundamentals and Practice, Summer School, Liverpool, United Kingdom, 20-24 July, 2015. Poster
- European Workshop on Phosphorus Chemistry (EWPC-12), Kassel, Germany. 16-18 March, 2015. Poster

Additional training and networking events:

- Open symposium on 10 years biomass conversion CatchBio, SugarCity, Halfweg, the Netherlands. 16th November, 2016
- Symposium Tailored Catalysis for Sustainability, Spoorwegmuseum, Utrecht, the Netherlands, 20th January, 2016

- SuBiCat Symposium II Sustainable Catalytic Conversions of Renewable Substrates, St. Andrews, United Kingdom, 2nd March, 2015

Abstract

This thesis deals with ligand design for a variety of applications in homogeneous catalysis with an overarching objective of advancing in the search for sustainable catalytic conversions and energy utilization. The first chapter is a general introduction that briefly describes the key features of bidentate xantphos ligands and its favorable modular structure, which can be applied in rational ligand design. Several examples are discussed to illustrate how careful ligand design in combination with mechanistic understanding leads to exquisite performance in different catalytic conversions.

The second chapter describes the use of heteroleptic copper(I) complexes bearing modified xantphos and neocuproine as ligands and their application in the light driven C–C coupling reaction of 1,2,3,4-tetrahydro-2-phenyl isoquinoline with nitromethane. In particular, a series of new electronically tuned complexes has been synthesized and used as photocatalysts to establish structure - activity relationships in photocatalysis. It was found that electronic features were crucial to significantly enhance the stability and therefore the catalytic activity of this type of complexes. Mechanistic insights were also obtained, suggesting that the reaction studied likely involves oxidative and reductive quenching pathways according to the correlations between the catalytic results and the photophysical features of the complexes.

The third chapter of this thesis focuses on lignin depolymerization. For this purpose, the use of ionic liquids as reaction media has gained a lot of attention due to their unique properties compared to classical solvents. In the context of sustainable catalytic processes, recovery of the solvent and catalyst is very important. This chapter aims at using imidazolium-tagged ligands to achieve catalyst and solvent recyclability. A robust synthesis of ion-tagged ligands based on the xantphos backbone was developed and optimized. Their use in the ruthenium catalyzed C–O bond cleavage of a lignin model compound was briefly studied. This methodology follows the principle of bringing catalyst and lignin substrate together by rendering a suitable environment, such as protected ionic liquids, which could dissolve lignin efficiently allowing its catalytic transformation.

The aim of the fourth chapter of this thesis is to combine the findings of the two previous chapters by introducing imidazolium-tags in a copper based photosensitizer for the photocatalytic reduction of carbon dioxide to carbon monoxide in ionic liquids. The functionalized complex proved to be active in this transformation but catalyst recovery was not achieved. Nevertheless, a system containing unmodified ligands exhibited better performance than the concurrent systems reported in the literature using ionic liquids as reaction media.

The last chapter corresponds to the experimental section. It gives a full step by step description of all the relevant experiments and synthetic procedures to support the conclusions of this doctoral thesis. In addition, full characterization involving ^1H , ^{13}C , ^{31}P and ^{19}F NMR spectroscopy, High Resolution Mass Spectroscopy, infrared spectroscopy, elemental analysis and melting points of new synthesized compounds are described to support their identity and purity when applicable and possible.

Table of contents

| | |
|---|----|
| Chapter I. General introduction | 5 |
| 1.1 Phosphine ligands development | 5 |
| 1.1.1 Tertiary phosphine ligands | 5 |
| 1.1.2 Electronic and steric properties of phosphine ligands | 5 |
| 1.1.3 Xantphos | 9 |
| 1.1.4 Influence of bite angle in catalysis | 10 |
| 1.1.5 Influence of electronic ligand effects in catalysis | 16 |
| 1.1.6 Steric and electronic effects studies in biomass conversion | 17 |
| 1.1.7 Functionalized ligands | 18 |
| 1.2 Thesis outline | 21 |
| 1.3 References | 22 |
| Chapter II: Electronic phosphine ligand effects on the photochemistry of heteroleptic Cu(I) complexes: A comprehensive study. | 25 |
| 2.1 Introduction | 25 |
| 2.1.1 Heteroleptic copper complexes in the context of energy utilization | 25 |
| 2.1.2 Applications of $[\text{Cu}(\text{N}^{\wedge}\text{N})(\text{P}^{\wedge}\text{P})]^+$ complexes | 31 |
| 2.2 Justification and project aims | 41 |
| 2.3 Results and discussion | 43 |
| 2.3.1 Synthesis of ligands and complexes | 43 |
| 2.3.2 Dissociative equilibria studies | 46 |
| 2.3.3 Structural features | 47 |
| 2.3.4 Electrochemistry | 52 |
| 2.3.5 UV-Vis absorption | 55 |
| 2.3.6 Solution photophysics | 56 |
| 2.3.7. HOMO and LUMO contributions | 57 |
| 2.3.8 Photocatalysis | 59 |
| 2.4 Conclusions | 70 |
| 2.5 References | 71 |
| Chapter III: Modified xantphos ligands for lignin depolymerization in ionic liquid media | 79 |
| 3.1 Introduction | 79 |
| 3.1.1 Lignocellulosic biomass: Properties and opportunities | 79 |

Table of contents

| | |
|--|-----|
| 3.1.2 Lignocellulosic biomass composition | 81 |
| 3.1.3 Methodologies for the depolymerization of lignin | 86 |
| 3.1.4 Ionic liquids and biphasic catalysis | 104 |
| 3.2 Justification and project aims | 107 |
| 3.3 Results and discussion | 109 |
| 3.3.1 Synthesis of 2,7-bis(5-(3-methylimidazolium)pentyl)-9,9-dimethyl -4,5-bis(2,8-dimethyl-10-phenoxaphosphino)xanthene hexafluoro phosphate (Imidazolium/Ion-Tagged Ligand) | 109 |
| 3.3.2 Catalysis in ionic liquids | 129 |
| 3.4 Conclusions | 132 |
| 3.5 References | 133 |
| Chapter IV: Photocatalytic CO ₂ reduction in ionic liquid media | 139 |
| 4.1 Introduction | 139 |
| 4.1.1 The importance of carbon dioxide utilization | 139 |
| 4.1.2 Overview of homogeneous photocatalytic approaches for CO ₂ reduction | 141 |
| 4.1.3 Solubilization and photoreduction of CO ₂ in ionic liquids | 144 |
| 4.2 Justification and project aims | 148 |
| 4.3 Results and discussion | 150 |
| 4.3.1 Synthesis and characterization of complexes | 150 |
| 4.3.3 High-purity conditions | 161 |
| 4.4 Conclusions | 163 |
| 4.5 References | 164 |
| Thesis Conclusion | 171 |
| Chapter V: Experimental section | 173 |
| 5.1 Chapter II: Electronic phosphine ligand effects on the photochemistry of heteroleptic Cu(I) complexes: A comprehensive study. | 173 |
| General information | 173 |
| Synthesis and characterization of compounds | 173 |
| X-Ray characterization | 219 |
| Stability experiments | 225 |
| Photocatalysis | 225 |
| 5.2 Chapter III: Modified xantphos ligands for lignin depolymerization in ionic liquid media | 229 |

Table of contents

| | |
|--|-----|
| General information | 229 |
| Synthesis and characterization of compounds | 230 |
| Catalytic experiments | 261 |
| 5.3 Chapter IV: Photocatalytic CO ₂ reduction in ionic liquid media | 263 |
| General information | 263 |
| Synthesis of ligands and complexes | 263 |
| Photocatalytic experiments | 272 |
| 5.4 References | 278 |

List of abbreviations

| | |
|---------------|--|
| Å | Angstrom(s) |
| β_n | bite angle |
| ϕ | quantum yield |
| σ_p | Hammett parameter |
| ϵ | absorption coefficient |
| τ | lifetime |
| χ | Tolman electronic parameter |
| Δ | heat |
| 5-HMF | 5-(hydroxymethyl) furfural |
| ea | equatorial-apical |
| bcp | 4,7-diphenyl-1,10-phenanthroline 2,9-dimethyl-4,7-diphenyl-1,10-phenanthroline |
| BDE | Bond Dissociation Enthalpy |
| bFAP | (tris(heptafluoropropyl)trifluorophosphate) |
| BID | Barrier Ionization Discharge Detector |
| BIH | dimethylphenylbenzimidazoline |
| BINAP | 2,2'-Bis(diphenylphosphino)-1,1'-binaphthalene |
| BISBI | 2,2'-bis(diphenylphosphinomethyl)-1,1'-biphenyl |
| bmim | 1-butyl-3-methylimidazolium |
| Bphen | 4,7-diphenyl-1,10-phenanthroline |
| bmpyrr | 1-methylpyrrolidinium |
| bpy | 2,2'-bipyridine |
| CDC | cross-dehydrogenative coupling |
| COD | cyclooctadiene |
| CzCPs | Carbazolic Porous Organic Frameworks |
| d | doublet |
| D:A | donor: acceptor ratio |
| dap | anisylphenanthroline |

| | |
|------------------------------|--|
| DCA | dicyanamide |
| DDQ | 2,3-dichloro-5,6-dicyano-1,4-benzoquinone |
| dF(CF₃)ppy | 2-(2,4-difluorophenyl)-5-trifluoro-methylpyridine) |
| DFT | Density Functional Theory |
| diop | (4R-trans)-[(2,2-dimethyl-1,3-dioxolane-4,5-diyl)bis(methylene)]bis(diphenylphosphine) |
| DIPEA | N,N-diisopropylethylamine |
| dipp | 2,9-diisopropyl-1,10-phenanthroline |
| dmp | 2,9-dimethyl-1,10-phenanthroline |
| dpep | 2,9-diphenylethan-1,10-phenanthroline |
| DPEphos | bis[(2-diphenylphosphino)phenyl] ether |
| dpp | 2,9-diphenyl-1,10-phenanthroline |
| dppb | 1,2-bis(diphenylphosphino)benzene |
| dppe | bis(diphenylphosphino)ethane |
| dppf | 1,1'-ferrocenediyl-bis(diphenylphosphine) |
| dppm | bis(diphenylphosphino)methane |
| dppp | bis(diphenylphosphino)propane |
| dtbbpy | 4,4'-di-tertbutyl-2,2'-bipyridyl |
| E_R | steric repulsive energy parameter |
| ee | Bisequatorial |
| eFAP | (tris(pentafluoroethyl)trifluorophosphate) |
| emim | 1-ethyl-3-methylimidazolium |
| FDCA | 2,5-furandicarboxylic acid |
| FID | Flame Ionization Detector |
| fl | Fluorescence |
| GHG | greenhouse gas |
| GVL | γ-valerolactone |
| HOMO | Highest Occupied Molecular Orbital |
| hmim | 1-hexyl-3-methylimidazolium |
| IL | ionic liquid |
| ILCT | Intra Ligand Charge Transfer |

| | |
|-----------------------|--|
| IR | infrared spectroscopy |
| ISC | intersystem crossing |
| <i>J</i> | coupling constant |
| L | neutral ligand |
| l:b | linear to branch ratio |
| LA | levulinic acid |
| LC | Ligand Centered |
| LUMO | Lowest Unoccupied Molecular Orbital |
| m | multiplet |
| MFC | Mass Flow Controllers |
| MLCT | Metal to Ligand Charge Transfer |
| mp | melting point |
| N[^]N | phenanthroline-type ligand |
| NHC | N-heterocyclic carbene |
| NHPI | N-hydroxyphthalimide |
| NMP | N-methyl-2-pyrrolidone |
| NMR | Nuclear Magnetic Resonance |
| omim | 1-octyl-3-methylimidazolium |
| p | Pentet |
| P[^]P | diphosphine ligand |
| ph | Phosphorescence |
| phen | 1,10-phenanthroline |
| PLQY | Photo Luminescence Quantum Yields |
| pmim | 1-propyl-3-methylimidazolium |
| POP | 10-chloro-2,8-dimethylphenoxaphosphine |
| PPE | phenethyl phenyl ether |
| ppy | 2-phenylpyridine |
| PS | photosensitizer |
| pftpb | tetrakis[3,5-bis(trifluoromethyl)phenyl]borate |
| q | quartet |
| s | singlet |

List of abbreviations

| | |
|--------------|--|
| SCE | Saturated Calomel Electrode |
| sept | septet |
| SET | Single Electron Transfer |
| SIPr | 1,3-bis(2,6-diisopropylphenyl)imidazolidene |
| SR | sacrificial electron donor |
| t | triplet |
| TCB | Tetracyanoborate |
| TDDFT | Time-Dependent Density Functional Theory |
| TEA | Trimethylamine |
| TEOA | Triethylethanolamine |
| tfpb | tetrakis(bis- 3,5-trifluoromethylphenyl)borate |
| THF | Tetrahydrofuran |
| TOF | turnover frequency |
| TON | turnover number |
| tpy | terpyridine |
| WRC | water reduction catalyst |
| X | Counterion |

Chapter I. General introduction

1.1 Phosphine ligands development

1.1.1 Tertiary phosphine ligands

A ligand is an organic, main-group molecule or ion that binds to a metal generating a coordination complex. The nature of the ligand influences both the bond interaction with the metal center and the steric environment around it, thus the reactivity of the metal complex.¹ Understanding the electronic and steric contributions of the ligand to the metal – phosphine bond and overall reactivity of the complex is therefore an essential tool for a rational design approach.² Among the various molecules studied, tertiary phosphines have been widely investigated in this field. They are ancillary neutral ligands that coordinate to transition metals by σ -donation from the lone pair of their phosphorus atom to the empty orbitals of the metal center. They also accept π -backdonation from the d -orbitals of the metal to their antibonding P–C σ^* orbitals.³⁻⁴ These two contributions are the basis for the stability of the formed complex, especially with late transition metals due to their soft nature. The success of phosphine ligands goes beyond fundamental chemistry and their metal complexes remain the catalysts of choice for many successful processes based on homogeneous catalysis, numerous of them applied at industrial level.⁵⁻⁷ Nowadays, a wide library of phosphines is available; they can be classified, for example, by their denticity which refers to the number of sites of attachment the ligand has with the metal. The most studied classes are monodentate and bidentate (or chelating) phosphines, the latter provide increased stability and better control over the coordination sphere of the metal compared with the former ones.⁸ The focus of this thesis is based on bidentate phosphine ligands.

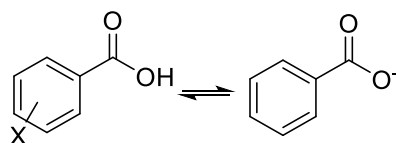
1.1.2 Electronic and steric properties of phosphine ligands

1.1.2.1 Monodentate phosphines

The main tool for quantifying the electronic properties of the phosphine ligand is measuring the CO stretching in a metal carbonyl complex. This is called the Tolman electronic parameter (χ) named after its inventor in 1970.⁹⁻¹⁰ It employs the A1 IR stretching frequencies (ν_{A1}) of carbonyl ligands in $[\text{Ni}(\text{CO})_3\text{L}]$ as probe by using $\text{P}(t\text{-Bu})_3$ as reference ligand. Therefore, χ is defined as the difference between the stretching frequencies of $[\text{Ni}(\text{CO})_3\text{L}]$ and the one of $[\text{Ni}(\text{CO})_3\text{P}(t\text{-Bu})_3]$ in cm^{-1} . The coordination of the ligand (L) to the metal

center (M) causes donation of electron density from L to M, which is then transferred as π -backdonation to the carbonyl's anti-bonding orbital (π^*). This causes a stretching of the C–O triple bond that is associated with the donor ability of L. An alternative approach consists of measuring the coupling constant between the phosphorous atom and another NMR active nucleus like rhodium, platinum or selenium. Stronger donating ligands result in stronger bond with the transition metal and, therefore, in larger coupling constants.¹¹⁻¹³ One of the convenient options is the measurement of the coupling constant in phosphinoselenides between phosphorous and selenium.¹⁴⁻¹⁵ The advantage of this method lies in the straightforward synthesis of these compounds that are air-stable solids, thus facilitating their manipulation compared to most transition metal complexes.

Another important approach to determine the phosphine basicity can be described by using the Hammett parameters σ . These parameters are determined according to the ionization constants of substituted benzoic acids. The substituent has an effect on the acid dissociation constants and the corresponding equation can be used to determine the Hammett σ value where K_X is the corresponding constant for a *meta* (m) or *para* (p) substituted benzoic acid and K_H is the ionization constant of benzoic acid at 25 °C (Equation 1, Scheme 1). The Hammett σ_p values (Hammett parameter σ_p) relate to the *para* substitution of benzoic acid, describing the resonance and inductive effects of the substituent.⁴⁸⁻⁴⁹ This thesis uses the Hammett σ_p values in order to discuss the effect of the *para* substituents present on the aryl ring attached to the phosphorus atom for the discussions corresponding to chapter II.



$$\sigma_X = \log K_X - \log K_H \quad (1)$$

Scheme 1. Determination of Hammett values.

The steric properties of phosphine ligands are usually quantified using the Tolman cone angle which is defined as the angle formed at the apex of a cone centered at a metal positioned 2.28 Å from the phosphorous atom (a typical Ni–P bond distance). The cone is framed embracing all the atoms of the ligand; this parameter is based on space filling models (Figure 1).⁹ The

major limitation of this approach is that usually the shape of a ligand is different from a perfect cone and when more complex and different ligands are bound to a metal center an introduction of strain is induced. Such fact makes it difficult to determine when a minimum cone has been accomplished and how much it compares with the behavior of the real molecule. In order to overcome these drawbacks, other models have been proposed based on crystal structures and/or calculations such as the solid angle by White and co-workers,¹⁶⁻¹⁷ and the steric repulsive energy parameter (E_R) by Brown and co-workers.¹⁸⁻¹⁹

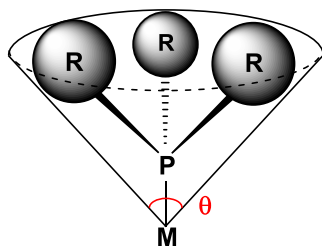


Figure 1. Tolman's definition of the cone angle.

1.1.2.2 Bidentate phosphines

Bidentate phosphine ligands possess two tertiary phosphines linked by a backbone (Figure 2) and usually chelate the metal center providing increased stability. The backbone can contain a carbon skeleton (dppe, BISBI), heteroatoms (diop, DPEphos) and transition metals (dppf). Moreover, it can be used to produce chiral ligands (BINAP). This thesis will be focused on the chemistry of xantphos, which will be covered in detail in the next section.

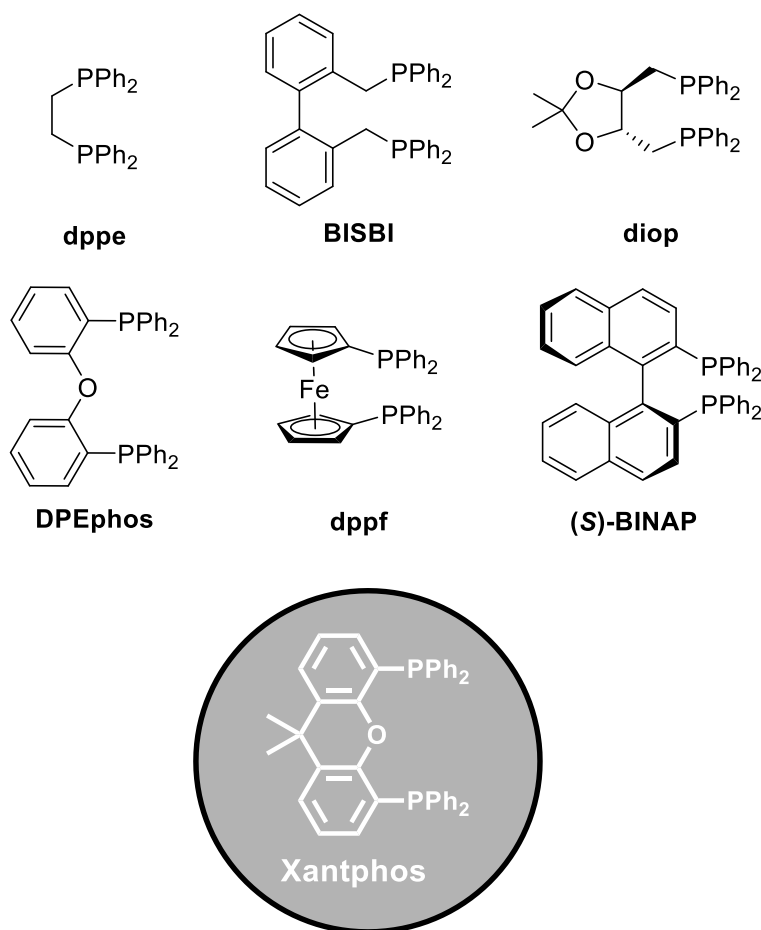


Figure 2. Selected examples of bidentate phosphine ligands.

The classification of this type of ligands is problematic by using the aforementioned parameters of cone angle and χ . In order to compare bidentate ligands in a systematic fashion, the *natural bite angle* is used in addition to other former parameters and it refers to the P–M–P angle in a transition metal complex that is determined by the backbone of the ligand.²⁰ It was introduced by Casey and co-workers and calculated by molecular modelling placing a central dummy atom at a distance of 2.135 Å from both phosphorous atoms.²¹ As alternative it can be measured by an X-ray structure and this is called crystallographic bite angle, which has been shown to be in agreement with the calculated one.²⁰⁻²¹ The bite angle affects the properties of the metal complex via an electronic effect on the metal and via a steric effect induced by the ligand. The term of *electronic bite angle effect* refers to the electronic changes at the metal as consequence of the natural bite angle of bidentate phosphines.²² It can also be described as *metal-preferred bite angle* defined as the P–M–P angle of the lowest energy

conformation in a metal complex in the absence of steric effects.²⁰ For example, square planar and octahedral complexes prefer ligands with a natural bite angle of 90°, whereas a tetrahedral complex prefers ligands with a natural bite angle of 109°. The closer the natural bite angle of a ligand is to the metal-preferred bite angle, the better the stabilization of the resulting complex is. On the other hand, deviations from these values result in electronic destabilization of the complex. The *steric bite angle effect* describes the variation in steric interactions around the metal complex when the backbone of the ligand is modified. The final properties of a diphosphine-metal complex are always dependent on both electronic and steric bite angle effects that cause a particular electron density of the metal center and a specific environment around it. These leads to different interactions with a given substrate, consequently to different performances in catalysis.^{8, 22}

1.1.3 Xantphos

This versatile ligand is the object of this thesis and was first reported by van Leeuwen and co-workers in 1995 with the goal of obtaining high selectivity and understanding the effect of the bite angle on catalytic transformations such as the rhodium catalyzed hydroformylation.²³ This ligand is based on the xanthene type backbone, which can be modified to vary its features (Figure 3). The three common sites used to modify this ligand are the bridgehead position (blue circle), the substituents on the phosphorous atoms (green circle) and the positions in the para position to the oxygen atom of the backbone (red circle). Such synthetic modifications enable the effective tuning of the properties of the ligand as well as the generation of ligand libraries.²⁴

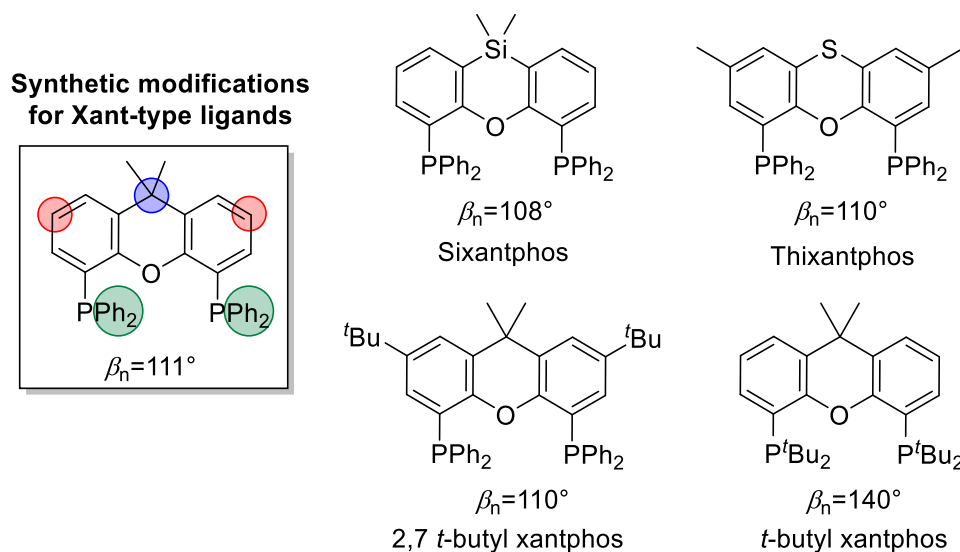
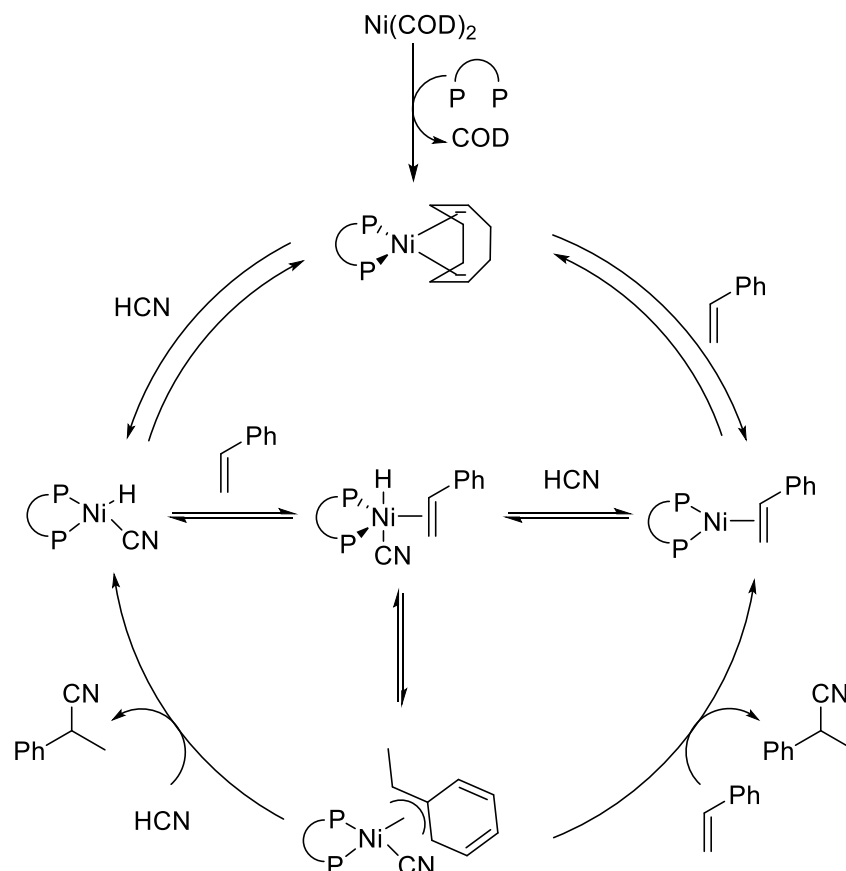


Figure 3. Synthetic modifications of xant-type ligands in order to tune their features.

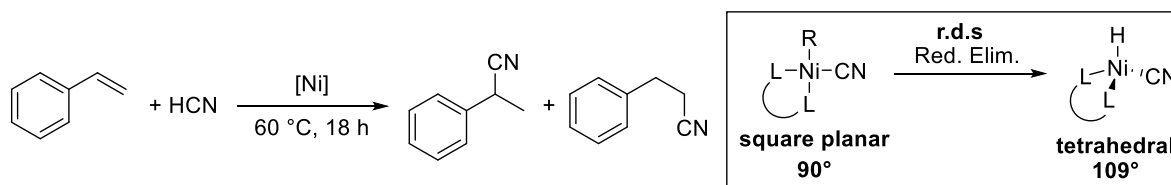
1.1.4 Influence of bite angle in catalysis

The influence of the bite angle in catalysis involving xant-type ligands has been studied for different reactions. This introduction reports three selected examples (*vide infra*) hydrocyanation,²⁵ hydroformylation of alkenes²⁶⁻²⁷ and C–O bond cleavage of aryl ethers.²⁸ In addition to these, other studies have been reported in many different transformations, for example for allylic alkylation,²⁹⁻³⁰ amination of aryl halides³¹⁻³² and cross coupling.³³ In the addition of HCN to double bonds, the rate determining step is reported to be the reductive elimination of RCN from the square planar Ni(II) complex to form the tetrahedral Ni(0) species.³⁴ Moloy reported that nickel diphosphine complexes with large bite angles enhanced the rate of the reductive elimination step.³⁵ Studies on the hydrocyanation of styrene highlighted the utility of xant-type ligands with a natural bite angle of 105–106° in stabilizing the tetrahedral Ni(0) complex, thus facilitating the reductive elimination (Scheme 2).²⁵



Scheme 2. Nickel-catalyzed hydrocyanation of styrene.²²

It was reported that bidentate ligands displaying large bite angles are able to destabilize the square planar geometry of $\text{Ni}(\text{II})$ intermediates, stabilizing tetrahedral $\text{Ni}(\text{0})$ species by enforcing coordination geometries.¹ Higher yields and selectivity were always obtained when using xantphos-type derivatives compared to the use of PPh_3 or other diphosphine like DPEPhos, dppe and BINAP (Table 1).

Table 1. Nickel-catalyzed hydrocyanation of styrene using bidentate phosphines.

| Ligand | Bite angle β_n (°) | Yield (%) ^a | Branched product (%) |
|------------------|--------------------------|------------------------|----------------------|
| PPh ₃ | | 0 | |
| Dppe | 79 | <1 | ca. 40 |
| BINAP | 85 | 4 | 29 |
| DPEPhos | 101 | 35–41 | 88–91 |
| Sixantphos | 105 | 94–95 | 97–98 |
| Thixantphos | 106 | 69–92 | 96–98 |
| Xantphos | 109 | 27–75 | 96–99 |

Reaction conditions: Styrene/Ni = 28.5, HCN/Ni = 17.5, [Ni] = 73.3 mM, T = 60 °C, t = 18 h. ^aYields are based on HCN.

In a different study, van Leeuwen and co-workers synthetically modified the xanthene backbone at the 9-position, obtaining a wide library of xant-type ligands with different natural bite angles and applied them in the hydroformylation reaction (Figure 4).²⁷

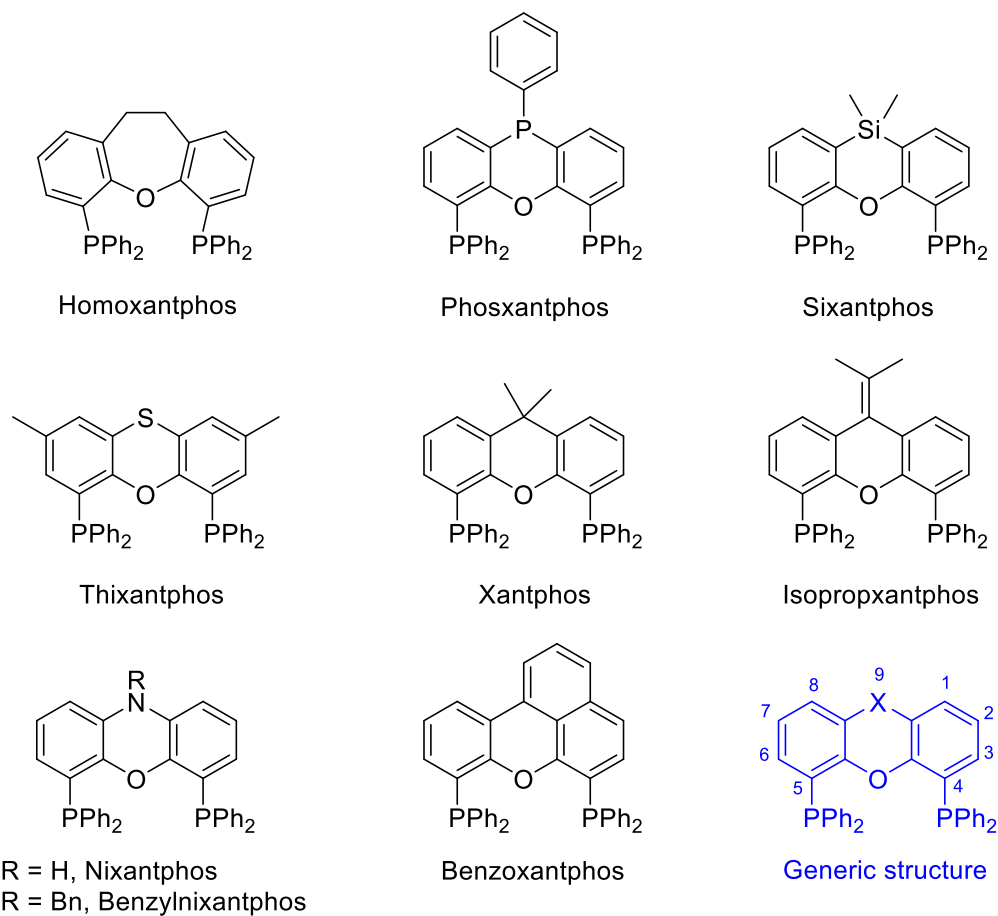


Figure 4. Modified xantphos ligands to evaluate bite angle effects.²⁷

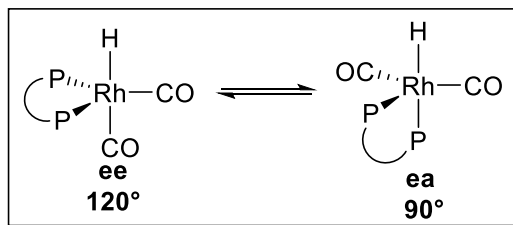
It was demonstrated that the rate of the reaction and the selectivity for the linear aldehyde as main product, increases when the natural bite angle of the xant-type ligand becomes wider, being 102° for homoxantphos and 121° for benzoxantphos (Table 2).

Table 2. Hydroformylation of 1-octene. The bite angle effect.

| Ligand | Bite angle β_n (°) | l:b ratio | % linear aldehyde | % isomer | TOF |
|------------------|-----------------------------|-----------------|----------------------|----------------|----------------|
| Homoxantphos | 102.0 | 8.50 ± 0.16 | 88.2 ± 0.4 | 1.4 ± 0.3 | 36.9 ± 4.8 |
| Phosxantphos | 107.9 | 14.6 ± 0.9 | 89.7 ± 0.4 | 4.2 ± 0.1 | 74.2 ± 1.6 |
| Sixantphos | 108.5 | 34.3 ± 0.6 | 94.4 ± 0.2 | 2.9 ± 0.2 | 76.5 ± 8.8 |
| Thixantphos | 109.6 | 56.6 ± 0.2 | 93.7 ± 0.1 | 4.7 ± 0.03 | 94.1 ± 0.4 |
| Xantphos | 111.4 | 52.2 ± 1.4 | 94.5 ± 0.2 | 3.7 ± 0.2 | 187 ± 4 |
| Isopropxantphos | 113.2 | 49.8 ± 0.3 | 94.3 ± 0.1 | 3.8 ± 0.1 | 162 ± 7 |
| Nixantphos | 114.1 | 50.6 ± 1.3 | 94.3 ± 0.3 | 3.9 ± 0.3 | 154 ± 12 |
| Benzylnixantphos | 114.2 | 69.4 ± 3.2 | 94.9 ± 0.4 | 3.7 ± 0.5 | 160 ± 5 |
| Benzoxantphos | 120.6 | 50.2 ± 0.4 | 96.5 ± 0.04 | 1.6 ± 0.02 | 343 ± 7 |

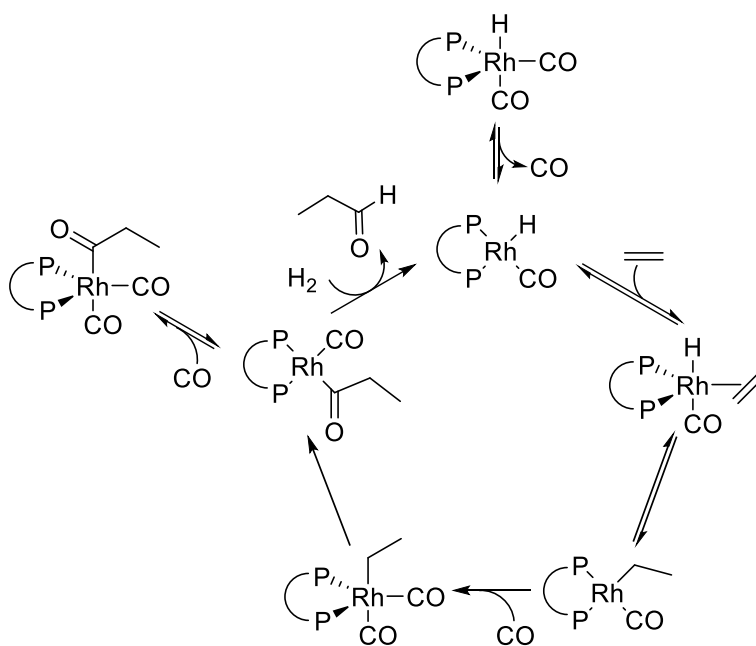
^aReaction conditions: CO/H₂ = 1, P(CO/H₂) = 20 bar, ligand/Rh = 5, substrate/Rh = 637, [Rh] = 1.00 mM, number of experiments = 3. In none of the experiments hydrogenation was observed. ^bLinear over branched ratio, percent selectivity for linear aldehyde, percent isomerization to 2-octene, and turnover frequency were determined at 20% alkene conversion. ^cTurnover frequency = (mol of aldehyde) (mol of Rh)⁻¹ h⁻¹.

When using bidentate phosphines for this transformation, such ligands can coordinate to the metal center in bisequatorial (ee) or equatorial-apical (ea) fashion (Scheme 3) depending on their bite angle. The benzoxantphos ligand exhibits a low ee:ea isomer ratio, fact that could be attributed to the higher rigidity of the backbone resulting from the introduction of the extra phenyl ring. Ligands with the presence of nitrogen as heteroatom in the backbone showed lower activity, perhaps by the donating ability of the nitrogen moiety and/or their higher flexibility.



Scheme 3. Bisequatorial (ee) or equatorial-apical (ea) fashion ligand coordination for (diphosphine)Rh(CO)₂H.

The expansion of the steric bulk of the bidentate phosphine by increasing its natural bite angle explains the selectivity towards the linear aldehyde. The reason that favors the formation of the linear product over the branched one relies on the formation of a sterically congested rhodium center that forms more selectively the less sterically hindered linear rhodium alkyl species (Scheme 4).²⁷ As suspected from related studies by the same group, the selectivity of the reaction yielding linear aldehyde as major product of the catalytic process depends on the natural bite angle and on the electronic features of the ligand.²⁶



Scheme 4. Rhodium-catalyzed hydroformylation of alkenes.²⁴

1.1.5 Influence of electronic ligand effects in catalysis

The electronic properties of xant-type ligands can be tuned by changing the substituent on the phosphorous atom and it has been shown to impact the catalytic performance of the modified complexes. For example, in the rhodium catalyzed hydroformylation of 1-octene the *para* substitution of thixantphos influenced the activity of the catalyst but not the selectivity which is dictated by the natural bite-angle.²⁶

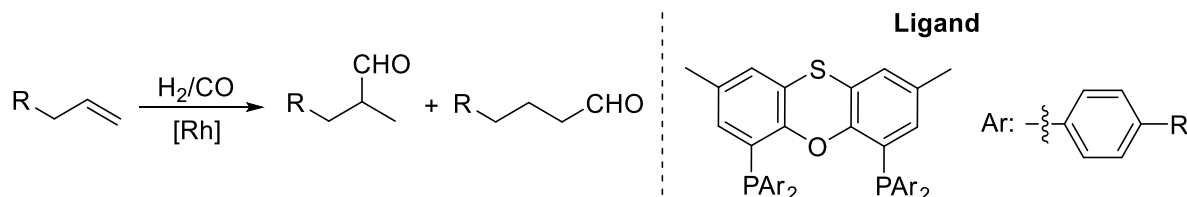
Important previous work by Christenson,³⁶ reported the effect of electron donation from the phosphine ligand in hydroformylation. The results were obtained by testing a series of 1,1'-bis(*p*-R-diphenylphosphino)ferrocene ligands. The outcome from this study stated that less donating phosphine ligands exhibited higher linear aldehyde (l:b) ratios as well as higher reaction rates.

Casey and co-workers compared the iridium complexes of BISBI and DIPHOS noticing that the former assumes only an ee coordination (ee:ea = 100:0) to the metal center, whereas the latter is only ae (ee:ea = 0:100).³⁷ The same ligands were applied in the Rh-catalyzed hydroformylation of 1-hexene, forming the catalyst in situ from the diphosphine ligand and Rh(CO)₂(acac). The BISBI-Rh catalyst showed higher l:b ratio (66.5±0.5) than DIPHOS-Rh (1.3±0.1), leading to the assumption that selectivity was dictated by the coordination of the diphosphine ligand. However, the scenario is not so simple, in fact the selectivity was doubled (l:b = 123±3) by using BISBI-(3,5-CF₃) that shows only ee coordination, showcasing that the electronic effect of the ligand play an important role and higher selectivity is achieved with electron withdrawing substituents.

Later, a series of modified thixantphos ligands forming a Hammett series was studied by van Leeuwen and co-workers.²⁶ The authors reported that the equilibrium between the ee and ea coordination for the pentacoordinated rhodium intermediate (diphosphine)Rh(CO)₂H depends on the donation from the phosphorus ligand. Again, it was described that electron withdrawing substituents favored the equilibrium towards the ee coordination and in higher l:b ratio in the hydroformylation of 1-octene (Table 3).³⁷ Other observations from the authors are that faster dissociation of the carbonyl ligand by weaker donation from the phosphine ligand in the (diphosphine)Rh(CO)₂H complex enhances the coordination of the substrate, increasing the reaction rates. The more electrophilic the rhodium center is, more CO

dissociation is observed and β -hydride elimination can take place after the formation of the Rh-alkyl intermediate.²⁶

Table 3. Hydroformylation of 1-octene. The electronic ligand effect.



| R | Bite-angle β_n (°) | σ_p | l:b ratio ^b | % selectivity ^b | % isomer ^b | TOF ^{b,c} |
|----------------------------------|-----------------------------|------------|------------------------|-------------------------------|--------------------------|--------------------|
| N(CH ₃) ₂ | 109.1 | -0.83 | 44.6 | 93.1 | 4.8 | 28 |
| OCH ₃ | 106.9 | -0.27 | 36.9 | 92.1 | 5.3 | 45 |
| CH ₃ | 106.7 | -0.17 | 44.4 | 93.2 | 4.7 | 78 |
| H | 106.4 | 0.00 | 50.0 | 93.2 | 4.9 | 110 |
| F | 106.6 | 0.06 | 51.5 | 92.5 | 5.7 | 75 |
| Cl | 107.8 | 0.23 | 67.5 | 91.7 | 6.9 | 66 |
| CF ₃ | 109.3 | 0.54 | 86.5 | 92.1 | 6.8 | 158 |

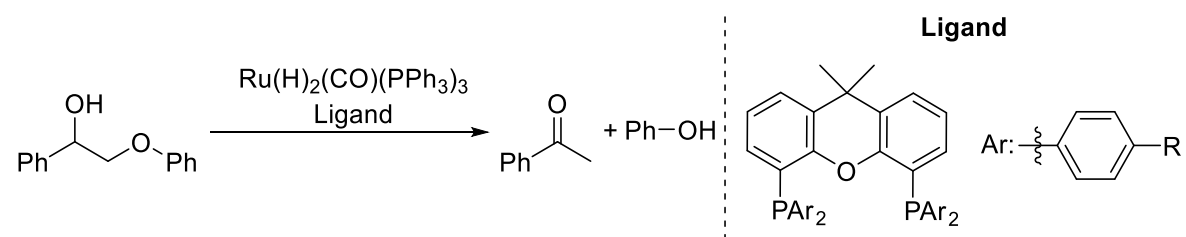
^aReaction conditions: CO/H₂ = 1, $P(\text{CO}/\text{H}_2)$ = 20 bar, ligand/Rh = 5, substrate/Rh = 637, [Rh] = 1.00 mM, number of experiments = 3. In none of the experiments hydrogenation was observed. ^bLinear over branched ratio, percent selectivity for linear aldehyde, percent isomerization to 2-octene, and turnover frequency were determined at 20% alkene conversion. ^cTurnover frequency = (mol of aldehyde) (mol of Rh)⁻¹ h⁻¹.

1.1.6 Steric and electronic effects studies in biomass conversion

A ruthenium-xantphos system has been applied in the catalytic C–O bond cleavage of aryl ethers in model compounds for biomass conversion through a hydrogen borrowing mechanism. Ellman et al. reported xantphos as the best ligand from the screening when compared to other mono and bidentate phosphines, displaying quantitative conversions of lignin model compounds and a synthetic polymer.³⁸

Kamer and co-workers studied the system from the perspective of the influence of the electronic and natural bite angle effects by ligand modification.²⁸ Variation of the bite angle from 102° to 121° showed the unmodified xanthene backbone as the optimal one for this transformation. Better conversions were achieved by increasing the phosphine basicity, fact that led the authors to propose oxidative addition as the rate limiting step in the catalytic process (Table 4 and scheme 12, chapter III).

Table 4. Electronic effect on C–O bond cleavage of 2-phenoxy-1-phenylethanol.



| R | σ_p^b | Conversion (%) ^c |
|------------------|--------------|-----------------------------|
| OCH ₃ | -0.27 | 47.6 |
| CH ₃ | -0.17 | 46.5 |
| H | 0.00 | 44.6 |
| F | 0.06 | 26.2 |
| CF ₃ | 0.54 | 5.1 |

^aConditions: 0.25 mmol of 2-phenoxy-1-phenylethanol with 2 mol% catalyst loading (0.005 mmol of $\text{Ru}(\text{H})_2(\text{CO})(\text{PPh}_3)_3$, 0.005 mmol of ligand and 0.125 mmol of 1,2,4,5-tetramethylbenzene as the internal standard in anhydrous xylenes in a closed microwave vial, 135 °C, 45 min. ^bHammett σ_p values. ^cConversion determined by gas chromatography.

1.1.7 Functionalized ligands

Catalyst separation and recyclability are important research topics contemplated to overcome major drawbacks of homogeneous catalysis. Despite the high activity and selectivity exhibited by many organometallic complexes, the separation of the reaction products from the reaction media and the catalyst is often troublesome. In addition, catalyst recyclability remains a challenge. One important approach to reach a general solution to these limitations, consists of the structural rational modification of the catalyst to favor its solubility in a

specific type of solvent or phase. Such solvent/phase should be immiscible or allow the extraction of the products under certain conditions, creating in this manner a biphasic system.³⁹

Synthetic tailoring of the ligand/catalyst depends on the requirements of the catalytic system. Examples of modified xantphos-type ligands suitable for biphasic catalysis have been described as water-soluble ligands,⁴⁰ amphiphilic ligands,⁴¹⁻⁴² fluorous-based ligands⁴³ and imidazolium-tagged ligands.⁴⁴⁻⁴⁷ Among them, this thesis will focus on ion-tagged ligands with imidazolium cores in their structure.

1.1.7.1 Imidazolium-tagged ligands suitable for biphasic catalysis

The modular structure of the xantphos ligand gives the opportunity of performing synthetic transformations that achieve demonstrable changes in reactivity and overall performance of its complexes by rational ligand design. It has been proven that such changes facilitate various processes and/or help with the understanding of reaction mechanisms.

van Leeuwen and co-workers reported ligand **1** (Figure 5) for the hydroformylation of 1-octene in butyl-3-methylimidazolium hexafluorophosphate with high reaction rates and low catalyst leaching (5 ppb). The system could be recycled up to seven times.⁴⁷ Cole-Hamilton and co-workers applied ligand **2** (Figure 5) in the continuous flow homogeneous hydroformylation of long chain alkenes using supercritical fluids in 1-butyl-3-methylimidazolium and 1-n-octyl-3-methylimidazolium triflimide as ionic liquids.⁴⁵ The results were comparable to commercial systems. Optimization of the aforementioned system provided rates and selectivities to the desired linear aldehyde that are of commercial interest.⁴⁶

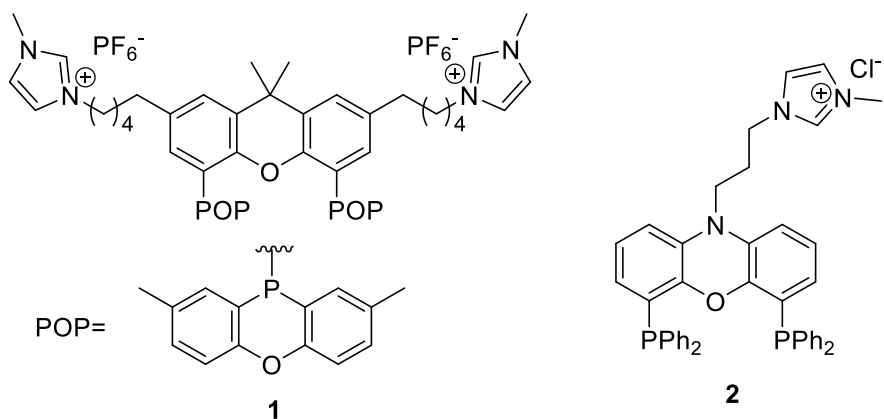


Figure 5. Ion-tagged modified ligands. **1:** Imidazolium-tagged xantphos-type ligand: 2,7-bis(5-(3-methylimidazolium)pentyl)-9,9-dimethyl-4,5-bis(2,8-dimethyl-10-phenoxaphosphino)xanthene hexafluorophosphate, **2:** Imidazolium-tagged nixantphos ligand: 4,6-bis(diphenylphosphino)-10-propyl-methylimidazolium-phenoxazine chloride.

In this section the effectiveness and importance of rational ligand design in catalytic transformations has been highlighted in selected examples and it is intended to aid the discussion of the research chapters. This thesis will specifically focus on *p*-substituted xantphos ligands (Hammett series) and imidazolium-tagged ligands of the xantphos family with the presence of imidazolium cores in their structure applied to different catalytic processes.

1.2 Thesis outline

Ligand design is a very interesting and widely studied topic in homogeneous catalysis, it has been presented as a brief general introduction in Chapter I, contemplating selected examples using xantphos as bidentate ligand for different catalytic processes. The incentive was to highlight the importance of the optimization of existing catalytic reactions, advancement towards catalyst stability as well as development of sustainable and efficient methodologies; areas which are the main focus of this thesis.

Each research chapter contains its own specialized introduction to contextualize and familiarize the reader with the topic and content of the section.

The synthesis and complexation of *para*-modified xantphos ligands for the evaluation of the phosphine ligand effect in photocatalytic applications is discussed in Chapter II. The selected model reaction was the Cross Dehydrogenative Coupling (CDC) of 1,2,3,4-tetrahydro-2-phenyl isoquinoline with nitromethane photocatalyzed by $[\text{Cu}(p\text{-R-xantphos})(\text{dmp})]\text{BF}_4$ complexes.

The synthesis of potentially recyclable imidazolium-tagged xant-type ligands and their application in the Ruthenium Catalyzed C–O bond cleavage of 2-phenoxy-1-phenylethanol in ionic liquids is discussed in chapter III.

Towards energy utilization, the last research section, Chapter IV, discusses the photocatalytic CO_2 reduction in ionic liquid media by $[\text{Cu}(\text{xantphos})(\text{bcp})]\text{PF}_6$, $[\text{Cu}(\text{POP-xantphos})(\text{bcp})]\text{PF}_6$ and $[\text{Cu}(\text{Imidazolium-tagged POP-xantphos})(\text{bcp})]\text{PF}_6$ complexes. This chapter faces the challenges of performing photocatalysis in alternative solvents.

Lastly, Chapter V contains the experimental sections corresponding to each research chapter.

1.3 References

1. Kamer, P. C. J.; van Leeuwen, P. W. N. M.; Reek, J. N. H. Wide Bite Angle Diphosphines: Xantphos Ligands in Transition Metal Complexes and Catalysis. *Acc. Chem. Res.* **2001**, *34* (11), 895-904.
2. Gillespie, J. A.; Dodds, D. L.; Kamer, P. C. J. Rational design of diphosphorus ligands - a route to superior catalysts. *Dalton Trans.* **2010**, *39* (11), 2751-2764.
3. Leyssens, T.; Peeters, D.; Orpenb, G.; Harvey, N.J. Insight into metal-phosphorus bonding from analysis of the electronic structure of redox pairs of metal-phosphine complexes. *New J. Chem.* **2005**, *29*, 1424-1430.
4. Marynick, D. S. π -Accepting abilities of phosphines in transition-metal complexes. *J. Am. Chem. Soc.* **1984**, *106* (14), 4064-4065.
5. Knowles, W. S., Asymmetric hydrogenations (Nobel Lecture). *Angew. Chem. Int. Ed.* **2002**, *41* (12), 1998-2007.
6. Noyori, R. Asymmetric catalysis: science and opportunities (Nobel Lecture). *Angew. Chem. Int. Ed.* **2002**, *41* (12), 2008-2022.
7. Nicolaou, K. C.; Bulger, P. G.; Sarlah, D. Palladium-catalyzed cross-coupling reactions in total synthesis. *Angew. Chem. Int. Ed.* **2005**, *44* (29), 4442-4489.
8. Kamer, P. C. J.; van Leeuwen, P. W. N. M. Phosphorus(III)Ligands in Homogeneous Catalysis: Design and Synthesis. *Wiley*. **2012**, 978-0-470-66627-2.
9. Tolman, C. A. Steric effects of phosphorus ligands in organometallic chemistry and homogeneous catalysis. *Chem. Rev.* **1977**, *77* (3), 313-348.
10. Tolman, C. A. Electron donor-acceptor properties of phosphorus ligands. Substituent additivity. *J. Am. Chem. Soc.* **1970**, *92* (10), 2953-2956.
11. Mann, B. E.; Musco, A. A phosphorus-31 nuclear magnetic resonance investigation of the structure, equilibria, and kinetics of $[\text{Pt}(\text{PR}_3)_n]$ in solution. *J. Chem. Soc., Dalton Trans.* **1980**, (5), 776-785.
12. Roodt, A.; Otto, S.; Steyl, G. Structure and solution behaviour of rhodium(I) Vaska-type complexes for correlation of steric and electronic properties of tertiary phosphine ligands. *Coord. Chem. Rev.* **2003**, *245* (1-2), 121-137.
13. Banger, K. K.; Brisdon, A. K.; Herbert, C. J.; Ghaba, H. A.; Tidmarsh, I. S. Fluoroalkenyl, fluoroalkynyl and fluoroalkyl phosphines. *J. Fluorine Chem.* **2009**, *130* (12), 1117-1129.
14. Allman, T.; Goel, R. G. The basicity of phosphines. *Can. J. Chem.* **1982**, *60* (6), 716-722.
15. Beckmann, U.; Sueslueyan, D.; Kunz, P. Is the $^1J_{\text{PSe}}$ Coupling Constant a Reliable Probe for the Basicity of Phosphines? A ^{31}P NMR Study. *Phosphorus, Sulfur Silicon Relat. Elem.* **2011**, *186* (10), 2061-2070.
16. White, D.; Tavener, B. C.; Leach, P. G. L.; Coville, N. J. Solid angles I. The radial profile. *J. Organomet. Chem.* **1994**, *478* (1-2), 205-211.
17. White, D.; Tavener, B. C.; Coville, N. J.; Wade, P. W. Solid angles. III. The role of conformers in solid angle calculations. *J. Organomet. Chem.* **1995**, *495* (1-2), 41-51.
18. Brown, T. L.; Lee, K. J. Ligand steric properties. *Coord. Chem. Rev.* **1993**, *128* (1-2), 89-116.
19. Bilbrey, J. A.; Kazez, A. H.; Locklin, J.; Allen, W. D. Exact Ligand Solid Angles. *J. Chem. Theory Comput.* **2013**, *9* (12), 5734-5744.

20. Dierkes, P.; van Leeuwen, P. W. N. M. The bite angle makes the difference: a practical ligand parameter for diphosphine ligands. *J. Chem. Soc., Dalton Trans.* **1999**, (10), 1519-1530.
21. Casey, C. P.; Whiteker, G. T. The natural bite angle of chelating diphosphines. *Isr. J. Chem.* **1990**, 30 (4), 299-304.
22. Freixa, Z.; Van Leeuwen, P. W. N. M. Bite angle effects in diphosphine metal catalysts: steric or electronic? *Dalton Trans.* **2003**, (10), 1890-1901.
23. Kranenburg, M.; van der Burgt, Y. E. M.; Kamer, P. C. J.; van Leeuwen, P. W. N. M.; Goubitz, K.; Fraanje, J. New Diphosphine Ligands Based on Heterocyclic Aromatics Inducing Very High Regioselectivity in Rhodium-Catalyzed Hydroformylation: Effect of the Bite Angle. *Organometallics*. **1995**, 14 (6), 3081-3089.
24. van Leeuwen, P. W. N. M.; Kamer, P. C. J. Featuring Xantphos. *Catal. Sci. Technol.* **2018**, 8 (1), 26-113.
25. Kranenburg, M.; Kamer, P. C. J.; van Leeuwen, P. W. N. M.; Vogt, D.; Keim, W. Effect of the bite angle of diphosphine ligands on activity and selectivity in the nickel-catalyzed hydrocyanation of styrene. *J. Chem. Soc., Chem. Commun.* **1995**, (21), 2177-2178.
26. Van der Veen, L. A.; Boele, M. D. K.; Bregman, F. R.; Kamer, P. C. J.; Van Leeuwen, P. W. N. M.; Goubitz, K.; Fraanje, J.; Schenk, H.; Bo, C. Electronic Effect on Rhodium Diphosphine Catalyzed Hydroformylation: The Bite Angle Effect Reconsidered. *J. Am. Chem. Soc.* **1998**, 120 (45), 11616-11626.
27. Van der Veen, L. A.; Keeven, P. H.; Schoemaker, G. C.; Reek, J. N. H.; Kamer, P. C. J.; Van Leeuwen, P. W. N. M.; Lutz, M.; Spek, A. L. Origin of the Bite Angle Effect on Rhodium Diphosphine Catalyzed Hydroformylation. *Organometallics*. **2000**, 19 (5), 872-883.
28. Shaw, L.; Somisara, D. M. U. K.; How, R. C.; Westwood, N. J.; Bruijninx, P. C. A.; Weckhuysen, B. M.; Kamer, P. C. J. Electronic and bite angle effects in catalytic C-O bond cleavage of a lignin model compound using ruthenium Xantphos complexes. *Catal. Sci. Technol.* **2017**, 7 (3), 619-626.
29. Van Haaren, R. J.; Oevering, H.; Coussens, B. B.; Van Strijdonck, G. P. F.; Reek, J. N. H.; Kamer, P. C. J.; Van Leeuwen, P. W. N. M. On the influence of the bite angle of bidentate phosphane ligands on the regioselectivity in allylic alkylation. *Eur. J. Inorg. Chem.* **1999**, (8), 1237-1241.
30. Kranenburg, M.; Kamer, P. C. J.; Van Leeuwen, P. W. N. M. The effect of the bite angle of diphosphine ligands on activity and selectivity in palladium-catalyzed allylic alkylation. *Eur. J. Inorg. Chem.* **1998**, (1), 25-27.
31. Harris, M. C.; Geis, O.; Buchwald, S. L. Sequential N-arylation of primary amines as a route to alkyl diarylamines. *J. Org. Chem.* **1999**, 64 (16), 6019-6022.
32. Guari, Y.; Van Es, D. S.; Reek, J. N. H.; Kamer, P. C. J.; Van Leeuwen, P. W. N. M. An efficient, palladium-catalyzed amination of aryl bromides. *Tetrahedron Lett.* **1999**, 40 (19), 3789-3790.
33. Kranenburg, M.; Kamer, P. C. J.; Van Leeuwen, P. W. N. M. The effect of the bite angle of diphosphine ligands on activity and selectivity in palladium-catalyzed cross-coupling. *Eur. J. Inorg. Chem.* **1998**, (2), 155-157.
34. McKinney, R. J.; Roe, D. C. The mechanism of nickel-catalyzed ethylene hydrocyanation. Reductive elimination by an associative process. *J. Am. Chem. Soc.* **1986**, 108 (17), 5167-5173.

35. Marcone, J. E.; Moloy, K. G. Kinetic Study of Reductive Elimination from the Complexes (Diphosphine)Pd(R)(CN). *J. Am. Chem. Soc.* **1998**, *120* (33), 8527-8528.
36. Unruh, J. D.; Christenson, J. R. A study of the mechanism of rhodium/phosphine-catalyzed hydroformylation: use of 1,1'-bis(diarylphosphino)ferrocene ligands. *J. Mol. Catal.* **1982**, *14* (1), 19-34.
37. Casey, C. P.; Paulsen, E. L.; Beuttenmueller, E. W.; Proft, B. R.; Petrovich, L. M.; Matter, B. A.; Powell, D. R. Electron Withdrawing Substituents on Equatorial and Apical Phosphines Have Opposite Effects on the Regioselectivity of Rhodium Catalyzed Hydroformylation. *J. Am. Chem. Soc.* **1997**, *119* (49), 11817-11825.
38. Nichols, J. M.; Bishop, L. M.; Bergman, R. G.; Ellman, J. A. Catalytic C-O Bond Cleavage of 2-Aryloxy-1-arylethanol and Its Application to the Depolymerization of Lignin-Related Polymers. *J. Am. Chem. Soc.* **2010**, *132* (36), 12554-12555.
39. Cole-Hamilton, D. J. Homogeneous Catalysis--New Approaches to Catalyst Separation, Recovery, and Recycling. *Science* **2003**, *299* (5613), 1702-1706.
40. Schreuder Goedheijt, M.; Kamer, P. C. J.; van Leeuwen, P. W. N. M. A water-soluble diphosphine ligand with a large 'natural' bite angle for two-phase hydroformylation of alkenes. *J. Mol. Catal. A: Chem.* **1998**, *134* (1-3), 243-249.
41. Desset, S. L.; Cole-Hamilton, D. J. Carbon dioxide induced phase switching for homogeneous-catalyst recycling. *Angew. Chem. Int. Ed.* **2009**, *48* (8), 1472-1474.
42. Buhling, A.; Elgersma, J. W.; Nkrumah, S.; Kamer, P. C. J.; van Leeuwen, P. W. N. M. Novel amphiphilic diphosphines: synthesis, rhodium complexes, use in hydroformylation and rhodium recycling. *Dalton Trans.* **1996**, (10), 2143-2154.
43. Adams, D. J.; Cole-Hamilton, D. J.; Harding, D. A. J.; Hope, E. G.; Pogorzelec, P.; Stuart, A. M. Towards the synthesis of perfluoroalkylated derivatives of Xantphos. *Tetrahedron.* **2004**, *60* (18), 4079-4085.
44. Bronger, R. P. J.; Silva, S. M.; Kamer, P. C. J.; van Leeuwen, P. W. N. M. A novel dicationic phenoxaphosphino-modified Xantphos-type ligand: a ligand for highly active and selective, biphasic, rhodium catalysed hydroformylation in ionic liquids. *Dalton Trans.* **2004**, (10), 1590-1596.
45. Webb, P. B.; Kunene, T. E.; Cole-Hamilton, D. J. Continuous flow homogeneous hydroformylation of alkenes using supercritical fluids. *Green Chem.* **2005**, *7* (5), 373-379.
46. Kunene, T. E.; Webb, P. B.; Cole-Hamilton, D. J. Highly selective hydroformylation of long-chain alkenes in a supercritical fluid ionic liquid biphasic system. *Green Chem.* **2011**, *13* (6), 1476-1481.
47. Bronger, R. P. J.; Silva, S. M.; Kamer, P. C. J.; Leeuwen, P. W. N. M. A novel dicationic phenoxaphosphino-modified Xantphos-type ligand—a unique ligand specifically designed for a high activity, selectivity and recyclability. *Chem. Commun.* **2002**, (24), 3044-3045.
48. Hansch, C.; Leo, A.; Taft, R. W. A Survey of Hammett Substituent Constants and Resonance and Field Parameters. *Chem. Rev.* **1991**, *97*, 165-195.
49. Allman, T.; Goel, R. The basicity of phosphines. *Can. J. Chem.* **1982**, *60*, 716-722.

Chapter II: Electronic phosphine ligand effects on the photochemistry of heteroleptic Cu(I) complexes: A comprehensive study.

2.1 Introduction

2.1.1 Heteroleptic copper complexes in the context of energy utilization

The increasing global consumption of energy encourages the search for solutions to supply and efficiently utilize it. Those are major challenges the human population is facing. World energy statistics and projections underline the increased consumption of energy from 13.5 TW in 2001 to 27.6 TW in 2050, reaching 43.0 TW in 2100.¹ In 2013, 86% of this energy was produced from fossil fuels, thus impacting the environment due to the increase in the CO₂ levels and the well-known related problems.² Therefore, the development of more efficient systems able to produce and use carbon-neutral energy (solar, eolic, geothermal, etc.) is of great demand. Among the various sources of energy, solar radiation is one of the most attractive; significant progress has been achieved for its capture, conversion and storage.³ Moreover, it can also be used to promote chemical reactions (photoreaction) which can be accelerated by a catalyst (photocatalyst). In this field several transition metal complexes have been utilized as photocatalyst mainly based on expensive transition metals such as iridium and ruthenium.⁴⁻⁷ It has been recently shown that copper can promote several transformations being an attractive alternative to more precious metals.⁸ The advantage of using copper lies notably in its cheaper price and higher abundancy when compared with other elements.⁹

This part of this thesis is focused on cationic heteroleptic copper(I) complexes bearing bidentate nitrogen and phosphorous ligands with general formula $[\text{Cu}(\text{N}^{\wedge}\text{N})(\text{P}^{\wedge}\text{P})]^+$, where neocuproine or bathocuproine are the N[^]N ligand and xantphos the P[^]P ligand. In the next sections an overview of the characteristics of these complexes and their applications in photocatalysis is presented.

2.1.1.1 Homoleptic $[\text{Cu}(\text{N}^{\wedge}\text{N})_2]^+$ complexes

Copper(I) coordination compounds bearing identical ligands, proved to be of great interest due to their comparable excited state properties with the more expensive $[\text{Ru}^{\text{II}}(\text{bpy})_3]^{2+}$ (Figure 1).⁹ Among them, copper(I) phenanthroline complexes usually absorb UV-Vis light in a range between 350-650 nm with high extinction coefficients ($\epsilon \sim 10^3\text{--}10^4 \text{ M}^{-1}\text{cm}^{-1}$). The excited states are metal to ligand charge transfer states (MLCT),¹⁰ accessible upon light absorption and promotion of an electron from the d orbitals of copper to the π^* orbitals of the ligand, it is formally a Cu(II) metal center coordinated to a reduced ligand, $[\text{Cu}^{\text{II}}(\text{N}^{\wedge}\text{N})(\text{N}^{\wedge}\text{N}^{\cdot-})]^{+*}$. These MLCT excited states are emissive with lifetimes $\tau = 10^{-9}\text{--}10^{-7}$ s at room temperature in CH_2Cl_2 solution.¹¹⁻¹³

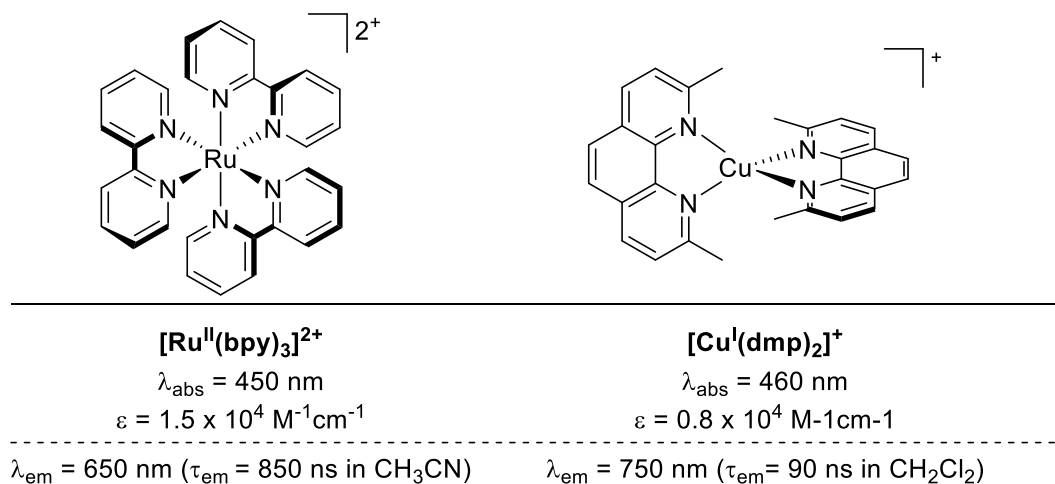
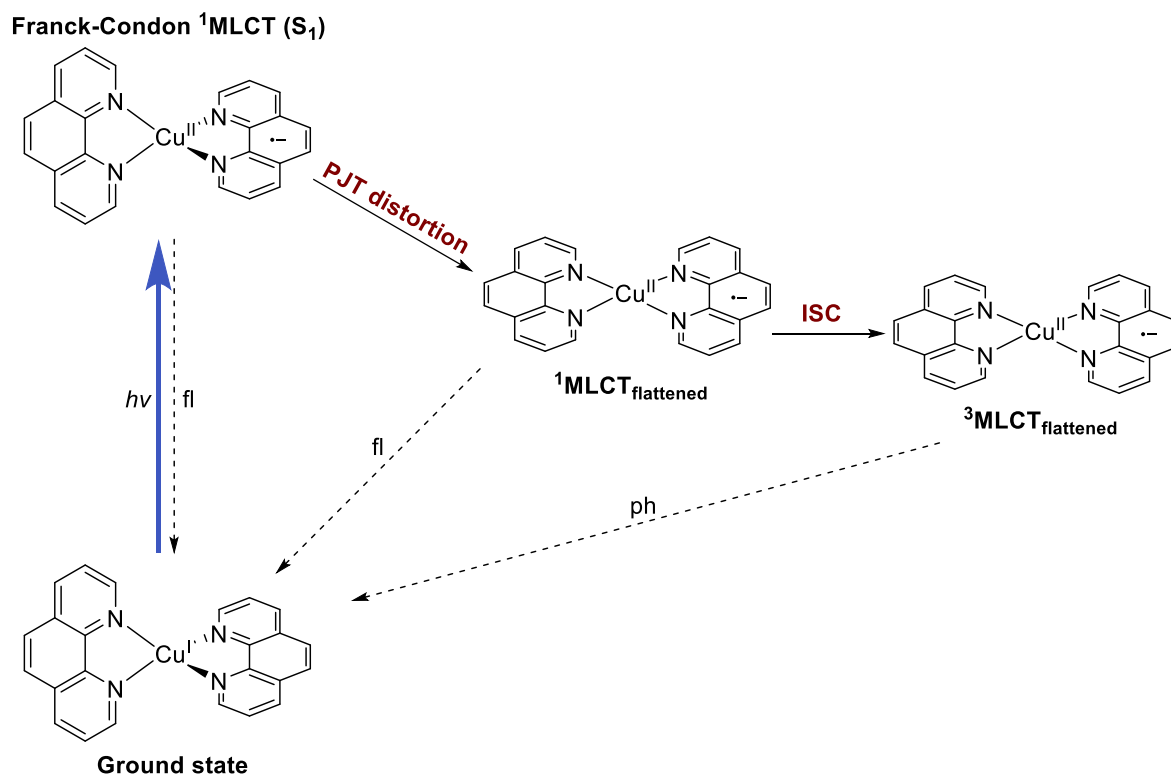


Figure 1. Comparison between the photophysical properties of $[\text{Ru}^{\text{II}}(\text{bpy})_3]^{2+}$ and $[\text{Cu}^{\text{I}}(\text{dmp})_2]^+$.⁹

When absorbing light, the copper center formally oxidizes from Cu(I) to Cu(II) and therefore possesses different structural and electrochemical properties. Regarding their geometry, Cu(I) is d^{10} and prefers a tetrahedral geometry, on the other hand Cu(II) is d^9 and adopts a Jahn-Teller distorted square planar arrangement. Therefore, when Cu(I) is excited it has to undergo a structural reorganization and this can be hampered by increasing the steric bulk of the phenanthroline ligand at the 2,9 positions (adjacent to the nitrogen). In fact, it was found that it is easier to oxidize $\text{Cu}^{\text{I}}(\text{phen})_2$ than $\text{Cu}^{\text{I}}(\text{dmp})_2$, with a 400 mV difference in redox potential, because the former can change geometry more easily than the latter. Apart from steric factors, their redox chemistry is also solvent dependent. For example, the $E_{1/2}$ for the

couple Cu(I)/Cu(II) is 0.93 V in CH₂Cl₂, 0.77 V in CH₃CN and 0.64 V in DMSO with a common electrolyte versus a silver wire reference.¹⁰ A proposed model accounting for their relaxation is presented below (Scheme 1).



Scheme 1. Schematic model for photoexcitation and the relaxation of [Cu^{II}(phen)₂]⁺ type complexes. General geometrical changes of homoleptic bis-diimine Cu(I) complexes upon excitation. Radiative transitions (fluorescence (fl) and phosphorescence (ph)) are shown as dashed lines and non-radiative transitions as thin solid lines.¹⁴⁻¹⁶

Upon excitation the Franck-Condon ¹MLCT state is populated, which is necessarily a singlet state and undergoes vibrational relaxation in the form of pseudo Jahn-Teller distortion to ¹MLCT_{flattened}.¹⁷⁻¹⁸ This relaxation causes a significant red shift in the emission spectra of these complexes.¹⁹ The system populates the triplet ³MLCT_{flattened} state by intersystem crossing (ISC). Finally, as a result of this flattening, it opens the coordination sphere around the copper center for coordination of a donor molecule, usually solvent, forming an exciplex and quenching their emission.²⁰⁻²¹ Radiative relaxation to the ground state as emission is

possible either from $^1\text{MLCT}_{\text{flattened}}$ or $^3\text{MLCT}_{\text{flattened}}$, the former as fluorescence (fl) and the latter as phosphorescence (ph).

2.1.1.2 Heteroleptic $[\text{Cu}(\text{N}^{\wedge}\text{N})(\text{PPh}_3)_2]^+$ complexes

In addition to homoleptic complexes, heteroleptic complexes where the metal binds to different types of ligands have been explored. The first family of related heteroleptic complexes studied is described by the general formula $[\text{Cu}(\text{N}^{\wedge}\text{N})(\text{PPh}_3)_2]\text{X}$. Their behavior in solution is complex and their photophysical properties depend on the nature of the phenanthroline ligand, the solvent and the counterion. Moreover, defining their speciation in solution is not straightforward due to their tendency to undergo ligand redistribution reactions. For example, the comparison between $[\text{Cu}(\text{dmp})(\text{PPh}_3)_2]^+$ and $[\text{Cu}(\text{phen})(\text{PPh}_3)_2]^+$ is illustrative, where dmp is 2,9-dimethyl-1,10-phenanthroline and phen an unsubstituted phenanthroline.²² They exist as heteroleptic complexes due to the synergic effect associated with the σ -donating PPh_3 and π -acceptor phenanthroline, but steric factors play a role. The complex $[\text{Cu}(\text{dmp})(\text{PPh}_3)_2]^+$ possesses methyl groups on the phenanthroline ligand, which leads to unfavorable steric interactions with the phenyl groups of the phosphines and promotes their dissociation. Overall, the combination of steric constraints and coordinating factors make the preparation of a CH_2Cl_2 solution in which $[\text{Cu}(\text{dmp})(\text{PPh}_3)_2]^+$ is the only complex present difficult to characterize, whereas it is possible with $[\text{Cu}(\text{phen})(\text{PPh}_3)_2]^+$. These two complexes are comparable emitters in the solid state. In solution, their emission is quenched by solvent-induced exciplex quenching upon transient coordination of the solvent and the coordination number of the copper center increases from four to five. Therefore, the emission of $[\text{Cu}(\text{phen})(\text{PPh}_3)_2]^+$ is lower in methanol ($\phi = 2.8 \times 10^{-5}$) than in CH_2Cl_2 ($\phi = 6.6 \times 10^{-4}$) because the former is more nucleophilic, thus more efficient as quencher. In methanol the emission of $[\text{Cu}(\text{dmp})(\text{PPh}_3)_2]^+$ ($\phi = 1.4 \times 10^{-3}$) is higher than the one of $[\text{Cu}(\text{phen})(\text{PPh}_3)_2]^+$ ($\phi = 2.8 \times 10^{-5}$) because the steric crowding around the copper center prevents coordination of the quencher.

These comparisons highlight the importance of choosing the right combination of ligands in order to achieve stability and high emissions. Apart from varying the steric crowding around the metal center by substituting the 2,9 positions of the phenanthroline, the electronic properties of the phosphine have been investigated for a series of $[\text{Cu}(\text{dmp})(p\text{-R-PPh}_3)_2]\text{BF}_4$ ($\text{R} = \text{Me}, \text{H}, \text{Cl}$) complexes. McMillin et al. studied the effect of the phosphine ligand on the

stability of Cu(I) complexes. In this study the ligand dmp was kept constant while the triphenylphosphine ligand was varied for a family of $[\text{Cu}(\text{dmp})(p\text{-R-PPh}_3)_2]\text{BF}_4$ complexes. They observed systematic changes on the emission responding to variation in donor strength of the phosphine where more basic phosphine donors increased the electron density of the copper center, affecting the charge transfer excited states by lowering their energy.²³

2.1.1.3 Heteroleptic $[\text{Cu}(\text{N}^{\wedge}\text{N})(\text{P}^{\wedge}\text{P})]^+$ complexes based on chelating diphosphines

Two major drawbacks of the $[\text{Cu}(\text{N}^{\wedge}\text{N})(\text{PPh}_3)_2]^+$ complexes are the exciplex quenching in nucleophilic solvents and the poor control of speciation in non-coordinating media.²²⁻²³ In order to overcome these problems, bidentate chelating phosphines have been studied and $[\text{Cu}(\text{N}^{\wedge}\text{N})(\text{DPEphos})]^+$ was the first example.²⁴⁻²⁵ DPEphos shows improved photophysical properties when compared to its triphenylphosphine analogues (Table 1). The emission properties depend on the steric bulk of the phenanthroline used, in fact comparable values were measured for the unsubstituted $[\text{Cu}(\text{phen})(\text{DPEphos})]^+$ and $[\text{Cu}(\text{phen})(\text{PPh}_3)_2]^+$, whereas $[\text{Cu}(\text{dmp})(\text{DPEphos})]^+$ possesses higher emission with remarkable longer lifetime.

Table 1. Photophysical data for heteroleptic copper(I) complexes in CH_2Cl_2 at room temperature.

| Complex | λ_{abs} (nm) | λ_{em} (nm) | Φ | τ , μs |
|--|-----------------------------|----------------------------|--------|------------------------|
| $[\text{Cu}(\text{phen})(\text{DPEphos})]^+$ | 391 | 700 | 0.0018 | 0.19 |
| $[\text{Cu}(\text{dmp})(\text{DPEphos})]^+$ | 383 | 570 | 0.15 | 14.3 |
| $[\text{Cu}(\text{phen})(\text{PPh}_3)_2]^+$ | 370 | 680 | 0.0007 | 0.22 |
| $[\text{Cu}(\text{dmp})(\text{PPh}_3)_2]^+$ | 365 | 560 | 0.0014 | 0.33 |
| $[\text{Cu}(\text{dmp})(\text{dppe})]^+$ | 400 | 630 | 0.010 | 1.33 |

An interesting observation is that solvent-induced exciplex quenching is less effective for DPEphos complexes than the for those bearing PPh_3 . In fact, the life time of $[\text{Cu}(\text{dmp})(\text{DPEphos})]^+$ in methanol is 2.4 μs whereas the one of $[\text{Cu}(\text{dmp})(\text{PPh}_3)_2]^+$ is just 330 ns and its emission perseveres in acetone ($\tau = 3.8 \mu\text{s}$) and acetonitrile ($\tau = 1.1 \mu\text{s}$). The superior emission properties of $[\text{Cu}(\text{dmp})(\text{DPEphos})]^+$ might result from the introduction of the bidentate phosphine which hampers ligand dissociation and favors the pseudo tetrahedral geometry instead the flattened one resisting the typical distortion.²⁵ Another reason for this fact could be attributed to the better interlocking caused by ligand-ligand interactions of

bulkier ligands, which could suppress exciplex quenching and provide major rigidity when compared to the one with two PPh_3 , similarly to the previously reported effect present in homoleptic $[\text{Cu}(\text{N}^{\wedge}\text{N})]_2^+$ bearing biquinoline ligands.²⁶

2.1.1.4 Modification of $[\text{Cu}(\text{N}^{\wedge}\text{N})(\text{P}^{\wedge}\text{P})]^+$: phenanthroline

After the discovery of the superior photophysical performances achievable when using bidentate phosphines, the search for the best combination of $\text{N}^{\wedge}\text{N}$ and $\text{P}^{\wedge}\text{P}$ ligand started. The functionalization of the phenanthroline scaffold has been intensively considered in order to rationalize factors that augment stability, photochemical properties and catalytic performance of the heteroleptic $[\text{Cu}(\text{N}^{\wedge}\text{N})(\text{P}^{\wedge}\text{P})]^+$ type complexes. A detailed study investigating the stability of these complexes was reported by Armaroli and co-workers using an extensive combination of different $\text{P}^{\wedge}\text{P}$ and $\text{N}^{\wedge}\text{N}$ ligands (Figure 2).²⁷

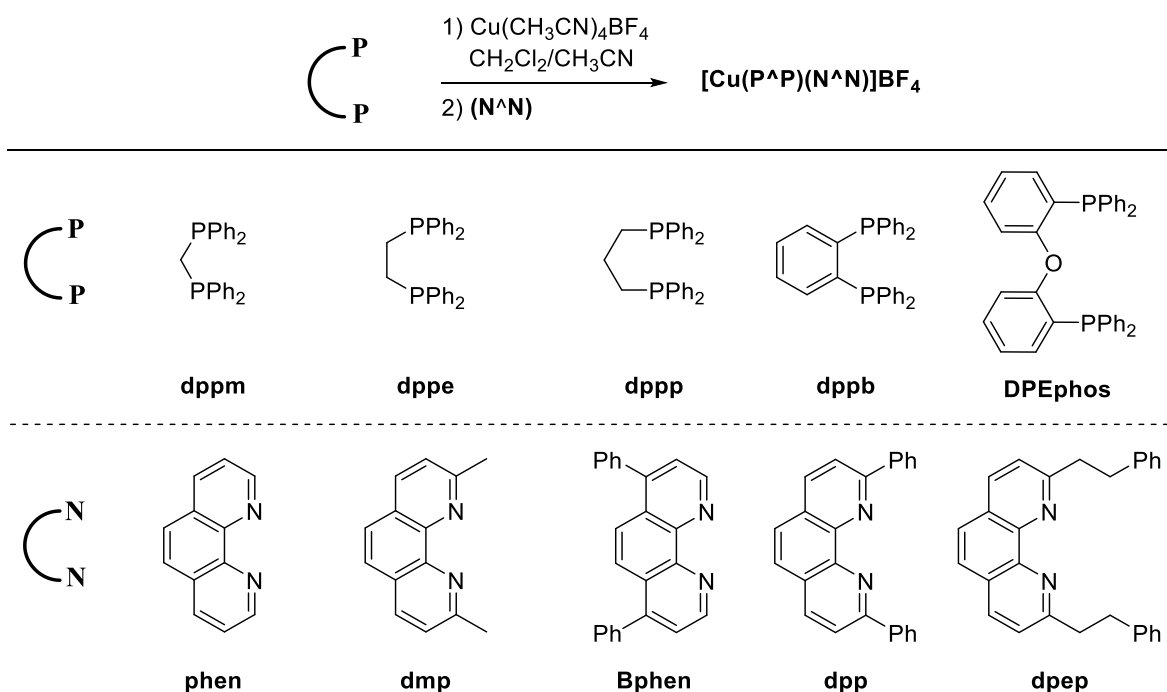


Figure 2. $\text{N}^{\wedge}\text{N}$ and $\text{P}^{\wedge}\text{P}$ ligands used for preparation of heteroleptic $[\text{Cu}(\text{N}^{\wedge}\text{N})(\text{P}^{\wedge}\text{P})]^+$ complexes.

The authors concluded that stable heteroleptic complexes were always formed with all the $\text{P}^{\wedge}\text{P}$ ligands tested in combination with unsubstituted **phen** or with the 4,7 substituted **Bphen**. Conversely, bulkier substituents at the 2,9 positions resulted in more labile complexes (Table 2). Complexes bearing **dmp** could be isolated. Although stable in the solid state, these

complexes undergo disproportionation in solution even in apolar solvents such as CD₂Cl₂. Homoleptic/heteroleptic ratios are highly dependent on the bidentate ligand. It was also found that increasing the size of the substituent at the 2 and 9 positions of the N[^]N ligand (e.g. from methyl of **dmp** to phenyl in **dpp**) led to the exclusive formation of the homoleptic complexes. This instability is due to the steric interaction between the 2,9 substituents of the phenanthroline and the PPh₂ groups of the phosphine, which increases in the order **dmp** < **dpep** < **dpp**. Noteworthy, **DPEphos** is able to form almost exclusively heteroleptic complex with both **dmp** and **dpep** due to the destabilization of the [Cu(P[^]P)₂]⁺ and favorable orientation of PPh₂ groups limiting the steric interaction with the 2,9 substituents of the N[^]N ligand. Therefore, it is not surprising that similar P[^]P ligands, such as xantphos, have been used in different applications, which are presented in the following sections.

Table 2. Proportion of heteroleptic complex as deduced from integration of the ¹H NMR spectra of the crude product mixture.

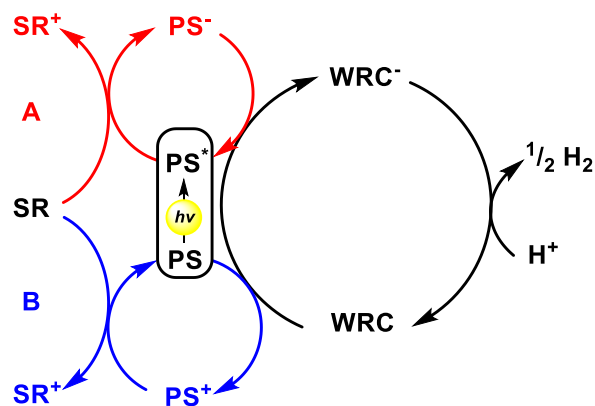
| | dmp | dpep | dpp |
|----------------|------------|-------------|------------|
| dppm | 30% | 10% | traces |
| dppe | 80% | 15% | traces |
| dppp | 80% | 10% | traces |
| dppb | 65% | 5% | traces |
| DPEphos | >99.5% | >99.5% | traces |

2.1.2 Applications of [Cu(N[^]N)(P[^]P)]⁺ complexes

2.1.2.1 Catalysis

Water reduction

The main motivation for these investigations on this topic lies in the utilization of solar energy being the most abundant energy source to produce hydrogen from water. This is a clean and sustainable approach for hydrogen production which does not affect the environment by causing pollution.²⁸ The catalytic reduction of water to hydrogen is one of the most studied reactions catalyzed by [Cu(N[^]N)(P[^]P)]⁺ complexes. In this transformation, the aforementioned complexes are used as photosensitizers (PS) in combination with a water reduction catalyst (WRC) and a sacrificial electron donor (SR)²⁹ (Scheme 2).



Scheme 2. Cycles for the photocatalytic proton reduction. Pathway A (red): reductive quenching cycle; Pathway B (blue): oxidative quenching cycle.³⁰

A common feature throughout the different reports is the methodical modification of the phenanthroline ligand. The first study was reported in 2013 by Beller and co-workers, who used $[\text{Fe}_3(\text{CO})_{12}]$ as the WRC in combination with triethylamine as SR.³⁰ Firstly, they investigated the effect of the functionalization of the N^N ligand in combination with DPEphos. Among the nitrogen donor ligands tested, bathocuproine (bcp) showed significant activity ($\text{TON} = 477$) due to both steric and electronic factors. The methyl groups of bathocuproine help to reduce the non-radiative decay, and prevent exciplex quenching by obstructing the expansion of the coordination sphere around the metal center. The electronegative phenyl groups may provide π^* states lower in energy that facilitate MLCT. After showing the superior performance of bcp, different P^P ligands have been tested (Figure 3).

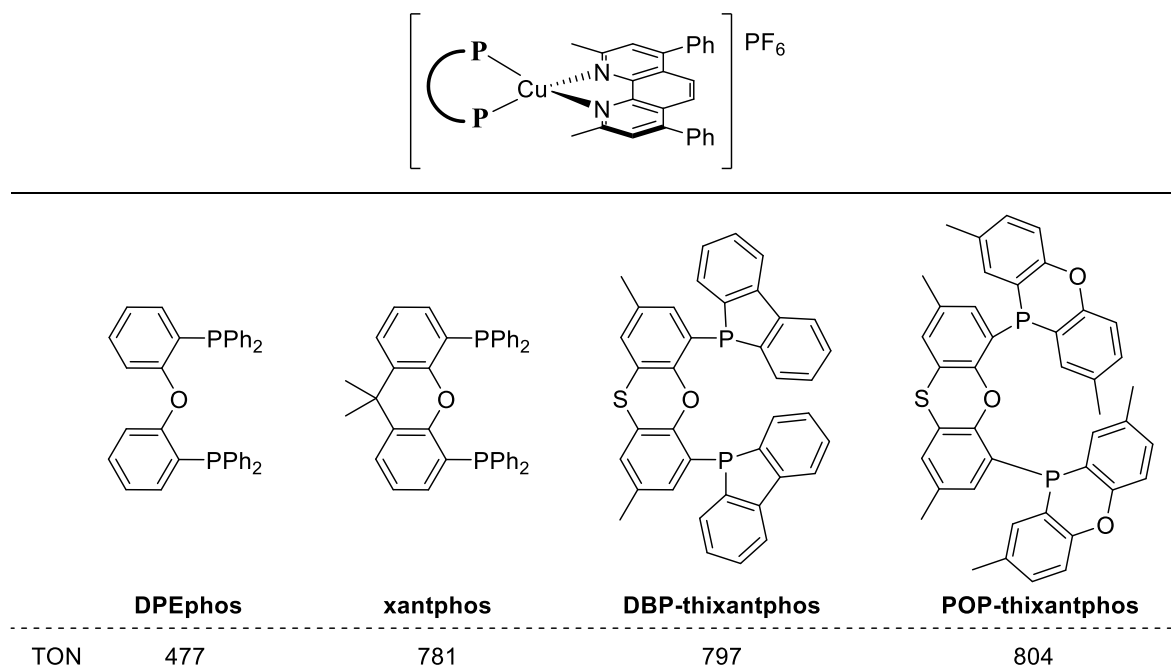


Figure 3. Activity of $[\text{Cu}(\text{N}^{\wedge}\text{N})(\text{P}^{\wedge}\text{P})]^+$ photosensitizers in water reduction.

Xantphos gave better performance (TON = 781) with respect to DPEphos due to the larger bite angle and higher rigidity. The highest activities were achieved with DBP-thixantphos (TON = 797) and POP-thixantphos (TON = 804). It is worth mentioning that under their reaction conditions these three copper complexes outperformed the classic and more expensive $[\text{Ru}(\text{bipy})_3]\text{Cl}_2$ (TON = 58) and $[\text{Ir}(\text{bipy})(\text{ppy})_2]\text{PF}_6$ (TON = 576).

After this first report, major efforts were made in tuning the phenanthroline scaffold. Beller and co-workers reported a comprehensive library of phenanthroline ligands with different steric and electronic properties.³¹ The related copper complexes were formed in situ using xantphos or POP-thixantphos as the $\text{P}^{\wedge}\text{P}$ ligand and they were compared in catalysis. In all cases the latter showed better performances presumably because of the lower steric hindrance between the phenanthroline and the phosphine ligand resulting from the more rigid structure around the phosphorus atoms. The steric bulk of the 2,9 substituents of the phenanthroline ligands was analyzed using **A–E**, and the optimal structure was found using *s*-Bu (Figure 4, top). The electronic effects were probed using **I–O**, which possess an olefin spacer to place the substituents far from the metal center in order to avoid any extra steric contribution (Figure 4, bottom). A linear correlation between the Hammett parameter and activity exist

for this series of compounds, with electron donating groups being the less active, presumably due to the destabilization of the excited state.

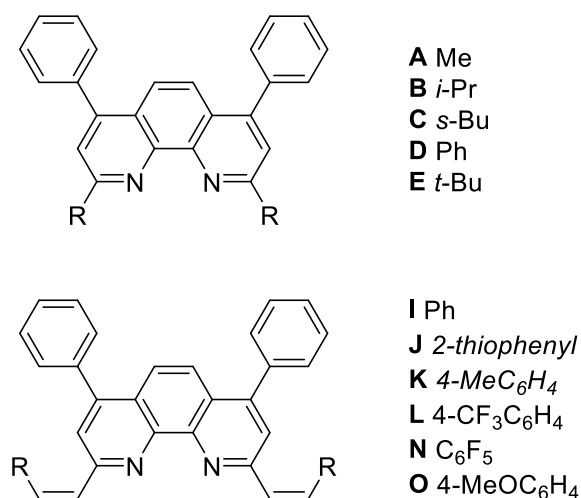


Figure 4. Phenanthroline ligands tested in water reduction mediated by [Cu(N[^]N)(P[^]P)]⁺ photosensitizers.

Finally, phenyl substituents in the 4,7 positions, such as the bathocuproine structure, provided one of the choices to achieve high TONs. Overall, the best catalyst proved to be the one bearing POP-thixantphos as P[^]P ligand and **C** as N[^]N ligand, which is a bulkier phenanthroline possessing *sec*-butyl groups at the 2,9 positions. A further improvement of the performance of the CuPSs was made by incorporating a triphenylamine substituent instead of the phenyl moiety at the 4,7 position (Figure 5), which generates intra-ligand charge transfer (ILCT) excited states resulting in outstanding absorption and excited-state lifetime. This is reflected in superior performances with an astonishing TON = 19000 and TOF = 1800 h⁻¹.³²

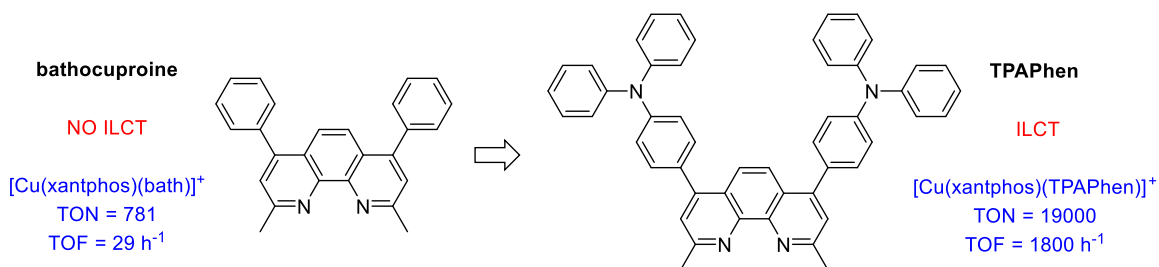


Figure 5. Structure of TPAPhen in comparison with bathocuproine structure and activity of the related CuPSs.

Recently, two diimine ligands possessing extended π -system in the backbone (Figure 6) have been tested with the aim of increasing conjugation, consequently augment the extinction coefficients and induce a redshifted absorption.³³ Experimentally, these complexes revealed very weak emissions, which implies rapid deactivation processes. As a consequence, copper complexes using these diamine ligands performed poorly in the reduction of water to hydrogen.

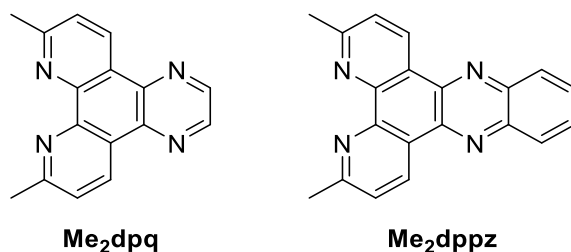
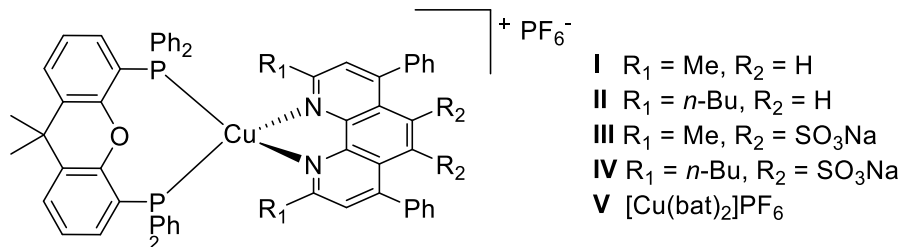


Figure 6. Structures of the diimine ligands with extended π -system in the backbone.

In parallel to the search for a high performing PSs, researchers investigated the various steps of the photocatalysis involving these species. Lochbrunner and co-workers reported a detailed time-resolved spectroscopic analysis of several heteroleptic copper sensitizers $[\text{Cu}(\text{N}^{\wedge}\text{N})(\text{P}^{\wedge}\text{P})]^+$ concerning their initial light-induced intramolecular electron transfer and their relaxation steps in order to compare them with the parent homoleptic $[\text{Cu}(\text{N}^{\wedge}\text{N})_2]^+$ and rationalize their higher performances.³⁴ The excitation of the $[\text{Cu}(\text{N}^{\wedge}\text{N})_2]^+$ depends on the wavelength used and can populate directly the S_1 (singlet state) or excite the S_n (where $n \geq 2$) state followed by fast population of the S_1 state in ~ 100 fs.³⁵⁻³⁶ Subsequently, the “flattening” of the complex structure from a pseudo-tetrahedral to a distorted square planar geometry occurs in $\tau_1 \sim 0.8$ ps, followed by intersystem crossing (ISC) to the respective T_1 (triplet state)

in $\tau_2 \sim 10$ ps.³⁷⁻³⁹ As final step, the relaxation from T_1 to the ground state takes place on a microsecond timescale, partially as emission. TDDFT calculations on $[\text{Cu}(\text{bcp})(\text{xantphos})]^+$ (**I**) revealed that excitations from the copper d orbitals to the π^* of the phenanthroline ligand are involved in the transitions from $S_0 \rightarrow S_1$ and from $S_0 \rightarrow S_2$, whereas xantphos does not have any positive contribution in harvesting radiation. Since a single charge transfer is possible in the heteroleptic complexes from the copper center to the only phenanthroline ligand (with respect to two in the homoleptic congeners), smaller extinction coefficients are characteristic for $[\text{Cu}(\text{N}^{\wedge}\text{N})(\text{P}^{\wedge}\text{P})]^+$ species. The following distortion and ISC processes have been evaluated for different complexes (Table 3). The flattening from pseudo tetrahedral to square planar arrangements is always slower for heteroleptic complexes ($1.0 \text{ ps} \leq \tau_1 \leq 1.4 \text{ ps}$) and depends on the molecular weight and size of the surrounding ligands. Finally, faster ISC was detected with phenanthroline bearing the substituent SO_3Na (**III** and **IV**), whereas the *n*-butyl moiety increases this time (τ_2 (**II**) = 8.4 ps).

Table 3. Time constants for the distortion (τ_1) and ISC (τ_2) processes in $[\text{Cu}(\text{N}^{\wedge}\text{N})(\text{P}^{\wedge}\text{P})]^+$ **I**-**IV** ($\text{P}^{\wedge}\text{P}$ = xantphos) and $[\text{Cu}(\text{N}^{\wedge}\text{N})_2]^+$ ($\text{N}^{\wedge}\text{N}$ = bathocuproine, bcp) **V**.



| Complex | τ_1 (ps) | τ_2 (ps) |
|------------|---------------|---------------|
| I | 1.1 | 7.4 |
| II | 1.0 | 8.4 |
| III | 1.4 | 6.5 |
| IV | 1.4 | 6.8 |
| V | 0.7 | 7.5 |

Overall this study pointed out that the first initial step after photoexcitation is very fast (in the order of picoseconds) and the small differences cannot account for the superior performances of the heteroleptic PSs in hydrogen evolving systems. Therefore, their

decomposition during the photocatalysis was investigated. The excited CuPSs* can undergo both pathways, reductive or oxidative quenching depending on how the electron transfer occurs.⁴⁰ Among them, oxidative quenching pathway is dominant, resulting in the formation of the oxidized CuPS which decomposes by dissociation of xantphos and formation of the homoleptic $[\text{Cu}(\text{N}^{\wedge}\text{N})_2]^+$. This has been confirmed by a combination of UV-Vis, Raman spectroscopy and electrochemistry techniques.⁴¹

CO₂ reduction

Another interesting application of these CuPSs involves the reduction of CO₂ to CO described by Beller and co-workers (Figure 7).⁴² The CuPSs were combined with cyclopentadienone iron complexes as catalyst and dimethylphenylbenzimidazoline (BIH) as sacrificial donor. Again, $[\text{Cu}(\text{bcp})(\text{xantphos})]\text{PF}_6$ (**I**) was found to be the best PS among the ones tested, with a TON (CO) = 487 and selectivity of 99%. In order to investigate the possible pathway for the photoinduced electron transfer in this catalytic system, quenching experiments using Stern–Volmer analysis were performed between the CuPS and the iron catalyst or the SR (BIH). These experiments showed the reductive quenching between CuPS and the iron catalyst pathway to operate in this transformation

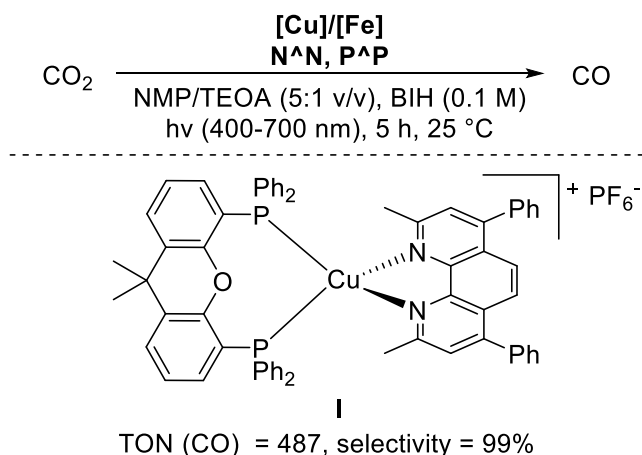
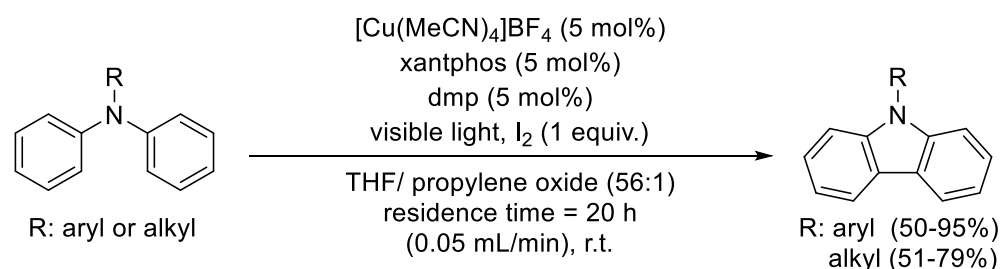


Figure 7. CO₂ reduction to CO catalyzed by iron complexes using $[\text{Cu}(\text{N}^{\wedge}\text{N})(\text{xantphos})]^+$ as PS and BIH and SR.

Other catalytic applications

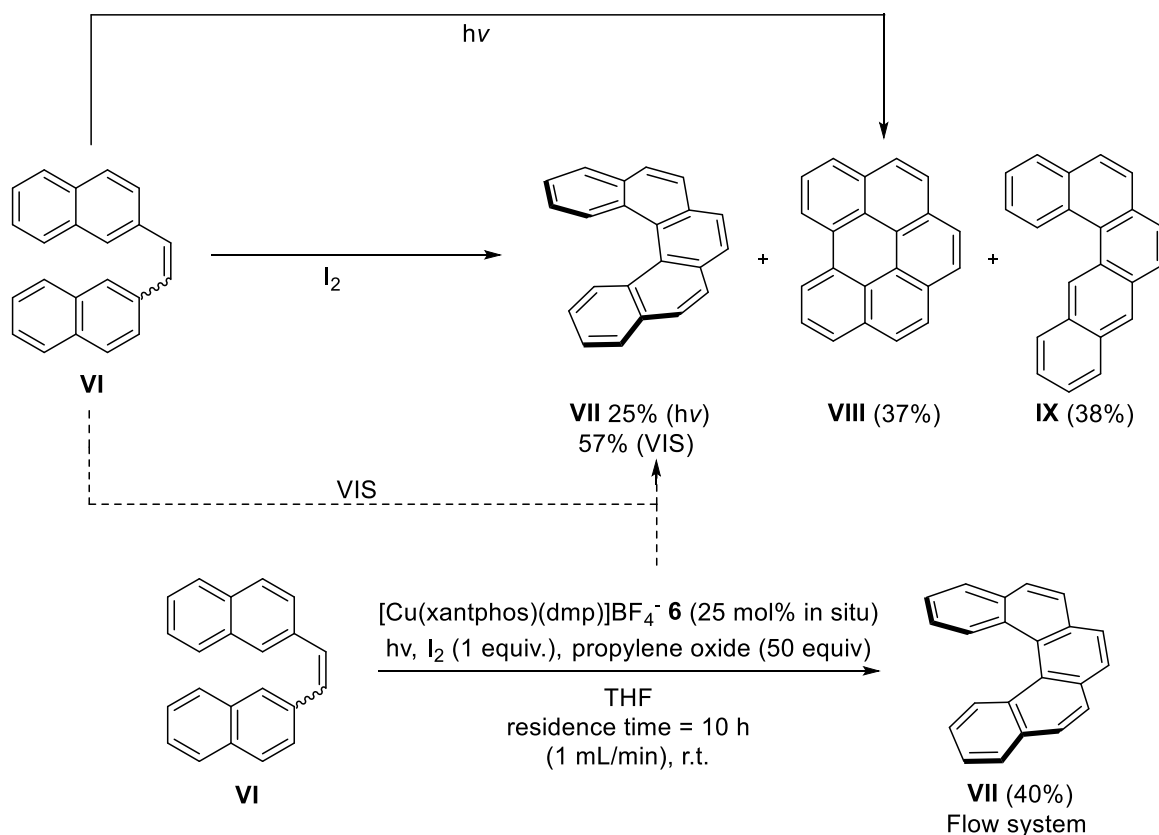
The complexes with formula $[\text{Cu}(\text{N}^{\wedge}\text{N})(\text{P}^{\wedge}\text{P})]^+$ have been applied for the synthesis of carbazoles from tertiary amines via C–C bond formation (Scheme 3),⁴³ which is

complementary to the more explored C–N bond formation using transition metal catalysts with palladium or copper in combination with strong oxidants.⁴⁴⁻⁴⁶ The active catalyst, [Cu(xantphos)(dmp)]BF₄, was formed *in situ* and it successfully catalyzed the formation of a broad range of carbazoles bearing both N-aromatic or N-alkylic substituents under visible light. The reaction rates were increased by using a continuous flow system, lowering the reaction time from 120 h in batch to 10 h when using triphenylamine as starting material. Moreover, the optimized procedure uses I₂ as oxidant, but it can be replaced with molecular oxygen with a slightly lower yield (75% with I₂ and 55 % with O₂ when triphenylamine was used as substrate).



Scheme 3. Synthesis of carbazole using the *in situ* preformed [Cu(xantphos)(dmp)]BF₄ catalyst under flow conditions and visible light irradiation.

Another application comprises the synthesis of helicenes, which are interesting materials due to their chirality and conjugated nature. The classical approach for their synthesis is the UV light-mediated photocyclodehydrogenative cyclization of stilbenes (Mallory reaction)⁴⁷ coupled with an *in situ* oxidation to restore the aromaticity. This methodology encounters selectivity problems when applied to higher helicenes such as [5]helicene **VII**. It can be obtained by irradiation of the stilbenyl starting material **VI** with a high intensity mercury lamp, using molecular iodine as oxidant. The low yield of 25% obtained, was due to the formation of the over oxidized polycyclic aromatic species **VIII** (37%) and the regioisomeric product dibenzo[*b,g*]phenanthrene **IX** (38%). Attempts to improve selectivity were achieved by obtaining 57% yield of the desired product **VII** using the *in situ* preformed [Cu(xantphos)(dmp)]BF₄ under irradiation in the visible region (Scheme 4).⁴⁸ Importantly, a clean reaction was obtained without the formation of any byproduct. The reaction time can be shortened using flow conditions from 120 h to 10 h (flow reactor, 40% yield) with comparable yield and complete selectivity.



Scheme 4. Synthesis of [5]helicene using [Cu(xantphos)(dmp)]BF₄.

Finally, these complexes have been also applied in photoredox transformations of organic halides, such as reduction and cyclization.⁴⁹ In those cases, the complex bearing xantphos was less active than the one using DPEphos and in all cases bathocuproine performed better than all the other phenanthrolines tested.

2.1.2.2 Sensors

These complexes have been also studied as oxygen sensors since their emission intensity diminishes as the concentration of oxygen increases, which can be measured by Stern–Volmer analysis (K_{SV}). An efficient sensor requires two features: long excited-state lifetimes and accessibility to oxygen.⁵⁰ Mann and coworkers reported crystalline [Cu(xantphos)(dmp)]tfpb, [Cu(xantphos)(dipp)]tfpb, and [Cu(xantphos)(dipp)]pftpb (dipp = 2,9-diisopropyl-1,10-phenanthroline; tfpb = tetrakis(bis-3,5-trifluoromethylphenyl)borate; pftpb = tetrakis(pentfluorophenyl)borate) and their performances correlate with the amount of void space calculated from their crystal structure (Table 4).⁵¹

Table 4. Photophysical, % void space and oxygen sensing data.

| Complex | K_{SV} | Φ (N ₂) | Φ (O ₂) | τ (μ s, N ₂) | τ (μ s, O ₂) | % void |
|---------------------------|----------|--------------------------|--------------------------|---------------------------------------|---------------------------------------|-----------|
| [Cu(xantphos)(dmp)]tfpb | 5.65(8) | 0.66(5) | 0.084(3) | 30.2 | 5.0 | 3.3% |
| [Cu(xantphos)(dipp)]tfpb | 3.41(9) | 0.95(5) | 0.22(1) | 38.5 | 9.6 | 2.0% |
| [Cu(xantphos)(dipp)]pftpb | 0.153(2) | 0.47(4) | 0.31(3) | 19.5 | 15.6 | 2.0% |

The better performances of the complexes bearing tfpb were ascribed to the alignment of the void cavities in their solid structure, which were separated by highly mobile CF₃ groups creating a sort of channel and allowing higher contact with oxygen (Figure 8). On the other hand, [Cu(xantphos)(dipp)]pftpb crystals contain void spaces as distinct pockets, thus limiting its efficiency. Later, the same authors incorporated [Cu(xantphos)(dmp)]PF₆ on solid support AP200/19 obtaining similar efficiency ($K_{SV} = 5.59$) as with [Cu(xantphos)(dmp)]tfpb ($K_{SV} = 5.65(8)$).⁵²

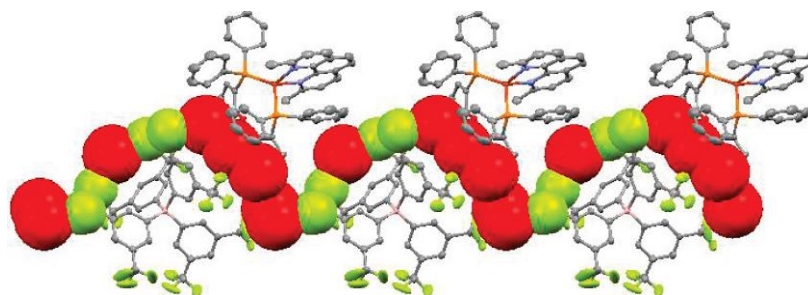


Figure 8. Representation of the calculated void space as red space filling spheres for compound [Cu(xantphos)(dmp)]tfpb. The fluorine atoms of the disordered CF₃ groups that clutter the void cavities are shown in green.⁵¹

2.2 Justification and project aims

Heteroleptic copper(I) complexes with general formula $[\text{Cu}(\text{P}^{\wedge}\text{P})(\text{N}^{\wedge}\text{N})]^+$ containing bidentate phosphine ($\text{P}^{\wedge}\text{P}$) and phenanthroline ($\text{N}^{\wedge}\text{N}$) ligands are an emerging class of photocatalysts and photosensitizers in several applications (*vide supra*).^{30, 34, 42-43, 53-58, 48, 51-52,}

⁵⁹ In comparison with the benchmark Ru(II) polypyridyl complexes, which have been intensively studied for the past decades,⁶⁰⁻⁶¹ the understanding of the electronic and structural requirements governing their photophysical performance is far from complete. The modular structure of these scaffolds provides unique opportunities to fine-tune the photophysical, structural and electrochemical properties of the complexes by independent modification of the ($\text{P}^{\wedge}\text{P}$) or ($\text{N}^{\wedge}\text{N}$) ligands.^{29, 62-63} Among the different combinations of ($\text{P}^{\wedge}\text{P}$) and ($\text{N}^{\wedge}\text{N}$) ligands reported in the literature, complexes bearing xantphos and phenanthroline derivatives have shown the most promising results in photocatalysis. In order to improve the performance of these copper complexes, either as photocatalysts or photosensitizers, fine-tuning of both steric and electronic properties is needed. Thus, comprehension of the underlying steric and electronic features influencing their properties is essential. Up to date, modification of the phenanthroline scaffold remains the most common strategy compared to the bidentate phosphine component.^{30, 33, 40} Nevertheless, the xanthene backbone offers more options for the fine tuning of both, electronic and steric properties, but this has remained relatively unexplored.

With respect to catalyst development, a systematic study of the properties of the bidentate phosphine ligand and their effect on the photophysical and photochemical features of this type of heteroleptic copper complexes has not been yet reported. Predominantly, commercially available phosphines have been used to assess their photocatalytic performance.⁶² The modification of these ligands typically requires challenging synthetic procedures as they tend to oxidize easily in the presence of air which requires laborious preparation methods.⁶⁴ Nevertheless, such ligands have found widespread use in the field of homogeneous catalysis and their modular structure allows tweaking their steric and electronic properties.⁶⁵⁻⁶⁶ Especially, xantphos derivatives possess rigid backbones and large bite angles, which disfavor the square planar geometry and stabilize the tetrahedral arrangement of metal complexes.⁶⁷⁻⁶⁸ This feature in particular makes them promising candidates for photocatalytic applications, where conservation of a tetrahedral geometry in

the excited states has been found to be crucial.⁶⁹ Furthermore, the structure of this versatile bidentate phosphine allows very subtle electronic fine-tuning while keeping the steric properties intact.⁷⁰ Therefore, in this research chapter we studied a Hammett series of five well-defined [Cu(*p*-R-xantphos)(neocuproine)]BF₄ (R = CF₃, F, H, Me, OMe) complexes (**1–5**, Figure 9) by systematic electronic modification of the xantphos scaffold at the *para* position of the arylphosphine moiety. Their structural characterization, determination of photophysical properties and application in the aerobic photocatalyzed cross-dehydrogenative coupling of 1,2,3,4-tetrahydro-2-phenyl isoquinoline with nitromethane enabled us to expand the current knowledge regarding these species through the assessment of their structure-activity relationships.

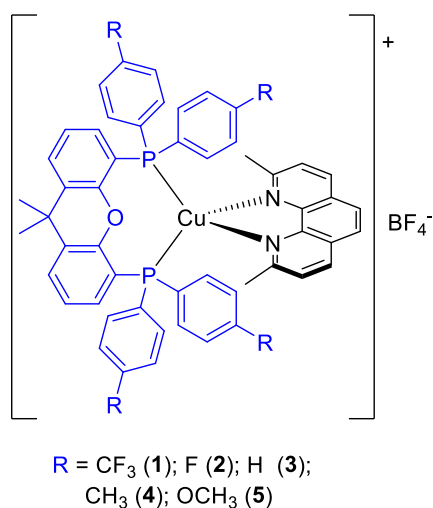
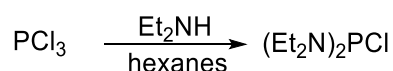


Figure 9. Modifications of the xantphos ligand presented in this work. Hammett series of [Cu(*p*-R-xantphos)(dmp)]BF₄ complexes.

2.3 Results and discussion

2.3.1 Synthesis of ligands and complexes

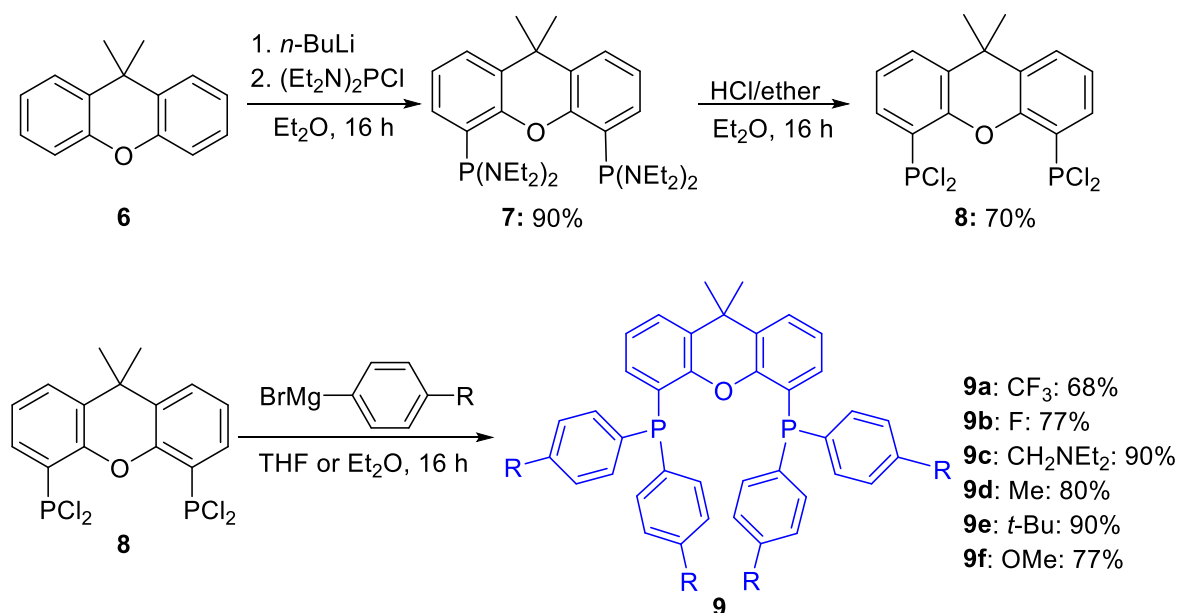
Chloroamino phosphines are important intermediates in phosphorus synthesis; the bis(diethylamino)chlorophosphine precursor is extremely moisture sensitive and a pyrophoric diethylamino derivate. It had to be obtained reliably in large amounts as it is a crucial reagent for xantphos ligand synthesis. It has to be noted that its synthesis requires strict inert conditions and dry reagents. This compound was obtained by the reaction between diethylamine and PCl_3 .⁷¹⁻⁷² During its synthesis, formation of mono(dialkyl)aminodichlorophosphine and trisubstituted phosphines have to be avoided as they cannot be easily separated by distillation. It was found that the most effective methodology required the use of mechanical stirring; while the most suitable solvent was hexanes. Using these conditions, the synthetic precursor was obtained in a good 80% isolated yield (Scheme 5).



Scheme 5. Synthesis of bis(diethylamino)chlorophosphine.

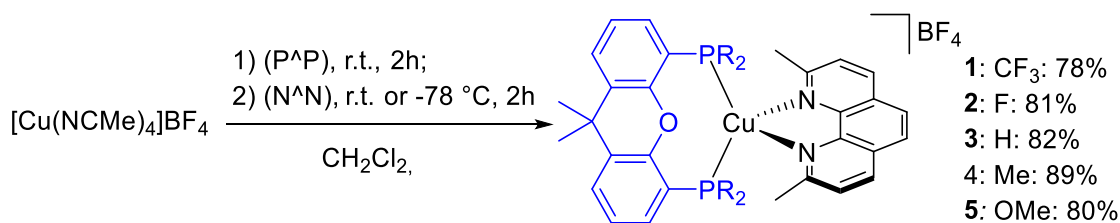
The synthesis of the xantphos-based Hammett ligand series started from 9,9-dimethyl xanthene **6** as the free backbone (Scheme 6) by performing ortho-dilithiation followed by reaction with bis(diethylamino)chlorophosphine to afford the intermediate **7** in excellent 90% yield.⁷³ In the second step, the methodology of Zhu and co-workers was implemented to obtain the intermediate 4,5-bis(dichlorophosphino)-9,9-dimethylxanthene **8** by chlorination of the previous synthetic intermediate in the presence of hydrogen chloride in ether in 70% yield.⁷⁴ In the first three steps of the synthesis, mechanical stirring is required when performing the reactions in multigram scale due to the presence of large quantities of salts. Lastly, a Grignard reaction with the corresponding *p*-substituted aryl bromide afforded the desired phosphine ligand **9** in generally good yields of 68–90%.⁷⁵ This last step requires to be handled with caution when using fluorinated aryl bromides as they can explosively decompose yielding metal fluorides.⁷⁶ These family of ligands used for complexation were previously reported by Kamer and co-workers.⁷⁵ During the development of this thesis an optimized synthetic route was achieved. Avoiding side reactions during the synthesis is

crucial to obtain these synthetic intermediates in few steps and multigram scales, thereby making them highly accessible. Careful monitoring of those reactions by ^{31}P NMR spectroscopy is essential to avoid impurities such as remaining starting material or decomposition products, which form after extended reaction times, in order to obtain reproducible results. All these procedures have been performed multiple times with high reproducibility. Importantly, none of the synthetic intermediates and ligands required separation by chromatography and only recrystallization was employed to afford them in high purity and isolated yields. When compared with the reported methodologies, yields have been improved from 16 to 31% for the synthesis of intermediates and final products. Multigram scale synthesis of the precursor bis(diethylamino)chlorophosphine and intermediates **7** and **8** was possible and the described procedures of this thesis can be scaled up successfully.



Scheme 6. Synthesis of *p*-substituted xantphos-type ligands.

With these ligands in hand, the corresponding $\text{Cu}(\text{P}^*\text{P})(\text{N}^*\text{N})\text{BF}_4$ ($(\text{N}^*\text{N}) = 2,9\text{-dimethyl-1,10-phenanthroline dmp}$; (P^*P) = *para* modified xantphos ligand) complexes were synthesized by stoichiometric reaction of the tetrakis acetonitrile copper tetrafluoroborate precursor, $[\text{Cu}(\text{MeCN})_4]\text{BF}_4$, with the chelating phosphine ligand, followed by addition of the diimine ligand in dichloromethane (Scheme 7).



Scheme 7. Synthesis of [Cu(P[^]P)(N[^]N)]BF₄ complexes.

The major hurdle in the synthesis of these complexes is their disproportionation in solution with the formation of homoleptic species [Cu(N[^]N)₂]⁺ and [Cu(P[^]P)₂]⁺, of which the former possesses a remarkable thermodynamic stability.⁷⁷⁻⁷⁹ When the phosphine ligand is strongly electron donating (*p*-OMe) or electro withdrawing (*p*-CF₃) the synthesis of the complexes is more problematic, probably being governed by the higher thermodynamic stability of the homoleptic complex, which was observed in significant amounts at room temperature. Moreover, the two species (homoleptic and heteroleptic complexes) were difficult to separate by routine purification techniques. Manual separation of the crystals led to a tedious and low yielding purification. In order to displace the equilibrium towards the formation of the heteroleptic complex (kinetic product of the reaction) and suppress any equilibration to the homoleptic complex, the synthesis and purification were performed at -78°C. With this strategy, it was possible to hamper the formation of the thermodynamically more stable homoleptic species. Analytically pure complexes were isolated by precipitation with diethyl ether from a dichloromethane solution of the crude complex, followed by recrystallization from a 1:1 mixture of diethyl ether/dichloromethane.

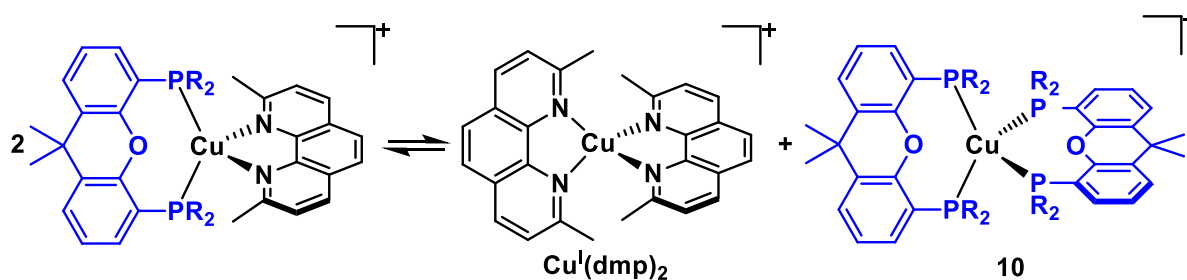
The complexes were characterized by multinuclear NMR spectroscopy. The ³¹P NMR spectra of all the complexes present a broad singlet at around – 13 ppm, which is shifted at low field (ca. 7 ppm) with respect to the signal of the free ligand upon to the coordination to the metal center. No trend exists between chemical shift and electronic nature of the *para* substituent at the aryl ring of the phosphorous ligand. The ¹H NMR spectra of all the complexes show in the aromatic region the two characteristic deshielded peaks of dmp at around 8.3 ppm and 7.8 ppm, in addition to the other peaks of dmp and xantphos ligand. In the aliphatic region the singlet belonging to the methyl of dmp at 2.2 ppm and the singlet of the methyl of the xantphos backbone are present at around 1.8 ppm. The ¹⁹F NMR signals of

the tetrafluoroborate anion (BF_4^-) consist of two singlet signals at ca. 153.3 ppm with ratio 1:4, corresponding to the isotope ^{10}B and ^{11}B respectively.

The ligands *p*-*tert*-Butyl **9e** (Scheme 7) and *tert*-Butyl xantphos (commercially available) could not form this type of heteroleptic complexes due to steric hindrance under our complexation conditions and only the homoleptic phenanthroline complex was obtained in both cases. The ligand *p*-(diethylamino)methyl xantphos (xantham) **9c** complexed successfully but the corresponding complex was not used for catalysis as it was not stable under reaction conditions due to its easily oxidizable amino substituents.

2.3.2 Dissociative equilibria studies

Dynamic ligand exchange in solution has been observed for various heteroleptic copper complexes obtained from dmp and bidentate phosphines, which are however stable in the solid state. As described by Armaroli and co-workers the homoleptic/heteroleptic ratio is highly dependent on the bidentate phosphine chelating the copper center (Scheme 8).²⁷ In order to observe the magnitude of the disproportionation of isolated complexes in solution, stability experiments were performed by quantitative ^{31}P NMR spectroscopy with triphenylphosphine oxide as internal standard during a period of eight hours in deuterated dichloromethane at room temperature. The formation of homoleptic complexes product of ligand exchange was not observed for any of the electronically modified ligands **1–5**. It shows the distinctive stability of the complexes bearing xantphos derivatives compared to other chelating ligands previously reported with dmp as diimine ligand.²⁷



Scheme 8. Dissociative equilibria for $[\text{Cu}(\text{P}^{\wedge}\text{P})(\text{N}^{\wedge}\text{N})]^+$ complexes.

During the course of this project it was possible to synthesize the homoleptic species $[\text{Cu}(\text{xantphos})_2]\text{BF}_4$ (**10**) to confirm its structure and that it can be formed despite large steric hindrance of the xantphos ligands. We were also successful in obtaining an X-ray crystal structure of this complex (Figure 10).

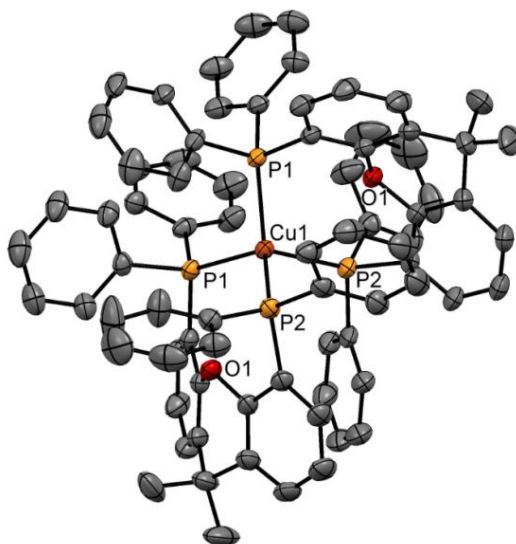


Figure 10. Thermal ellipsoid representation of complex **10**. Anion, hydrogen atoms and co-crystallized solvent molecules have been omitted for clarity. Displacement ellipsoids correspond to 50% probability.

2.3.3 Structural features

All the complexes have been fully characterized and crystals suitable for X-ray analysis (Figure 11-15) were grown by slow diffusion of diethyl ether into a saturated solution of the complex in dichloromethane (**1**, **2**, **3** and **4**), and by slow evaporation of a solution of the compound in dichloromethane (**5**).

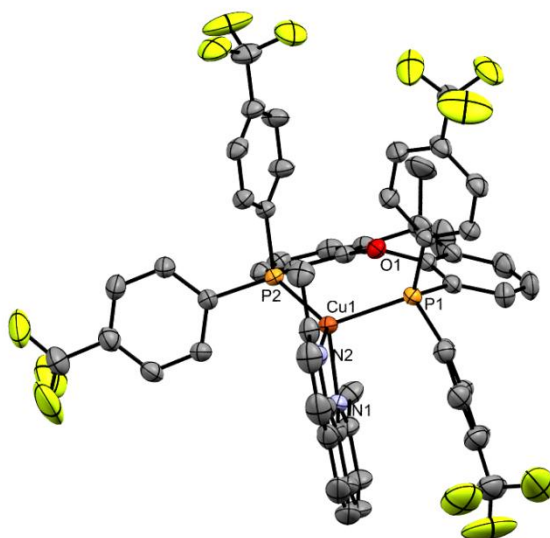


Figure 11. Thermal ellipsoid representation of complex **1**. Anion, hydrogen atoms and co-crystallized solvent molecules have been omitted for clarity. Displacement ellipsoids correspond to 50% probability.

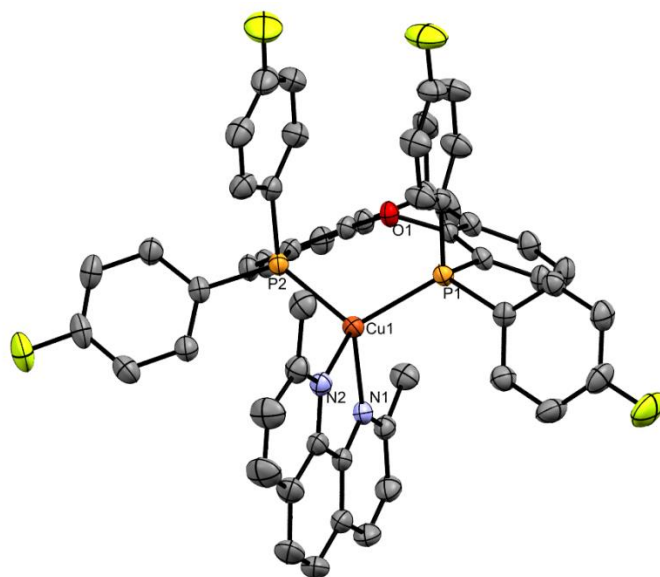


Figure 12. Thermal ellipsoid representation of complex **2**. Anion, hydrogen atoms and co-crystallized solvent molecules have been omitted for clarity. Displacement ellipsoids correspond to 50% probability.

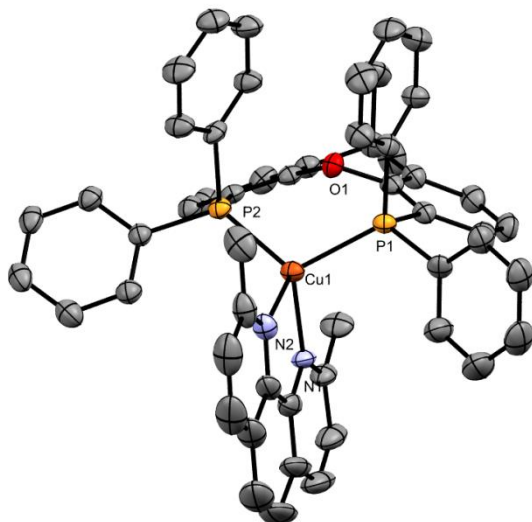


Figure 13. Thermal ellipsoid representation of complex **3**. Anion, hydrogen atoms and co-crystallized solvent molecules have been omitted for clarity. Displacement ellipsoids correspond to 50% probability.

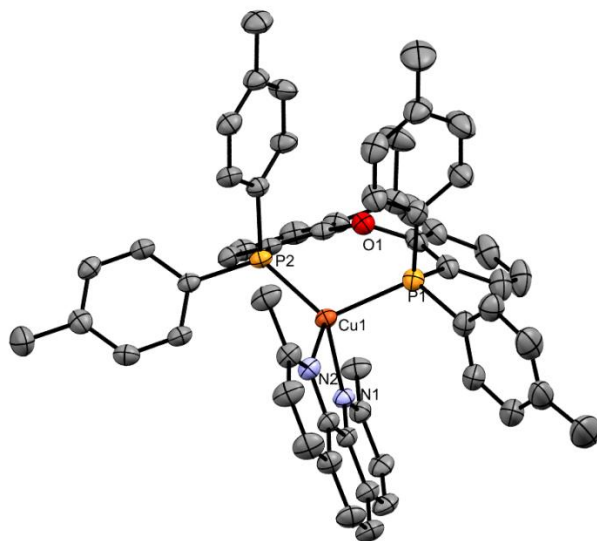


Figure 14. Thermal ellipsoid representation of complex **4**. The second independent molecule, anions, hydrogen atoms and co-crystallized solvent molecules have been omitted for clarity. Displacement ellipsoids correspond to 50% probability.

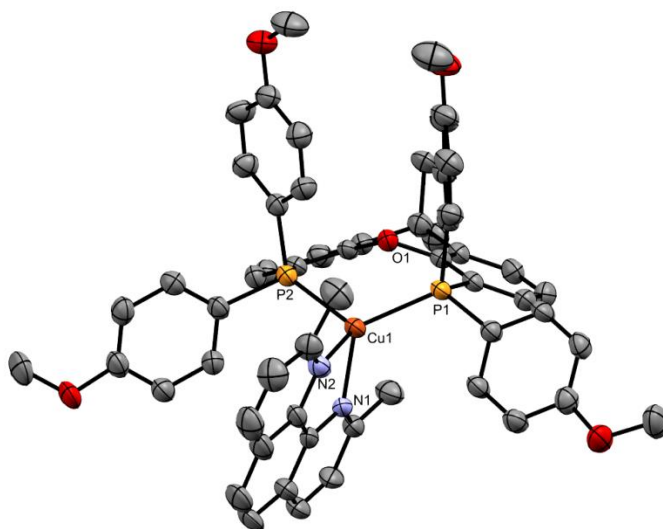


Figure 15. Thermal ellipsoid representation of complex **5**. Anion, hydrogen atoms and co-crystallized solvent molecules have been omitted for clarity. Displacement ellipsoids correspond to 50% probability.

Each structure except **4** (Me) comprises one complex cation, a tetrafluoroborate anion, and, other than in the case of **2** (F), various solvent molecules. In the case of **4** (Me) the structure comprises two independent complex cations, and CH₂Cl₂ solvent. In all the species, the copper atom possesses the expected distorted tetrahedral geometry, coordinated by the two nitrogens of dmp and the two phosphorus of the xantphos derivative. The Cu–N bond lengths [2.080(3)–2.127(4) Å] fall into the typical range, although several of them are towards the longer end of the range. Conversely, while the majority of the Cu–P bond lengths [2.2562(9)–2.3274(9) Å] are also within the typical range, several of these exceed the range of bond lengths commonly seen (2.23–2.29 Å), without any noticeable trend in particular regarding to phosphine basicity.

The structures show two general arrangements of the xantphos derivative; where the two aryl rings of the xantphos derivative in proximity to each other are either approximately parallel or approximately orthogonal. Complexes **2** (F), **3** (H) and **4** (Me) show a parallel arrangement, and while the rings in **3** (H) and **4** (Me) are not close enough to take part in π - π stacking, those in **2** (F) are, although around the limit of distances for such interactions [centroid \cdots centroid distance 3.804(15) Å]. Complexes **1** (CF₃) and **5** (OMe) show a near-orthogonal arrangement of rings, the two rings inclined at 70° **5** (OMe) and 85° **1** (CF₃) with

respect to each other. The greater deviation from orthogonality in **5** (OMe) positions the rings too far apart to take part in CH $\cdots\pi$ interactions, but they are close enough in complex **1** (CF₃) to form a very weak interaction (C–H \cdots centroid distance 2.96 Å). This distance is slightly larger than the conventional van der Waals limit, but CH $\cdots\pi$ interactions have been suggested to be effective at distances greater than this value.⁹⁸ In addition to the changes within the arrangement of the xantphos derivative, the complexes also show variation in relative arrangements of the xantphos and dmp. In complexes **2** (F) and **3** (H) the dmp sits centrally relative to the two PR₂ groups of the xantphos derivative, the aryl rings that form this cavity lying approximately orthogonal to the plane of the dmp, but not close enough to give rise to CH $\cdots\pi$ interactions. The methyl of the dmp lying closest to the xanthene core is close enough to form weak CH $\cdots\pi$ interactions involving two different hydrogens on the same methyl in both cases (C–H \cdots centroid distances 2.79–2.87 Å). In contrast, complexes **1** (CF₃), **4** (Me) and **5** (OMe) show the dmp positioned closer to one aryl ring of the xantphos derivative than the other, although these three complexes do show variations on this arrangement. Both complexes **4** (Me) and **5** (OMe) have the aryl ring of the xantphos closest to being approximately orthogonal to the dmp plane, and positioned to form a CH $\cdots\pi$ interaction, at C–H \cdots centroid distances of 2.75 and 2.68 Å, respectively. In both these cases the dmp is again positioned with a methyl group in proximity to the xanthene, and able to form CH $\cdots\pi$ interactions, although these are likely weaker than those seen in **2** (F) and **3** (H) (C–H \cdots centroid distances for **4** (Me) 2.87–2.89 Å, for **5** (OMe) 2.97 Å), and in the case of **5** (OMe) may be regarded as extremely weak due to their length. Complex **1** (CF₃), although it does show inclination of the dmp towards one aryl ring, in this case the two ring systems are parallel, although not close enough to be involved in π - π stacking. Unlike the other four complexes, however, the dmp is inclined differently, and the methyl proximal to the xanthene is not close enough to form any CH $\cdots\pi$ interaction.

All five complexes show some intermolecular interactions between cationic complexes. For complexes **2** (F), **3** (H), **4** (Me) and **5** (OMe) these are CH $\cdots\pi$ interactions involving predominantly aryl hydrogens, although in **4** (Me) and **5** (OMe) interactions are seen involving the methyl hydrogens of the dmp (C–H \cdots centroid distances 2.63–2.94 Å). In contrast, in **1** (CF₃) no CH $\cdots\pi$ interactions between complexes are seen, instead the primary interactions are mutually supporting $\pi\cdots\pi$ interactions between adjacent dmp

[centroid...centroid distances 3.523(2) and 3.639(2) Å]. These interactions between complexes are additionally supported by a variety of CH...F interactions with the tetrafluoroborate anions, where the anion can often bridge adjacent complexes. The solvent molecules, where present, also form similar interactions with both cations, anions and other solvent molecules. The analysis corresponding to the structural features was performed by Dr. David B. Cordes at the University of St Andrews.

2.3.4 Electrochemistry

For the sections 2.3.4 - 2.3.6, electrochemical and photophysical characterizations of **1–5** were carried out and analyzed by Chenfei Li under the supervision of Dr. Eli Zysman-Colman at the University of St Andrews. The analysis of the phosphine ligand effect on UV-Vis absorption features (Section 2.3.5) was analyzed at Leibniz Institute for Catalysis (LIKAT) in Rostock by Paola Andrea Forero Cortés and Dr. Esteban Mejía. The electrochemistry of **1–5** was studied by cyclic voltammetry (CV) in order to discern the redox behavior of the complexes. Measurements were carried out in degassed HPLC grade dichloromethane (CH_2Cl_2) and acetonitrile (MeCN) under a nitrogen atmosphere with 0.1 M TBAPF₆ as the supporting electrolyte using a glassy carbon working electrode, a platinum wire counter electrode, a Ag/Ag⁺ pseudo-reference electrode and referenced vs. SCE using Fc/Fc⁺ as an internal standard (0.46 V in CH_2Cl_2)⁸⁰ and scan rate: 50 mV s⁻¹. The CV and DPV traces are resumed in Table 5 (CH_2Cl_2) and Table 6 (MeCN).

Table 5. Ground and excited state electrochemical data of **1–5** in CH₂Cl₂.

| Complex | σ_p | E_{ox}/V^a | E_{red}/V^a | $\Delta E_{redox}/V^a$ | E_{opt}/V^b | E^*_{ox}/V^c | E^*_{red}/V^c |
|----------|------------|--------------|---------------|------------------------|---------------|----------------|-----------------|
| 1 | 0.54 | 1.51 | -1.74 | 3.25 | 2.89 | -1.38 | 1.15 |
| 2 | 0.06 | 1.32 | -1.96 | 3.28 | 2.78 | -1.46 | 0.82 |
| 3 | 0 | 1.18 | -2.03 | 3.21 | 2.62 | -1.44 | 0.59 |
| 4 | -0.17 | 1.25 | / | / | 2.56 | -1.35 | / |
| 5 | -0.27 | 1.12 | -1.71 | 2.92 | 2.70 | -1.58 | 0.99 |

a) Electrochemical measurements carried out in a degassed HPLC grade CH₂Cl₂ with glassy carbon working electrode, Ag/Ag⁺ reference electrode and a platinum wire counter electrode. Fc/Fc⁺ was used as the internal standard and the data reported versus SCE (0.46 V vs SCE in CH₂Cl₂);⁸¹ b) optical gap inferred from the onset of the absorption of the MLCT band, defined as the energy at 10% relative intensity of the maximum on the low energy tail; c) excited state redox potentials calculated with equation $E^*_{ox} = E_{ox} - E_{opt}$, $E^*_{red} = E_{red} + E_{opt}$.⁸² σ_p : Hammett parameter.

Table 6. Ground and excited state electrochemical data of **1–5** in MeCN.

| Complex | σ_p | E_{ox}/V^a | E_{red}/V^a | $\Delta E_{redox}/V^a$ | E_{opt}/V^b | E^*_{ox}/V^c | E^*_{red}/V^c |
|----------|------------|--------------|---------------|------------------------|---------------|----------------|-----------------|
| 1 | 0.54 | 1.51 | -1.63 | 3.14 | 2.79 | -1.28 | 1.16 |
| 2 | 0.06 | 1.20 | -1.73 | 2.93 | 2.66 | -1.46 | 0.93 |
| 3 | 0 | 1.21 | -1.74 | 2.95 | 2.61 | -1.40 | 0.87 |
| 4 | -0.17 | 1.19 | -1.72 | 2.91 | 2.58 | -1.39 | 0.86 |
| 5 | -0.27 | 1.17 | -1.75 | 2.92 | 2.53 | -1.36 | 0.78 |

a) Electrochemical measurements carried out in a degassed HPLC grade MeCN with glassy carbon working electrode, Ag/Ag⁺ reference electrode and a platinum wire counter electrode. Fc/Fc⁺ was used as the internal standard and the data reported versus SCE (0.38 V vs SCE in MeCN);³¹ b) optical gap inferred from the intersection points of the normalized absorption spectra and the tangent of the onset of the normalized emission spectra in MeCN, defined as the energy at 10% relative intensity of the maximum on the low energy tail; c)

excited state redox potentials calculated with equation $E^*_{ox} = E_{ox} - E_{opt}$, $E^*_{red} = E_{red} + E_{opt}$.⁸² σ_p : Hammett parameter.

All the complexes studied show irreversible oxidation and quasi-reversible reduction waves when studied in CH_2Cl_2 and MeCN, with the exception of complex **4** (*p*-Me) where the reduction wave was not detected. It should be noted that small differences in oxidation waves were observed for all complexes in the two solvents but that for complexes **2** (*p*-F) and **3** (*p*-H), significantly more negative reduction potentials were obtained in CH_2Cl_2 when compared to MeCN. The excited state oxidation potentials of **1–5** vary from $E^*_{ox} = -1.58$ V for **5** to $E^*_{ox} = -1.28$ V for **1**. These values are higher than that of $[Ru(bpy)_3]^{2+}$ ($E^*_{ox} = -0.81$ V), which is widely used in photoredox catalysis reactions following oxidative quenching pathways.⁸³ Comparing **1–5** with $[Cu(dap)_2]Cl$ (*dap* = anisylphenanthroline) ($E^*_{ox} = -1.43$ V), a well-studied copper-based photoreductant,⁸⁴ one of the five complexes was found to be a stronger photoreductant ($E^*_{ox} = -1.46$ for **2**). On the other hand, these copper complexes also have the potential of being photooxidants. The excited state reduction potentials of **1–5** vary from 0.59 V (for **3**) to 1.16 V (for **1**). The E^*_{red} for **1** is close to that of the photocatalyst $[Ir(dF-CF_3-ppy)_2(dtbbpy)]^+$ ($E^*_{red} = 1.21$ V),⁸⁵ while most of the complexes have larger E^*_{red} than $[Ru(bpy)_3]^{2+}$ ($E^*_{red} = 0.77$ V).⁸³

The electrochemical measurements in CH_3CN were plotted versus the Hammett parameter (σ_p) and was observed an increase of ΔE_{red} , E_{opt} , E^*_{ox} and E^*_{red} going from complexes possessing negative σ_p (electron donating substituents) to the ones with positive σ_p (electron withdrawing substituent). Contrarily, complexes bearing more positive σ_p have lower E_{red} (Figure 16). Poor correlations were observed when using the electrochemical data in CH_2Cl_2 .

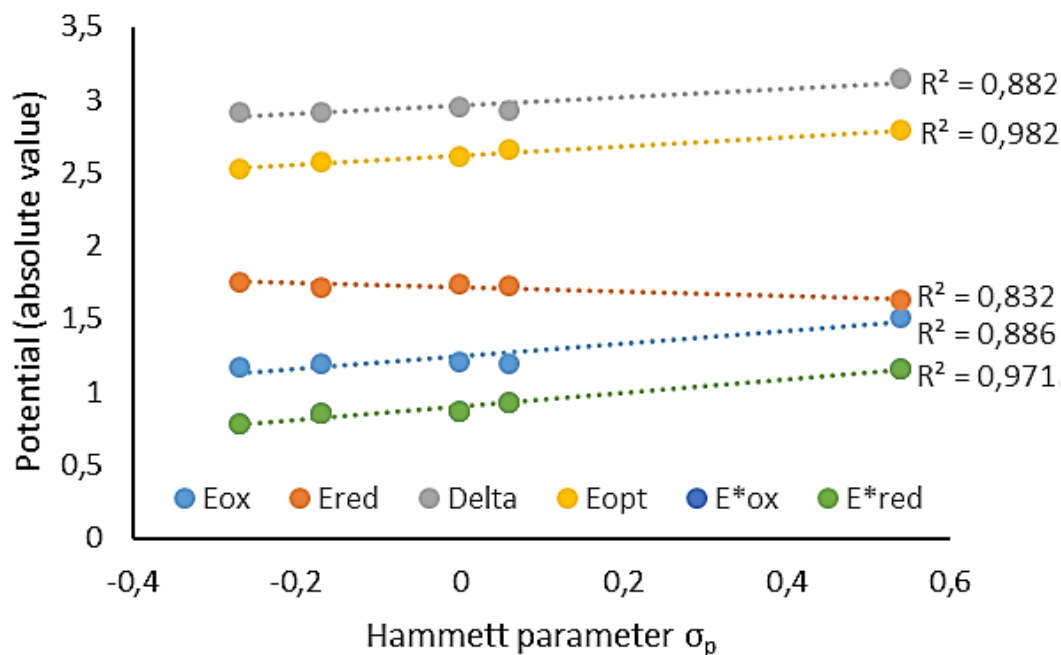


Figure 16. Hammett plot of the electrochemical data in CH₃CN for **1–5**.

2.3.5 UV-Vis absorption

The absorption data for **1–5** are compiled in Table 7. The absorption spectra are dominated by two features: an intense ($\epsilon \approx 37000 \text{ M}^{-1}\text{cm}^{-1}$) high energy (250–300 nm), ligand-centered (^1LC) $\pi - \pi^*$ transition and a low energy (350–450 nm), ($\epsilon \approx 2000 \text{ M}^{-1}\text{cm}^{-1}$) metal to ligand charge transfer ($^1\text{MLCT}$) transition. These absorption profiles mimic literature reports of $[\text{Cu}(\text{N}^{\wedge}\text{N})(\text{P}^{\wedge}\text{P})]^+$ complexes.⁴⁰

All complexes of the Hammett series show a similar CT absorption band ~376–403 nm (Table 7) and emission band ~520–558 nm (Table 8). These bands shifted slightly to longer wavelengths when the Hammett value changed from positive to negative values due to the increased donation ability of the phosphine. The trend observed correlates with the energy gap between the phenanthroline π^* orbital and the copper d orbital which in turn decreases as the Hammett value becomes more positive, lowering the energy of the CT excited states (Figure 17).^{23, 86}

Table 7. Relevant absorption data for complex **1–5**

| Complex | σ_p | $\lambda_{\text{abs}} / \text{nm}$ | $(\epsilon / *10^3 \text{M}^{-1} \text{cm}^{-1})^a$ |
|----------|------------|------------------------------------|---|
| | | LC | CT |
| 1 | 0.54 | 278(41) | 376 (3.3) |
| 2 | 0.06 | 275(40) | 385 (2.8) |
| 3 | 0 | 276(38) | 393 (2.7) |
| 4 | -0.17 | 276(41) | 392 (3.2) |
| 5 | -0.27 | 274(36) | 403 (1.9) |

a) Absorption data for complexes **1–5**, all measurements were carried out in HPLC grade CH_2Cl_2 at 298K. σ_p : Hammett parameter.

2.3.6 Solution photophysics

The photophysical properties of **1–5** were studied in degassed CH_2Cl_2 at 298 K. Their photophysical data are given in Table 8. All five complexes showed broad and unstructured CT emission profiles and emit over a narrow range in the green-yellow color range from 520 for **1** to 558 nm for **5**. The emission energies fit a Hammett trend, demonstrating that modulation of the electronics of the P[^]P ligand can tune the emission energy of the complex in a controlled manner (Figure 17).

Table 8. Relevant solution state photophysical data for complexes **1–5**^a

| Complex | σ_p | $\lambda_{\text{em}} (\text{nm})^b$ | $\Phi_{\text{PL}} (\%)^c$ | $\tau_{\text{PL}} (\mu\text{s})^d$ | $k_r \times 10^4 \text{ s}^{-1}$ | $k_{\text{nr}} \times 10^4 \text{ s}^{-1}$ |
|----------|------------|-------------------------------------|---------------------------|------------------------------------|----------------------------------|--|
| | | | | | 1 | 1 |
| 1 | 0.54 | 520 | 8.0 | 3.09 | 2.60 | 29.77 |
| 2 | 0.06 | 537 | 11.8 | 3.37 | 3.50 | 29.67 |
| 3 | 0 | 550 | 12.5 | 3.00 | 4.17 | 33.33 |
| 4 | -0.17 | 550 | 9.3 | 6.17 | 1.51 | 16.21 |
| 5 | -0.27 | 558 | 14.5 | 6.83 | 2.12 | 14.64 |

a) Measurements at 298 K in deaerated CH_2Cl_2 ; b) $\lambda_{\text{exc}} = 360 \text{ nm}$; c) Quinine sulfate used as the reference ($\Phi_{\text{PL}} = 54.6\%$ in 0.5 M H_2SO_4 at 298 K);¹⁸ d) $\lambda_{\text{exc}} = 369 \text{ nm}$. Φ_{PL} : Photoluminescence quantum yield, τ_{PL} : excited state life time, k_r : radiative decay constant, k_{nr} : non-radiative decay constant. σ_p : Hammett parameter.

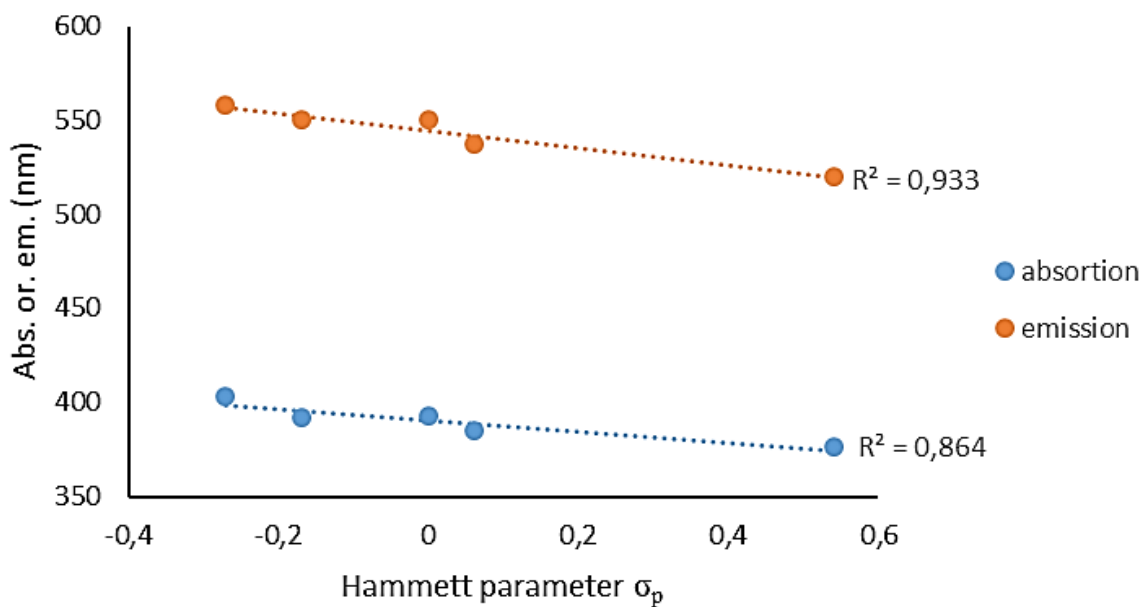


Figure 17. Hammett plot of absorption and emission energies in CH_2Cl_2 for **1–5**.

As a result of the large degree of steric hindrance around the metal center induced by both the dmp and the bulky xantphos ligands, photoluminescence quantum yields between 8–14.5% were observed for **1–5**. The excited state lifetimes, τ_{PL} , of **1–5** range from 3.00 to 6.83 μs . Complexes bearing electron-donating substituents on the xantphos ligand (**4** and **5**) show decreased k_{nr} compared to the other complexes within the series.

It is now possible to cross-compare the photophysical properties of **1–5** with other Cu-based photocatalysts. For instance, $[\text{Cu}(\text{dmp})(\text{DPEPhos})]^+$ shows a marginally higher Φ_{PL} in CH_2Cl_2 (15%) and significantly longer life time τ_{PL} (14.3 μs) than **1–5**. However, E^*_{ox} of $[\text{Cu}(\text{dmp})(\text{DPEPhos})]^+$ is -1.35 V, which is the same as complex **4** (Table 5) and less reducing than the remaining four complexes in the series.²⁵ In the context of photoredox catalysis, an analysis of the excited state redox behavior of **1–5** reveals the attractive potential of **5** as it has the highest excited state oxidation potential, highest solution state Φ_{PL} and longest τ_{PL} .

2.3.7. HOMO and LUMO contributions

Density functional theory (DFT) calculations indicated that the lowest unoccupied molecular orbital (LUMO) of **1–5** is located on the dmp ligand while the highest occupied molecular orbital (HOMO) consists of a combination of copper d-orbitals and P[^]P ligand orbitals. These

calculations were performed by Professor Michael Bühl, Robert Dickson and Chenfei Li at the University of St Andrews.

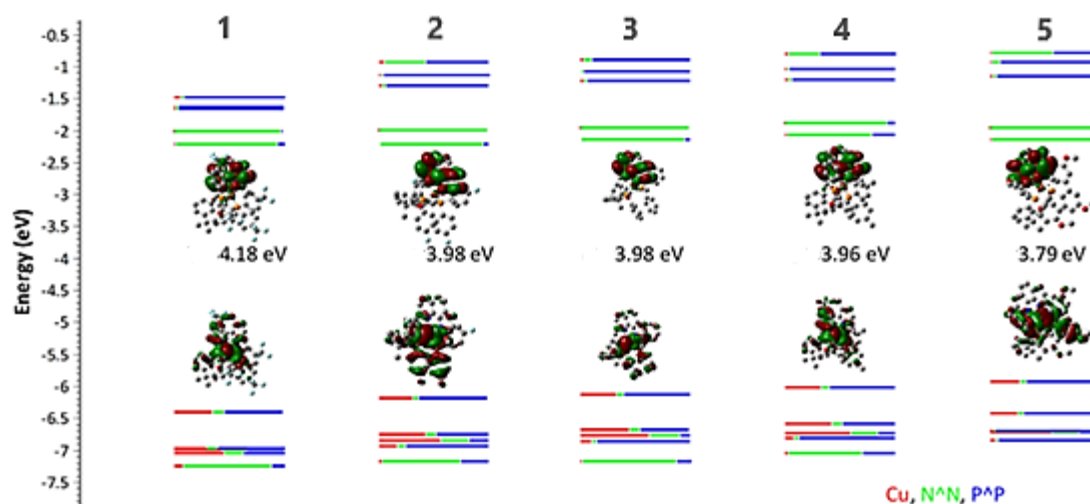
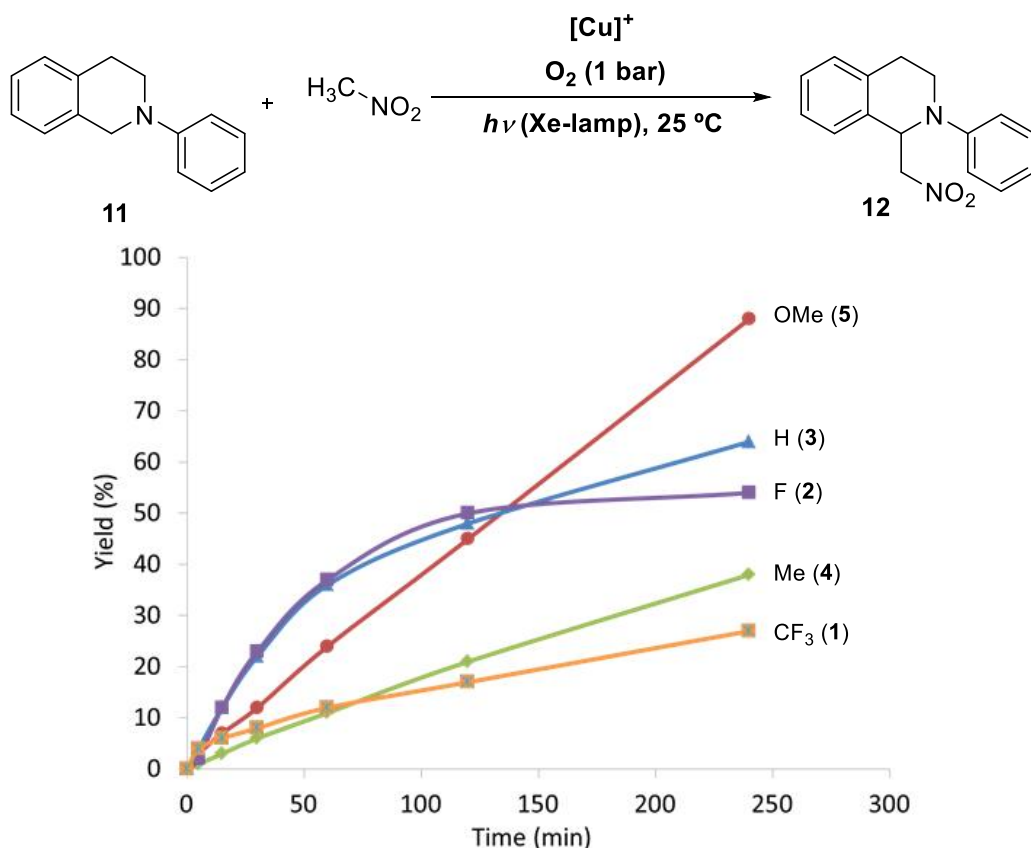


Figure 18. Kohn-Sham energy diagram for **1–5** with electron density distribution of HOMO and LUMO (PBE0 level of DFT calculations). Red bars represent copper orbitals, green bars represent orbitals on the N^N ligand and blue bars represent orbitals on the P^P ligand.

The trend in HOMO energies follows the Hammett trend, it was observed that complexes **4** and **5** have the highest HOMO and smaller ΔE between HOMO and LUMO compared to complexes bearing electron-withdrawing substituents (**1** and **2**) according to DFT-calculated HOMO-LUMO gaps). It can be deduced that the electronic phosphine effect on the LUMO is less evident when compared to the HOMO (Figure 18).

2.3.8 Photocatalysis

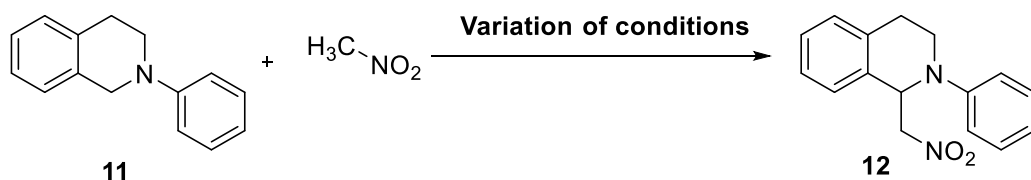
In order to assess the influence of the electronic phosphine ligand effect in the photocatalytic performance of these complexes, the aerobic photocatalyzed cross-dehydrogenative coupling (CDC) between N-phenyl-tetrahydroisoquinoline **11** and nitromethane was selected as model reaction, based on the previous report by Wang and co-workers which used a carborane-based phosphine ligands.⁸⁷ This simple reaction allowed us kinetic profiling and comparison between our series of complexes (Scheme 9).



Scheme 9. CDC of 1,2,3,4-tetrahydro-2-phenyl isoquinoline with nitromethane photocatalyzed by $[Cu(P^P)(dmp)]BF_4$ complexes. *Reaction conditions:* **11** (0.2 mmol), $[Cu]^+$ (0.003 mmol, 1.5 mol%), CH_3NO_2 (10 mL), O_2 atmosphere. Reaction profiles taken within 4 hours and yields were determined by quantitative 1H NMR analysis of the crude reaction mixture using naphthalene as external standard based on **11**. Irradiation: 300 W xenon lamp at ambient temperature (25 °C). Wavelength 300–600 nm.

The five complexes studied gave yields of product **12** varying from 26 to 88% after four hours of irradiation by a 300 W xenon lamp operating in the 300-600 nm range. Very fast reaction rates were obtained initially for complexes **2** and **3**, but conversion stalled after only two hours of reaction, suggesting fast deactivation of the catalyst. Complexes **4** and **5** gave slower initial rates of reaction but these rates remained constant over longer periods of times, suggesting that the catalyst remained active over the course of the experiments. A series of control experiments were conducted in order to confirm the requirement of all the components of the reaction (Table 9).

Table 9. Control experiments for the CDC of 1,2,3,4-tetrahydro-2-phenyl isoquinoline with nitromethane.



| Entry | Variation | Yield (%) |
|-------|---|-----------|
| 1 | 0.003 mmol xantphos, 0.003 mmol [Cu(MeCN) ₄]BF ₄ | 8 |
| 2 | 0.003 mmol dmp, 0.003 mmol [Cu(MeCN) ₄]BF ₄ | 8 |
| 3 | 0.003 mmol [Cu(MeCN) ₄]BF ₄ | 4 |
| 4 | Only substrate | 4 |
| 5 | No irradiation | 0 |

Reaction conditions: **11** (0.2 mmol), CH₃NO₂ (10 mL), O₂ atmosphere. Reaction time: 8 hours and yields were determined by quantitative ¹H NMR analysis of the crude reaction mixture using naphthalene as external standard based on **11**. Irradiation: 300 W xenon lamp at ambient temperature (25 °C). Wavelength 300–600 nm.

It was observed that the reaction does not proceed in the dark (Table 9, entry 5) and only 4 % of the product was observed in the presence of the copper salt without addition of any of the ligand (entry 3) as well as with only substrate in absence of the metal precursor and ligands upon irradiation (entry 4). It was also observed that a yield of only 8% of the desired product was obtained when the homoleptic xantphos and dmp complexes were formed in situ (entries 1 and 2). Moreover, kinetic profiles of each catalyst were obtained using a long pass filter Cut-On 422 nm and a decrease of the reaction rates for all complexes was observed; the maximum product yield obtained by complex **5** was 21% after four hours (Figure 9, Chapter V). It suggests the reaction does not work in optimal conditions when the complexes are not irradiated at their wavelength of maximum absorbance, as expected.

2.3.8.1 Structure – reactivity relationships

The correlations between photophysical, structural parameters and the conversion for each catalyst (**1–5**) at four hours reaction time are reported in Table 10. The full electrochemistry and photophysical data in dichloromethane were selected in this chapter to address the discussion due to the lower interference of this solvent in terms of complex stability. Redox potentials in acetonitrile serve as reference for comparison of the complexes with those in literature but their full photophysical characterization in this solvent is still needed in order to showcase their behavior. Overall activity has been considered for the established correlations which can differ from the initial catalyst activity due to secondary processes.

Table 10. Correlations between photophysics, structural parameters and activity of [Cu(*p*-R-xantphos)(dmp)]⁺ complexes.

| Entry | <i>p</i> -R | σ_p | τ_{PL} (μ s) | Φ_{PL} (%) | E*Ox (V) | Yield at 4h (%) |
|-------|------------------------------|------------|------------------------|-----------------|----------|-----------------|
| 1 | OMe (5) | -0.27 | 6.83 | 14.5 | -1.58 | 88.4 |
| 2 | H (3) | 0 | 3.0 | 12.5 | -1.44 | 64 |
| 3 | F (2) | 0.06 | 3.37 | 11.8 | -1.46 | 53.6 |
| 4 | Me (4) | -0.17 | 6.17 | 9.3 | -1.35 | 38.4 |
| 5 | CF ₃ (1) | 0.54 | 3.09 | 8.0 | -1.38 | 26.8 |

p-R: para substituent, σ_p : Hammett parameter, τ_{PL} : Life time, Φ_{PL} : photoluminescence quantum yield, E*ox: Excited state oxidation potential. Yield at 4h (%): *Reaction conditions*: **11** (0.2 mmol), [Cu]⁺ (0.003 mmol, 1.5 mol%), CH₃NO₂ (10 mL), O₂ atmosphere. Yields were determined by quantitative ¹H NMR analysis of the crude reaction mixture using naphthalene as external standard based on **11**. Irradiation: 300 W xenon lamp at ambient temperature (25 °C). Wavelength 300–600 nm.

Geometry

It has been observed that conservation of the tetrahedral geometry is a very important requirement for the optimal performance of Cu(I) photosensitizers as stated by Beller and co-workers.^{40,42} As previously discussed in section 2.3.3, all complexes display a pseudo tetrahedral geometry in the ground state. These results are in agreement with the previously reported strategy employed to stabilize the Cu(I) excited state using sterically hindered ligands that preserve the tetrahedral geometry by preventing the Jahn-Teller distortion and concomitant flattening of the complex to the square planar geometry, thus favoring the radiative relaxation pathway.⁴¹ By forcing the excited state into a tetrahedral environment, the energy gap between the copper *d*-orbitals and the π^* orbitals from the ligand increases, slowing down the premature non-radiative deactivation of the photosensitizer.²⁶ This effect on the catalysis can be illustrated by comparing the results of the catalytic reaction performed by the homoleptic Cu(N[^]N)₂ complex with neocuproine as ligand. This complex does not

have the xantphos ligand which enforces 109° bond angle and readily undergoes Jahn-Teller distortion to a flattened excited state. When the complex is formed *in situ* and used for catalysis, it only results in 8% yield after four hours of irradiation. By contrast, the heteroleptic complexes **1–5** possess the xant-type ligand that forces the metal center into a tetrahedral geometry and all of them perform significantly better under identical catalytic conditions. Even complex **1**, the least efficient of the series, gives more than a three-fold increase in yield up to 26%. The homoleptic complex Cu(P[^]P)₂ formed *in situ* performs poorly, in this case geometry would not be the drawback but instead the MLCT process could be different from the synergic xantphos-dmp combination affecting the catalytic outcome.

Electronic phosphine ligand effect

In addition to the geometric factor, the stability of these species is dictated also by an electronic component. This constitutes the synergic effect associated with a good σ -donor (phosphine ligand) in combination with the π -acceptor dimethylphenanthroline which helps to hamper ligand dissociation.^{22-23, 88} In principle, higher donation from the phosphine results in more stable complexes. Such correlation has not been previously proven for the [Cu(P[^]P)(N[^]N)]⁺ type of complexes containing xantphos as chelating ligand, despite their various applications. In our case, with better sigma donors such as **4** and **5** the conversion rate did not change over the course of the reaction, indicating negligible deactivation of the catalyst. In contrast, the presence of the most electron withdrawing ligand in complex **1** deactivates faster than its analogues giving the lowest conversion after four hours. Despite the high activity that the unmodified xantphos complex **3** exhibits, catalyst decomposition is still observed, as evidenced by the sharp decrease in reaction rate after 2 hours of irradiation which also occurs in a similar fashion to complex **2** (Scheme 9). Importantly, here we show for the first time how the electronic effects of the diphosphine ligand influences the excited state stability in these type of photosensitizers. We observed that complexes bearing electron donating groups (negative Hammett values) exhibit longer excited state life times (**5** (6.83 μ s), **4** (6.17 μ s)) (Table 10, entries 4 and 1). This observation confirms that the design of photosensitizers with longer state lifetimes not only depends on the geometry but also on the electronic features which undoubtedly play a crucial role enhancing the stability of the complexes.

Solvation

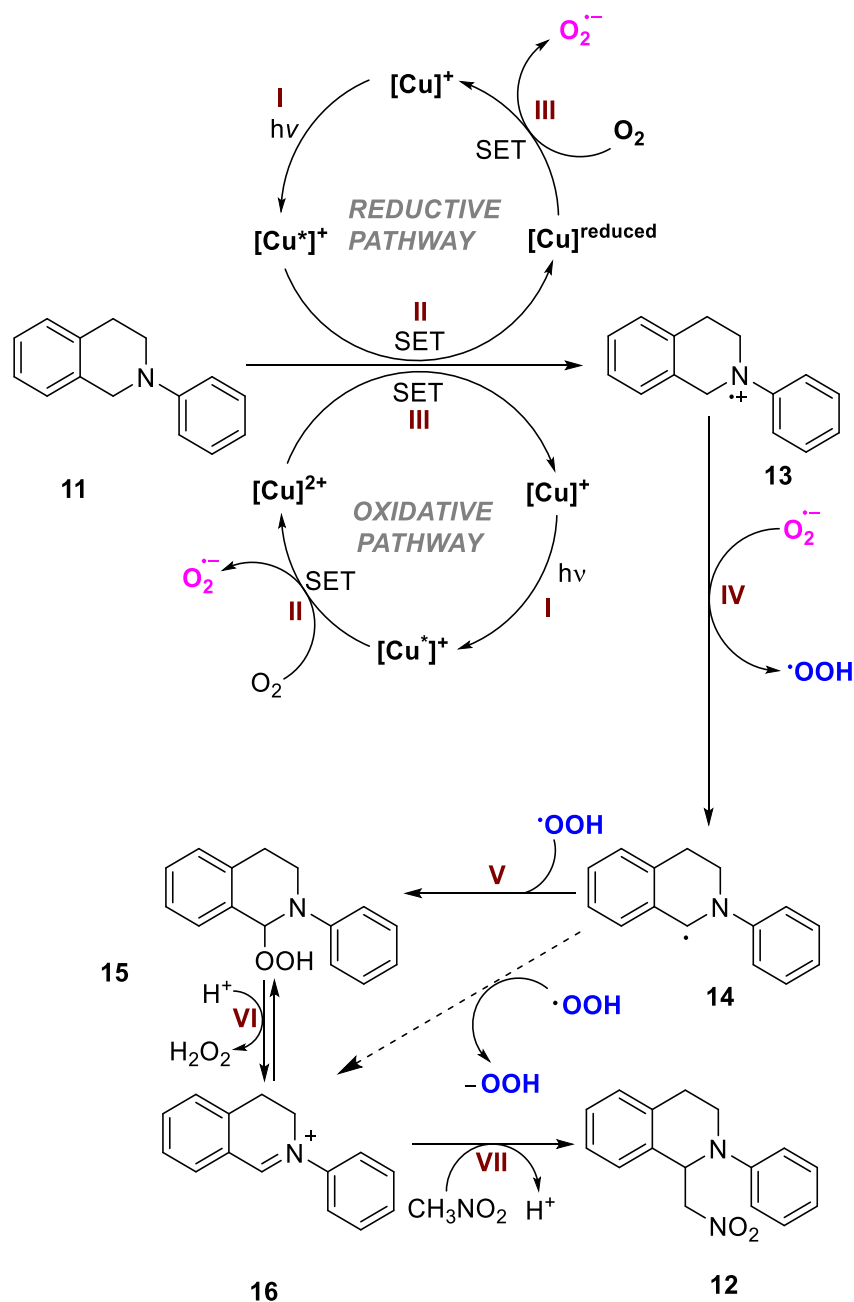
It has been shown that one of the major deactivation pathways of the Cu(I) complexes of the type studied in this chapter involves a solvent induced exciplex quenching of their excited states. In general, the bulky xant-like ligands prevent Cu(I) complexes against solvation, therefore slowing non radiative decay processes of the excited states. Since solvation of Cu(I) complexes depends not only on the geometry around the copper center but also on the electrostatic interactions of such cationic compounds with the solvent, electronics of the ligand play a decisive role. More donating phosphines decrease the positive character of the Cu(I) metal center,⁸⁹ thus reducing the destabilizing complex-solvent interaction leading to more stable complexes and enhancing their photochemical activity.

Among all the complexes tested, [Cu(*p*-OMe-xantphos)(dmp)]BF₄ (**5**) represents the ideal combination between σ donation from the chelating phosphine ligand making this photosensitizer highly stable. The complex in mention exhibits the highest Φ_{PL} , the lowest non radiative decay rate constant k_{nr} , the longest excited state life time τ_{PL} , more negative Hammett parameter and most negative E^*_{ox} potential among the Hammett series (Table 10). As a result of this, the reaction reaches full conversion within 5 hours, yielding 93% of the desired product.

Mechanistic insights

For this transformation a dominant reductive quenching pathway has been previously proposed in which the excited Cu(I) species is reduced to a radical anion copper intermediate “Cu^{reduced}”, oxidizing the amine substrate **II** and the photocatalyst being regenerated by molecular oxygen (Scheme 10, upper catalytic cycle), yielding the superoxide anion as byproduct **III**.⁸⁷ An alternative mechanism can be envisaged based on a oxidative quenching pathway (Scheme 10, lower catalytic cycle). In this case, the excited Cu(I) undergoes an electron transfer with molecular oxygen, yielding the oxidized Cu(II) species **II** which can be reduced back to Cu(I) by the amine substrate **III**. It should be noted that in both of these mechanisms, the radical cation of the amine substrate is formed along with the superoxide anion O₂^{•-} and the major difference lies in the initial electron transfer to the excited photocatalyst from the amine in a reductive quenching pathway, or from the excited photocatalyst to molecular oxygen in an oxidative quenching pathway.

Analysis of the photophysics of the complexes (**1–5**), showed a strong correlation between the photocatalyst performance and E^*_{ox} potentials, but no significant correlation with E^*_{red} potentials, suggesting an oxidative quenching in the catalytic cycle as the preferred pathway (Scheme 10). As observed by Walton and co-workers, complexes with tetrahedral structures exhibit the higher E^*_{ox} potentials due to their resistance to undergo the Jahn-Teller distortion for the appropriated flattened geometry of complexes with formal Cu(II) oxidation state, which is the case for our series of complexes.²⁵ Among them, photocatalyst **5** has the most negative E^*_{ox} potential ($E^*_{ox} = -1.58$ V Vs SCE) within the series which explains its superior activity in this reaction. Indeed, both reduction of oxygen to the superoxide anion ($E_{red(O_2/O_2^{\cdot-})} = -0.75$ V Vs SCE)⁹⁰ by the photoexcited Cu(I) complex and the oxidation of the tetrahydroisoquinoline ($E_{ox} = 0.83$ V to 0.88 V Vs SCE depending on solvent)⁹¹⁻⁹³ by the oxidized Cu(II) ($E_{ox} = 1.12$ V Vs SCE) are highly favored. In another illustrative case, complex **3** has a $E^*_{red} = 0.59$ V (Vs SCE in CH_2Cl_2) which should prevent any reductive quenching pathway via electron transfer from the amine, but the catalytic reaction proceeds in 53% yield after four hours suggesting the preferred oxidative quenching pathway.



Scheme 10. Proposed mechanism for the aerobic photocatalyzed cross-dehydrogenative coupling between N-phenyl-tetrahydroisoquinoline and nitromethane performed by $[Cu(p\text{-R-xantphos})(dmp)]^+$ complexes.

We therefore propose the following mechanism for this transformation (Scheme 10). After light irradiation, the excited state of the heteroleptic copper complex is quenched by molecular oxygen, generating a Cu(II) species and the superoxide radical anion $O_2^{\cdot-}$ **II**. Single

electron transfer between this Cu(II) and **11** regenerates the photocatalyst along with the formation of the radical cation **13 III** (Scheme 10, lower cycle). Deprotonation from the benzylic position of **13** by $\text{O}_2^{\cdot-}$ forms the radical **14** along with the hydroperoxyl radical HOO^{\cdot} **IV**. Reaction of those two species, either by direct recombination **V** or single electron transfer, leads to an equilibrating mixture of hydroperoxide **15** and iminium ion **16 VI**.⁹⁴⁻⁹⁶ Finally, nucleophilic attack of nitromethane on the highly electrophilic **16** leads to the formation of the CDC product **12 VII**.

The existence of the oxidative pathway under our reaction conditions was further supported by emission quenching experiments. Therefore, the emission intensity of a 41.66 μM solution of **5** was determined in the absence and in the presence of the quenchers **11** and O_2 (2.6mM each)⁹⁷, respectively (Figure 19). The emission was quenched by ca. 18.2% in the presence of **11** (red line) and by ca. 95.9% in the presence of O_2 (blue line), pointing out to the preferential interaction between **5** and O_2 than between **5** and **11**. It is important, however, to state that the quenching of emission does not necessarily mean an electron transfer.

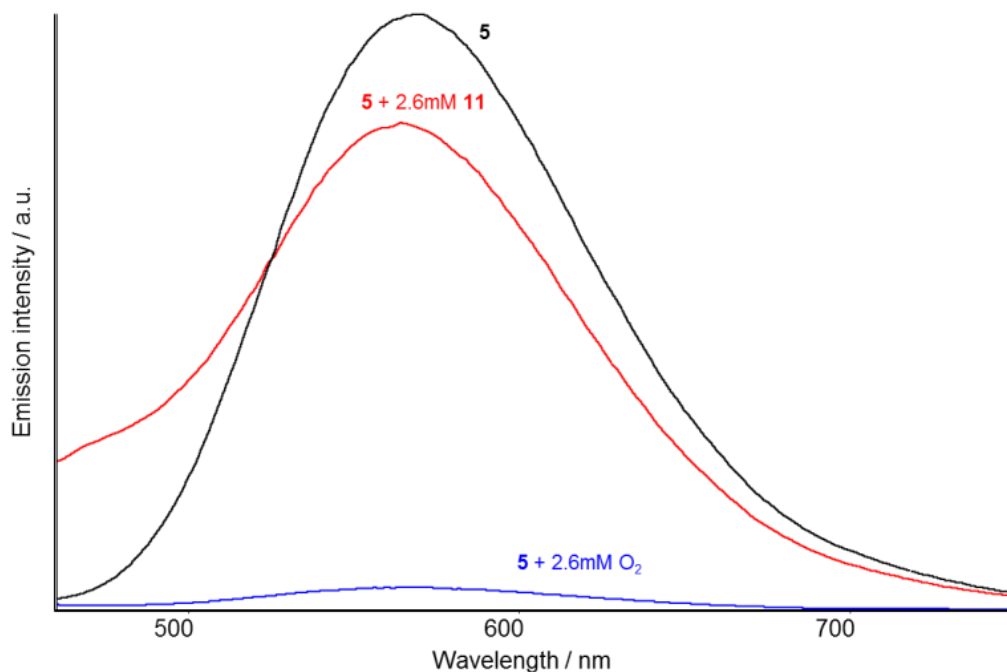


Figure 19. Steady-state emission spectra of **5** in the absence of any quencher (black), in the presence of 2.6 mM **11** (red) and in the presence of 2.6 mM O₂ (blue). Note that in the presence of O₂, almost all of the emission is quenched. Steady-state emission spectra were recorded using a Cary Eclipse Fluorescence spectrophotometer (Agilent Technologies) with an excitation wavelength of 390 nm, a slit width of 10 nm for excitation and of 20 nm for emission and an averaging time of 0.1s. The studies were performed in a sealable 10x10 mm quartz glass cuvette. The oxygen amount was adjusted by addition of the corresponding amount of an O₂-saturated acetonitrile solution⁹⁷ (2.6 mM O₂) to the solution of **5**.

According to the quenching experiment a reductive pathway is also possible and has to be considered where the copper complex is excited by light **I**, then performs SET with the substrate **11 II** and the yielded reduced copper gets oxidized by oxygen regenerating the catalyst **III** (Scheme 10, upper cycle). In order to compare the likelihood of both pathways under reaction conditions, it is possible to compare the favorability of the initial electron transfer by looking at the potentials of these components. The redox potentials of the excited state of the complexes reveal that a reduction of oxygen by the complexes is favorable, complexes **1-5** having consistently more negative E^*_{ox} potentials, ranging between -1.35 V and -1.58 V in dichloromethane (Table 5) and -1.28 V to -1.46 V in acetonitrile (Table 6), allowing the facile reduction of oxygen with potential of -0.75 V Vs SCE⁹⁰ (II). On the other

hand, the excited state reduction potential E^*_{red} of complexes **1–5** range from 0.59 V to 1.15 V in dichloromethane and 0.78 V to 1.16 V in acetonitrile. These values are only slightly more positive, or even less positive in the case of complex **3** in CH_2Cl_2 , than the reported oxidation potential from 0.83 to 0.88 V Vs SCE depending on the solvent⁹¹⁻⁹³ for the oxidation of tetrahydroisoquinoline **11** to the radical cation. Collectively, this suggests that the oxidative quenching process would be favored for all the complexes studied in this section but that, although unlikely, a minor contribution of the reductive quenching pathway could be operating for some complexes.

It is also important to consider that analysis of this catalytic process is also affected by contribution not only from the well-defined catalyst but also from the homoleptic complexes formed during the reaction, which showed to be slightly active when formed *in situ* under reaction conditions (Table 9). Other non-radiative pathways may be taking place during this catalytic process but there is not enough experimental evidence at this stage supporting such processes. At the current state of our investigations, quenching of the excited photosensitizers by oxygen forming singlet oxygen cannot be discarded and the result from the steady-state emission experiments cannot be fully attributed to an oxidative quenching (Figure 16, blue line). Identification of singlet oxygen under reactions conditions and its role not only as a quencher of the excited photosensitizer but as a reactant that yields the product in this specific catalytic process requires additional experimental work which is not covered in this PhD thesis. Therefore, this chapter focused on the discussion of the phosphine ligand effects and oxidative and reductive pathways based on redox potentials and experimental evidence. Other processes that could be operating in competition are not discussed in the present manuscript but research on the topic is ongoing in order to conclude the project.

2.4 Conclusions

The Hammett series of xantphos ligands was synthesized by an optimized methodology, reliably obtaining precursors and synthetic intermediates in multigram scale. Additionally, the synthetic procedures reported in this thesis do not require tedious purification protocols such as column chromatography for sensitive compounds and these can be obtained by recrystallization in high purity and in good to excellent yields.

Donating substituents at the *para* position of modified xantphos ligands play a key role in stabilizing heteroleptic copper(I) photosensitizers and have a significant impact on their catalytic performance. The more negative the Hammett parameter σ_p is, the higher the stability of the photosensitizer is. Evidently, the choice of the chelating phosphine ligand is relevant for the optimization of the performance of Cu(I) complexes in photocatalytic applications. With the application of the Hammett series of complexes in the aerobic photocatalyzed Cross-Dehydrogenative Coupling (CDC) between N-phenyl-tetrahydroisoquinoline and nitromethane as model reaction, it has been shown that structure, photophysical properties and stability of the photosensitizers are all important components to consider for the achievement of high catalytic performance. Interestingly, it has been shown that, although some photophysical properties correlate with the Hammett parameter, their influence on the photocatalytic performance is more complex and contemplates several interdependent variables. Among the complexes tested, **5** achieved the highest catalytic activity, due to the synergistic combination of all these factors. Fine-tuning of the electronic properties of the phosphine ligand resulted in the enhanced catalytic performance of the photosensitizer. Moreover, the systematic investigations presented in this work helped to understand the reaction mechanisms for the photocatalytic process.

In particular, a direct correlation between activity and E^*_{ox} potentials, along with emission quenching experiments proved that oxidative and reductive quenching pathways are involved in the aerobic photocatalyzed CDC between N-phenyl-tetrahydroisoquinoline and nitromethane. Overall, this detailed study showcased that systematic investigations are a powerful tool to achieve more efficient systems by understanding of reaction mechanisms and complex interactions in photocatalytic transformations.

2.5 References

1. Hoffert, M. I.; Caldeira, K.; Jain, A. K.; Haites, E. F.; Harvey, L. D. D.; Potter, S. D.; Schlesinger, M. E.; Schneider, S. H.; Watts, R. G.; Wigley, T. M. L.; Wuebbles, D. J. Energy implications of future stabilization of atmospheric CO₂ content. *Nature* **1998**, 395 (6705), 881-884.
2. US Dept of Energy, W., DC, Energy Information Administration (2015) Annual Energy Outlook with projections to 2040. **2015**.
3. Lewis, N. S. Research opportunities to advance solar energy utilization. *Science* **2016**, 351 (6271), 353.
4. Teegardin, K.; Day, J. I.; Chan, J.; Weaver, J. Advances in Photocatalysis: A Microreview of Visible Light Mediated Ruthenium and Iridium Catalyzed Organic Transformations. *Org. Process Res. Dev.* **2016**, 20 (7), 1156-1163.
5. Campagna, S.; Puntoriero, F.; Nastasi, F.; Bergamini, G.; Balzani, V. Photochemistry and photophysics of coordination compounds: ruthenium. (Photochemistry and Photophysics of Coordination Compounds I). *Top. Curr. Chem.* **2007**, 280, 117-214.
6. Zeitler, K. Photoredox Catalysis with Visible Light. *Angew. Chem. Int. Ed.* **2009**, 48 (52), 9785-9789.
7. Rau, S.; Walther, D.; Vos, J. G. Inspired by nature: light driven organometallic catalysis by heterooligonuclear Ru(II) complexes. *Dalton Trans.* **2007**, (9), 915-919.
8. Paria, S.; Reiser, O. Copper in photocatalysis. *ChemCatChem* **2014**, 6 (9), 2477-2483.
9. Sandroni, M.; Kayanuma, M.; Rebarz, M.; Akdas-Kilig, H.; Pellegrin, Y.; Blart, E.; Le Bozec, H.; Daniel, C.; Odobel, F. Heteroleptic diimine copper(I) complexes with large extinction coefficients: synthesis, quantum chemistry calculations and physico-chemical properties. *Dalton Trans.* **2013**, 42 (40), 14628-14638.
10. Ruthkosky, M.; Castellano, F. N.; Meyer, G. J. Photodriven Electron and Energy Transfer from Copper Phenanthroline Excited States. *Inorg. Chem.* **1996**, 35 (22), 6406-6412.
11. Horvath, O. Photochemistry of copper(I) complexes. *Coord. Chem. Rev.* **1994**, 135-136, 303-324.
12. Kutal, C. Spectroscopic and photochemical properties of d¹⁰ metal complexes. *Coord. Chem. Rev.* **1990**, 99, 213-252.
13. Ruthkosky, M.; Kelly, C. A.; Castellano, F. N.; Meyer, G. J. Electron and energy transfer from CuI MLCT excited states. *Coord. Chem. Rev.* **1998**, 171, 309-322.
14. Scaltrito, D. V.; Thompson, D. W.; O'Callaghan, J. A.; Meyer, G. J. MLCT excited states of cuprous bis-phenanthroline coordination compounds. *Coord. Chem. Rev.* **2000**, 208, 243-266.
15. Zhang, Y.; Schulz, M.; Waechtler, M.; Karnahl, M.; Dietzek, B. Heteroleptic diimine-diphosphine Cu(I) complexes as an alternative towards noble-metal based photosensitizers: Design strategies, photophysical properties and perspective applications. *Coord. Chem. Rev.* **2018**, 356, 127-146.
16. Chen, L. X.; Shaw, G. B.; Novozhilova, I.; Liu, T.; Jennings, G.; Attenkofer, K.; Meyer, G. J.; Coppens, P. MLCT State Structure and Dynamics of a Copper(I) Diimine Complex Characterized by Pump-Probe X-ray and Laser Spectroscopies and DFT Calculations. *J. Am. Chem. Soc.* **2003**, 125 (23), 7022-7034.

17. Garakyaraghi, S.; Danilov, E. O.; McCusker, C. E.; Castellano, F. N. Transient Absorption Dynamics of Sterically Congested Cu(I) MLCT Excited States. *J. Phys. Chem. A* **2015**, *119* (13), 3181-3193.
18. Mara, M. W.; Jackson, N. E.; Huang, J.; Stickrath, A. B.; Zhang, X.; Gothard, N. A.; Ratner, M. A.; Chen, L. X. Effects of Electronic and Nuclear Interactions on the Excited-State Properties and Structural Dynamics of Copper(I) Diimine Complexes. *J. Phys. Chem. B* **2013**, *117* (6), 1921-1931.
19. Siddique, Z. A.; Yamamoto, Y.; Ohno, T.; Nozaki, K. Structure-Dependent Photophysical Properties of Singlet and Triplet Metal-to-Ligand Charge Transfer States in Copper(I) Bis(diimine) Compounds. *Inorg. Chem.* **2003**, *42* (20), 6366-6378.
20. Moudam, O.; Kaeser, A.; Delavaux-Nicot, B.; Duhayon, C.; Holler, M.; Accorsi, G.; Armaroli, N.; Seguy, I.; Navarro, J.; Destruel, P.; Nierengarten, J.F. Electrophosphorescent homo- and heteroleptic copper(I) complexes prepared from various bis-phosphine ligands. *Chem. Commun.* **2007**, (29), 3077-3079.
21. Armaroli, N. Photoactive mono- and polynuclear Cu(I)-phenanthrolines. A viable alternative to Ru(II)-polypyridines?. *Chem. Soc. Rev.* **2001**, *30* (2), 113-124.
22. Palmer, C. E. A.; McMillin, D. R. Singlets, triplets, and exciplexes: complex, temperature-dependent emissions from (2,9-dimethyl-1,10-phenanthroline)bis(triphenylphosphine)copper(1+) and (1,10-phenanthroline)(triphenylphosphine)copper(1+). *Inorg. Chem.* **1987**, *26* (23), 3837-3840.
23. Casadonte, D. J., Jr.; McMillin, D. R. Dual emissions from (2,9-dimethyl-1,10-phenanthroline)bis(tertiary phosphine)copper(1+) systems in a rigid glass: influence of the phosphine donor strength. *Inorg. Chem.* **1987**, *26* (23), 3950-3952.
24. Kuang, S. M.; Cuttell, D. G.; McMillin, D. R.; Fanwick, P. E.; Walton, R. A. Synthesis and Structural Characterization of Cu(I) and Ni(II) Complexes that Contain the Bis[2-(diphenylphosphino)phenyl]ether Ligand. Novel Emission Properties for the Cu(I) Species. *Inorg. Chem.* **2002**, *41* (12), 3313-3322.
25. Cuttell, D. G.; Kuang, S.-M.; Fanwick, P. E.; McMillin, D. R.; Walton, R. A. Simple Cu(I) Complexes with Unprecedented Excited-State Lifetimes. *J. Am. Chem. Soc.* **2002**, *124* (1), 6-7.
26. Riesgo, E. C.; Hu, Y.-Z.; Bouvier, F.; Thummel, R. P.; Scaltrito, D. V.; Meyer, G. J. Crowded Cu(I) Complexes Involving Benzo[h]quinoline: π -Stacking Effects and Long-Lived Excited States. *Inorg. Chem.* **2001**, *40* (14), 3413-3422.
27. Kaeser, A.; Mohankumar, M.; Mohanraj, J.; Monti, F.; Holler, M.; Cid, J.-J.; Moudam, O.; Nierengarten, I.; Karmazin-Brelot, L.; Duhayon, C.; Delavaux-Nicot, B.; Armaroli, N.; Nierengarten, J. F. Heteroleptic Copper(I) Complexes Prepared from Phenanthroline and Bis-Phosphine Ligands. *Inorg. Chem.* **2013**, *52* (20), 12140-12151.
28. Tee, S. Y.; Win, K. Y.; Koh, L. D.; Liu, S.; Teng, C. P.; Han, M.-Y.; Tee, S. Y.; Koh, L.-D.; Teng, C. P.; Han, M. Y.; Teo, W. S. Recent Progress in Energy-Driven Water Splitting. *Adv. Sci.* **2017**, *4* (5), 1600337.
29. Junge, H.; Rockstroh, N.; Fischer, S.; Brueckner, A.; Ludwig, R.; Lochbrunner, S.; Kuehn, O.; Beller, M. Light to hydrogen: photocatalytic hydrogen generation from water with molecularly-defined iron complexes. *Inorganics*. **2017**, *5* (1), 14, 1-21.
30. Luo, S. P.; Mejia, E.; Friedrich, A.; Pazidis, A.; Junge, H.; Surkus, A.-E.; Jackstell, R.; Denurra, S.; Gladiali, S.; Lochbrunner, S.; Beller, M. Photocatalytic Water Reduction

with Copper-Based Photosensitizers: A Noble-Metal-Free System. *Angew. Chem. Int. Ed.* **2013**, 52 (1), 419-423.

31. Chen, N.-Y.; Xia, L.-M.; Lennox, A. J. J.; Sun, Y.-Y.; Chen, H.; Jin, H.-M.; Junge, H.; Wu, Q.-A.; Jia, J.-H.; Beller, M.; Luo, S. P. Structure-Activated Copper Photosensitizers for Photocatalytic Water Reduction. *Chem. Eur. J.* **2017**, 23 (15), 3631-3636.

32. Kim, J.; Whang, D. R.; Park, S. Y. Designing Highly Efficient CuI Photosensitizers for Photocatalytic H₂ Evolution from Water. *ChemSusChem* **2017**, 10 (9), 1883-1886.

33. Heberle, M.; Tschierlei, S.; Rockstroh, N.; Ringenberg, M.; Frey, W.; Junge, H.; Beller, M.; Lochbrunner, S.; Karnahl, M. Heteroleptic copper photosensitizers: Why an extended π -system does not automatically lead to enhanced hydrogen production. *Chem. Eur. J.* **2017**, 23 (2), 312-319.

34. Tschierlei, S.; Karnahl, M.; Rockstroh, N.; Junge, H.; Beller, M.; Lochbrunner, S. Substitution-Controlled Excited State Processes in Heteroleptic Copper(I) Photosensitizers Used in Hydrogen Evolving Systems. *ChemPhysChem* **2014**, 15 (17), 3709-3713.

35. Zgierski, M. Z. Cu(I)-2,9-dimethyl-1,10-phenanthroline: Density functional study of the structure, vibrational force-field, and excited electronic states. *J. Chem. Phys.* **2003**, 118 (9), 4045-4051.

36. Iwamura, M.; Watanabe, H.; Ishii, K.; Takeuchi, S.; Tahara, T. Coherent nuclear dynamics in ultrafast photoinduced structural change of bis(diimine)copper(I) complex. *J. Am. Chem. Soc.* **2011**, 133 (20), 7728-7736.

37. Huang, J.; Buyukcakil, O.; Mara, M. W.; Coskun, A.; Dimitrijevic, N. M.; Barin, G.; Kokhan, O.; Stickrath, A. B.; Ruppert, R.; Tiede, D. M.; Stoddart, J. F.; Sauvage, J. P.; Chen, L. X. Highly Efficient Ultrafast Electron Injection from the Singlet MLCT Excited State of Copper(I) Diimine Complexes to TiO₂ Nanoparticles. *Angew. Chem. Int. Ed.* **2012**, 51 (51), 12711-12715.

38. Iwamura, M.; Takeuchi, S.; Tahara, T. Real-Time Observation of the Photoinduced Structural Change of Bis(2,9-dimethyl-1,10-phenanthroline)copper(I) by Femtosecond Fluorescence Spectroscopy: A Realistic Potential Curve of the Jahn-Teller Distortion. *J. Am. Chem. Soc.* **2007**, 129 (16), 5248-5256.

39. Leydet, Y.; Bassani, D. M.; Jonusauskas, G.; McClenaghan, N. D. Equilibration between Three Different Excited States in a Bichromophoric Copper(I) Polypyridine Complex. *J. Am. Chem. Soc.* **2007**, 129 (28), 8688-8689.

40. Mejia, E.; Luo, S.-P.; Karnahl, M.; Friedrich, A.; Tschierlei, S.; Surkus, A. E.; Junge, H.; Gladiali, S.; Lochbrunner, S.; Beller, M. A Noble-Metal-Free System for Photocatalytic Hydrogen Production from Water. *Chem. Eur. J.* **2013**, 19 (47), 15972-15978.

41. Zhang, Y.; Heberle, M.; Waechtler, M.; Karnahl, M.; Dietzek, B. Determination of side products in the photocatalytic generation of hydrogen with copper photosensitizers by resonance Raman spectroelectrochemistry. *RSC Adv.* **2016**, 6 (107), 105801-105805.

42. Rosas-Hernandez, A.; Steinlechner, C.; Junge, H.; Beller, M. Earth-abundant photocatalytic systems for the visible-light-driven reduction of CO₂ to CO. *Green Chem.* **2017**, 19 (10), 2356-2360.

43. Hernandez-Perez, A. C.; Collins, S. K. A Visible-Light-Mediated Synthesis of Carbazoles. *Angew. Chem., Int. Ed.* **2013**, 52 (48), 12696-12700.

44. Cho, S. H.; Yoon, J.; Chang, S. Intramolecular Oxidative C-N Bond Formation for the Synthesis of Carbazoles: Comparison of Reactivity between the Copper-Catalyzed and Metal-Free Conditions. *J. Am. Chem. Soc.* **2011**, 133 (15), 5996-6005.

45. Jordan-Hore, J. A.; Johansson, C. C. C.; Gulias, M.; Beck, E. M.; Gaunt, M. J. Oxidative Pd(II)-Catalyzed C-H Bond Amination to Carbazole at Ambient Temperature. *J. Am. Chem. Soc.* **2008**, *130* (48), 16184-16186.
46. Tsang, W. C. P.; Zheng, N.; Buchwald, S. L. Combined C-H functionalization/C-N bond formation route to carbazoles. *J. Am. Chem. Soc.* **2005**, *127* (42), 14560-14561.
47. Joergensen, K. B., Photochemical oxidative cyclisation of stilbenes and Stilbenoids - the Mallory-reaction. *Molecules* **2010**, *15*, 4334-4358.
48. Hernandez-Perez, A. C.; Vlassova, A.; Collins, S. K. Toward a Visible Light Mediated Photocyclization: Cu-Based Sensitizers for the Synthesis of [5]Helicene. *Org. Lett.* **2012**, *14* (12), 2988-2991.
49. Michelet, B.; Deldaele, C.; Kajouj, S.; Moucheron, C.; Evano, G. A General Copper Catalyst for Photoredox Transformations of Organic Halides. *Org. Lett.* **2017**, *19* (13), 3576-3579.
50. Nishikawa, M.; Wakita, Y.; Nishi, T.; Miura, T.; Tsubomura, T. Long-lived and oxygen-responsive photoluminescence in the solid state of copper(I) complexes bearing fluorinated diphosphine and bipyridine ligands. *Dalton Trans.* **2015**, *44* (19), 9170-9181.
51. Smith, C. S.; Branham, C. W.; Marquardt, B. J.; Mann, K. R. Oxygen Gas Sensing by Luminescence Quenching in Crystals of Cu(xantphos)(phen)+ Complexes. *J. Am. Chem. Soc.* **2010**, *132* (40), 14079-14085.
52. Medina-Rodriguez, S.; Orriach-Fernandez, F. J.; Poole, C.; Kumar, P.; de la Torre-Vega, A.; Fernandez-Sanchez, J. F.; Baranoff, E.; Fernandez-Gutierrez, A. Copper(I) complexes as alternatives to iridium(III) complexes for highly efficient oxygen sensing. *Chem. Commun.* **2015**, *51* (57), 11401-11404.
53. Zhang, Y.; Schulz, M.; Wächtler, M.; Karnahl, M.; Dietzek, B. Heteroleptic diimine-diphosphine Cu(I) complexes as an alternative towards noble-metal based photosensitizers: Design strategies, photophysical properties and perspective applications. *Coord. Chem. Rev.* **2018**, *356*, 127-146.
54. Lennox, A. J. J.; Fischer, S.; Jurrat, M.; Luo, S. P.; Rockstroh, N.; Junge, H.; Ludwig, R.; Beller, M. Copper-Based Photosensitisers in Water Reduction: A More Efficient In Situ Formed System and Improved Mechanistic Understanding. *Chem. Eur. J.* **2016**, *22* (4), 1233-1238.
55. Fischer, S.; Hollmann, D.; Tschierlei, S.; Karnahl, M.; Rockstroh, N.; Barsch, E.; Schwarzbach, P.; Luo, S. P.; Junge, H.; Beller, M.; Lochbrunner, S.; Ludwig, R.; Brueckner, A. Death and rebirth: Photocatalytic hydrogen production by a self-organizing copper-iron system. *ACS Catal.* **2014**, *4* (6), 1845-1849.
56. Karnahl, M.; Mejia, E.; Rockstroh, N.; Tschierlei, S.; Luo, S. P.; Grabow, K.; Kruth, A.; Brueser, V.; Junge, H.; Lochbrunner, S.; Beller, M. Photocatalytic Hydrogen Production with Copper Photosensitizer-Titanium Dioxide Composites. *ChemCatChem* **2014**, *6* (1), 82-86.
57. Sun, Y. Y.; Wang, H.; Chen, N.-Y.; Lennox, A. J. J.; Friedrich, A.; Xia, L. M.; Lochbrunner, S.; Junge, H.; Beller, M.; Zhou, S.; Luo, S.P. Efficient photocatalytic water reduction using in situ generated Knoelker's iron complexes. *ChemCatChem* **2016**, *8* (14), 2340-2344.
58. Hernandez-Perez, A. C.; Caron, A.; Collins, S. K. Photochemical Synthesis of Complex Carbazoles: Evaluation of Electronic Effects in Both UV and Visible-Light Methods in Continuous Flow. *Chem. Eur. J.* **2015**, *21* (46), 16673-16678.

59. Xiao, P.; Dumur, F.; Zhang, J.; Fouassier, J. P.; Gimes, D.; Lalevee, J. Copper Complexes in Radical Photoinitiating Systems: Applications to Free Radical and Cationic Polymerization upon Visible LEDs. *Macromolecules* **2014**, *47* (12), 3837-3844.
60. Balzani, V.; Juris, A. Photochemistry and photophysics of Ru(II)polypyridine complexes in the Bologna group. From early studies to recent developments. *Coord. Chem. Rev.* **2001**, *211* (1), 97-115.
61. Juris, A.; Balzani, V.; Barigelletti, F.; Campagna, S.; Belser, P.; von Zelewsky, A. Ru(II) polypyridine complexes: photophysics, photochemistry, electrochemistry, and chemiluminescence. *Coord. Chem. Rev.* **1988**, *84*, 85-277.
62. Hernandez-Perez, A. C.; Collins, S. K. Heteroleptic Cu-Based Sensitizers in Photoredox Catalysis. *Acc. Chem. Res.* **2016**, *49* (8), 1557-1565.
63. Weber, M. D.; Viciano-Chumillas, M.; Armentano, D.; Cano, J.; Costa, R. D. σ -Hammett parameter: a strategy to enhance both photo- and electro-luminescence features of heteroleptic copper(I) complexes. *Dalton Trans.* **2017**, *46* (19), 6312-6323.
64. Rinehart, N. I.; Kendall, A. J.; Tyler, D. R. A Universally Applicable Methodology for the Gram-Scale Synthesis of Primary, Secondary, and Tertiary Phosphines. *Organometallics* **2018**, *37* (2), 182-190.
65. Adams, G. M.; Weller, A. S. POP-type ligands: Variable coordination and hemilabile behaviour. *Coord. Chem. Rev.* **2018**, *355*, 150-172.
66. van Leeuwen, P. W. N. M.; Kamer, P. C. J. Featuring Xantphos. *Catal. Sci. Technol.* **2018**, *8* (1), 26-113.
67. Goertz, W.; Keim, W.; Vogt, D.; Englert, U.; Boele, M. D. K.; van der Veen, L. A.; Kamer, P. C. J.; van Leeuwen, P. W. N. M. Electronic effects in the nickel-catalyzed hydrocyanation of styrene applying chelating phosphorus ligands with large bite angles. *J. Chem. Soc., Dalton Trans.* **1998**, (18), 2981-2988.
68. Kranenburg, M.; Kamer, P. C. J.; van Leeuwen, P. W. N. M.; Vogt, D.; Keim, W. Effect of the bite angle of diphosphine ligands on activity and selectivity in the nickel-catalyzed hydrocyanation of styrene. *J. Chem. Soc., Chem. Commun.* **1995**, (21), 2177-8.
69. McMillin, D. R.; Kirchhoff, J. R.; Goodwin, K. V. Exciplex quenching of photo-excited copper complexes. *Coord. Chem. Rev.* **1985**, *64*, 83-92.
70. Van der Veen, L. A.; Boele, M. D. K.; Bregman, F. R.; Kamer, P. C. J.; Van Leeuwen, P. W. N. M.; Goubitz, K.; Fraanje, J.; Schenk, H.; Bo, C. Electronic Effect on Rhodium Diphosphine Catalyzed Hydroformylation: The Bite Angle Effect Reconsidered. *J. Am. Chem. Soc.* **1998**, *120* (45), 11616-11626.
71. Punji, B.; Mague, J. T.; Balakrishna, M. S. Thioether-Functionalized Ferrocenyl-bis(phosphonite), $\text{Fe}\{(\text{C}_5\text{H}_4)\text{P}(-\text{OC}_{10}\text{H}_6(\mu\text{-S})\text{C}_{10}\text{H}_6\text{O-})\}_2$: Synthesis, Coordination Behavior, and Application in Suzuki-Miyaura Cross-Coupling Reactions. *Inorg. Chem.* **2007**, *46* (24), 10268-10275.
72. Khabbass, N. D. A. H. A study of the reactions between halamines and varieties of phosphorus species. *Durham theses* **1981**, Durham University.
73. Goertz, W.; Kamer, P. C. J.; Van Leeuwen, P. W. N. M.; Vogt, D. Asymmetric nickel-catalyzed hydrocyanation of vinylarenes by applying homochiral xantphos ligands. *Chem. Eur. J.* **2001**, *7* (8), 1614-1618.
74. Zhu, Y.; Rawal, V. H. Palladium-catalyzed C3-benzoylation of indoles. *J. Am. Chem. Soc.* **2012**, *134* (1), 111-114.

75. Shaw, L.; Somisara, D. M. U. K.; How, R. C.; Westwood, N. J.; Bruijninx, P. C. A.; Weckhuysen, B. M.; Kamer, P. C. J. Electronic and bite angle effects in catalytic C-O bond cleavage of a lignin model compound using ruthenium Xantphos complexes. *Catal. Sci. Technol.* **2017**, 7 (3), 619-626.
76. Ashby, E. C.; Al-Fekri, D. M. The reaction of benzotrihalides and benzal halides with magnesium. Synthetic and mechanistic studies. *J. Organomet. Chem.* **1990**, 390 (3), 275-292.
77. Mohankumar, M.; Holler, M.; Nierengarten, J. F.; Sauvage, J. P. Preparation of Copper(I) Pseudo-rotaxanes from Bis-phosphine Ligands. *Chem. Eur. J.* **2012**, 18 (39), 12192-12195.
78. Siankevich, S.; Mozzettini, S.; Bobbink, F.; Ding, S.; Fei, Z.; Yan, N.; Dyson, P. J. Influence of the Anion on the Oxidation of 5-Hydroxymethylfurfural by Using Ionic-Polymer-Supported Platinum Nanoparticle Catalysts. *ChemPlusChem* **2018**, 83 (1), 1.
79. James, B. R.; Williams, R. J. P. 383. The oxidation-reduction potentials of some copper complexes. *J. Chem. Soc.* **1961**, (0), 2007-2019.
80. Connelly, N. G.; Geiger, W. E. Chemical Redox Agents for Organometallic Chemistry. *Chem. Rev.* **1996**, 96 (2), 877-910.
81. Banus, M. G., A design for a saturated calomel electrode. *Science* **1941**, 93, 601-602.
82. Braslavsky, S. E.; Acuna, A. U.; Adam, W.; Amat, F.; Armesto, D.; Atvars, T. D. Z.; Bard, A.; Bill, E.; Bjoern, L. O.; Bohne, C.; Bolton, J.; Bonneau, R.; Bouas-Laurent, H.; Braun, A. M.; Dale, R.; Dill, K.; Doepp, D.; Duerr, H.; Fox, M. A.; Gandolfi, T.; Grabowski, Z. R.; Griesbeck, A.; Kutateladze, A.; Litter, M.; Lorimer, J.; Mattay, J.; Michl, J.; Miller, R. J. D.; Moggi, L.; Monti, S.; Nonell, S.; Ogilby, P.; Olbrich, G.; Oliveros, E.; Olivucci, M.; Orellana, G.; Prokorenko, V.; Naqvi, K. R.; Rettig, W.; Rizzi, A.; Rossi, R. A.; San Roman, E.; Scandola, F.; Schneider, S.; Thulstrup, E. W.; Valeur, B.; Verhoeven, J.; Warman, J.; Weiss, R.; Wirz, J.; Zachariasse, K. Glossary of Terms Used in Photochemistry, 3rd edition (IUPAC recommendations 2006). *Pure Appl. Chem.* **2007**, 79 (3), 293-465.
83. Prier, C. K.; Rankic, D. A.; MacMillan, D. W. C. Visible Light Photoredox Catalysis with Transition Metal Complexes: Applications in Organic Synthesis. *Chem. Rev.* **2013**, 113 (7), 5322-5363.
84. Pirtsch, M.; Paria, S.; Matsuno, T.; Isobe, H.; Reiser, O. [Cu(dap)₂Cl] As An Efficient Visible-Light-Driven Photoredox Catalyst in Carbon-Carbon Bond-Forming Reactions. *Chem. Eur. J.* **2012**, 18 (24), 7336-7340.
85. Lowry, M. S.; Goldsmith, J. I.; Slinker, J. D.; Rohl, R.; Pascal, R. A., Jr.; Malliaras, G. G.; Bernhard, S. Single-Layer Electroluminescent Devices and Photoinduced Hydrogen Production from an Ionic Iridium(III) Complex. *Chem. Mater.* **2005**, 17 (23), 5712-5719.
86. Sakaki, S.; Mizutani, H.; Kase, Y.-i.; Inokuchi, K.-j.; Arai, T.; Hamada, T. Photoinduced electron transfer between [Cu(dmphen)L₂]⁺ [dmphen = 2,9-dimethyl-1,10-phenanthroline, L = PPhn(C₆H₄)Me-p)_{3-n} (n = 0-3)] and methylviologen. *J. Chem. Soc., Dalton Trans.* **1996**, 0, 1909-1914.
87. Wang, B.; Shelar, D. P.; Han, X. Z.; Li, T.-T.; Guan, X.; Lu, W.; Liu, K.; Chen, Y.; Fu, W. F.; Che, C. M. Long-Lived Excited States of Zwitterionic Copper(I) Complexes for Photoinduced Cross-Dehydrogenative Coupling Reactions. *Chem. Eur. J.* **2015**, 21 (3), 1184-1190.
88. Helmut, S., Ternary Cu²⁺ Complexes: Stability, Structure, and Reactivity. *Angew. Chem. Int. Ed.* **1975**, 14 (6), 394-402.

89. Sakaki, S.; Hashimoto, S.; Koga, G.; Ohkubo, K. Significant phosphine ligand effect on the photochemical reactivity of $[\text{Cu}(\text{N-N})\text{L}_2]^+$ ($\text{N-N} = 1,10\text{-phenanthroline}$ or $2,9\text{-dimethyl-1,10-phenanthroline}$; $\text{L} = \text{tertiary phosphine}$). *Dalton Trans.* **1988**, (6), 1641-1644.
90. Sawyer, D. T.; Gibian, M. J.; Morrison, M. M.; Seo, E. T. On the chemical reactivity of superoxide ion. *J. Am. Chem. Soc.* **1978**, *100* (2), 627-628.
91. Willms, J. A.; Gleich, H.; Schrempp, M.; Menche, D.; Engeser, M. Investigations of the Copper-Catalyzed Oxidative Cross-Coupling of Tetrahydroisoquinolines with Diethylzinc by a Combination of Mass Spectrometric and Electrochemical Methods. *Chem. Eur. J.* **2018**, *24* (11), 2663-2668.
92. Yang, Q.; Zhang, L.; Ye, C.; Luo, S.; Wu, L.-Z.; Tung, C. H. Visible-Light-Promoted Asymmetric Cross-Dehydrogenative Coupling of Tertiary Amines to Ketones by Synergistic Multiple Catalysis. *Angew. Chem. Int. Ed.* **2017**, *56* (13), 3694-3698.
93. Bartling, H.; Eisenhofer, A.; König, B.; Gschwind, R. M. The Photocatalyzed Aza-Henry Reaction of N-Aryltetrahydroisoquinolines: Comprehensive Mechanism, $\text{H}\cdot$ - versus H^+ -Abstraction, and Background Reactions. *J. Am. Chem. Soc.* **2016**, *138* (36), 11860-11871.
94. Boess, E.; Sureshkumar, D.; Sud, A.; Wirtz, C.; Fares, C.; Klussmann, M. Mechanistic Studies on a Cu-Catalyzed Aerobic Oxidative Coupling Reaction with N-Phenyl Tetrahydroisoquinoline: Structure of Intermediates and the Role of Methanol As a Solvent. *J. Am. Chem. Soc.* **2011**, *133* (21), 8106-8109.
95. Boess, E.; Schmitz, C.; Klussmann, M. A Comparative Mechanistic Study of Cu-Catalyzed Oxidative Coupling Reactions with N-Phenyltetrahydroisoquinoline. *J. Am. Chem. Soc.* **2012**, *134* (11), 5317-5325.
96. Ratnikov, M. O.; Doyle, M. P. Mechanistic Investigation of Oxidative Mannich Reaction with tert-Butyl Hydroperoxide. The Role of Transition Metal Salt. *J. Am. Chem. Soc.* **2013**, *135* (4), 1549-1557.
97. Quaranta, M.; Murkovic, M.; Klimant, I. A new method to measure oxygen solubility in organic solvents through optical oxygen sensing. *Analyst* **2013**, *138* (21), 6243-6245.
98. Nishio, M.; Umezawa, Y.; Honda, K.; Tsuboyama, S.; Suezawa, H. CH/π hydrogen bonds in organic and organometallic chemistry. *CrystEngComm* **2009**, *11* (9), 1757-1788.

Chapter III: Modified xantphos ligands for lignin depolymerization in ionic liquid media

3.1 Introduction

3.1.1 Lignocellulosic biomass: Properties and opportunities

3.1.1.1 Lignocellulosic biomass as alternative to oil

Currently humanity depends on carbon-based compounds derived from petroleum to obtain liquid fuels and chemicals; however, this feedstock is unfortunately a limited source due to its non-renewability (Figure 1, left side).¹ From an economic point of view, its cost is raising due to the large demand and the depletion of exploitable reserves. In this scenario, finding an alternative is mandatory and researchers have started to focus their attention towards biomass as a renewable feedstock (Figure 1, right side), especially for the production of chemicals since electrical energy can be provided from other sources such as wind, sun and hydroelectric plants.²

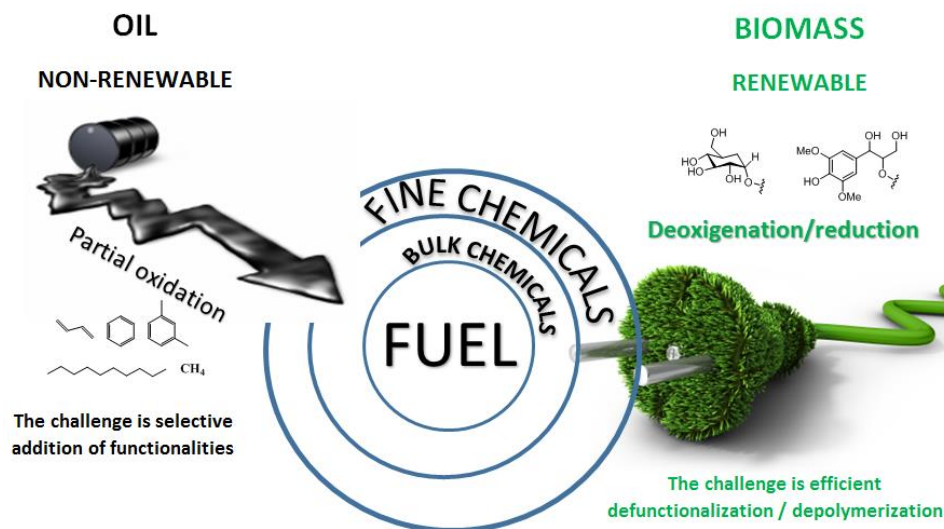


Figure 1. Petroleum and biomass conversion processes. Adapted from Barta.³

For example, in North America, the idea of increasing the use of biomass for domestic energy consumption and production of chemicals is gaining importance. In the U.S the volume of chemical commodities derived from biomass was set to increase by 25% by 2030 as

estimated in 2005 according to the goals of the U.S. Department of Energy. Lately, the goal was modified and currently it is expected an increase of 30%.⁴⁻⁵

Among the various types of biomass, this introduction is focused on lignocellulose derived from plants. This feedstock cannot be used directly as it is comprised of many different components with robust structures and therefore requires different separation processes. In an ideal bio-refinery process, the complex matrix needs to be first pre-treated in order to extract polysaccharides with ethanol for the generation of bio-based fuels. During this process, lignin is generated as a by-product which is used as a low quality fuel to provide heat for other procedures in the refinery. Discovering novel methodologies for its depolymerization will allow lignin to enter in the cycle for the production of bio based aromatic chemicals after fractionation and further conversion of the lignocellulosic biomass components (Figure 2).⁶

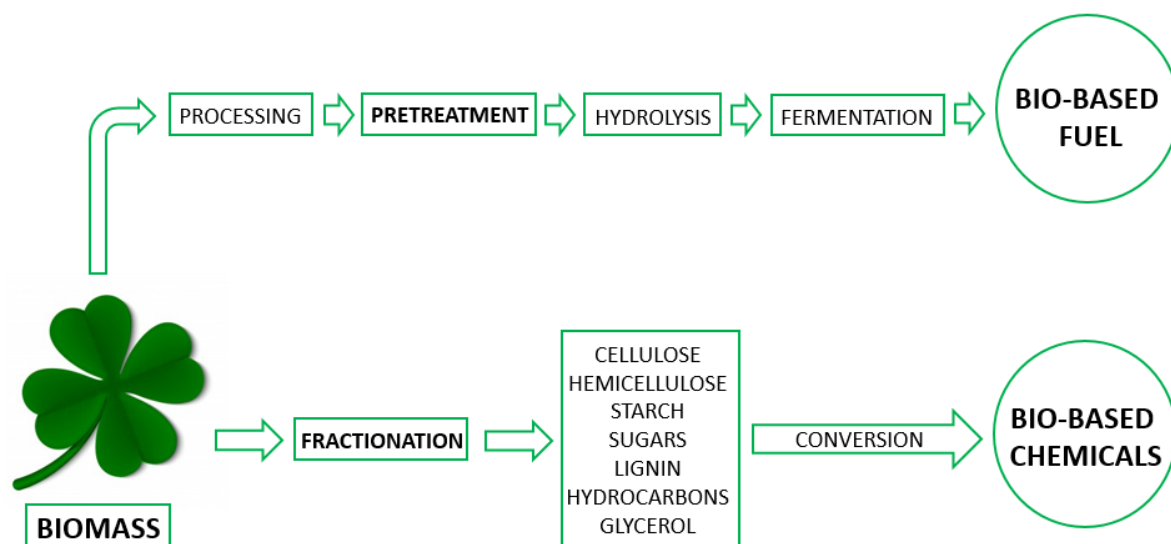


Figure 2. Integrated ideal bio refinery process for lignocellulosic biomass conversion Adapted from Bozell.⁵

3.1.1.2 Ethical Considerations

Regarding the use of waste, chemical processes play a vital role in this challenging area but politics, economics and psychology cannot be ignored when making decisions, so “win-win” solutions have to be designed.

“We can make our waste more treasure than trash. But it also reveals that to achieve that goal, we’ll have to work with our waste more than ever. Luckily, a growing number of researchers appear to be interested in getting their hands dirty”.⁷

Another critical point is that the use of agricultural crops as sources of biofuels could be in competition with food/feed needs and industrial purposes. Currently, there is a debate about the deficiency of agricultural land and its adequate use. In particular, where food production levels are low the use of land for food is a priority and biomass as a source of chemicals and energy takes second place.⁸ In this context it is important to underline that lignin is not applicable for nutrition purposes, it already exists in surplus and is underutilized thus its use does not induce more competition in the use of agriculture lands. Therefore lignin could be exploited in bio refinery processes from the non-edible biomass sources like forest products, grass, straw, etc.,⁹ for the production of second generation bioproducts. Moreover, if the monomers extracted from lignin can be successfully isolated they will be already functionalized, then the synthesis of chemicals based on them will require fewer than using alkanes as starting materials. It is well known that bio-based molecules have shown unique properties in terms of biocompatibility and biodegradability in comparison with their synthetic analogues, for that reason, their higher benefit and “bio” or “natural” label is better accepted in the market.¹⁰

3.1.2 Lignocellulosic biomass composition

Lignocellulosic biomass is a potential feedstock containing three major components in its structure: cellulose, hemicelluloses and lignin (Figure 3). This renewable resource could be used for the production of a variety of valuable chemicals, fuel and energy.¹¹ Despite the chemical attractiveness of all these fractions, this chapter will only focus on lignin structure, properties, and valorization methodologies of this potentially important feedstock.



Figure 3. Components of plant cells. Adapted from Weckhuysen.¹¹

3.1.2.1 Hemi (cellulose) fraction

Cellulose and hemicellulose are formed by plants via the polymerization of monosaccharides which are formed from the photosynthesis process, resulting in cellulose from glucose (Figure 4) and hemicellulose as the polymeric product of glucose and xylose. The cellulosic reserve is one of the world's largest biomass resources contributing up to almost 720 billion tons of material per year.¹¹ Currently, only about 200 million tons are used industrially, mainly as a raw material for paper and packaging industries.¹² The very large amount of material available, and the increasing interest in biomass as a renewable resource, means the valorization of this lignocellulosic fraction has attracted huge attention from the scientific community in the last decades.

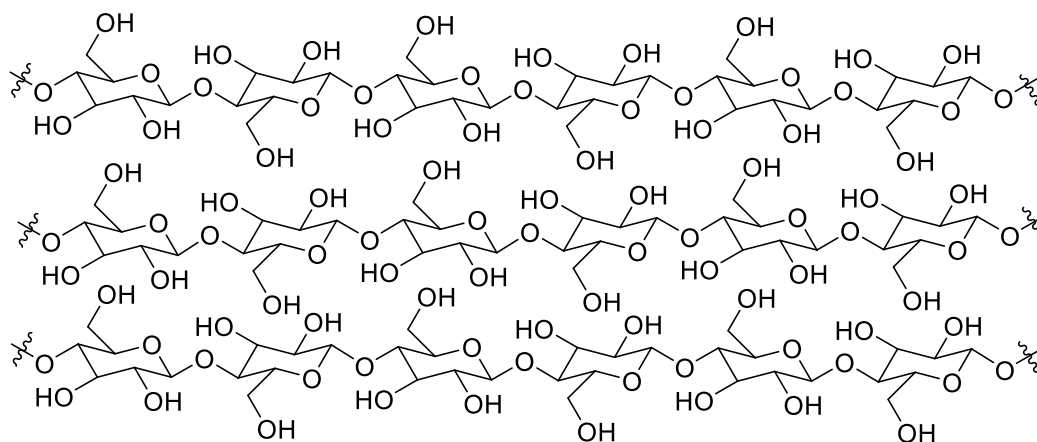


Figure 4. Cellulose polymer.

Hydrolysis of glycosidic bonds mediated by acid is the predominant process for the valorization of these types of biopolymers.¹³ Several biofuels can be formed starting from this biomass fraction such as bioethanol, furan-based biofuels such as 5-(hydroxymethyl) furfural (5-HMF) and valeric biofuels such as levulinic acid (LA).¹⁴ Moreover, LA can be further converted to γ -valerolactone (GVL),¹⁵ a precursor that could be potentially used for adipic acid synthesis.¹⁶ Additionally, 5-HMF can be used as starting material for the synthesis of 2,5-furandicarboxylic acid (FDCA), which is under study as a replacement for terephthalic acid in polyesters synthesis.¹⁷

3.1.2.2 Lignin fraction

Lignin is a three-dimensional amorphous polymer formed by random radical coupling of aromatic monomers (monolignols) at many different positions due to electron delocalization of the aromatic ring, oxo-functionalities and the olefin of the side chain (phenylpropane monomers); giving the highly cross-linked polymer.¹⁸ The rigidity of the plant is conferred by the interaction through chemical bonding between lignin with cellulose and hemicellulose micro fibrils. In particular, lignin serves as a permanent glue to give rigidity, water transport and defense for plants, making it very resistant to chemical transformations.¹⁹⁻²⁰ As described above lignin is formed by different monomers linked together to form a complex 3D polymer. The most common sub-units in lignin are derived from the constituent monolignols: coniferyl alcohol, sinapyl alcohol and coumaryl alcohol (Figure 5). The ratio of these building blocks mainly depends on the plant source. Lignin sources are divided into softwood and hardwood.

The composition of softwood and hardwood lignin varies in the relative abundance of the *p*-coumaryl, coniferyl, and sinapyl alcohols. Coniferyl alcohols constitute approximately 90% of softwood lignin, while similar amount of coniferyl and sinapyl alcohol appear in hardwood lignin.¹¹

Lignin is a waste product of various industrial processes, primarily the pulping and paper industries. It has been found that in residual lignin, the condensed phenolic units are formed in greater abundance in softwood compared to hardwood.²¹ All these characteristics are important when considering different plant materials as feedstock in order to obtain the desired chemicals.

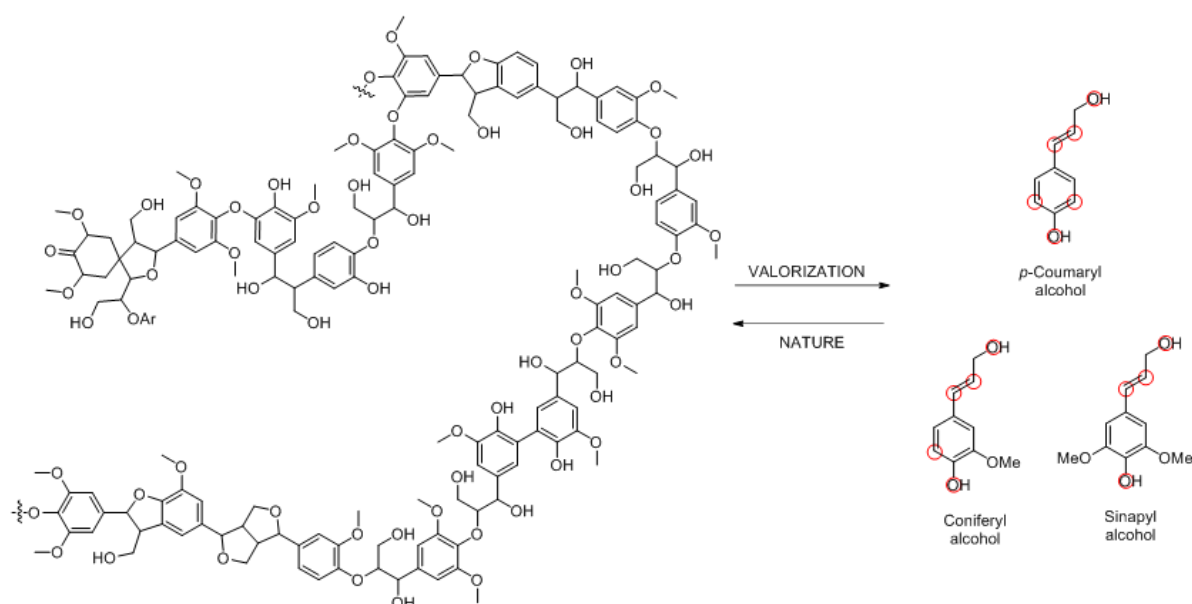


Figure 5. Model structure of lignin and monolignols with their points of polymerization. Adapted from Weckhuysen¹¹ and Barta.²²

Other important feature is the variety of linkages encountered in the lignin matrix (Figure 6). In addition to the variation in monolignol composition, there is a varying proportion of the different linkages in both hardwood and softwood lignin (Table 1),¹¹ with the β -O-4 type being most common. For this reason, the β -O-4 is the most studied linkage as its cleavage should lead to the most efficient depolymerization of the lignin matrix.

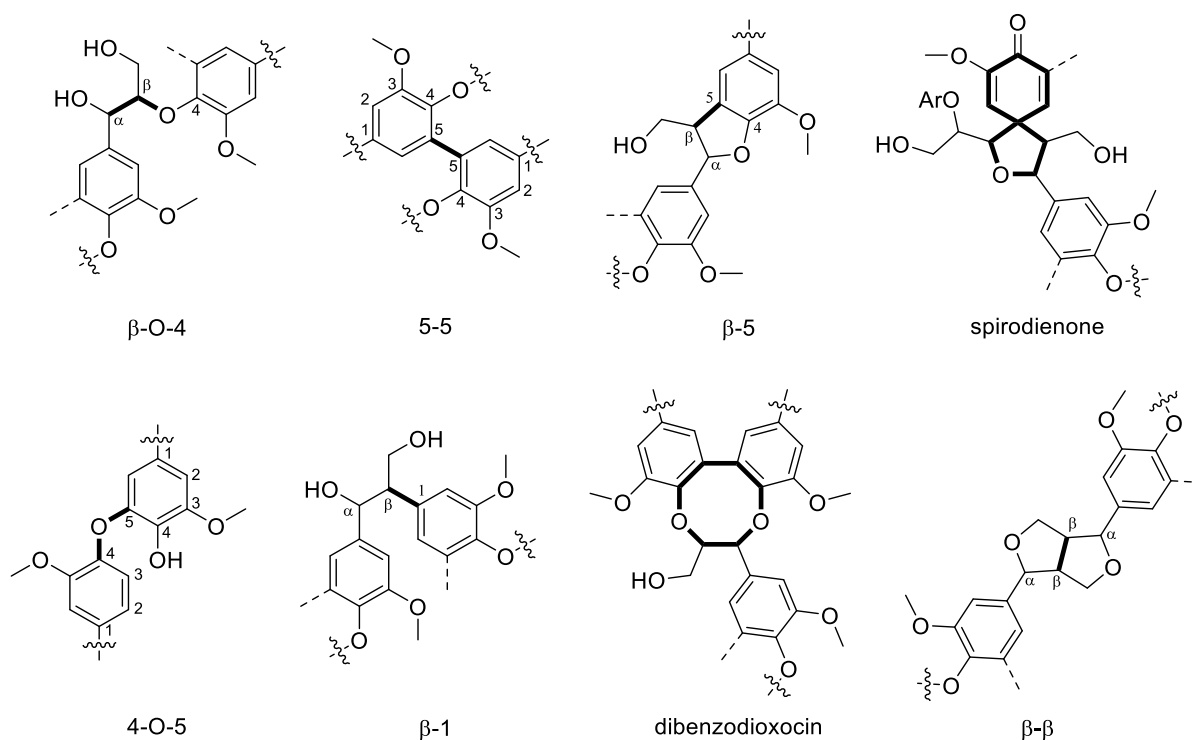


Figure 6. Linkages present in lignin. Taken from Weckhuysen.¹¹

Table 1. Different linkages present in softwood and hardwood lignin.

| Linkage (%) ^a | β -O-4 | 5-5 | β -5 | 4-O-5 | β -1 | β - β |
|--------------------------|--------------|-------|------------|-------|------------|-------------------|
| Spruce (Softwood) | 45–50 | 19–22 | 9–12 | 4–7 | 7–9 | 2–4 |
| Birch (Hardwood) | 60 | 9 | 6 | 6.5 | 7 | 3 |

a) Spirodienone and dibenzodioxocin linkages: n.d.

Nowadays, the use of lignin is mostly limited to be used as an adhesive binder or as a fuel for direct combustion simply being burned to provide heat for other processes, but it has remarkable potential to produce various forms of aromatic hydrocarbons which can be useful for the chemical industry.²³ Design of new long term conversion technologies for the depolymerization of lignin could provide a source of low-molecular weight starting materials and very important aromatic chemicals.²⁴

Valorization of lignin in a controlled fashion has been limited by difficulties in the dissolution of the material caused by its complex 3D structure and the resistance of phenolic ethers

toward hydrolysis.⁹ Its conversion is therefore particularly challenging and has been studied by different disciplines in order to access the monolignols as building blocks for more complex, valuable and useful molecules.^{11,22}

3.1.3 Methodologies for the depolymerization of lignin

As mentioned above, the β -O-4 linkage is the predominant one and therefore the most promising to target in order to achieve efficient depolymerization. In this section the chemical properties of this type of linkage are discussed and an overview of different methodologies developed in order to cleave this bond is presented.

3.1.3.1 β -O-4 linkage

This linkage consists of an aryl-ether structure, which can be cleaved at the undesired C-C bond or the desired C-O bond position depending on the strategy applied. It is worth underlining that many studies were not made on real lignin, but on smaller molecules that mimic this substructure of the biopolymer.¹¹ These molecules are used in order to understand the chemical properties, reaction mechanism and conditions that can be further applied on native lignin. The simplest model compound commonly used for β -O-4 linkage is phenethyl phenyl ether (PPE) (**1**) (Figure 7).

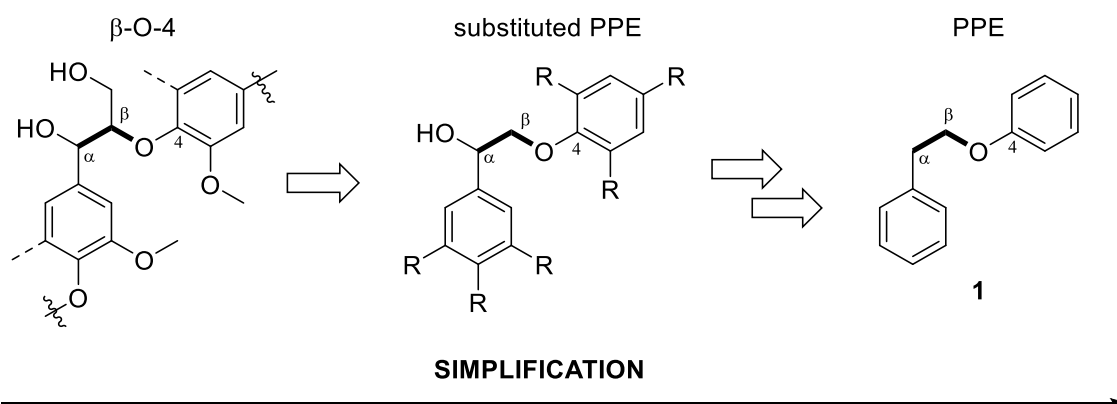


Figure 7. Simplification of the β -O-4 linkage in corresponding model compounds.

Beckham and co-workers reported the calculation of C-O bond dissociation enthalpies for β -O-4 lignin model compounds and other related oxo-substituted derivatives. Computational studies have shown that β -O-4 (70 Kcal mol⁻¹) and α -O-4 (55 kcal mol⁻¹) linkages are

the most accessible in terms of BDE with respect to the others types like biphenyl (115 kcal mol⁻¹) and β -5 (105 kcal mol⁻¹) (Figure 8).²⁵

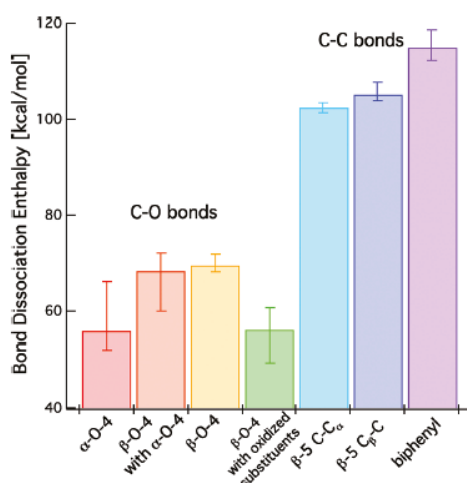


Figure 8. Bond Dissociation Enthalpies for different lignin linkages.²⁵

The authors also presented calculations for β -O-4 linkages with a ketone functionality in the α position since this type of intermediate has been reported in a number of different studies on the catalytic cleavage of β -O-4 model compounds.²⁶ By oxidizing the benzylic alcoholic groups of the molecule to carbonyl groups, the potential for hydrogen bonding is completely suppressed in lignin model compounds. Indeed, phenethyl phenyl ether model compounds which have methoxy substitution close to the β -O-4 linkage show higher cleavage rates of the ether bond.²⁵

3.1.3.2 Depolymerization approaches of ether-aryl linkages

Oxidative approaches

Oxidative depolymerization is a methodology inspired by the natural cleavage of C-C bonds and C-O bonds in lignin. The mechanism of degradation is not well understood but it has been reported to involve the formation of non-stable radicals, which disintegrate in the presence of oxygen.²⁷ A brief overview of this topic with selected examples of different methodologies is discussed below.

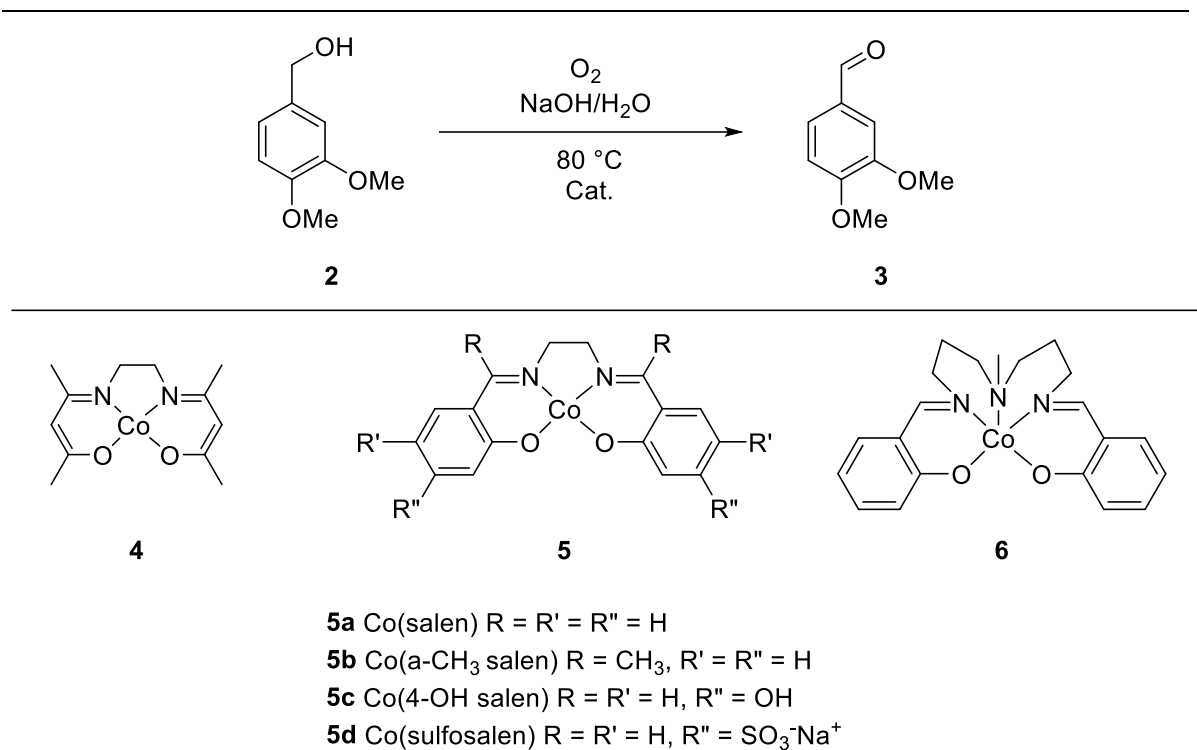
Enzymatic

Bacterial degradation of humic acids has shown that manganese oxides formed by microbial catalysis surround bacterial cells and can promote lysis of the complex humic structures to

yield low molecular weight organic substrates.²⁸ This is a good inspiration for lignin degradation research due to its related structure, in terms of aromatic monomers linked together, to humic matter. Manganese peroxidase is a lignin-modifying enzyme secreted by ligninolytic fungi. It oxidizes Mn^{II} to Mn^{III} which is very reactive and able to attack phenolic compounds present in lignin allowing the formation of free unstable radicals that finally decompose spontaneously under aerobic conditions.²⁹ Laccases have been identified as copper-containing extracellular oxidases that can perform lignin oxidation. These enzymes also oxidize Mn^{II} to Mn^{III} producing H_2O_2 that can be used by manganese peroxidases in cooperation towards an enzymatic pathway for lignin biodegradation.³⁰ The activity of these lignin-oxidizing enzymes is extremely specific, they use lignin as substrate and cellulose remains untouched.³¹ The challenge that this methodology faces is the space time yields for a very slow process. In addition to these enzymes, β -etherases hold encouraging prospects due to their high selectivity in the cleavage of C–O bonds.³² The oxidation of the C_α -hydroxyl groups of the β -O-4 aryl ether bonds in lignin is required first, as β -etherases require a carbonyl group adjacent to the aryl ether linkage.³³

Metal catalysts

Veratryl alcohol (**2**) has been studied as a model substrate for oxidative approaches to lignin depolymerization. It was chosen since it has been considered as a model compound for lignin reactivity studies in enzymatic systems. Co(salen) complexes have been studied and it was shown that unsubstituted salens were most efficient with the sulfonated structures (**5d**) as exception (Scheme 1).³⁴ Water-soluble salen metal complexes (**7**) bearing bulky substituents (Figure 9) yielded aldehydes from the benzylic alcohol substrates. Unfortunately, these catalysts showed low selectivity, forming mixtures of products from coniferyl alcohol substrates.³⁵



Scheme 1. Co(salen) type complexes for benzylic oxidation of the lignin model compound **2**.³⁰

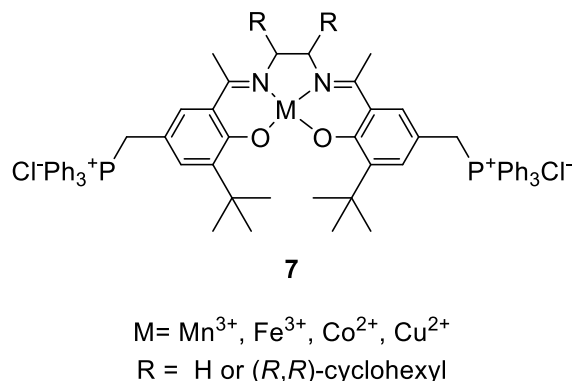
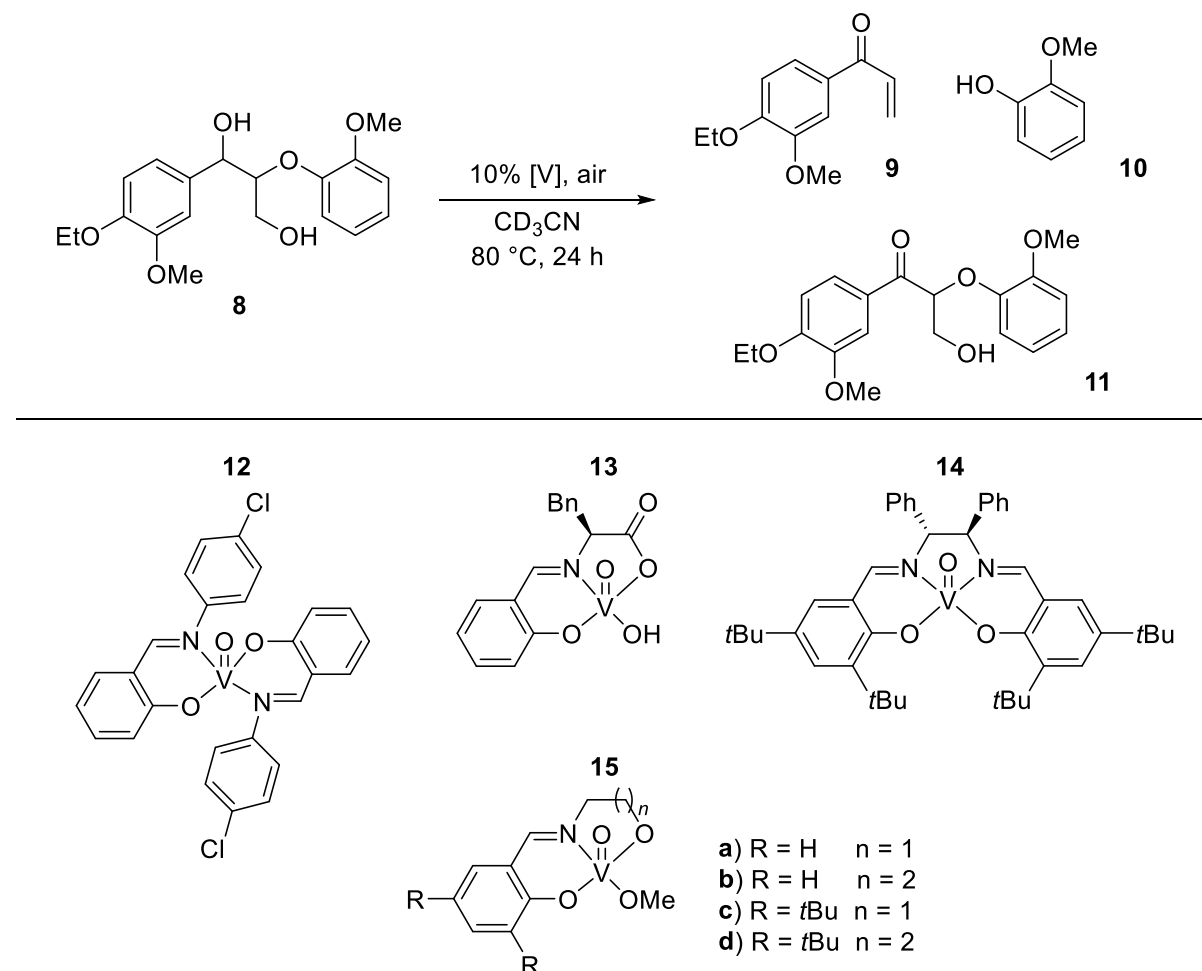


Figure 9. Bulky water soluble Co-salen catalysts.

In addition to salen complexes, other species were tested in oxidation of lignin model compounds. For example, vanadium catalysts using tridentate Schiff base ligands (**12–15**) are able to perform oxidation catalysis using dimeric lignin model compounds containing a β -O-4 linkage as substrate (e.g. **8**) (Scheme 2). Benzylic oxidation provides the major product (**11**) and only small amounts of C–O bond cleavage products from the redox neutral transformation (**9** and **10**) are obtained. Surprisingly, it was found that vanadium catalysts

using tridentate Schiff base ligands prefer C–O cleavage over the typical benzylic oxidation which is an unprecedented kind of reactivity.³⁶

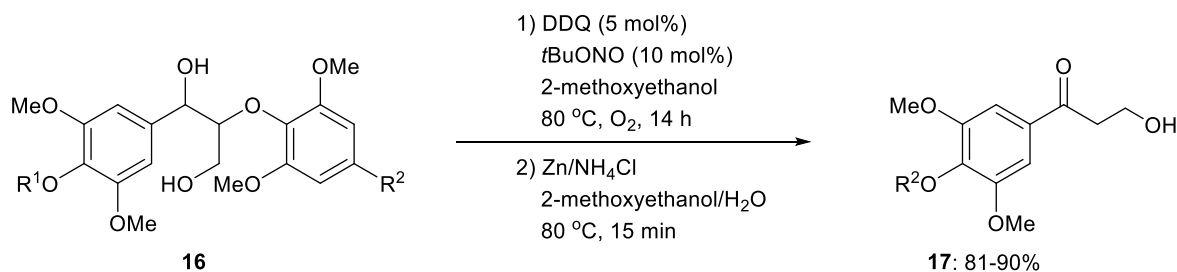


Scheme 2. Vanadium catalysts using tridentate Schiff base ligands for oxidation of β -O-4 model compounds.³⁶

Metal-free oxidation

More effective oxidative routes have been reported with more realistic model compounds. It has been shown that benzylic oxidation favors the β -O-4 cleavage not only in lignin model compounds but also in real lignin in the presence of molecular oxygen and catalytic amounts of 2,3-dichloro-5,6-dicyano-1,4-benzoquinone (DDQ) and *tert*-butyl nitrite at 80°C (Scheme 3). After finding a solvent system suitable for dissolving lignin, the catalytic depolymerization was achieved with an excess of zinc as reductant giving the respective

phenolic products. Around 5% of β -Hydroxypropiosyringone was obtained when this methodology was applied to real lignin.³⁷

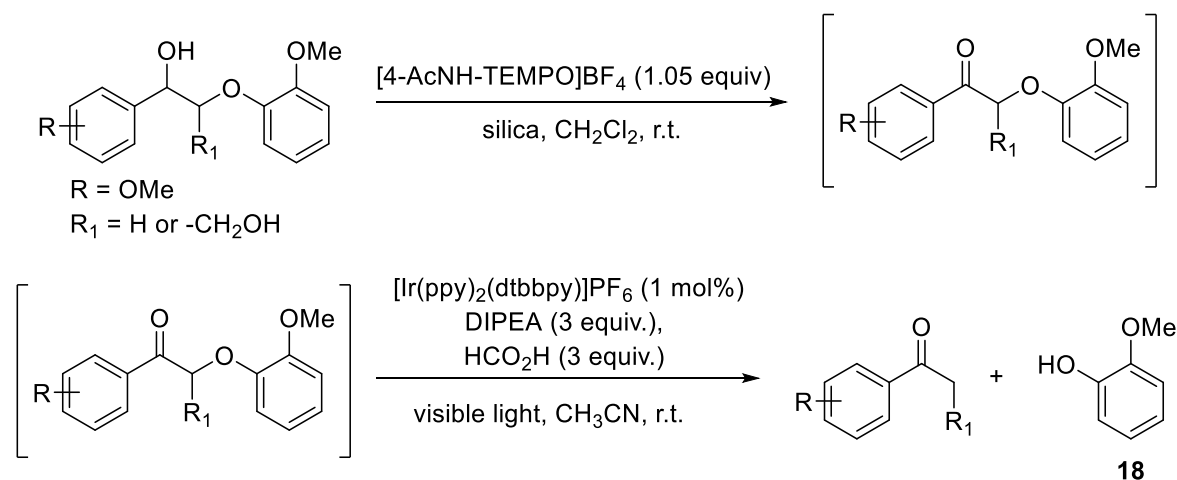


Scheme 3. Oxidation of β -O-4 model compound using DDQ.

A common drawback of the oxidative approaches discussed above is the increased oxygen content of the products, making this methodology less attractive. To overcome this problem, catalytic hydrogenolysis (i.e. reductive cleavage) of β -O-4 model compounds has been postulated as a suitable methodology for lignin conversion³⁸ and this strategy is discussed in the next section.

Photocatalytic lignin degradation

Photocatalytic approaches have been studied in order to reduce the temperature needed for the degradation of lignin and lignin model compounds (usually > 80 °C), thus augmenting the selectivity of the process. It requires previous oxidation step of the model compound which decreases the bond dissociation enthalpy (BDE) of the ether linkage. The first example was developed by Stephenson and coworkers utilizing lignin model compounds (Scheme 4).³⁹ This is a two-step protocol involving first an oxidation of the starting material using [4-AcNH-TEMPO]BF₄ and silica in CH₂Cl₂. Subsequently, DIPEA, formic acid, [Ir(ppy)₂(dtbbpy)]PF₆ (1 mol%) (where ppy= 2-phenylpyridine and dtbbpy = 4,4'-di-tertbutyl-2,2'-bipyridyl), and CH₃CN were added and the reaction mixture was irradiated with blue LEDs to produce the fragmentation products in high yields. Moreover, a batch-to-flow setup was developed where the oxidation was performed in batch and the reductive cleavage in flow, increasing the substrate consumption (1.8 mmol/h in flow from 0.050 mmol/h in batch) and lowering the catalyst loading (1.0 mol% batch to 0.030 mol% in flow).

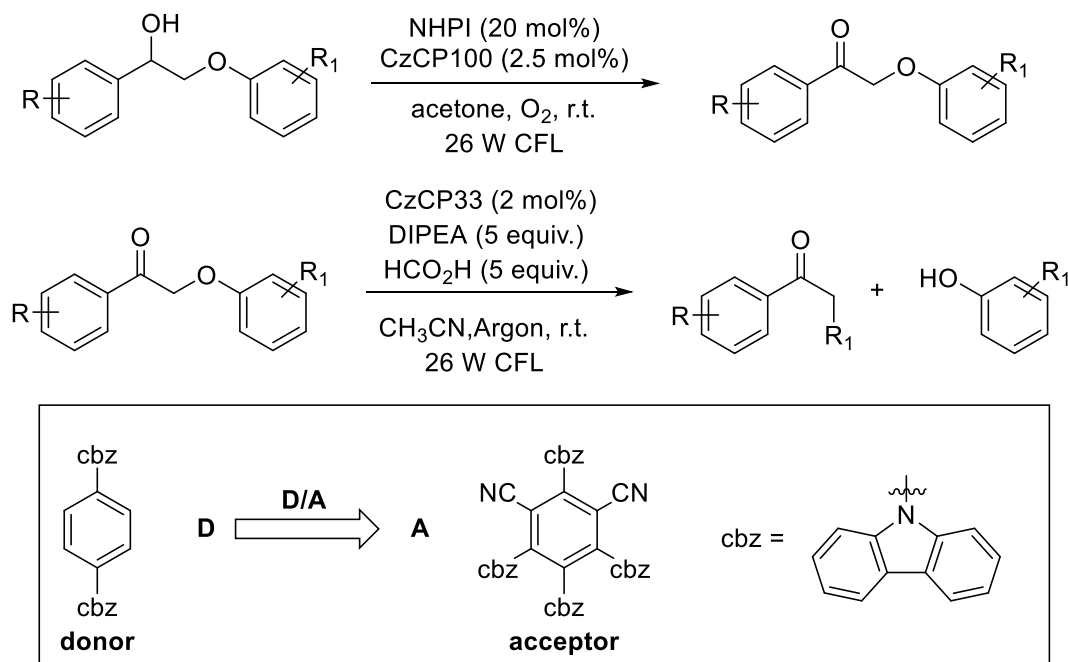


Scheme 4. Two-steps protocol for the cleavage of lignin model compounds involving photocatalysis.

The stoichiometric amount of [4-AcNH-TEMPO]BF₄ in the oxidation step can be replaced by a dual catalysis approach involving palladium acetate (10 mol%) in the presence of sodium persulfate (2 equiv.) combined with 1 mol % [Ir(dF(CF₃)ppy)₂(dtbbpy)]PF₆ (where (dF(CF₃)ppy) = 2-(2,4-difluorophenyl)-5-trifluoro-methylpyridine) as photocatalyst, which was irradiated using blue LEDs, affording the desired β-O-4 cleavage.⁴⁰ Finally, these chemical oxidation steps can also be replaced using electrocatalysis with N-hydroxyphthalimide (10 mol %), and 2,6-lutidine (10 mol %) in oxygen-saturated acetonitrile at 0.64 V (vs Fc⁺/Fc).⁴¹ After irradiation it yielded the products. Interestingly, this last methodology was successfully applied to native lignin isolated from pine giving monomeric and oligomeric units.

Another interesting example was reported by Zhang and co-workers utilizing the possibility to tune the redox potential of Carbazolic Porous Organic Frameworks (CzCPs) by changing their donor:acceptor ratio (D:A) (Scheme 5). This enabled performing both oxidation of the starting materials and reductive cleavage of the resulting ketones in two separated steps.⁵² The former step is accomplished using 2.5 mol% of CzCP100 in conjunction with N-hydroxyphthalimide (NHPI) and molecular oxygen, which possess the strongest oxidative capability (D:A = 0:100), whereas the latter step is catalyzed by 2 mol % of CzCP33 (D:A = 66:33) and uses a combination of DIPEA and formic acid as reductant. Despite the fact that

both reactions can be performed at room temperature under irradiation with a 26 W white compact fluorescent lamp, the major drawback of this method is the need for isolation of the oxidized starting material in order to be able to perform the reductive cleavage step.



Scheme 5. Cleavage of lignin model compounds using Carbazolic Porous Organic Frameworks (CzCPs).

Reductive approaches

Acid promoted cleavage

Acid catalyzed ether bond cleavage is the classic method used for lignin depolymerization. It became an attractive strategy and lignin isolation processes are commonly based on using strong acids. This methodology has been important for the characterization of the biopolymer, as it allowed the identification of various monomers in the lignin structure.⁴² Regarding the β -O-4 cleavage of model compounds, this approach leads to aromatic aldehydes, ketones, phenols, and dehydrated intermediates leading to olefinic products.⁴³ However, under acidic conditions, the carbonyl products also repolymerize to yield complex mixtures.

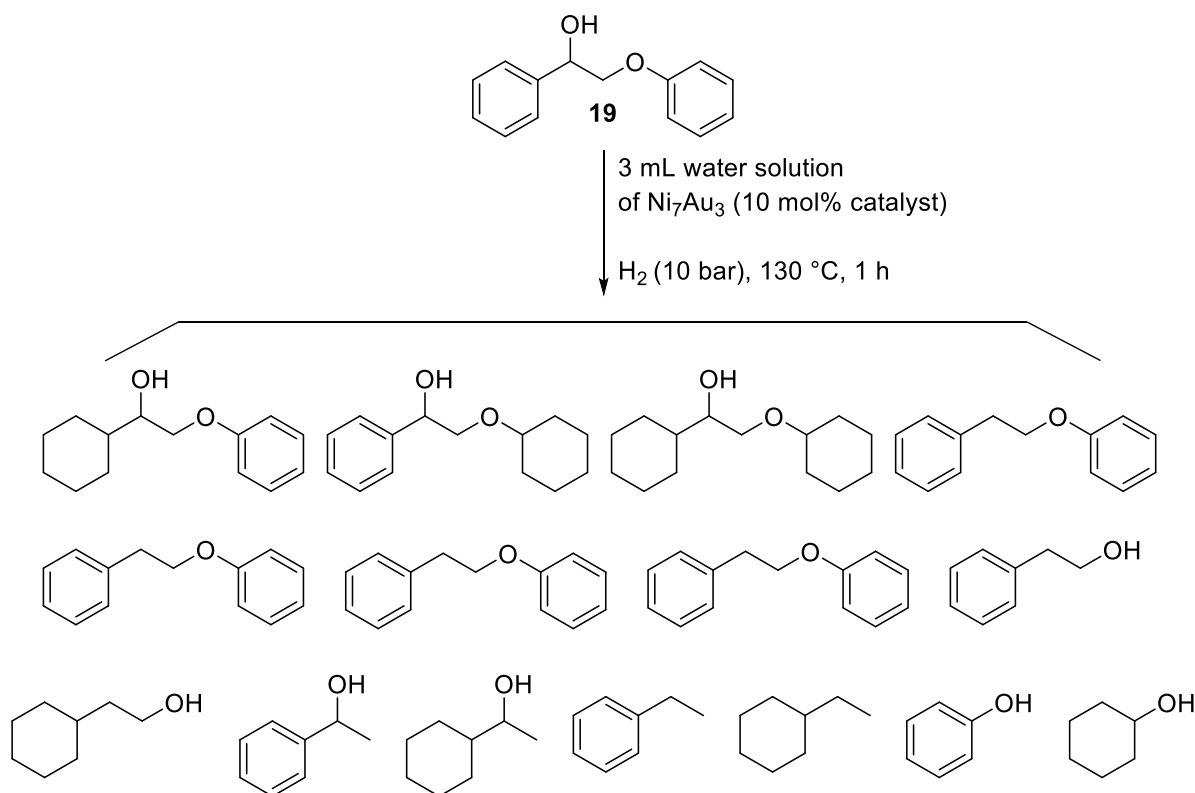
Base promoted cleavage

Cleavage of lignin and lignin model compounds in presence of base has been studied as such but also in presence of transition metals and using supercritical fluids providing aromatic products including ketones, aldehydes and alcohols. It has been found that the presence of base without any other additives leads to condensation and polymerization processes of the products rendering the isolation of the monomeric units challenging.⁴⁴ Miller reported the depolymerization of lignin in supercritical methanol and ethanol using KOH at 290 °C for ten to fifteen minutes. Alkylated aromatic ethers and phenols as monomeric products were obtained using excess of base, but product decomposition became a problem when using high temperatures. Side reactions cannot be controlled and new C–C bond formation is favored together with coke and tar formation, which is impractical for commercial applications of lignin valorization.⁴⁵

Heterogeneous approaches

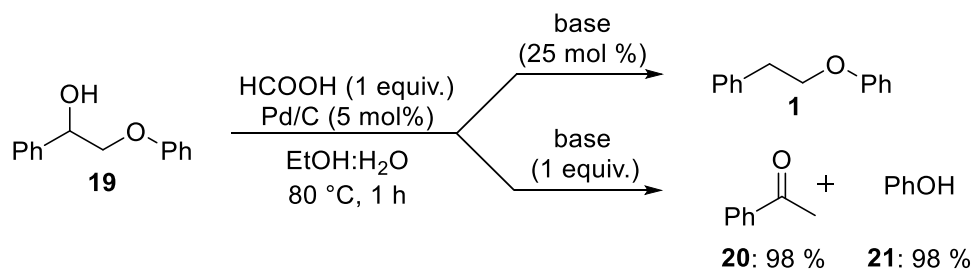
In general, acid and base based methodologies require harsh conditions and have the common drawback of the recondensation of the monomers leading to complex polymers, sometimes with higher molecular weight than the lignin starting material. For that reason, more selective and milder approaches have been studied in order to achieve a satisfactory depolymerization system. One of these strategies is heterogeneous catalysis. Among all the possible metals, nickel is gaining increasing attention due to its good performance in the C–O bond cleavage of lignin model compounds and real lignin. As a selected example, Xu and co-workers showed that Ni/C catalysts achieved up to 80% selectivity in C–O bond cleavage.⁴⁶ Later, Yan and co-workers tested bimetallic NiM catalysts (M= Ru, Rh, Pd, Pt or Au) using 2-phenoxy-1-phenylethanol (**19**) as a model compound. Among these catalysts, Ni₇Au₃ showed the best performance converting 87% of the model compound in just one hour; unfortunately, the selectivity is low, leading to a mixture of dimeric and monomeric products (Scheme 6).⁴⁷⁻

48



Scheme 6. Dimers and monomers formed using Ni₇Au₃ catalyst.⁴⁸

In addition to nickel methodologies other metal catalysts such as palladium have been tested. Samec and co-workers described an effective system for cleavage of **19** using a heterogeneous palladium catalyst and formic acid as a reducing agent in air affording high yields via β -O-4 linkage cleavage (Scheme 7). Interestingly, when applying this system in native lignin, lower molecular weight species were obtained making this methodology attractive for further developments.⁴⁹



Scheme 7. Heterogeneous palladium catalyzed cleavage of β -O-4 model compound using formic acid.⁴⁹

The main drawback of the hydrogenolysis of aromatic C–O bonds performed by heterogeneous catalysts is that it usually requires harsh conditions leading to a mixture of products because of the competition with the hydrogenation of the aromatic ring.⁵⁰

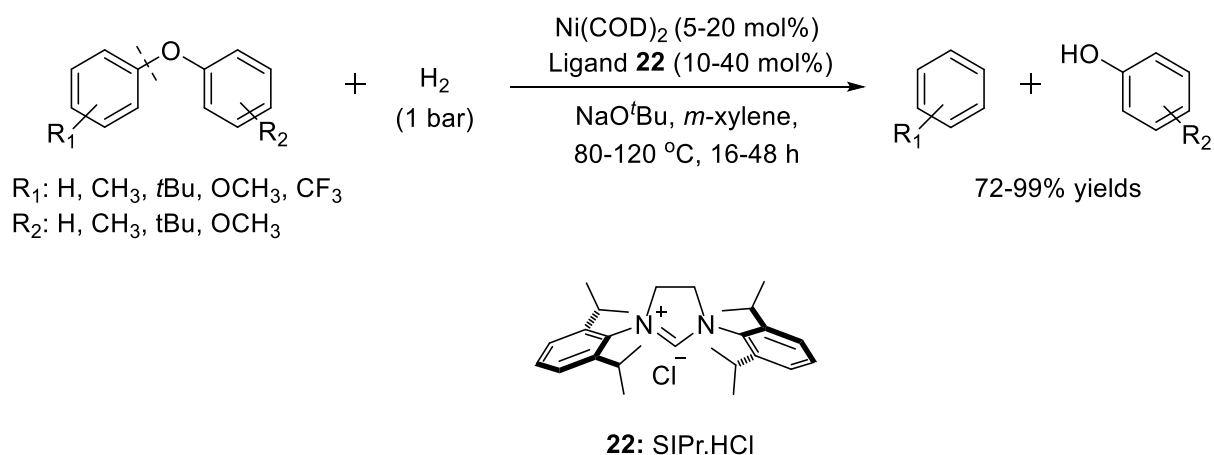
The same catalyst, Pd/C (5 mol%), was used by Hartwig and co-workers for the fragmentation of more complex β -O-4 model compounds. In this case, a temperature as high as 200 °C is needed for the reaction to occur.⁵¹ Interestingly, no external H₂ is needed because the hydrogen for the reduction of the C–O bond is provided by the benzylic alcohol of the starting materials.

Homogeneous Catalysis

Nickel and iridium catalysts

Homogeneous catalysis has some advantages over heterogeneous systems in the form of very good activity and selectivity. When the catalyst is soluble, important spectroscopic and kinetic data can be easily obtained, therefore providing a good understanding of the reactions mechanisms. This information is vital for catalyst design, enabling tuning of activity and selectivity of the catalytic system. A particularly important feature of homogeneous catalysts in the context of using lignin as a substrate is their ability to penetrate the complex 3D structure of the biopolymer reaching the targeted linkages, which make them very attractive for depolymerization catalysis.¹¹

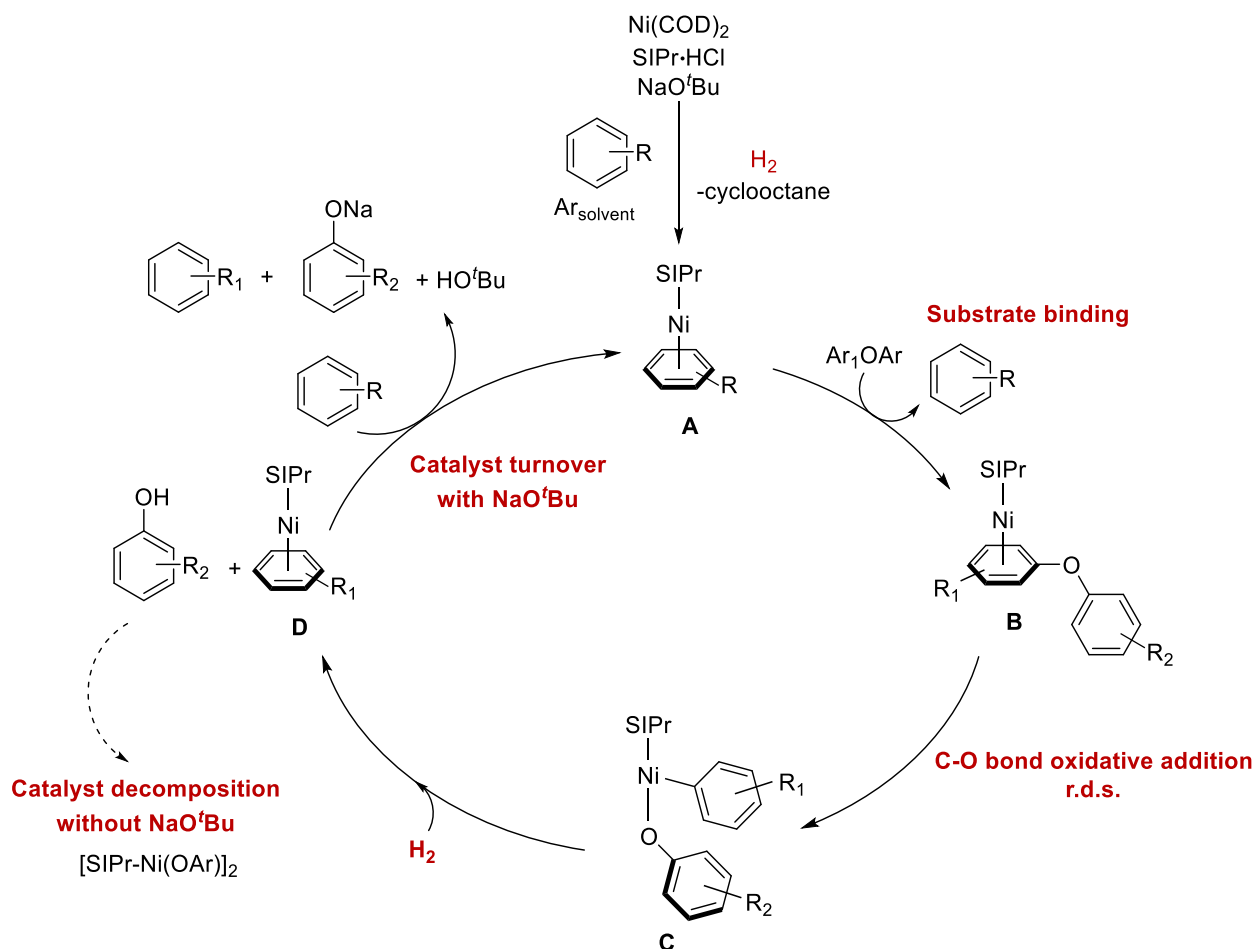
Hartwig reported that diaryl ethers were selectively cleaved by hydrogenolysis using nickel complexes of NHC ligands (**22**) under mild conditions (Scheme 8). Despite the strength and stability of the C–O bond, arenes and phenols were obtained in good to excellent yields.⁵³



Scheme 8. Ni(NHC) system for the cleavage of aryl–ether bond.⁵³

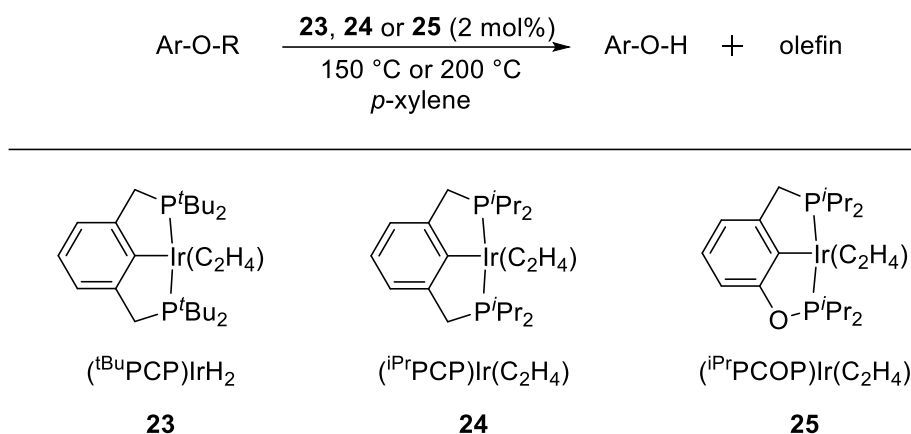
In a later study, the same authors found that a ligand-free system was more active than the SIPr–Ni catalyst. To generate a suitable system for the hydrogenolysis of lignin the authors developed a heterogeneous system with nickel as a metal without the use of any additional ligands, noticing that the nickel acts not as a homogeneous catalyst anymore but as a heterogeneous one.⁵⁴

The mechanism of the homogeneous Nickel-catalyzed reaction has been investigated using DFT calculations⁵⁵⁻⁵⁶ and was later unraveled experimentally (Scheme 9).⁵⁷ First, SIPr–Ni(η^6 –Ar_{solvent}) (**A**) is formed by sequential deprotonation of SIPr·HCl by NaO^tBu, coordination of free SIPr to the Ni⁰, hydrogenation of COD and association of the aromatic solvent (Ar_{solvent}) used in the reaction. **A** is the resting state of the catalyst and reacts with the diaryl ether starting material (Ar₁OAr) forming the η^6 –diaryl ether complex SIPr–Ni(η^6 –Ar₁OAr) (**B**), which undergoes C–O bond cleavage affording the tri-coordinated SIPr–Ni(Ar₁) (OAr) (**C**). This was found to be the rate-determining step of the catalytic reaction. Successively, **C** reacts with H₂ forming ArOH and SiPr–Ni(η^6 –Ar₁) (**D**) which replace the bound Ar₁ with Ar_{solvent} regenerating the resting state **A**. NaO^tBu is also required to deprotonate the released ArOH, avoiding decomposition of the catalyst by reaction of phenol with SIPr–Ni(η^6 –Ar₁) giving the dimeric [SIPr–Ni(μ –OAr)]₂.



Scheme 9. Proposed Mechanism for the Ni-Catalyzed C–O bond cleavage with NHC as ligand.⁵⁷

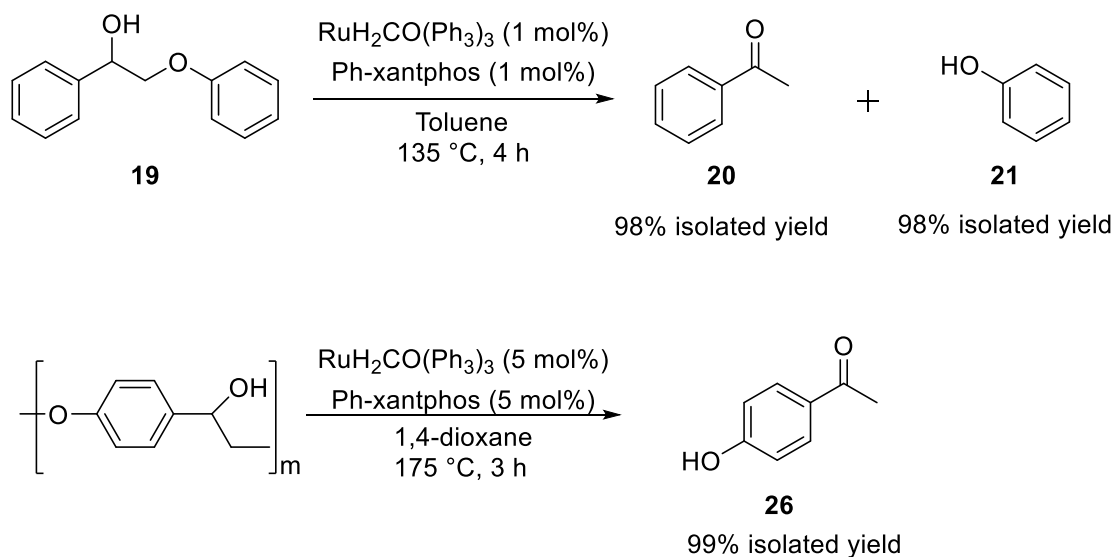
Goldman and co-workers performed stoichiometric studies on iridium pincer complexes showing that the C–O bond cleavage in simple methyl aryl ether molecules could be achieved.⁵⁸ Later, the same author reported the first example of an atom-economical catalytic cleavage of the C–O bond of an alkyl aryl ether by (PCP)Ir-type catalysts (**23-25**) (Scheme 10).⁵⁹



Scheme 10. (PCP)Ir-type catalysts for the cleavage of C–O bond in alkyl-aryl ethers.⁵⁹

Redox neutral ruthenium-catalyzed C–O bond cleavage

Bergman reported the redox neutral ruthenium catalyzed cleavage of alkyl aryl ethers, assisted by an alcohol group as internal H₂ donor.²⁶ It is a very attractive fully atom-economical approach (Scheme 11). Using a Ru/xantphos system, simple and polymeric model compounds based on 2-aryloxy-1-arylethanols structures were successfully converted to the ketones and alcohols, giving 98% and 99% yields, respectively.



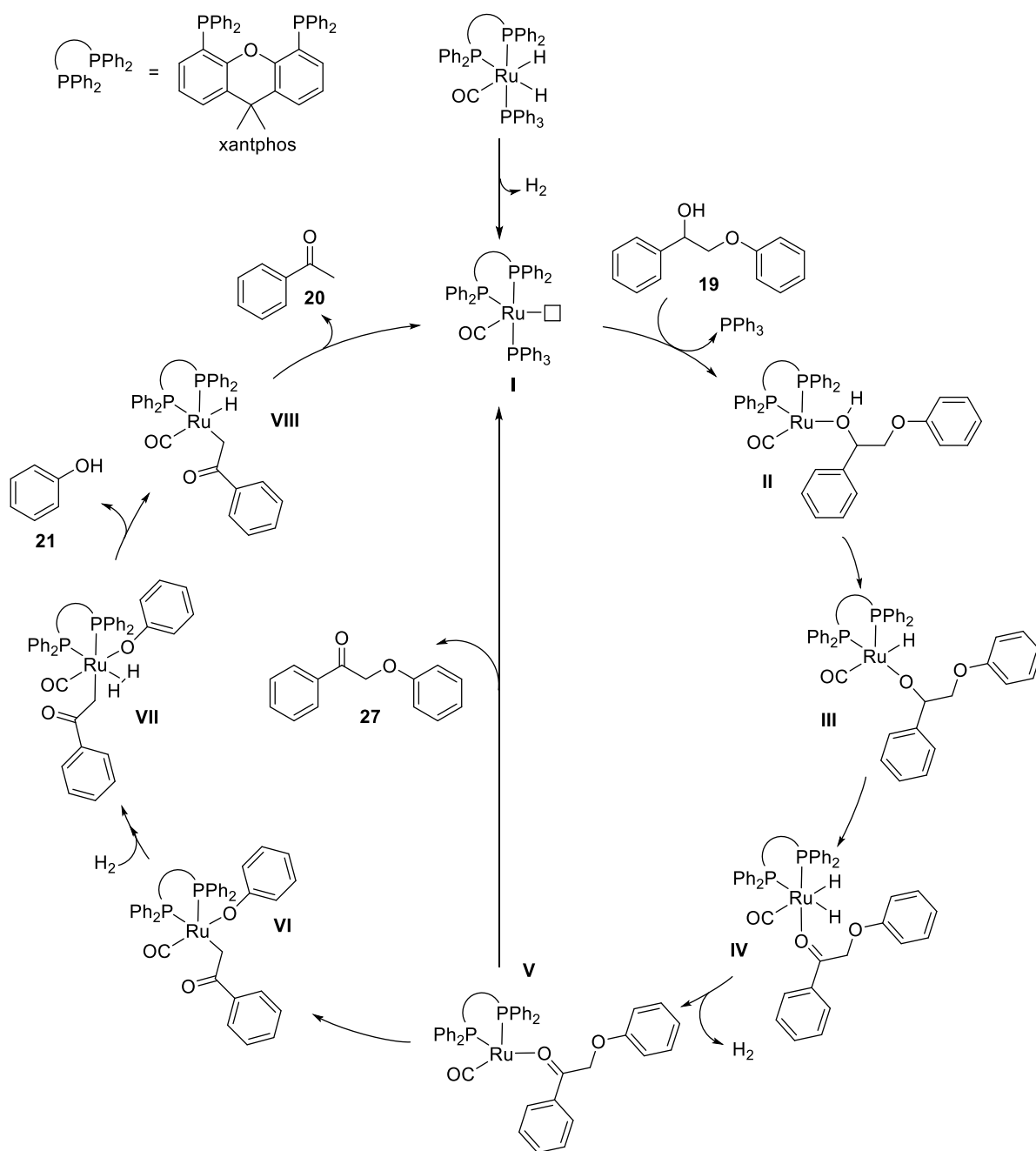
Scheme 11. Ru/xantphos catalyzed cleavage of β–O–4 model compounds.²⁶

The reported methodology requires a catalytic system, which is able to perform the needed hydrogen shuttling and subsequent bond cleavage processes in tandem to be successful and

the ruthenium complex $\text{RuH}_2(\text{CO})(\text{PPh}_3)_3$ is known for performing both reactions efficiently. Further reaction optimization and mechanistic insights were reported by Kamer and co-workers (Section 1.6, Chapter I).

Mechanism of the Ru/xantphos-catalyzed cleavage of aryl ether linkages

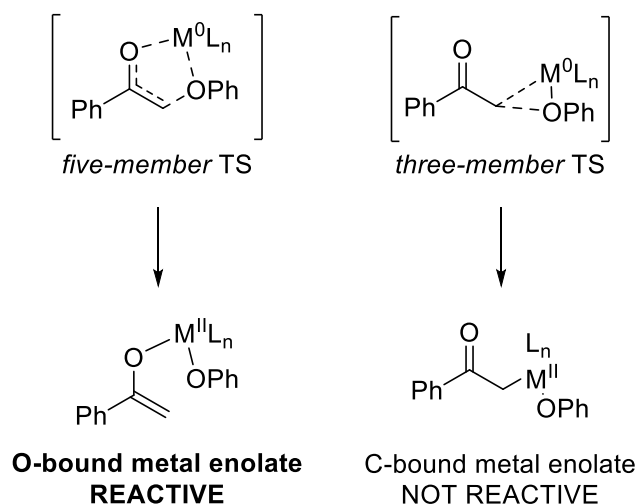
A first proposed mechanism for Ru/xantphos catalyzed cleavage of aryl ether bond was reported by Bergman and co-workers, postulating a benzylic ketone as intermediate. The final reductive elimination step involves first the elimination of acetophenone (**20**) followed by phenol (**21**).²⁶ Later, Beckham and co-workers studied this mechanism further (Scheme 12), using computational DFT calculations. They reached the same conclusions as Bergman about the elementary steps and the ketone as intermediate, but proposed the reverse order of releasing of the products.⁶⁰



Scheme 12. Detailed mechanism for Ru/xantphos aryl-ether cleavage.⁶⁰

The mechanism proposed by Beckham starts with the loss of H₂ to form [Ru(xantphos)(CO)(PPh₃)] after losing PPh₃ and coordinating 2-phenoxy-1-phenylethan-1-ol (**19**) forming **II**. In this intermediate, the Ru center is in close proximity to both the protic hydrogen attached to the O-atom for oxidative addition to form **III** as well as the hydrogen attached to the α-C-atom for subsequent β-hydride elimination to form **IV**. The consequent

reductive elimination of H_2 leads to **V** which contains the intermediate ketone (**27**) that can either be released and re-enter the catalytic cycle, or undergo the desired C–O bond cleavage. This cleavage is proposed to pass through a concerted oxidative addition with a 5-membered transition state (Scheme 13), leading to **VI** which is an O-bound enolate that is less stable than the corresponding C-bound analogue derived from the classically accepted 3-membered transition state. The authors proposed that it is this O-bound enolate that can further react with H_2 giving the dissociation of the desired products; the more stable C-bound enolate is inactive to further transformations.⁶⁰



Scheme 13. Concerted oxidative addition of C–O bond giving **VI**.⁶⁰

After coordination of H_2 by complex **VI**, the desired products phenol and acetophenone are released by reductive elimination. While the order of product release was originally proposed to occur via the successive reductive eliminations of acetophenone (**20**) followed by phenol (**21**), Beckham considered the feasibility of both sequences of product release, concluding it proceeds with initial phenol and subsequent acetophenone release. The first reductive step is similar in energy for both products, but the second reductive elimination step is much more facile for release of acetophenone with respect to the phenol leading to the first elimination of phenol (**21**) followed by acetophenone (**20**) and the regeneration of $[\text{Ru}]$ **I** to restart the catalytic cycle.⁶⁰

This elegant approach counts with a very important drawback, the Ru-xantphos catalyst did not perform when tested in more complex model compounds within the efforts to simulate the native lignin structure. The catalyst suffers partial deactivation to **28** by coordination of catechol type moieties (Figure 10).⁶¹

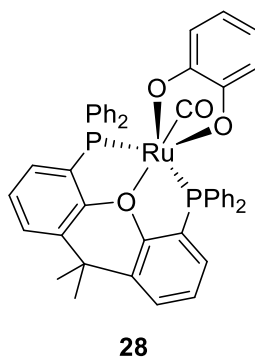


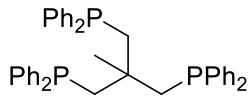
Figure 10. Structure of Ru(CO)(xantphos)(OC₆H₄O)(CO).

In order to overcome this limitation James and co-workers performed the reaction with γ -acetylated model compounds. As products from this process, unsaturated ketone dimers as well as the desired monomeric products were confirmed. Depolymerization products from kraft lignin as substrate were detected.⁶²

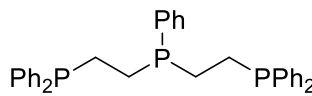
Ru(triphos) system

Triphos ligands have been also explored in the homogeneous catalytic cleavage of β -O-4 linkages using [Ru(COD)(methylallyl)₂] as metal precursor. Interestingly, with this system PPh₃, dppe and xantphos did not give significant amounts of phenyl-ether bond cleavage (Table 2, entries 1–3). On the other hand, using 1,1,1-tris(diphenylphosphinomethyl)ethane (triphos B) or bis(diphenylphosphinoethyl)phenylphosphine (triphos C) led to good yields of the desired products (Table 2, entry 4).⁶³

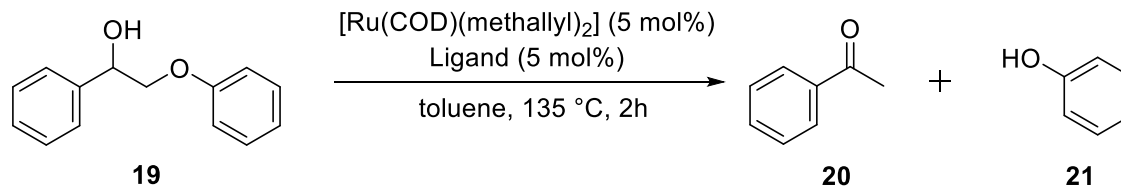
Table 2. Homogeneous catalytic cleavage of β -O-4 linkages using $[\text{Ru}(\text{COD})(\text{methallyl})_2]$ and phosphines.⁶³



triphos B



triphos C



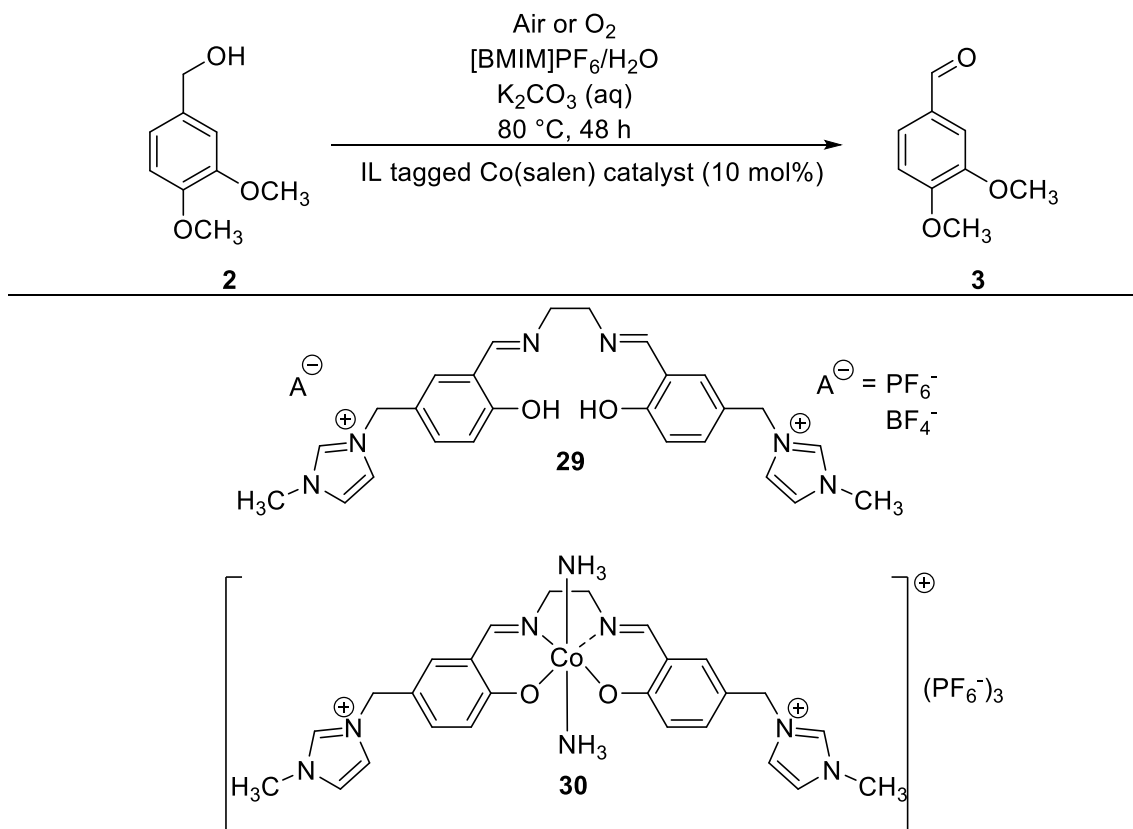
Reaction scheme showing the conversion of 19 to 20 and 21 using $[Ru(COD)(methallyl)_2]$ (5 mol%) and a Ligand (5 mol%) in toluene at 135 °C, 2h.

| Entry | Ligand | Yield of 20 (%) | Yield of 21 (%) |
|-------|------------------|-----------------|-----------------|
| 1 | PPh ₃ | 5 | 5 |
| 2 | dppe | 2 | 1 |
| 3 | xantphos | 11 | 12 |
| 4 | triphos B | 67 | 65 |
| 5 | triphos C | 93 | 84 |

3.1.4 Ionic liquids and biphasic catalysis

Ionic liquids have been extensively studied by cause of their properties as reaction media. From a more chemical point of view, they exhibit more properties and applicability in green methodologies and ligand design due to their tunable character. In particular, their coordinating abilities become a very attractive characteristic that can be modified with different variations of the cationic core, counter ion and substituents.⁶⁴ Disruption of the strong and diverse non-covalent interactions in the lignin structure can be performed by some ionic liquids leading to its dissolution as a result of hydrogen bonding disruption in the lignin network. Other parameters which play an important role, are interaction and solvation of the aromatic moieties of lignin by π - π and n - π interactions generally set by the cationic part of the ionic liquid.⁶⁵⁻⁶⁶

Ion-tagged ligands could offer better interaction of the final metal complex with an ionic liquid in which it is dissolved achieving not only good solubility and product separation processes but also offering the potential for catalyst recycling. As an important example, selective oxidation of veratryl alcohol (**2**) to veratraldehyde (**3**) under air was achieved by a cationic salen ligand (**29**). This transformation is a good example of potential applications of this type of cationic ligands (Scheme 14).⁶⁷



Scheme 14. Cationic Cobalt with ion-tagged salen ligand for the conversion of **2**.

The biphasic catalytic system reported contained the imidazolium ion tagged Co(salen) (**30**) as catalyst and 1-butyl-3-methylimidazolium hexafluorophosphate as ionic liquid using water as a co-solvent. It showed that the introduction of the imidazolium core to a ligand is a great way to improve the solubility of the complex in the ionic liquid. An IL/H₂O system allowed the authors to reach efficient product separation and catalyst recyclability.⁶⁸

Another example of a recyclable ligand is 2,7-bis(5-(3-methylimidazolium)pentyl)-9,9-dimethyl-4,5-bis(2,8-dimethyl-10-phenoxaphosphino)xanthene hexafluorophosphate (**31**)

(Figure 11) which has been reported by Kamer and co-workers as a suitable ligand for the Rhodium-catalyzed hydroformylation of 1-hexene and 1-octene performed in ionic liquids. The reaction proceeded with an excellent combination of regioselectivity, activity and recyclability of the catalyst.⁶⁹

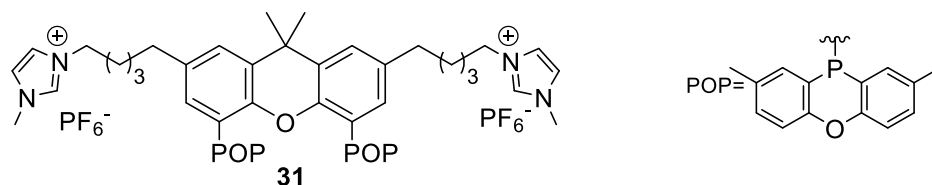


Figure 11. 2,7-bis(5-(3-methylimidazolium)pentyl)-9,9-dimethyl-4,5-bis(2,8-dimethyl-10-phenoxaphosphino)xanthene hexafluorophosphate ligand (**31**).⁶⁹

Another related structure was reported by Cole-Hamilton and co-workers, which was used in combination of ionic liquids as solvent and supercritical carbon dioxide (scCO₂) as transport vector for the substrates and products.⁷⁰ This system was very effective for the hydroformylation of long chain alkenes with rhodium and the imidazolium-tagged ligand nixantphos (**32**) (Figure 12) in [alkMIM][NTf₂] in a flow system and it was based on the insolubility of ionic liquids in scCO₂. In homogeneous catalysis, biphasic systems are a great alternative to isolate the products and recycle the catalyst.

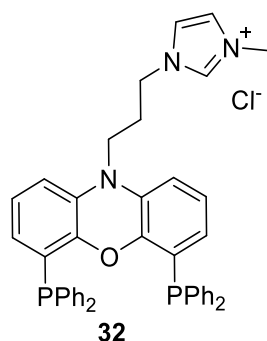


Figure 12. Imidazolium-tagged nixantphos ligand (**32**).⁷⁰

3.2 Justification and project aims

The wide bite angle diphosphine ligand xantphos has been reported by Bergman as a ligand that exhibits great activity in the ruthenium catalyzed cleavage of lignin β -O-4 linkages; these ligands perform well in the tandem Oppenauer oxidation and C-O aryl ether hydrogenolysis.²⁶ Ligand effects in the reactivity of the complexes can be expected as both the transfer hydrogenation and the C-O bond activation steps need to be optimized. The bite angle and electronic effects on the Ru/xantphos system-catalyzed ether bond cleavage of the model compound 2-phenoxy-1-phenylethanol for the β -O-4 linkage have been investigated in our group with a series of different xant-type ligands. It has been observed that substrate conversions can be enhanced when using ligands with increased σ -donor ability affording better conversion when compared to xantphos.⁷¹

The homogeneous catalytic depolymerization of lignin towards efficient valorization of lignocellulosic biomass faces an important bottleneck in the capability to dissolve lignin, which remains a challenge. Several solvents and extraction strategies have been recently explored to dissolve biomass and separate it into its components. Ionic liquids have recently become very popular solvents for the dissolution of biomass. Weckhuysen reported an interesting development in recent years studying the catalytic cleavage of lignin and model compounds in this kind of alternative solvents. They observed a reaction media effect on the catalytic activity caused by stabilization of reactive intermediates.^{11, 72} For the redox neutral cleavage method based on the Ru/xantphos system described before (Section 1.6, Chapter I), the substitution of volatile solvents for recyclable ones and the use of biomass as starting material for chemical conversions is an important approach for chemical sustainability.

The catalytic Ru/xantphos system has been based on hydrophobic ligands so far. To achieve effective catalyst separation and recyclability, xantphos ion-tagged phosphine ligands containing imidazolium cores derived from xantphos (Figure 13)⁶⁹ and nixantphos (Figure 14)⁷⁰ were part of the screening. Ion-tagged ligands were specifically used aiming at the implementation of the ruthenium-catalyzed C-O bond cleavage of lignin β -O-4 linkages in ionic liquids. This chapter focuses mainly on the synthesis of a previously reported modified xant-type ligand,⁶⁹ as well as new derivatives and preliminary results of their application in the catalytic aryl ether bond cleavage of a lignin model compound in ionic liquid media.

The aim of the present work is to optimize catalyst performance in the catalytic ether bond cleavage of lignin by both optimizing ligand structure and solubility in ionic liquids as ideal solvent for lignin dissolution.

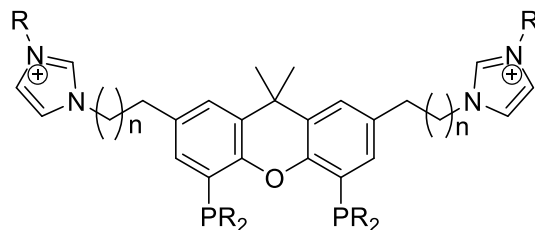


Figure 13. Imidazolium-tagged xantphos-type ligands.

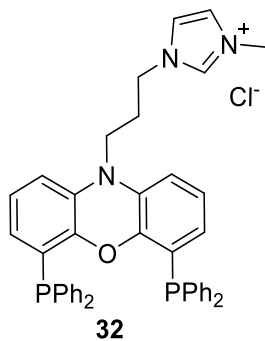
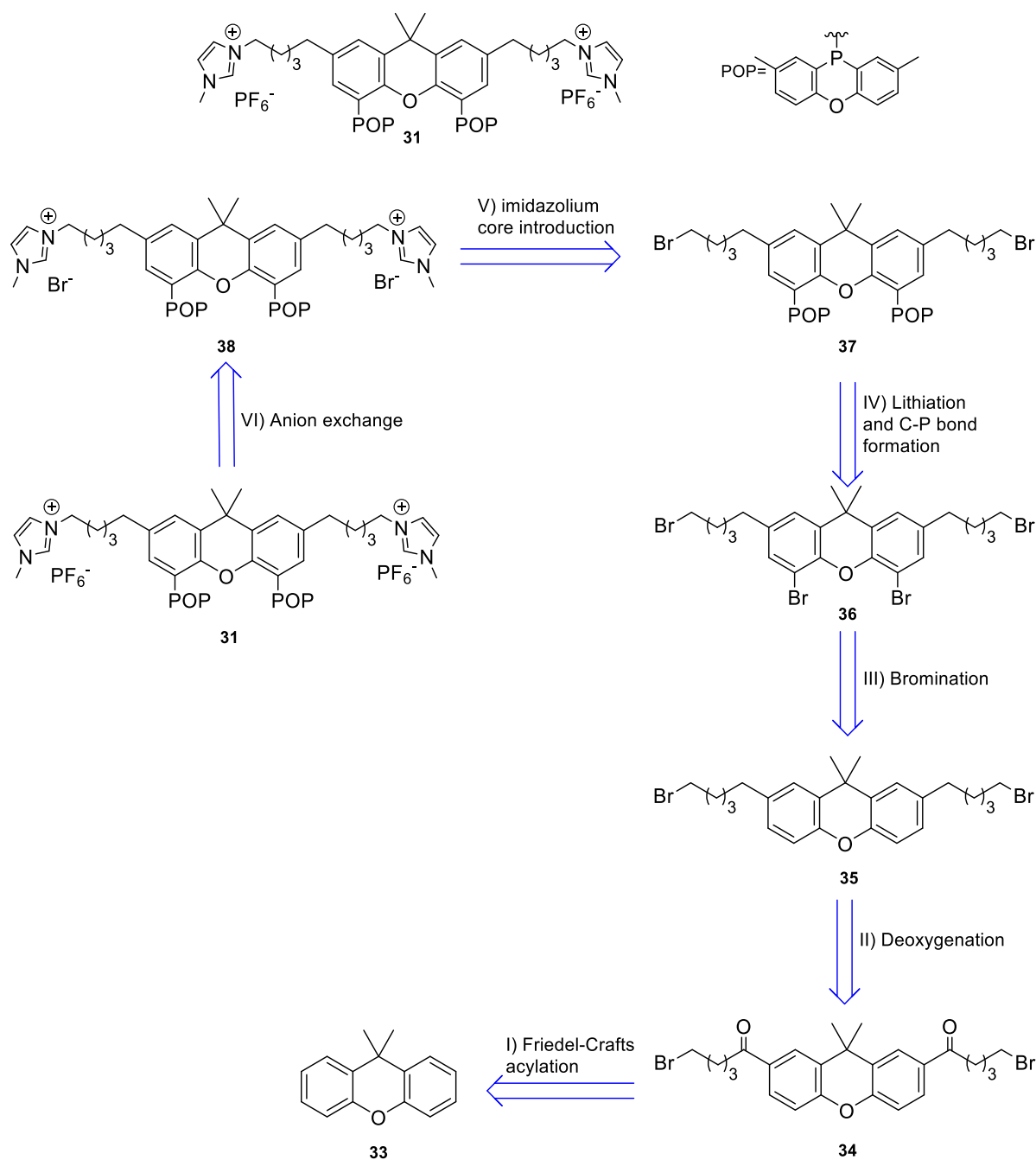


Figure 14. Imidazolium-tagged nixantphos ligand.

3.3 Results and discussion

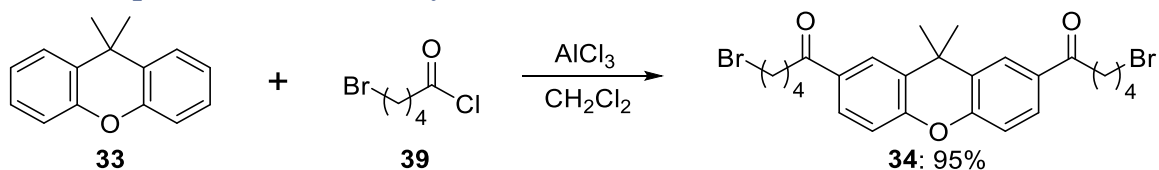
3.3.1 Synthesis of 2,7-bis(5-(3-methylimidazolium)pentyl)-9,9-dimethyl - 4,5-bis(2,8-dimethyl-10-phenoxaphosphino)xanthene hexafluoro phosphate (Imidazolium/Ion-Tagged Ligand)

Ionic liquids have been shown to be an alternative reaction media to classic solvents, such as DMSO⁷³ for lignin solubilization.⁶⁵ Our interest in cationic ligands is based on the possibility of improving the interaction of the catalyst with the substrate and the alternative reaction media, ionic liquids. In this respect, an ion-tagged ligand, containing imidazolium groups in its structure was published in 2004 by Bronger.⁶⁹ However, the published synthesis turned out not to be reproducible. In this thesis, we report a reproducible and robust synthesis for imidazolium tagged ligands. This kind of functionalization is very attractive for ligand design due to the possibility of changing substituents and different parameters in order to obtain a library of ligands to test in different reactions. The retrosynthetic route for this type of ligand is shown below (Scheme 15). The initial aim was to synthesize the known ligand to check the robustness of its chemistry under our reaction conditions.



Scheme 15. 2,7-bis(5-(3-methylimidazolium)pentyl)-9,9-dimethyl-4,5-bis(2,8-dimethyl-10-phenoxaphosphino)xanthene hexafluorophosphate ligand and its retrosynthetic strategy proposed by the authors.⁶⁹

3.3.1.1 Step I) Friedel-Crafts Acylation

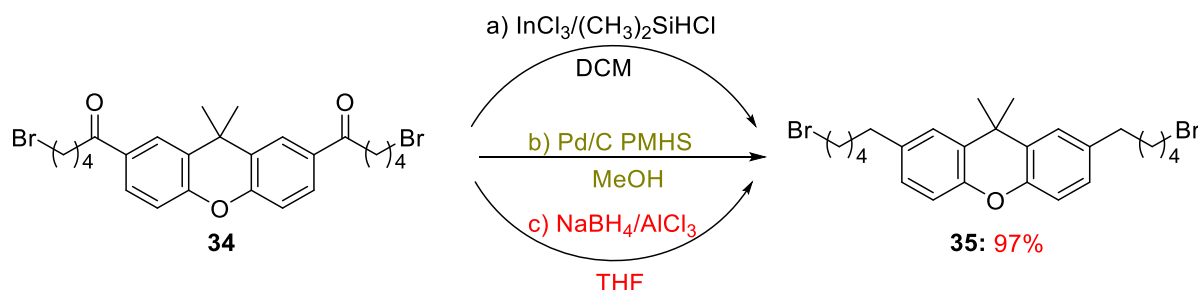


Scheme 16. Synthesis of the intermediate 2,7-di(5-bromopentanoyl)-9,9-dimethylxanthene (**34**).

The first step is a Friedel-Crafts acylation which gives the desired product with high selectivity according to the procedure reported by Bronger et al.⁶⁹ The regioselectivity of the acylation is determined by the presence of the oxygen on the xanthene ring (mesomeric activation towards the *para*-position). The product 2,7-bis(5-bromopentanoyl)-9,9-dimethylxanthene (**34**) was successfully obtained in 95% isolated yield (Scheme 16).

3.3.1.2 Step II) Deoxygenation

Acylated products can be converted to the corresponding alkanes via classical protocols such as Clemmensen or Wolff-Kishner reductions.⁷⁴ However, these procedures generally do not tolerate halogen groups well. The procedure reported in the initial synthesis of the ligand, uses InCl_3 and chlorodimethylsilane in a catalytic deoxygenation that is tolerant to the alkyl bromide substituents.⁶⁹ This procedure gives the desired product, but also various unidentified silicon containing impurities which are difficult to separate, making this methodology less attractive due to long and tedious chromatographic separation (Table 3, procedure A). In particular, two successive columns with a large amount of eluent are required due to the very similar retention factors of the different species, obtaining only 11% isolated yield of the pure deoxygenated product. Moreover, the procedure lacks reproducibility depending on the scale of the reaction, which is not convenient to achieve a general and scalable methodology. In order to achieve a straightforward optimal synthetic route, different strategies were tested (Table 3) and ^1H -NMR spectra of the crude mixtures are shown in order to compare the feasibility of the different approaches (Figure 15).

Table 3. Reaction conditions for the deoxygenation of 2,7-bis(5-bromopentanoyl)-9,9-dimethylxanthene (**34**).

| Procedure | Conditions | NMR Conversion (%) | Isolated yield (%) |
|-----------------|--|--|--------------------|
| A ⁶⁹ | InCl_3 (11 mol%), Chlorodimethylsilane (4.8 eq.), CH_2Cl_2 , r.t., rx followed by IR | >99 - By-products observed - Silicon-based impurities | 11 |
| B ⁷⁵ | Pd/C (5 mol%), PMHS (10 eq.), MeOH, 65 °C, 16 h. | No full conversion - By-products observed - Silicon-based impurities | - |
| C ⁷⁶ | NaBH_4 (9.71 eq.), AlCl_3 (5.44 eq.), THF, reflux, 5h | >99 - Only desired product | 97 |

The ^1H NMR spectrum of the hydrosilylation procedure using InCl_3 shows full conversion of the starting material, but with formation of different species (Figure 15, spectrum A). When Pd/C^{75} is used as catalysts (Table 3, procedure B), the ketone is not fully converted and also formation of by-products is observed similar to the previous discussed methodology (Figure 15, spectrum B). As aforementioned, the separation of these different species is difficult, mainly due to the large amount of silicon impurities present (red rectangle in Figure 15). Gratifyingly, using AlCl_3 in combination with NaBH_4^{76} (Table 3, procedure C) gave complete conversion towards the desired product (Figure 15, spectrum C). It is worth to underline that this straightforward methodology only requires a simple extraction in order to obtain the pure product in excellent isolated yields of 97%, in contrast with the other tested procedures.

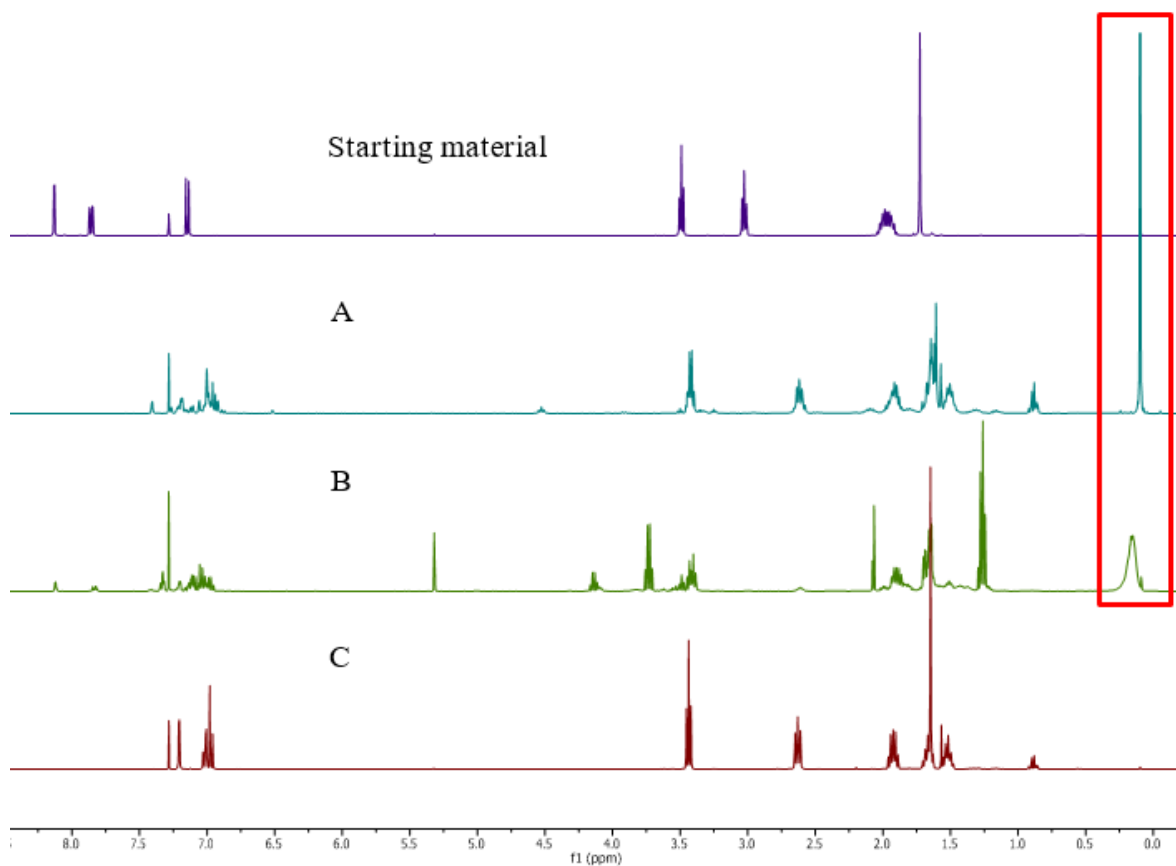


Figure 15. ^1H -NMR spectra (400 MHz, CDCl_3) of the crude mixtures of the different deoxygenation methodologies; from top to bottom: reference spectrum of the starting material, method A, method B, method C. In the red rectangle the silicon impurities are highlighted.

3.3.1.3 Step III) Bromination

Aryl halides are important intermediates in synthetic chemistry as they facilitate the regioselective functionalization of aromatic rings. In phosphorus chemistry in particular, they allow the formation of the new C–P bond required for phosphine synthesis.⁷⁷

Previous attempts in our group to obtain the pure dibrominated intermediate (**36**) were unsuccessful and a mixture of products was always observed. For this step, the authors reported a selective bromination by dropwise addition of bromine diluted in hexanes at 0 °C to the substrate dissolved in CH_2Cl_2 .⁶⁹ When trying to reproduce this method a complex mixture of products was obtained and the desired product was not clearly observed (Figure 16, spectrum A). A test adding bromine diluted in hexanes dropwise as reported, but in which

the reactants were diluted in double amount of solvent was carried out. Again, no traces of the desired product were observed (Figure 16, spectrum B).

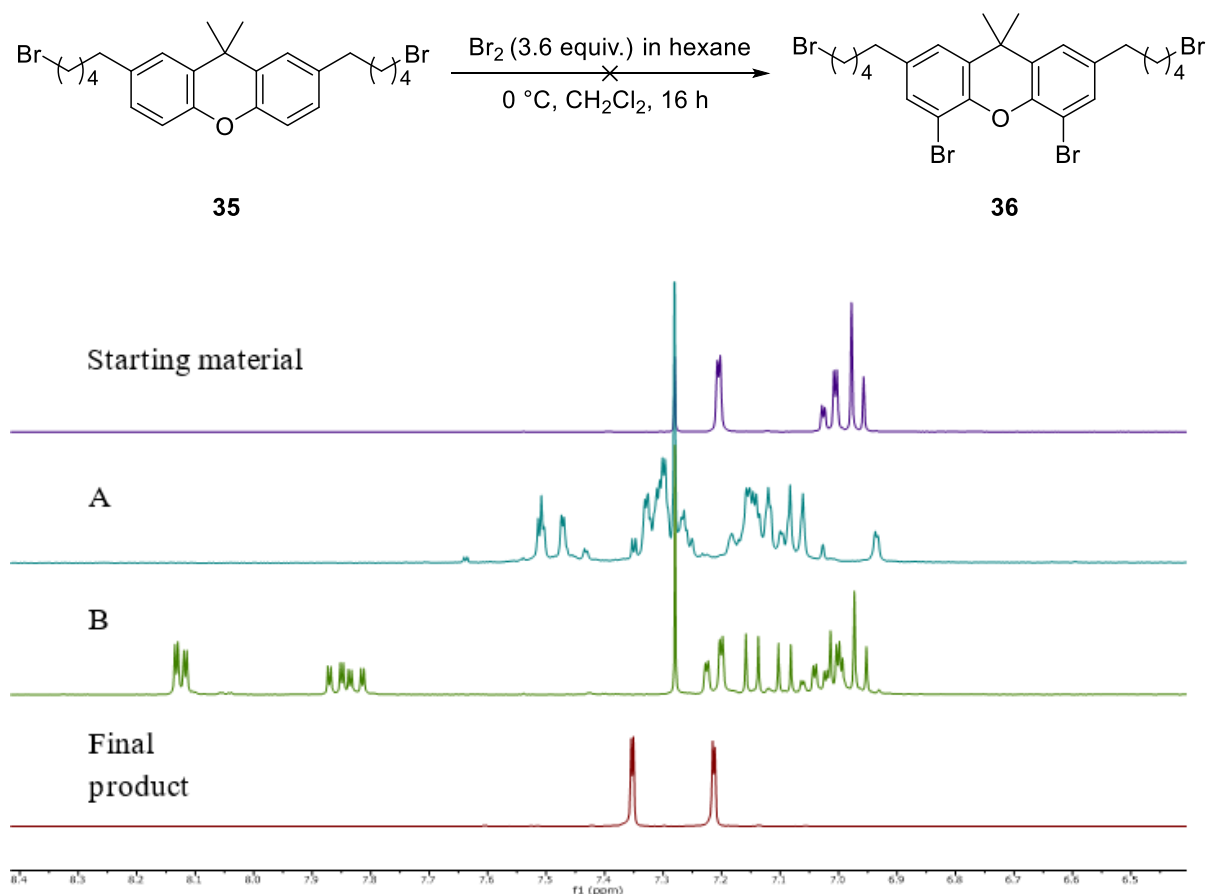


Figure 16. Aromatic region of ^1H -NMR spectra (400 MHz, CDCl_3) of the crude mixtures of the bromination step. From top to bottom: reference spectrum of the starting material, A) Reaction following the reported methodology,⁶⁹ B) Reaction in more diluted conditions, C) Reference spectrum of the product.

After these problems with the reported methodology were encountered, a different bromine source was tested using HBr in DMSO (Figure 17).⁷⁸ Unfortunately, no conversion towards the product was observed.

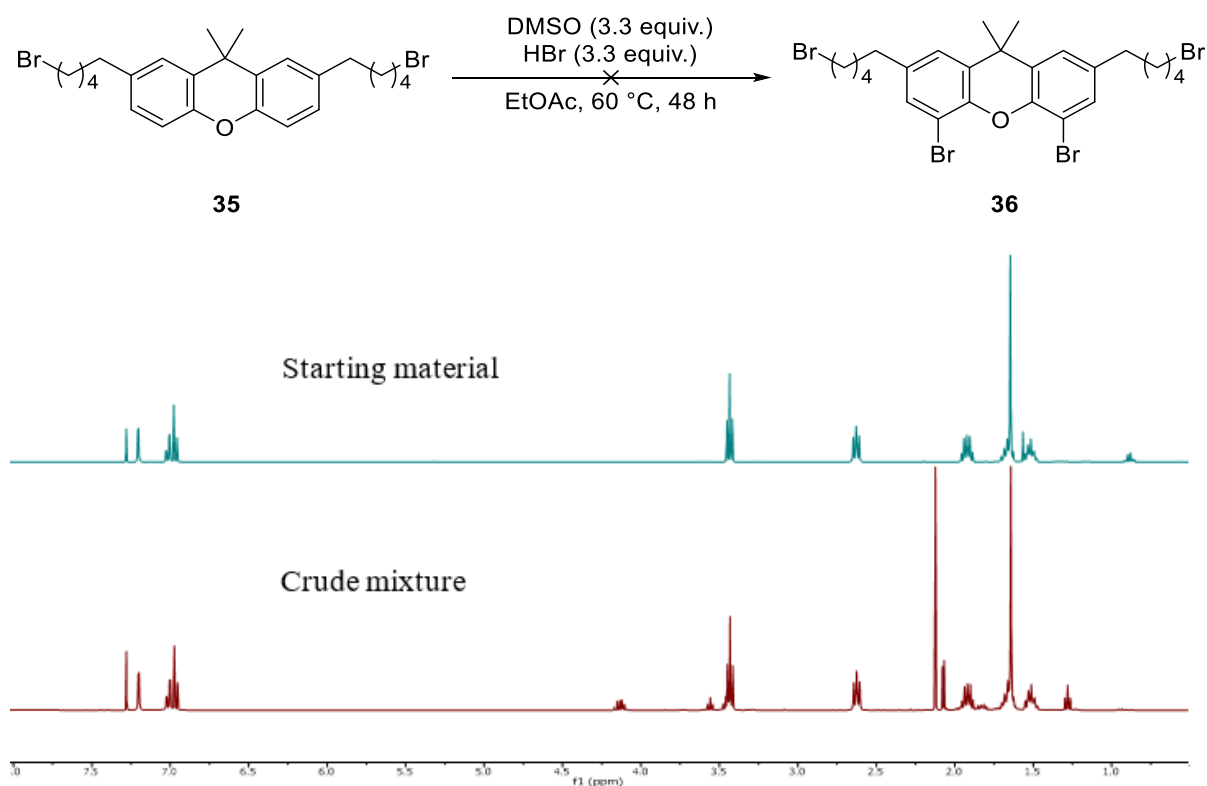


Figure 17. ^1H -NMR spectra (400 MHz, CDCl_3) of the crude mixtures of the reaction using HBr/DMSO.

Br_2 -based halogenation

Considering the inactivity of the previously tested brominating agent, non-diluted elemental bromine was used in order to achieve the desired reactivity. Unfortunately, when using this reagent the formation of undesirable by-products could not be prevented using the reported methodology.⁶⁹ With the need of obtaining a pure brominated product to perform the C–P bond formation, an optimization of the method using elemental bromine was performed and a selected set of experiments is shown below to discuss the main parameters involved in the selective bromination of 2,7-bis(5-bromopentyl)-9,9-dimethylxanthene and their corresponding ^1H -NMR spectra are reported.

Rebek and co-workers reported a procedure using iron powder to catalyze dibromination of 2,7 substituted xanthene structures.⁷⁹ Under these conditions, an important consideration is that the reaction should be followed by NMR spectroscopy to prevent the formation of undesired products.

First NMR tube reactions were performed using 5 mol% of iron powder in deuterated dichloromethane as solvent in order to follow product formation. The reaction gave the dibrominated product with good selectivity and the formation of by-products was hampered (Figure 18A). Unfortunately, when scaling it up to 100 mg, using the same reaction conditions, formation of impurities was observed (Figure 18B). The reported methodology is substrate dependent and each xanthene derivate requires an amount of bromine from 2.9 to 4 equiv. and iron catalyst loading from 5 to 10 mol%. In particular, the most similar xanthene structure with respect to our molecule requires 4 equiv. of bromine and 10 mol% of iron. Using these conditions, the amount of by-products remarkably increased (Figure 18C). It is important to mention that the yielded impurities are very difficult to remove from the desired product by column chromatography as retention factors are very similar for all the species formed. This fact strongly affects the isolated yields and the purity of the final compound.

FeCl_3 and FeBr_3 were tested resulting in lower selectivity. A blank test without catalyst was then performed (Figure 18D) using the same amount of bromine (4 equiv.), but impurities were also observed and it was the turning point to avoid the use of catalytic dibromination procedures. For expansion of the aromatic area Figure 19 is presented.

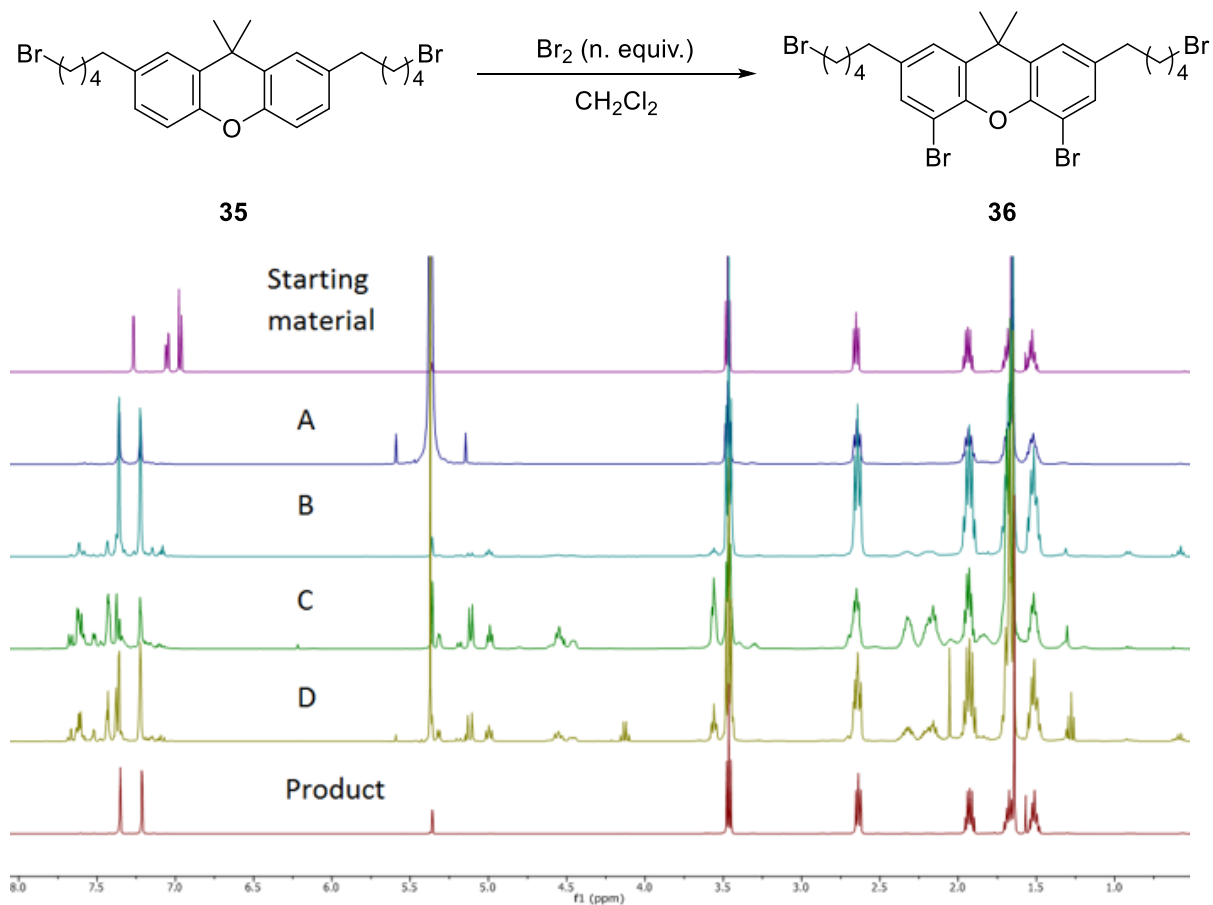


Figure 18. ^1H -NMR spectra (400 MHz, CD_2Cl_2) of the crude mixtures of the bromination step using variations of Rebek's methodology, expansion of the aromatic area; from top to bottom: reference spectrum of the starting material, A) NMR reaction using Fe (5 mol%) and Br_2 (2.9 equiv.), B) scaling up using Fe (5 mol%) and Br_2 (2.9 equiv.), C) Fe (10 mol%), Br_2 (4 equiv), D) Br_2 (4 equiv) without catalyst. All the reactions were performed at 0°C .

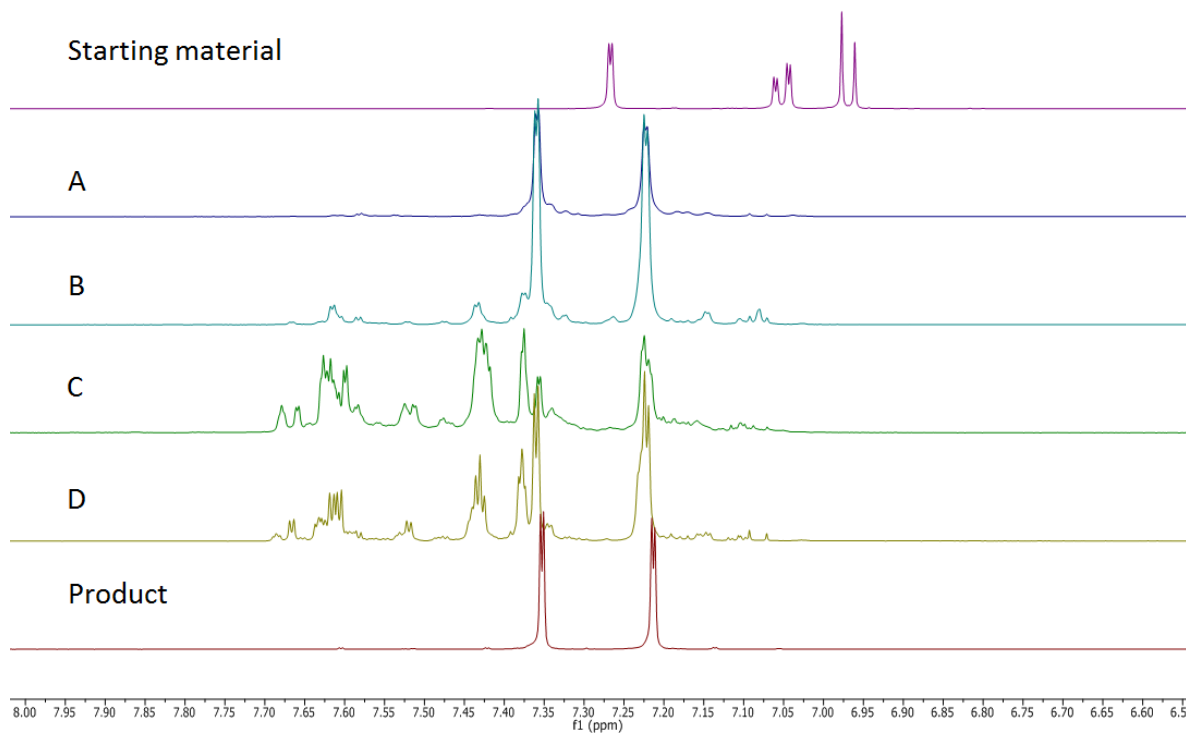


Figure 19. ^1H -NMR spectra (400 MHz, CD_2Cl_2) of crude mixtures for the bromination step using variations of Rebek's methodology, expansion of the aromatic area; from top to bottom: reference spectrum of the starting material, A) NMR reaction using Fe (5 mol%) and Br_2 (2.9 equiv.), B) scaling up using Fe (5 mol%) and Br_2 (2.9 equiv.), C) Fe (10 mol%), Br_2 (4 equiv), D) Br_2 (4 equiv) without catalyst. All reactions were performed at 0°C .

A literature report indicated that selectivity issues are common for the bromination of functionalized aromatic compounds of the xanthene family.⁸⁰ This patent describes an industrial protocol for the selective bromination of fluorescein (**40**) (Figure 20). The patent mentioned describes the perbromination and purification problems for the production of substantially pure dibromofluorescein. The authors stated that the synthesis of dibromofluorescein gave a reaction mixture composed of a variety of brominated products. In order to obtain selective bromination in positions 4 and 5, the pH of the medium has to be increased under refluxing conditions in the presence of elemental bromine. These conditions could not be applied to the target molecule due to chemical reactivity. In our case this protocol would potentially lead to side reactions in the side chains of the molecule.

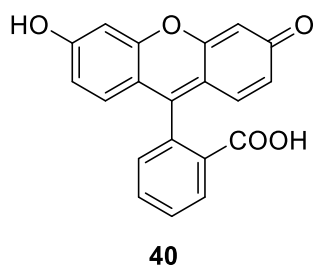


Figure 20. Structure of fluorescein (**40**).

Subsequently, a modification of the procedure reported by Bronger⁶⁹ was performed. Cooling down the reaction mixture to -20 °C instead of 0 °C and adding just three equivalents instead of 3.6 equiv. of bromine in hexanes afforded the product with fewer extra peaks in addition to the expected ones (Figure 21). It shows that temperature and the amount of bromine are crucial and that by optimizing these parameters the selectivity of the reaction could be improved.

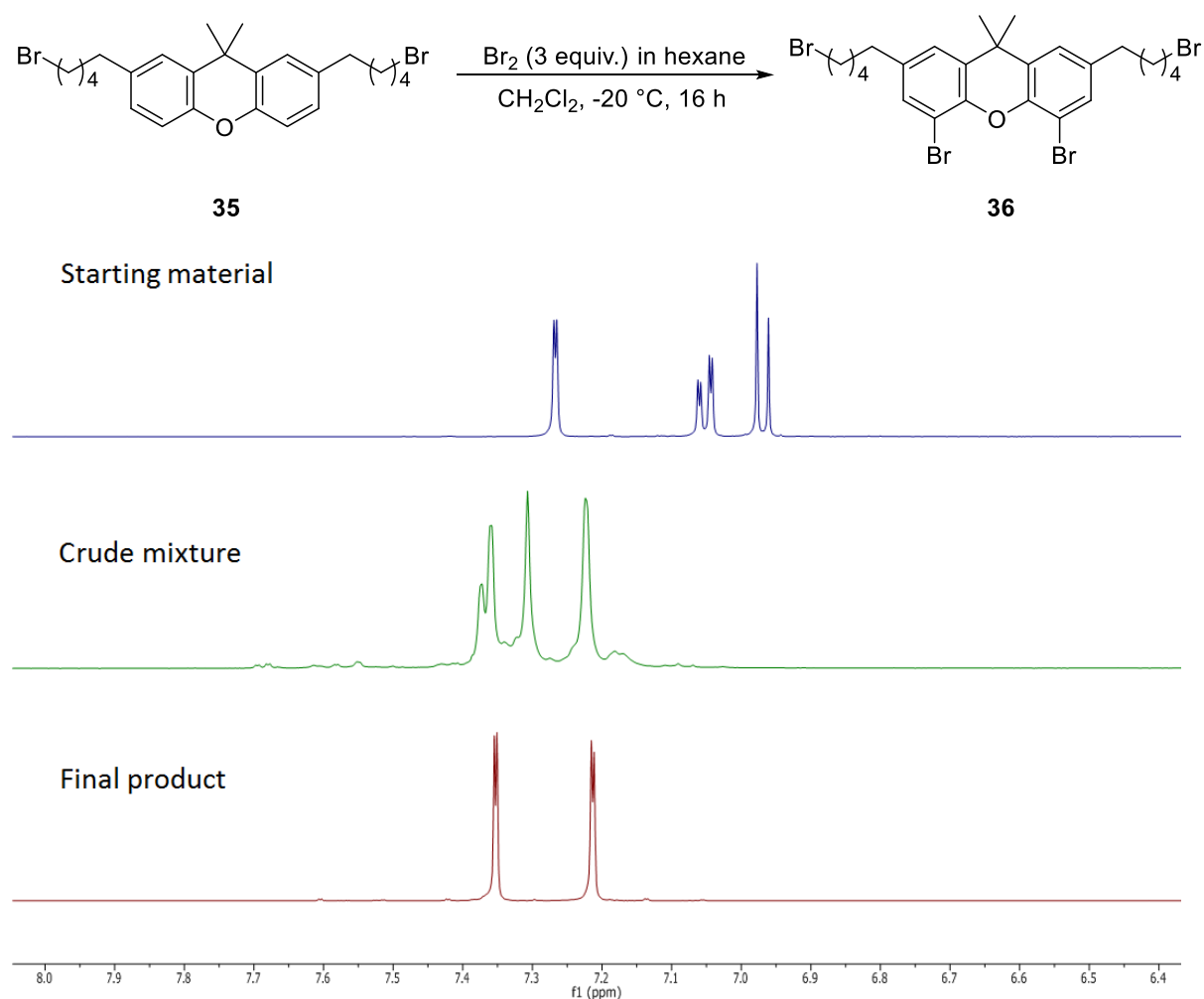


Figure 21. ^1H -NMR spectra (400 MHz, CD_2Cl_2) of the crude mixtures of the bromination step using a variation of the reported methodology⁶⁹ at -20°C , expansion of the aromatic area.

Lowering the temperature to -78°C and using non-diluted elemental bromine as adapted from Osakada's methodology;⁸¹ great selectivity was achieved towards the desired product (Figure 22). When scaling up the reaction to 200 mg side products were observed. For this example, the use of column chromatography with hexane/acetone (99:1) as eluent system was performed for 50 mg of compound and only $\sim 42\%$ of the pure dibrominated product was obtained.

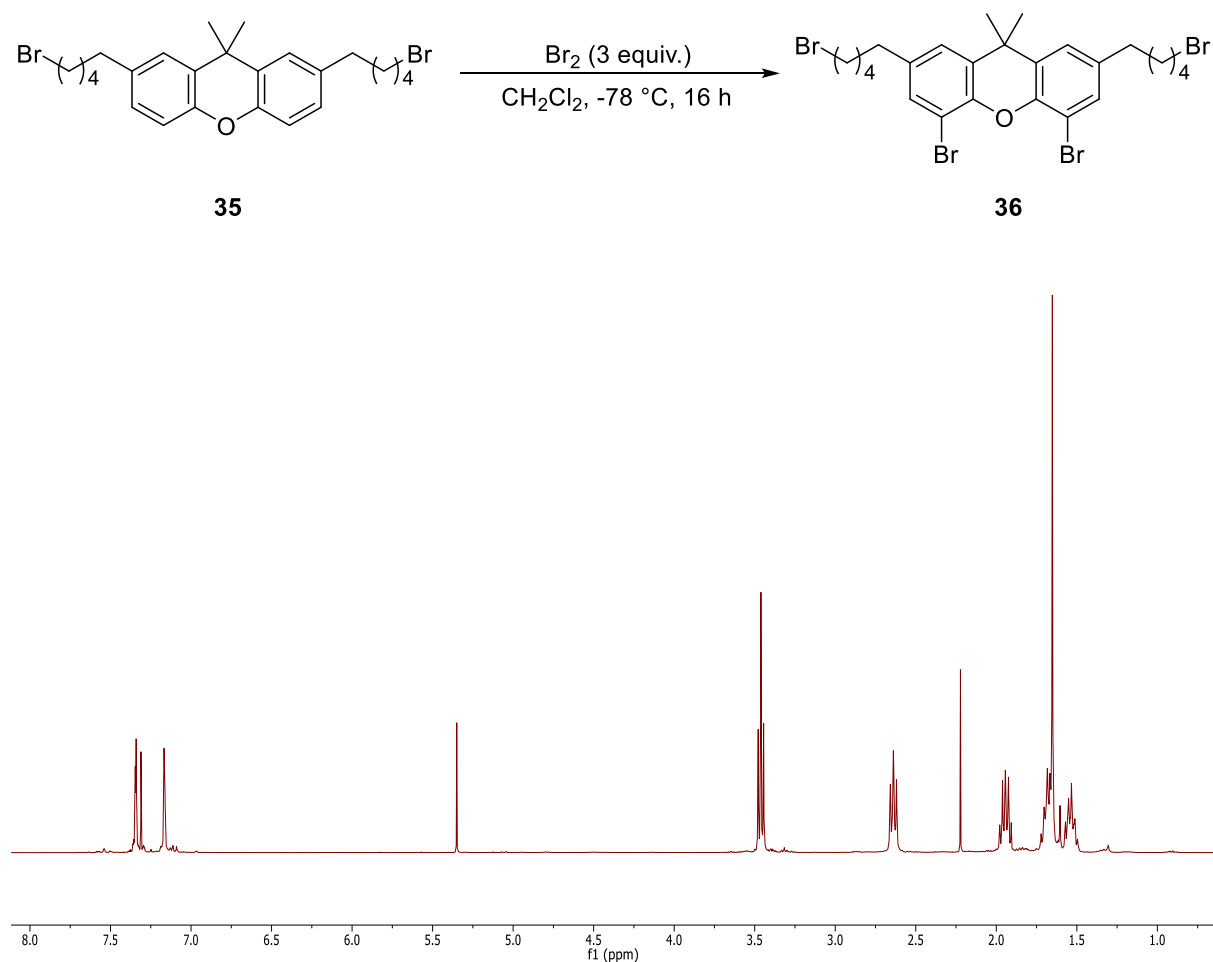


Figure 22. ^1H -NMR spectra (400 MHz, CD_2Cl_2) of the crude product after work up.

Following the successful trend of lowering both temperature and amount of bromine, the desired product was obtained by dropwise addition of 2.7 equivalents of bromine to a CH_2Cl_2 solution of the starting material at -78°C . Under these conditions, the reaction is completely selective and does not require further purification after the work up, obtaining 4,5-dibromo-2,7-bis(5-bromopentyl)-9,9-dimethylxanthene (**36**) in 98% isolated yield (Figure 23).

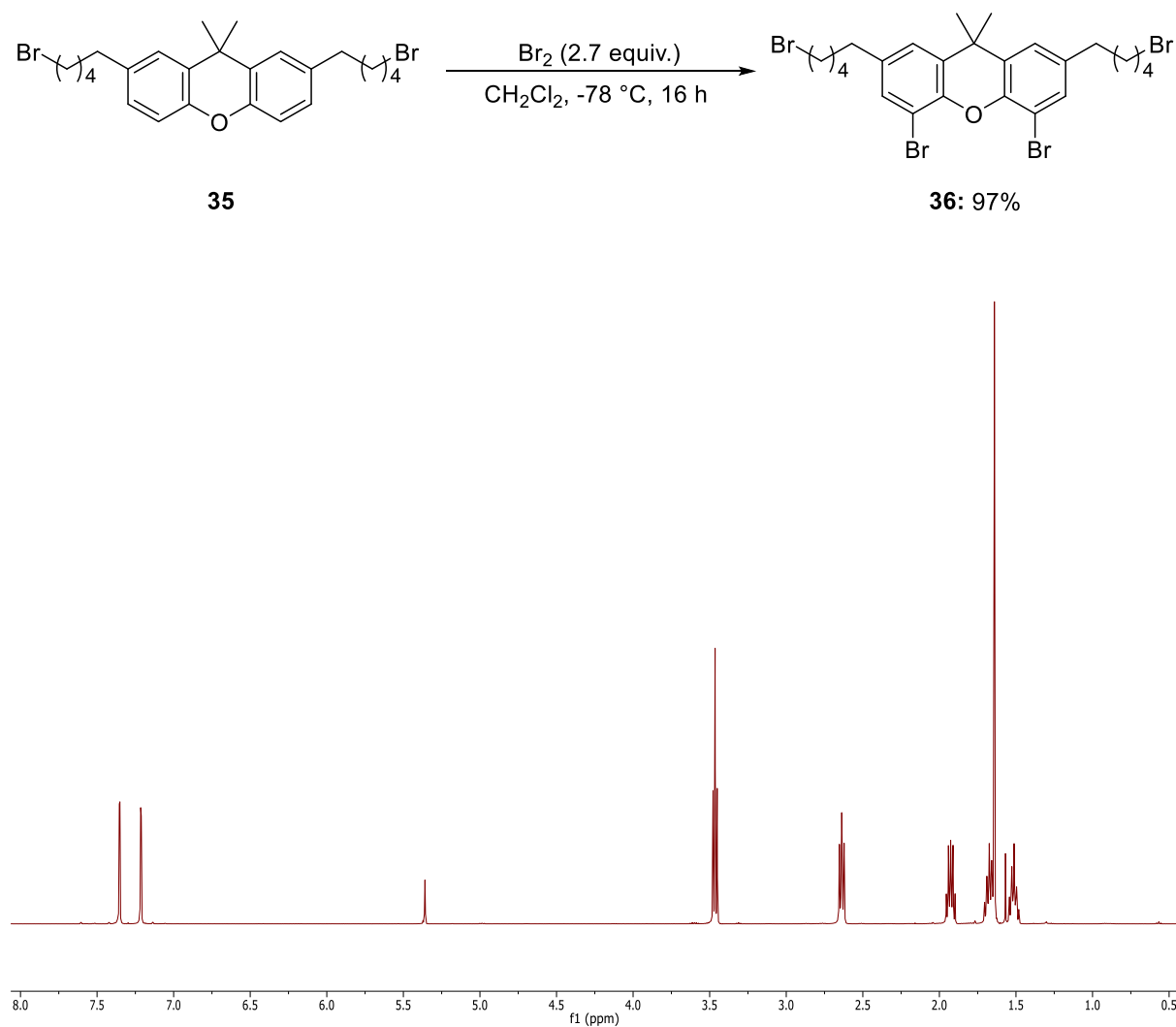
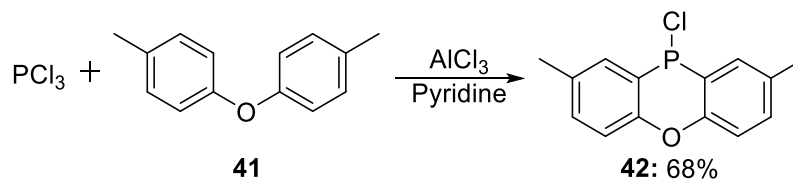


Figure 23. ^1H -NMR spectra (400 MHz, CD_2Cl_2) of isolated brominated product.

Synthesis of 10-chloro-2,8-dimethylphenoxaphosphine (POP)



Scheme 17. Synthesis of POP-Cl (**42**).

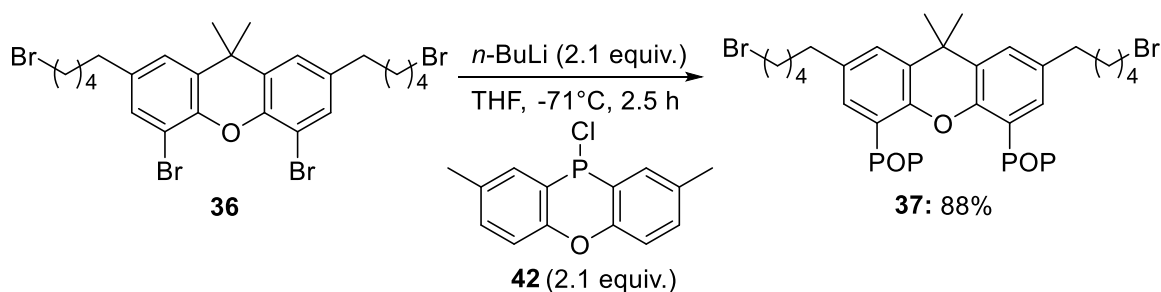
The halophosphine 10-chloro-2,8-dimethylphenoxaphosphine (POP-Cl) which is a substituent for the synthesis of our tagged ligand was synthesized following a protocol described by Herwig and coworkers (Scheme 17).⁸² The reaction occurs via electrophilic

aromatic substitution between phosphorus trichloride and *p*-tolyl ether following a Friedel-Crafts type mechanism. The final part requires addition of pyridine to cleave the complex formed between the halophosphine with the Lewis acid after reaction completion. Once the Lewis acid-amine adduct is removed by filtration, the synthetic intermediate is extensively extracted with toluene and washed with diethyl ether to remove the remaining impurities. This method allows the access to the synthetic intermediate 10-chloro-2,8-dimethylphenoxaphosphine (**42**) in high purity and 68% yield.

3.3.1.4 Step IV) Lithiation and C–P bond formation

One of the most widely used methods to synthesize phosphines by carbon-phosphorus bond formation, contemplates the reaction of halophosphines with organolithium species. Stoichiometric amounts of the reagents are required. The reaction requires strict inert conditions not only because of the sensitive nature of intermediates and final product, but also because many halophosphines are flammable and corrosive.⁸³

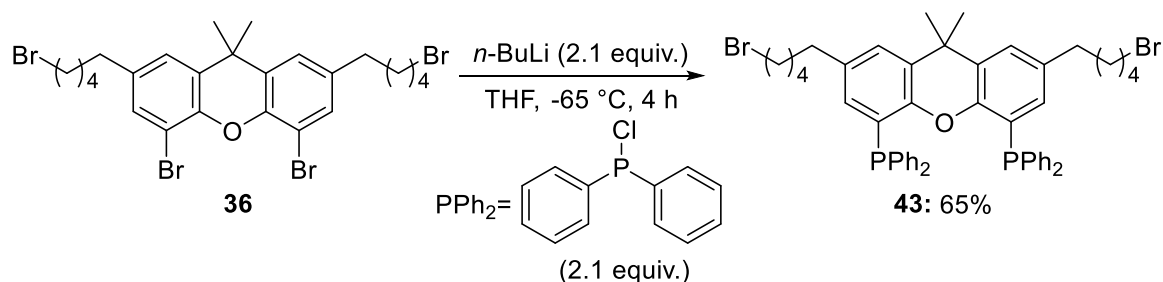
In order to afford the intermediate 2,7-bis(5-bromopentyl)-9,9-dimethyl-4,5-bis(2,8-dimethyl-10-phenoxaphosphino)xanthene (**37**), the dilithiation of 4,5-dibromo-2,7-bis(5-bromopentyl)-9,9-dimethylxanthene (**36**) in THF at low temperature followed by reaction with the halophosphine **42** was performed (Scheme 18). The new desired C–P bond was achieved by halogen–lithium exchange and the intermediate was obtained in 88% yield.



Scheme 18. Synthesis of the phosphine (**37**).

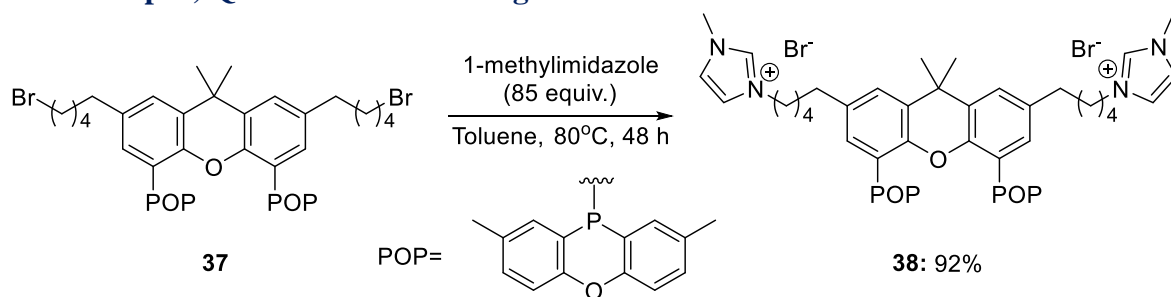
For comparison we also synthesized the xantphos analogue 2,7-bis(5-(3-methylimidazolium)pentyl)-9,9-dimethyl-4,5-bis-(diphenylphosphino)xanthene triflate (**47**) (Ion-tagged ligand).

For the synthesis of the synthetic precursor 2,7-bis(5-bromopentyl)-9,9-dimethyl-4,5-bis(diphenylphosphino)xanthene (Scheme 19) the same procedure was followed using chlorodiphenylphosphine instead of 2,8-dimethyl-10-phenoxaphosphino chloride. The phosphine intermediate 2,7-bis(5-bromopentyl)-9,9-dimethyl-4,5-bis(diphenylphosphino)xanthene (**43**) was obtained.



Scheme 19. Synthesis of the phosphine 2,7-bis(5-bromopentyl)-9,9-dimethyl-4,5-bis(diphenylphosphino) xanthene (**43**).

3.3.1.5 Step V) Quaternarization – Ligand functionalization



Scheme 20. Imidazolium functionalization step for the synthesis of 2,7-bis(5-(3-methylimidazolium)pentyl)-9,9-dimethyl-4,5-bis(2,8-dimethyl-10-phenoxaphosphino) xanthene bromide (**38**).

The introduction of the imidazolium cores in the modified xanthene backbone was possible following the methodology reported by Cole-Hamilton and co-workers.⁷⁰ The *N*-alkylation reaction of 1-methylimidazole with the precursor **37** gave full conversion towards the functionalized ligand **38** (Scheme 20) despite using lower amounts of 1-methylimidazole. Initially we followed the reaction by ³¹P NMR spectroscopy in order to observe product selectivity and estimated reaction time (Figure 24).

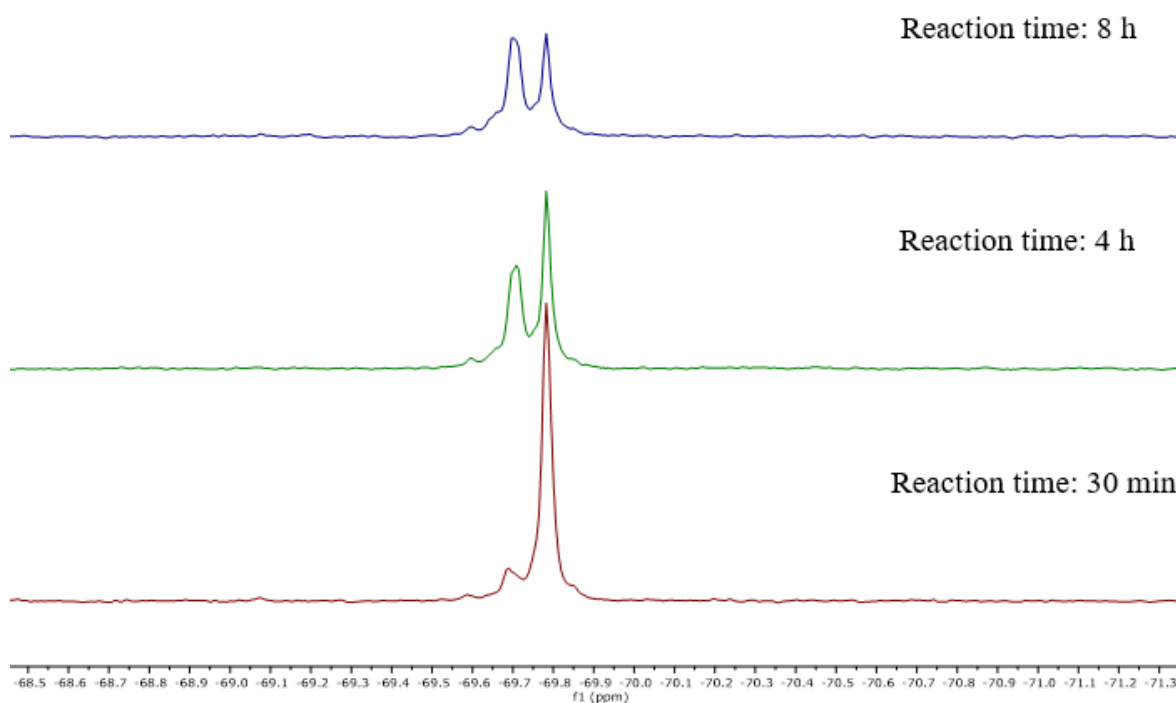


Figure 24. Monitoring of quaternarization by ^{31}P NMR (202 MHz, $\text{C}_6\text{D}_5\text{CD}_3$).

This method avoids long reaction times (48 h instead of 8 days) and does not require further purification due to the low solubility of POP-xantphos ligands in organic solvents. The compound crashes out from the reaction mixture as a white crystalline powder.

A crystal structure of the product was obtained (Figure 25). It was possible to identify the two imidazolium rings that were introduced by quaternarization. However, the counterion could not be identified as bromide. The counterion chloride was used as they could have been introduced by using chlorinated solvents at some point during compound manipulation. The identification of the anion is difficult to confirm because of the low quality of the crystal; therefore, it is unsuitable for detailed analysis.

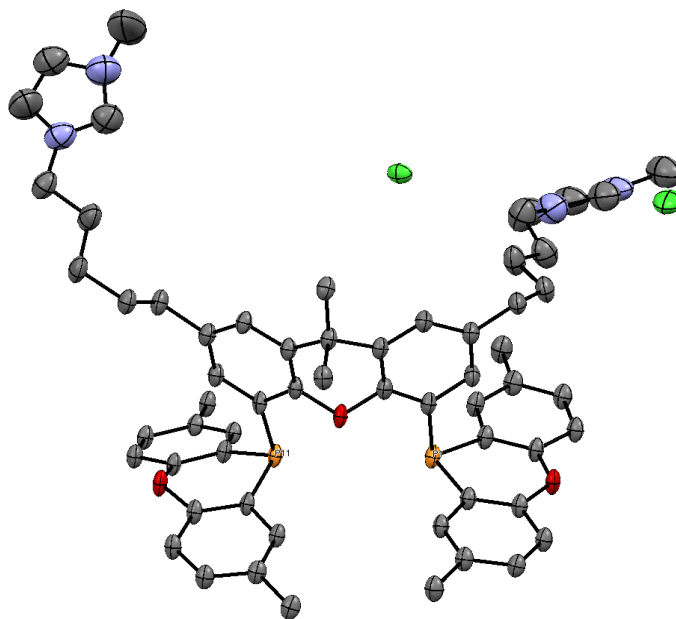
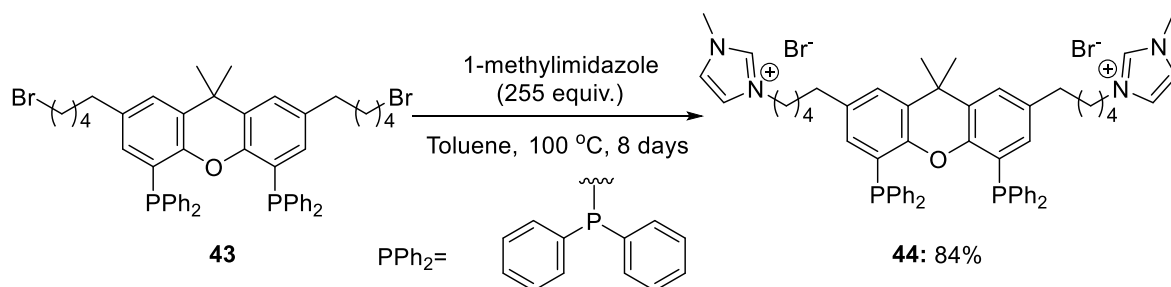


Figure 25. Thermal ellipsoid representation of ligand **38**. Hydrogen atoms and co-crystallized solvent molecules have been omitted for clarity. Displacement ellipsoids correspond to 20% probability.

For the synthesis of the synthetic precursor 2,7-bis(5-(3-methylimidazolium)pentyl)-9,9-dimethyl-4,5-bis-(diphenylphosphino)xanthene bromide (**44**) a modification of the previously described protocol was necessary (Scheme 21). An important feature of POP-xantphos derivatives is their crystallization properties and the lack of solubility. The POP-xantphos ion-tagged precursor crashed out from the reaction mixture and this fact drove the reaction to completion in short reaction times. This was not the case for the current precursor and product formation as well as purification were challenging. It requires long reaction time, followed by extensive washing with toluene and diethyl ether to afford the product.



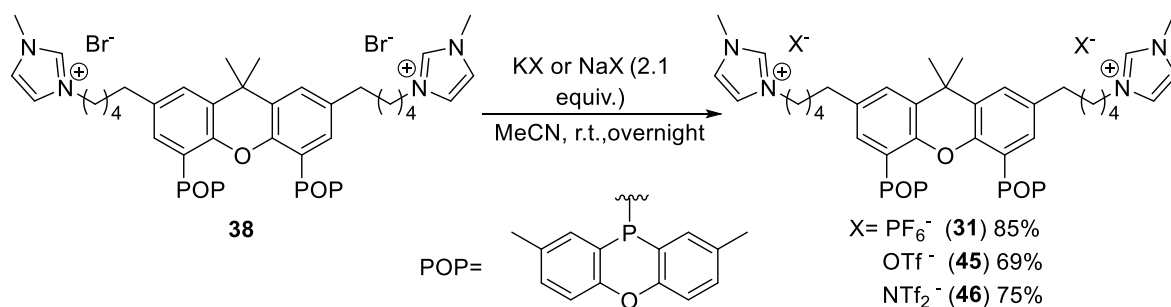
Scheme 21. Imidazolium functionalization step for synthetic precursor **44**.

3.3.1.6 Step VI) Counterion exchange

Counterion exchange was necessary to finalize our synthesis because for catalytic applications it is important, considering that halides can be detrimental to catalyst performance. Non-coordinating anions such as hexafluorophosphate, triflate and triflimide which usually do not interact with the metal center are the ones of choice for catalytic applications.⁸⁴

Initially, the original methodology reported to obtain this ligand was applied performing the counterion exchange in water in presence of the corresponding potassium salt.⁶⁹ Product impurities were observed and water removal under inert conditions is not ideal. Importantly, the ligand could not be extracted in the presence of water from the reaction mixture because it was present in both phases. The separation of the layers was not possible. Subsequently, it was observed that the use of ammonium salts as counterion source was not favorable, despite the byproduct crystallization from the reaction mixture. Ammonium salts are slightly soluble in organic solvents and contamination from the salt precursor was always detected.

Subsequently, sodium or potassium salts were used to achieve the counterion exchange in acetonitrile (Scheme 22). The suspension gives the desired product after overnight reaction. Next, removal of the solvent and filtration of the salts followed by extensive extraction of the ligand with various organic solvents afforded the target ligands.



Scheme 22. Counterion exchange reaction for ligands **31**, **45** and **46**.

The reaction was followed by ³¹P NMR spectroscopy in order to assess product formation and reaction times (Figure 26 and 27). Despite the conversion towards the product is quantitative, the poor solubility of the ligand in organic solvents considerable reduces the

isolated yield. The counterion exchange can occur in both dichloromethane or acetonitrile as solvents.

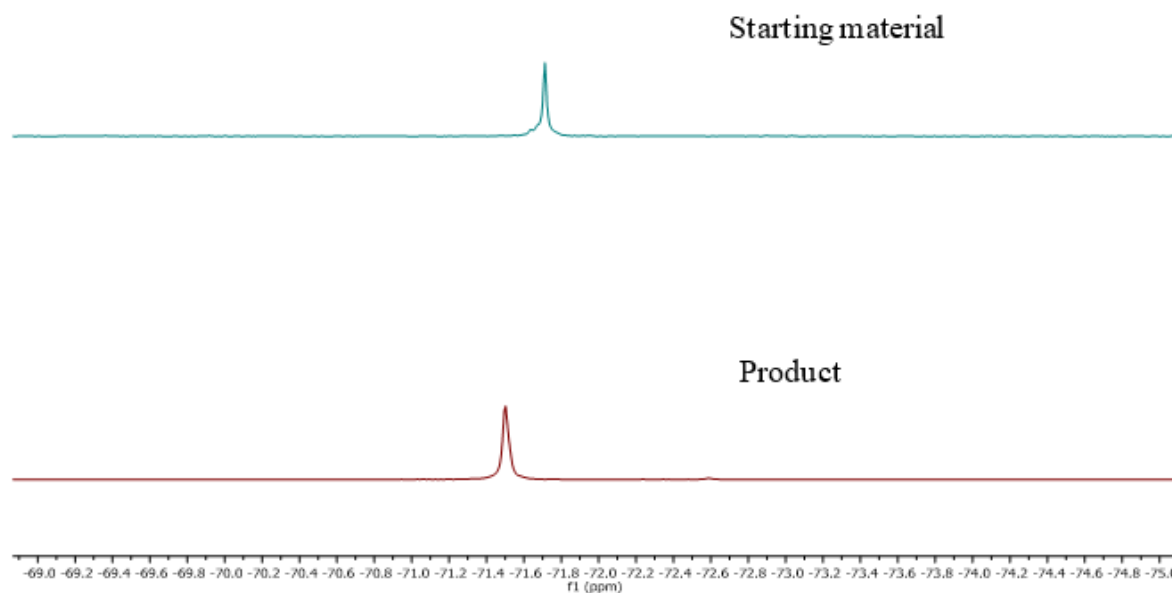


Figure 26. Monitoring of counterion exchange of **31** by ^{31}P NMR (202 MHz, CD_2Cl_2).

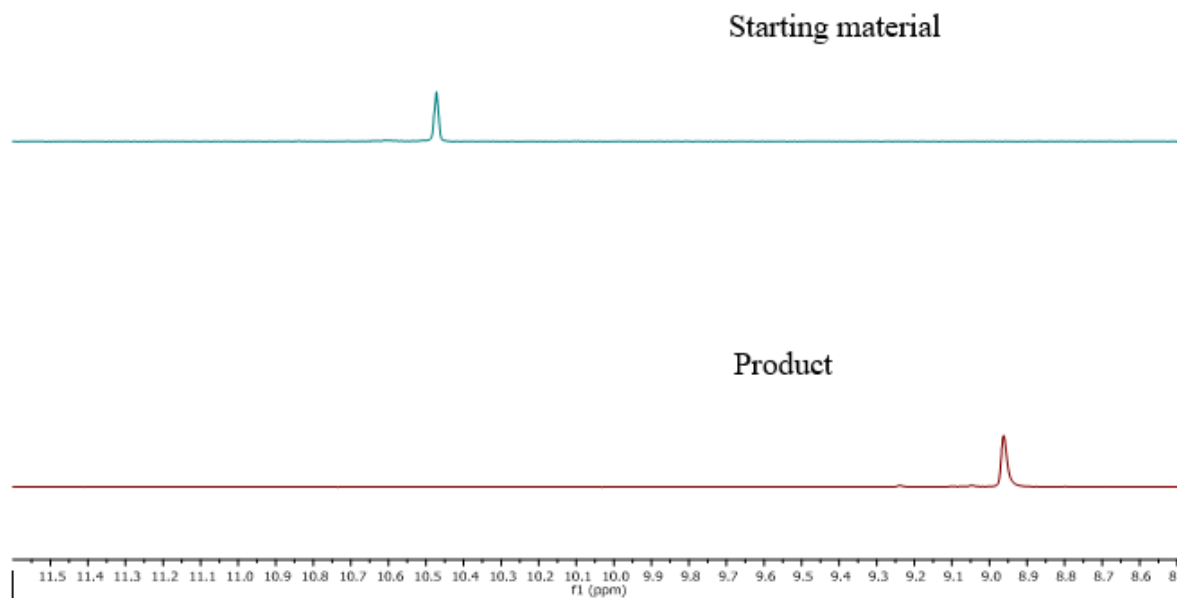
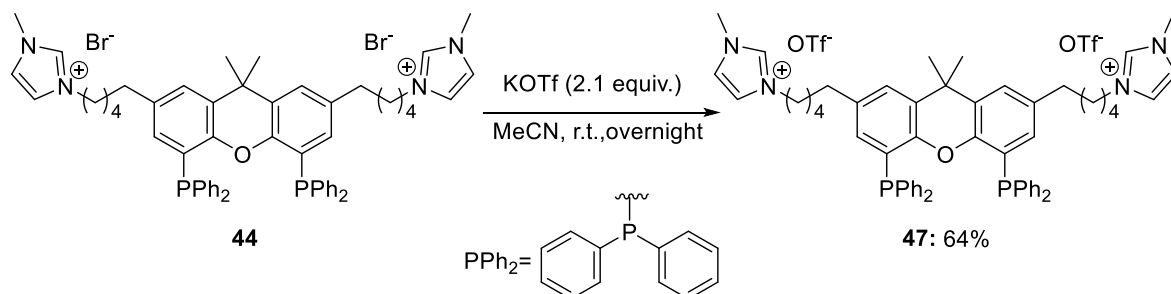


Figure 27. Monitoring of counterion exchange of **31** by ^1H NMR (400 MHz, CD_2Cl_2).

For the synthesis of the ligand 2,7-bis(5-(3-methylimidazolium)pentyl)-9,9-dimethyl-4,5-bis(diphenylphosphino)xanthene triflate (**47**), the reaction was performed as previously described for the aforementioned ligand (Scheme 23).



Scheme 23. Counterion exchange reaction for ligand **47**.

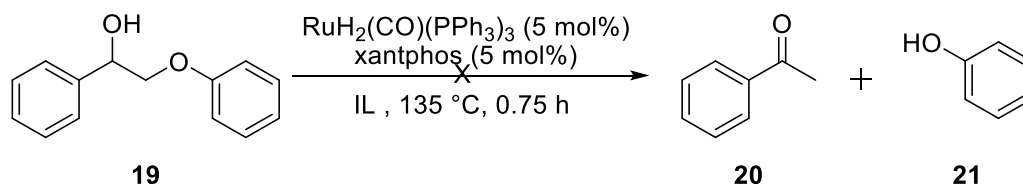
Additionally, the imidazolium-tagged nixantphos ligand **32** was synthesized according to the procedure of Cole-Hamilton and co-workers.⁷⁰

3.3.2 Catalysis in ionic liquids

Our goal in catalysis was to assess the performance of the synthesized imidazolium-tagged ligands in the ruthenium-catalyzed C–O bond cleavage of lignin model compounds in ionic liquids to establish a potential recyclable system for lignin depolymerization.

Lignin solubilization is a challenge, such feature is problematic for its characterization and valorization purposes. This recalcitrant biopolymer exhibits low solubility in most organic solvents. Homogeneous catalysts require that lignin goes into solution in the reaction media in order to have significant activity toward the conversion of the biopolymer.^{73, 85} Ionic liquids have been reported as alternative solvents to solubilize lignin.⁷² Because of their modular structural components, tuning of solute-solvent interactions can lead to high lignin solubility. It has been shown that electrostatic interactions with the solvent can disrupt the intra molecular polymer interactions and drive lignin into solution.⁶⁵ In order to evaluate our reaction conditions in this kind of alternative solvent, the ionic liquids selected for this studies due to their reported capability to solubilize lignin^{11, 65, 72} were: 1-ethyl-3-methylimidazolium diethyl phosphate, 1,3-dimethylimidazolium methyl sulfate, 1,3-ethyl-3-methylimidazolium trifluoromethanesulfonate and 1-ethyl-3-methylimidazolium chloride.

Reaction conditions were selected according to the reported procedure for the catalytic C–O bond cleavage of a lignin model compound using xant-type ligands, initially using commercially available xantphos.⁷¹ The reaction was carried out at 0.75 h in order to compare our results with the reported data in the literature (Scheme 24). The ionic liquids were dried before use (Chapter V, Section 5.2).



Scheme 24. Catalytic C–O bond cleavage of 2-phenoxy-1-phenylethanol compound using ruthenium xantphos ligands.

Under our reaction conditions, only 5% conversion towards the products was observed, while in xylenes xantphos achieves 44.6% conversion of **19** at 2 mol%.⁷¹ Poor solubility of the non-modified ligand was discarded by performing the experiments with imidazolium-tagged ligands. The nixantphos and xantphos analogues also gave 5% conversion towards the product under the same conditions. The imidazolium-tagged POP-xantphos derivative did not give any conversion. We believe the acidic proton of the imidazolium present in the ionic liquid structure reacted with the ruthenium precatalyst and/or other ruthenium species hampering the formation of the desired active complex (Scheme 12, section 3.1.3.2), causing its deactivation by forming carbene species. Although, the complex formed by side reactivity was not isolated, phosphorus NMR of the reaction mixture does not show the signals corresponding to the expected complex (Figure 28).

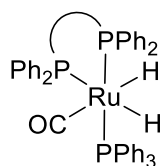
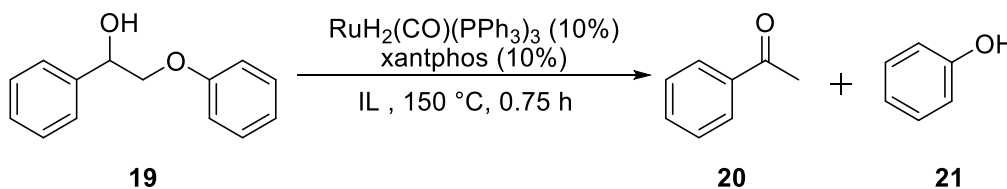


Figure 28. Expected ruthenium complex (Scheme 12, section 3.1.3.2).

Therefore, we decided then to use C2 protected ionic liquids. The ionic liquids tested were 1-ethyl-2,3-methylimidazolium hexafluorophosphate and 1-ethyl-2,3-methylimidazolium bis(trifluoromethanesulfonyl)imide.

As preliminary results for the catalytic transformation, when using commercial xantphos, full conversion of **19** towards the desired products **20** and **21** is achieved in 0.75 hours with 10% catalyst loading in both ionic liquids (Table 4). The extraction of the products and internal standard from the reaction media was achieved by washing the ionic liquid phase with organic solvents.

Table 4. Catalytic C–O bond cleavage of 2-phenoxy-1-phenylethanol in ionic liquids.

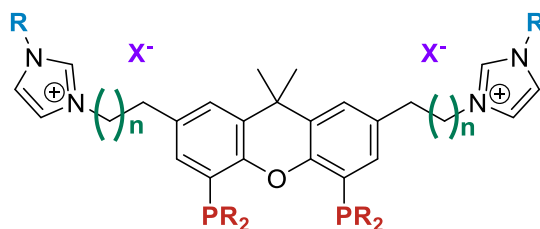


| Ionic liquid | Catalyst loading (mol%) | Conversion of 19 (%) |
|--|-------------------------|-----------------------------|
| 1-ethyl-2,3 methylimidazolium hexafluorophosphate | 10 | >99% |
| 1-ethyl-2,3 methylimidazolium Bis(trifluoromethanesulfonyl)imide | 10 | >99% |

Reaction conditions: 0.25 mmol of 2-phenoxy-1-phenylethan-1-ol with 10 mol% catalyst loading (0.025 mmol of $\text{RuH}_2\text{CO}(\text{PPh}_3)_3$, 0.025 mmol of xantphos ligand and 0.125 mmol of 1,2,4,5-tetramethylbenzene as the internal standard in 2 mL of the selected ionic liquid in a closed microwave vial provided with a magnetic stirrer. The reaction mixture was sealed and heated to 150 °C, 45 minutes after which the reaction mixture was cooled to room temperature, washed with 5 mL of toluene, 5 mL of diethyl ether and 5 mL of ethyl acetate. The yield was determined by gas chromatography. Results presented are the averages of reactions carried out in triplicate.

3.4 Conclusions

The optimized synthetic route reported in this thesis enables the functional modification of xantphos ligands suitable for catalysis in ionic liquid media by the introduction of imidazolium-tagged cores in their structure. This improved, robust and reliable synthetic procedure allows modular access to a variety of functionalized xant-type ligands.



Preliminary catalytic results in C2 protected ionic liquids showed promising results to perform the catalytic C–O bond cleavage of 2-phenoxy-1-phenylethanol in ionic liquids media.

In order to achieve effective biphasic catalytic systems, further investigations will determine the activity for each new tagged ligand in the homogeneous ruthenium-catalyzed C–O bond cleavage of the lignin model compound 2-phenoxy-1-phenylethanol. Reaction optimization and recyclability experiments still need to be performed in future investigations in our research group to allow product separation and catalyst recycling for lignin depolymerization into useful monomers. Once the candidate catalyst and optimized conditions are established, the catalytic system will be applied to more complicated lignin model compounds and real lignin could be also considered in the long term aim of the present project.

3.5 References

1. Tuck, C. O.; Perez, E.; Horvath, I. T.; Sheldon, R. A.; Poliakoff, M. Valorization of Biomass: Deriving More Value from Waste. *Science* **2012**, *337* (6095), 695-699.
2. Huber, G. W.; Iborra, S.; Corma, A. Synthesis of Transportation Fuels from Biomass: Chemistry, Catalysts, and Engineering. *Chem. Rev.* **2006**, *106* (9), 4044-4098.
3. Barta, K.; Ford, P. C. Catalytic Conversion of Nonfood Woody Biomass Solids to Organic Liquids. *Acc. Chem. Res.* **2014**, *47* (5), 1503-1512.
4. U. S. Department of Energy. 2016 Billion-Ton Report: Advancing Domestic Resources for a Thriving Bioeconomy. Volume 1: Economic Availability of Feedstocks of the 2016 Billion-Ton. <https://www.energy.gov/eere/bioenergy/downloads/2016-billion-ton-report-advancing-domestic-resources-thriving-bioeconomy>. **2016**.
5. Perlack, R. D. W., L. L.; Turhollow, A. F.; Graham, R. L.; Stokes, B. J.; Erbach, D. C. U. S. Department of Energy, Biomass as Feedstock for a bioenergy and bioproducts industry: the technical feasibility of a billion-ton annual supply. **2005**.
6. Bozell, J. J.; Astner, A.; Baker, D.; Biannic, B.; Cedenio, D.; Elder, T.; Hosseinaei, O.; Delbeck, L.; Kim, J. W.; O'Lenick, C. J.; Young, T. Integrating Separation and Conversion-Conversion of Biorefinery Process Streams to Biobased Chemicals and Fuels. *BioEnergy Res.* **2014**, *7* (3), 856-866.
7. Wigginton, N.; Yeston, J.; Malakoff, D. Working with waste. More treasure than trash. Introduction. *Science* **2012**, *337* (6095), 662-663.
8. Nonhebel, S. Renewable energy and food supply: will there be enough land? *Renew. Sustain. Energy. Rev.* **2005**, *9* (2), 191-201.
9. Azadi, P.; Inderwildi, O. R.; Farnood, R.; King, D. A. Liquid fuels, hydrogen and chemicals from lignin: A critical review. *Renew. Sustain. Energy. Rev.* **2013**, *21*, 506-523.
10. Gallezot, P. Catalytic conversion of biomass: challenges and issues. *ChemSusChem* **2008**, *1* (8-9), 734-737.
11. Zakzeski, J.; Bruijninx, P. C. A.; Jongerius, A. L.; Weckhuysen, B. M. The Catalytic Valorization of Lignin for the Production of Renewable Chemicals. *Chem. Rev.* **2010**, *110* (6), 3552-3599.
12. Van de Vyver, S.; Geboers, J.; Jacobs, P. A.; Sels, B. F. Recent advances in the catalytic conversion of cellulose. *ChemCatChem* **2011**, *3* (1), 82-94.
13. Fan, L. T. G., M. M.; and Lee, Y. H. Cellulose Hydrolysis. *Springer*. **1987**, 57. ISBN 978-3-642-72575-3.
14. Qi, L.; Horvath, I. T. Catalytic Conversion of Fructose to γ -Valerolactone in γ -Valerolactone. *ACS Catal.* **2012**, *2* (11), 2247-2249.
15. Metzker, G.; Burtoloso, A. C. B. Conversion of levulinic acid into γ -valerolactone using $\text{Fe}_3(\text{CO})_{12}$: mimicking a biorefinery setting by exploiting crude liquors from biomass acid hydrolysis. *Chem. Commun.* **2015**, *51* (75), 14199-14202.
16. Van de Vyver, S.; Roman-Leshkov, Y. Emerging catalytic processes for the production of adipic acid. *Catal. Sci. Technol.* **2013**, *3* (6), 1465-1479.
17. Ait Rass, H.; Essayem, N.; Besson, M. Selective Aerobic Oxidation of 5-HMF into 2,5-Furandicarboxylic Acid with Pt Catalysts Supported on TiO_2 - and ZrO_2 -Based Supports. *ChemSusChem* **2015**, *8* (7), 1206-1217.
18. Knothe, G.; Krah, J.; Gerpen, J. The Biodiesel Handbook. *Academic Press and AOCS Press* **2010**. ISBN: 9780983507260

19. Collinson, S. R.; Thielemans, W. The catalytic oxidation of biomass to new materials focusing on starch, cellulose and lignin. *Coord. Chem. Rev.* **2010**, 254 (15-16), 1854-1870.
20. Shmulsky, R.; Jones, D. P. Forest products and wood science: an introduction. *Wiley*, **2011**. ISBN:9780470960035.
21. Heitner, C.; Dimmel, D.; Schmidt, J. Lignin and Lignans: Advances in Chemistry. *CRC Press*, **2010**. ISBN 9781574444865.
22. Deuss, P. J.; Barta, K. From models to lignin: Transition metal catalysis for selective bond cleavage reactions. *Coord. Chem. Rev.* **2016**, 306, 510-532.
23. Fernando, S.; Adhikari, S.; Chandrapal, C.; Murali, N. Biorefineries: Current Status, Challenges, and Future Direction. *Energy Fuels* **2006**, 20 (4), 1727-1737.
24. Calvo-Flores, F. G.; Dobado, J. A. Lignin as Renewable Raw Material. *ChemSusChem* **2010**, 3 (11), 1227-1235.
25. Kim, S.; Chmely, S. C.; Nimlos, M. R.; Bomble, Y. J.; Foust, T. D.; Paton, R. S.; Beckham, G. T. Computational Study of Bond Dissociation Enthalpies for a Large Range of Native and Modified Lignins. *J. Phys. Chem. Lett.* **2011**, 2 (22), 2846-2852.
26. Nichols, J. M.; Bishop, L. M.; Bergman, R. G.; Ellman, J. A. Catalytic C-O Bond Cleavage of 2-Aryloxy-1-arylethanol and Its Application to the Depolymerization of Lignin-Related Polymers. *J. Am. Chem. Soc.* **2010**, 132 (36), 12554-12555.
27. Hammel, K. E. Extracellular free radical biochemistry of ligninolytic fungi. *New J. Chem.* **1996**, 20 (2), 195-198.
28. Sunda, W. G.; Kieber, D. J. Oxidation of humic substances by manganese oxides yields low-molecular-weight organic substrates. *Nature* **1994**, 367 (6458), 62-64.
29. Hofrichter, M. Review: lignin conversion by manganese peroxidase (MnP). *Enzyme Microb. Technol.* **2002**, 30 (4), 454-466.
30. Schlosser, D.; Hofer, C. Laccase-catalyzed oxidation of Mn^{2+} in the presence of natural Mn^{3+} chelators as a novel source of extracellular H_2O_2 production and its impact on manganese peroxidase. *Appl. Environ. Microbiol.* **2002**, 68 (7), 3514-3521.
31. Bajpai, P.; Anand, A.; Bajpai, P. K. Bleaching with lignin-oxidizing enzymes. *Biotechnol. Annu. Rev.* **2006**, 12, 349-378.
32. Husarcikova, J.; Voss, H.; Dominguez de Maria, P.; Schallmeyer, A. Microbial β -etherases and glutathione lyases for lignin valorisation in biorefineries: current state and future perspectives. *Appl. Microbiol. Biotechnol.* **2018**, 102 (13), 5391-5401.
33. Picart, P.; Mueller, C.; Mottweiler, J.; Wiermans, L.; Bolm, C.; Dominguez de Maria, P.; Schallmeyer, A. From Gene Towards Selective Biomass Valorization: Bacterial β -Etherases with Catalytic Activity on Lignin-Like Polymers. *ChemSusChem* **2014**, 7 (11), 3164-3171.
34. Kervinen, K.; Korpi, H.; Leskelae, M.; Repo, T. Oxidation of veratryl alcohol by molecular oxygen in aqueous solution catalyzed by cobalt salen-type complexes: the effect of reaction conditions. *J. Mol. Catal. A: Chem.* **2003**, 203 (1-2), 9-19.
35. Haikarainen, A.; Sipila, J.; Pietikainen, P.; Pajunen, A.; Mutikainen, I. Salen complexes with bulky substituents as useful tools for biomimetic phenol oxidation research. *Bioorg. Med. Chem.* **2001**, 9 (6), 1633-1638.
36. Son, S.; Toste, F. D. Non-Oxidative Vanadium-Catalyzed C-O Bond Cleavage: Application to Degradation of Lignin Model Compounds. *Angew. Chem., Int. Ed.* **2010**, 49 (22), 3791-3794.

37. Lancefield, C. S.; Ojo, O. S.; Tran, F.; Westwood, N. J. Isolation of Functionalized Phenolic Monomers through Selective Oxidation and C-O Bond Cleavage of the β -O-4 Linkages in Lignin. *Angew. Chem. Int. Ed.* **2015**, *54* (1), 258-262.
38. Zaheer, M.; Kempe, R. Catalytic hydrogenolysis of aryl ethers: A key step in lignin valorization to valuable chemicals. *ACS Catal.* **2015**, *5* (3), 1675-1684.
39. Nguyen, J. D.; Matsuura, B. S.; Stephenson, C. R. J. A Photochemical Strategy for Lignin Degradation at Room Temperature. *J. Am. Chem. Soc.* **2014**, *136* (4), 1218-1221.
40. Karkas, M. D.; Bosque, I.; Matsuura, B. S.; Stephenson, C. R. J. Photocatalytic Oxidation of Lignin Model Systems by Merging Visible-Light Photoredox and Palladium Catalysis. *Org. Lett.* **2016**, *18* (19), 5166-5169.
41. Bosque, I.; Magallanes, G.; Rigoulet, M.; Karkas, M. D.; Stephenson, C. R. J. Redox Catalysis Facilitates Lignin Depolymerization. *ACS Cent. Sci.* **2017**, *3* (6), 621-628.
42. Cramer, A. B.; Hunter, M. J.; Hibbert, H. Lignin and related compounds. XXXV. Ethanolysis of spruce wood. *J. Am. Chem. Soc.* **1939**, *61*, 509-516.
43. Sturgeon, M. R.; Kim, S.; Lawrence, K.; Paton, R. S.; Chmely, S. C.; Nimlos, M.; Foust, T. D.; Beckham, G. T. A Mechanistic Investigation of Acid-Catalyzed Cleavage of Aryl-Ether Linkages: Implications for Lignin Depolymerization in Acidic Environments. *ACS Sustain. Chem. Eng.* **2014**, *2* (3), 472-485.
44. Roberts, V. M.; Stein, V.; Reiner, T.; Lemonidou, A.; Li, X.; Lercher, J. A. Towards Quantitative Catalytic Lignin Depolymerization. *Chem. Eur. J.* **2011**, *17* (21), 5939-5948.
45. Miller, J. E.; Evans, L.; Littlewolf, A.; Trudell, D. E. Batch microreactor studies of lignin and lignin model compound depolymerization by bases in alcohol solvents. *Fuel* **1999**, *78* (11), 1363-1366.
46. Song, Q.; Cai, J.; Zhang, J.; Yu, W.; Wang, F.; Xu, J. Hydrogenation and cleavage of the C-O bonds in the lignin model compound phenethyl phenyl ether over a nickel-based catalyst. *Chinese J. Catal.* **2013**, *34* (4), 651-658.
47. Zhang, J.; Teo, J.; Chen, X.; Asakura, H.; Tanaka, T.; Teramura, K.; Yan, N., A Series of NiM (M = Ru, Rh, and Pd) Bimetallic Catalysts for Effective Lignin Hydrogenolysis in Water. *ACS Catal.* **2014**, *4* (5), 1574-1583.
48. Zhang, J.; Asakura, H.; van Rijn, J.; Yang, J.; Duchesne, P.; Zhang, B.; Chen, X.; Zhang, P.; Saeys, M.; Yan, N. Highly efficient, NiAu-catalyzed hydrogenolysis of lignin into phenolic chemicals. *Green Chem.* **2014**, *16* (5), 2432-2437.
49. Galkin, M. V.; Sawadjoon, S.; Rohde, V.; Dawange, M.; Samec, J. S. M. Mild Heterogeneous Palladium-Catalyzed Cleavage of β -O-4'-Ether Linkages of Lignin Model Compounds and Native Lignin in Air. *ChemCatChem* **2014**, *6* (1), 179-184.
50. Serrano-Ruiz, J. C.; Dumesic, J. A. Catalytic routes for the conversion of biomass into liquid hydrocarbon transportation fuels. *Energy Environ. Sci.* **2011**, *4* (1), 83-99.
51. Gao, F.; Webb, J. D.; Sorek, H.; Wemmer, D. E.; Hartwig, J. F. Fragmentation of Lignin Samples with Commercial Pd/C under Ambient Pressure of Hydrogen. *ACS Catal.* **2016**, *6* (11), 7385-7392.
52. Luo, J.; Zhang, X.; Lu, J.; Zhang, J. Fine Tuning the Redox Potentials of Carbazolic Porous Organic Frameworks for Visible-Light Photoredox Catalytic Degradation of Lignin β -O-4 Models. *ACS Catal.* **2017**, *7* (8), 5062-5070.
53. Sergeev, A. G.; Hartwig, J. F. Selective, Nickel-Catalyzed Hydrogenolysis of Aryl Ethers. *Science* **2011**, *332* (6028), 439-443.

54. Sergeev, A. G.; Webb, J. D.; Hartwig, J. F. A Heterogeneous Nickel Catalyst for the Hydrogenolysis of Aryl Ethers without Arene Hydrogenation. *J. Am. Chem. Soc.* **2012**, *134* (50), 20226-20229.
55. Xu, L.; Chung, L. W.; Wu, Y. D. Mechanism of Ni-NHC Catalyzed Hydrogenolysis of Aryl Ethers: Roles of the Excess Base. *ACS Catal.* **2016**, *6* (1), 483-493.
56. Sawatlon, B.; Wititsuwannakul, T.; Tantirungrotechai, Y.; Surawatanawong, P. Mechanism of Ni N-heterocyclic carbene catalyst for C-O bond hydrogenolysis of diphenyl ether: a density functional study. *Dalton Trans.* **2014**, *43* (48), 18123-18133.
57. Saper, N. I.; Hartwig, J. F. Mechanistic Investigations of the Hydrogenolysis of Diaryl Ethers Catalyzed by Nickel Complexes of N-Heterocyclic Carbene Ligands. *J. Am. Chem. Soc.* **2017**, *139* (48), 17667-17676.
58. Kundu, S.; Choi, J.; Wang, D. Y.; Choliy, Y.; Emge, T. J.; Krogh-Jespersen, K.; Goldman, A. S. Cleavage of ether, ester, and tosylate C(sp³)-O bonds by an iridium complex, initiated by oxidative addition of C-H bonds. Experimental and computational studies. *J. Am. Chem. Soc.* **2013**, *135* (13), 5127-5143.
59. Haibach, M. C.; Lease, N.; Goldman, A. S. Catalytic cleavage of ether C-O bonds by pincer iridium complexes. *Angew. Chem. Int. Ed.* **2014**, *53* (38), 10160-10163.
60. Chmely, S. C.; Kim, S.; Ciesielski, P. N.; Jimenez-Oses, G.; Paton, R. S.; Beckham, G. T. Mechanistic Study of a Ru-Xantphos Catalyst for Tandem Alcohol Dehydrogenation and Reductive Aryl-Ether Cleavage. *ACS Catal.* **2013**, *3* (5), 963-974.
61. Wu, A.; Patrick, B. O.; Chung, E.; James, B. R. Hydrogenolysis of β -O-4 lignin model dimers by a ruthenium-xantphos catalyst. *Dalton Trans.* **2012**, *41* (36), 11093-11106.
62. Wu, A.; Lauzon, J. M.; James, B. R. Hydrogenolysis of a γ -Acetylated Lignin Model Compound with a Ruthenium-Xantphos Catalyst. *Catal. Lett.* **2015**, *145* (2), 511-518.
63. vom Stein, T.; Weigand, T.; Merken, C.; Klankermayer, J.; Leitner, W. Trimethylenemethane-Ruthenium(II)-Triphos Complexes as Highly Active Catalysts for Catalytic C-O Bond Cleavage Reactions of Lignin Model Compounds. *ChemCatChem* **2013**, *5* (2), 439-441.
64. Lee, S. Functionalized imidazolium salts for task-specific ionic liquids and their applications. *Chem. Commun.* **2006**, (10), 1049-1063.
65. Hart, W. E. S.; Harper, J. B.; Aldous, L. The effect of changing the components of an ionic liquid upon the solubility of lignin. *Green Chem.* **2015**, *17* (1), 214-218.
66. da Costa Lopes, A. M.; Joao, K. G.; Morais, A. R. C.; Bogel-Lukasik, E.; Bogel-Lukasik, R. Ionic liquids as a tool for lignocellulosic biomass fractionation. *Sustainable Chem. Processes* **2013**, *1*:3, 1-31.
67. Sonar, S.; Ambrose, K.; Hendsbee, A. D.; Masuda, J. D.; Singer, R. D. Synthesis and application of Co(salen) complexes containing proximal imidazolium ionic liquid cores. *Can. J. Chem.* **2012**, *90* (1), 60-70.
68. Ambrose, K.; Hurisso, B. B.; Singer, R. D. Recyclable ionic liquid tagged Co(salen) catalysts for the oxidation of lignin model compounds. *Can. J. Chem.* **2013**, *91* (12), 1258-1261.
69. Bronger, R. P. J.; Silva, S. M.; Kamer, P. C. J.; van Leeuwen, P. W. N. M. A novel dicationic phenoxaphosphino-modified Xantphos-type ligand: a ligand for highly active and selective, biphasic, rhodium catalysed hydroformylation in ionic liquids. *Dalton Trans.* **2004**, (10), 1590-1596.

70. Webb, P. B.; Kunene, T. E.; Cole-Hamilton, D. J. Continuous flow homogeneous hydroformylation of alkenes using supercritical fluids. *Green Chem.* **2005**, 7 (5), 373-379.
71. Shaw, L.; Somisara, D. M. U. K.; How, R. C.; Westwood, N. J.; Bruijninx, P. C. A.; Weckhuysen, B. M.; Kamer, P. C. J. Electronic and bite angle effects in catalytic C–O bond cleavage of a lignin model compound using ruthenium Xantphos complexes. *Catal. Sci. Technol.* **2017**, 7 (3), 619-626.
72. Zakzeski, J.; Jongerius, A. L.; Weckhuysen, B. M. Transition metal catalyzed oxidation of Alcell lignin, soda lignin, and lignin model compounds in ionic liquids. *Green Chem.* **2010**, 12 (7), 1225-1236.
73. Zhao, W.; Xiao, L.-P.; Song, G.; Sun, R.-C.; He, L.; Singh, S.; Simmons, B. A.; Cheng, G. From lignin subunits to aggregates: insights into lignin solubilization. *Green Chem.* **2017**, 19 (14), 3272-3281.
74. Kabalka, G. W.; Chandler, J. H. Deoxygenation of Aldehydes and Ketones: An Improved Procedure. *Synth. Commun.* **1979**, 9 (4), 275-279.
75. Volkov, A.; Gustafson, K. P. J.; Tai, C.-W.; Verho, O.; Baeckvall, J.-E.; Adolfsson, H. Mild Deoxygenation of Aromatic Ketones and Aldehydes over Pd/C Using Polymethylhydrosiloxane as the Reducing Agent. *Angew. Chem. Int. Ed.* **2015**, 54 (17), 5122-5126.
76. Ono, A.; Suzuki, N.; Kamimura, J. Hydrogenolysis of diaryl and aryl alkyl ketones and carbinols by sodium borohydride and anhydrous aluminum(III) chloride. *Synthesis* **1987**, (8), 736-738.
77. Clayden, J. Organolithiums: Selectivity for Synthesis. First Edition. **2002**, 23, ISBN: 0-08043261-1.
78. Song, S.; Sun, X.; Li, X.; Yuan, Y.; Jiao, N.; Jiao, N. Efficient and Practical Oxidative Bromination and Iodination of Arenes and Heteroarenes with DMSO and Hydrogen Halide: A Mild Protocol for Late-Stage Functionalization. *Org. Lett.* **2015**, 17 (12), 2886-2889.
79. Nowick, J. S.; Ballester, P.; Ebmeyer, F.; Rebek, J. Convergent functional groups. 9. Complexation in new molecular clefts. *J. Am. Chem. Soc.* **1990**, 112 (24), 8902-8906.
80. Ashmead, L. T. Bromination of fluorescein, United States Patent 3111528. *Sun Chemical Corporation* **1963**, (Staten Island, New York, N.Y.).
81. Takeuchi, D.; Chiba, Y.; Takano, S.; Osakada, K. Double-Decker-Type Dinuclear Nickel Catalyst for Olefin Polymerization: Efficient Incorporation of Functional Comonomers. *Angew. Chem. Int. Ed.* **2013**, 52 (48), 12536-12540.
82. Herwig, J.; Skutta, P.; Sturm, S. Process for the production of substituted 10-chlorophenoxaphosphines or 10-Bromo-phenoxaphosphines. *United States, Patent Application Publication* **2001**, US 2001/0047114A1.
83. Wauters, I.; Debrouwer, W.; Stevens, C. V. Preparation of phosphines through C-P bond formation. *Beilstein J. Org. Chem.* **2014**, 10, 1064-1096.
84. Bochmann, M. "Non-Coordinating" Anions: Underestimated Ligands. *Angew. Chem. Int. Ed* **1992**, 31 (9), 1181-1182.
85. Mu, L.; Shi, Y.; Wang, H.; Zhu, J. Lignin in Ethylene Glycol and Poly(ethylene glycol): Fortified Lubricants with Internal Hydrogen Bonding. *ACS Sustain. Chem. Eng.* **2016**, 4 (3), 1840-1849.

Chapter IV: Photocatalytic CO₂ reduction in ionic liquid media

4.1 Introduction

4.1.1 The importance of carbon dioxide utilization

Carbon dioxide concentrations in the atmosphere have been increasing by 280 ppm over the past century reaching 403 ppm in 2016, a value that is 40% higher than the levels corresponding to the pre-industrial era. The major reason for this increase lies in the use of fossil fuels as primary source (82% in 2015) to supply the increasing demand of energy, which grew by almost 150% between 1971 and 2015. Each source of energy (*i.e.* oil, coal, gas etc.) account for CO₂ emission related to their content of carbon (Figure 1, left), therefore coal represents the source with the highest emission of CO₂ (45% of the total) despite being less used than oil for energy supply. As consequence, countries that utilize coal as major energy supply are also the ones producing more CO₂. Noticeable, the first ten countries in order of emission accounted for 21.7 Gt of the 32.3 Gt of CO₂ emanations in total in 2015, with China emitting 28% of the entire amount. Regarding the emission by sector in 2015, electricity and heat accounted for 41% of the total, followed by transport (24%), industry (19%), residential (6%), services (3%) and other (7%) (Figure 1, right).¹⁻²

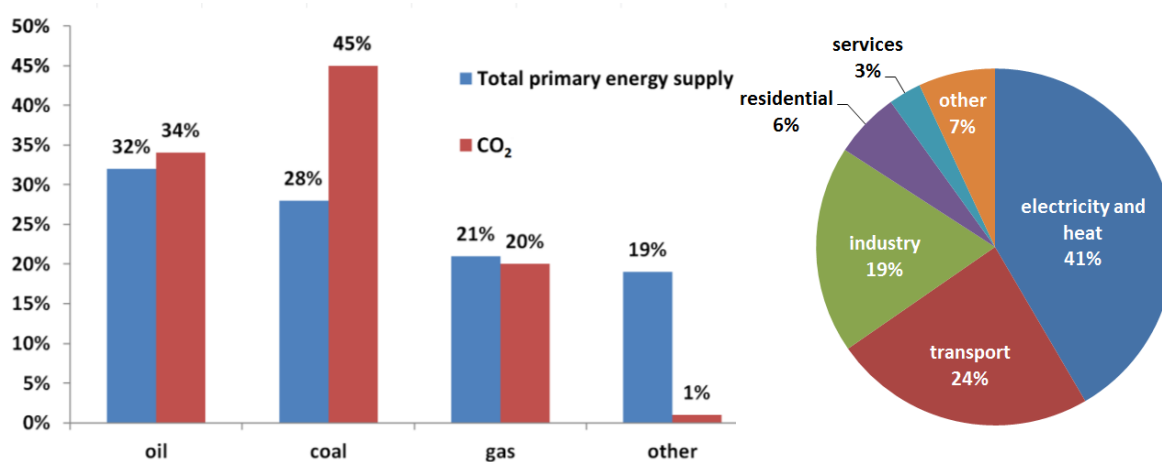


Figure 1. Fuel contributions to world primary energy supply and CO₂ emissions (left). World CO₂ emissions from fuel combustion by sector (right).²

Three strategies have been envisioned for the reduction of CO₂ production.³ The first approach consists in reaching higher efficiency in energy production, especially in the sectors that contribute more to the emissions. Therefore, better insulation of buildings, new or refurbished industrial plants based on low-emission technologies and fuel-efficient vehicles are on the top of the priorities. The major problem for the implementation of this strategy consists in the high cost and long time needed for the conversion of the existing low-efficient buildings, plants and vehicles. The second strategy is shifting from fossil fuels to renewable energy sources like sun, wind and geothermal energy. The third strategy fundamentally differs from the two previous ones because it is based on the concept of utilization of CO₂ rather than avoiding its production. In this context, CO₂ is utilized as C1 carbon source to obtain chemicals, but CO₂ is a stable molecule ($\Delta G_f^\circ = -396$ kJ/mol) and energy is needed for its conversion into species in which the O/C ratio is lower than 2 or the H/C ratio is increased from zero. Thermal energy combined with stoichiometric (*i.e.* synthesis of urea⁴ and salicylic acid⁵ or catalytic synthesis of organic carbonates,⁶ and carbamates⁷) protocols have been developed. More recently, the utilization of solar energy for the reduction of CO₂ started to gain increasing interest due to the desirable switch from fossil fuel to renewable energy sources. The one-electron reduction of CO₂ to form CO₂^{•-} is very difficult (-2.14 V *vs.* SCE)⁸⁻⁹ and an efficient process requires an overpotential of up to 0.6 V, due in part to the kinetic restrictions forced by the structural difference between linear CO₂ and bent CO₂^{•-}.^{8,10} A more accessible pathway consists of reducing CO₂ *via* proton-assisted multiple-electron transfer, which can afford different products (Table 1).⁹

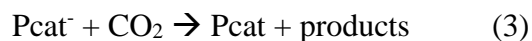
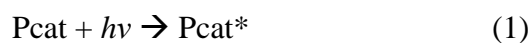
Table 1. CO₂ reduction potentials (E° potentials are reported at pH 7).¹¹

| Reaction | E° (V) <i>vs.</i> SCE |
|---|-----------------------|
| $\text{CO}_2 + 2\text{H}^+ + 2\text{e}^- \rightarrow \text{HCO}_2\text{H}$ | - 0.85 |
| $\text{CO}_2 + 2\text{H}^+ + 2\text{e}^- \rightarrow \text{CO} + \text{H}_2\text{O}$ | - 0.77 |
| $\text{CO}_2 + 4\text{H}^+ + 4\text{e}^- \rightarrow \text{C} + 2\text{H}_2\text{O}$ | - 0.44 |
| $\text{CO}_2 + 4\text{H}^+ + 4\text{e}^- \rightarrow \text{HCHO} + \text{H}_2\text{O}$ | - 0.72 |
| $\text{CO}_2 + 6\text{H}^+ + 6\text{e}^- \rightarrow \text{CH}_3\text{OH} + \text{H}_2\text{O}$ | - 0.62 |
| $\text{CO}_2 + 8\text{H}^+ + 8\text{e}^- \rightarrow \text{CH}_4 + 2\text{H}_2\text{O}$ | - 0.48 |

4.1.2 Overview of homogeneous photocatalytic approaches for CO₂ reduction

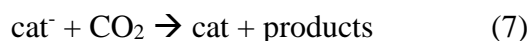
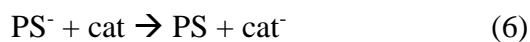
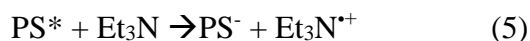
Two different systems can be envisioned to perform this reduction using homogeneous photocatalysis, the first strategy is based on a single molecule (Pcat) that acts both as photosensitizer (PS) and catalyst (cat), whereas in the second approach a photosensitizer (PS) and a transition metal catalyst (cat) work concertedly.¹¹

The complexes belonging to the first class are promoted to an excited state (Pcat*) upon light excitation. This excited state is then quenched by a sacrificial donor (S), such as triethylamine (TEA) or triethylethanolamine (TEOA), to give the reduced catalyst (Pcat⁻) that is responsible for the reduction of CO₂ (Equations 1-3)



In this context, metalloporphyrins and related metallomacrocycles have been studied because they are strong light absorbers with extremely large extinction coefficients in the visible spectral region.¹²⁻¹⁶ However, their excited states lifetimes are really short resulting in low concentrations of active catalyst in solution. In addition, they undergo unwanted hydrogenation of the macrocycle ring and these degradation products seem to preferentially catalyze the reduction of protons over CO₂.¹¹ In addition to metalloporphyrins, Re(CO)₃(bpy)X-based complexes have been intensely studied,¹⁷⁻¹⁹ but they suffer from narrow range of absorption in the visible region and sluggish reactivity with CO₂ which are reflected in poor turnover frequencies (TOF). More recently, mononuclear, binuclear and trinuclear terpyridine (tpy) 2-phenylpyridine (ppy) iridium complexes have been also applied for the reduction of CO₂ to CO.²⁰⁻²²

Examples of the second class of dual catalytic systems typically involve ruthenium or iridium complexes as photosensitizers, which are promoted to an excited state PS* upon light excitation. This excited state is then quenched by a sacrificial donor (S), such as triethylamine (TEA) or triethylethanolamine (TEOA), to give the reduced PS⁻ that is responsible for electron transfer to the catalyst, ultimately reducing CO₂ (Equations 4-7).¹¹⁻²³



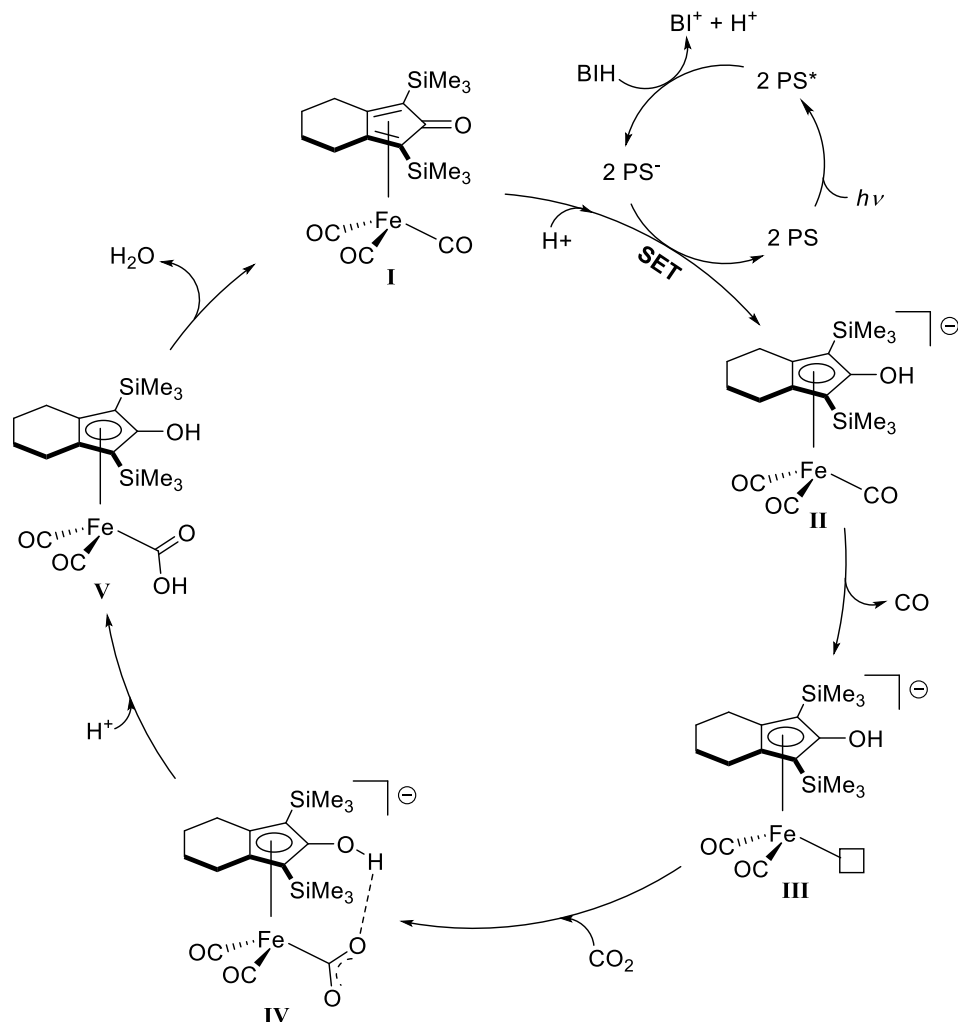
Catalysts based on Mn,²⁴⁻²⁶ Fe,^{24, 27-28} Co,²⁹⁻³⁰ or Ni and Ir³¹ proved to be able to reduce CO₂. In addition, photosensitizer and catalyst can be connected by a bridge forming a supramolecular complex.³²⁻³⁵

Recently Beller and co-workers reported a selective system from the reduction of CO₂ to CO applying (cyclopentadienone) iron–tricarbonyl complexes as catalysts due to their bifunctional nature, which translates to the presence of both a proton-donor site (ligand) and a hydride-donor site (metal center).³⁶ The chosen photosensitizer was [Ir(dF(CF₃)ppy)₂-(dtbbpy)]PF₆ (IrPS) (where dF(CF₃)ppy = cyclometalated 2-(2,4-difluorophenyl)-5-trifluoromethylpyridine and dtbbpy = 4,4'-di-tert-butyl-2,2'-bipyridyl).³⁷ They used TEOA as sacrificial donor and N-methyl-2-pyrrolidone (NMP) as solvent, irradiating the reaction mixture using a Hg-lamp (400–700 nm) at 2.5 W for 5 h at room temperature. Under these reaction conditions, a TON of 596 was obtained using 5 μM of catalyst, outperforming the structurally related [Fe(CO)₃(bpy)] that reached a TON of 129. The mechanism was investigated using FTIR measurements and Stern-Volmer analysis. Irradiating the sole (cyclopentadienone) iron tricarbonyl complex in solution under argon resulted in CO dissociation, whereas a new iron-hydride species is formed in the presence of IrPS. Stern-Volmer analysis showed that either the iron catalyst or TEOA can quench the emission of the excited state PS*. However, the former possess an irreversible reduction peak at -1.44 V vs. SCE that is more negative than the one of the couple [IrPS*/IrPS⁺] (-0.89 V vs. SCE), thus electron transfer from the PS to the iron catalyst is thermodynamically unfeasible. For this reasons, a reductive quenching mechanism between IrPS and TEOA was suggested.

Later, the same group replaced the iridium photosensitizer with the more economical and earth-abundant copper (CuPS) obtaining slightly lower TON of 487.³⁸ In this case 1,3-dimethyl-2-phenyl-2,3-dihydro-1H-benzo[d]imidazole (BIH) was used as sacrificial electron

donor and again a reductive quenching mechanism operating between CuPS* and BIH was proposed.

A combination of experimental studies and DFT calculations enabled the elucidation of the mechanism for this transformation (Scheme 1).^{27, 36, 39} According to calculations, removal of CO from **I** to form the corresponding neutral species is unfavorable ($\Delta G = 32.5 \text{ Kcal mol}^{-1}$), but decarbonylation is accessible after reduction of **I** by the photosensitizer to give **II**, followed by CO dissociation to afford **III**. CO₂ coordination is presumed to dictate the product distribution,⁴⁰ in particular effective formation of CO is associated with CO₂ bound *via* the carbon atom whereas η^1 -OCO coordination will finally lead to formic acid. It was calculated that coordination of CO₂ via carbon to give **IV** is facilitated by hydrogen bonding with the OH of the cyclopentadienyl ligand. Intermediate **IV** is in equilibrium with the protonated species **V** and this equilibrium is shifted toward the products by an exergonic and irreversible dehydration step that releases H₂O and regenerates **I**.



Scheme 1. Proposed mechanism for the photochemical reduction of CO₂ using the cyclopentadienone iron complex.

4.1.3 Solubilization and photoreduction of CO₂ in ionic liquids

All the aforementioned photocatalytic systems function using organic solvents, but in the perspective of a more environment-friendly processes these have to be replaced. Ionic liquids (ILs) have been explored as a greener alternative to molecular solvents. They possess several advantages such as negligible vapor pressure, great thermal stability, wide electrochemical stability window, tunable polarity, hydrophobicity and solvent miscibility behavior through variation of the cations and anions. Figure 2 shows the most common cations studied for CO₂ capture.⁴¹

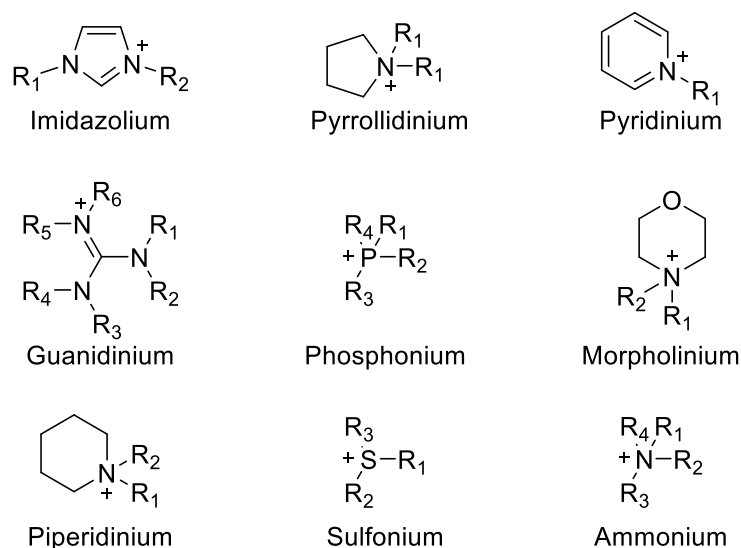


Figure 2. Commonly used cations of ILs for CO₂ capture.⁴¹

The solubility of CO₂ in ILs depends both on enthalpic and entropic effects.⁴¹ Enthalpic effects are mainly related to the interaction of CO₂ with the anion of the ILs, whereas the cation has a secondary role.⁴²⁻⁴⁴ These contributions were studied experimentally, finding that the solubility of CO₂ increases in order [NO₃]⁻ (= nitrate) < [SCN]⁻ (= thiocyanate) < [MeSO₄]⁻ (= methylsulphate) < [BF₄]⁻ (= tetrafluoroborate) < [DCA]⁻ (= dicyanoamide) < [PF₆]⁻ (= hexafluorophosphate) < [Tf₂N]⁻ (= bis(trifluoromethylsulfonyl)imide) < [Methide]⁻ (= tris(trifluoromethylsulfonyl)methide) < [C₇F₁₅CO₂]⁻ (= pentadecafluorooctanoate) (Figure 3a).^{44-45,46} Moreover, greater solubility is associated with higher number of fluorinated groups of the anion as shown in Figure 3b, with [BF₄]⁻ < [TfO]⁻ (= triflate) < [TfA]⁻ (= trifluoroacetate) < [PF₆]⁻ < [Tf₂N]⁻ < [methide]⁻ (=tris(trifluoromethylsulfonyl)methide) < [C₇F₁₅CO₂]⁻ < [eFAP]⁻ (tris(pentafluoroethyl)trifluorophosphate) < [bFAP]⁻ (tris(heptafluoropropyl)trifluorophosphate).⁴⁴⁻⁴⁵ Regarding the cation, the solubility of CO₂ increases with the increasing alkyl chain length on the imidazolium cation^{44, 47-48} (Figure 3c).⁴⁹

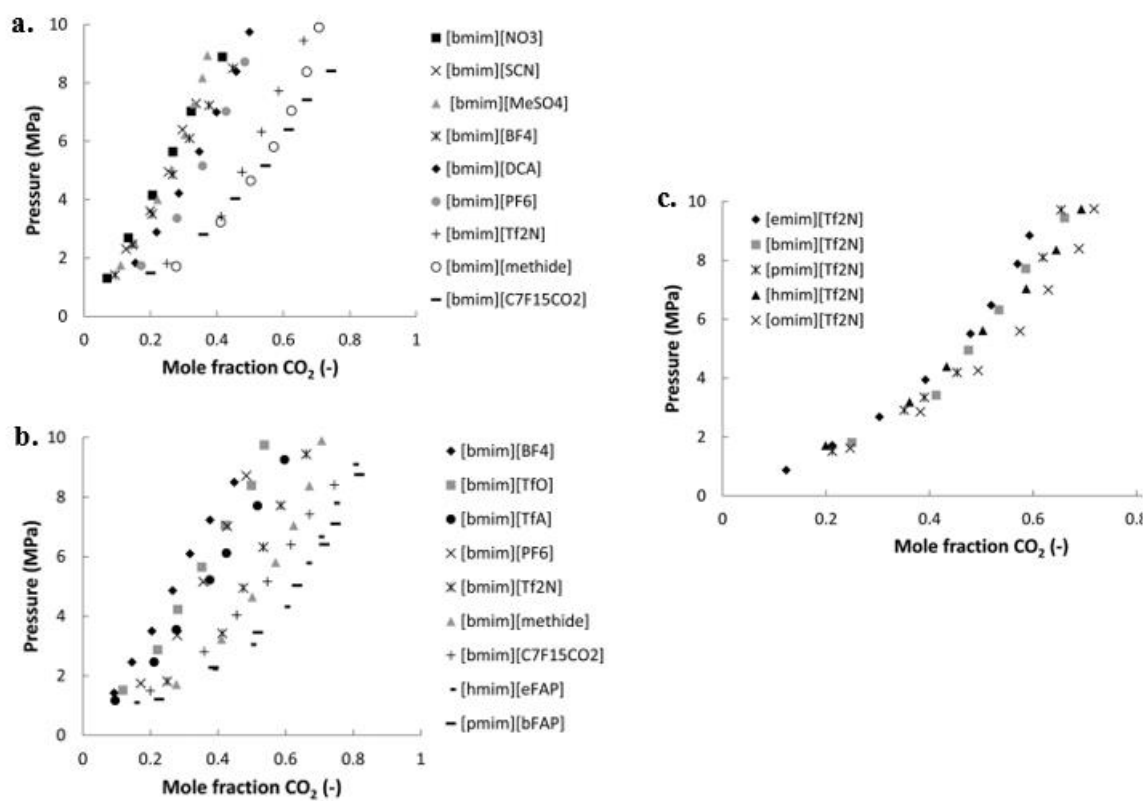


Figure 3. (a) Effect of anion on CO₂ solubility. (b) Effect of anion fluorination on CO₂ solubility. (c) Effect of alkyl chain length on CO₂ solubility.⁴¹ [emim] = 1-ethyl-3-methylimidazolium; [bmim] = 1-butyl-3-methylimidazolium; [pmim] = 1-propyl-3-methylimidazolium; [hmim] = 1-hexyl-3-methylimidazolium; [omim] = 1-octyl-3-methylimidazolium.

Recently, entropic effects were proven important for the dissolution of CO₂ in ILs and its solubility increases with increasing the ionic liquid molecular weight, molar volume and free volume (free cavities in the ILs).^{41, 50-51} For these solubilizing properties of ILs, they have been employed as reaction media in combination with heterogeneous⁵² and homogeneous⁵³ catalysts for the chemical reduction of CO₂ to CO. In addition, electrochemical reduction of CO₂ to fuels takes place in ILs due to their excellent electrochemical properties.⁵⁴⁻⁵⁹ Recently, Lin and co-workers reported the capture and activation of CO₂ to give CO by ILs coupled with photoredox catalysis using [Ru(bpy)₃]Cl₂ as PS and CoCl₂·6H₂O as catalyst.⁶⁰ The structures of the cations and anions of the imidazolium ILs had considerable effects on the

activation and reduction of CO₂ (Table 2). Better performances were obtained with [Tf₂N] and BF₄ as anions because the related IL has low viscosity, thus favoring the reaction kinetics.⁶¹ Decreased yields were correlated with ILs possessing longer chain lengths in their cation which shows an opposite trend respect to the previous studies regarding the sole solubility of CO₂ in ILs that states that longer chains show better solubility of the gas due to increased van der Waals interactions.⁴⁹ However, Wang and co-workers attributed this contradictory behavior to the higher molecular weights of the ILs that augment viscosity and steric hindrance, leading to low reactivity.⁶⁰

Table 2. The effect of various ILs on the photocatalytic conversion of CO₂ to CO.

| IL | CO/ μ mol | H ₂ / μ mol | CO + H ₂ / μ mol | Sel./% |
|----------------------------|---------------|----------------------------|---------------------------------|--------|
| [emim][Tf ₂ N] | 34.7 | 10.9 | 45.6 | 76.1 |
| [emim][l-l] | 3.7 | 1.1 | 4.8 | 77.1 |
| [emim][OTf] | 0.4 | 0.1 | 0.5 | 80.0 |
| [emim][ac] | n.d | n.d | / | / |
| [emim][dca] | 0.1 | 0.2 | 0.3 | 33.3 |
| [emim][BF ₄] | 31.0 | 4.1 | 35.1 | 88.3 |
| [bmim][BF ₄] | 28.0 | 1.6 | 29.6 | 94.6 |
| [hmim][BF ₄] | 13.1 | 0.5 | 13.6 | 96.3 |
| [omim][BF ₄] | 6.8 | 0.3 | 7.1 | 95.8 |
| [bdimim][BF ₄] | 13.7 | 1.1 | 14.8 | 92.3 |

Reaction conditions: IL (3.6 mL), H₂O (1.2 mL), CO₂ (1 atm), [Ru(bpy)₃]Cl₂ (7.8 mg), CoCl₂·6H₂O (1 mmol), TEOA (1.2 mL), $\lambda > 420$ nm, 30 °C, 2 h. [l-l] = 2-hydroxypropanoate, [ac] = acetate, [bdimim] = 1,2-methyl-3-butyylimidazolium.⁶⁰

4.2 Justification and project aims

Increasing of atmospheric levels of CO₂ is a worrying problem society is facing. Climate change has been well debated not only scientifically but also politically. It is known that the earth temperature is rising due to greenhouse gasses (GHGs) and it brings severe consequences for humanity. The global surface temperatures have already risen by 0.9 °C between 1880 and 2015.⁶² It has been stated that if society does not address the mitigation of such effects, by 2100 the global surface temperature could increase in a range from 1.4 °C to 5.8 °C compared to 1900.⁶³ The impacts of climate change should not be ignored and there are some devastating consequences for our planet such as rise of sea levels, change of weather patterns, extreme weather, and effects on human societies notably due to detrimental effects on global food production leading to political instability, security risks, human health risks and detrimental effects for wildlife and ecosystems.⁶⁴ Carbon dioxide constitutes 81% of the total amount of GHGs⁶⁵. Utilization of CO₂ captured from emissions is therefore mandatory to mitigate its negative effects on the atmosphere envisioning it as carbon source replacing fossil fuels.⁶⁶ The reduction of CO₂ to CO, generating an energy-rich commodity chemical is one of the strategies for CO₂ valorization.⁶⁷⁻⁶⁸

Energy utilization plays also a crucial role in the development of sustainable catalytic processes. Solar power is a sustainable source of energy. The amount of energy it provides our planet in one hour is the equivalent our humanity could spend in a year.⁶⁹ For the effective use of solar energy it is important to consider the alternatives to not only store but also deliver energy according to the demand. Low-cost storage methodologies covering variable atmospheric conditions are required in order to use solar energy as primary energy supply.⁷⁰ A feasible approach towards this direction is the development and optimization of photocatalytic processes that enable chemical transformations by the use of photonic energy as driving force.⁷¹

Combination of energy and CO₂ utilization towards catalytic sustainable approaches was the inspiration for this chapter. The search for photocatalytic systems that convert carbon dioxide to more valuable chemicals is an area of great interest. In this field transition metal complexes have been studied where Re,^{33, 35, 72-73} Ir²⁰⁻²² and Ru⁷⁴⁻⁷⁶ are known for being selective. Solving the problem of using expensive and less friendly transition metals, Beller and co-

workers developed a system based on the earth abundant, less toxic copper metal bearing bathocuproine and xantphos as ligands. Additionally, it was demonstrated to be a novel selective system for the visible-light-driven reduction of CO₂ to CO (Section 2.1.2.1).³⁸ Selective processes towards the production of CO from CO₂ are challenging since numerous by-products can be generated.⁷⁷ The reduction of CO₂ is also in competition with hydrogen formation, a process that usually requires less negative potentials, and therefore is difficult to avoid.⁷⁸⁻⁷⁹ Lastly, we were interested in the use of ionic liquids as an alternative for traditional molecular solvents. They exhibit incomparable features that make them the ideal reaction media for many applications. The substitution of volatile solvents hampers solvent losses to the atmosphere⁸⁰⁻⁸¹ or contamination of the final product.

This chapter shows the photocatalytic reduction of CO₂ to CO in ionic liquid media by well-defined earth-abundant metal complexes. Here, we have integrated the key points for sustainable catalytic methodologies combining a visible-light driven process in ionic liquids for the valorization of CO₂. We showcase the performance of ionic complexes in ionic liquid media for catalytic applications as well as the result from a rationally designed ion-tagged complex.

4.3 Results and discussion

4.3.1 Synthesis and characterization of complexes

4.3.1.1 Synthesis

The following compounds: Knölker complex,⁸² [Cu(bcp)(xantphos)]PF₆ (bcp: bathocuproine)⁸³ and BIH (dimethylphenylbenzimidazoline)⁸⁴ were prepared according to literature procedures. These compounds were provided for the project by the group of Professor. Matthias Beller/Dr. Henrick Junge. The imidazolium-tagged ligand for the preparation of complex **3** was synthesized according to the corresponding procedure (Chapter III, section 3.3.1). The complexes studied in this chapter are depicted in Figure 4.

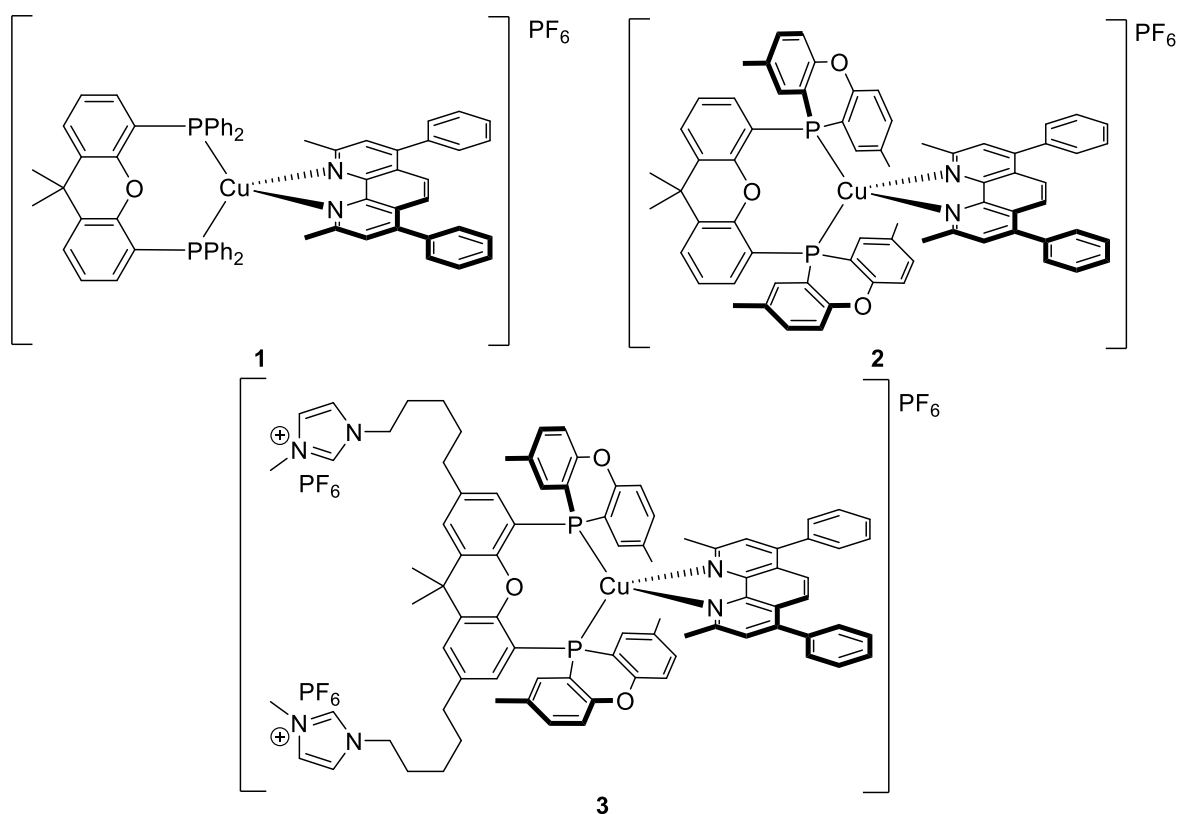


Figure 4. Heteroleptic complexes **1,2,3**. Complex **1**: [Cu(bcp)(xantphos)]PF₆. Complex **2**: [Cu(bcp)(POP-xantphos)]PF₆; POP-xantphos 4,5-bis(2,8-dimethyl-10-phenoxaphosphino)-9,9-dimethylxanthene. Complex **3**: [Cu(bcp)(Imidazolium-tagged POP-xantphos)]PF₆, Imidazolium-tagged POP-xantphos: 2,7-bis(5-(3-methylimidazolium)pentyl)-9,9-dimethyl-4,5-bis(2,8-dimethyl-10-phenoxaphosphino)xanthene hexafluorophosphate.

Initially, the synthesis of copper complexes to be used as photosensitizers in comparison with the reported [Cu(xantphos)(bcp)]PF₆ **1** was assessed. A more rigid and sterically demanding ligand was used to form complex **2** as its similar analogue POP-thixantphos has been reported to give exceptional performance in photocatalytic applications.⁸⁵ Complex **2** was successfully synthesized by reaction of 4,5-bis(2,8-dimethyl-10-phenoxaphosphino)-9,9-dimethylxanthene (POP-xantphos) with the metal precursor copper(I) tetrakis(acetonitrile) hexafluorophosphate in CH₂Cl₂, followed by the addition of the bathocuproine ligand. The complex is stable in solution, allowing its full characterization.

Complex **3** was introduced in this study due to the expected higher solubility of ionic-tagged complexes in ionic liquids, as well as to potentially achieve catalyst recovery. Complex **3** decomposes rapidly in solution in a wide range of molecular solvents, which made its characterization very challenging. Complex **3** could be only identified by HRMS, ³¹P NMR spectroscopy and electrochemistry due to its low solubility and stability.

The ³¹P NMR spectrum of **2** present two peaks belonging to the phosphorous atom of the ligand (broad singlet at 53.46 ppm) and to the PF₆ anion (septet at -144.53 ppm with $J = 710.1$ Hz). Comparable chemical shifts were observed for the ³¹P signals in **3** (broad singlet at -52.90 ppm and multiplet -144.50). No additional spectroscopic data of **3** were obtained due to its low solubility and stability in common deuterated solvents. On the other hand, ¹H NMR spectrum of **2** shows three singlet signals in the aliphatic region belonging to the methyl groups of dmp (2.25 ppm), POP (1.98 ppm) and xantphos (1.78 ppm). The ¹⁹F NMR spectrum of the PF₆ anion shows a doublet at -73.64 ppm with coupling constant $J = 710.1$ Hz.

4.3.1.2 Electrochemical and photophysical characterization of complexes

The solution absorption spectra of all three complexes (Figure 5) show intense absorption bands below 330 nm that can be assigned to ligand based transitions. Complexes **2** and **3** show the same absorption profile whereas the absorption profile of **1** is slightly different which is attributed to the different nature of the P[^]P chelating ligand. The broad absorption at around 395 nm arises from a metal to ligand charge transfer transition (MLCT) and is characteristic for this type of heteroleptic [Cu(P[^]P)(N[^]N)]⁺ complexes.⁸⁶ Upon excitation in the MLCT band all three compounds exhibit a broad unstructured emission (Figure 6). It is

noteworthy that **2** and **3** show almost the same emission maxima (539 and 541 nm respectively) whereas the emission of **1** is red-shifted by around 15 nm. We propose that this feature is related to the higher steric demand of the phosphine ligand used for the formation of **2** and **3**. The POP-xantphos ligand is less flexible than xantphos and therefore imposes greater steric bulk around the copper(I) center. After excitation in the MLCT band, copper is formally oxidized to copper(II), which prefers a square planar geometry. Steric hindrance restricts the geometry change and preserves the tetrahedral geometry upon excitation.⁸⁷

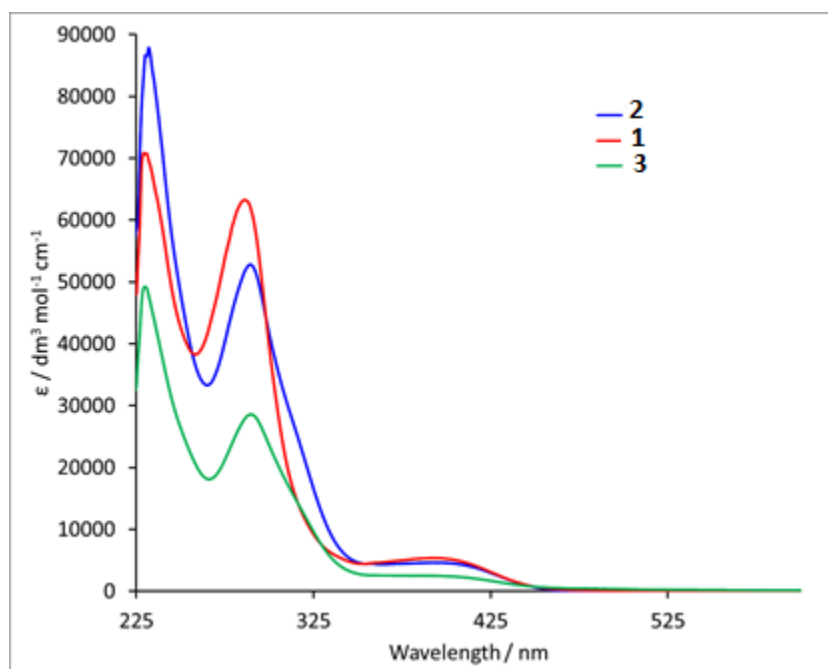


Figure 5: Solution absorption spectra of complexes **1**, **2** and **3** (CH₂Cl₂, 2.5 × 10⁻⁵ mol dm⁻³).

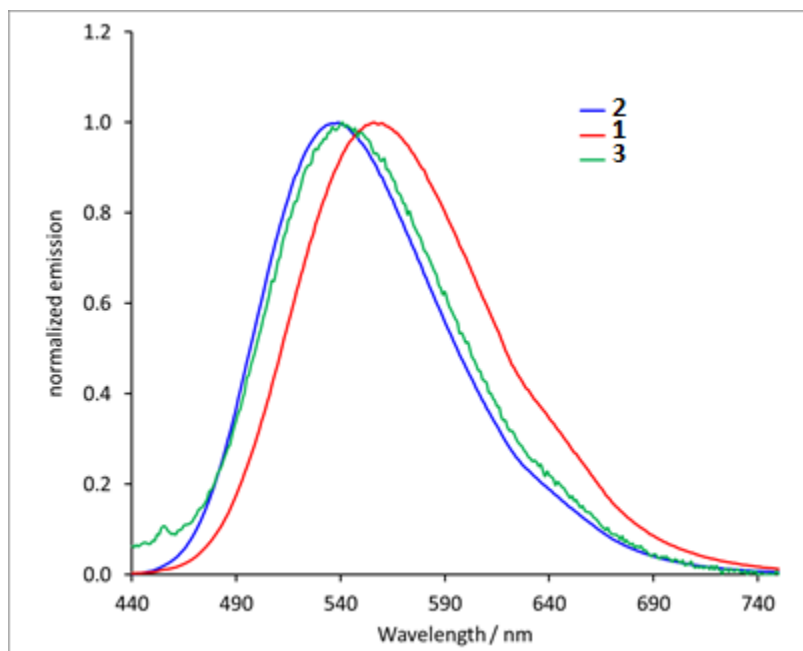


Figure 6: Normalized emission spectra of copper(I) complexes **1**, **2** and **3** ($\lambda_{\text{exc}} = 400$ nm, degassed CH₂Cl₂, 2.5×10^{-5} mol dm⁻³).

Complexes **1** and **2** show high photo luminescence quantum yields (PLQY) in deaerated solution (39.8 and 38.0%) and excited state lifetimes of 9.42 and 7.24 μs respectively. In contrast, complex **3** exhibits a lower PLQY of 9.9 % and an excited state lifetime of 3.43 μs . This drop in emission performance of **3** could be attributed to the presence of imidazolium moieties that facilitate non radiative decay pathways and therefore lower the PLQY. For all compounds, the PLQY and excited state lifetimes are shorter in aerated than deaerated solutions (Table 3).

Table 3: Photophysical properties of the complexes in CH₂Cl₂ solution at a concentration of 2.5×10^{-5} mol dm⁻³ excited at $\lambda_{\text{exc}} = 365$ nm.

| Complex | UV-Vis MLCT $\lambda_{\text{abs}}/\text{nm}$ | $\lambda_{\text{em}}/\text{nm}$ | PLQY (non- degassed/degassed ^a)% | $\tau_{1/2}$ (non- degassed/degassed ^a)/ μs |
|----------|--|---------------------------------|---|---|
| 1 | 393 | 555 | 1.1/38.0 | 0.338/7.24 |
| 2 | 398 | 539 | 1.3/39.8 | 0.446/9.42 |
| 3 | 395 | 541 | 1.5/9.9 | 0.373/3.43 |

^aDegassed by bubbling nitrogen stream through the solution for 20 min.

Redox potentials are summarized in Table 4. The three complexes **1**, **2** and **3** show quasi-reversible oxidations at 0.86, 0.83 and 0.79 V respectively. This signal can be assigned to a copper based oxidation. Additionally, **2** and **1** show a quasi-reversible reduction signal at –2.10 and –2.11 V respectively. In the case of **3** there is an irreversible reduction process observed at –1.98 V. Due to the low solubility of **3** in CH₂Cl₂, all electrochemical signals are very weak for this compound. It is noteworthy that **1** and **2** behave similarly in terms of oxidation and reduction potential. On the other hand, **3** shows a copper oxidation signal at significantly lower potential and an irreversible reduction at less negative potential (–1.98 V). This process probably relates to an imidazolium reduction, since it is not present in the case of **1** and **2**. Further analysis is needed to investigate the origin of this signal and its influence.

Table 4: Cyclic voltammetry data for copper(I) complexes referenced to internal Fc/Fc⁺ = 0 V; degassed HPLC grade CH₂Cl₂ solution with [nBu₄N][PF₆] as supporting electrolyte and a scan rate of 100 mV s^{–1}. Processes are quasi reversible unless otherwise stated (ir = irreversible).

| Complex | E ^{ox} _{1/2} /V (E _{pc} – E _{pa} /mV) | E ^{red} _{pa} /V | E ^{red} _{1/2} /V (E _{pa} – E _{pc} /mV) |
|----------|---|-----------------------------------|--|
| 1 | 0.86 (81) | | –2.11 (154) |
| 2 | 0.83 (72) | | –2.10 (127) |
| 3 | 0.79 (68) | –1.98 ^{ir} | |

Excited state redox potentials are calculated according to formulas (1) and (2)⁸⁸ and the results are summarized in Table 5 where E₀₀ is the (non-observable) energy difference between the lowest vibrational level of the electronic ground and electronic excited states and E_{ox}^{1/2} and E_{red}^{1/2} are the copper based oxidation and ligand based reduction potentials (Table 5). E₀₀ is estimated from the solution emission onset (5 % emission intensity) at room temperature. Note that for **3** a non-reversible ligand based reduction was observed and therefore no excited state reduction potential could be obtained.

$$E^*_{ox} = E_{ox}^{1/2} - E_{00} \quad (1)$$

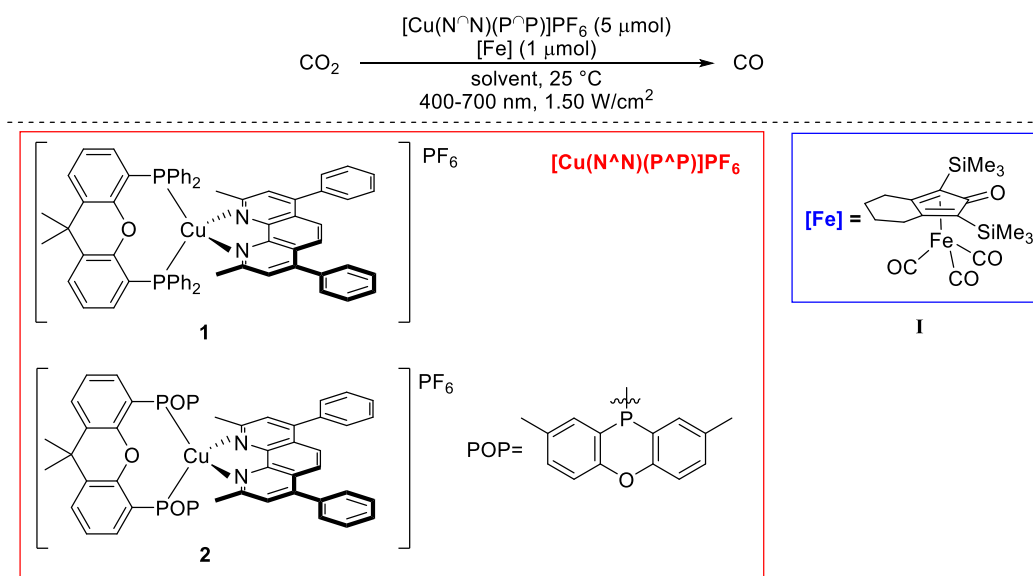
$$E^*_{red} = E_{red}^{1/2} + E_{00} \quad (2)$$

Table 5: Excited state redox potentials.

| Complex | E^*_{ox}/V | $E^*_{\text{red}}/\text{V}$ | E_{00}/eV |
|----------|----------------------------|-----------------------------|--------------------|
| 1 | −1.77 | 0.52 | 2.63 |
| 2 | −1.84 | 0.57 | 2.67 |
| 3 | −1.97 | - | 2.75 |

Electrochemical and photophysical characterization was performed and analyzed by Fabian Brunner from Professors Catherine Housecroft and Edwin Constable group at the University of Basel, Switzerland.

4.3.2 Photocatalysis

**Scheme 2.** Photocatalytic CO₂ reduction using [Cu(N[∧]N)(P[∧]P)]PF₆ as photosensitizers.

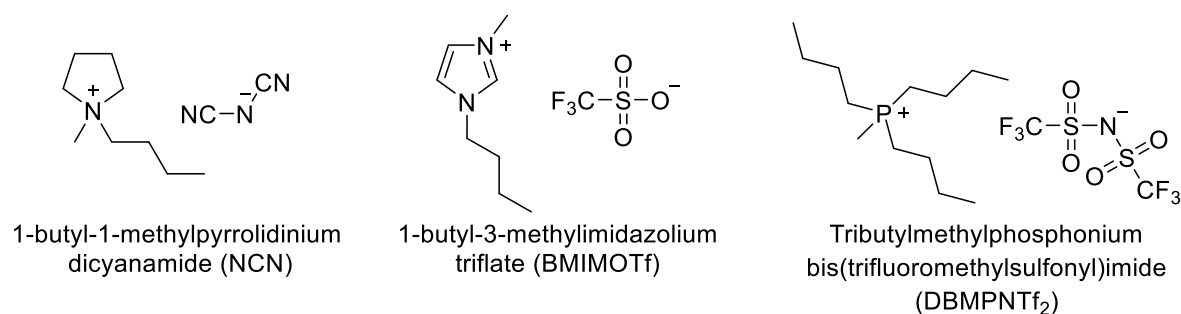
Our investigation started using the well-defined photosensitizers **1** and **2** in combination with the iron catalyst **I** and N-methyl-2-pyrrolidone (NMP) as molecular solvent (Scheme 2 and Table 6). Under these reaction conditions a TON (CO) of 427 was obtained with high selectivity toward CO ($\geq 98\%$) when using the well-defined PS **1** (Table 6, entry 1) in organic solvents.³⁸ A higher TON(CO) was observed when using **2**, despite a marginal decrease in selectivity (Table 6, entry 2).

Table 6. Iron photocatalyzed CO₂ reduction with [Cu(N[∧]N)(P[∧]P)]PF₆ complexes as PS in molecular solvent systems.

| Entry | Complex | Solvent | TON (CO) | TON (H ₂) | Selectivity [%] |
|-------|----------|---------------------|----------|-----------------------|-----------------|
| 1 | 1 | NMP/TEOA (5:1, v:v) | 427 | 5 | ≥ 98 |
| 2 | 2 | NMP/TEOA (5:1, v:v) | 508 | 23 | ≥ 95 |

Reaction conditions: [Fe] (1 μmol), [Cu(N[∧]N)(P[∧]P)]PF₆ (5 μmol), BIH (150 mg) and TEOA (1.25 mL) were illuminated at 400-700 nm (1.50 W) in 6.25 mL of solvent for 5 h. Results presented are the averages of reactions carried out in duplicate.

The CuPS/Fe systems were then tested using different ionic liquids as solvent (Table 7) in order to ascertain the impact of the latter on the catalytic performances. Interestingly, the activity and selectivity of the system was highly dependent on the ionic liquid used. A significant increase in selectivity was obtained using 1-butyl-1-methylpyrrolidinium dicyanamide (NCN) (Table 7, entries 1 and 2) compared to 1-butyl-3-methylimidazolium triflate (BMIMOTf) (Table 7, entries 3 and 4), independently from the CuPS used. In particular, almost equal TON(CO) and TON(H₂) were observed for **2** in BMIMOTf as solvent (Table 7, entry 3) and a significant overproduction of hydrogen was observed when **1** in BMIMOTf was used (Table 7, entry 4). This unwanted selectivity to hydrogen formation was even more pronounced when using **1** in DBMPNTf₂ (tributylmethylphosphonium bis(trifluoromethylsulfonyl)imide) (Table 7, entry 5). In summary, NCN was found to be the most suitable IL to selectively produce CO and **1** was identified as the best photosensitizer both in term of activity (TON(CO) = 80) and selectivity ($\geq 96\%$). Importantly the *in-situ* formation of the CuPS is ineffective when using ILs as solvents (Table 7, entry 6), in contrast to the catalytic outcome noticed in molecular solvents. Finally, the production of CO varies only marginally when the reaction time was increased from 5 h to 15 h which shows the catalyst is not active over longer reaction times (Table 7, entry 7).

Table 7 Iron photocatalyzed CO₂ reduction with [Cu(N[^]N)(P[^]P)]PF₆ complexes as PS in different ionic liquids.

| Entry | Complex | Solvent | TON (CO) | TON (H ₂) | Selectivity [%] |
|----------------|----------|---------------------------------------|-------------|--------------------------|--------------------|
| 1 | 2 | NCN/TEOA(4:1, v:v) | 32 | <3 | ≥91 |
| 2 | 1 | NCN/TEOA(4:1, v:v) | 80 | <3 | ≥96 |
| 3 | 2 | BMIMOTf/TEOA (4:1, v:v) | 174 | 171 | 50 |
| 4 | 1 | BMIMOTf/TEOA (4:1, v:v) | 63 | 124 | 33 |
| 5 | 1 | DBMPNTf ₂ /TEOA (4:1, v:v) | 63 | 274 | 19 |
| 6 ^a | 1 | NCN/TEOA (4:1, v:v) | 4 | <3 | ≥57 |
| 7 ^b | 1 | NCN/TEOA (4:1, v:v) | 82 | <3 | ≥96 |

Reaction conditions: [Fe] (1 μmol), [Cu(N[^]N)(P[^]P)]PF₆ (5.0 μmol), BIH (150 mg) and TEOA (1.5 mL) were illuminated at 400-700 nm (1.50 W) in 6.0 mL of solvent for 5 h. ^aAn *In situ* CuPS system consisting of [Cu(CH₃CN)₄]PF₆ (5.0 μmol), bathocuproine (5.1 μmol) and xantphos (15 μmol) has been utilized. ^b[Cu(N[^]N)(P[^]P)]PF₆ (5.2 μmol) and 15 h of reaction time were used. Results presented are the averages of reactions carried out in duplicate.

The only system described in the literature that reduces CO₂ to CO in pure ionic liquid is based on *fac*-ReCl(bpy)(CO)₃ and 1-methylpyrrolidinium tetracyanoborate ([bmpyrr][TCB]), using supercritical scCO₂ where CO₂ acts as both a solvent and reactant in order to avoid substrate solubility problems. The system showed a dramatically lower TON between 0.7 and 5 when compared with ours.⁸⁹ Moreover, the use of ionic liquid in combination with molecular solvent was reported to enhance the intrinsic activity of a

photocatalytic system based on [Ru(bpy)₃Cl₂] as photosensitizer and CoCl₂·6H₂O as catalyst. The chosen ionic liquid was 1-ethyl-3-methylimidazolium bis(trifluoromethylsulfonyl)imide ([Emim][NTf₂]), obtaining a TON(CO) of 34.7 and selectivity of 76 %, using water in the reaction mixture. Both values are lower than the ones achieved with our system.⁶⁰ Unfortunately, the authors do not report the activity in pure ionic liquid. At this stage of investigation, it is too speculative to propose the reasons for this huge improvement of our catalytic system compared to the reported ones, which is most likely a combination of both catalyst and ionic liquid choice. Nevertheless, it is already a competitive system with respect to the reported ones not only because of the performances, but also for the use of complexes based on the economical and abundant copper and iron complexes.

Control experiments were performed in order to confirm the necessity of all the components used in the aforementioned protocol (Table 8). First, irradiating the sole ionic liquid in the presence of CO₂ produced only traces of CO and H₂ (Table 8, entries 1 and 2). Similar results were obtained using either only **I** (Table 8, entry 3) or CuPS (Table 8, entry 4). Therefore, all the components need to be present in order to effectively convert CO₂, which does not proceed in the absence of light, confirming its photochemical nature (Table 8, entry 5). Finally, replacing CO₂ with argon atmosphere did not yield CO at the end of the reaction (Table 8, entry 6) proving this methodology forms CO from CO₂ and not from decomposition of the catalyst or other components of the reaction system.

Table 8. Blank reactions for evaluation of the necessity of the components of the catalytic system.

| Entry | [Fe] [μmol] | [CuPS] [μmol] | TON (CO) | TON (H ₂) | Selectivity [%] |
|----------------|--------------------------|----------------------------|----------|-----------------------|-----------------|
| 1 ^a | - | - | <1 | <3 | / |
| 2 | - | - | <1 | <3 | / |
| 3 | 1 | - | <1 | <3 | / |
| 4 | - | 5 | <1 | <3 | / |
| 5 ^b | 1 | 5 | <1 | <3 | / |
| 6 ^c | 1 | 5 | <1 | <3 | / |

Reaction conditions: [Fe] (1 μmol), **1** [Cu(N[^]N)(P[^]P)]PF₆ (5 μmol), BIH (150 mg) and TEOA (1.5 mL) were illuminated at 400-700 nm (1.50 W) in 6.0 mL of 1-Butyl-1-methylpyrrolidinium dicyanamide for 5 h. ^a1-Butyl-3-methylimidazolium triflate (6.0 mL) was applied as the solvent. ^bReaction conducted in the absence of light. ^cReaction performed under an atmosphere of argon. Results presented are the averages of reactions carried out in duplicate.

When complex **3** was used a lower TON of 27 was obtained compared to **2** (TON 32). It was observed from the electrochemical and photophysical characterization that the interference of the imidazolium tags affected the emission properties of the complex compared to the original ligand **2**. As expected, the PS bearing the functionalized 4,5-bis(2,8-dimethyl-10-phenoxaphosphino)-9,9-dimethylxanthene (imidazolium-tagged POP-xantphos) ligand **3** solubilized in the ionic liquid faster compared to **1** and **2** but its performance was poorer in the photocatalytic reaction. Complex **3** exhibited a major drawback, its extreme instability in organic solvents affected the potential recyclability of this particular photosensitizer discarding the required liquid-liquid extractions. We found that ionic unmodified complexes perform better overall and are significantly easier to prepare and handle. This finding suggests the imidazolium tag modification is not favourable for application in our specific photocatalytic system.

Complex **1** showed high solubility in the ionic liquid of choice and when the reaction mixture was washed with organic solvents in order to recycle the ionic liquid, it remained in the IL reaction media. It was the goal we had when applying the imidazolium-tagged complex in this reaction. Unfortunately, the complexes were deactivated after five hours reaction time and its removal from the ionic liquid was not successful. Recyclability of the ionic liquid and the photosensitizer was not achieved. More stable systems under the operating conditions are needed to enable efficient recycling.

4.3.3 High-purity conditions

High-purity experiments were carried out and analyzed at Leibniz Institute for Catalysis (LIKAT) by Dr. Nikolaos Moustakas from Dr. Jennifer Strunk group. Since CO₂ is a thermodynamically highly stable molecule,⁹⁰ it is expected that many other carbon-containing molecules can react faster under the selected experimental conditions. Therefore, it is very important for CO₂ reduction experiments to verify that neither hydrocarbons nor CO are produced from the catalyst, reaction media or any other C-containing impurities that could be present in the reaction chamber. If such outcomes are not analyzed carefully, the photocatalytic efficiency of the tested sample can be overestimated leading to altered conclusions.⁹¹⁻⁹²

The true formation of products from CO₂ as carbon source can be evidenced by the analysis of product formation in a blank experiment in the absence of this gas. Under identical reaction conditions CO₂ is replaced by an inert gas and the chromatogram is analyzed in order to identify possible catalyst decomposition, solvent or any other impurities present in the reaction set up.⁹³ Extensive baseline measurements without the presence of CO₂ should take place to determine that the production of hydrocarbons comes from the substrate and not from other potential sources of carbon that take place during the experiment.

4.3.3.1 CO₂ reduction to CO

The reaction chamber was flushed with CO₂ for one hour before it was filled up to final pressure of 1500 mbar. The sample was irradiated with the 200 W Hg/Xe lamp equipped with a 420 nm cut-off filter and a chromatogram was collected every 45 minutes for a total of six hours (Experimental set up, Chapter V/Figure 11-12). The sample did not decompose under the blank experiments meaning that the production of CO comes from CO₂.

High concentration of oxygen was identified when handling the sample into the reactor under helium atmosphere which is the conventional gas for these experiments. Oxygen was not previously observed under argon conditions because of the similar retention compared to argon. Even though oxygen was present, the catalytic system performed and CO was observed but in significantly lower concentration compared to our previously optimized conditions in batch reactors (Section 4.3.2). Further experiments with proper manipulation of the sample under inert conditions are recommended where helium is used as the baseline inert gas to ensure that no oxygen is present (avoiding the interference with the argon peak). The CO concentration over the six hours of the photocatalytic reduction of CO₂ to CO in ILs is presented in Figure 7. This experiment shows conversions not much higher than stoichiometric product formation. Further optimization of the reaction set up is needed and the respective experiments are undergoing in the laboratories of Dr. Jennifer Strunk to apply high purity conditions for our data analysis using complex **1** which was found to be the best candidate for this photocatalytic application. Oxygen is the current interference for product analysis and catalytic performance.

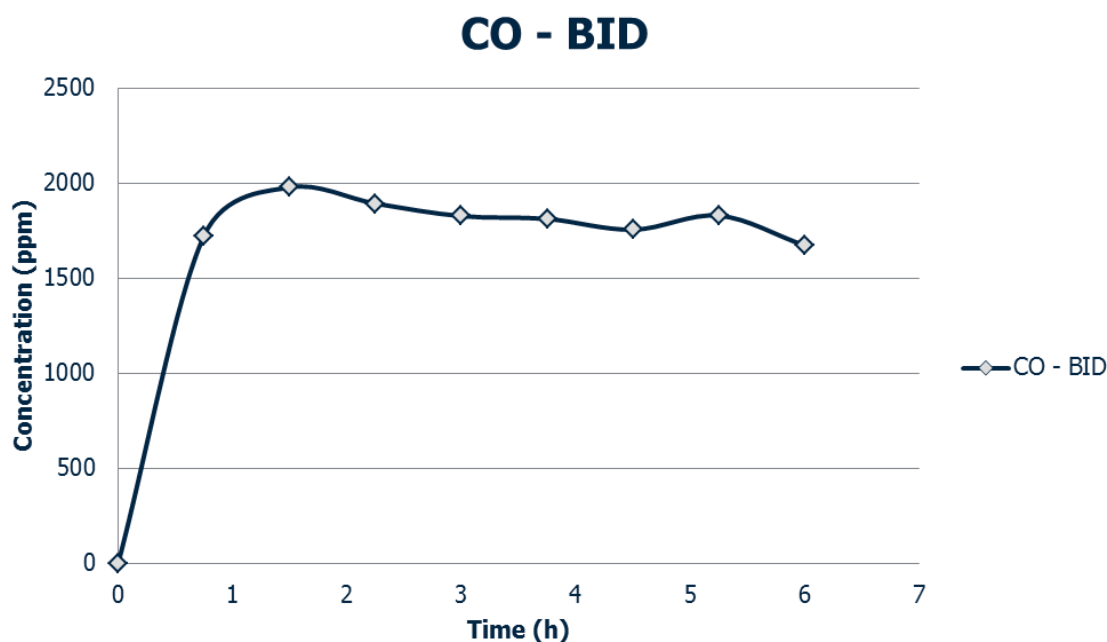


Figure 7. CO concentration over the 6 hours of the iron photocatalyzed CO₂ reduction with [Cu(N[^]N)(P[^]P)]PF₆ complexes as PS. PS: complex **2**.

4.4 Conclusions

Ionic liquids proved to be suitable solvents for the photocatalytic CO₂ reduction to CO using a reported system based on a copper photosensitizer and an iron catalyst. High selectivity for CO and moderate turnover numbers were achieved. Overall our results show that we have developed a superior system over those reported with rhenium⁸⁹ or ruthenium-cobalt⁶⁰ systems in ionic liquid media for the same reaction using unmodified xantphos as ligand.

Introduction of imidazolium tags in the xantphos ligands proved to be a disadvantageous strategy for this specific photocatalytic application under our reaction conditions. Photophysical properties of the resulting complex were dramatically affected by the imidazolium ring, as compared to unmodified ligands, and as a result the catalytic performance was poorer. In addition, despite its greater solubility in ionic liquid media, the stability of the complex was found to be low and catalyst recovery could not be performed after the catalytic experiments, disqualifying it as a viable candidate for further development.

4.5 References

1. Globally averaged marine surface annual mean expressed as a mole fraction in dry air. Earth System Research Laboratory Global Monitoring Division. Global Greenhouse Gas Reference Network. <https://www.esrl.noaa.gov/gmd/ccgg/trends/global.html>.
2. International Energy Agency (IEA), website: www.iea.org. CO₂ Emissions From Fuel Combustion Highlights. Statistics, 2017 Edition, <https://www.iea.org/publications/freepublications/publication/CO2EmissionsfromFuelCombustionHighlights2017.pdf>.
3. Aresta, M.; Dibenedetto, A.; Angelini, A. Catalysis for the Valorization of Exhaust Carbon: from CO₂ to Chemicals, Materials, and Fuels. Technological Use of CO₂. *Chem. Rev.* **2014**, *114* (3), 1709-1742.
4. Global CCS Institute, Accelerating the Uptake of CCS: Industrial Use of Captured Carbon Dioxide. March 2011, Parsons Brinckerhoff. <https://hub.globalccsinstitute.com/sites/default/files/publications/14026/accelerating-uptake-ccs-industrial-use-captured-carbon-dioxide.pdf>.
5. Schmitt, R.; Burkard, B. Naphtholcarboxylic acids. *Chem. Ber.* **1877**, *20*, 2699-2704.
6. Martin, C.; Fiorani, G.; Kleij, A. W. Recent Advances in the Catalytic Preparation of Cyclic Organic Carbonates. *ACS Catal.* **2015**, *5* (2), 1353-1370.
7. Belli Dell'Amico, D.; Calderazzo, F.; Labella, L.; Marchetti, F.; Pampaloni, G. Converting Carbon Dioxide into Carbamate Derivatives. *Chem. Rev.* **2003**, *103* (10), 3857-3897.
8. Won, D. I.; Lee, J. S.; Cheong, H. Y.; Cho, M.; Jung, W. J.; Son, H. J.; Pac, C.; Kang, S. O. Organic-inorganic hybrid photocatalyst for carbon dioxide reduction. *Faraday Discuss.* **2017**, *198*, 337-351.
9. Fujita, E. Photochemical carbon dioxide reduction with metal complexes. *Coord. Chem. Rev.* **1999**, *185-186*, 373-384.
10. Fujita, E.; Brunschwig, B. S. In: Catalysis of Electron Transfer, Heterogeneous and Gas-Phase Systems. ed Balzani V Wiley-VCH. **2001**, Vol 4, 88-126.
11. Morris, A. J.; Meyer, G. J.; Fujita, E. Molecular Approaches to the Photocatalytic Reduction of Carbon Dioxide for Solar Fuels. *Acc. Chem. Res.* **2009**, *42* (12), 1983-1994.
12. Grodkowski, J.; Neta, P.; Fujita, E.; Mahammed, A.; Simkhovich, L.; Gross, Z. Reduction of Cobalt and Iron Corroles and Catalyzed Reduction of CO₂. *J. Phys. Chem. A* **2002**, *106* (18), 4772-4778.
13. Grodkowski, J.; Neta, P. Cobalt Corrin Catalyzed Photoreduction of CO₂. *J. Phys. Chem. A* **2000**, *104* (9), 1848-1853.
14. Grodkowski, J.; Dhanasekaran, T.; Neta, P.; Hambright, P.; Brunschwig, B. S.; Shinozaki, K.; Fujita, E. Reduction of Cobalt and Iron Phthalocyanines and the Role of the Reduced Species in Catalyzed Photoreduction of CO₂. *J. Phys. Chem. A* **2000**, *104* (48), 11332-11339.
15. Behar, D.; Dhanasekaran, T.; Neta, P.; Hosten, C. M.; Ejeh, D.; Hambright, P.; Fujita, E. Cobalt Porphyrin Catalyzed Reduction of CO₂. Radiation Chemical, Photochemical, and Electrochemical Studies. *J. Phys. Chem. A* **1998**, *102* (17), 2870-2877.
16. Grodkowski, J.; Behar, D.; Neta, P.; Hambright, P. Iron Porphyrin-Catalyzed Reduction of CO₂. Photochemical and Radiation Chemical Studies. *J. Phys. Chem. A* **1997**, *101* (3), 248-254.

17. Takeda, H.; Koike, K.; Inoue, H.; Ishitani, O. Development of an Efficient Photocatalytic System for CO₂ Reduction Using Rhenium(I) Complexes Based on Mechanistic Studies. *J. Am. Chem. Soc.* **2008**, *130* (6), 2023-2031.
18. Liu, C.; Dubois, K. D.; Louis, M. E.; Vorushilov, A. S.; Li, G. Photocatalytic CO₂ Reduction and Surface Immobilization of a Tricarbonyl Re(I) Compound Modified with Amide Groups. *ACS Catal.* **2013**, *3* (4), 655-662.
19. Hawecker, J.; Lehn, J. M.; Ziessel, R. Photochemical and electrochemical reduction of carbon dioxide to carbon monoxide mediated by (2,2'-bipyridine)tricarbonylchlororhenium(I) and related complexes as homogeneous catalysts. *Helv. Chim. Acta.* **1986**, *69* (8), 1990-2012.
20. Sato, S.; Morikawa, T.; Kajino, T.; Ishitani, O. A Highly Efficient Mononuclear Iridium Complex Photocatalyst for CO₂ Reduction under Visible Light. *Angew. Chem. Int. Ed.* **2013**, *52* (3), 988-992.
21. Reithmeier, R. O.; Meister, S.; Rieger, B.; Siebel, A.; Tschurl, M.; Heiz, U.; Herdtweck, E. Mono- and bimetallic Ir(III) based catalysts for the homogeneous photocatalytic reduction of CO₂ under visible light irradiation. New insights into catalyst deactivation. *Dalton Trans.* **2014**, *43* (35), 13259-13269.
22. Reithmeier, R. O.; Meister, S.; Siebel, A.; Rieger, B. Synthesis and characterization of a trinuclear iridium(III) based catalyst for the photocatalytic reduction of CO₂. *Dalton Trans.* **2015**, *44* (14), 6466-6472.
23. Whitten, D. G. Photoinduced electron transfer reactions of metal complexes in solution. *Acc. Chem. Res.* **1980**, *13* (3), 83-90.
24. Guo, Z.; Cheng, S.; Cometto, C.; Anxolabehere-Mallart, E.; Ng, S. M.; Ko, C. C.; Liu, G.; Chen, L.; Robert, M.; Lau, T. C. Highly Efficient and Selective Photocatalytic CO₂ Reduction by Iron and Cobalt Quaterpyridine Complexes. *J. Am. Chem. Soc.* **2016**, *138* (30), 9413-9416.
25. Cheung, P. L.; Machan, C. W.; Malkhasian, A. Y. S.; Agarwal, J.; Kubiak, C. P. Photocatalytic reduction of carbon dioxide to CO and HCO₂H using fac-Mn(CN)(bpy)(CO)₃. *Inorg. Chem.* **2016**, *55* (6), 3192-3198.
26. Takeda, H.; Koizumi, H.; Okamoto, K.; Ishitani, O. Photocatalytic CO₂ reduction using a Mn complex as a catalyst. *Chem. Commun.* **2014**, *50* (12), 1491-1493.
27. Alsabeh, P. G.; Rosas-Hernandez, A.; Barsch, E.; Junge, H.; Ludwig, R.; Beller, M. Iron-catalyzed photoreduction of carbon dioxide to synthesis gas. *Catal. Sci. Technol.* **2016**, *6* (10), 3623-3630.
28. Bonin, J.; Robert, M.; Routier, M. Selective and Efficient Photocatalytic CO₂ Reduction to CO Using Visible Light and an Iron-Based Homogeneous Catalyst. *J. Am. Chem. Soc.* **2014**, *136* (48), 16768-16771.
29. Wang, F.; Cao, B.; To, W.-P.; Tse, C. W.; Li, K.; Chang, X. Y.; Zang, C.; Chan, S. L. F.; Che, C. M. The effects of chelating N₄ ligand coordination on Co(II)-catalysed photochemical conversion of CO₂ to CO: reaction mechanism and DFT calculations. *Catal. Sci. Technol.* **2016**, *6* (20), 7408-7420.
30. Chan, S. L. F.; Lam, T. L.; Yang, C.; Yan, S. C.; Cheng, N. M. A robust and efficient cobalt molecular catalyst for CO₂ reduction. *Chem. Commun.* **2015**, *51* (37), 7799-7801.
31. Thoi, V. S.; Kornienko, N.; Margarit, C. G.; Yang, P.; Chang, C. J. Visible-light photoredox catalysis: selective reduction of carbon dioxide to carbon monoxide by a nickel

- N-heterocyclic carbene-isoquinoline complex. *J. Am. Chem. Soc.* **2013**, *135* (38), 14413-14424.
32. Schneider, J.; Vuong, K. Q.; Calladine, J. A.; Sun, X. Z.; Whitwood, A. C.; George, M. W.; Perutz, R. N. Photochemistry and Photophysics of a Pd(II) Metalloporphyrin: Re(I) Tricarbonyl Bipyridine Molecular Dyad and its Activity Toward the Photoreduction of CO₂ to CO. *Inorg. Chem.* **2011**, *50* (23), 11877-11889.
33. Kato, E.; Takeda, H.; Koike, K.; Ohkubo, K.; Ishitani, O. Ru(II)-Re(I) binuclear photocatalysts connected by -CH₂XCH₂- (X = O, S, CH₂) for CO₂ reduction. *Chem. Sci.* **2015**, *6* (5), 3003-3012.
34. Nakada, A.; Koike, K.; Maeda, K.; Ishitani, O. Highly efficient visible-light-driven CO₂ reduction to CO using a Ru(II)-Re(I) supramolecular photocatalyst in an aqueous solution. *Green Chem.* **2016**, *18* (1), 139-143.
35. Sahara, G.; Ishitani, O. Efficient Photocatalysts for CO₂ Reduction. *Inorg. Chem.* **2015**, *54* (11), 5096-5104.
36. Rosas-Hernandez, A.; Alsabeh, P. G.; Barsch, E.; Junge, H.; Ludwig, R.; Beller, M. Highly active and selective photochemical reduction of CO₂ to CO using molecular-defined cyclopentadienone iron complexes. *Chem. Commun.* **2016**, *52* (54), 8393-8396.
37. Lowry, M. S.; Goldsmith, J. I.; Slinker, J. D.; Rohl, R.; Pascal, R. A.; Malliaras, G. G.; Bernhard, S. Single-Layer Electroluminescent Devices and Photoinduced Hydrogen Production from an Ionic Iridium(III) Complex. *Chem. Mater.* **2005**, *17* (23), 5712-5719.
38. Rosas-Hernandez, A.; Steinlechner, C.; Junge, H.; Beller, M. Earth-abundant photocatalytic systems for the visible-light-driven reduction of CO₂ to CO. *Green Chem.* **2017**, *19* (10), 2356-2360.
39. Rosas-Hernandez, A.; Junge, H.; Beller, M.; Roemelt, M.; Francke, R. Cyclopentadienone iron complexes as efficient and selective catalysts for the electroreduction of CO₂ to CO. *Catal. Sci. Technol.* **2017**, *7* (2), 459-465.
40. Collin, J. P.; Jouaiti, A.; Sauvage, J. P. Electrocatalytic properties of (tetraazacyclotetradecane)nickel(2+) and Ni₂(biscyclam)₄⁺ with respect to carbon dioxide and water reduction. *Inorg. Chem.* **1988**, *27* (11), 1986-1990.
41. Ramdin, M.; de Loos, T. W.; Vlucht, T. J. H. State-of-the-art of CO₂ Capture with Ionic Liquids. *Ind. Eng. Chem. Res.* **2012**, *51* (24), 8149-8177.
42. Cadena, C.; Anthony, J. L.; Shah, J. K.; Morrow, T. I.; Brennecke, J. F.; Maginn, E. J. Why Is CO₂ So Soluble in Imidazolium-Based Ionic Liquids?. *J. Am. Chem. Soc.* **2004**, *126* (16), 5300-5308.
43. Anthony, J. L.; Anderson, J. L.; Maginn, E. J.; Brennecke, J. F. Anion Effects on Gas Solubility in Ionic Liquids. *J. Phys. Chem. B* **2005**, *109* (13), 6366-6374.
44. Aki, S. N. V. K.; Mellein, B. R.; Saurer, E. M.; Brennecke, J. F. High-Pressure Phase Behavior of Carbon Dioxide with Imidazolium-Based Ionic Liquids. *J. Phys. Chem. B* **2004**, *108* (52), 20355-20365.
45. Muldoon, M. J.; Aki, S. N. V. K.; Anderson, J. L.; Dixon, J. K.; Brennecke, J. F. Improving Carbon Dioxide Solubility in Ionic Liquids. *J. Phys. Chem. B* **2007**, *111* (30), 9001-9009.
46. Kumelan, J.; Perez-Salado Kamps, A.; Tuma, D.; Maurer, G. Solubility of CO₂ in the Ionic Liquids [bmim][CH₃SO₄] and [bmim][PF₆]. *J. Chem. Eng. Data* **2006**, *51* (5), 1802-1807.

47. Carvalho, P. J.; Alvarez, V. H.; Machado, J. J. B.; Pauly, J.; Daridon, J. L.; Marrucho, I. M.; Aznar, M.; Coutinho, J. A. P. High pressure phase behavior of carbon dioxide in 1-alkyl-3-methylimidazolium bis(trifluoromethylsulfonyl)imide ionic liquids. *J. Supercrit. Fluids*. **2009**, *48* (2), 99-107.
48. Schilderman, A. M.; Raeissi, S.; Peters, C. J. Solubility of carbon dioxide in the ionic liquid 1-ethyl-3-methylimidazolium bis(trifluoromethylsulfonyl)imide. *Fluid Phase Equilibria* **2007**, *260* (1), 19-22.
49. Almantariotis, D.; Gefflaut, T.; Padua, A. A. H.; Coxam, J. Y.; Costa Gomes, M. F. Effect of Fluorination and Size of the Alkyl Side-Chain on the Solubility of Carbon Dioxide in 1-Alkyl-3-methylimidazolium Bis(trifluoromethylsulfonyl)amide Ionic Liquids. *J. Phys. Chem. B*. **2010**, *114* (10), 3608-3617.
50. Carvalho, P. J.; Coutinho, J. A. P. On the Nonideality of CO₂ Solutions in Ionic Liquids and Other Low Volatile Solvents. *J. Phys. Chem. Lett.* **2010**, *1* (4), 774-780.
51. Shannon, M. S.; Tedstone, J. M.; Danielsen, S. P. O.; Hindman, M. S.; Irvin, A. C.; Bara, J. E. Free Volume as the Basis of Gas Solubility and Selectivity in Imidazolium-Based Ionic Liquids. *Ind. Eng. Chem. Res.* **2012**, *51* (15), 5565-5576.
52. Wang, W.; Wang, S.; Ma, X.; Gong, J. Recent advances in catalytic hydrogenation of carbon dioxide. *Chem. Soc. Rev.* **2011**, *40* (7), 3703-3727.
53. Wang, S.; Wang, X. Imidazolium Ionic Liquids, Imidazolylidene Heterocyclic Carbenes, and Zeolitic Imidazolate Frameworks for CO₂ Capture and Photochemical Reduction. *Angew. Chem. Int. Ed.* **2016**, *55* (7), 2308-2320.
54. Rosen, B. A.; Zhu, W.; Kaul, G.; Salehi-Khojin, A.; Masel, R. I. Water enhancement of CO₂ conversion on silver in 1-ethyl-3-methylimidazolium tetrafluoroborate. *J. Electrochem. Soc.* **2013**, *160* (2), H138-H141.
55. Rosen, B. A.; Haan, J. L.; Mukherjee, P.; Braunschweig, B.; Zhu, W.; Salehi-Khojin, A.; Dlott, D. D.; Masel, R. I. In Situ Spectroscopic Examination of a Low Overpotential Pathway for Carbon Dioxide Conversion to Carbon Monoxide. *J. Phys. Chem. C*. **2012**, *116* (29), 15307-15312.
56. Rosen, B. A.; Salehi-Khojin, A.; Thorson, M. R.; Zhu, W.; Whipple, D. T.; Kenis, P. J. A.; Masel, R. I. Ionic Liquid-Mediated Selective Conversion of CO₂ to CO at Low Overpotentials. *Science* **2011**, *334* (6056), 643-644.
57. Chandrasekaran, K.; Bockris, J. O. M. In-situ spectroscopic investigation of adsorbed intermediate radicals in electrochemical reactions: carbon dioxide(1-) (CO₂⁻) on platinum. *Surf. Sci.* **1987**, *185* (3), 495-514.
58. Bockris, J. O. M.; Wass, J. C. The photoelectrocatalytic reduction of carbon dioxide. *J. Electrochem. Soc.* **1989**, *136* (9), 2521-2528.
59. Zhao, G.; Jiang, T.; Han, B.; Li, Z.; Zhang, J.; Liu, Z.; He, J.; Wu, W. Electrochemical reduction of supercritical carbon dioxide in ionic liquid 1-n-butyl-3-methylimidazolium hexafluorophosphate. *J. Supercrit. Fluids*. **2004**, *32* (1-3), 287-291.
60. Lin, J.; Ding, Z.; Hou, Y.; Wang, X. Ionic Liquid Co-catalyzed Artificial Photosynthesis of CO. *Scientific Reports* **2013**, *3*, 1056.
61. Baltus, R. E.; Culbertson, B. H.; Dai, S.; Luo, H.; DePaoli, D. W. Low-Pressure Solubility of Carbon Dioxide in Room-Temperature Ionic Liquids Measured with a Quartz Crystal Microbalance. *J. Phys. Chem. B*. **2004**, *108* (2), 721-727.
62. "Global Temperature" NASA's Goddard Institute for Space Studies (GISS). GISTEMP Team, **2018**: GISS Surface Temperature Analysis (GISTEMP). NASA Goddard

- Institute for Space Studies. *Dataset accessed 20YY-MM-DD* at <https://data.giss.nasa.gov/gistemp/>. Hansen, J., R. Ruedy, M. Sato, and K. Lo, **2010**: Global surface temperature change, *Rev. Geophys.* 48, RG4004, doi:10.1029/2010RG000345.
63. Gao, Y.; Gao, X.; Zhang, X. The 2 °C Global Temperature Target and the Evolution of the Long-Term Goal of Addressing Climate Change—From the United Nations Framework Convention on Climate Change to the Paris Agreement. *Engineering* **2012**, 3, 272-278.
64. Henderson, R. M.; Reinert, S. A.; Polina, D.; Migdal, A. Climate change in 2018: Implications for business. *Harvard Business School* **2018**. <https://www.hbs.edu/environment/Documents/climate-change-2018.pdf>
65. Climate Change Division. Overview of Greenhouse Gases. *United States Environmental Protection Agency* **2016**, <https://www.epa.gov/ghgemissions/overview-greenhouse-gases>.
66. Wenzel, M.; Rihko-Struckmann, L.; Sundmacher, K. Continuous production of CO from CO₂ by RWGS chemical looping in fixed and fluidized bed reactors. *Chemical Engineering Journal* **2018**, 336, 278-296.
67. Laitar, D. S.; Müller, P.; Sadighi, J. P. Efficient Homogeneous Catalysis in the Reduction of CO₂ to CO. *J. Am. Chem. Soc.* **2005**, 127 (49), 17196-17197.
68. DiMeglio, J. L.; Rosenthal, J. Selective Conversion of CO₂ to CO with High Efficiency Using an Inexpensive Bismuth-Based Electrocatalyst. *Journal of the American Chemical Society* **2013**, 135 (24), 8798-8801.
69. Lewis, N. S.; Nocera, D. G. Powering the planet: Chemical challenges in solar energy utilization. *PNAS*. **2006**, 103 (43), 15729-15735.
70. Cook, T. R.; Dogutan, D. K.; Reece, S. Y.; Surendranath, Y.; Teets, T. S.; Nocera, D. G. Solar Energy Supply and Storage for the Legacy and Nonlegacy Worlds. *Chem. Rev.* **2010**, 110 (11), 6474-6502.
71. Takanabe, K. Photocatalytic Water Splitting: Quantitative Approaches toward Photocatalyst by Design. *ACS Catalysis* **2017**, 7 (11), 8006-8022.
72. Nakada, A.; Koike, K.; Nakashima, T.; Morimoto, T.; Ishitani, O. Photocatalytic CO₂ Reduction to Formic Acid Using a Ru(II)-Re(I) Supramolecular Complex in an Aqueous Solution. *Inorg. Chem.* **2015**, 54 (4), 1800-1807.
73. Ettedgui, J.; Diskin-Posner, Y.; Weiner, L.; Neumann, R. Photoreduction of Carbon Dioxide to Carbon Monoxide with Hydrogen Catalyzed by a Rhenium(I) Phenanthroline-Polyoxometalate Hybrid Complex. *J. Am. Chem. Soc.* **2011**, 133 (2), 188-190.
74. Rosas-Hernandez, A.; Junge, H.; Beller, M. Photochemical reduction of carbon dioxide to formic acid using ruthenium(II)-based catalysts and visible light. *ChemCatChem* **2015**, 7 (20), 3316-3321.
75. Kuramochi, Y.; Itabashi, J.; Fukaya, K.; Enomoto, A.; Yoshida, M.; Ishida, H. Unexpected effect of catalyst concentration on photochemical CO₂ reduction by trans(Cl)-Ru(bpy)(CO)₂Cl₂: new mechanistic insight into the CO/HCOO⁻ selectivity. *Chem. Sci.* **2015**, 6 (5), 3063-3074.
76. Kuramochi, Y.; Kamiya, M.; Ishida, H. Photocatalytic CO₂ Reduction in N,N-Dimethylacetamide/Water as an Alternative Solvent System. *Inorg. Chem.* **2014**, 53 (7), 3326-3332.

-
77. Kortlever, R.; Shen, J.; Schouten, K. J. P.; Calle-Vallejo, F.; Koper, M. T. M. Catalysts and Reaction Pathways for the Electrochemical Reduction of Carbon Dioxide. *J. Phys. Chem. Lett.* **2015**, *6* (20), 4073-4082.
78. Peterson, A. A.; Noerskov, J. K. Activity Descriptors for CO₂ Electroreduction to Methane on Transition-Metal Catalysts. *J. Phys. Chem. Lett.* **2012**, *3* (2), 251-258.
79. Shaughnessy, C. I.; Jantz, D. T.; Leonard, K. C. Selective electrochemical CO₂ reduction to CO using in situ reduced In₂O₃ nanocatalysts. *J. Mater. Chem. A* **2017**, *5* (43), 22743-22749.
80. Flieger, J.; Grushka, E. B.; Czajkowska-Żelazko, A. Ionic Liquids as Solvents in Separation Processes. *Austin J Anal Pharm Chem* **2014**, *1*(2), 1009.
81. Ventura, S. P. M.; Silva, F. A.; Quental, M. V.; Mondal, D.; Freire, M. G.; Coutinho, J. A. P. Ionic-Liquid-Mediated Extraction and Separation Processes for Bioactive Compounds: Past, Present, and Future Trends. *Chem. Rev.* **2017**, *117* (10), 6984-7052.
82. Knoelker, H. J.; Heber, J.; Mahler, C. H., Transition metal-diene complexes in organic synthesis. Part 14. Regioselective iron-mediated [2+2+1] cycloadditions of alkynes and carbon monoxide: synthesis of substituted cyclopentadienones. *Synlett* **1992**, (12), 1002-1004.
83. Luo, S. P.; Mejia, E.; Friedrich, A.; Pazidis, A.; Junge, H.; Surkus, A. E.; Jackstell, R.; Denurra, S.; Gladiali, S.; Lochbrunner, S.; Beller, M. Photocatalytic Water Reduction with Copper-Based Photosensitizers: A Noble-Metal-Free System. *Angew. Chem. Int. Ed.* **2013**, *52* (1), 419-423.
84. Lee, I. S. H.; Jeoung, E. H.; Kreevoy, M. M. Marcus Theory of a Parallel Effect on α for Hydride Transfer Reaction between NAD⁺ Analogs. *J. Am. Chem. Soc.* **1997**, *119* (11), 2722-2728.
85. Mejia, E.; Luo, S. P.; Karnahl, M.; Friedrich, A.; Tschierlei, S.; Surkus, A. E.; Junge, H.; Gladiali, S.; Lochbrunner, S.; Beller, M. A Noble-Metal-Free System for Photocatalytic Hydrogen Production from Water. *Chem. Eur. J.* **2013**, *19* (47), 15972-15978.
86. Fresta, E.; Costa, R. D. Beyond traditional light-emitting electrochemical cells - a review of new device designs and emitters. *J. Mater. Chem. C* **2017**, *5* (23), 5643-5675.
87. Keller, S.; Prescimone, A.; Bolink, H.; Sessolo, M.; Longo, G.; Martínez-Sarti, L.; Junquera-Hernández, J. M.; Constable, E. C.; Ortí, E.; Housecroft, C. E. Luminescent copper(I) complexes with bisphosphane and halogen-substituted 2,2'-bipyridine ligands. *Dalton Trans.* **2018**, *47*, 14263-14276.
88. McCullough, B. J.; Neyhouse, B. J.; Schrage, B. R.; Reed, D. T.; Osinski, A. J.; Ziegler, C. J.; White, T. A. Visible-Light-Driven Photosystems Using Heteroleptic Cu(I) Photosensitizers and Rh(III) Catalysts To Produce H₂. *Inorg. Chem.* **2018**, *57* (5), 2865-2875.
89. Grills, D. C.; Fujita, E. New Directions for the Photocatalytic Reduction of CO₂: Supramolecular, scCO₂ or Biphasic Ionic Liquid-scCO₂ Systems. *J. Phys. Chem. Lett.* **2010**, *1* (18), 2709-2718.
90. Freund, H. J.; Roberts, M. W. Surface chemistry of carbon dioxide. *Surface Science Reports* **1996**, *25* (8), 225-273.
91. Yang, C. C.; Vernimmen, J.; Meynen, V.; Cool, P.; Mul, G. Mechanistic study of hydrocarbon formation in photocatalytic CO₂ reduction over Ti-SBA-15. *J. Catal.* **2011**, *284* (1), 1-8.

92. Yang, C. C.; Yu, Y. H.; van der Linden, B.; Wu, J. C. S.; Mul, G. Artificial Photosynthesis over Crystalline TiO₂-Based Catalysts: Fact or Fiction?. *J. Am. Chem. Soc.* **2010**, *132* (24), 8398-8406.
93. Moustakas, N. G.; Strunk, J., Photocatalytic CO₂ reduction on TiO₂-based materials under controlled reaction conditions: Systematic insights from literature study. *Chem. Eur. J.* **2018**, *24* (49), 12739-12746.

Thesis Conclusion

In this doctoral thesis, a combination of synthesis of xant-type phosphine ligands and their application in different areas of catalysis was achieved. For this purpose, a Hammett series and imidazolium-tagged ligands were synthesized by our optimized methodologies. This resulted in reliable and scalable synthetic procedures, giving access to those elusive structures in high yields and purity, only employing crystallization techniques for purification.

In the first chapter of this thesis, synthesis of a Hammett series of heteroleptic copper(I) complexes and its application in photocatalysis were pursued. In particular, the use of heteroleptic copper [Cu(*p*-R-xantphos)(dmp)]BF₄ complexes for the aerobic photocatalyzed Cross-Dehydrogenative Coupling (CDC) of 1,2,3,4-tetrahydro-2-phenyl isoquinoline with nitromethane was studied. After synthesis, characterization and application of the electronically tuned complexes, structure-activity relationships were established. This project allowed a better understanding of the underlying design principles to apply for these copper complexes in photocatalysis. Mechanistic insights revealed that the aforementioned complexes likely operate under both, oxidative and reductive quenching pathways in that particular reaction. However, energy transfer processes generating singlet oxygen could be taking place in this photocatalytic transformation. In order to assess the possible existence and role of singlet oxygen under our reaction conditions, additional experimental work is still needed.

The second chapter of this thesis studied the ligand functionalization for lignin depolymerization in ionic liquid media. In the context of sustainable catalytic processes, recovery of the solvent and catalyst is very important, a feature that makes the use of ionic liquids attractive compared to classical solvents. The synthesis of xantphos imidazolium-tagged ligands was profoundly optimized. Their use in the ruthenium-catalyzed C-O bond cleavage of a lignin model compound was briefly studied after solving side reactivity issues caused by the reaction media. This project requires further optimization of the reaction in ionic liquid media, as well as the application of this system in more complex substrates.

The final research chapter of this thesis intended to combine the findings of the previous chapters by employing imidazolium-tagged ligands in heteroleptic copper complexes as photosensitizers in the photocatalyzed CO₂ reduction to CO. The imidazolium-tagged complex was obtained and despite performing in this catalytic transformation, its recovery and recyclability were not achieved. While still less efficient than homogeneous systems in organic solvents, higher activity in ionic liquid media was achieved as compared to reported systems by the use of non-functionalized complexes. Further optimization of the complex structure aiming at major stability under irradiation conditions is still needed. More stable complexes could allow their recovery and recyclability. This approach could be not only applied for this specific reaction but also for other catalytic processes that are mediated by [Cu(N[^]N)(P[^]P)]⁺ photosensitizers.

Chapter V: Experimental section

5.1 Chapter II: Electronic phosphine ligand effects on the photochemistry of heteroleptic Cu(I) complexes: A comprehensive study.

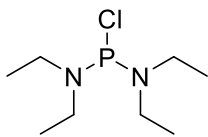
General information

For the synthesis of ligands and complexes all reactions were carried out using standard Schlenk techniques under argon atmosphere. All glassware was dried at 130 °C overnight and cooled under vacuum prior to use. ^1H , $^{13}\text{C}\{^1\text{H}\}$ and $^{31}\text{P}\{^1\text{H}\}$ Nuclear Magnetic Resonance (NMR) spectra were recorded at 298 K on either Bruker Avance 300, Avance II 400 and Bruker Avance II 500 spectrometers using the residual solvent peak for ^1H and $^{13}\text{C}\{^1\text{H}\}$ as reference. All NMR shifts are reported as δ in parts per million (ppm). A Gallenkamp melting point apparatus was used to determinate melting points. Toluene and TMEDA were distilled from sodium, THF and diethyl ether were distilled from sodium/benzophenone, hexanes from sodium/benzophenone/triglyme and dichloromethane and acetonitrile from calcium hydride. Diethylamine was dried over KOH powder. Anhydrous nitromethane was purchased from Sigma Aldrich. Aqueous reagents were degassed under argon before use for a minimum period of four hours. All reagents were purchased from commercial suppliers and used as received, unless otherwise noted. Mass spectrometry was carried out at National Mass Spectrometry Facility (NMSF-Swansea) and Leibniz Institute for Catalysis – LIKAT. Elemental analysis was carried out in the facilities at London Metropolitan University and Leibniz Institute for Catalysis – LIKAT. All reactions performed in this chapter require strict inert conditions. It has been observed that optimal results are obtained with freshly distilled solvents and that solvents from the SPS (Solvent purification system) can affect the yields for some synthetic procedures.

Synthesis and characterization of compounds

Synthesis of precursors

The synthesis of the highly sensitive compounds 9,9-dimethyl-4,5-bis(diethylaminophosphino)xanthene and 9,9-dimethyl-4,5-bis(dichlorophosphino)xanthene was followed by ^{31}P NMR spectroscopy of the crude mixture. The work-up of these compounds were performed quickly to avoid keeping the compounds in solution.

Synthesis of bis(diethylamino)chlorophosphine (I)

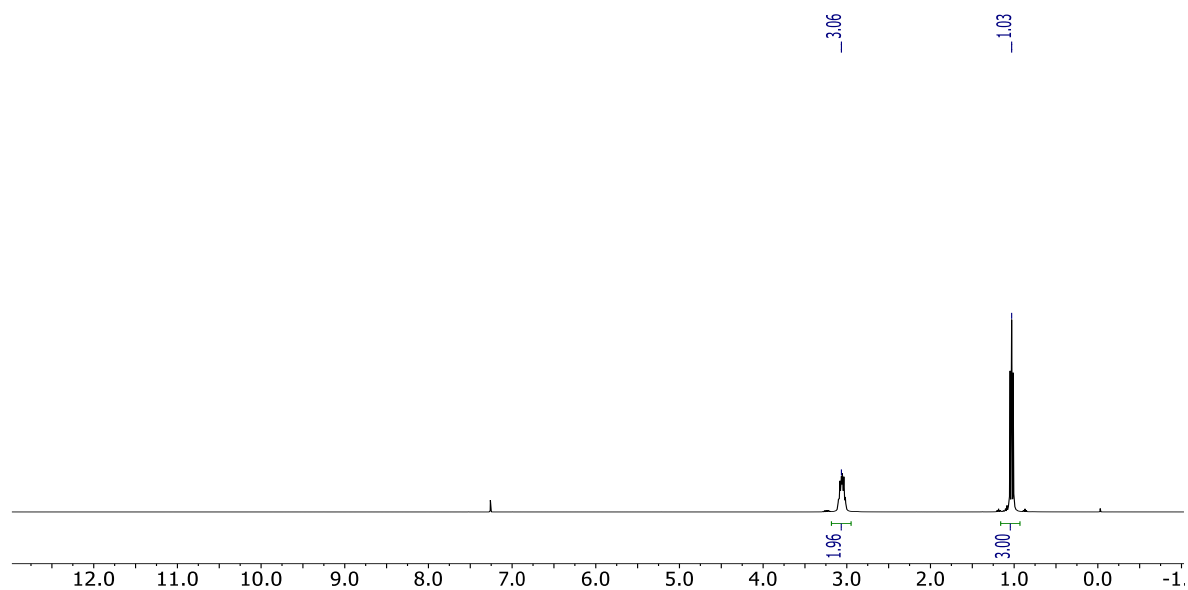
A modified procedure from the literature reports was performed.¹⁻² In a three-neck round-bottomed flask kept under inert atmosphere, the central neck was equipped with a mechanical stirrer and the third neck with a dropping funnel. Dried diethylamine (83 mL, 800 mmol) in hexanes (200 mL) was added dropwise to a solution of PCl_3 (17.5 mL, 200 mmol) in hexane (400 mL) at $-78\text{ }^\circ\text{C}$ over three hours. The reaction was then allowed to warm to room temperature overnight; the product was then filtered under an argon blanket and then concentrated under reduced pressure and distilled under reduced pressure. A viscous colorless liquid was obtained, which was used without further purification. Yield 88% (67 mL, 67 g). Analytical data were found to be consistent with the literature.

^1H NMR (CDCl_3 , 400 MHz, 298 K): δ (ppm) = 3.06 (qd, $J = 14.1$, $J = 7.0$ Hz, 8H, CH_2), 1.03 (t, $J = 7.2$ Hz, 12H, CH_3).

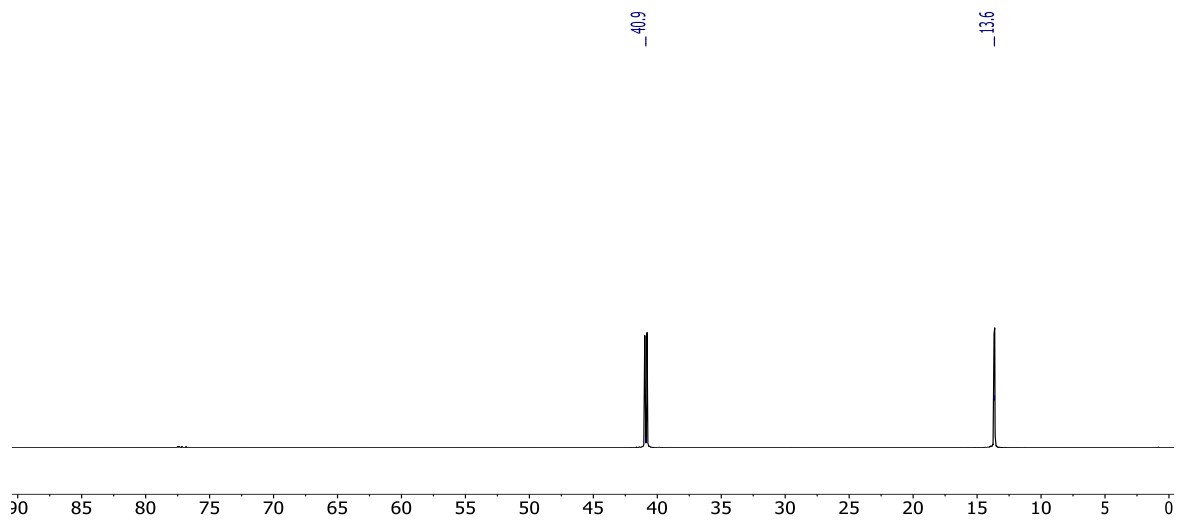
^{13}C - $\{^1\text{H}\}$ NMR (CDCl_3 , 100 MHz, 298 K): δ (ppm) = 40.9 (d, $J = 18.0$ Hz, CH_2), 13.6 (d, $J = 4.7$ Hz, CH_3).

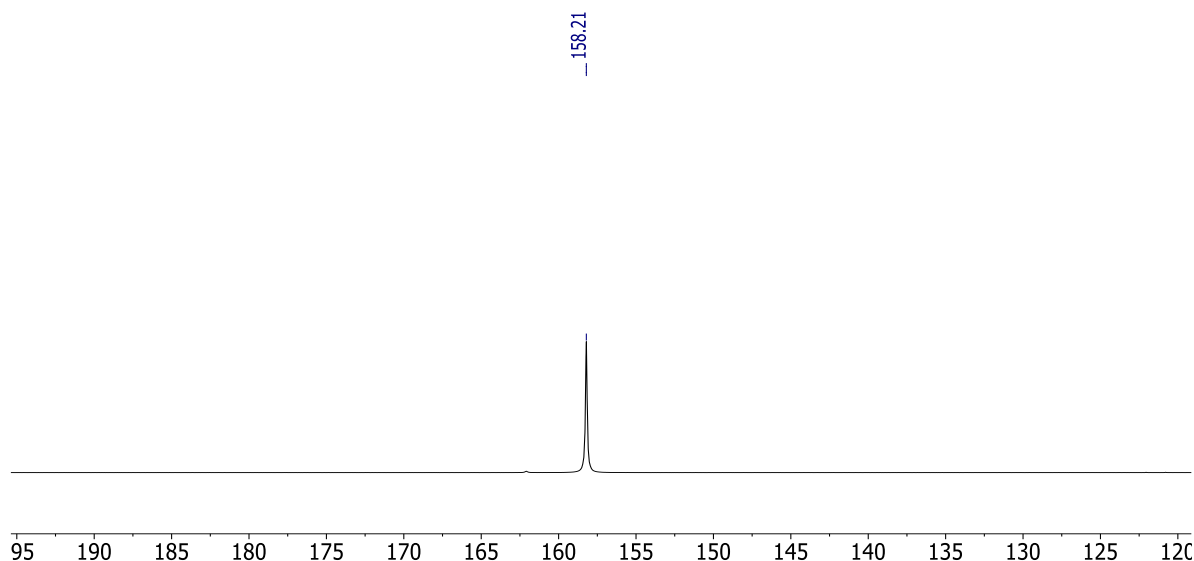
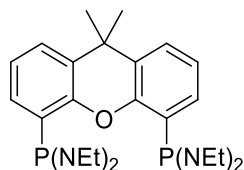
^{31}P - $\{^1\text{H}\}$ NMR (CDCl_3 , 162 MHz, 298 K): δ (ppm) = 158.2 (s).

^1H NMR (CDCl_3 , 400 MHz, 298 K)



$^{13}\text{C}\{-^1\text{H}\}$ NMR (CDCl_3 , 100 MHz, 298 K)

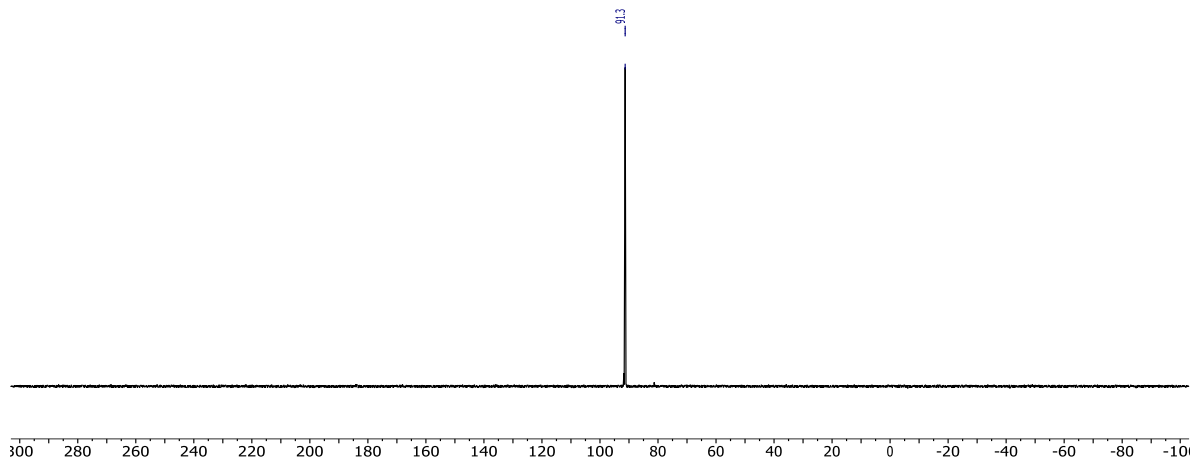


$^{31}\text{P}\{-^1\text{H}\}$ NMR (CDCl_3 , 162 MHz, 298 K)**Synthesis of 9,9-dimethyl-4,5-bis(diethylaminophosphino)xanthene (7)**

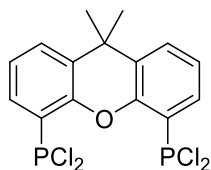
9,9-dimethylxanthene (4g, 19.06 mmol) and *N,N,N',N'*-tetramethylethylenediamine TMEDA (5.52 g, 7.12 mL, 47.6 mmol) were dissolved in diethyl ether (70 mL) in a two neck round-bottomed flask and cooled to $-78\text{ }^{\circ}\text{C}$. Then, *n*-butyllithium (21 mL of a 2.5 M solution in hexanes, 47.6 mmol) was added dropwise and the reaction mixture was stirred with a mechanical stirrer at room temperature overnight.³ Next, the resulting solution was added to a solution of bis(diethylamino)chlorophosphine (8.42 mL, 47.6 mmol) in pentane (40 mL) at $-78\text{ }^{\circ}\text{C}$. The mixture was transferred by cannula to a sintered filter and the colorless solution was concentrated under vacuum to give a pale yellow powder. The compound was crystallized from pentane providing a white powder which was used without further purification. This procedure was followed by ^{31}P NMR of the crude mixture. The work-up of this compound was performed quickly to avoid keeping the compound in solution. Yield: 90% (9.5 g).

 $^{31}\text{P}\{-^1\text{H}\}$ NMR (Et_2O , 162 MHz, 298 K): δ 91.3 (s).

$^{31}\text{P}\{-^1\text{H}\}$ NMR (Et_2O , 162 MHz, 298 K)



Synthesis of 9,9-dimethyl-4,5-bis(dichlorophosphino)xanthene (8)



The precursor of 9,9-dimethyl-4,5-bis(diethylaminophosphino)xanthene (7 g, 12.57 mmol) was dissolved in diethyl ether (150 mL) and cooled to $-78\text{ }^{\circ}\text{C}$ followed by the dropwise addition of hydrogen chloride (2 M solution in Et_2O , 62.6 mL, 125 mmol) over two hours.⁴ The reaction mixture was then warmed to room temperature and stirred with a mechanical stirrer overnight. The mixture was transferred by cannula to a sintered filter and the colorless solution was concentrated under vacuum to give a white powder which was used without further purification. The work-up of this compound was performed quickly to avoid keeping the compound in solution. Yield 70% (3.6 g)

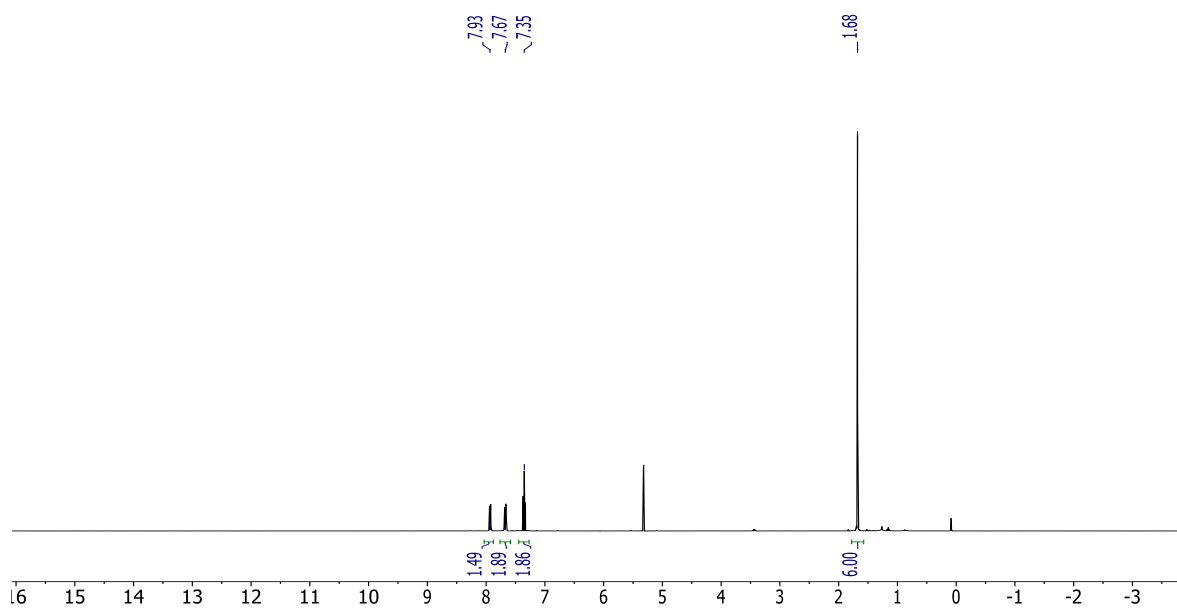
^1H NMR (CD_2Cl_2 , 400 MHz, 298 K): δ (ppm) = 7.93 (dq, $J = 7.6\text{ Hz}$, $J = 1.6\text{ Hz}$, 2H, CH_{Ar}), 7.67 (dd, $J = 7.8\text{ Hz}$, $J = 1.5\text{ Hz}$, 2H, CH_{Ar}), 7.35 (t, $J = 7.6\text{ Hz}$, 2H, CH_{Ar}), 1.68 (s, 6H, CH_3).

$^{13}\text{C}\{-^1\text{H}\}$ NMR (CD_2Cl_2 , 100 MHz, 298 K): δ (ppm) = 151.0 (s, C_q), 131.6 (t, $J = 2.6\text{ Hz}$, CH_{Ar}), 130.9 (s, C_q), 129.7 (s, CH_{Ar}), 128.1 (s, C_q), 125.4 (s, CH_{Ar}), 34.8 (s, C_q), 32.5 (s, CH_3).

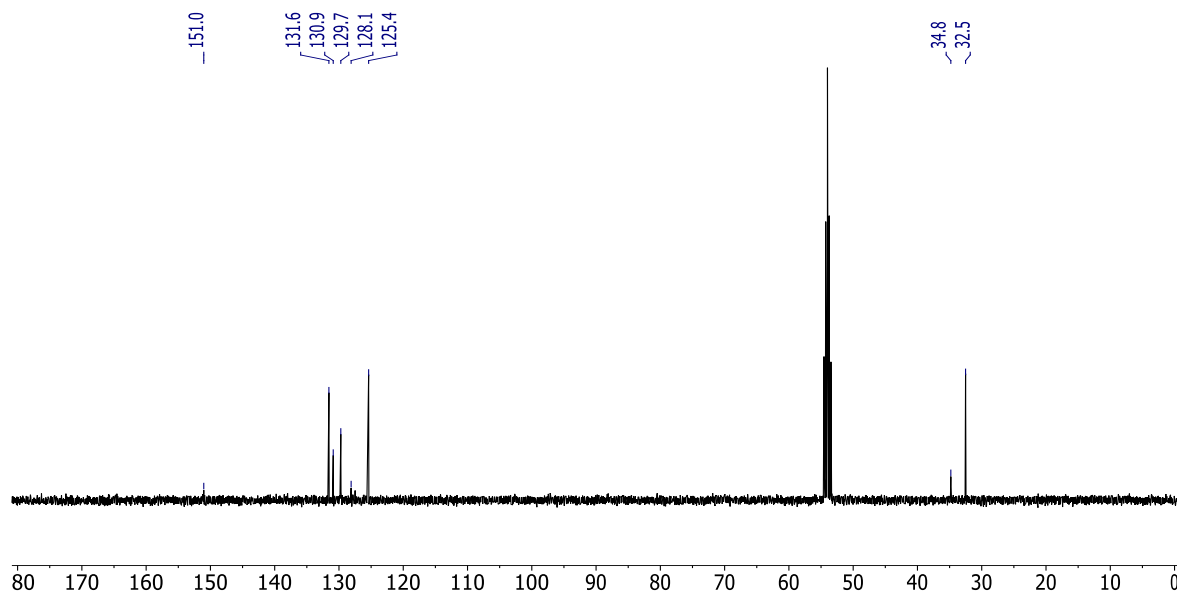
$^{31}\text{P}\{-^1\text{H}\}$ NMR (CD_2Cl_2 , 162 MHz, 298 K): δ (ppm) = 158.53 (s).

$^{31}\text{P}\{-^1\text{H}\}$ NMR (Et_2O , 162 MHz, 298 K): δ (ppm) = 157.6 (s).

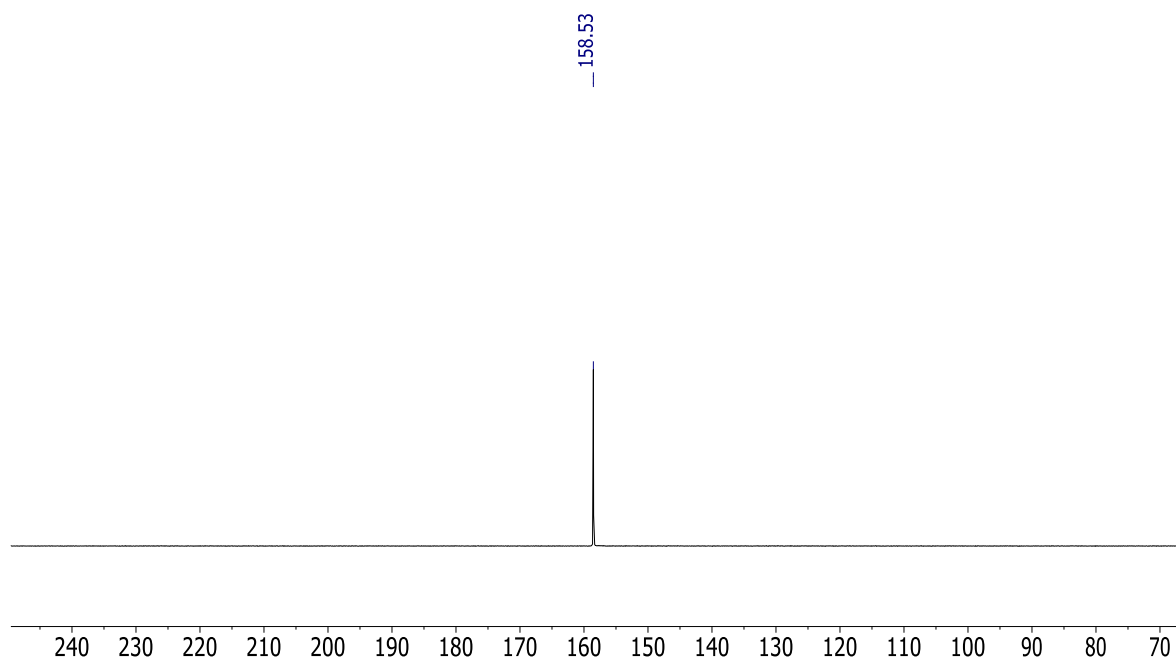
^1H NMR (CD_2Cl_2 , 400 MHz, 298 K)



$^{13}\text{C}\{-^1\text{H}\}$ NMR (CD_2Cl_2 , 100 MHz, 298 K)



$^{31}\text{P}\{-^1\text{H}\}$ NMR (CD_2Cl_2 , 162 MHz, 298 K)



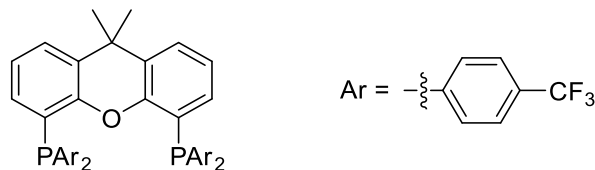
Synthesis of ligands

The last step of the synthesis (Grignard reaction) requires to be performed with caution when using fluorinated aryl bromides as they can explosively decompose yielding metal fluorides

The procedure was adapted from the methodology described by Kamer and co-workers.⁵ Conditions for the Grignard reaction as well as purification procedures have been modified. Et_2O was used for fluorinated ligands and THF for non-fluorinated ligands.

Activation of magnesium turnings for all ligands: A mixture of magnesium turnings (350 mg, 14.54 mmol) in Et_2O or THF (3 mL) activated with 1,2-dibromoethane (0.1 mL, 1.2 mmol) was stirred in a two neck Schlenk flask equipped with a condenser at room temperature for one hour, resulting in a suspension.

4,5-bis(di-*p*-trifluoromethylphenylphosphino)-9,9-dimethylxanthene (*p*-CF₃ xantphos ligand) (9a)



At room temperature, a solution of 4-bromobenzo trifluoride (1.36 g, 0.84 mL, 6.06 mmol) in Et₂O (4 mL) was added dropwise to the stirred suspension of the activated magnesium turnings. The reaction was followed by GCMS after quenching an aliquot of the reaction mixture with deuterated methanol. After affording the Grignard reagent, approximately after two hours, the product was filtered and added dropwise to a stirred solution of 9-dimethyl-4,5- bis(dichlorophosphino)xanthene (500 mg, 1.21 mmol) in Et₂O (10 mL) at -20 °C (ice bath with NaCl). The reaction mixture was stirred and allowed to warm to room temperature overnight. Subsequently, the reaction mixture was hydrolyzed with a solution of 1N HCl /Brine 1:1 (10 mL). The aqueous phase was separated, washed with CH₂Cl₂ (3x20 mL) and toluene (2x20 mL). The organic phases were combined, dried over Na₂SO₄ and volatiles were removed under vacuum. The resulting pale yellow powder was washed with cold pentane and recrystallized from the same solvent at 0°C affording a white crystalline powder. Yield: 700 mg, 68 %. Analytical data were found to be consistent with the literature.⁵

¹H NMR (500 MHz, CD₂Cl₂, 298 K): δ (ppm) = 7.56-7.51 (m, 10H, CH_{Ar}), 7.32-7.26 (m, 8H, CH_{Ar}), 7.04 (t, *J* = 7.8 Hz, 2H, CH_{Ar}), 6.49 (dd, *J* = 6.0 Hz, *J* = 1.2 Hz, 2H, CH_{Ar}), 1.67 (s, CH₃).

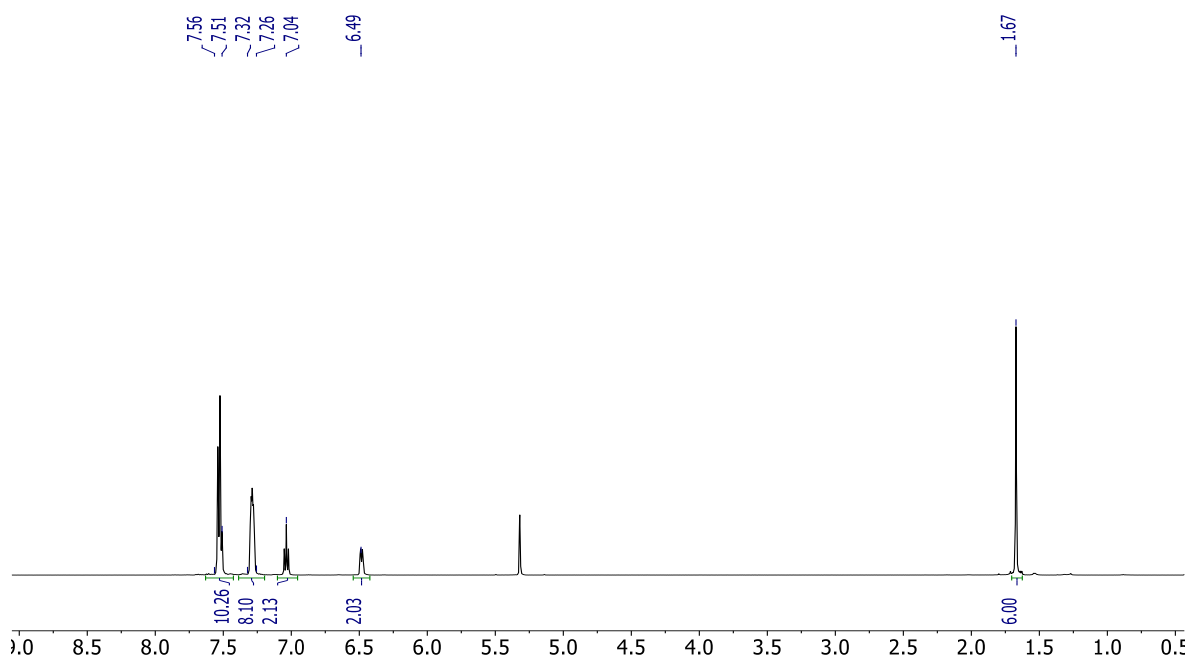
¹³C-{¹H} NMR (126 MHz, CD₂Cl₂, 298 K): δ (ppm) = 152.9 (t, *J* = 9.7 Hz, C_q), 142.1 (t, *J* = 7.3 Hz, C_q), 134.6 (t, *J* = 10.4 Hz, CH_{Ar}), 132.4 (s, CH_{Ar}), 131.2 (q, *J* = 32.2 Hz, C_q), 131.1 (s, C_q), 128.1 (s, CH_{Ar}), 125.6 (t, *J* = 3.4 Hz, CH_{Ar}), 124.8 (q, *J* = 273.9 Hz, C_q), 124.6 (s, CH_{Ar}), 123.7 (t, *J* = 8.4 Hz, C_q), 35.1 (s, C_q), 32.1 (s, CH₃).

³¹P-{¹H} NMR (202 MHz, CD₂Cl₂, 298 K): δ (ppm) = -17.67 (s).

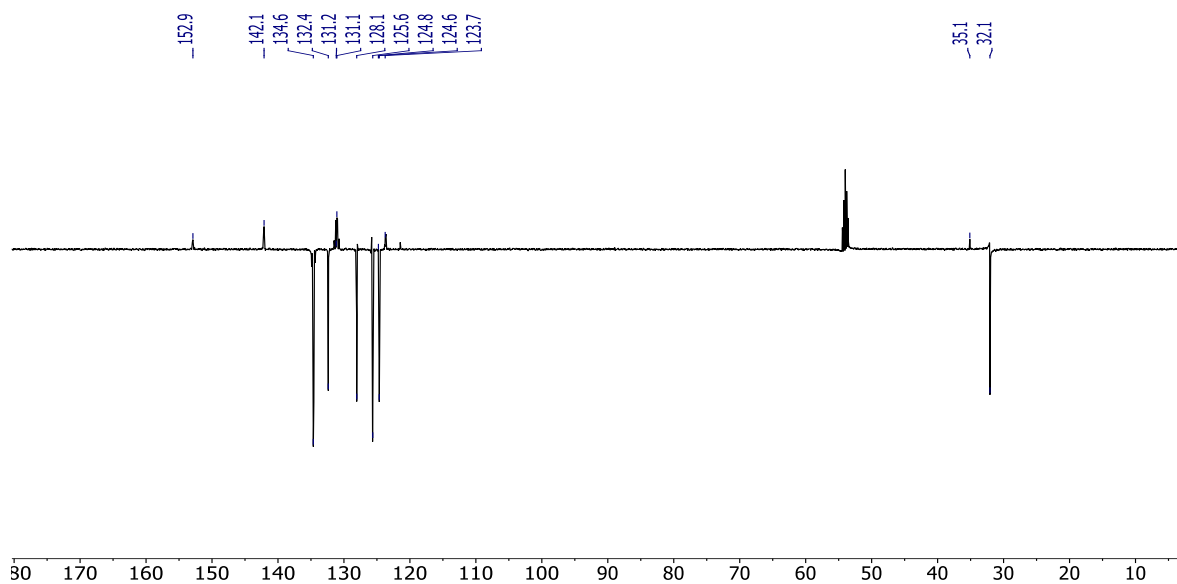
¹⁹F-{¹H} NMR (470 MHz, CD₂Cl₂, 298 K): δ (ppm) = -63.06 (s).

mp: 184-185 °C.

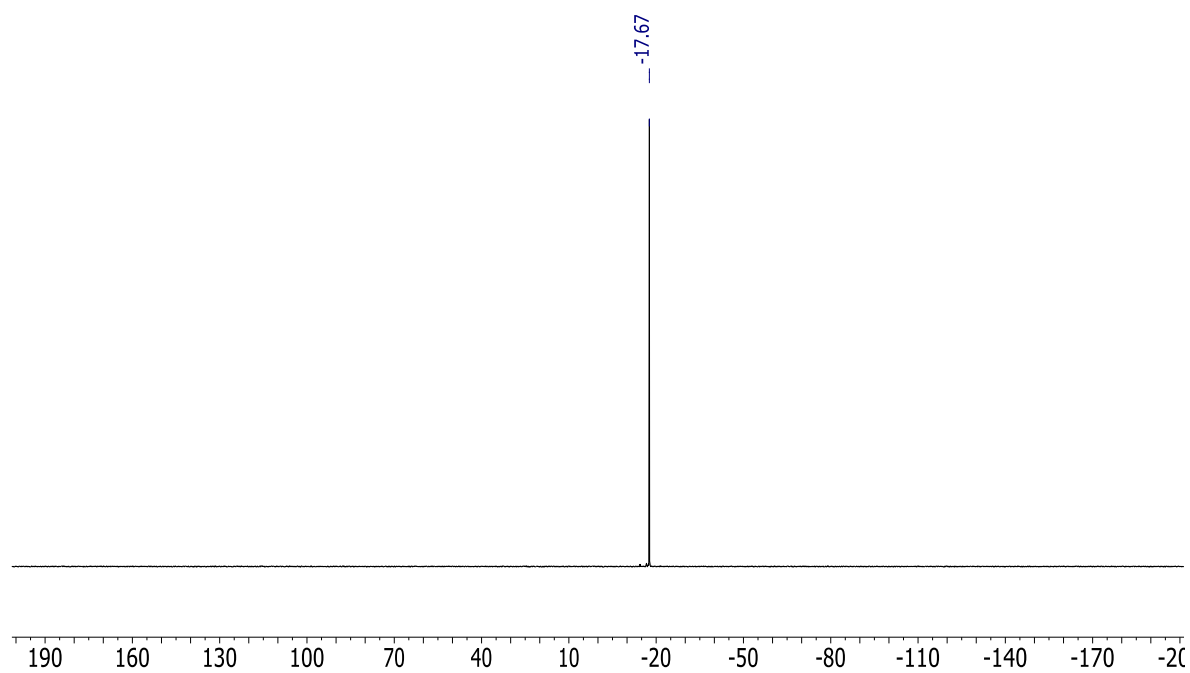
^1H NMR (500 MHz, CD_2Cl_2 , 298 K)



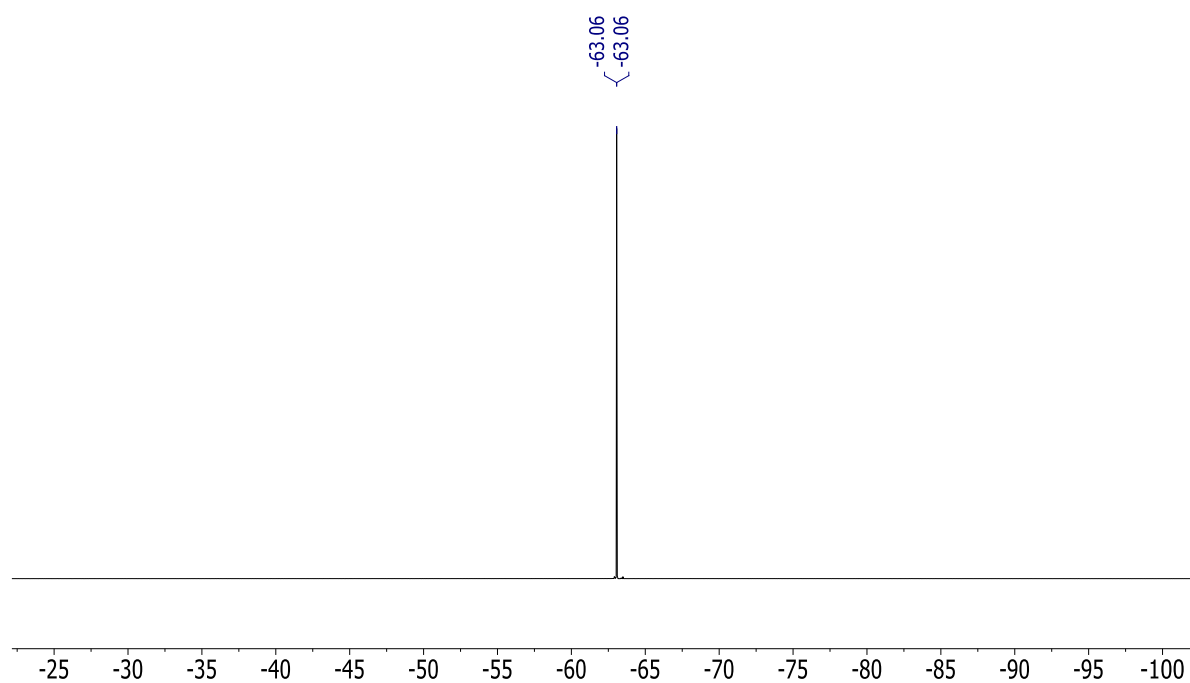
$^{13}\text{C}\{-^1\text{H}\}$ NMR (126 MHz, CD_2Cl_2 , 298 K)

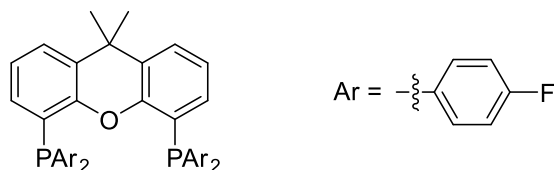


$^{31}\text{P}\{-^1\text{H}\}$ NMR (202 MHz, CD_2Cl_2 , 298 K)



$^{19}\text{F}\{-^1\text{H}\}$ NMR (470 MHz, CD_2Cl_2 , 298 K)



4,5-bis(di-*p*-fluorophenylphosphino)-9,9-dimethylxanthene (*p*-F xantphos ligand) (9b)

At room temperature, a solution of 1-bromo-4-fluorobenzene (1.0 g, 0.66 mL, 6.06 mmol) in Et₂O (4 mL) was added dropwise to the stirred suspension of the activated magnesium turnings. The reaction was followed by GCMS after quenching an aliquot of the reaction mixture with deuterated methanol. After affording the Grignard reagent, approximately after two hours, the product was filtered and added dropwise to a stirred solution of 9-dimethyl-4,5-bis(dichlorophosphino)xanthene (500 mg, 1.21 mmol) in Et₂O (10 mL) at -20 °C (Ice bath with NaCl). The reaction mixture was stirred and allowed to warm to room temperature overnight. Subsequently, the reaction mixture was hydrolyzed with a solution of 1N HCl /Brine 1:1 (10 mL). The aqueous phase was separated, washed with CH₂Cl₂ (3x20 mL) and toluene (2x20 mL). The organic phases were combined, dried over Na₂SO₄ and volatiles were removed under vacuum. The resulting white powder was washed with hexane and recrystallized from a saturated solution of the compound in CH₂Cl₂ layered with Isopropanol obtaining a white crystalline powder. Yield: 610 mg, 77 %. Analytical data were found to be consistent with the literature.⁵

¹H NMR (500 MHz, CD₂Cl₂, 298 K): δ (ppm) = 7.46 (dd, *J* = 7.8 Hz, *J* = 1.3 Hz, 2H, CH_{Ar}), 7.15-7.09 (m, 8H, CH_{Ar}), 6.99 (t, *J* = 7.6 Hz, 2H, CH_{Ar}), 6.96 (t, *J* = 7.6 Hz, 8H, CH_{Ar}), 6.46 (dq, *J* = 7.5 Hz, *J* = 1.6 Hz, 2H, CH_{Ar}), 1.64 (s, 6H, CH₃).

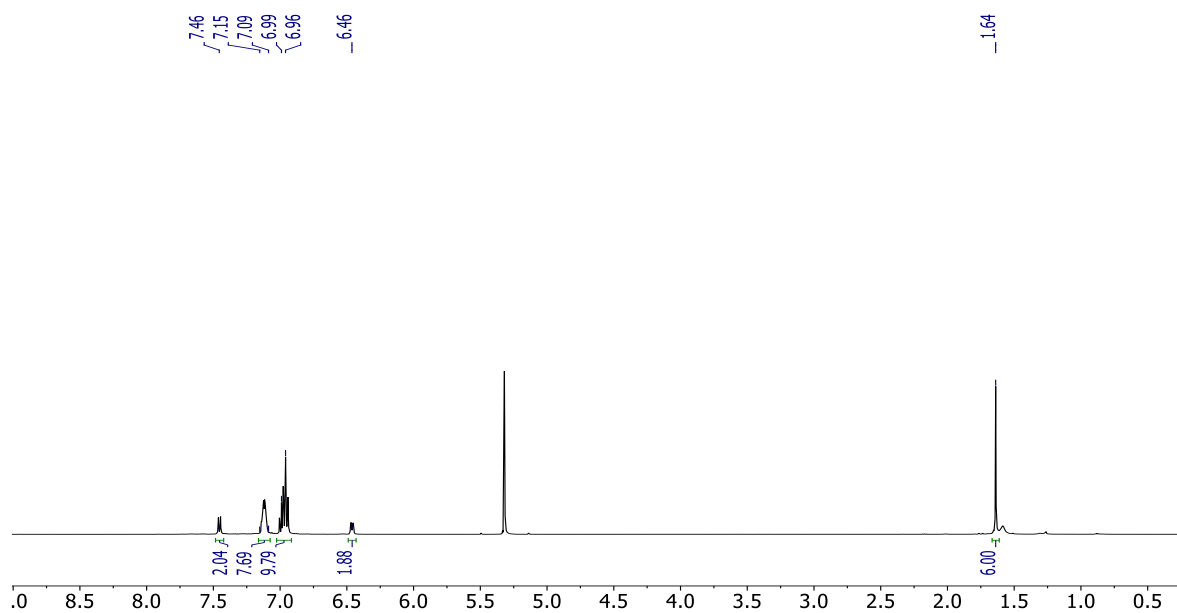
¹³C-{¹H} NMR (126 MHz, CD₂Cl₂, 298 K): δ (ppm) = 163.9 (d, *J* = 247.3 Hz, C_q), 152.7 (t, *J* = 9.6 Hz, C_q), 136.2 (m, CH_{Ar}), 133.2 (m, C_q), 132.1 (s, CH_{Ar}), 130.8 (s, C_q), 127.4 (s, CH_{Ar}), 125.6 (t, *J* = 8.3 Hz, C_q), 124.2 (s, CH_{Ar}), 116.0 (dt, *J* = 21.0 Hz, *J* = 3.8 Hz, CH_{Ar}), 35.0 (s, C_q), 32.1 (s, CH₃).

³¹P-{¹H} NMR (202 MHz, CD₂Cl₂, 298 K): δ (ppm) = -19.51 (s).

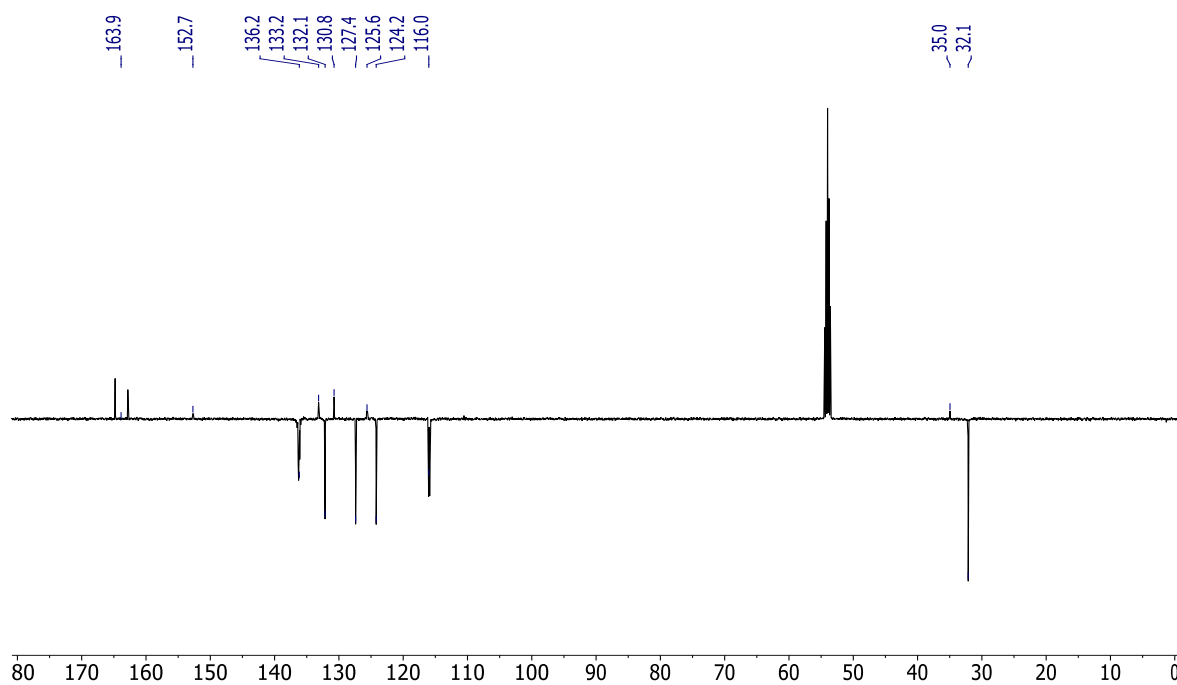
¹⁹F-{¹H} NMR (470 MHz, CD₂Cl₂, 298 K): δ (ppm) = -113.78 (t, *J* = 2.3 Hz).

mp: 196-197 °C.

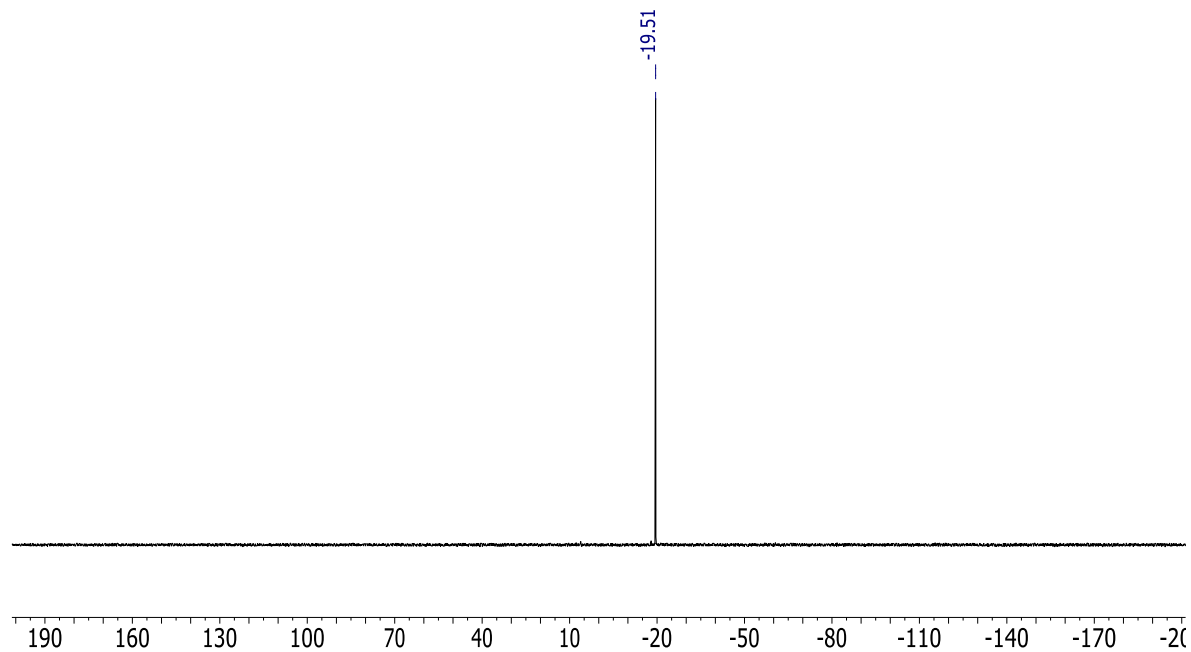
^1H NMR (500 MHz, CD_2Cl_2 , 298 K)



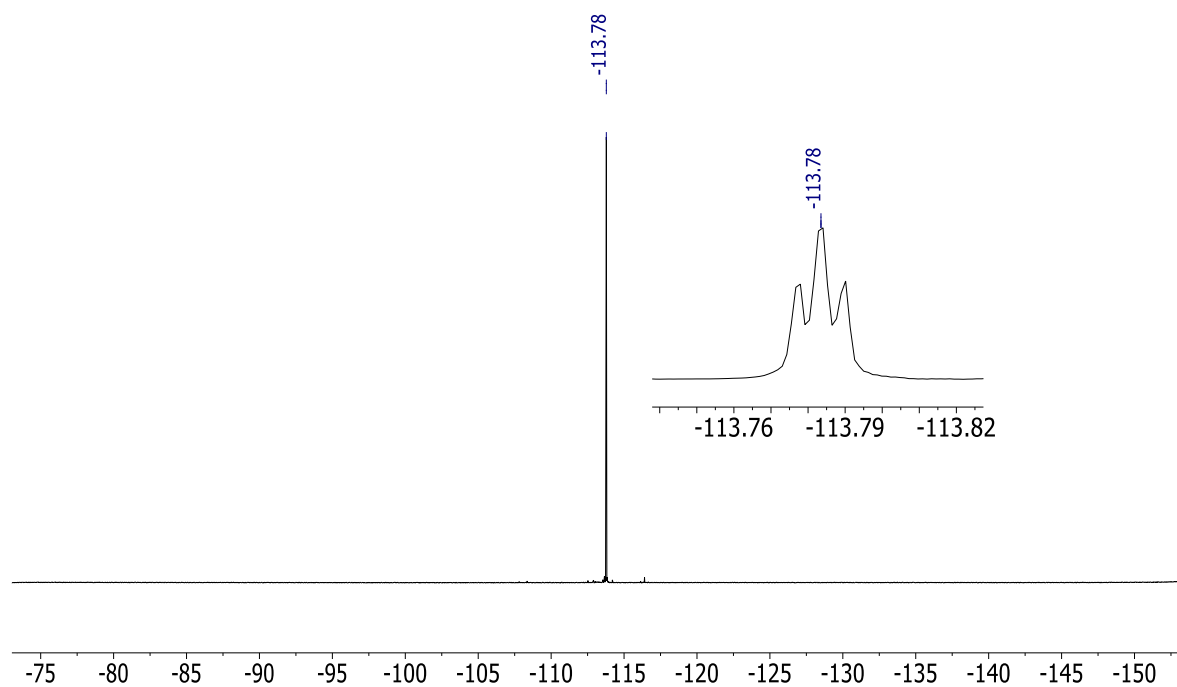
$^{13}\text{C}\{-^1\text{H}\}$ NMR (126 MHz, CD_2Cl_2 , 298 K)

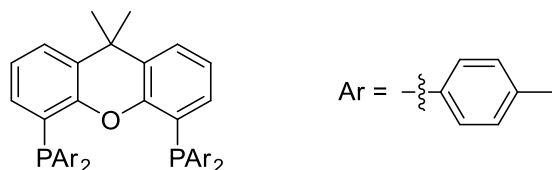


$^{31}\text{P}\{-^1\text{H}\}$ NMR (202 MHz, CD_2Cl_2 , 298 K)



$^{19}\text{F}\{-^1\text{H}\}$ NMR (470 MHz, CD_2Cl_2 , 298 K)



4,5-bis(di-*p*-tolylphosphino)-9,9-dimethylxanthene (*p*-Me xantphos ligand) (9d)

At room temperature, a solution of 4-bromo toluene (1.0 g, 0.74 mL, 6.06 mmol) in THF (4 mL) was added dropwise to the stirred suspension of the activated magnesium turnings. The reaction was followed by GCMS after quenching an aliquot of the reaction mixture with deuterated methanol. After affording the Grignard reagent, approximately after two hours, the product was filtered and added dropwise to a stirred solution of 9-dimethyl-4,5-bis(dichlorophosphino)xanthene (500 mg, 1.21 mmol,) in THF (10 mL) at -20 °C (ice bath with NaCl). The reaction mixture was stirred and allowed to warm to room temperature overnight. Subsequently, the reaction mixture was hydrolyzed with a solution of 1N HCl/Brine 1:1 (10 mL). The aqueous phase was separated, washed with CH₂Cl₂ (3x20 mL) and toluene (2x20 mL). The organic phases were combined, dried over Na₂SO₄ and volatiles were removed under vacuum. The resulting white powder was washed with hexane and recrystallized from a saturated solution of the compound in THF layered with hexanes obtaining a white crystalline powder. Yield: 620 mg, 80 %. Analytical data were found to be consistent with the literature.⁵

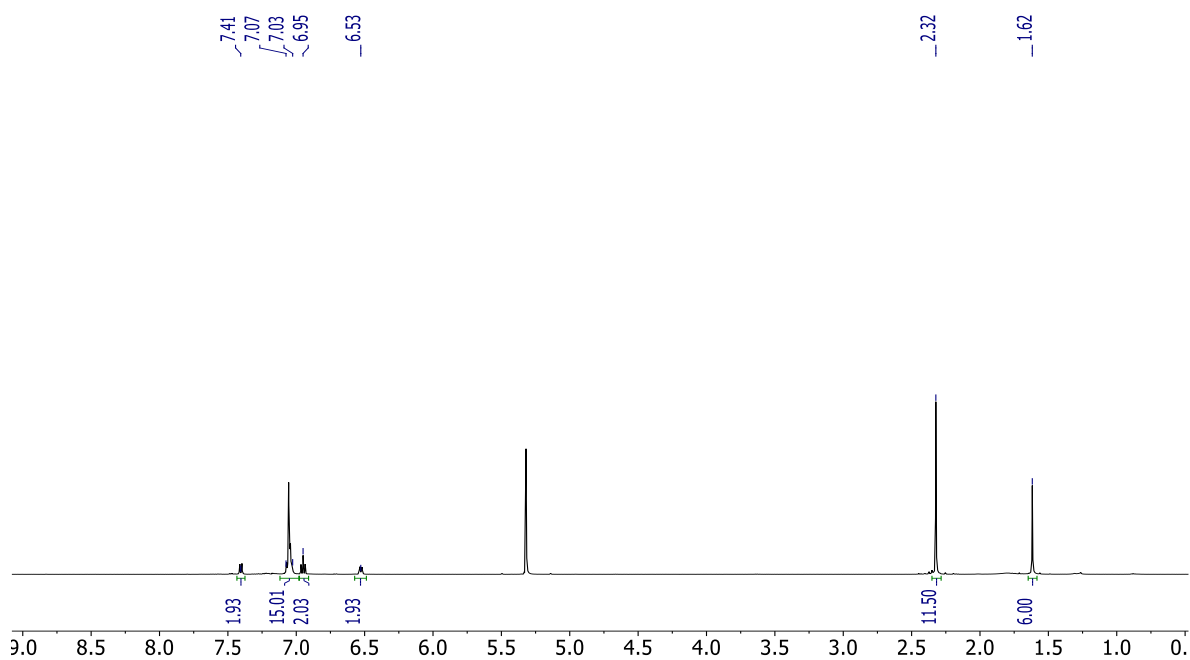
¹H NMR (500 MHz, CD₂Cl₂, 298 K): δ (ppm) = 7.41 (dd, J = 7.8 Hz, J = 1.4 Hz, 2H, CH_{Ar}), 7.07-7.03 (m, 16H, CH_{Ar}), 6.95 (t, J = 7.6 Hz, 2H, CH_{Ar}), 6.53 (dq, J = 7.5 Hz, J = 1.7 Hz, 2H, CH_{Ar}), 2.32 (s, 12H, CH₃), 1.62 (s, 6H, CH₃).

¹³C-{¹H} NMR (126 MHz, CD₂Cl₂, 298 K): δ (ppm) = 153.0 (t, J = 9.5 Hz, C_q), 138.5 (s, C_q), 134.5 (t, J = 6.0 Hz, C_q), 134.4 (t, J = 9.4 Hz, CH_{Ar}), 132.4 (s, CH_{Ar}), 130.6 (s, C_q), 129.5 (t, J = 3.5 Hz, CH_{Ar}), 126.9 (s, CH_{Ar}), 126.6 (t, J = 9.9 Hz, C_q), 123.8 (s, CH_{Ar}), 34.9 (s, C_q), 32.1 (s, CH₃), 21.6 (s, CH₃).

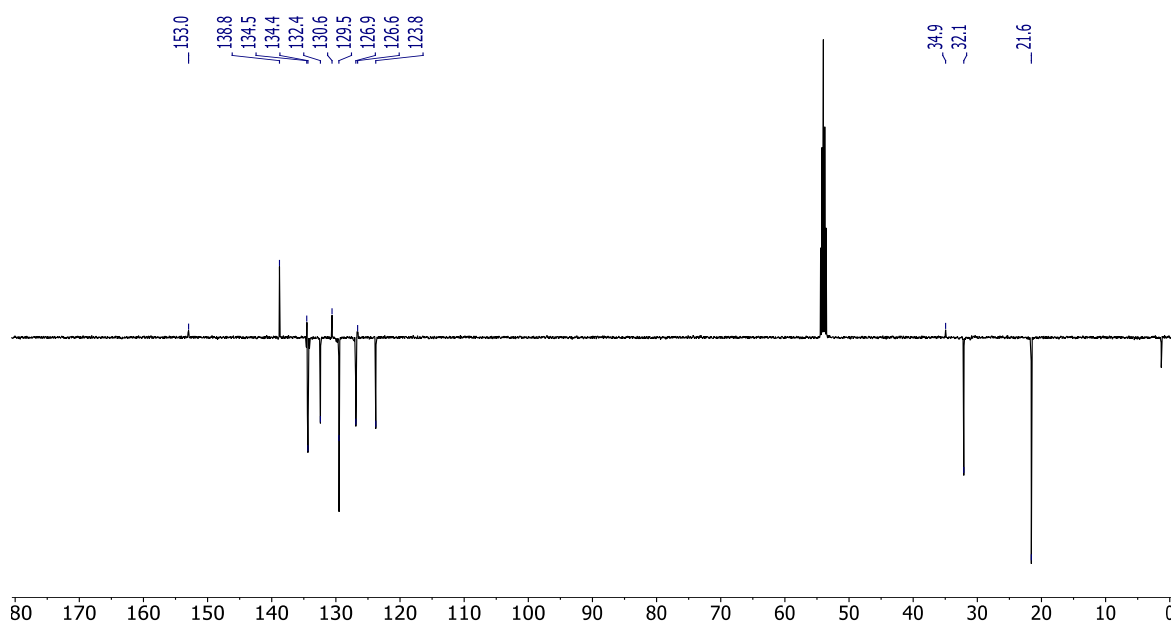
³¹P-{¹H} NMR (202 MHz, CD₂Cl₂, 298 K): δ (ppm) = -20.27 (s).

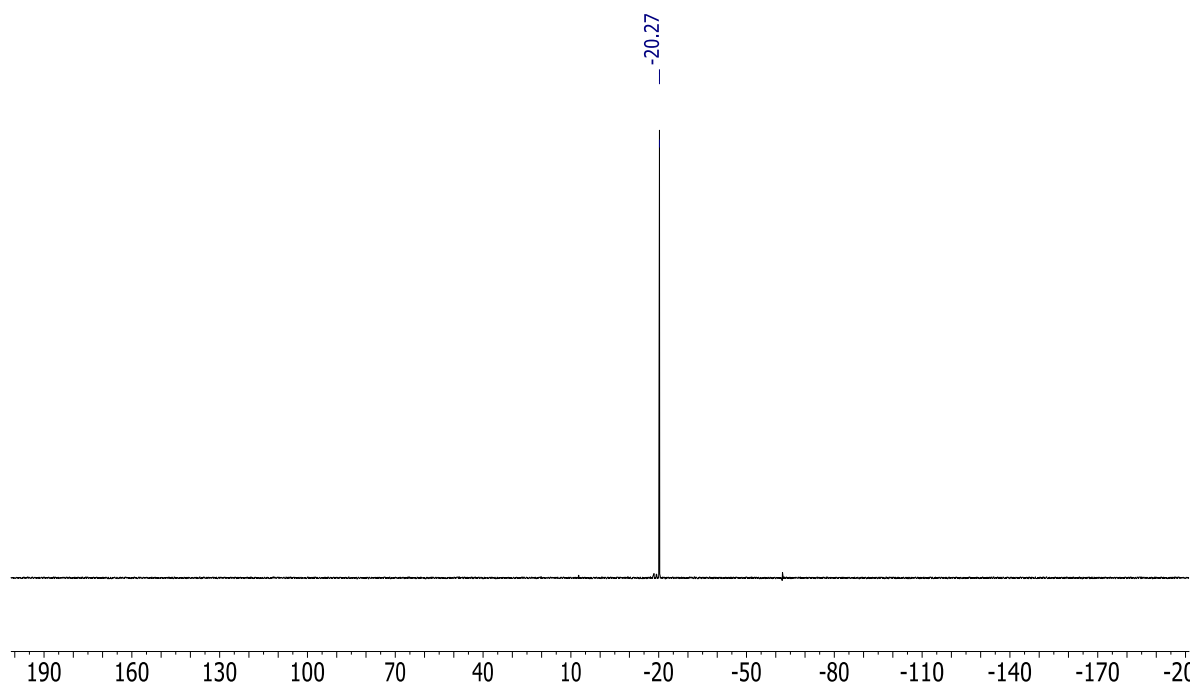
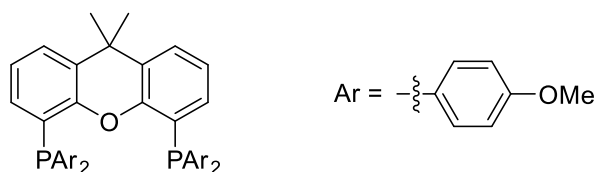
mp: 238-239 °C.

^1H NMR (500 MHz, CD_2Cl_2 , 298 K)



$^{13}\text{C}\{-^1\text{H}\}$ NMR (126 MHz, CD_2Cl_2 , 298 K)



$^{31}\text{P}\{-^1\text{H}\}$ NMR (202 MHz, CD_2Cl_2 , 298 K)**4,5-bis(di-*p*-anisylphosphino)-9,9-dimethylxanthene (*p*-OMe xantphos ligand) (9f)**

At room temperature, a solution of 4-bromo anisole (1.1 g, 0.75 mL, 6.06 mmol) in THF (4 mL) was added dropwise to the stirred suspension of the activated magnesium turnings. The reaction was followed by GCMS after quenching an aliquot of the reaction mixture with deuterated methanol. After affording the Grignard reagent, approximately after two hours, the product was filtered and added dropwise to a stirred solution of 9-dimethyl-4,5-bis(dichlorophosphino)xanthene (500 mg, 1.21 mmol) in THF (10 mL) at $-20\text{ }^{\circ}\text{C}$ (ice bath with NaCl). The reaction mixture was stirred and allowed to warm to room temperature overnight. Subsequently, the reaction mixture was hydrolyzed with a solution of 1N HCl/Brine 1:1 (10 mL). The aqueous phase was separated, washed with CH_2Cl_2 (3x20 mL) and toluene (2x20 mL). The organic phases were combined, dried over Na_2SO_4 and volatiles were removed under vacuum. The resulting white powder was washed with hexanes and recrystallized from a saturated solution of the compound in CH_2Cl_2 layered with ethanol

obtaining a white crystalline powder. Yield: 650 mg, 77 %. Analytical data were found to be consistent with the literature.⁵

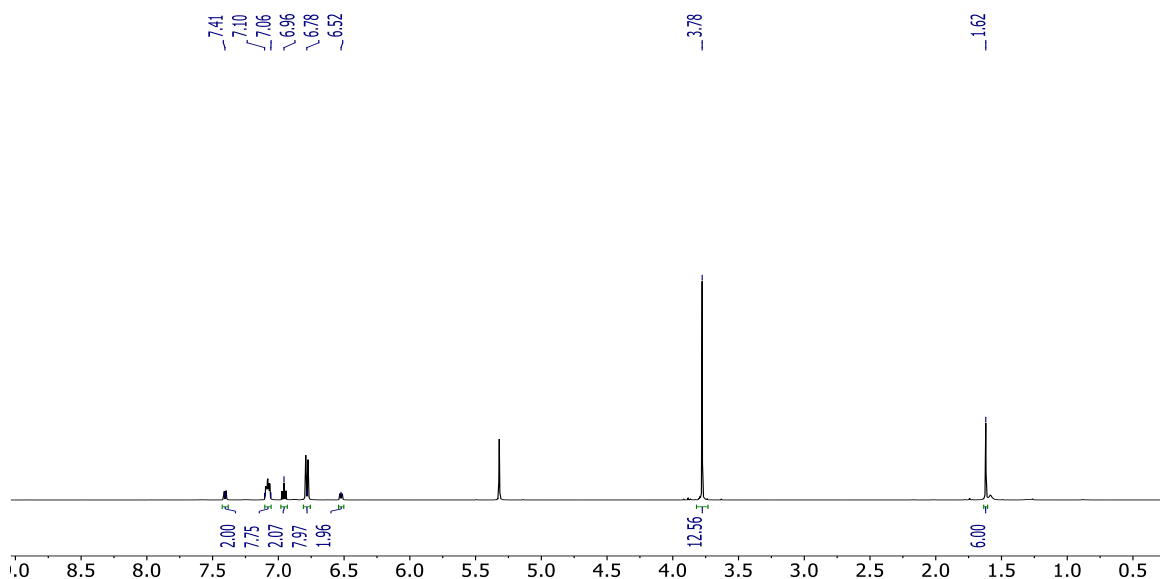
¹H NMR (500 MHz, CD₂Cl₂, 298 K): δ (ppm) = 7.41 (dd, J = 7.8 Hz, J = 1.4 Hz, 2H, CH_{Ar}), 7.10-7.06 (m, 8H, CH_{Ar}), 6.96 (t, J = 7.6 Hz, 2H, CH_{Ar}), 6.78 (d, J = 8.6 Hz, 8H, CH_{Ar}), 6.52 (dq, J = 7.7 Hz, J = 1.9 Hz, 2H, CH_{Ar}), 3.78 (s, 12H, OCH₃), 1.62 (s, 6H, CH₃).

¹³C-{¹H} NMR (126 MHz, CD₂Cl₂, 298 K): δ (ppm) = 160.5 (s, C_q), 152.8 (t, J = 9.4 Hz, C_q), 135.7 (t, J = 11.6 Hz, CH_{Ar}), 132.2 (s, CH_{Ar}), 130.6 (s, C_q), 129.0 (t, J = 4.9 Hz, C_q), 127.1-127.0 (m, C_q), 126.8 (s, CH_{Ar}), 123.8 (s, CH_{Ar}), 114.3 (s, CH_{Ar}), 55.6 (s, OCH₃), 34.9 (s, C_q), 32.1 (s, CH₃).

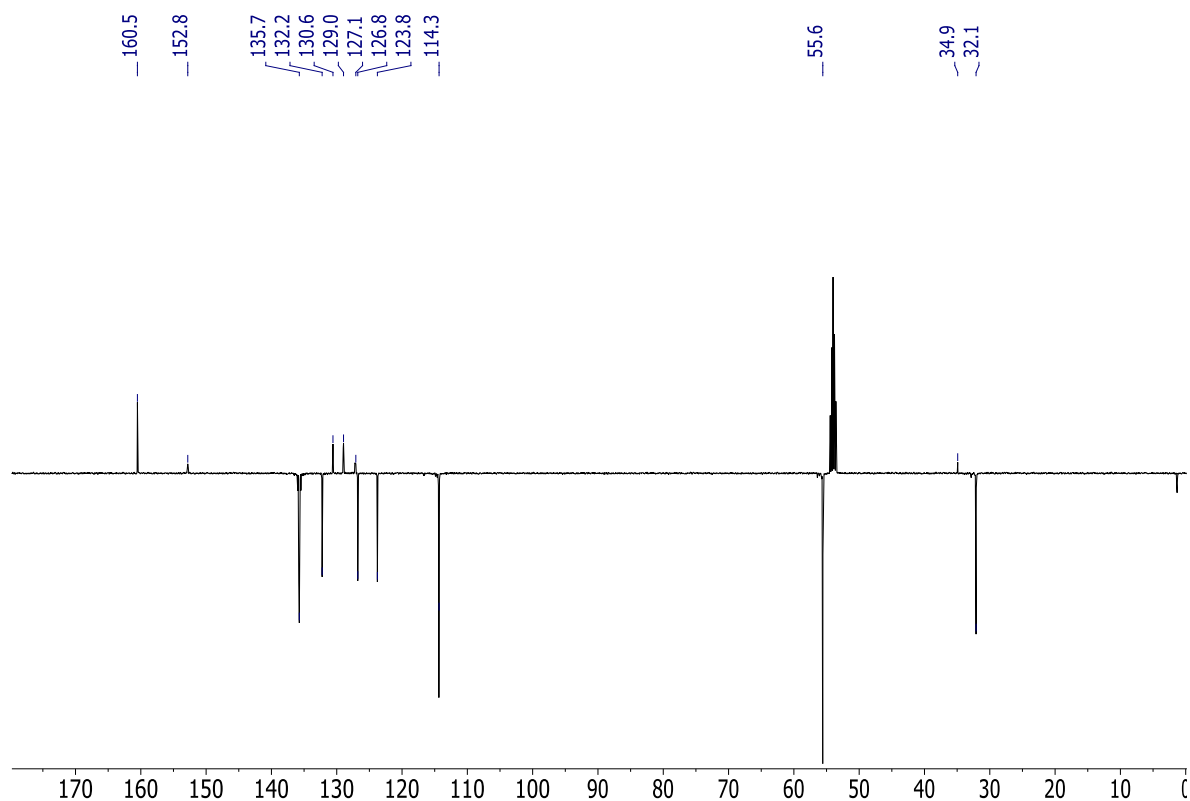
³¹P-{¹H} NMR (202 MHz, CD₂Cl₂, 298 K): δ (ppm) = -21.08 (s).

mp: 211-212 °C.

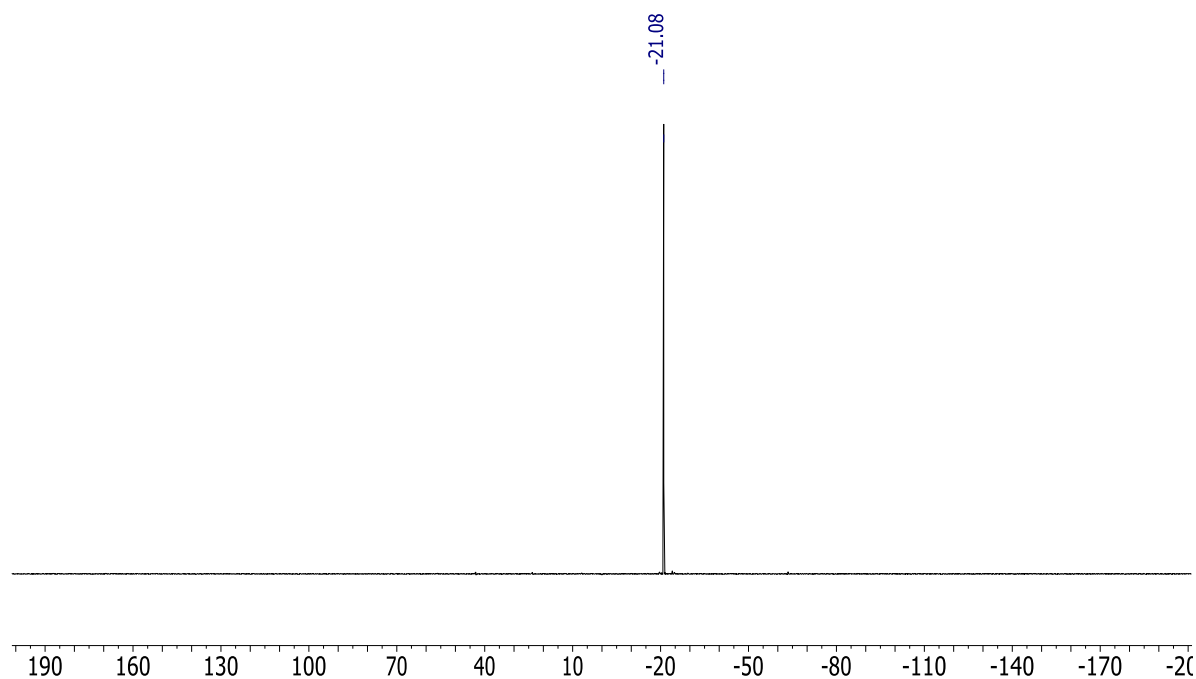
¹H NMR (500 MHz, CD₂Cl₂, 298 K)



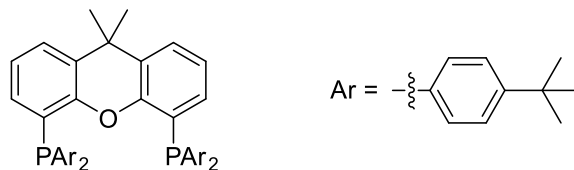
$^{13}\text{C}\{-^1\text{H}\}$ NMR (126 MHz, CD_2Cl_2 , 298 K)



$^{31}\text{P}\{-^1\text{H}\}$ NMR (202 MHz, CD_2Cl_2 , 298 K)



4,5-Bis(di-*p*-tert-butylphenylphosphino)-9,9-dimethylxanthene (*p*-*t*-Bu xantphos ligand) (9e)



At room temperature, a solution of 1-bromo-4-tert-butylbenzene (1.075 g, 0.88 mL, 5.05 mmol) in THF (4 mL) was added dropwise to the stirred suspension of the activated magnesium turnings. The reaction was followed by GCMS after quenching an aliquot of the reaction mixture with deuterated methanol. After affording the Grignard reagent, approximately after two hours, the product was filtered and added dropwise to a stirred solution of 9-dimethyl-4,5-bis(dichlorophosphino)xanthene (500 mg, 1.21 mmol) in THF (10 mL) at -20 °C (ice bath with NaCl). The reaction mixture was stirred and allowed to warm to room temperature overnight. Subsequently, the reaction mixture was hydrolyzed with a solution of 1N HCl/Brine 1:1 (10 mL). The aqueous phase was separated, washed with CH₂Cl₂ (3x20 mL) and toluene (2x20 mL). The organic phases were combined, dried over Na₂SO₄ and volatiles were removed under vacuum. The resulting white powder was washed with hexanes and recrystallized from a saturated solution of the compound in CH₂Cl₂ layered with ethanol obtaining a white crystalline powder. Yield: 870 mg, 90%.

¹H NMR (500 MHz, CD₂Cl₂, 298 K): δ (ppm) = 7.45(dd, J = 7.8 Hz, J = 1.3 Hz, 2H, CH_{Ar}), 7.37 (d, J = 8.1 Hz, 8H, CH_{Ar}), 7.24-7.15 (m, 8H, CH_{Ar}), 7.01 (t, J = 7.6 Hz, 2H, CH_{Ar}), 6.65 (dq, J = 7.5 Hz, J = 1.6 Hz, 2H, CH_{Ar}), 1.67 (s, 6H, CH₃), 1.35 (s, 36H, CH₃).

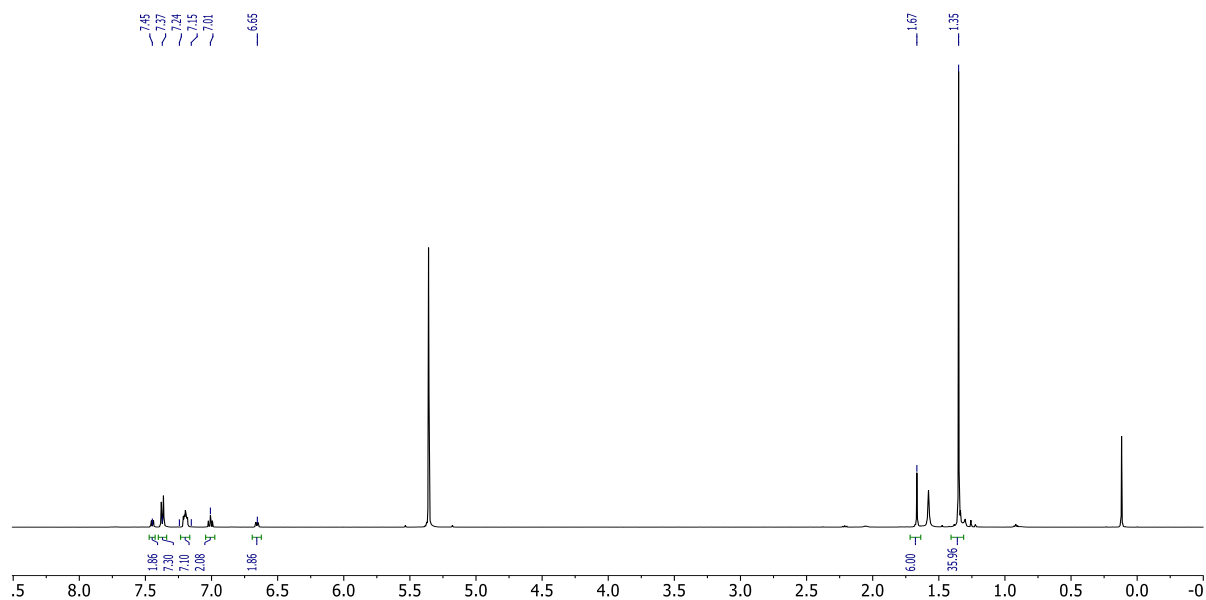
¹³C-{¹H} NMR (126 MHz, CD₂Cl₂, 298 K): δ (ppm) = 152.3 (m, C_q), 151.4 (s, C_q), 134.1 (t, J = 6.2 Hz, C_q), 133.7 (t, J = 10.9 Hz, CH_{Ar}), 132.1 (s, CH_{Ar}), 129.9 (s, C_q), 126.5 (s, CH_{Ar}), 125.2 (t, J = 3.8 Hz, CH_{Ar}), 123.2 (s, CH_{Ar}), 34.5 (s, C_q), 31.8 (s, CH₃), 31.0 (s, CH₃). 2 C_q missing.

³¹P-{¹H} NMR (202 MHz, CD₂Cl₂, 298 K): δ (ppm) = -22.24 (s).

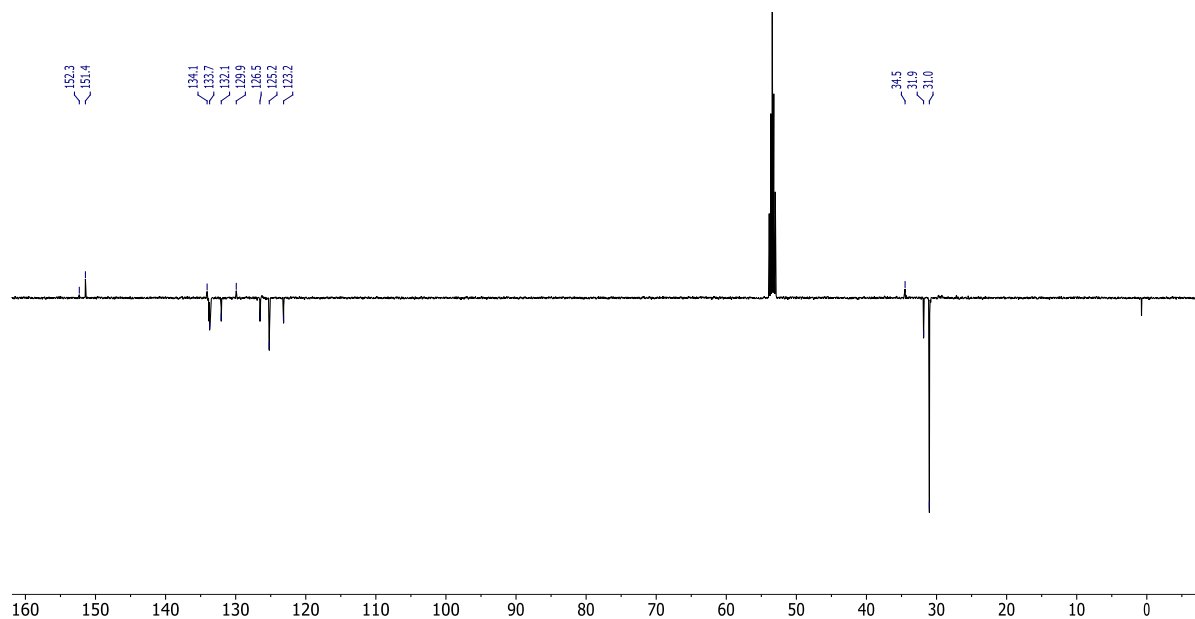
Anal. Calcd C₅₅H₆₄OP₂: C, 82.26; H, 8.03 Found: C, 82.13; H, 7.85.

mp: 208-209 °C.

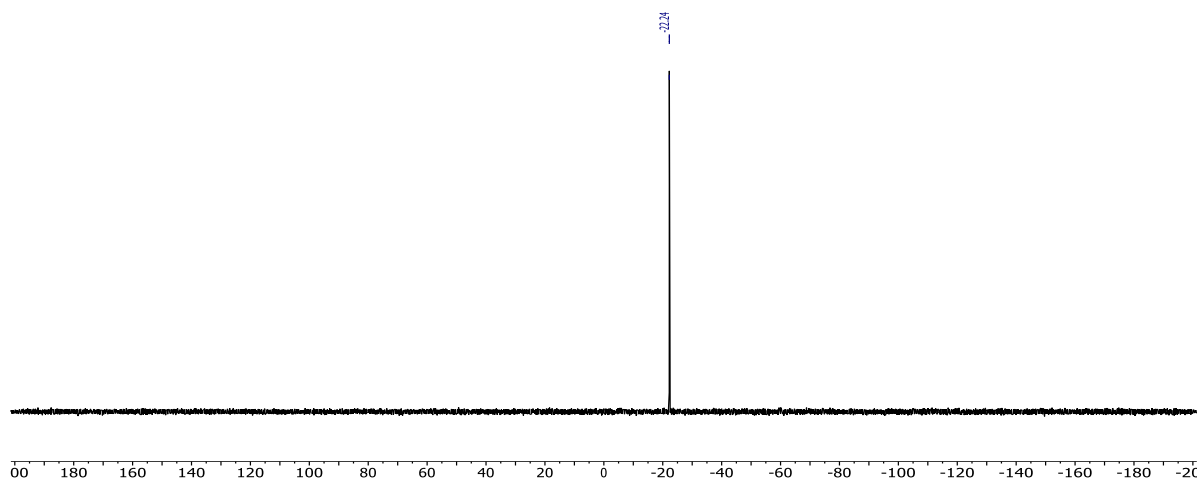
^1H NMR (500 MHz, CD_2Cl_2 , 298 K)



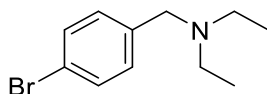
$^{13}\text{C}\{-^1\text{H}\}$ NMR (126 MHz, CD_2Cl_2 , 298 K)



$^{31}\text{P}\{-^1\text{H}\}$ NMR (202 MHz, CD_2Cl_2 , 298 K)

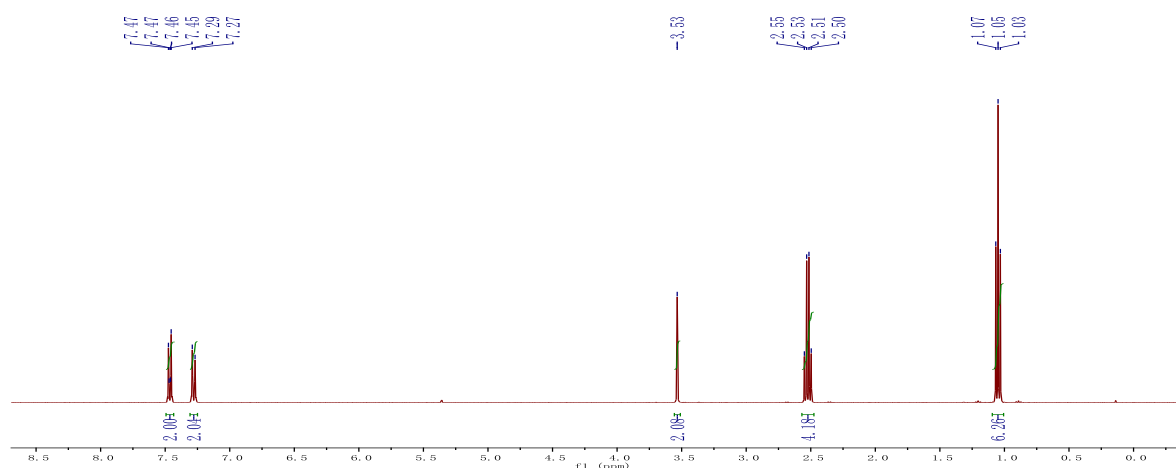


(p-bromobenzyl)diethylamine (VII)

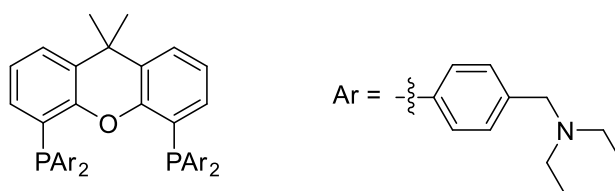


At $-20\text{ }^\circ\text{C}$ a solution of 4-bromobenzyl bromide (60 mmol, 15 g) in Et_2O (38 mL) was added to an excess of diethyl amine (540 mmol, 56.25 mL) over 1 hour. The reaction is slightly exothermic. After stirring for 2 hours the precipitate which formed was filtered off and washed three times with Et_2O . The filtrate was concentrated and the product was purified by flash column chromatography (silica gel, 400 g, EtOAc /hexane 25/75) giving a yellowish oil. Yield 85% (12.48 g).

^1H NMR (CD_2Cl_2 , 400 MHz, 298 K): δ (ppm) = 7.51 – 7.42 (m, 2H, CH_{Ar}), 7.32 – 7.24 (m, 2H, CH_{Ar}), 3.53 (s, 2H, CH_2), 2.52 (q, $J = 7.1$ Hz, 4H, CH_2), 1.05 (t, $J = 7.1$ Hz, 3H, CH_3). Data were found to match literature.⁶

^1H NMR (CDCl_3 , 400 MHz, 298 K)

4,5-bis[bis(4-((diethylamino)methyl)phenyl)phosphino]-10,10'-dimethylxanthene, xantham (9c)



At room temperature, a solution of (4-bromobenzyl)diethylamine (7.26 g, 30 mmol, 5.85 mL) in THF (30 mL) was added dropwise to a stirred mixture of magnesium turnings (1.75 g, 72 mmol) activated with 1,2-dibromoethane (0.54 mL) in THF (16 mL), the reaction was followed by GCMS and after 3 hours the product was filtered and added dropwise to a stirred solution of 9-dimethyl-4,5-bis(dichlorophosphino)xanthene (2.76 g, 6 mmol) in THF (54 mL) at 0 °C, then allowed to warm to room temperature and stirred overnight., the reaction mixture was hydrolyzed with 0.15 M H_2SO_4 (100 mL). The aqueous phase was separated, washed with CH_2Cl_2 (3x50 mL), toluene (2x50 mL) and neutralized with a saturated solution of NaHCO_3 . Extraction with CH_2Cl_2 (4x50 mL) and evaporation of the combined organic phases resulted in a yellowish powder which was crystallized from acetonitrile giving a white powder. Yield 90% (4.1 g).

^1H NMR (C_6D_6 , 400 MHz, 298 K): δ (ppm) = 7.57 – 7.50 (m, 8H, CH_{Ar}), 7.31 (d, J = 8.0 Hz, 8H, CH_{Ar}), 7.08 (dd, J = 7.8, J = 1.5 Hz, 2H, CH_{Ar}), 6.99 (dd, J = 7.5, J = 1.6 Hz, 2H,

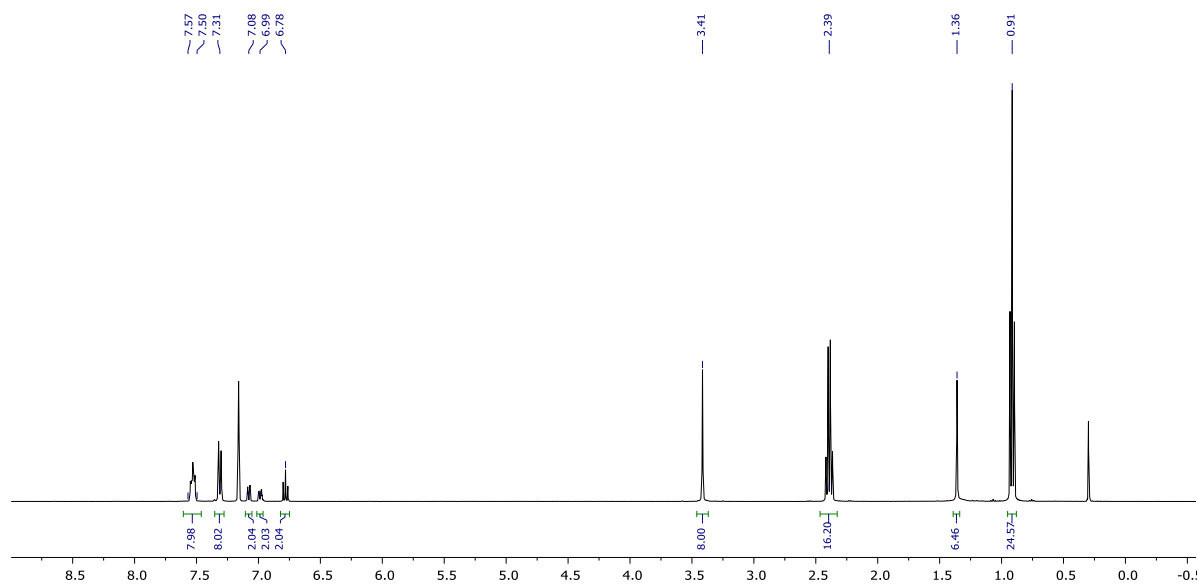
CH_{Ar}), 6.78 (t, $J = 7.6$ Hz, 2H, CH_{Ar}), 3.41 (s, 8H, CH_2), 2.39 (q, $J = 7.1$ Hz, 16H, CH_2), 1.36 (s, 6H, CH_3), 0.91 (t, $J = 7.1$ Hz, 24H, CH_3).

$^{13}\text{C}\{-^1\text{H}\}$ NMR (C_6D_6 , 100 MHz, 298 K): δ (ppm) = 153.1 (s, C_q), 141.2 (s, C_q), 136.5 (t, $J = 7.1$ Hz, C_q), 134.6 (t, $J = 9.9$ Hz, CH_{Ar}), 132.6 (s, CH_{Ar}), 130.2 (s, C_q), 129.0 (t, $J = 3.6$ Hz, CH_{Ar}), 126.6 (s, CH_{Ar}), 123.7 (s, CH_{Ar}), 58.0 (s, CH_2), 47.1 (s, CH_2), 34.2 (HMBC, C_q), 31.9 (s, CH_3), 12.3 (s, CH_3), 1 C_q missing.

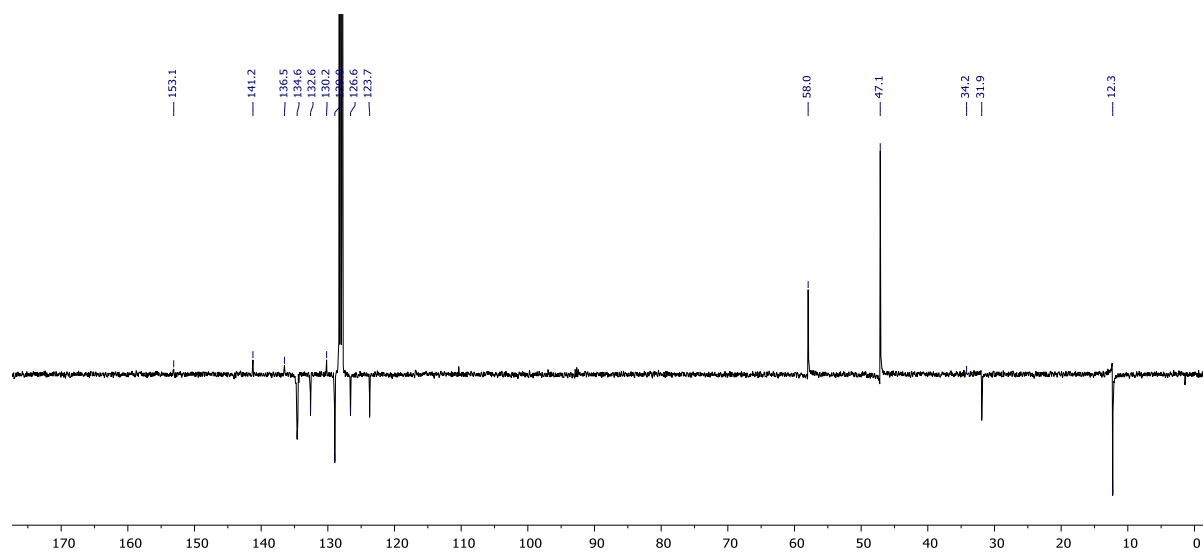
$^{31}\text{P}\{-^1\text{H}\}$ NMR (C_6D_6 , 162 MHz, 298 K): δ (ppm) = -19.3 (s). Data was found to match with literature⁶

mp: 287-288°C.

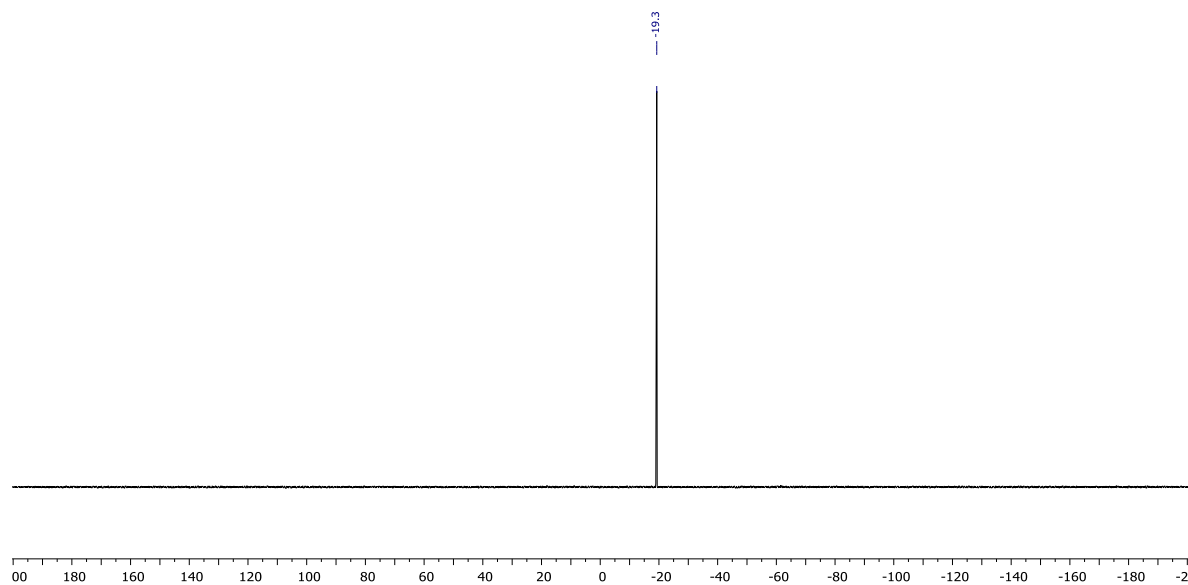
^1H NMR (400 MHz, C_6D_6 , 298 K)



$^{13}\text{C}\{-^1\text{H}\}$ NMR (100 MHz, C_6D_6 , 298 K)

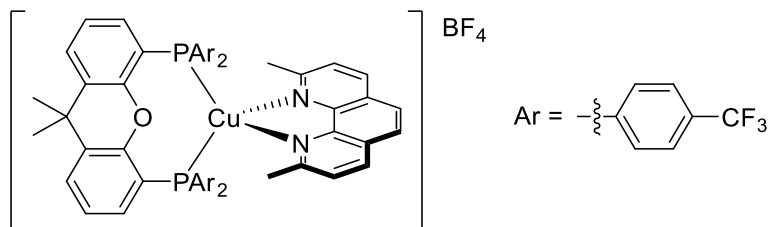


$^{31}\text{P}\{-^1\text{H}\}$ NMR (162 MHz, C_6D_6 , 298 K)



Synthesis of complexes

[Cu(neocuproine)(p-CF₃ xantphos)]BF₄ (1)



[Cu(MeCN)₄]₂BF₄ (0.11 mmol, 34.6 mg) was dissolved in CH₂Cl₂ (5 mL) in an Schlenk flask equipped with a magnetic stirrer. Then a solution of *p*-CF₃ xantphos ligand (0.11 mmol, 100 mg) in CH₂Cl₂ (5 mL) was added dropwise at -78 °C (dry ice/acetone bath), the whole procedure was carried out at this temperature. The mixture was stirred for two hours resulting in a colorless solution. Then, a solution of neocuproine (0.11 mmol, 22.9 mg) in CH₂Cl₂ (7 mL) was added dropwise and the resulting yellow solution was stirred for two hours. The resulting solution was filtered through celite in inert atmosphere. Solvents were evaporated and the complex redissolved in 2 mL of CH₂Cl₂ and precipitated by the addition of 25 mL of Et₂O. The mixture was stirred for two hours. The yellow precipitate was washed with Et₂O. The complex was recrystallized by slow diffusion of Et₂O in a saturated solution of the complex in CH₂Cl₂. The pale yellow crystals were washed with pentane and dried under vacuum overnight providing a pale orange powder. Yield: 110 mg, 78%.

¹H NMR (400 MHz, CD₂Cl₂, 298 K): δ (ppm) = 8.36 (d, *J* = 8.3 Hz, 2H, CH_{Ar}), 7.87 (s, 2H, CH_{Ar}), 7.78 (dd, *J* = 7.9 Hz, *J* = 1.5 Hz, 2H, CH_{Ar}), 7.58 (d, *J* = 8.2 Hz, 2H, CH_{Ar}), 7.32 (d, *J* = 8.2 Hz, 8H, CH_{Ar}), 7.28 (t, *J* = 7.8 Hz, 2H, CH_{Ar}), 7.18-7.11 (m, 8H, CH_{Ar}), 6.88-6.81 (m, 10H, CH_{Ar}), 2.26 (s, 6H, CH₃), 1.79 (s, 6H, CH₃).

¹³C-{¹H} NMR (100 MHz, CD₂Cl₂, 298 K): δ (ppm) = 159.1 (s, C_q), 155.4 (t, *J* = 6.6 Hz, C_q), 143.2 (s, C_q), 138.9 (s, CH_{Ar}), 136.0 (t, *J* = 15.2 Hz, C_q), 134.8 (t, *J* = 1.8 Hz, C_q), 133.9 (t, *J* = 8.1 Hz, C_q), 132.8 (q, *J* = 33.1 Hz, C_q), 130.8 (s, CH_{Ar}), 129.3 (s, CH_{Ar}), 128.5 (s, C_q), 126.8 (s, CH_{Ar}), 126.7 (t, *J* = 2.1 Hz, CH_{Ar}), 126.2 (s, CH_{Ar}), 126.1 (s, CH_{Ar}), 124.0 (q, *J* = 272.8 Hz, C_q), 119.6 (t, *J* = 14.1 Hz, C_q), 36.8 (s, C_q), 28.8 (s, CH₃), 27.9 (s, CH₃).

³¹P-{¹H} NMR (162 MHz, CD₂Cl₂, 298 K): δ (ppm) = -12.59 (br s).

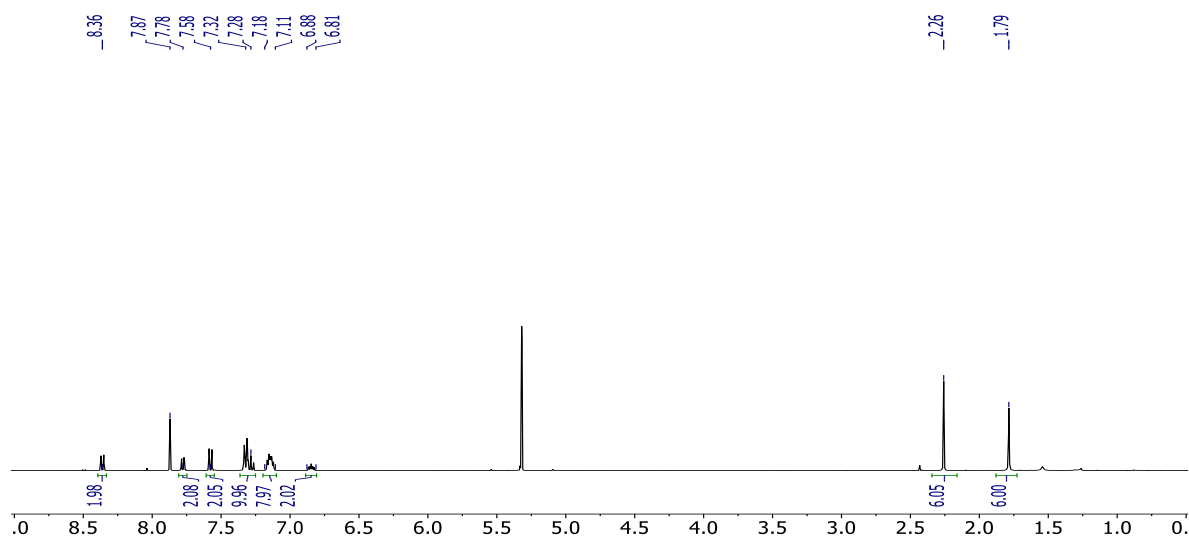
¹⁹F-{¹H} NMR (282 MHz, CD₂Cl₂, 298 K): δ (ppm) = -62.64 (s), -153.28 (s).

Anal. Calcd C₅₇H₄₀BCuF₁₆N₂OP₂: C, 56.62; H, 3.33 N, 2.32 Found: C, 56.52; H, 3.48 N, 2.52.

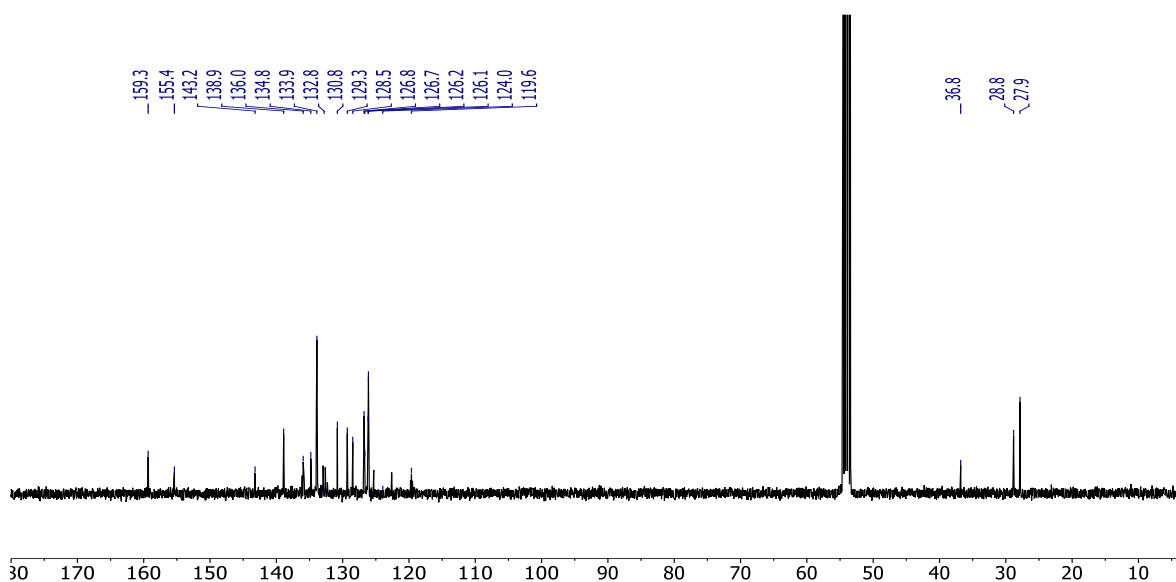
HRMS (ESI) *m/z*: [M-BF₄]⁺ Calcd for C₅₇H₄₀CuF₁₂N₂OP₂: 1121.1713; Found 1121.1713.

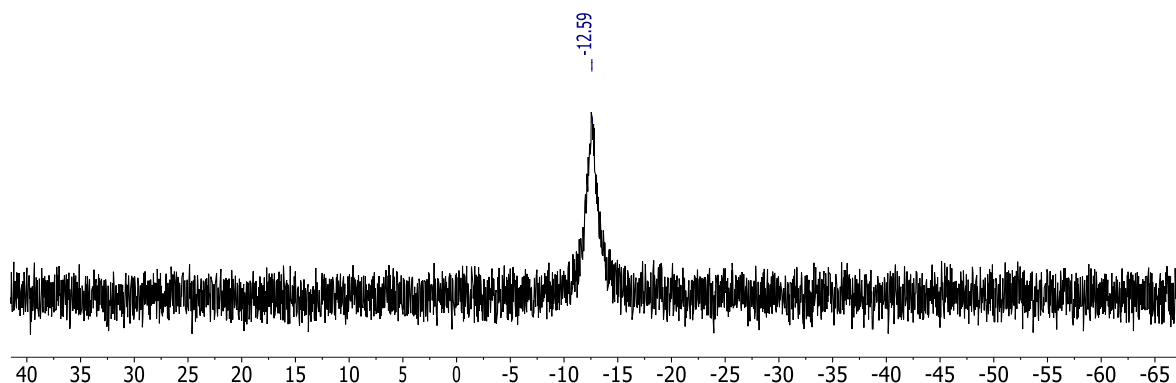
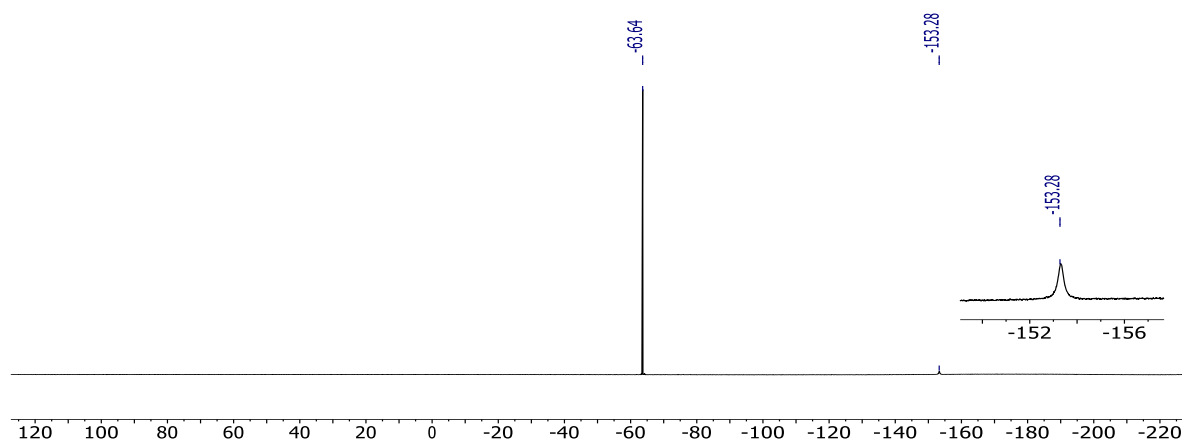
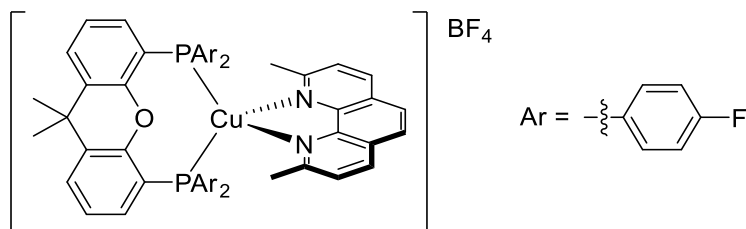
ATR-IR ν (cm⁻¹): 1409 (w), 1322 (m), 1124 (w), 1059 (m), 1013 (w), 831 (w), 697 (w), 600 (w), 510 (w), 411 (vw).

¹H NMR (400 MHz, CD₂Cl₂, 298 K)



¹³C-{¹H} NMR (100 MHz, CD₂Cl₂, 298 K)



$^{31}\text{P}\{-^1\text{H}\}$ NMR (162 MHz, CD_2Cl_2 , 298 K) $^{19}\text{F}\{-^1\text{H}\}$ NMR (282 MHz, CD_2Cl_2 , 298 K)***[Cu(neocuproine)(p-F xantphos)]BF₄ (2)***

$[\text{Cu}(\text{MeCN})_4]\text{BF}_4$ (0.15 mmol, 47.1 mg) was dissolved in CH_2Cl_2 (5 mL) in a Schlenk flask provided with a magnetic stirrer. Then a solution of *p*-F xantphos ligand (0.15 mmol, 100 mg) in CH_2Cl_2 (5 mL) was added dropwise at room temperature. The mixture was stirred for two hours resulting in a colorless solution. Then, a solution of neocuproine (0.15 mmol, 31.2 mg) in CH_2Cl_2 (7 mL) was added dropwise and the resulting yellow solution was stirred for two hours. The resulting solution was filtered through celite in inert atmosphere. Solvents were evaporated and the complex redissolved in 2 mL of CH_2Cl_2 and precipitated by the

addition of 25 mL of Et₂O. The mixture was stirred for two hours. The yellow precipitate was washed with Et₂O. The complex was recrystallized by slow diffusion of Et₂O in a saturated solution of the complex in CH₂Cl₂. The pale yellow crystals were washed with pentane and dried under vacuum overnight providing a yellow powder. Yield: 125 mg, 81%.

¹H NMR (400 MHz, CD₂Cl₂, 298 K): δ (ppm) = 8.37 (d, J = 8.3 Hz, 2H, CH_{Ar}), 7.91 (s, 2H, CH_{Ar}CH_{Ar}), 7.71 (dd, J = 7.8 Hz, J = 1.5 Hz, 2H, CH_{Ar}), 7.55 (d, J = 8.2 Hz, 2H, CH_{Ar}), 7.23 (t, J = 7.8 Hz, 2H, CH_{Ar}), 7.04-6.95 (m, 8H, CH_{Ar}), 6.82-6.74 (m, 10H, CH_{Ar}), 2.23 (s, 6H, CH₃), 1.76 (s, 6H, CH₃).

¹³C-{¹H} NMR (100 MHz, CD₂Cl₂, 298 K): δ (ppm) = 164.4 (d, J = 254.1 Hz, C_q), 159.4 (s, C_q), 155.4 (t, J = 6.6 Hz, C_q), 143.4 (s, C_q), 138.6 (s, CH_{Ar}), 135.6 (q, J = 8.5 Hz, CH_{Ar}), 134.6 (s, C_q), 130.6 (s, CH_{Ar}), 128.4 (s, CH_{Ar}), 127.4 (td, J = 17.5 Hz, J = 3.8 Hz, C_q), 126.7 (s, CH_{Ar}), 126.2 (t, J = 2.3 Hz, CH_{Ar}), 125.9 (s, CH_{Ar}), 121.6 (t, J = 13.5 Hz, C_q), 116.6 (dt, J_{F-C} = 21.4 Hz, J = 5.0 Hz, CH_{Ar}), 36.7 (s, C_q), 28.6 (s, CH₃), 27.7 (s, CH₃). 1C_q missing.

³¹P-{¹H} NMR (162 MHz, CD₂Cl₂, 298 K): δ (ppm) = -13.89 (br s).

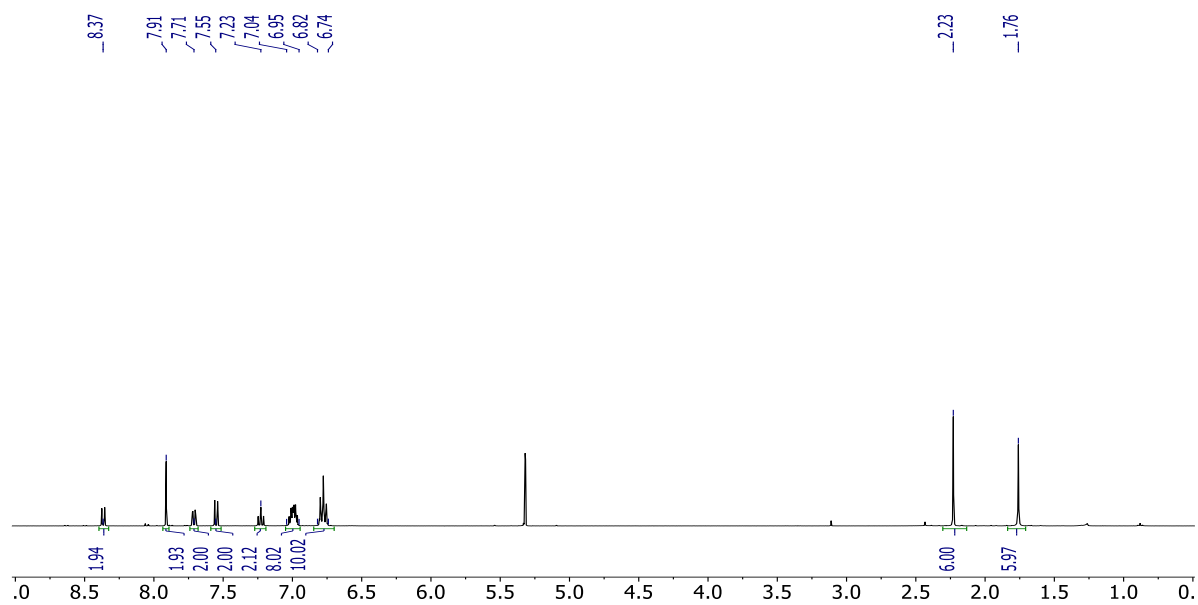
¹⁹F-{¹H} NMR (282 MHz, CD₂Cl₂, 298 K): δ (ppm) = -110.05 (m), -153.22 (s), -153.28 (s)

Anal. Calcd C₅₃H₄₀BCuF₈N₂OP₂: C, 63.08; H, 4.00; N, 2.78 Found: C, 62.90; H, 3.84; N, 2.84.

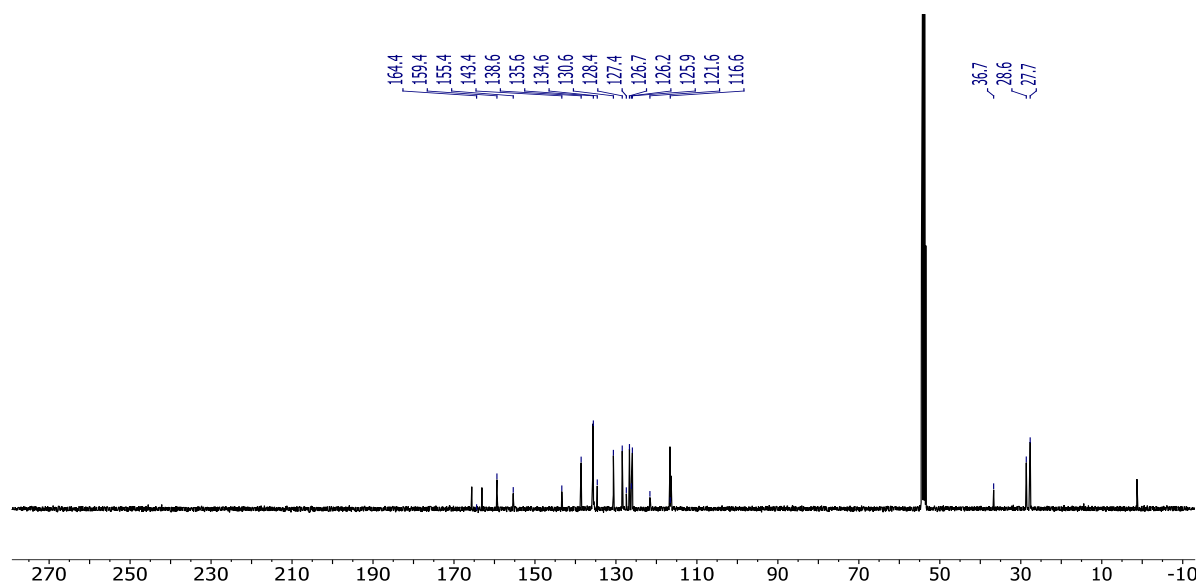
HRMS (ESI) m/z : [M-BF₄]⁺ Calcd for C₅₃H₄₀CuF₄N₂OP₂: 921.1840; Found 921.1840.

ATR-IR ν (cm⁻¹): 1590 (w), 1495 (w), 1405 (m), 1221 (m), 1162 (w), 1049 (m), 858 (w), 829 (m), 753 (w), 532 (w), 515 (m), 452 (w), 442 (w), 389 (w).

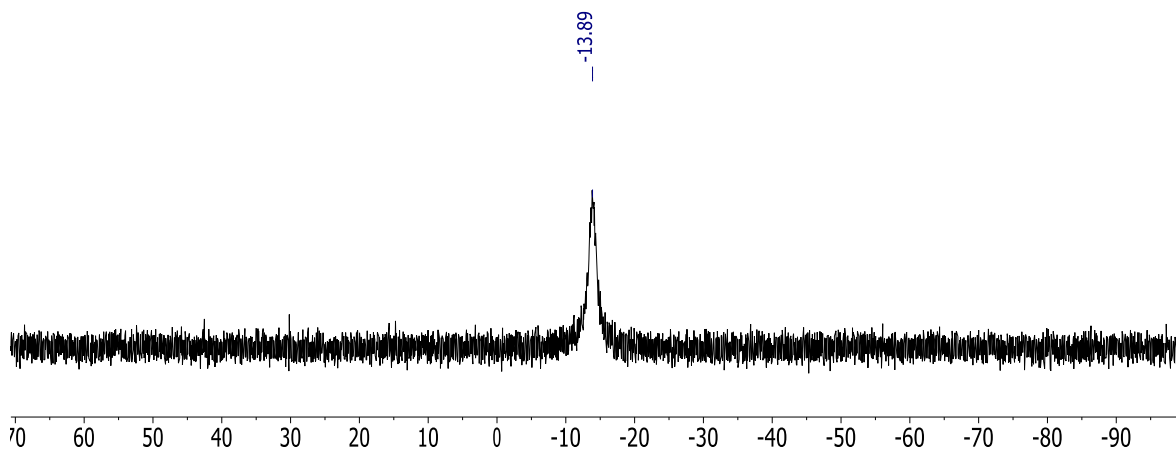
^1H NMR (400 MHz, CD_2Cl_2 , 298 K)



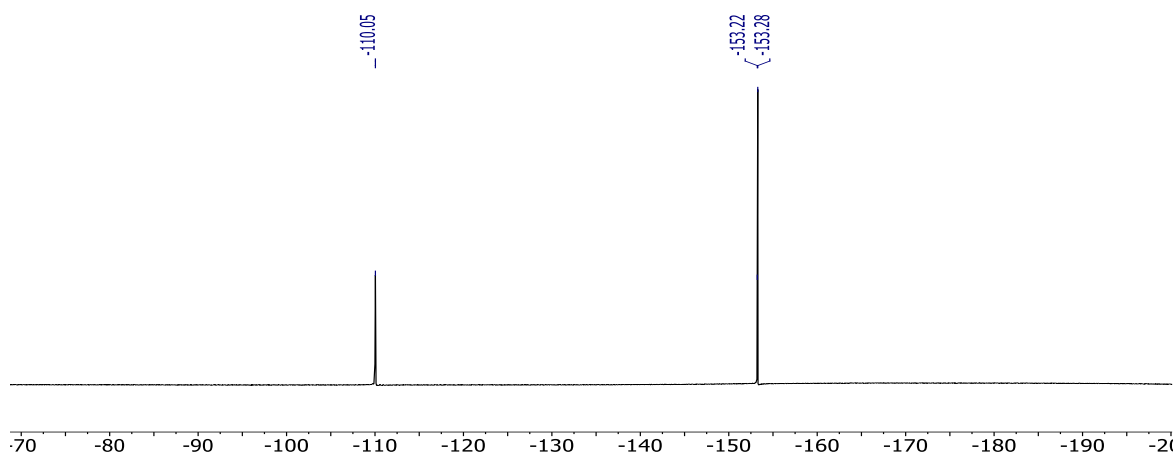
$^{13}\text{C}\{-^1\text{H}\}$ NMR (100 MHz, CD_2Cl_2 , 298 K)



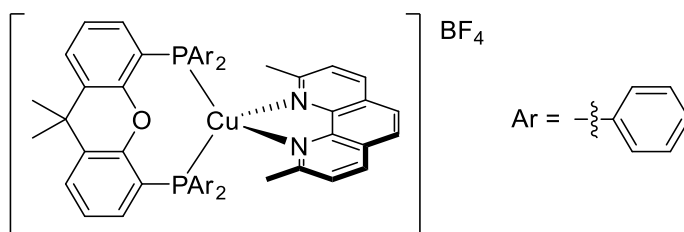
$^{31}\text{P}\{-^1\text{H}\}$ NMR (162 MHz, CD_2Cl_2 , 298 K)



$^{19}\text{F}\{-^1\text{H}\}$ NMR (282 MHz, CD_2Cl_2 , 298 K)



[Cu(neocuproine)(xantphos)]BF₄ (3)



$[\text{Cu}(\text{MeCN})_4]\text{BF}_4$ (0.17 mmol, 53.4 mg) was dissolved in CH_2Cl_2 (5 mL) in a Schlenk flask equipped with a magnetic stirrer. Then a solution of xantphos (0.17 mmol, 100 mg) in CH_2Cl_2 (5 mL) was added dropwise at room temperature. The mixture was stirred for two hours resulting in a colorless solution. Then, a solution of neocuproine (0.17 mmol, 35.4 mg) in CH_2Cl_2 (7 mL) was added dropwise and the resulting yellow solution was stirred for two

hours. The resulting solution was filtered through celite under inert atmosphere. Solvents were evaporated and the complex dissolved in 2 mL of CH₂Cl₂ and precipitated by the addition of 25 mL of Et₂O. The mixture was stirred for two hours. The yellow precipitate was washed with Et₂O. The complex was recrystallized by slow diffusion of Et₂O in a saturated solution of the complex in CH₂Cl₂. The pale yellow crystals were washed with pentane and dried under vacuum overnight obtaining a yellow powder. Yield: 133 mg, 82%.

¹H NMR (500 MHz, CD₂Cl₂, 298 K): δ (ppm) = 8.26 (d, *J* = 8.3 Hz, 2H, CH_{Ar}), 7.80 (s, 2H, CH_{Ar}), 7.68 (dd, *J* = 8.0 Hz, *J* = 1.5 Hz, 2H, CH_{Ar}), 7.48 (d, *J* = 8.3 Hz, 2H, CH_{Ar}), 7.25-7.17 (m, 6H, CH_{Ar}), 7.08-6.98 (m, 16H, CH_{Ar}), 6.94-6.88 (m, 2H, CH_{Ar}), 2.26 (s, 6H, CH₃), 1.74 (s, 6H, CH₃).

¹³C-{¹H} NMR (126 MHz, CD₂Cl₂, 298 K): δ (ppm) = 159.2 (s, C_q), 155.6 (s, C_q), 143.4 (s, C_q), 138.1 (s, CH_{Ar}), 134.4 (s, C_q), 133.5 (t, *J* = 7.8 Hz, CH_{Ar}), 132.0 (t, *J* = 16.5 Hz, C_q), 130.9 (s, CH_{Ar}), 130.4 (s, C_q), 129.1 (t, *J* = 4.1 Hz, CH_{Ar}), 128.3 (s, C_q), 128.1 (s, CH_{Ar}), 126.4 (s, CH_{Ar}), 125.8 (s, CH_{Ar}), 125.6 (s, CH_{Ar}), 121.9 (s, C_q), 35.5 (HMBC, C_q), 28.8 (s, CH₃), 27.6 (s, CH₃).

³¹P-{¹H} NMR (202 MHz, CD₂Cl₂, 298 K): δ (ppm) = -12.76 (br s).

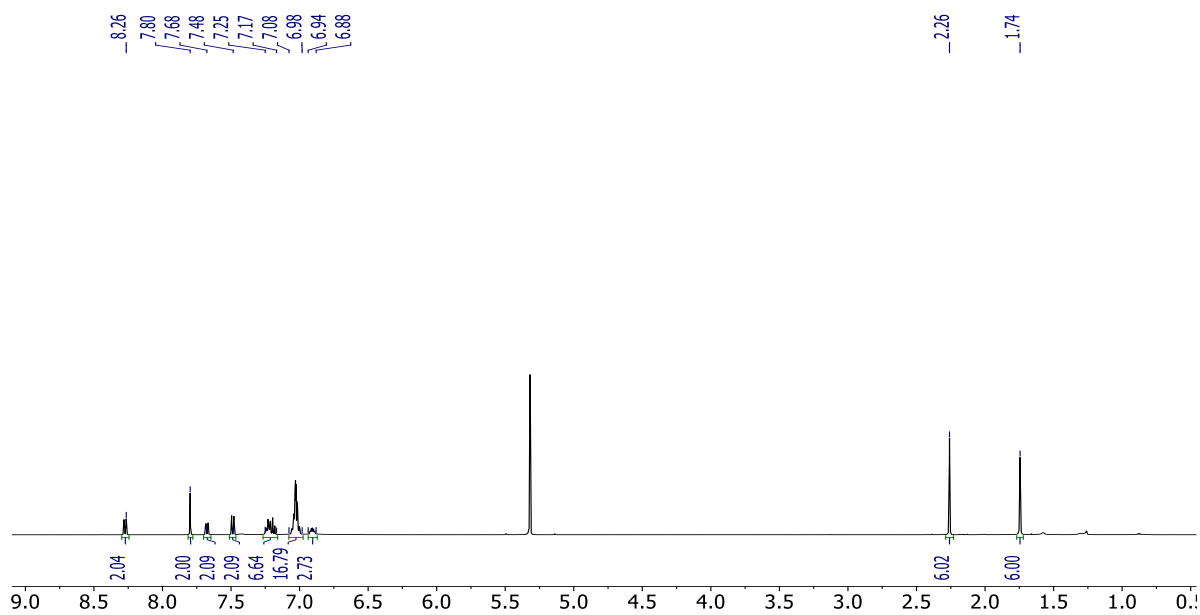
¹⁹F-{¹H} NMR (470 MHz, CD₂Cl₂, 298 K): δ (ppm) = -153.40 (s), -153.45 (s).

Anal. Calcd C₅₃H₄₄BCuF₄N₂OP₂: C, 67.92; H, 4.73; N, 2.99 Found: C, 67.81; H, 4.67; N, 2.95.

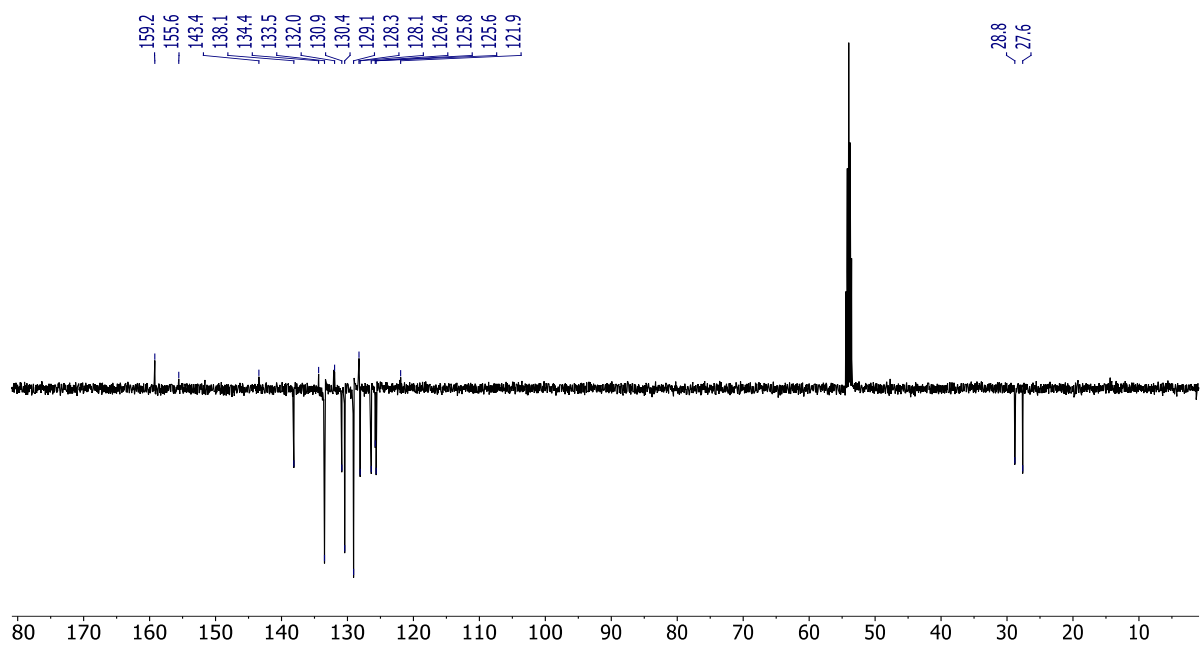
HRMS (ESI) *m/z*: [M-BF₄]⁺ Calcd for C₅₃H₄₄CuN₂OP₂: 849.2215; Found 849.2215.

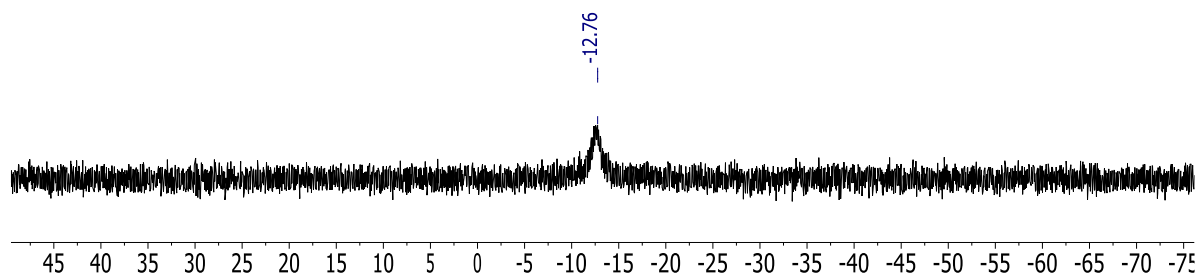
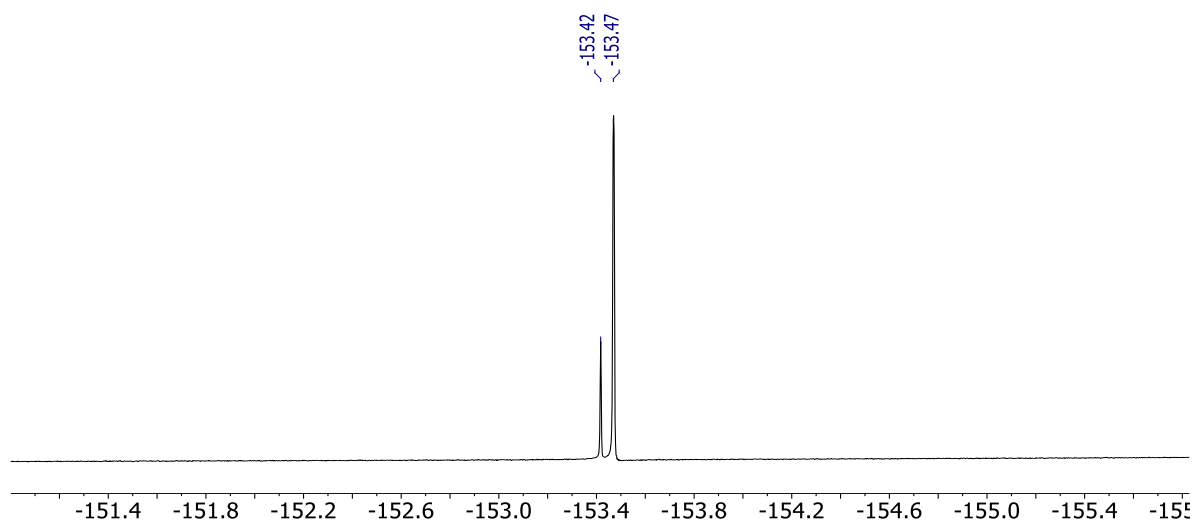
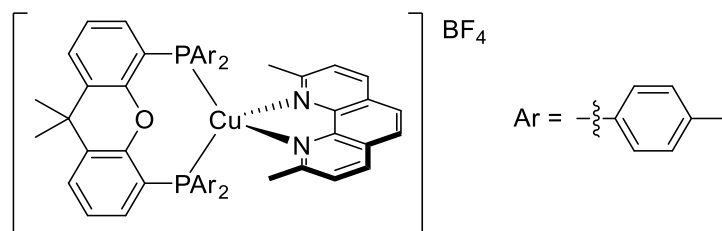
ATR-IR ν (cm⁻¹): 1434 (w), 1402 (m), 1224 (w), 1048 (m), 857 (w), 742 (m), 693 (m), 512 (m), 456 (m).

^1H NMR (500 MHz, CD_2Cl_2 , 298 K)



$^{13}\text{C}\{-^1\text{H}\}$ NMR (126 MHz, CD_2Cl_2 , 298 K)



$^{31}\text{P}\{-^1\text{H}\}$ NMR (202 MHz, CD_2Cl_2 , 298 K) $^{19}\text{F}\{-^1\text{H}\}$ NMR (470 MHz, CD_2Cl_2 , 298 K)***[Cu(neocuproine)(*p*-Me xantphos)]BF₄ (4)***

$[\text{Cu}(\text{MeCN})_4]\text{BF}_4$ (0.15 mmol, 47.1 mg) was dissolved in CH_2Cl_2 (5 mL) in a Schlenk flask equipped with magnetic stirrer. Then a solution of *p*-Me xantphos ligand (0.15 mmol, 100 mg) in CH_2Cl_2 (5 mL) was added dropwise at room temperature. The mixture was stirred for two hours resulting in a colorless solution. Then, a solution of neocuproine (0.15 mmol, 31.2 mg) in CH_2Cl_2 (7 mL) was added dropwise and the resulting yellow solution was stirred for two hours. The resulting solution was filtered through celite under inert atmosphere. Solvents

were evaporated, the complex redissolved in 2 mL of CH₂Cl₂ and precipitated by the addition of 25 mL of Et₂O. The mixture was stirred for two hours. The yellow precipitate was washed with Et₂O. The complex was recrystallized by slow diffusion of Et₂O in a saturated solution of the complex in CH₂Cl₂. The pale yellow crystals were washed with pentane and dried under vacuum overnight obtaining a dark yellow powder. Yield: 140 mg, 89%.

¹H NMR (500 MHz, CD₂Cl₂, 298 K): δ (ppm) = 8.28 (d, J = 8.2 Hz, 2H, CH_{Ar}), 7.81 (s, 2H, CH_{Ar}), 7.64 (dd, J = 7.9 Hz, J = 1.4 Hz, 2H, CH_{Ar}), 7.47 (d, J = 8.2 Hz, 2H, CH_{Ar}), 7.17 (t, J = 7.8 Hz, 2H, CH_{Ar}), 6.92-6.85 (m, 10H, CH_{Ar}), 6.81 (d, 3J = 7.5 Hz, 8H, CH_{Ar}), 2.23 (s, 18H, CH₃), 1.74 (s, 6H, CH₃).

¹³C-{¹H} NMR (126 MHz, CD₂Cl₂, 298 K): δ (ppm) = 159.2 (s, C_q), 155.5 (t, J = 6.6 Hz, C_q), 143.4 (s, C_q), 140.7 (s, C_q), 137.9 (s, CH_{Ar}), 134.3 (s, C_q), 133.4 (t, J = 8.3 Hz, CH_{Ar}), 130.7 (s, CH_{Ar}), 129.7 (t, J = 4.5 Hz, CH_{Ar}), 128.6 (t, J = 17.8 Hz, C_q), 128.2 (s, C_q), 127.8 (s, CH_{Ar}), 126.2 (s, CH_{Ar}), 125.6 (s, two signals overlap, CH_{Ar}), 122.5 (t, J = 12.6 Hz, C_q), 36.6 (s, C_q), 28.8 (s, CH₃), 27.6 (s, CH₃), 21.5 (s, CH₃).

³¹P-{¹H} NMR (202 MHz, CD₂Cl₂, 298 K): δ (ppm) = -13.67 (br s).

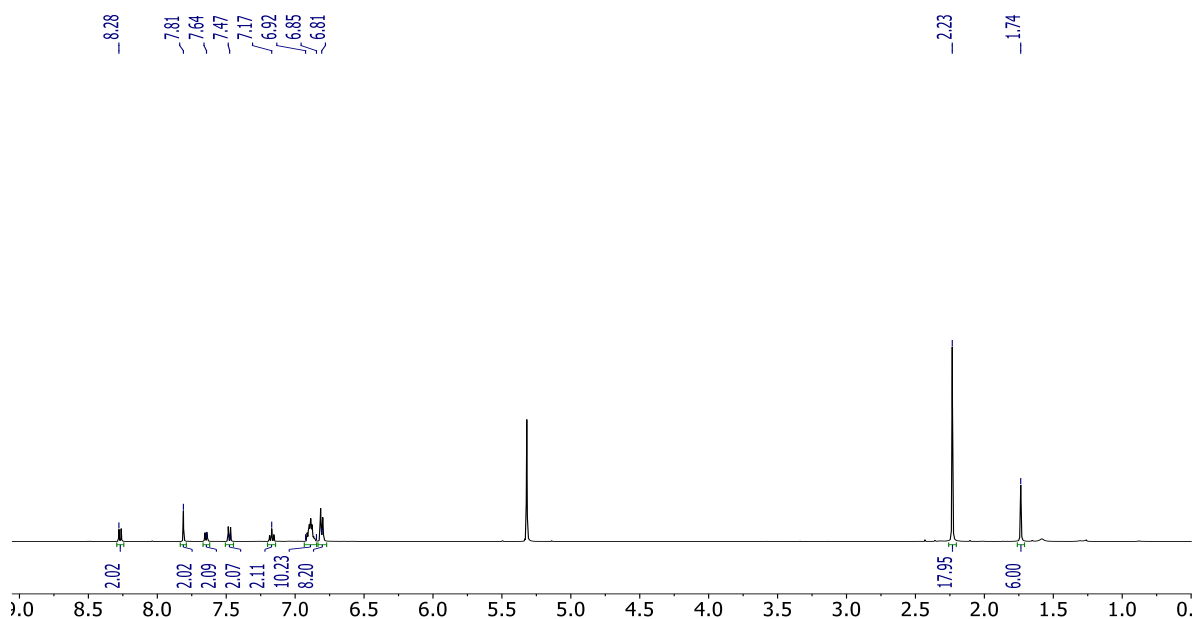
¹⁹F-{¹H} NMR (470 MHz, CD₂Cl₂, 298 K): δ (ppm) = -153.37 (s), -153.42 (s).

Anal. Calcd C₅₇H₅₂BCuF₄N₂OP₂: C, 68.92; H, 5.28; N, 2.82 Found: C, 68.86; H, 5.18; N, 2.97.

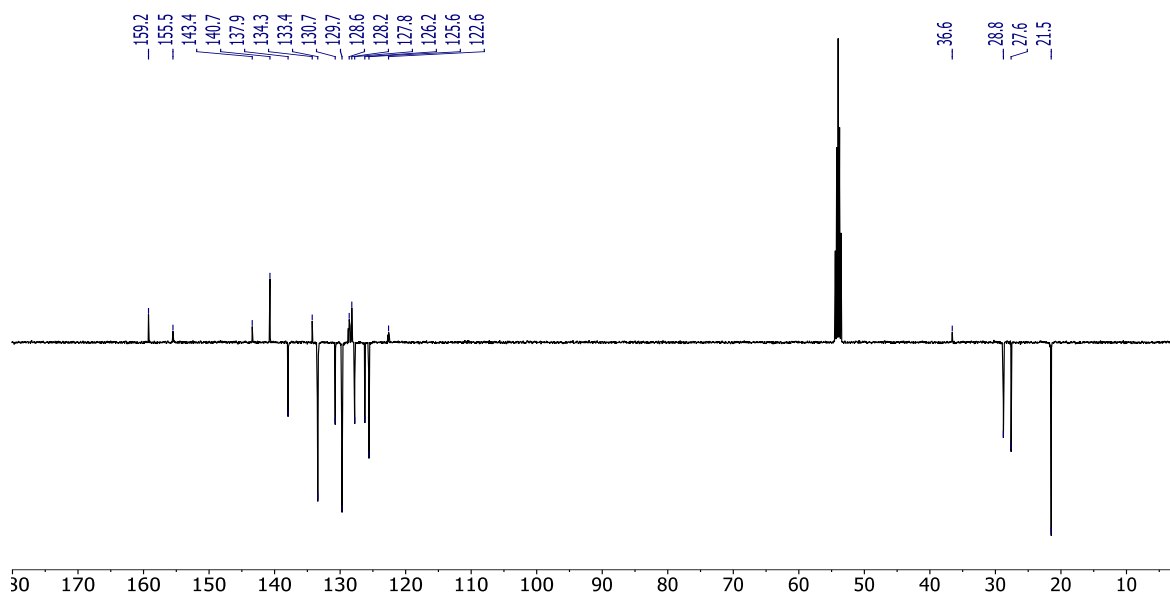
HRMS (ESI) m/z : [M-BF₄]⁺ Calcd for C₅₇H₅₂CuN₂OP₂: 905.2848; Found 905.2848.

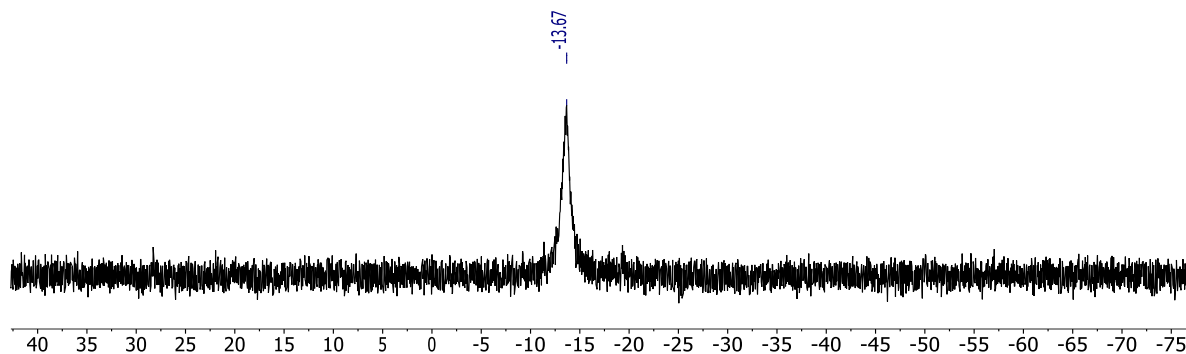
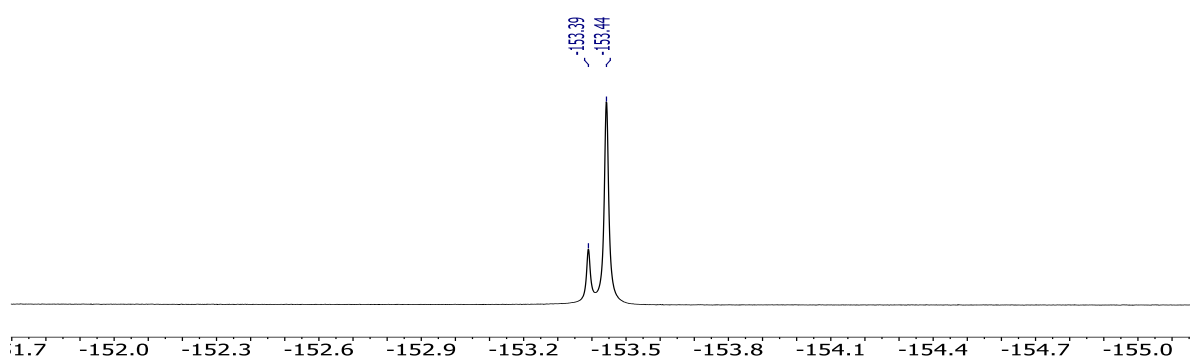
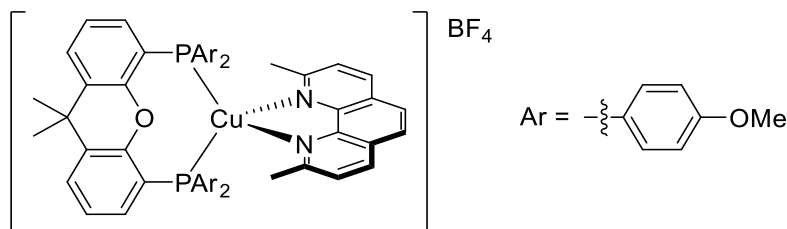
ATR-IR ν (cm⁻¹): 1403 (m), 1224 (m), 1048 (m), 857 (m), 803 (m), 750 (m), 730 (m), 616 (m), 507 (m), 444 (m).

^1H NMR (500 MHz, CD_2Cl_2 , 298 K)



$^{13}\text{C}\{-^1\text{H}\}$ NMR (126 MHz, CD_2Cl_2 , 298 K)



$^{31}\text{P}\{-^1\text{H}\}$ NMR (202 MHz, CD_2Cl_2 , 298 K) $^{19}\text{F}\{-^1\text{H}\}$ NMR (470 MHz, CD_2Cl_2 , 298 K)***[Cu(neocuproine)(p-OMe xantphos)]BF₄ (5)***

$[\text{Cu}(\text{MeCN})_4]\text{BF}_4$ (0.14 mmol, 44 mg) was dissolved in CH_2Cl_2 (5 mL) in a Schlenk flask equipped with a magnetic stirrer. Then a solution of *p*-OMe xantphos ligand (0.14 mmol, 100 mg) in CH_2Cl_2 (5 mL) was added dropwise at -78°C (dry ice/acetone bath), the whole procedure was carried out at this temperature. The mixture was stirred for two hours resulting in a colorless solution. Then, a solution of neocuproine (0.14 mmol, 29.1 mg) in CH_2Cl_2 (7 mL) was added dropwise and the resulting yellow solution was stirred for two hours. The resulting solution was filtered through celite under inert atmosphere. Solvents were evaporated and the complex redissolved in 2 mL of CH_2Cl_2 and precipitated by the addition of 25 mL of Et_2O . The mixture was stirred for two hours. The yellow precipitate was washed

with Et₂O. The complex was recrystallized by slow diffusion of diethyl ether into a saturated solution of the complex in CH₂Cl₂. The pale yellow crystals were washed with pentane and dried under vacuum overnight obtaining a light yellow powder. Yield: 121 mg, 80%.

¹H NMR (400 MHz, CD₂Cl₂, 298 K): δ (ppm) = 8.31 (d, J = 8.2 Hz, 2H, CH_{Ar}), 7.86 (s, 2H, CH_{Ar}), 7.64 (dd, J = 7.8 Hz, J = 1.5 Hz, 2H, CH_{Ar}), 7.50 (d, J = 8.2 Hz, 2H, CH_{Ar}), 7.17 (t, J = 7.8 Hz, 2H, CH_{Ar}), 6.96-6.88 (m, 8H, CH_{Ar}), 6.85-6.79 (m, 2H, CH_{Ar}), 6.56-6.51 (m, 8H, CH_{Ar}), 3.71 (s, 12H, OCH₃), 2.23 (s, 6H, CH₃), 1.74 (s, 6H, CH₃).

¹³C-{¹H} NMR (100 MHz, CD₂Cl₂, 298 K): δ (ppm) = 161.4 (s, C_q), 159.4 (s, C_q), 155.5 (s, C_q), 143.5 (s, C_q), 138.1 (s, CH_{Ar}), 135.0 (t, J = 8.5 Hz, CH_{Ar}), 134.3 (s, C_q), 130.6 (s, CH_{Ar}), 128.3 (s, C_q), 127.6 (s, CH_{Ar}), 126.4 (s, CH_{Ar}), 125.7 (m, two signals overlap, CH_{Ar}), 123.2 (t, J = 12.0 Hz, C_q), 122.8 (t, J = 18.6 Hz, C_q), 114.6 (t, J = 5.0 Hz, CH_{Ar}), 55.7 (s, OCH₃), 36.6 (s, C_q), 28.6 (s, CH₃), 27.6 (s, CH₃).

³¹P-{¹H} NMR (162 MHz, CD₂Cl₂, 298 K): δ (ppm) = -14.29 (br s).

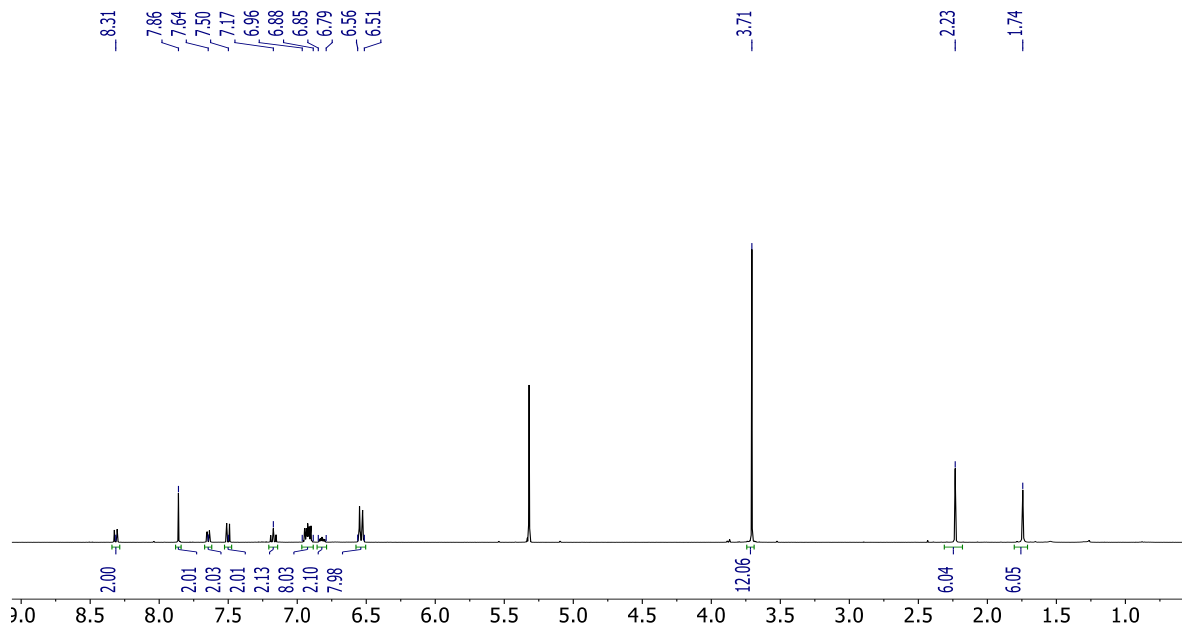
¹⁹F-{¹H} NMR (282 MHz, CD₂Cl₂, 298 K): δ (ppm) = -153.43 (s).

Anal. Calcd C₅₇H₅₂BCuF₄N₂O₅P₂: C, 64.75; H, 4.96; N, 2.65 Found: C, 64.76; H, 4.72; N, 2.29.

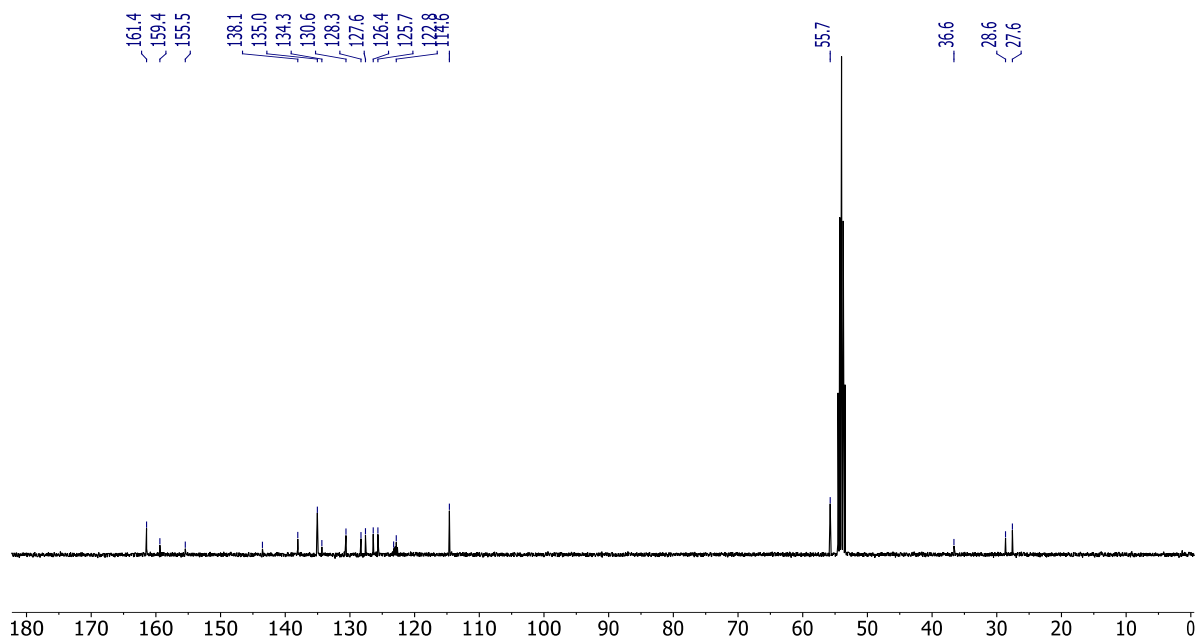
HRMS (ESI) m/z : [M-BF₄]⁺ Calcd for C₅₇H₅₂CuN₂O₅P₂: 969.2642; Found 969.26355

ATR-IR ν (cm⁻¹): 1593 (w), 1499 (m), 1404 (m), 1285 (w), 1251 (m), 1179 (m), 1097 (m), 1055 (m), 1023 (m), 826 (w), 797 (w), 752 (w), 534 (m), 433 (w).

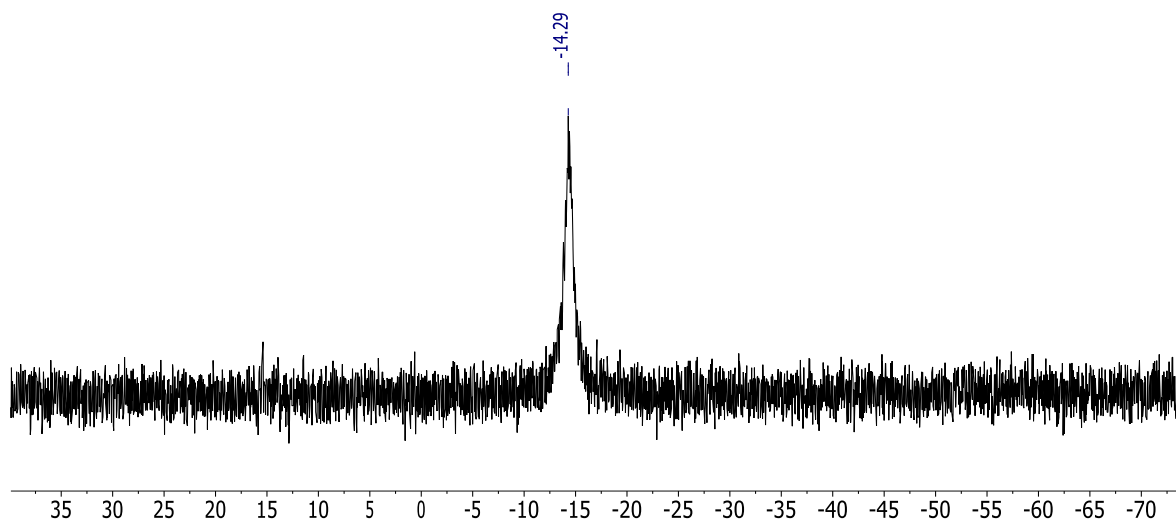
^1H NMR (400 MHz, CD_2Cl_2 , 298 K)



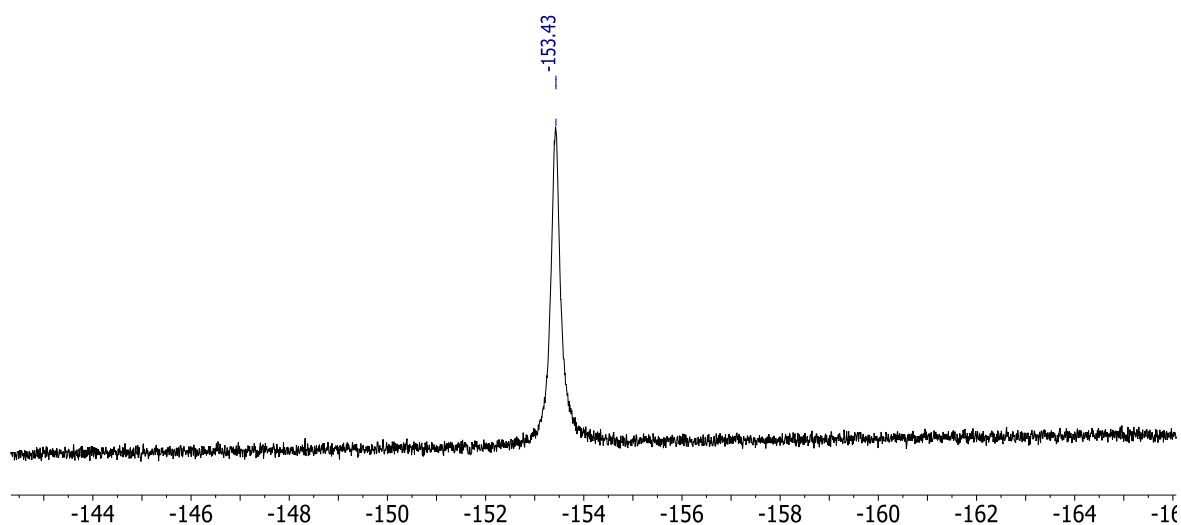
$^{13}\text{C}\{-^1\text{H}\}$ NMR (100.6 MHz, CD_2Cl_2 , 298 K)



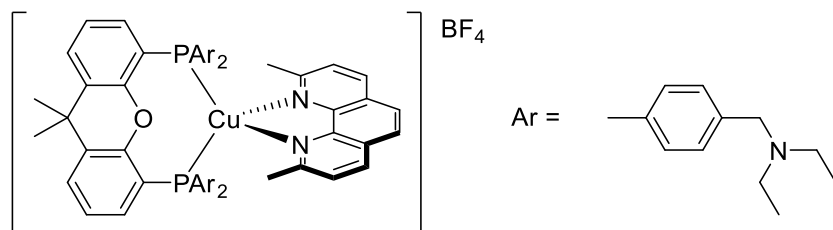
$^{31}\text{P}\{-^1\text{H}\}$ NMR (162 MHz, CD_2Cl_2 , 298 K)



$^{19}\text{F}\{-^1\text{H}\}$ NMR (282 MHz, CD_2Cl_2 , 298 K)



[Cu(neocuproine)(*p*-CH₂N(Et)₂ xantphos)]BF₄ (IX)



$[\text{Cu}(\text{MeCN})_4]\text{BF}_4$ (0.15 mmol, 47.1 mg) was dissolved in CH_2Cl_2 (5 mL) in a Schlenk flask equipped with a magnetic stirrer. Then a solution of *p*-CH₂N(Et)₂ xantphos ligand (0.15 mmol, 137.88 mg) in CH_2Cl_2 (5 mL) was added dropwise at room temperature. The mixture

was stirred for two hours resulting in a colorless solution. Then, a solution of neocuproine (0.15 mmol, 31.2 mg) in CH₂Cl₂ (7 mL) was added dropwise and the resulting green-yellow solution was stirred for two hours. The resulting solution was filtered through celite under inert atmosphere. Solvents were evaporated and the complex redissolved in 2 mL of CH₂Cl₂ and precipitated by the addition of 25 mL of Et₂O. The mixture was stirred for two hours. Solvents were removed by syringe and 25 mL of hexanes were added, the complex was sonicated for 20 minutes. The green-yellow precipitate was washed with Et₂O. It was not possible to obtain crystals suitable for X-ray analysis. The product was finally washed with pentane and dried under vacuum overnight obtaining a green-yellow powder. Yield: 145 mg, 76%.

¹H NMR (500 MHz, CD₂Cl₂, 298 K): δ (ppm) = 8.29 (d, J = 8.3 Hz, 2H, CH_{Ar}), 7.81 (s, 2H, CH_{Ar}), 7.69 (dd, J = 7.7 Hz, J = 1.4 Hz, 2H, CH_{Ar}), 7.51 (d, J = 8.3 Hz, 2H, CH_{Ar}), 7.23 (t, J = 7.8 Hz, 2H, CH_{Ar}), 7.07-6.97 (m, 18H, CH_{Ar}), 3.48 (s, 8H, CH₂), 2.49 (q, J = 7.3 Hz, 16H, CH₂), 2.29 (s, 6H, CH₃), 1.77 (s, 6H, CH₃), 1.01 (t, J = 7.3 Hz, 24H, CH₃).

¹³C-{¹H} NMR (126 MHz, CD₂Cl₂, 298 K): δ (ppm) = 158.6 (s, C_q), 155.1 (t, J = 6.5 Hz, C_q), 142.8 (s, C_q), 137.4 (s, CH_{Ar}), 133.8 (s, C_q), 132.8 (t, J = 8.1 Hz, CH_{Ar}), 130.3 (s, CH_{Ar}), 129.6 (m, C_q), 128.6 (s, CH_{Ar}), 127.5 (s, C_q), 127.3 (s, CH_{Ar}), 125.7 (s, CH_{Ar}), 125.1 (s, CH_{Ar}), 122.0 (m, C_q), 57.0 (s, CH₂), 46.8 (s, CH₂), 36.1 (s, C_q), 28.3 (s, CH₃), 27.0 (s, CH₃), 11.5 (s, CH₃). 1 CH_{Ar} and 1 C_q missing.

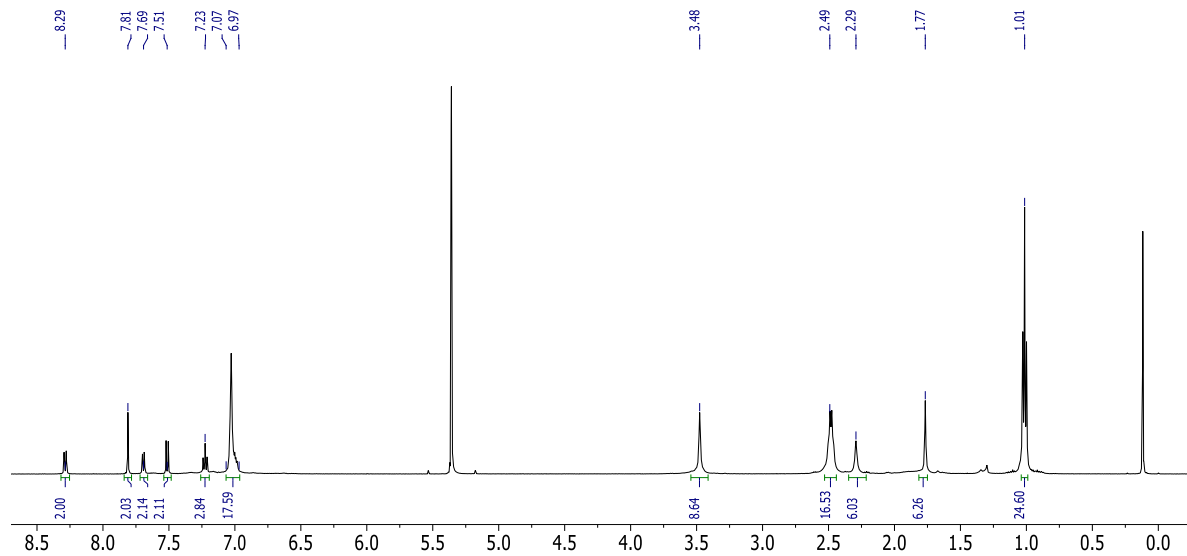
³¹P-{¹H} NMR (202 MHz, CD₂Cl₂, 298 K): δ (ppm) = -14.23 (br s).

¹⁹F-{¹H} NMR (470 MHz, CD₂Cl₂, 298 K): δ (ppm) = -152.80 (s), -152.83 (s).

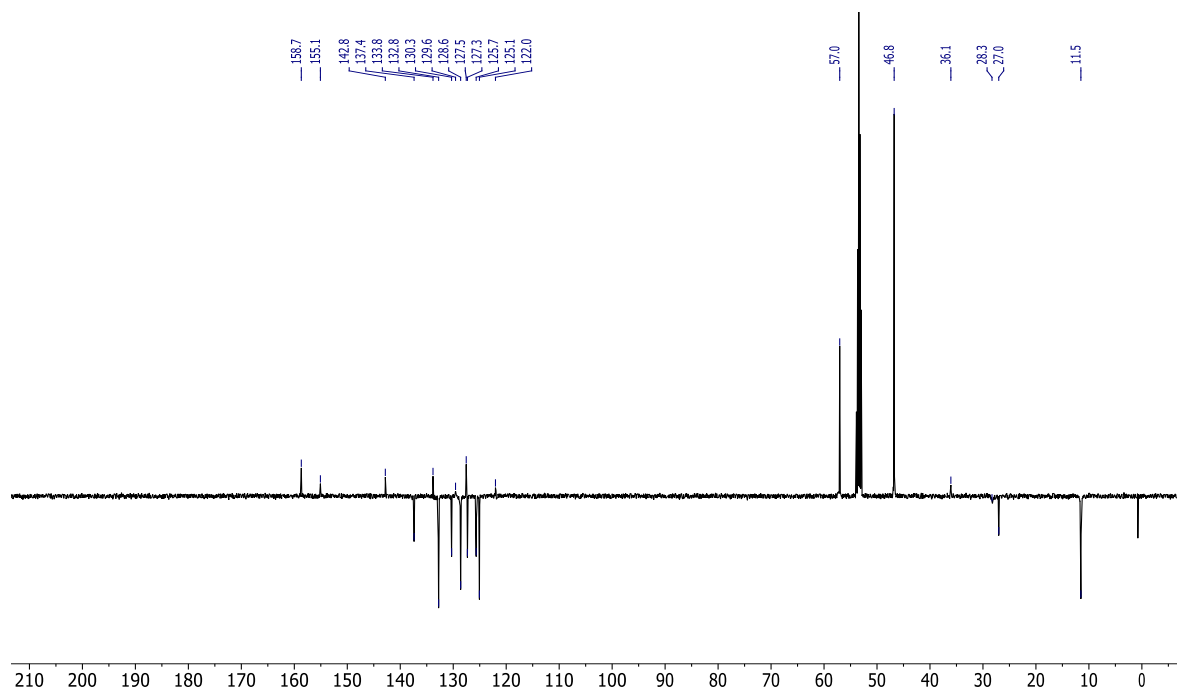
Anal. Calcd C₇₃H₈₈BCuF₄N₆OP₂ + 1CH₂Cl₂: C, 65.03; H, 6.66; N, 6.17 Found: C, 65.00; H, 6.31; N, 6.16.

HRMS (ESI) m/z : [M-BF₄]⁺ Calcd for C₇₃H₈₈BCuF₄N₆OP₂: 1189.5779; Found 1189.5779.

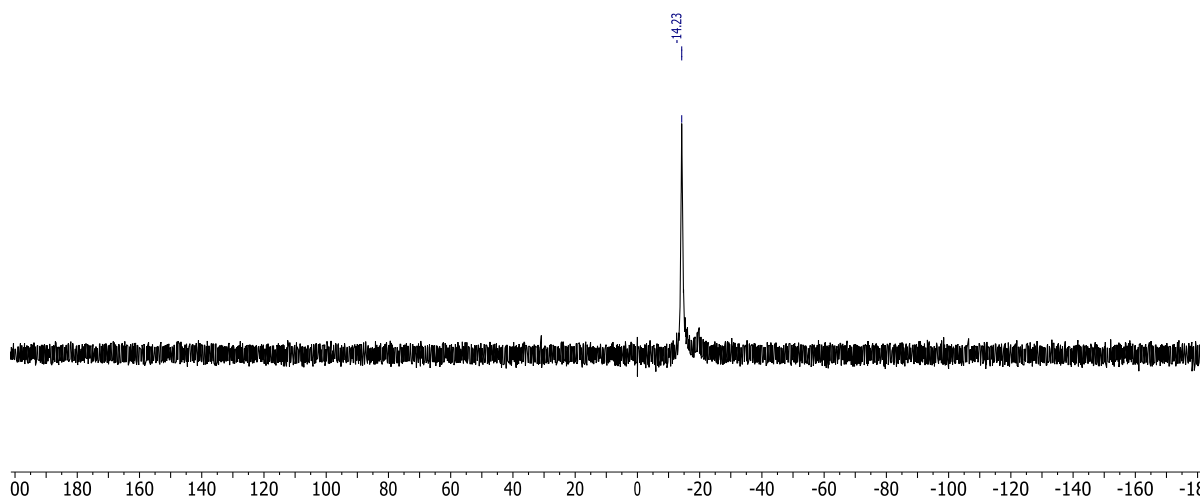
^1H NMR (500 MHz, CD_2Cl_2 , 298 K)



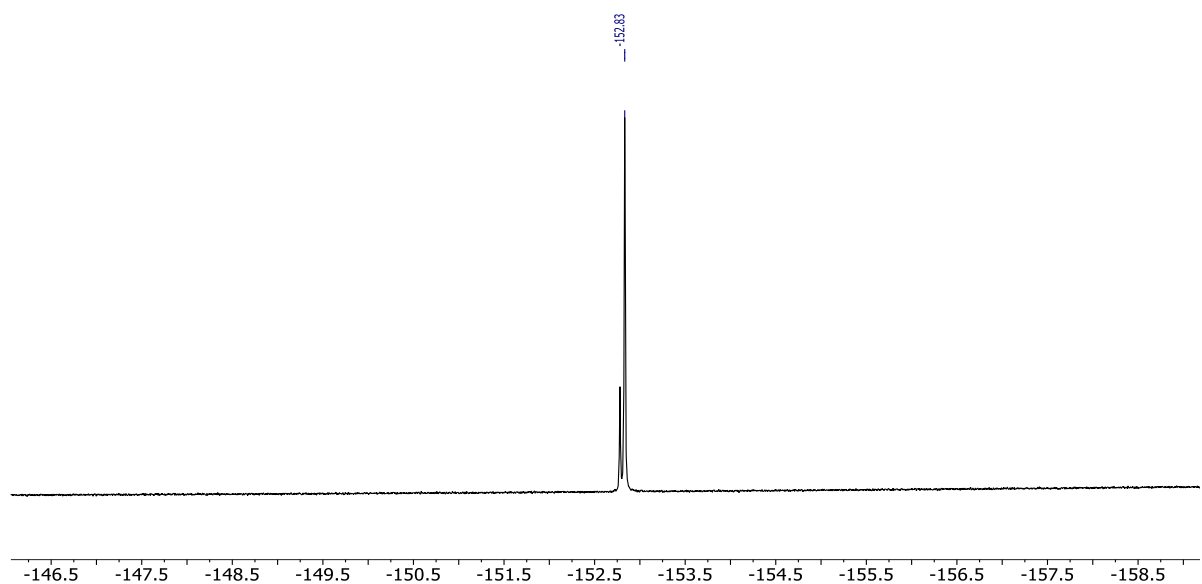
$^{13}\text{C}\{-^1\text{H}\}$ NMR (126 MHz, CD_2Cl_2 , 298 K)



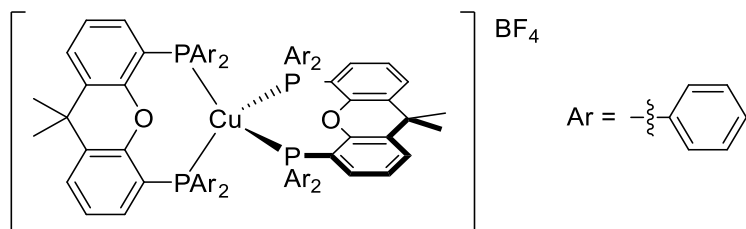
$^{31}\text{P}\{-^1\text{H}\}$ NMR (202 MHz, CD_2Cl_2 , 298 K)



$^{19}\text{F}\{-^1\text{H}\}$ NMR (470 MHz, CD_2Cl_2 , 298 K)



[Cu-bis(xantphos)]BF₄, homoleptic xantphos complex (10)



$[\text{Cu}(\text{MeCN})_4]\text{BF}_4$ (0.17 mmol, 54.2 mg) was dissolved in CH_2Cl_2 (10 mL) in a Schlenk flask equipped with magnetic stirrer. Then a solution of xantphos (0.34 mmol, 200 mg) in CH_2Cl_2

(5 mL) was added dropwise at room temperature. The reaction mixture was refluxed overnight resulting in a colorless solution. The solution was filtered through celite under inert atmosphere to remove any fine precipitate which sometimes forms. Solvents were evaporated and the complex suspended in 2 mL of CH₂Cl₂ and the remaining solute precipitated by addition of 25 mL of Et₂O. The white precipitate was washed with Et₂O. The complex was suspended in a 1:1 mixture CH₂Cl₂/THF. The supernatant was removed by syringe and *n*-hexane was added to it (1:1 mixture) to crystallize the product by slow diffusion. The white crystals were washed with pentane and dried under vacuum overnight obtaining a white powder. Yield: 388 mg, 86%. This compound is not soluble in hexanes, pentanes, DMSO, Et₂O, toluene, H₂O, CH₃OH, benzene and ethyl acetate and poorly soluble in CH₂Cl₂ and THF.

³¹P-{¹H} NMR (162 MHz, CD₂Cl₂, 298 K): δ (ppm) = -15.01 (br s).

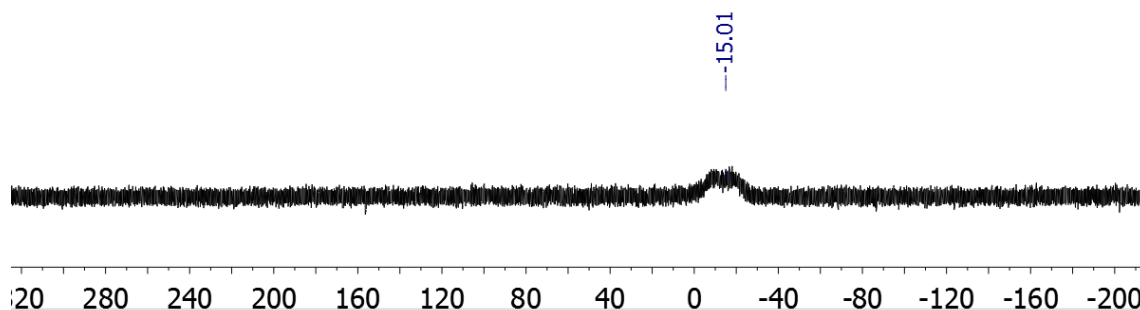
Anal. Calcd C₇₈H₆₄CuO₂P₄: C, 71.65; H, 4.93 Found: C, 71.66; H, 4.89.

HRMS (ESI) *m/z*: [M-BF₄]⁺ Calcd for C₇₈H₆₄CuO₂P₄: 1219.3158; Found 1219.3187

ATR-IR ν (cm⁻¹): 1565 (vw), 1478 (w), 1433 (w), 1404 (m), 1360 (vw), 1312 (vw), 1225 (m), 1199 (vw), 1158 (vw), 1090 (w), 1056 (m), 1030 (m), 997 (w), 875 (w), 848 (vw), 791 (w), 777 (vw), 742 (m), 694 (m), 666 (w), 607 (w), 587 (vw), 534 (w), 512 (m), 497 (m), 454 (m), 411 (w).

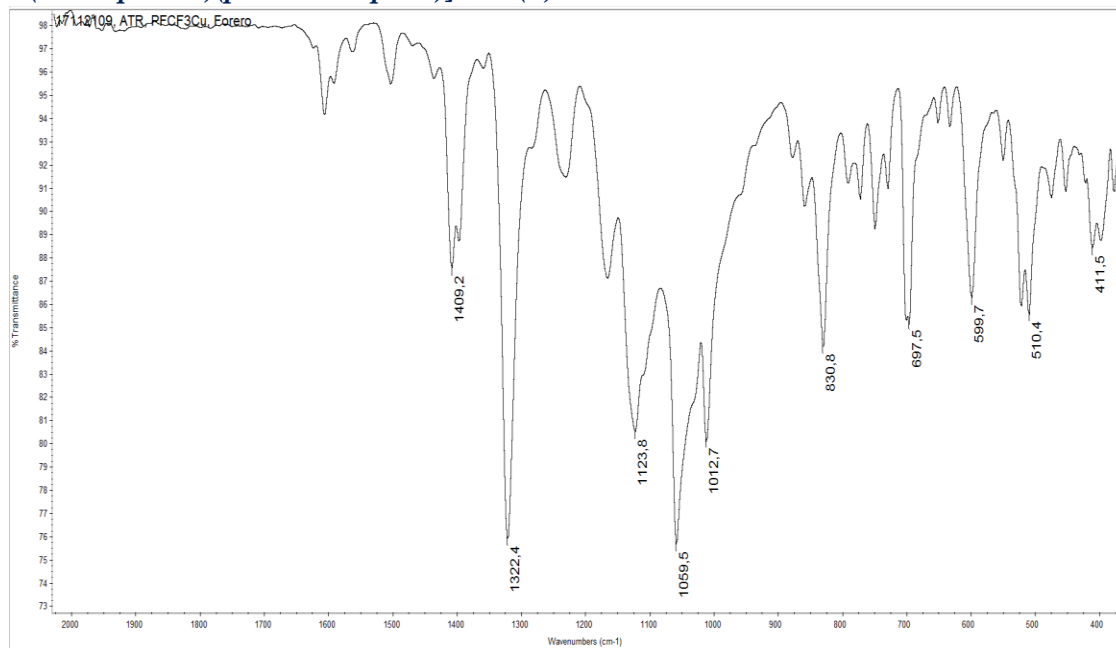
mp: 343-344 °C (dec.)

³¹P-{¹H} NMR (162 MHz, CD₂Cl₂, 298 K)

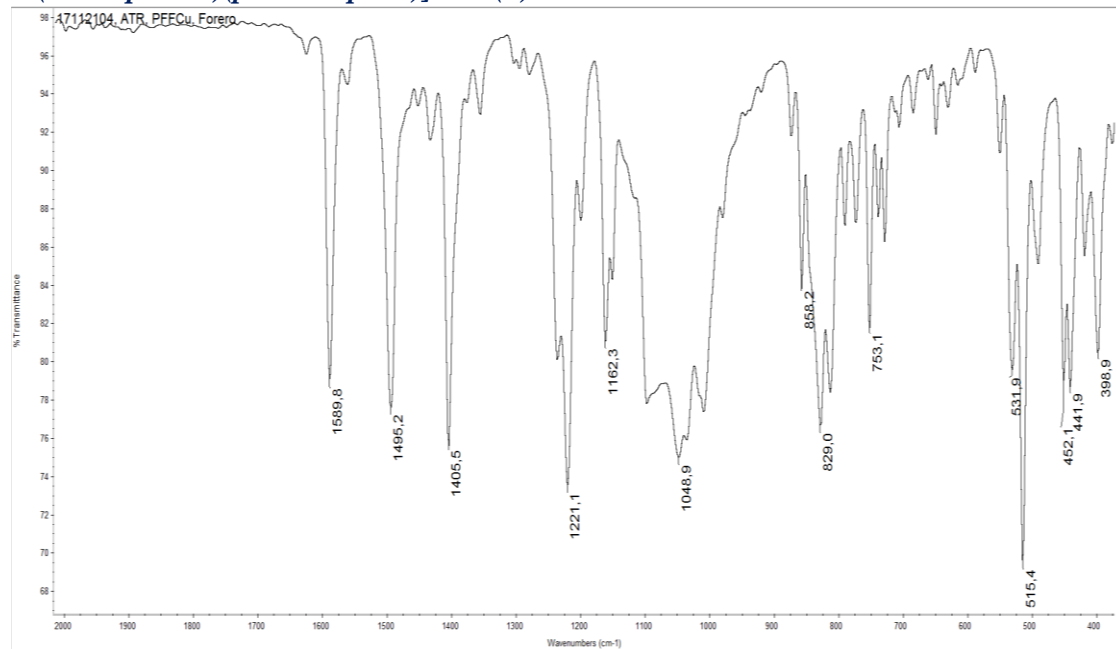


IR spectra of copper complexes

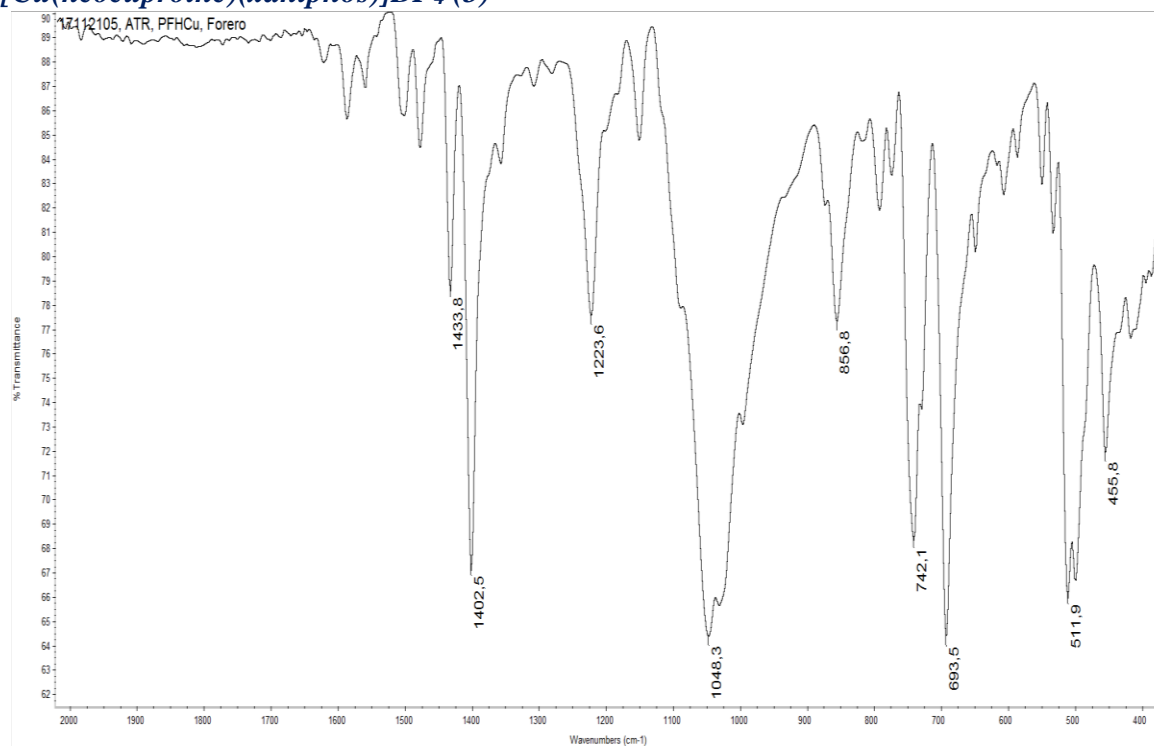
[Cu(neocuproine)(p-CF₃ xantphos)]BF₄ (1)



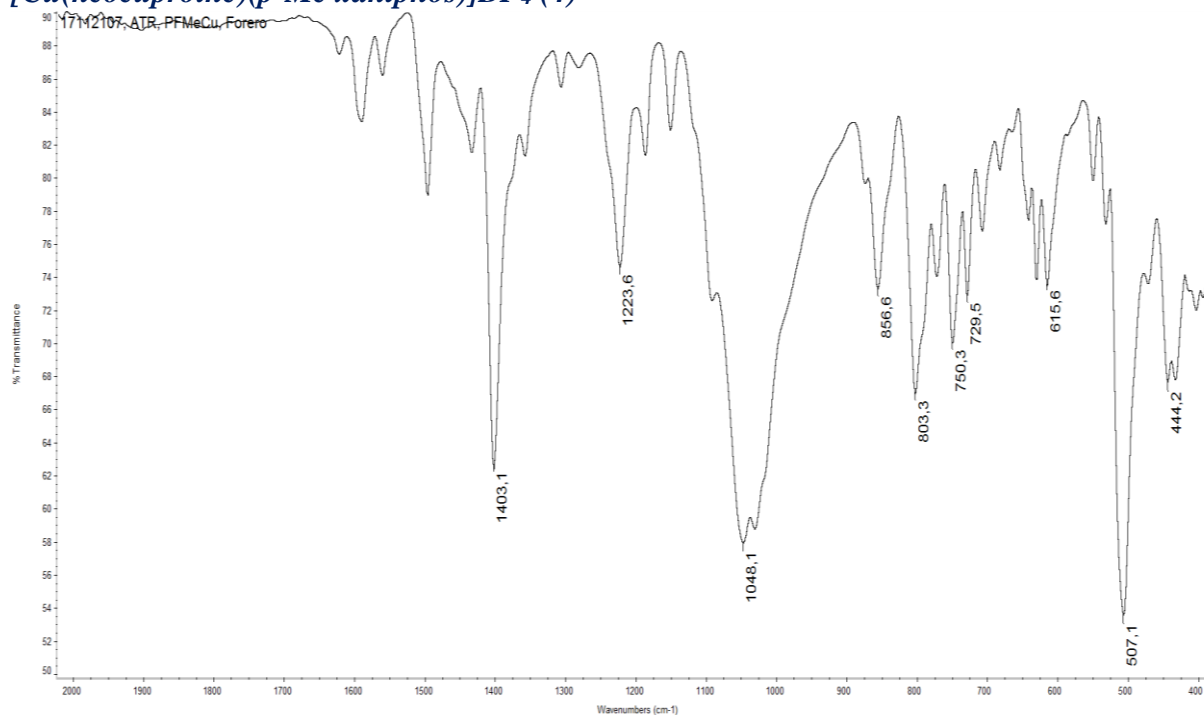
[Cu(neocuproine)(p-F xantphos)]BF₄ (2)



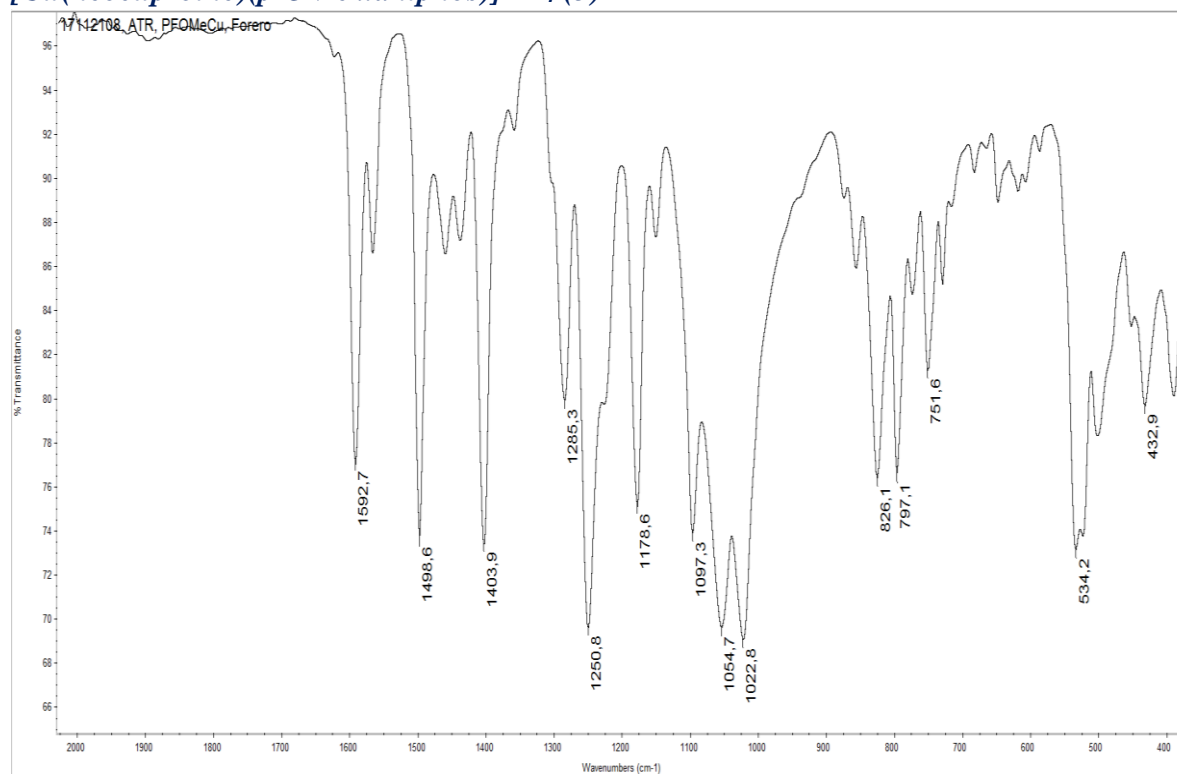
[Cu(neocuproine)(xantphos)]BF₄ (3)



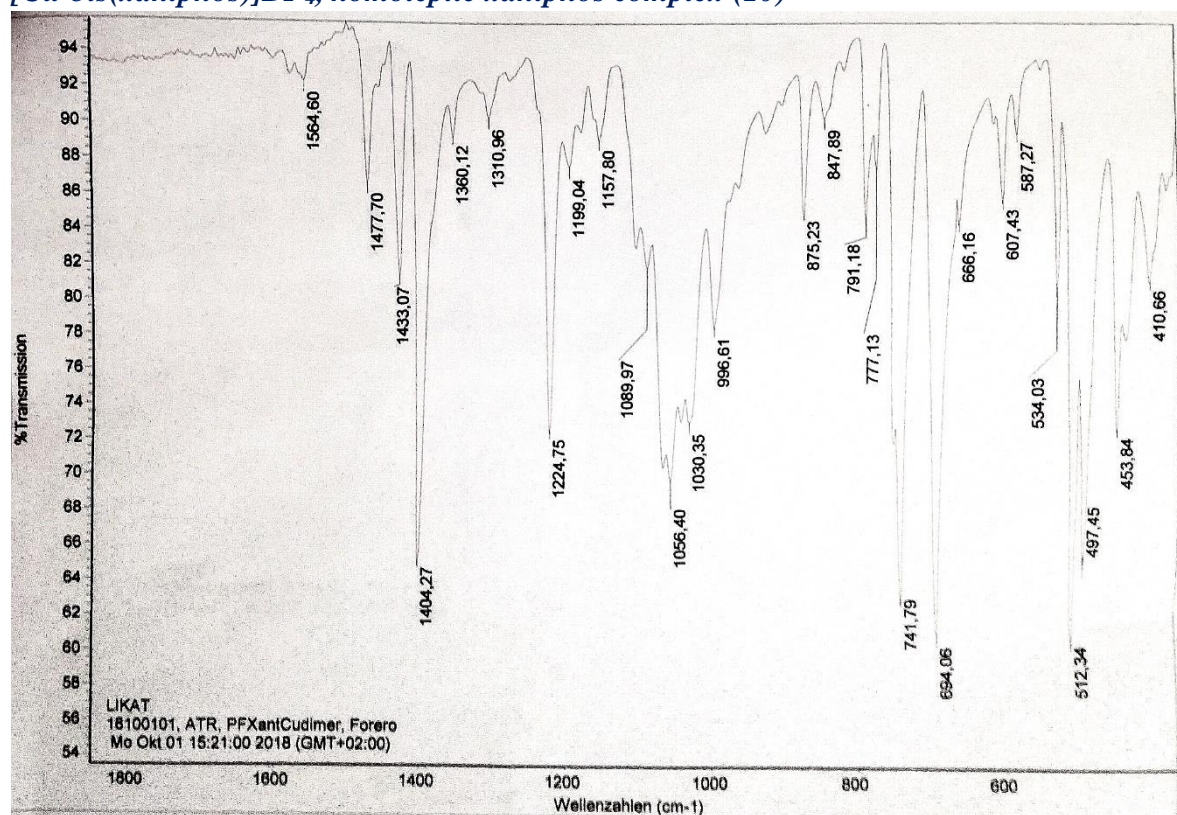
[Cu(neocuproine)(p-Me xantphos)]BF₄ (4)



[Cu(neocuproine)(p-OMe xantphos)]BF₄ (5)

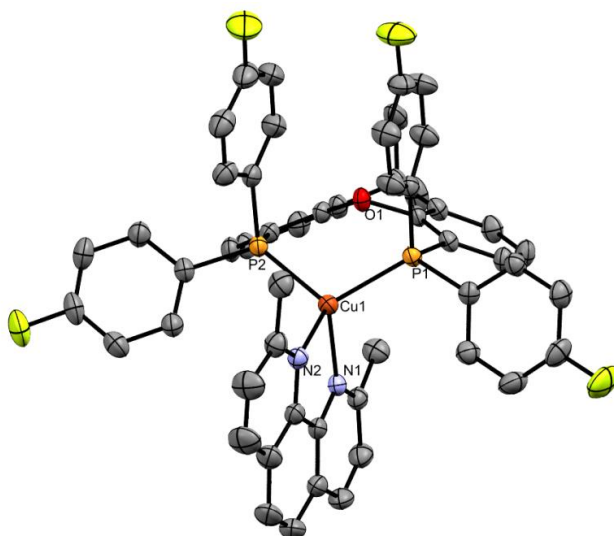
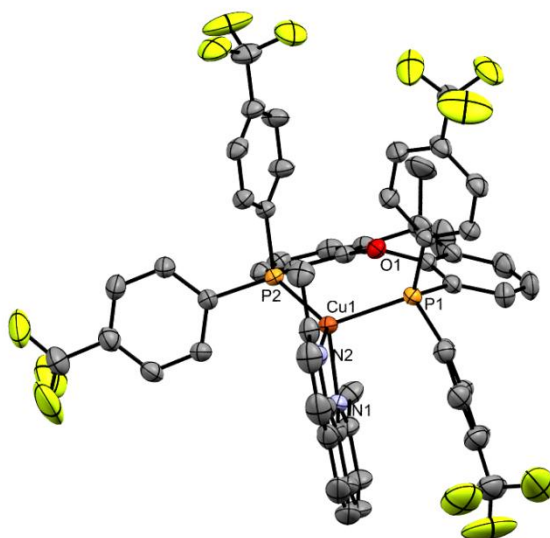


[Cu-bis(xantphos)]BF₄, homoleptic xantphos complex (10)



X-Ray characterization

Crystals of **1**, **2**, **3** and **4** were obtained by vapor diffusion of diethyl ether into a solution of the compound in dichloromethane. Crystals of **5** were obtained from a solution of the compound in dichloromethane. X-ray diffraction data for compounds **1–5** were collected at 173 K using a Rigaku FR-X Ultrahigh Brilliance Microfocus RA generator/confocal optics with XtaLAB P200 diffractometer [Mo K α radiation ($\lambda = 0.71075$ Å)]. Intensity data were collected using ω steps accumulating area detector images spanning at least a hemisphere of reciprocal space. Data for all compounds analyzed were collected and processed (including correction for Lorentz, polarization and absorption) using CrystalClear⁷ or CrysAlisPro.⁸ Structures were solved by direct methods (SIR2011⁹ and SIR2004¹⁰) and refined by full-matrix least-squares against F² (SHELXL-2018¹¹). Non-hydrogen atoms were refined anisotropically, and hydrogen atoms were refined using a riding model. All calculations were performed using the CrystalStructure¹² interface. For compound **10** data were collected on a Bruker Kappa APEX II Duo diffractometer. The structure was solved by direct methods (SHELXS-97)¹⁴ and refined by full-matrix least-squares procedures on F^2 (SHELXL-2014).¹⁵ The τ_4 parameters were calculated using the method of Houser et al.¹³ Selected crystallographic data are presented in Table 2. CCDC 1844671-1844675 contains the supplementary crystallographic data for this thesis. The data can be obtained free of charge from The Cambridge Crystallographic Database.



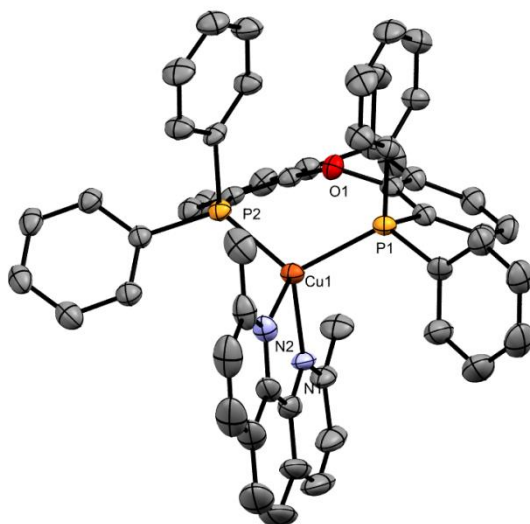


Figure 3. Thermal ellipsoid representation of complex $[Cu(neocuproine)(xantphos)]BF_4$ (**3**). Anion, hydrogen atoms and co-crystallized solvent molecules have been omitted for clarity. Displacement ellipsoids correspond to 50% probability.

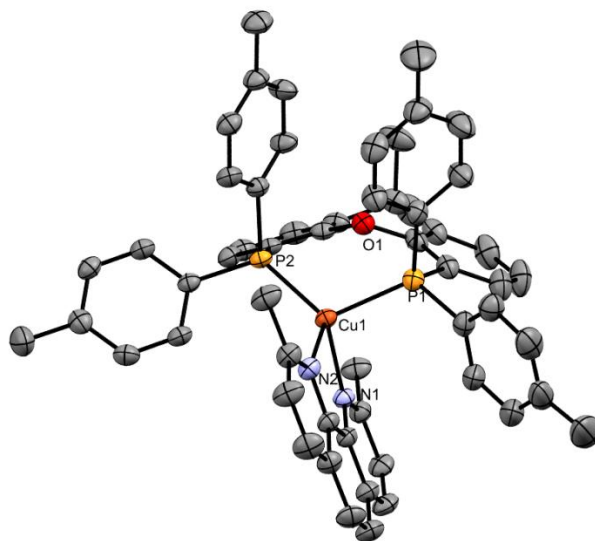


Figure 4. Thermal ellipsoid representation of complex $[Cu(neocuproine)(p\text{-}Me\text{-}xantphos)]BF_4$ (**4**). The second independent molecule, anions, hydrogen atoms and co-crystallized solvent molecules have been omitted for clarity. Displacement ellipsoids correspond to 50% probability.

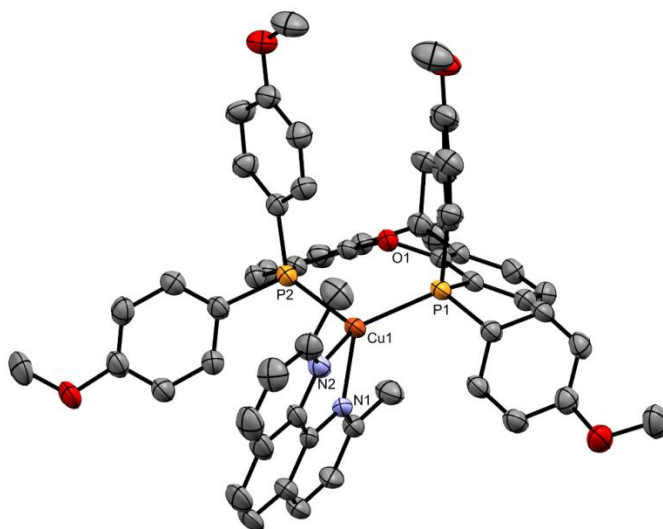


Figure 5. Thermal ellipsoid representation of complex $[Cu(neocuproine)(p\text{-OMe } xantphos)]BF_4$ (**5**). Anion, hydrogen atoms and co-crystallized solvent molecules have been omitted for clarity. Displacement ellipsoids correspond to 50% probability.

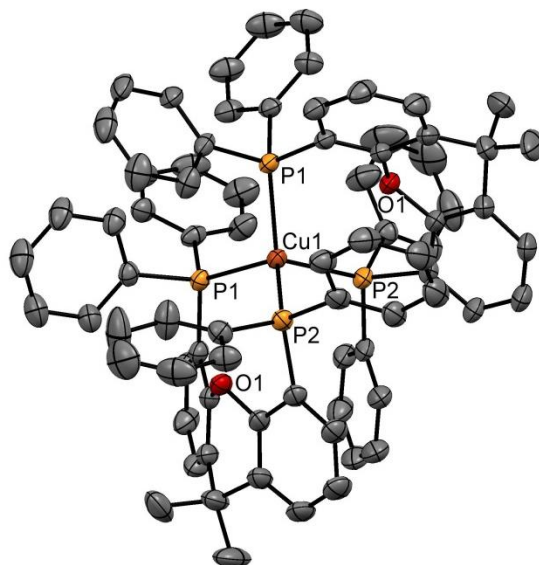


Figure 6. Thermal ellipsoid representation of complex $[Cu\text{-bis}(xantphos)]BF_4$, homoleptic *xantphos* complex (**10**). Anion, hydrogen atoms and co-crystallized solvent molecules have been omitted for clarity. Displacement ellipsoids correspond to 50% probability.

Table 1. Selected bond lengths (Å) and angles (°) for complexes **1-5** with estimated standard deviations in parenthesis.

| Complex | <i>p</i> -R | Cu-P1 | Cu-P2 | Cu-N1 | Cu-N2 | N2-Cu-N1 | N2-Cu-P1 | N1-Cu-P1 | N2-Cu-P2 | N1-Cu-P2 | P1-Cu-P2 |
|----------|-----------------|------------|------------|------------|------------|-----------|------------|------------|------------|------------|-----------|
| 1 | CF ₃ | 2.3274(9) | 2.2562(9) | 2.080(3) | 2.106(3) | 80.66(12) | 98.05(8) | 102.57(8) | 129.74(8) | 120.40(9) | 117.54(3) |
| 2 | F | 2.2792(6) | 2.2928(6) | 2.1130(16) | 2.1013(16) | 80.56(6) | 120.55(5) | 113.58(4) | 112.67(5) | 115.76(4) | 110.88(2) |
| 3 | H | 2.2812(16) | 2.2680(16) | 2.127(4) | 2.081(5) | 80.7(2) | 115.69(14) | 111.10(14) | 116.29(15) | 117.47(14) | 112.17(6) |
| 4 | Me | 2.2957(10) | 2.2670(10) | 2.115(3) | 2.091(3) | 80.33(11) | 110.42(8) | 102.10(8) | 120.85(8) | 124.45(8) | 113.61(4) |
| 5 | OMe | 2.2623(14) | 2.2964(16) | 2.092(4) | 2.121(5) | 80.19(18) | 122.35(13) | 120.53(12) | 107.39(13) | 103.70(12) | 116.38(6) |

Table 2. Selected crystallographic data.

| | 1 | 2 | 3 | 4 | 5 | 10 |
|---|---|--|--|--|--|---|
| empirical formula | C ₆₂ H ₅₂ BCl ₂ CuF ₁₆ N ₂ O ₂ P ₂ | C ₅₃ H ₄₀ BCuF ₈ N ₂ OP ₂ | C ₅₈ H ₅₆ BCl ₂ CuF ₄ N ₂ O ₂ P ₂ | C ₅₈ H ₅₄ BCl ₂ CuF ₄ N ₂ OP ₂ | C ₅₉ H ₅₆ BCl ₄ CuF ₄ N ₂ O ₅ P ₂ | C ₇₈ H ₆₄ BCuF ₄ O ₂ P ₄ |
| fw | 1368.29 | 1009.20 | 1096.30 | 1078.28 | 1227.21 | 1307.52 |
| crystal description | orange prism | yellow platelet | yellow prism | yellow platelet | yellow prism | colorless prism |
| crystal size [mm ³] | 0.26×0.12×0.10 | 0.18×0.06×0.01 | 0.24×0.12×0.09 | 0.39×0.36×0.03 | 0.09×0.04×0.03 | 0.36×0.24×0.23 |
| space group | <i>P</i> 2 ₁ / <i>n</i> | <i>P</i> $\bar{1}$ | <i>P</i> $\bar{1}$ | <i>P</i> $\bar{1}$ | <i>P</i> $\bar{1}$ | <i>Pbcn</i> |
| <i>a</i> [Å] | 11.3020(13) | 11.7321(17) | 11.3777(4) | 16.5704(15) | 11.9350(16) | 18.4171(11) |
| <i>b</i> [Å] | 20.369(2) | 12.9600(17) | 15.0152(4) | 18.1146(11) | 14.3801(16) | 18.2925(11) |
| <i>c</i> [Å] | 27.981(3) | 16.476(2) | 18.1082(5) | 19.5207(15) | 18.621(3) | 18.6510(12) |
| α [°] | | 94.2324(17) | 109.384(2) | 66.953(5) | 109.354(10) | 90 |
| β [°] | 99.268(3) | 104.489(3) | 92.589(3) | 89.911(8) | 105.071(17) | 90 |
| γ [°] | | 109.042(2) | 111.203(3) | 78.794(7) | 96.740(14) | 90 |
| vol [Å ³] | 6357.4(12) | 2259.4(5) | 2672.23(16) | 5270.9(8) | 2838.0(8) | 6283.4(7) |
| <i>Z</i> | 4 | 2 | 2 | 4 | 2 | 4 |
| ρ (calc) [g/cm ³] | 1.429 | 1.486 | 1.362 | 1.359 | 1.436 | 1.382 |
| μ [mm ⁻¹] | 0.568 | 0.631 | 0.627 | 0.633 | 0.693 | 0.511 |
| F(000) | 2784 | 1032 | 1136 | 2232 | 1264 | 2712 |
| reflections collected | 136743 | 28024 | 34800 | 128778 | 34650 | 168877 |
| independent reflections (<i>R</i> _{int}) | 15373 (0.0356) | 8223 (0.0213) | 11646 (0.0355) | 19250 (0.0509) | 10351 (0.0542) | 7599 (0.0614) |
| data/restraints/parameters | 15373/21/797 | 8223/0/617 | 11646/0/655 | 19250/0/1295 | 10351/0/711 | 7599/2/375 |
| GOF on <i>F</i> ² | 1.084 | 1.013 | 1.129 | 1.059 | 1.053 | 1.257 |
| <i>R</i> _I [<i>I</i> > 2σ(<i>I</i>)] | 0.0694 | 0.0306 | 0.0891 | 0.0602 | 0.0764 | 0.0660 |
| <i>wR</i> ₂ (all data) | 0.2239 | 0.0820 | 0.2689 | 0.1717 | 0.2369 | 0.1530 |
| largest diffraction peak/hole [e/Å ³] | 2.09, -1.03 | 0.32, -0.26 | 2.27, -0.95 | 1.67, -0.97 | 1.52, -0.68 | 0.69/-0.57 |
| τ_4 | 0.78 | 0.88 | 0.89 | 0.81/0.82 | 0.83 | 0.93 |

Stability experiments

250 μL of a 0.012 M solution of triphenylphosphine oxide in CH_2Cl_2 was added to a solution of the complex (0.003 mmol) in 300 μL of deuterated CH_2Cl_2 . Quantitative ^{31}P NMR was measured each hour for a period of eight hours at room temperature.

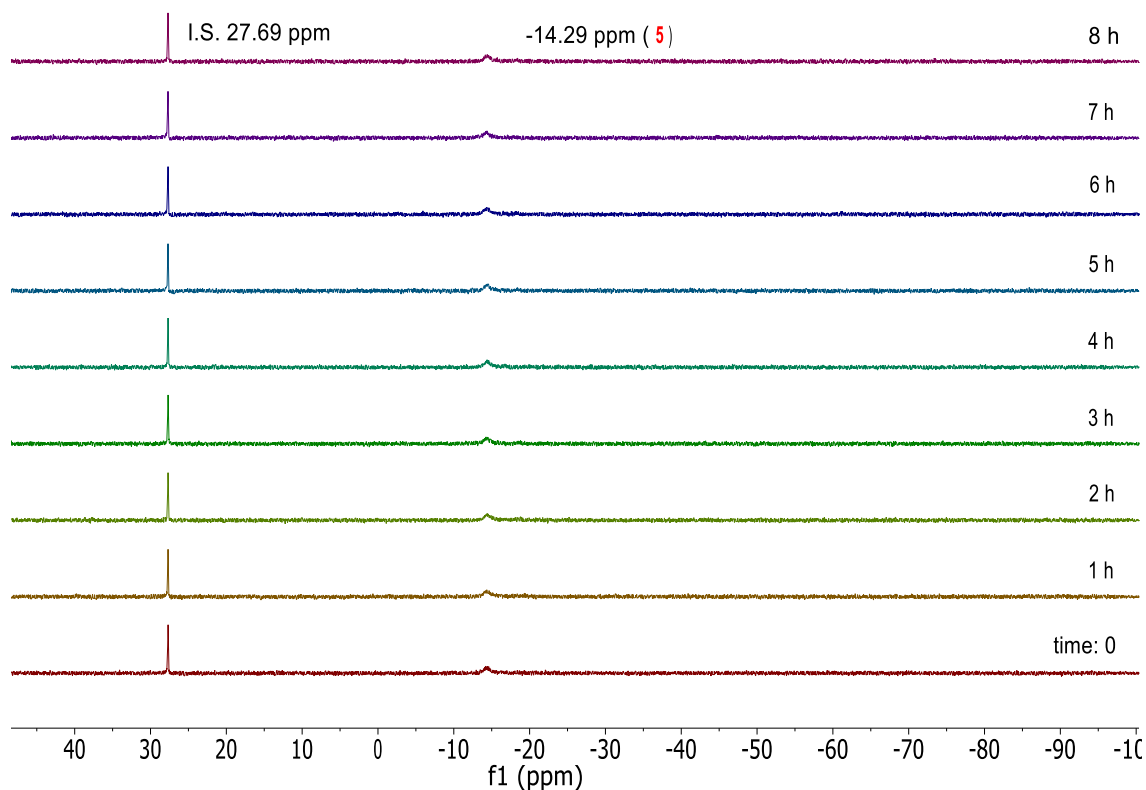


Figure 7. Stability experiment performed by quantitative ^{31}P NMR with triphenylphosphine oxide as internal standard during a period of eight hours in deuterated dichloromethane at room temperature. Integrals: 1.00 for internal standard (I.S.) at 27.69 ppm, 1.01 for complex 5 at -14.29 ppm, remained unchanged during the experiment. Representative example complex 5.

Photocatalysis

General procedure for the photoinduced cross-dehydrogenative coupling (CDC) reaction of nitromethane with tetrahydroisoquinoline: A 15 mL Pyrex tube equipped with a rubber septum and a magnetic stirring bar was charged with $[\text{Cu}(\text{neocuproine})(p\text{-R xantphos})]\text{BF}_4$ complex (0.003 mmol), 2-phenyl-1,2,3,4-tetrahydroisoquinoline (41.85 mg, 0.2 mmol), and nitromethane (10 mL). Oxygen was bubbled through the mixture for 30 min. The tube was provided with a balloon filled with oxygen and irradiated with a 300 W xenon lamp MAX 303 at ambient temperature (25 $^{\circ}\text{C}$), wavelength 300-600 nm.

After irradiation, the solvent was removed under vacuum and the residue dissolved in deuterated dichloromethane using naphthalene as internal standard for quantitative ^1H NMR analysis of the crude mixture. For kinetic profiles samples were taken by syringe.

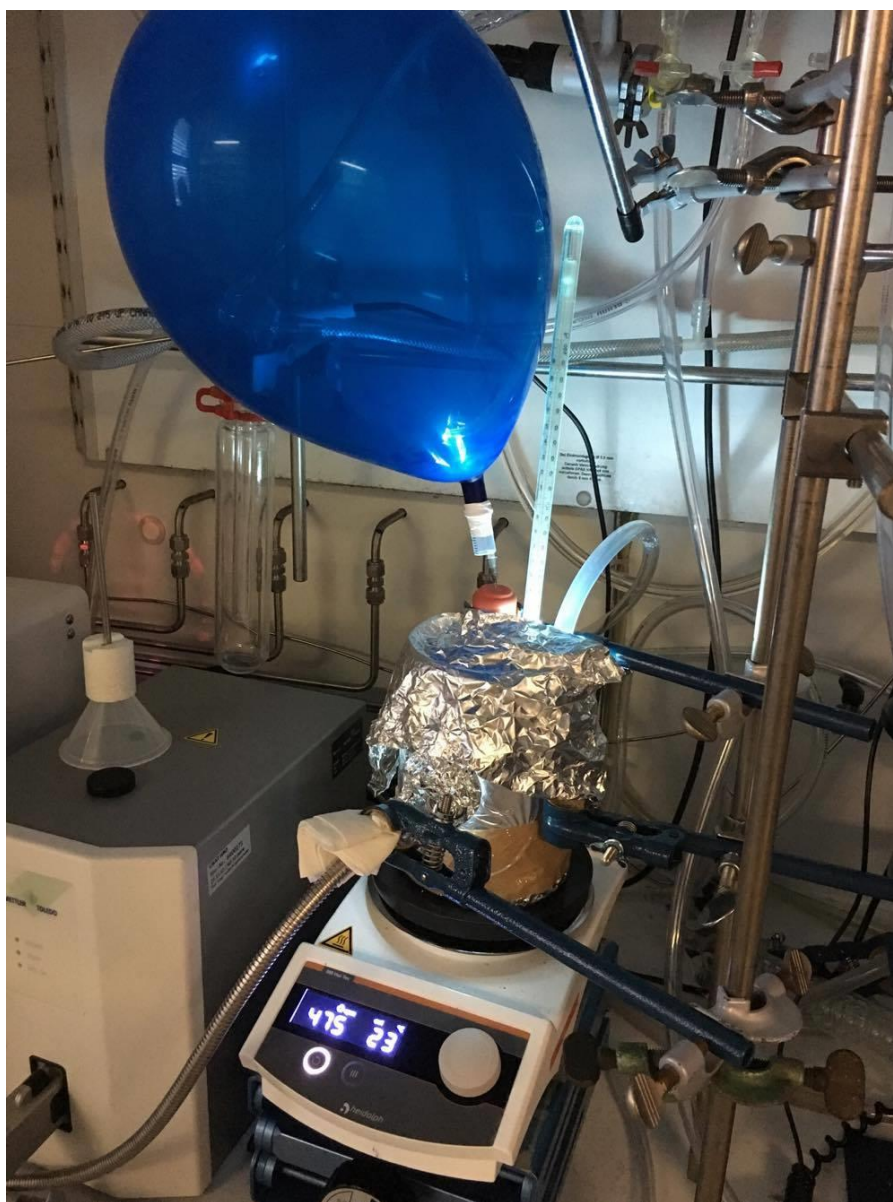


Figure 8. Set up for photocatalysis.

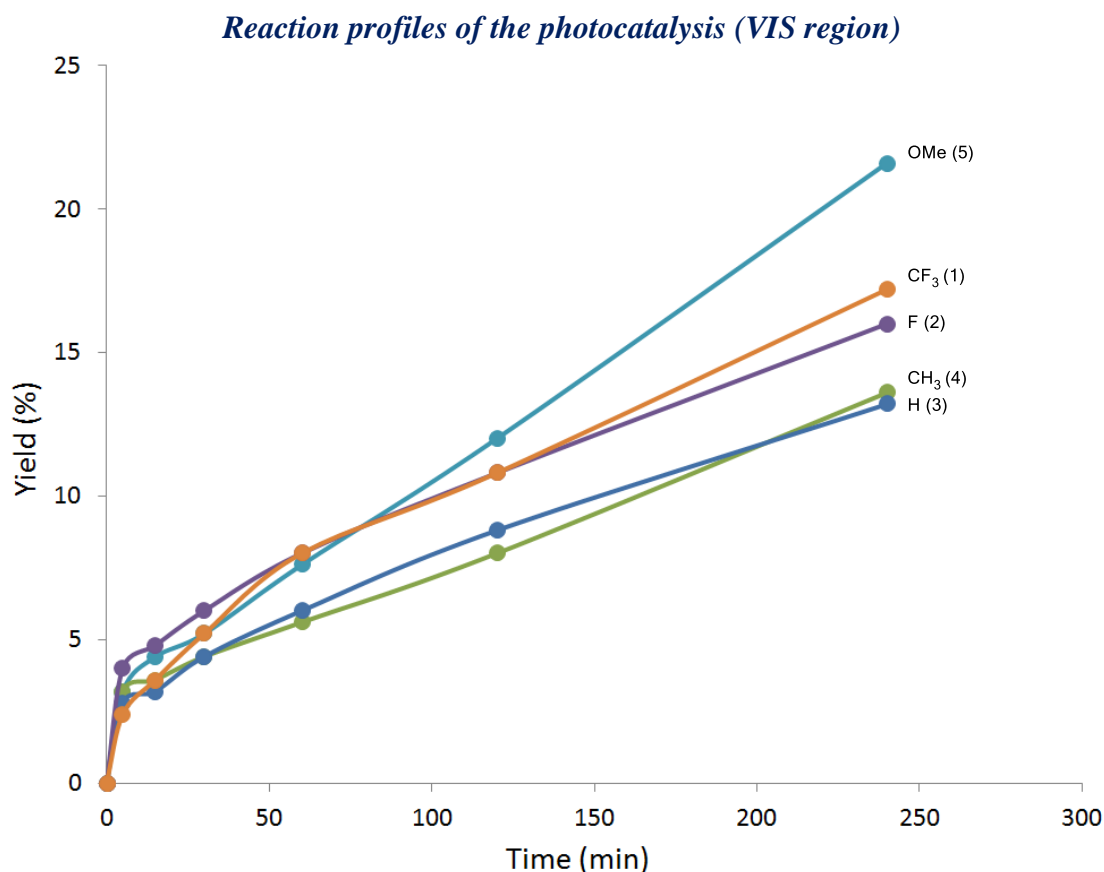


Figure 9. Kinetic profiles for the CDC reaction using a long pass filter Cut-On 420 nm. CDC of 1,2,3,4-tetrahydro-2-phenyl isoquinoline with nitromethane photocatalyzed by [Cu(P[^]P)(dmp)]BF₄ complexes with a long pass filter Cut-On 420 nm. *Reaction conditions:* **11** (0.2 mmol), [Cu]⁺ (0.003 mmol, 1.5 mol%), CH₃NO₂ (10 mL), O₂ atmosphere. Reaction profiles taken within 4 hours and yields were determined by quantitative ¹H NMR of the crude reaction mixture using naphthalene as external standard. Conversions are based on **11**. Irradiation: 300 W xenon lamp at ambient temperature (25 °C). Wavelength: 420-600 nm.

Emission quenching experiments

Steady state emission spectra were recorded using a Cary Eclipse Fluorescence spectrophotometer (Agilent Technologies) with an excitation wavelength of 390 nm, a slit width of 10 nm for excitation and of 20 nm for emission and an averaging time of 0.1 s. The studies were performed in a sealable 10x10 mm quartz glass cuvette. The oxygen amount was adjusted by addition of the corresponding amount of an O₂-saturated acetonitrile solution (2.6 mM O₂)¹⁶ to the solution of **5**.

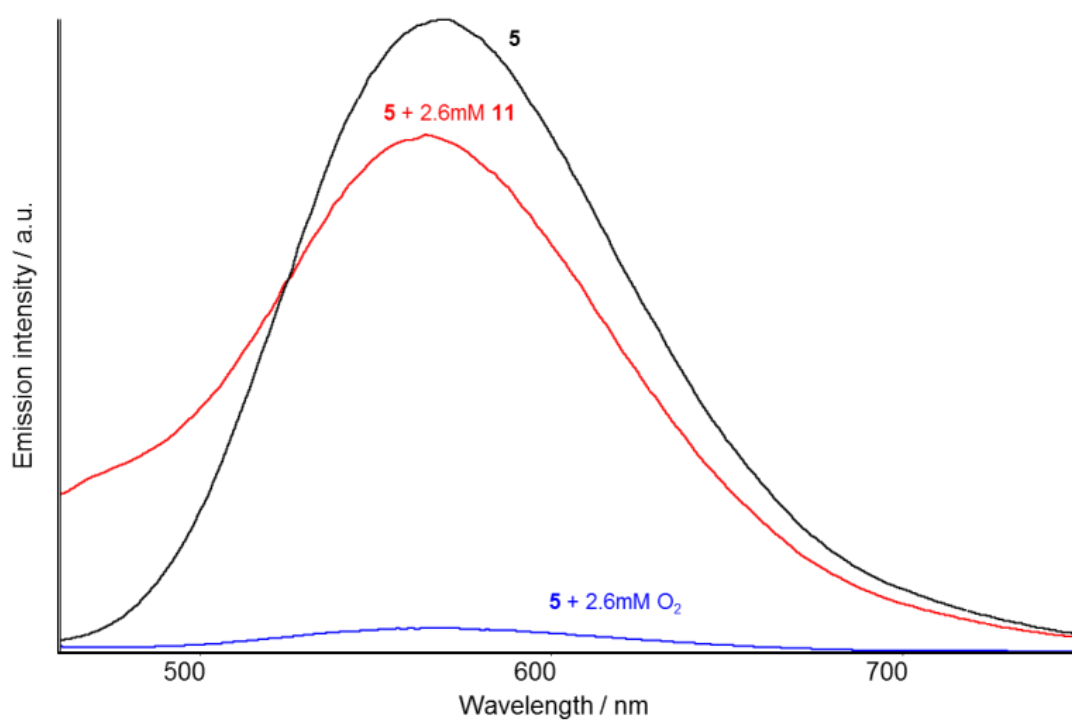


Figure 10. Steady state emission spectra of **5** in the absence of any quencher (black), in the presence of 2.6 mM **11** (red) and in the presence of 2.6 mM O₂ (blue). Note that in the presence of O₂, almost all of the emission is quenched.

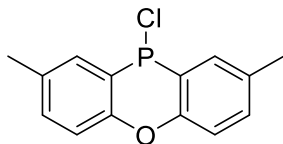
5.2 Chapter III: Modified xantphos ligands for lignin depolymerization in ionic liquid media

General information

All reactions were carried out using standard Schlenk techniques under argon atmosphere. All glassware was dried at 130 °C overnight prior to use. Gas chromatography was performed on a Thermo Scientific Trace 1300 system (split/split less injector) equipped with a Restek Rxi® 1-ms column (100% dimethyl polysiloxane, 30m x 0.25mm x 0.1µm dimensions, carrier gas – He, F.I.D. detector). Infrared spectra (vmax) were recorded on a Shimadzu Fourier transform IR Affinity-1 infrared spectrophotometer using the MIRacle™ single reflection horizontal ATR accessory from Pike (ANSe single crystal). Only the characteristic peaks are quoted. Samples were directly placed on the crystal (ATR). ^1H , $^{13}\text{C}\{-^1\text{H}\}$ and $^{31}\text{P}\{-^1\text{H}\}$ Nuclear Magnetic Resonance (NMR) spectra were recorded at 298 K on either Bruker Avance 400 Ultrashield or Bruker Avance 500 Ultrashield spectrometer using the residual solvent peak for ^1H and $^{13}\text{C}\{-^1\text{H}\}$ as reference. All NMR shifts are reported as δ in parts per million (ppm). Mass spectra were recorded from a Micromass LCT, which is a high performance orthogonal acceleration reflecting TOF mass spectrometer, coupled to a Water 2795 HPLC and Water 2996 photodiode array detector. A Gallenkamp melting point apparatus was used to determine melting points. Toluene and TMEDA were distilled from sodium, THF and diethyl ether were distilled from sodium/benzophenone, hexanes from sodium/benzophenone/triglyme and dichloromethane and acetonitrile from calcium hydride. Diethylamine was dried over KOH powder. Aqueous reagents were degassed by argon bubbling before use for a minimum period of four hours. All reagents were purchased from commercial suppliers and used as received, unless otherwise noted. Elemental analysis was conducted at London Metropolitan University using a Carlo Erba Flash 2000 Elemental Analyzer and at Leibniz-Institut Für Katalyse e. V. (LIKAT, Rostock). The internal standard, 1,2,4,5-tetramethylbenzene (Durene) used in the GC analysis for catalytic tests, was recrystallized from dichloromethane/ethanol. Ionic liquids were dried for two days at 80 °C under vacuum, degassed overnight by bubbling argon through the liquids and stored under argon. All reactions performed in this chapter require strict inert conditions. It has been observed that optimal results are obtained with freshly distilled solvents and that solvents from the SPS (Solvent purification system) can affect the yields for some synthetic procedures.

Synthesis and characterization of compounds

2,8-dimethyl-10-phenoxaphosphino chloride, POP-Cl (42)

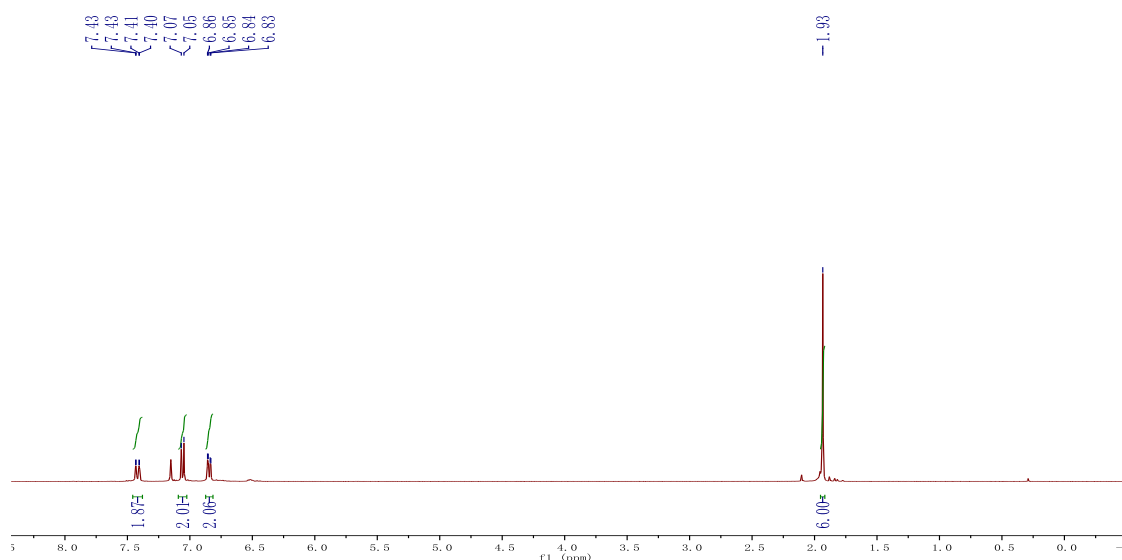


A mixture of *p*-tolyl ether (5.0 g, 25.2 mmol) and phosphorus trichloride (3.3 ml, 37.8 mmol) was prepared. To this solution, anhydrous aluminium chloride (5.1 g, 37.8 mmol) was added portion-wise. The mixture was heated overnight under gentle reflux. Residual phosphorus trichloride was then removed under vacuum.¹⁷ Toluene (10 mL) was added with vigorous stirring and removed under vacuum. Toluene (20 mL) was then added again and pyridine (5.1 mL, 63.6 mmol) added dropwise at -20 °C (ice-water/NaCl bath). After slow warming to room temperature the resulting Lewis-adduct precipitate was removed and the crude product washed with toluene (3x40 mL). The yellow-white crystalline product (4.5 g, 17.1 mmol, 68%) was isolated.

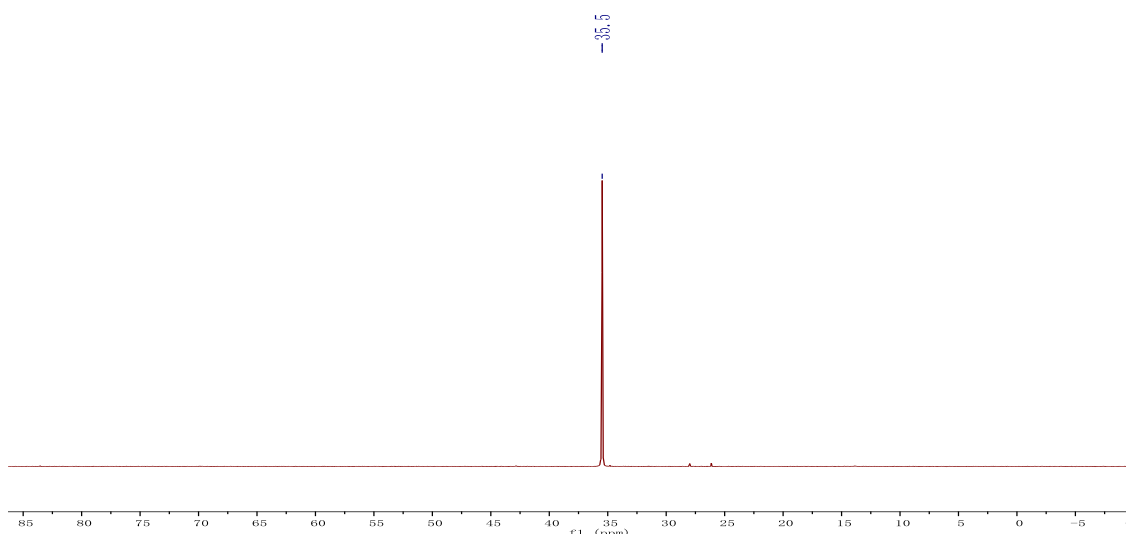
¹H NMR (C₆D₆, 400 MHz, 298 K): δ (ppm) = 7.42 (dd, $J = 10.9$, $J = 1.1$ Hz, 2H, CH_{Ar}), 7.06 (d, $J = 8.4$ Hz, 2H, CH_{Ar}), 6.85 (dd, $J = 8.4$, $J = 2.2$ Hz, 2H, CH_{Ar}), 1.93 (s, 6H, CH₃).

³¹P-{¹H} NMR (C₆D₆, 162 MHz, 298 K): δ (ppm) = 35.5 (s).

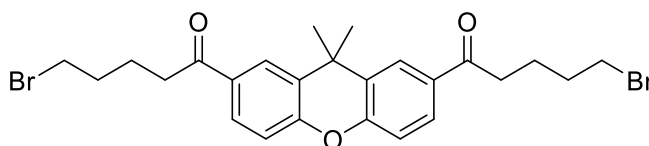
¹H NMR (C₆D₆, 400 MHz, 298 K)



$^{31}\text{P}\{-^1\text{H}\}$ NMR (C_6D_6 , 162 MHz, 298 K)



2,7-bis(5-bromopentanoyl)-9,9-dimethylxanthene (34)

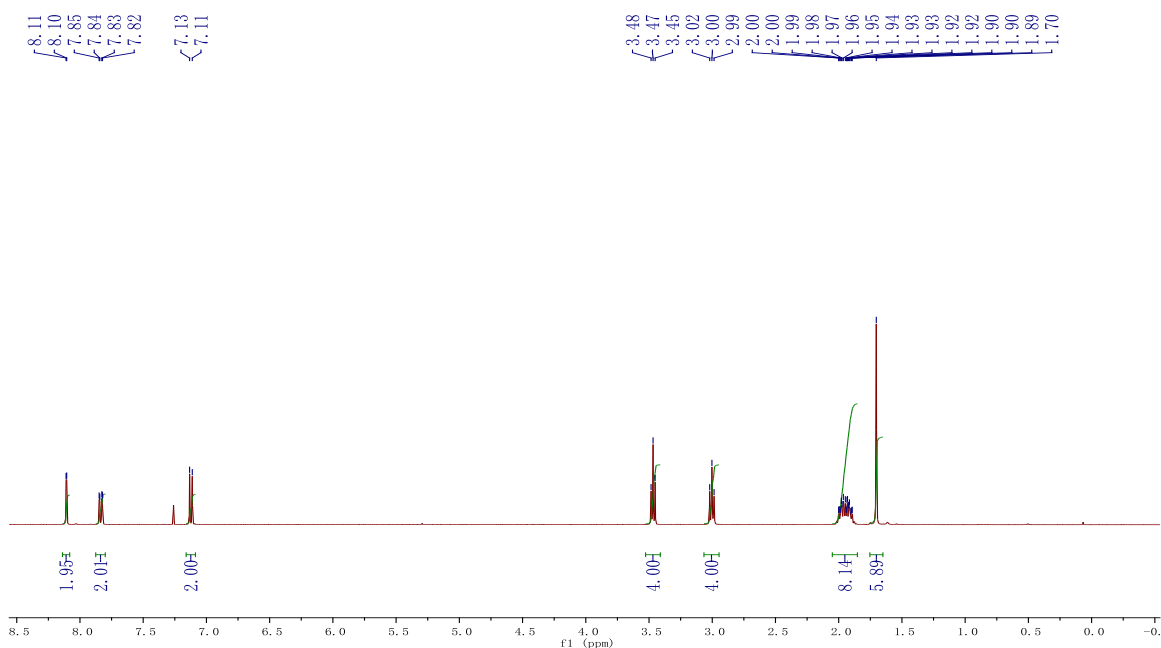
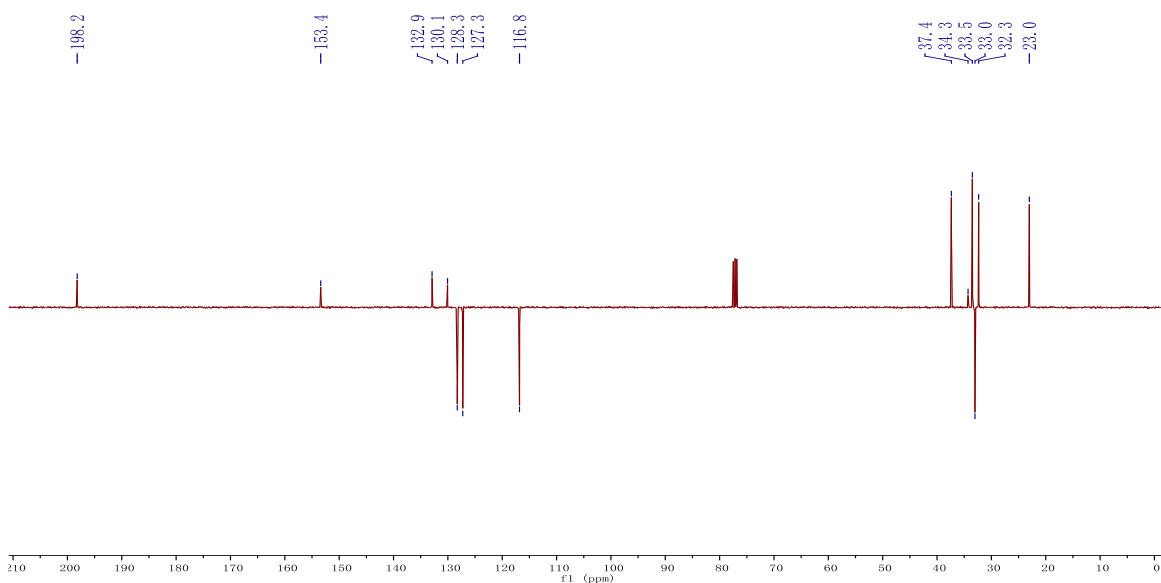
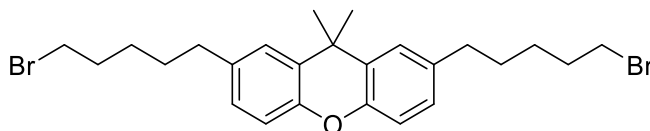


At $-20\text{ }^{\circ}\text{C}$ AlCl_3 (10 g, 75 mmol) was added slowly to a stirred solution of 9,9-dimethylxanthene (6.82 g, 32.5 mmol) and 5-bromovaleric chloride (10 mL, 75.10 mmol) in CH_2Cl_2 (100 mL).¹⁸ After overnight stirring, the reaction mixture was slowly poured into an ice-saturated solution of potassium sodium tartrate (Rochelle Salts) (80 mL) and extracted with CH_2Cl_2 ($3 \times 60\text{ mL}$), washed with NaHCO_3 ($2 \times 60\text{ mL}$). Next, then NaHCO_3 aqueous phase was extracted with CH_2Cl_2 ($2 \times 60\text{ mL}$). Subsequently, the organic layer was dried over Na_2SO_4 . The solvents were removed under vacuum and the resulting light green solid was washed with hexanes providing pale yellow crystals. Yield: 16.4 g, 95%.

^1H NMR (CDCl_3 , 400 MHz, 298 K): δ (ppm) = 8.11 (d, $J = 2.1\text{ Hz}$, 2H, CH_{Ar}), 7.84 (dd, $J = 8.5$, $J = 2.1\text{ Hz}$, 2H, CH_{Ar}), 7.12 (d, $J = 8.5\text{ Hz}$, 2H, CH_{Ar}), 3.47 (t, $J = 6.4\text{ Hz}$, 4H, CH_2), 3.00 (t, $J = 6.9\text{ Hz}$, 4H, CH_2), 2.05 – 1.85 (m, 8H, CH_2), 1.70 (s, 6H, CH_3).

$^{13}\text{C}\{-^1\text{H}\}$ NMR (CDCl_3 , 100 MHz, 298 K): δ (ppm) = 198.2 (s, C_q), 153.4 (s, C_q), 132.9 (s, C_q), 130.1 (s, C_q), 128.3 (s, CH_{Ar}), 127.3 (s, CH_{Ar}), 116.8 (s, CH_{Ar}), 37.4 (s, CH_2), 34.3 (s, C_q), 33.5 (s, CH_2), 33.0 (s, CH_3), 32.3 (s, CH_2), 23.0 (s, CH_2). Data were found to match the literature.¹⁸

mp: 83-84 $^{\circ}\text{C}$.

^1H NMR (CDCl_3 , 400 MHz, 298 K) ^{13}C - $\{^1\text{H}\}$ NMR (CDCl_3 , 100 MHz, 298 K)**2,7-bis(5-bromopentyl)-9,9-dimethylxanthene (35)**

In a three neck bottom flask at $-20\text{ }^{\circ}\text{C}$, 2,7-bis(5-bromopentyl)-9,9-dimethylxanthene (5.2 g, 9.69 mmol) was dissolved with (3.5 g, 94.15 mmol) of sodium borohydride in THF (90 ml), then AlCl_3 anhydrous (7.0 g, 52.79 mmol) was added portion wise to the mixture. *This step has to be handled carefully as the reaction is violent and highly exothermic, making sure the solvent does not evaporate during the refluxing time and that*

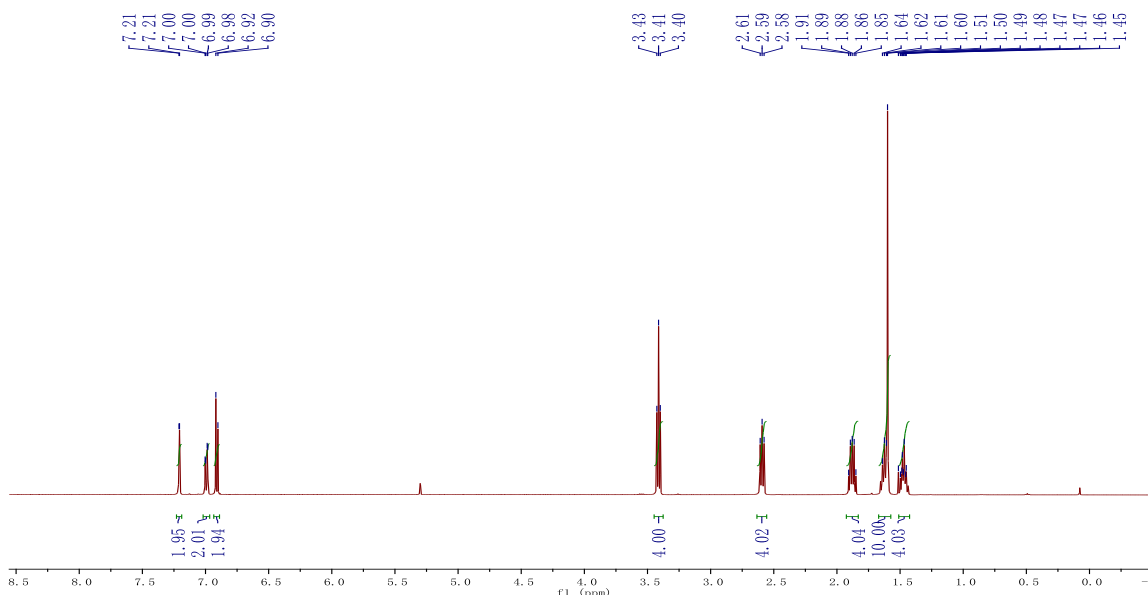
addition of AlCl₃ is slow. The reaction mixture was allowed to reach room temperature and then refluxed for 5 hours.¹⁹ The reaction mixture was cooled down and quenched slowly with ice-cold saturated solution of potassium sodium tartrate (Rochelle Salts) (150 mL). The product was extracted with CH₂Cl₂ (3x100 mL) and EtOAc (1x50 mL), the organic layers were dried over Na₂SO₄ and filtered through 40 g of silica affording a colorless oil. Yield: 4.7 g, 97%.

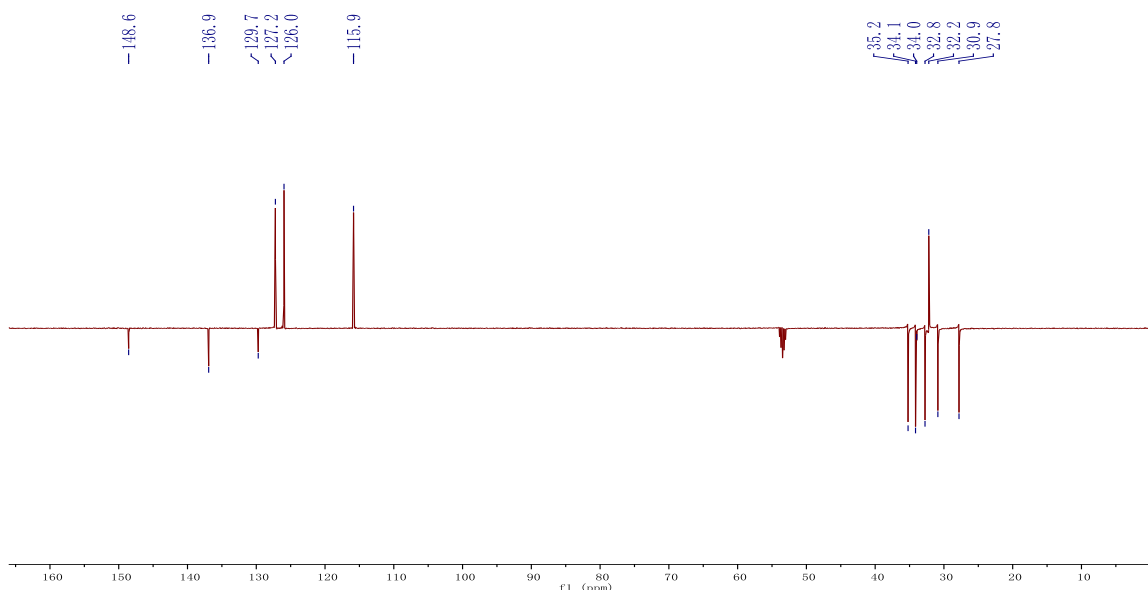
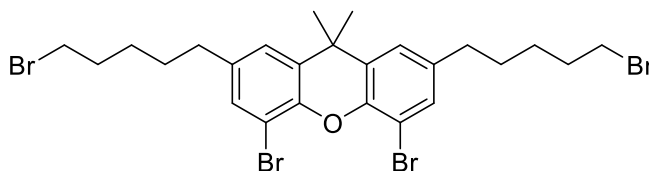
¹H NMR (CD₂Cl₂, 500 MHz, 298 K): δ (ppm) = 7.21 (d, J = 2.0 Hz, 2H, CH_{Ar}), 6.99 (dd, J = 8.2, J = 2.1 Hz, 2H, CH_{Ar}), 6.91 (d, J = 8.2 Hz, 2H, CH_{Ar}), 3.41 (t, J = 6.8 Hz, 2H, CH₂), 2.63 – 2.56 (m, 4H, CH₂), 1.93 – 1.83 (m, 4H, CH₂), 1.67 – 1.57 (m, 4H, CH₂), 1.60 (s, 6H, CH₃), 1.51 – 1.42 (m, 4H, CH₂).

¹³C-{¹H} NMR (CD₂Cl₂, 126 MHz, 298 K): δ (ppm) = 148.6 (s, C_q), 135.9 (s, C_q), 129.7 (s, C_q), 127.2 (s, CH_{Ar}), 126.0 (s, CH_{Ar}), 116.2 (s, CH_{Ar}), 35.2 (s, CH₂), 34.1 (s, CH₂), 34.0 (s, C_q), 32.8 (s, CH₂), 32.2 (s, CH₃), 30.9 (s, CH₂), 27.8 (s, CH₂). Data were found to match literature.¹⁸

Anal. Calcd for C₂₅H₃₂Br₂O: C, 59.05; H, 6.42; Found: C, 59.12; H, 6.40.

¹H NMR (CD₂Cl₂, 500 MHz, 298 K)



$^{13}\text{C}\{-^1\text{H}\}$ NMR (CD_2Cl_2 , 126 MHz, 298 K)**4,5-dibromo-2,7-bis(5-bromopentyl)-9,9-dimethylxanthene (36)**

To a $-78\text{ }^{\circ}\text{C}$ cooled solution of 2,7-bis-5-bromopentyl-9,9-dimethylxanthene²⁰ (3 g, 5.6 mmol) dissolved in CH_2Cl_2 (25 mL) and Br_2 was added slowly using a gas tight syringe (0.84 mL, 16.5 mmol) (The reaction was performed in a Schlenk tube and elemental bromine was previously cooled down to $-20\text{ }^{\circ}\text{C}$ in an ice-water/ NaCl bath in order to handle it easily). The reaction mixture was allowed to warm to room temperature, covered with aluminium foil and stirred overnight. *After addition of elemental bromine the Schlenk vessel was closed and disconnected from the Schlenk line in order to avoid the leaking of bromine vapor.* The excess of Br_2 was then quenched with a saturated solution of aqueous Na_2SO_3 , and the aqueous phase extracted with CH_2Cl_2 (3x50 mL) and EtOAc (1x80). Subsequently, the organic layer was dried over Na_2SO_4 and filtered through silica affording a white-yellow powder that was washed with pentanes. Yield: 3.85 g, 98%.

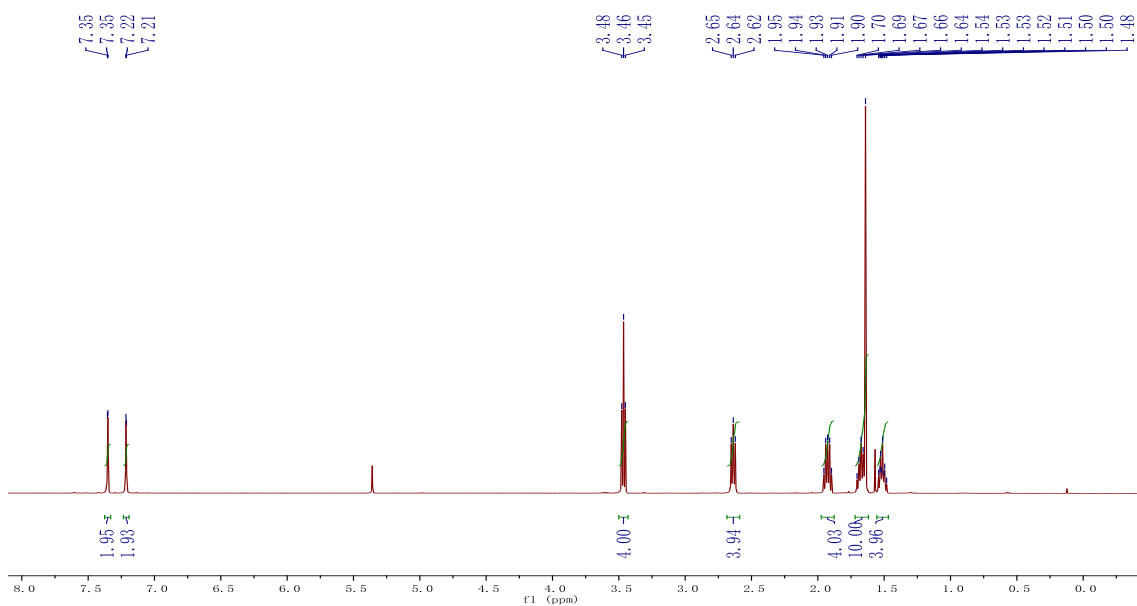
^1H NMR (CD_2Cl_2 , 500 MHz, 298 K): δ (ppm) = 7.35 (d, $J = 2.0$ Hz, 2H, CH_{Ar}), 7.21 (d, $J = 2.0$ Hz, 2H, CH_{Ar}), 3.46 (t, $J = 6.8$ Hz, 4H, CH_2), 2.68 – 2.59 (m, 4H, CH_2), 1.97 – 1.88 (m, 4H, CH_2), 1.72 – 1.62 (m, 4H, CH_2), 1.64 (s, 6H, CH_3), 1.56 – 1.47 (m, 4H, CH_2).

$^{13}\text{C}\{-^1\text{H}\}$ NMR (CD_2Cl_2 , 126 MHz, 298 K): δ (ppm) = 145.4 (s, C_q), 138.7 (s, C_q), 131.6 (s, C_q), 130.9 (s, CH_Ar), 125.1 (s, CH_Ar), 110.2 (s, C_q), 35.4 (s, C_q), 34.9 (s, CH_2), 34.0 (s, CH_2), 32.6 (s, CH_2), 31.7 (s, CH_3), 30.6 (s, CH_2), 27.7 (s, CH_2). Data were found to match literature.¹⁸

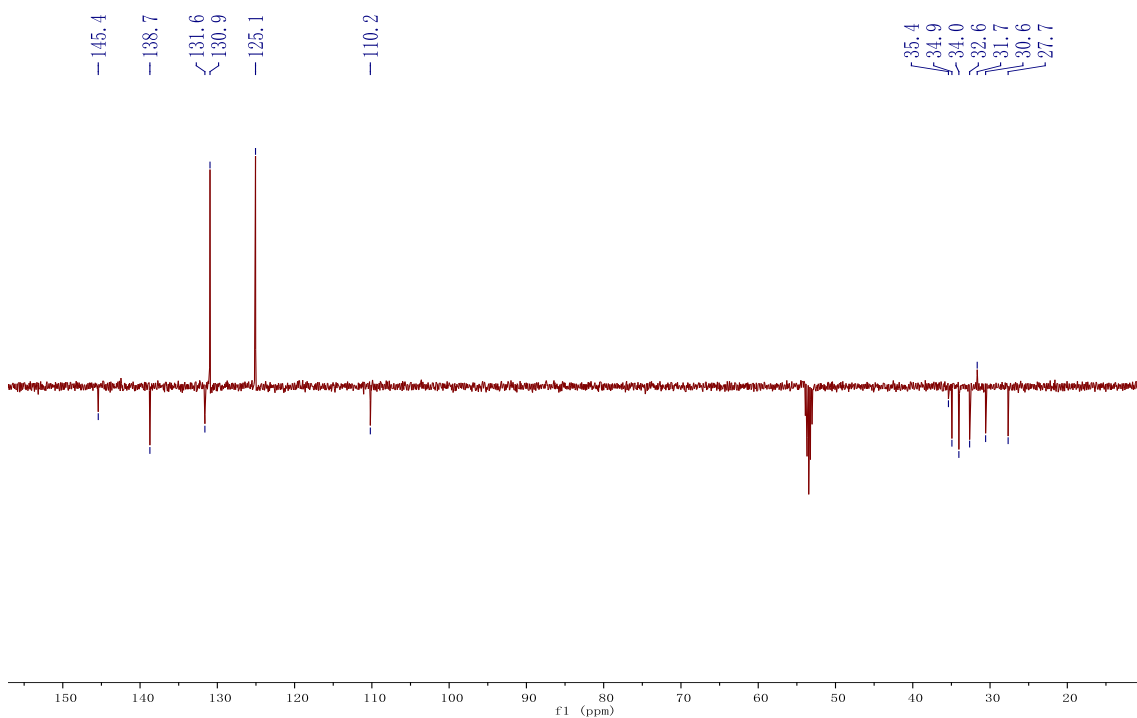
HRMS (ESI) m/z : $[\text{M}+\text{H}]^+$ Calcd for 662.90; Found 662.97.

mp: 66-68 $^\circ\text{C}$.

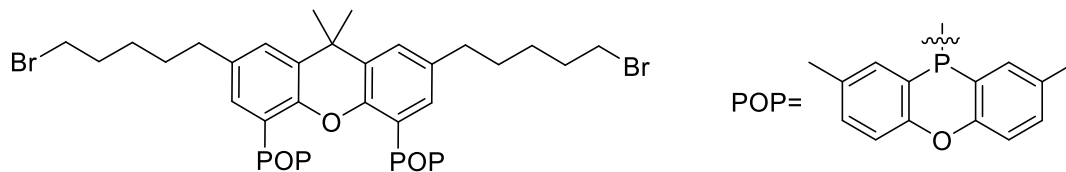
^1H NMR (CD_2Cl_2 , 500 MHz, 298 K)



$^{13}\text{C}\{-^1\text{H}\}$ NMR (CD_2Cl_2 , 126 MHz, 298 K)



2,7-bis(5-bromopentyl)-9,9-dimethyl-4,5-bis(2,8-dimethyl-10-phenoxaphosphino)xanthene (37)



Any xanthene synthetic precursor has been azeotropically dried three times with toluene under vacuum prior to lithiation. At $-71\text{ }^{\circ}\text{C}$ (ethanol/dry ice bath), 0.4 mL of *n*-butyllithium (2.5 M in hexanes, 0.98 mmol) was added dropwise to a stirred solution of azeotropically dried 4,5-dibromo-2,7-bis(5-bromopentyl)-9,9-dimethylxanthene (0.3 g, 0.45 mmol) in THF (8 mL). The resulting solution was stirred for 2.5 h. Subsequently, a suspension of 2,8-dimethyl-10-chlorophenoxaphosphine (0.25 g, 0.98 mmol) in toluene (3 mL) was added dropwise. The reaction mixture was slowly warmed to room temperature and stirred overnight. Next the THF was removed under vacuum and the mixture was diluted with CH_2Cl_2 (15 mL) and hydrolyzed with a 10% HCl aqueous solution (5 mL). The organic layer was removed and additional CH_2Cl_2 was added to the aqueous layer (extraction repeated 2 times). The organic layers were combined and dried over Na_2SO_4 and filtered using a cannula. The reaction mixture was then concentrated, washed with hexanes and concentrated again. The crude mixture was dissolved in a minimum amount of toluene and then isopropanol was gently layered on top (1:1). The mixture was allowed to slowly diffuse to give a white solid, which was isolated by filtration and dried under vacuum. Yield: 0.38 g, 88%.

^1H NMR (500 MHz, CD_2Cl_2 , 298 K): δ (ppm) = 7.93 (d, $J = 6.7$ Hz, 4H, CH_{Ar}), 7.21 (dd, $J = 8.3$ Hz, $J = 1.4$ Hz, 4H, CH_{Ar}), 7.14-7.09 (m, 6H, CH_{Ar}), 6.49 (s, 2H, CH_{Ar}), 3.35 (t, $J = 7$ Hz, 4H, CH_2), 2.39 (t, $J = 7.5$ Hz, 4H, CH_2), 2.35 (s, 12H, CH_3), 1.77 (p, $J = 7$ Hz, 4H, CH_2), 1.53 (s, 6H, CH_3), 1.41 (p, $J = 7.5$ Hz, 4H, CH_2), 1.33-1.24 (m, 4H, CH_2).

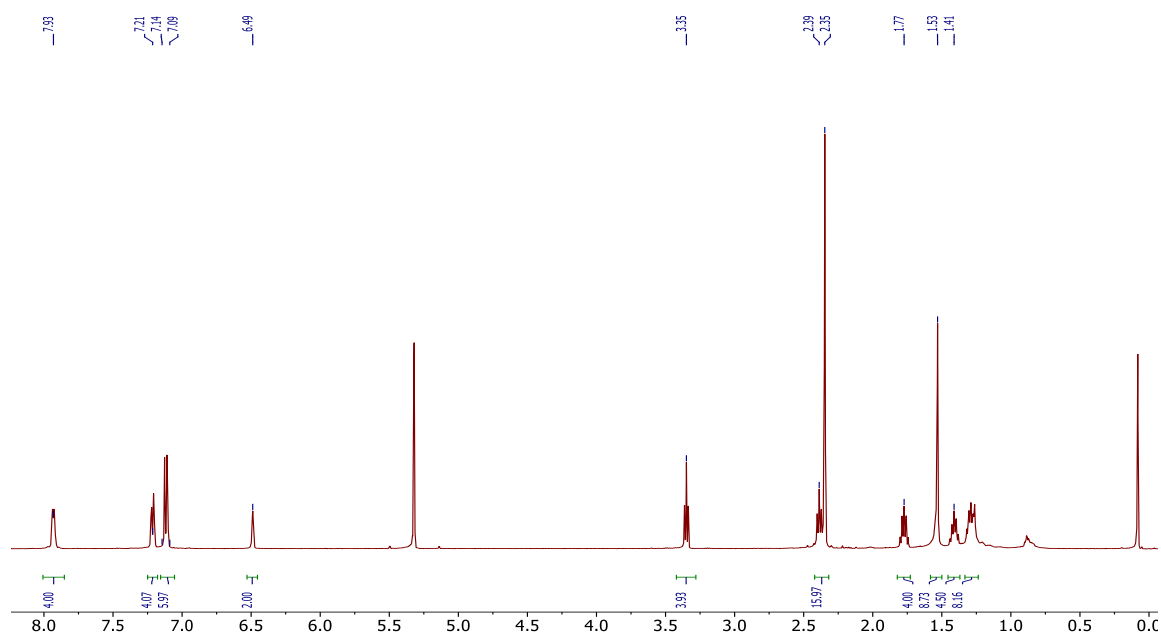
^{13}C NMR (126 MHz, CD_2Cl_2 , 298 K): δ (ppm) = 154.5 (s, C_q), 150.5 (HMBC, C_q), 137.6 (s, C_q), 135.9 (t, $J = 21.8$ Hz, CH_{Ar}), 133.6 (t, $J = 5.3$ Hz, C_q), 132.1 (s, CH_{Ar}), 131.9 (s, CH_{Ar}), 130.5 (s, C_q), 127.7 (s, CH_{Ar}), 118.4 (s, C_q), 117.9 (s, CH_{Ar}), 35.3 (s, CH_2), 35.0 (s, C_q), 34.5 (s, CH_2), 33.2 (s, CH_2), 32.7 (s, CH_3), 30.7 (s, CH_2), 28.0 (s, CH_2), 20.9 (s, CH_3). 1C_q missing.

^{31}P NMR (202 MHz, CD_2Cl_2 , 298 K): δ (ppm) = -71.7 (s). Data were found to match literature.¹⁸

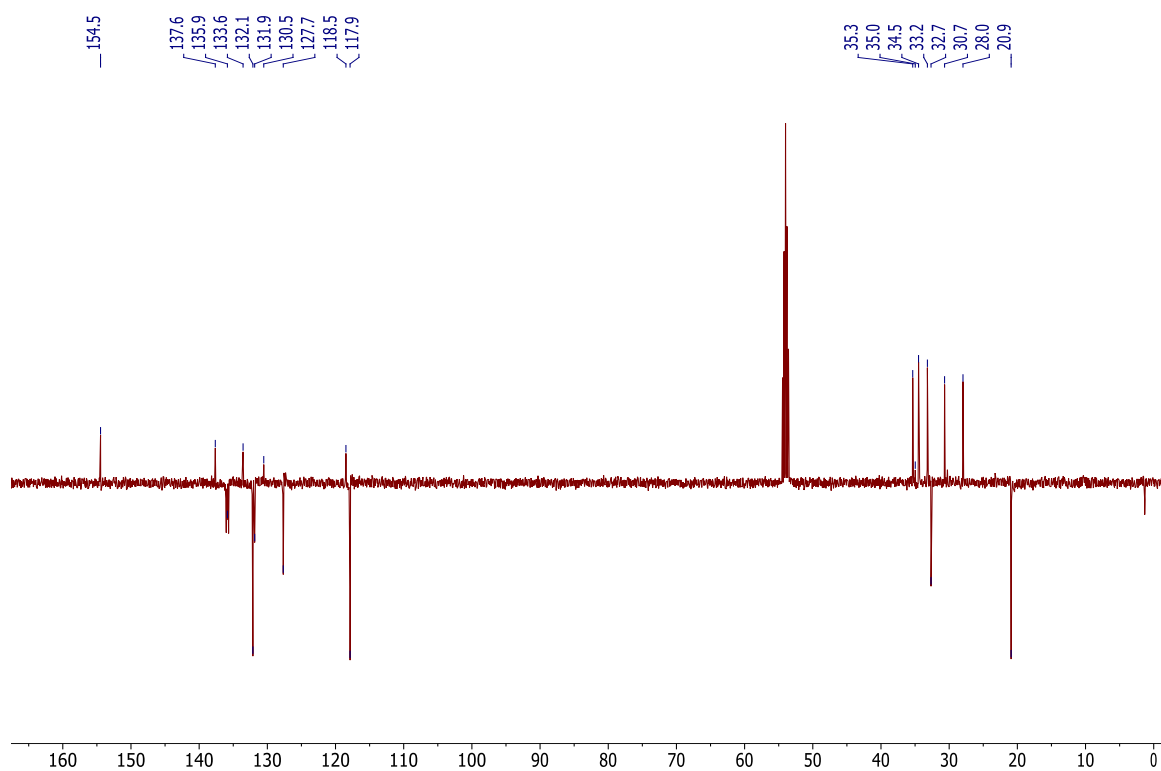
Anal. Calcd $\text{C}_{59}\text{H}_{54}\text{Br}_2\text{O}_3\text{P}_2$: C, 66.26; H, 5.67 Found: C, 66.38; H, 5.502.

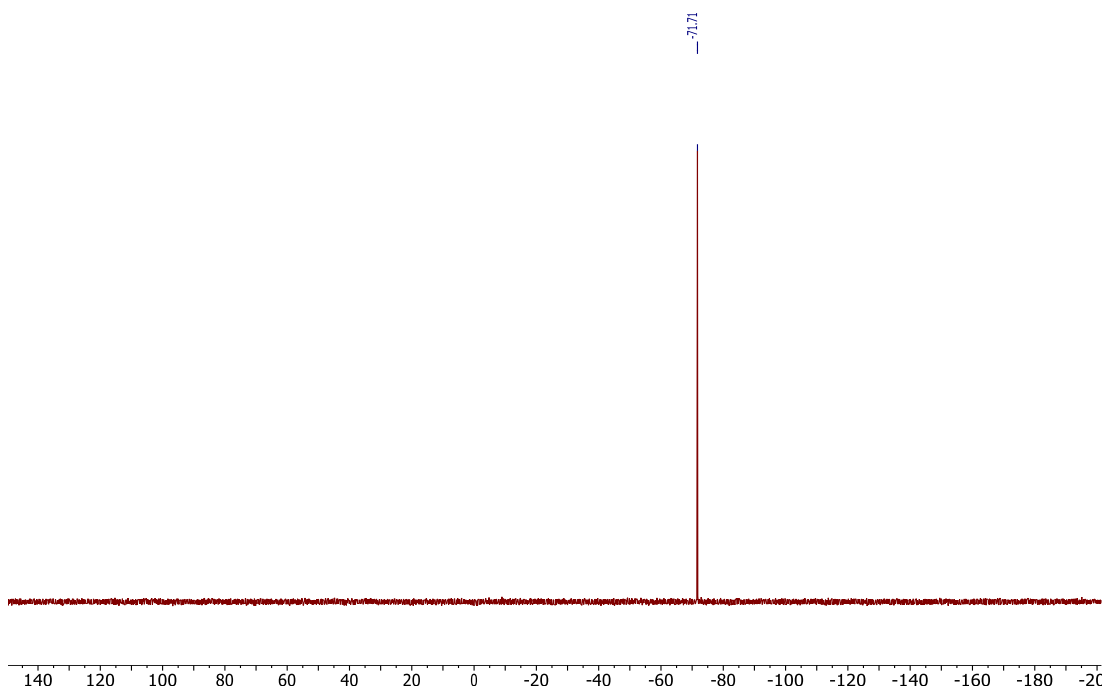
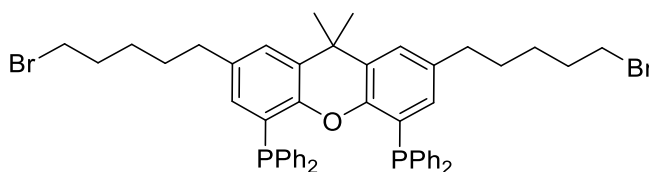
mp: 206-207 °C.

^1H NMR (CD_2Cl_2 , 500 MHz, 298 K)



^{13}C - $\{^1\text{H}\}$ NMR (CD_2Cl_2 , 126 MHz, 298 K)



$^{31}\text{P}\{-^1\text{H}\}$ NMR (CD_2Cl_2 , 202 MHz 298 K)**2,7-bis(5-bromopentyl)-9,9-dimethyl-4,5-bis(diphenylphosphino)xanthene (43)**

Any xanthene synthetic precursor prior lithiation has been azeotropically dried three times with toluene under vacuum. At $-71\text{ }^{\circ}\text{C}$ (ethanol/dry ice bath), 2.13 mL of *n*-butyllithium (2.5 M in hexanes, 5.32 mmol) was added dropwise to a stirred solution of azeotropically dried 4,5-dibromo-2,7-bis(5-bromopentyl)-9,9-dimethylxanthene (1.72 g, 2.58 mmol) in THF (86 mL). The resulting solution was stirred for 2.5 h. Subsequently, a solution of chlorodiphenylphosphine (0.96 mL, 5.35 mmol, density for chlorodiphenylphosphine: 1.229 g/mL) in THF (3.71 mL) was added dropwise. The reaction mixture was slowly warmed to room temperature and stirred overnight. Next, the THF was removed under vacuum and the mixture was diluted with CH_2Cl_2 (50 mL) and hydrolyzed with a 10% HCl aqueous solution (20 mL). The organic layer was removed and additional CH_2Cl_2 was added to the aqueous layer (extraction repeated 2 times). The organic layers were combined, dried over Na_2SO_4 and filtered using a cannula. The reaction mixture was then concentrated, washed with hexanes and concentrated again. The crude mixture was dissolved in a minimum amount of chloroform and then isopropanol was gently layered on top (1:1). The mixture was allowed to slowly diffuse

to give a white solid, which was isolated by filtration and dried under vacuum. Yield: 1.4 g, 65%. The compound was used without further purification.

^1H NMR (400 MHz, CD_2Cl_2 , 298 K): δ (ppm) = 7.36-7.11 (m, 22H, CH_{Ar}), 6.35 (q, J = 1.9 Hz, 2H, CH_{Ar}), 3.35 (t, J = 6.8 Hz, 4H, CH_2), 2.43 (t, J = 7.5 Hz, 4H, CH_2), 1.2-1.71 (m, 4H, CH_2), 1.63 (s, 6H, CH_3), 1.49-1.40 (m, 4H, CH_2), 1.36-1.26 (m, 4H, CH_2).

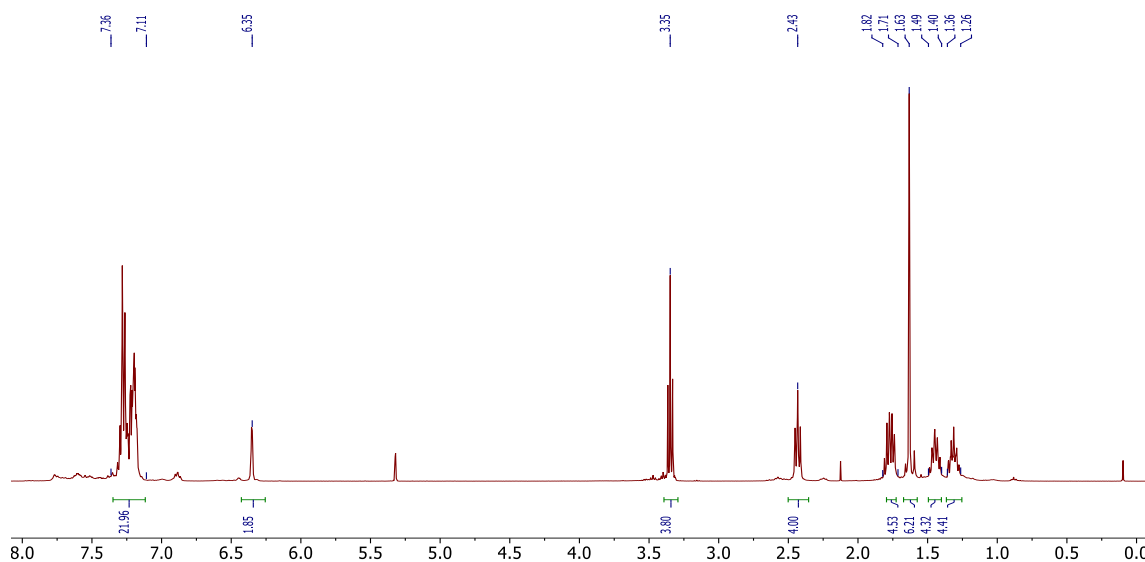
^{13}C NMR (101 MHz, CD_2Cl_2 , 298 K): δ (ppm) = 151.3 (t, J = 9.8 Hz, C_{q}), 137.9 (s, C_{q}), 137.5 (t, J = 6.0 Hz, C_{q}), 134.4 (t, J = 12.8 Hz, CH_{Ar}), 132.3 (s, CH_{Ar}), 130.3 (s, C_{q}), 128.9 (t, J = 3.5 Hz, CH_{Ar}), 128.7 (s, CH_{Ar}), 127.1 (s, CH_{Ar}), 35.50 (s, CH_2), 35.03 (s, C_{q}), 34.55 (s, CH_2), 33.15 (s, CH_2), 32.23 (s, CH_3), 30.91 (s, CH_2), 27.97 (s, CH_2). 1 C_{q} missing.

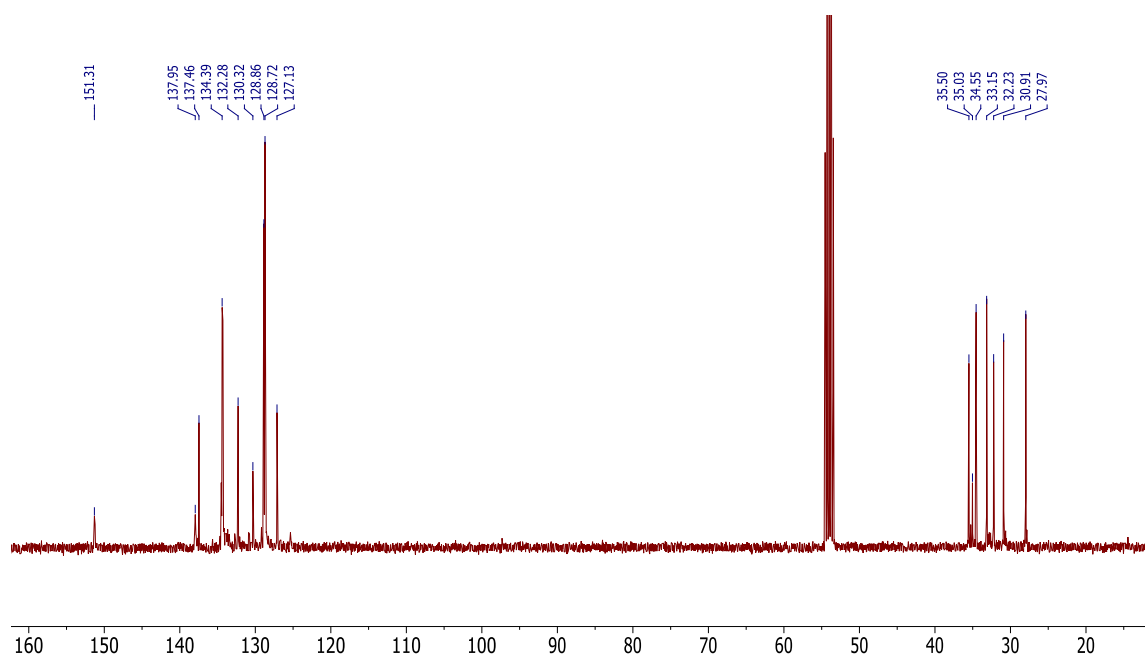
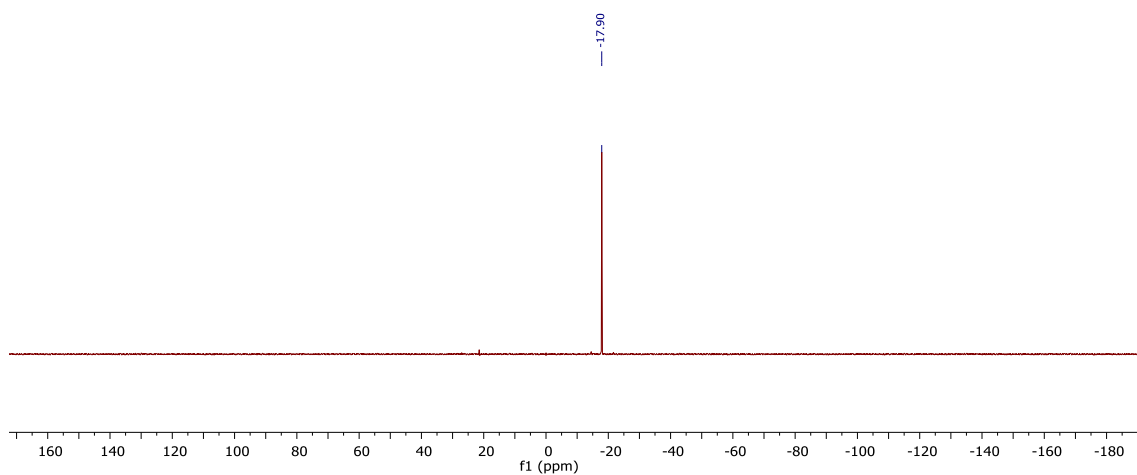
^{31}P NMR (162 MHz, CD_2Cl_2 , 298 K): δ (ppm) = - 17.9 (s).

Anal. Calcd $\text{C}_{49}\text{H}_{50}\text{Br}_2\text{OP}_2$: C, 67.13; H, 5.75 Found: C, 67.13; H, 5.599.

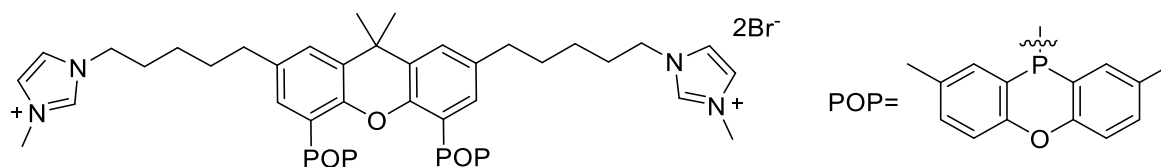
mp: 111-112 $^\circ\text{C}$.

^1H NMR (CD_2Cl_2 , 400 MHz, 298 K)



$^{13}\text{C}\{-^1\text{H}\}$ NMR (CD_2Cl_2 , 101 MHz, 298 K) $^{31}\text{P}\{-^1\text{H}\}$ NMR (CD_2Cl_2 , 162 MHz, 298 K)

2,7-bis(5-(3-methylimidazolium)pentyl)-9,9-dimethyl-4,5-bis(2,8-dimethyl-10-phenoxaphosphino)xanthene bromide (38)



2,7-bis(5-bromopentyl)-9,9-dimethyl-4,5-bis(2,8-dimethyl-10-phenoxaphosphino)xanthene (0.104 mmol, 100 mg) and 0.7 mL of 1-methylimidazole (8.78 mmol, 720 mg, 85 eq.) were dissolved in freshly distilled toluene (7 mL) in a Schlenk tube equipped with

a magnetic stirrer and a condenser. The reaction was then warmed to 80 °C for 48 hours.²¹ Formation of shiny white crystals was observed. The reaction mixture was cooled down. The supernatant was removed by syringe and the product extensively washed with toluene, diethyl ether and *n*-pentane. The compound was dried under vacuum at 40 °C. Yield: 107 mg, 92%. A low quality single crystal was obtained (Figure 11).

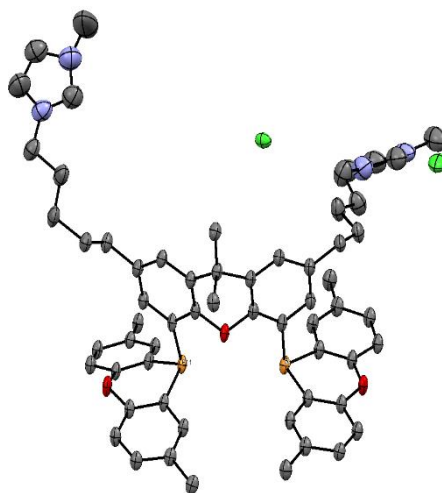


Figure 11. Thermal ellipsoid representation of ligand **38**. Hydrogen atoms have been omitted for clarity. Displacement ellipsoids correspond to 20% probability.

¹H NMR (300 MHz, CDCl₃, 298 K): δ (ppm) = 10.55 (s, 2H, CH_{Ar}), 7.96 (d, J = 7.2 Hz, 4H, CH_{Ar}), 7.25-7.06 (m, 14H, CH_{Ar}), 6.49 (q, J = 2.0 Hz, 2H, CH_{Ar}), 4.20 (t, J = 7.5 Hz, 4H, CH₂), 3.99 (s, 6H, CH₃), 2.39 (t, J = 7.5 Hz, 4H, CH₂), 2.35 (s, 12H, CH₃), 1.83 (p, J = 7.5 Hz, 4H, CH₂), 1.51 (s, 6H, CH₃), 1.46 (p, J = 7.5 Hz, 4H, CH₂), 1.22 (p, J = 7.5 Hz, 4H, CH₂).

¹³C NMR (126 MHz, CD₂Cl₂, 298 K): δ (ppm) = 154.6 (s, C_q), 151.2 (HMBC, C_q), 138.6 (s, CH_{Ar}), 137.5 (s, C_q), 135.9 (t, J = 22.5 Hz, CH_{Ar}), 133.6 (t, J = 6.5 Hz, C_q), 132.2 (s, CH_{Ar}), 131.8 (s, CH_{Ar}), 130.8 (s, C_q), 127.7 (s, CH_{Ar}), 123.4 (s, CH_{Ar}), 122.0 (s, CH_{Ar}), 118.5 (t, J = 2.9 Hz, C_q), 117.9 (s, CH_{Ar}), 50.3 (s, CH₂), 37.0 (s, CH₃), 35.3 (s, CH₂), 32.4 (s, CH₃), 30.7 (s, CH₂), 30.4 (s, CH₂), 30.2 (s, C_q), 25.7 (s, CH₂), 20.9 (s, CH₃). 1 C_q missing.

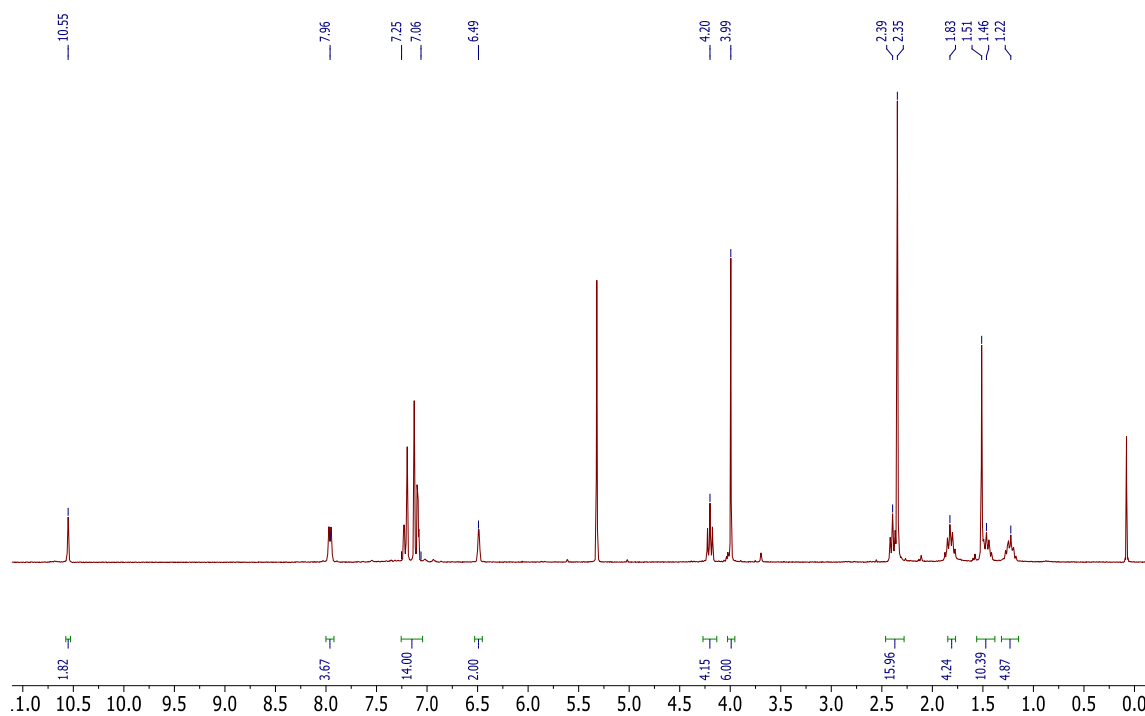
³¹P NMR (202 MHz, CD₂Cl₂, 298 K): δ (ppm) = - 71.6 (s). Data were found to match literature.¹⁸

Anal. Calcd C₆₁H₆₆N₄O₃P₂: C, 65.13; H, 5.91; N, 4.98 Found: C, 65.18; H, 5.692; N, 5.440.

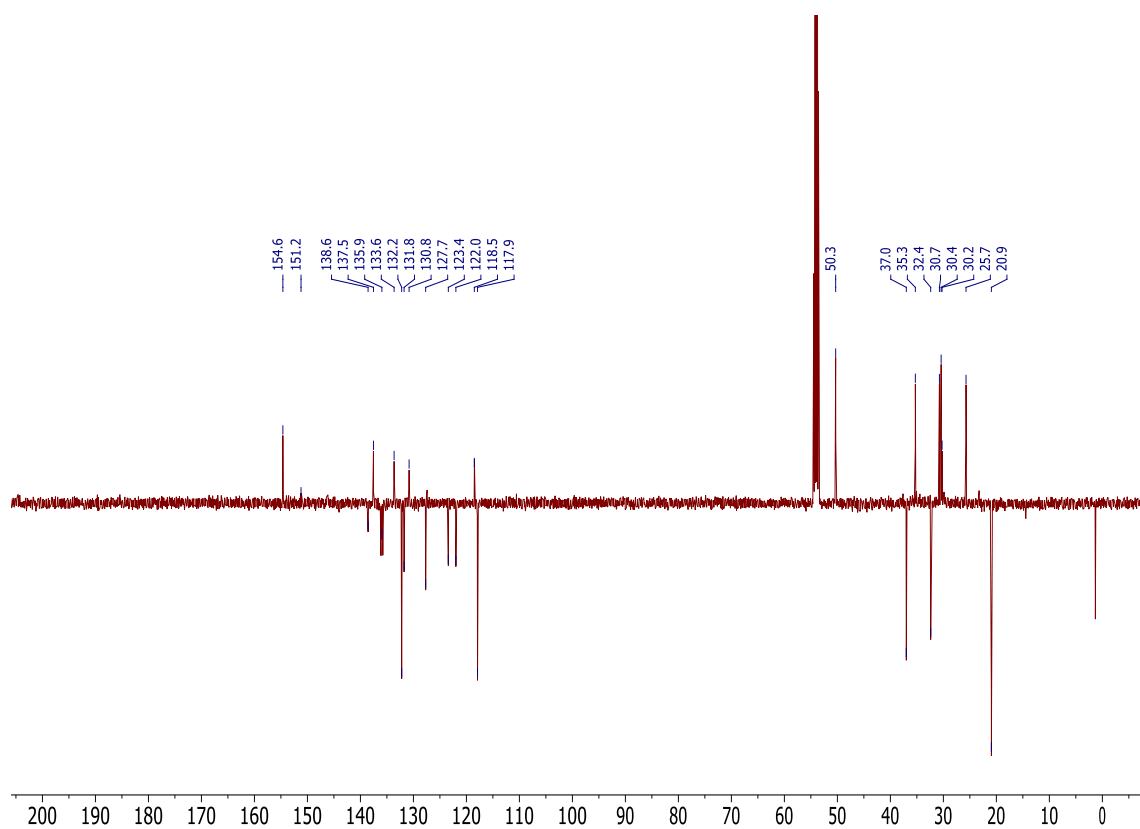
HRMS (ESI) m/z : $[M-2Br]^{2+}$ Calcd for $C_{61}H_{66}N_4O_3P_2$: 482.2310; Found 482.2312.

mp: 240-241°C.

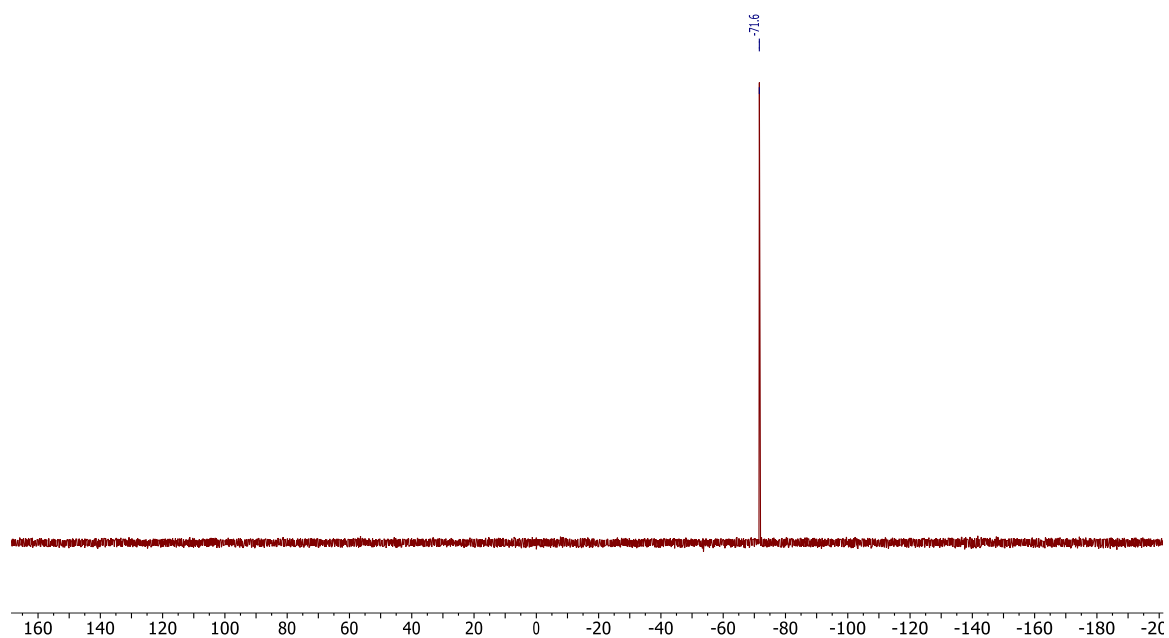
1H NMR (300 MHz, $CDCl_3$, 298 K)



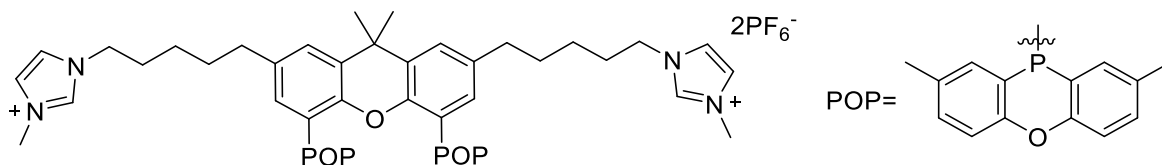
^{13}C NMR (126 MHz, CD_2Cl_2 , 298 K)



^{31}P NMR (202 MHz, CD_2Cl_2 , 298 K)



2,7-bis(5-(3-methylimidazolium)pentyl)-9,9-dimethyl-4,5-bis(2,8-dimethyl-10-phenoxaphosphino)xanthene hexafluorophosphate (31)



Potassium hexafluorophosphate (0.18 mmol, 33.86 mg, 2.1 eq.) and 2,7-Di(5-(3-methylimidazolium)pentyl)-9,9-dimethyl-4,5-di-(2,8-dimethyl-10-phenoxaphosphino) xanthene bromide (0.08 mmol, 100 mg) were dissolved in MeCN (3 mL) at room temperature in a Schlenk tube equipped with a magnetic stirrer. The reaction mixture was stirred overnight. Subsequently, 12 mL of CH₂Cl₂ were added and the product was filtered through celite. The celite was washed with CH₂Cl₂/MeCN (1:3) 5 times and CH₂Cl₂/THF (3:1) once. The solvents were removed and the compound was dried under vacuum at 40 °C giving a white powder. Yield: 95 mg, 85%. Data were found to match literature.¹⁸

¹H NMR (400 MHz, CD₃CN, 298 K): δ (ppm) = 8.61 (s, 2H, CH_{Ar}), 7.96 (d, J = 7.0 Hz, 4H, CH_{Ar}), 7.34 (s, 4H, CH_{Ar}), 7.26 (dd, J = 7.8 Hz, J = 2.3 Hz, 4H, CH_{Ar}), 7.23 (d, J = 2.3 Hz, 4H, CH_{Ar}), 7.13 (m, 2H, CH_{Ar}), 4.07 (t, J = 7.6 Hz, 4H, CH₂), 3.82 (s, 6H, CH₃), 2.39-2.31 (m, 4H, CH₂), 2.34 (s, 12H, CH₃), 1.75 (p, J = 7.6 Hz, 4H, CH₂), 1.49 (s, 6H, CH₃), 1.40 (p, J = 7.6 Hz, 4H, CH₂), 1.23-1.13 (m, 4H, CH₂). Data were found to match the literature.¹⁸

¹⁹F NMR (377 MHz, CD₂Cl₂, 298 K): δ (ppm) = -72.82 (d, J = 710.2 Hz).

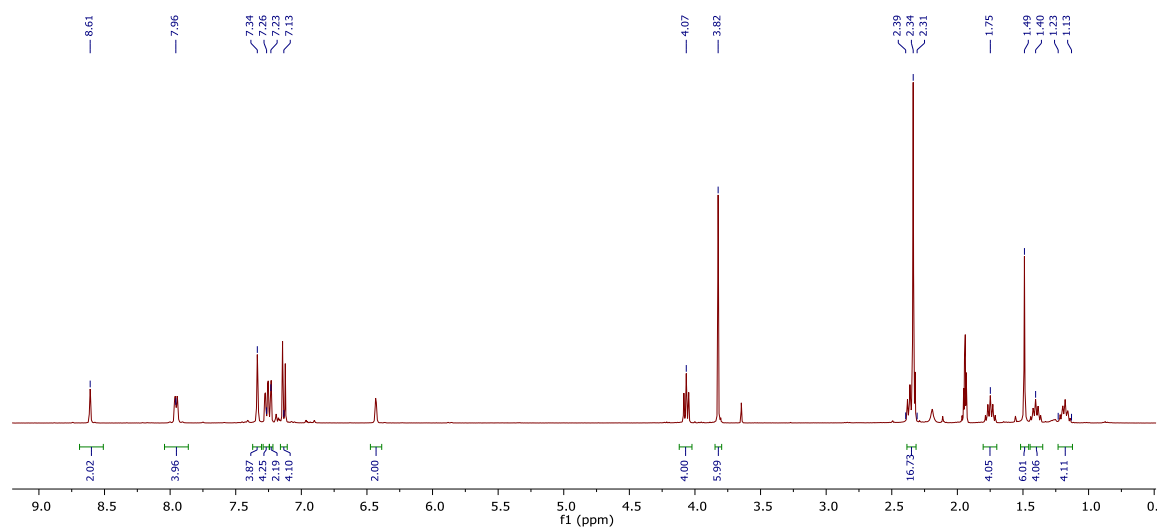
³¹P NMR (162 MHz, CD₃CN, 298 K): δ -71.97 (s), -144.62 (sept, J = 710.2 Hz).

HRMS (ESI) m/z : [M-2PF₆]²⁺ Calcd for C₆₁H₆₆N₄O₃P₂: 482.2310; Found 482.2292.

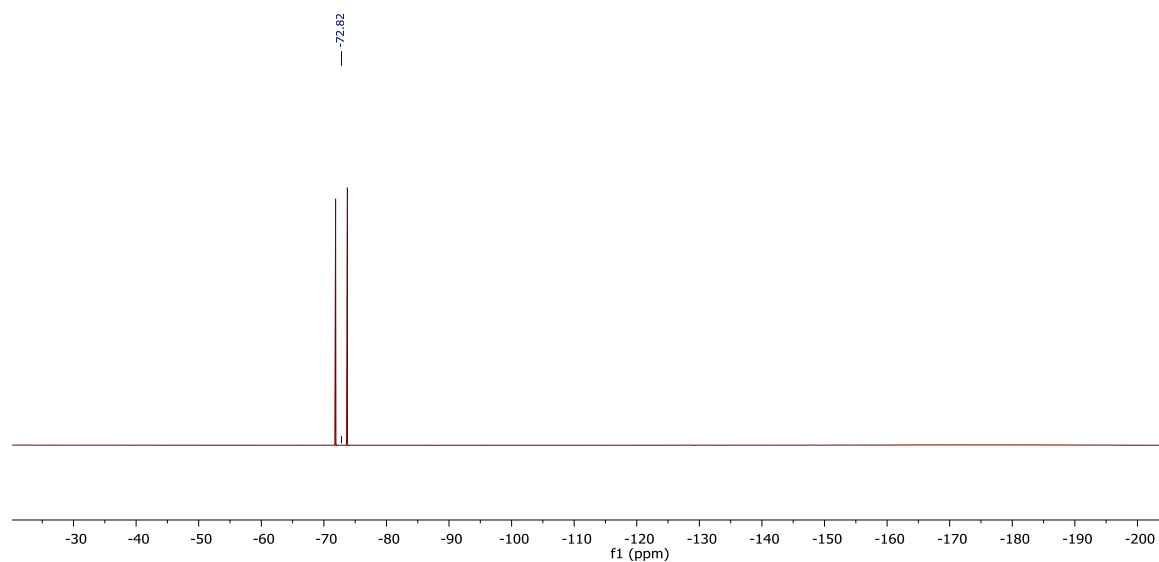
HRMS (ESI, negative ion mode) m/z : [M]⁻ Calcd for F₆P: 144.9642; Found: 144.9646.

mp: 221-222 °C.

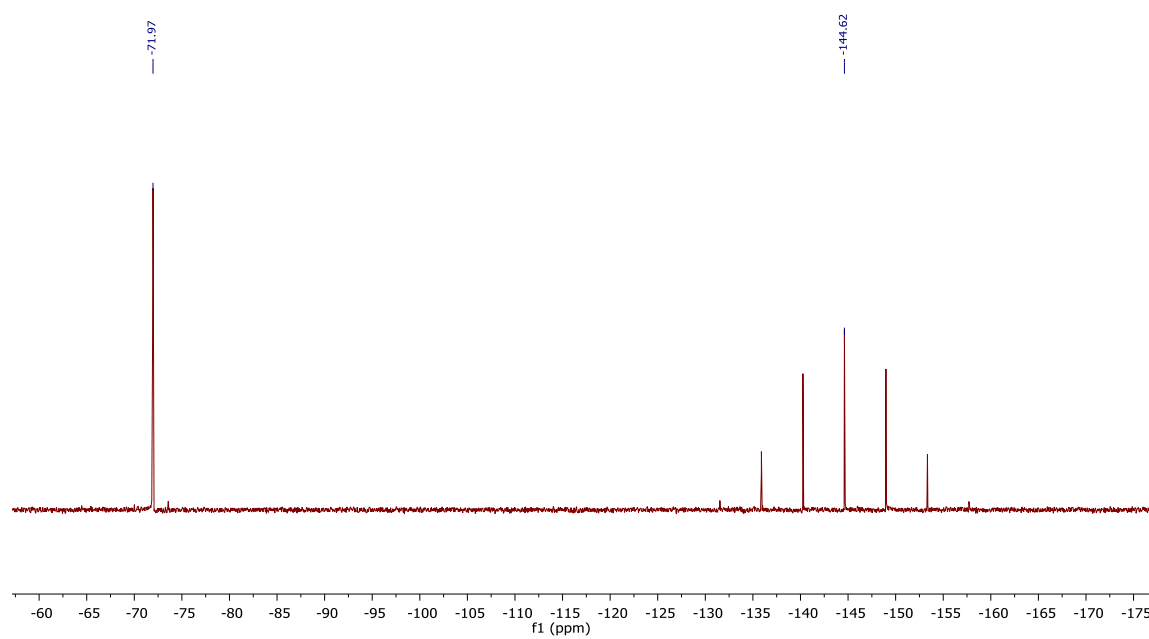
^1H NMR (400 MHz, CD_3CN , 298 K)



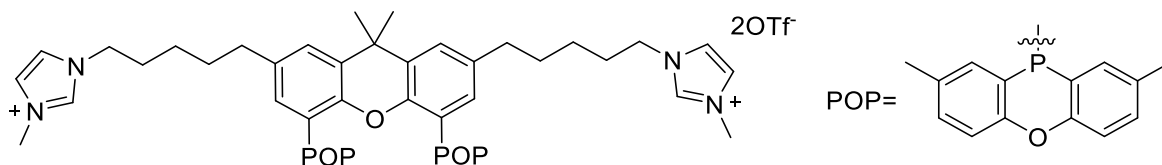
^{19}F NMR (377 MHz, CD_2Cl_2 , 298 K)



^{31}P NMR (162 MHz, CD_3CN , 298 K)



2,7-bis(5-(3-methylimidazolium)pentyl)-9,9-dimethyl-4,5-bis(2,8-dimethyl-10-phenoxaphosphino)xanthene trifluoromethanesulfonate (45)



Potassium trifluoromethanesulfonate KOTf (0.18 mmol, 34.62 mg, 2.1 eq.) and 2,7-bis(5-(3-methylimidazolium)pentyl)-9,9-dimethyl-4,5-di(2,8-dimethyl-10-phenoxaphosphino)xanthene bromide (0.08 mmol, 100 mg) were dissolved in MeCN (3 mL) at room temperature in a Schlenk tube equipped with a magnetic stirrer. The reaction mixture was stirred overnight. Subsequently, 12 mL of CH₂Cl₂ were added and the product was filtered through celite. The celite was washed with CH₂Cl₂/MeCN (1:3) 5 times and CH₂Cl₂/THF (3:1) once. The solvents were removed and the compound was dried under vacuum at 40 °C giving a white powder. Yield: 75 mg, 69%.

¹H NMR (500 MHz, CD₂Cl₂, 298 K): δ (ppm) = 8.46 (s, 2H, CH_{Ar}), 7.97 (d, *J* = 6.5 Hz, 4H, CH_{Ar}), 7.21 (dd, *J* = 8.3 Hz, *J* = 1.8 Hz, 4H, CH_{Ar}), 7.15 (bt, *J* = 1.8 Hz, 2H, CH_{Ar}), 7.13-7.09 (m, 8H, CH_{Ar}), 6.50 (s, 2H, CH_{Ar}), 4.05 (t, *J* = 7.4 Hz, 4H, CH₂), 3.83 (s, 6H, CH₃), 2.39 (t, *J* = 7.6 Hz, 4H, CH₂), 2.35 (s, 12H, CH₃), 1.77 (p, *J* = 7.8 Hz, 4H, CH₂), 1.45 (s, 12H, CH₃), 1.20 (p, *J* = 7.8 Hz, 4H, CH₂).

¹³C NMR (126 MHz, CD₂Cl₂, 298 K): δ (ppm) = 154.7 (s, C_q), 150.8 (HMBC, C_q), 137.5 (s, C_q), 136.3 (s, CH_{Ar}), 135.9 (t, *J* = 22.3 Hz, CH_{Ar}), 133.7 (t, *J* = 5.8 Hz, C_q), 132.2 (s, CH_{Ar}), 131.7 (s, CH_{Ar}), 130.8 (s, C_q), 127.6 (s, CH_{Ar}), 124.0 (s, CH_{Ar}), 122.7 (s, CH_{Ar}), 120.4 (q, *J* = 321.7 Hz, C_q), 118.4 (t, *J* = 2.4 Hz, C_q), 117.9 (s, CH_{Ar}), 50.5 (s, CH₂), 36.9 (s, CH₂), 35.2 (s, CH₃), 35.0 (s, C_q), 32.2 (s, CH₂), 30.6 (s, CH₂), 30.2 (s, CH₃), 25.6 (s, CH₂), 20.9 (s, CH₃).

³¹P NMR (202 MHz, CD₂Cl₂, 298 K): δ (ppm) = -71.5(s).

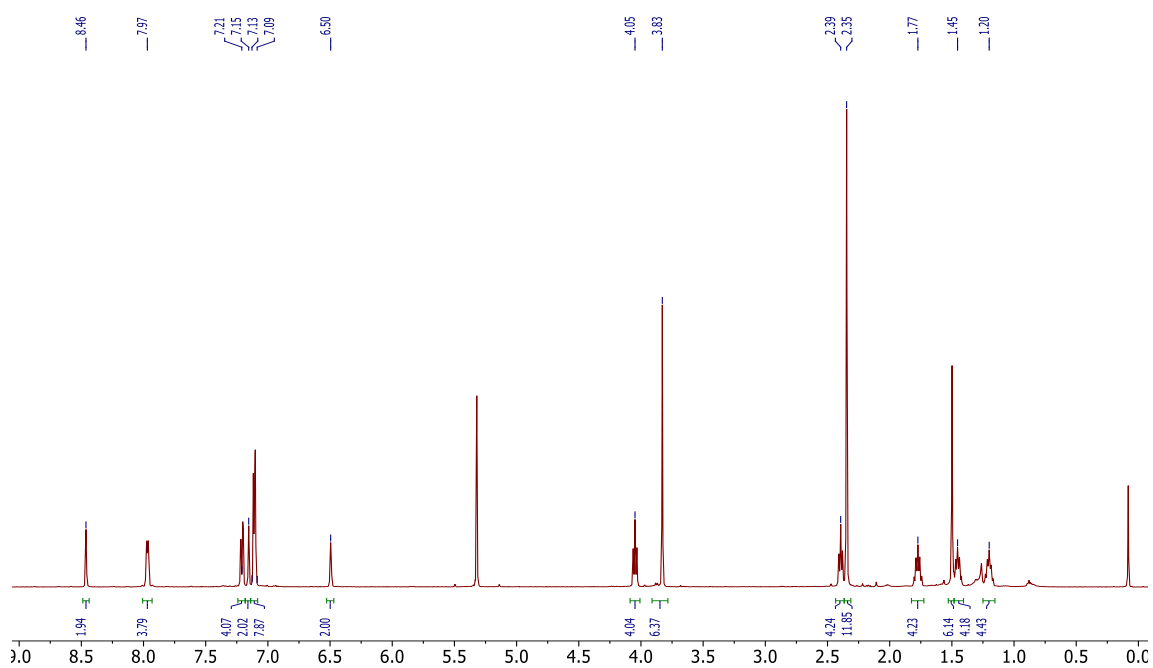
¹⁹F NMR (470 MHz, CD₂Cl₂, 298 K): δ (ppm) = -79.5 (s).

HRMS (ESI) *m/z*: [M-2OTf]²⁺ Calcd for C₆₁H₆₆N₄O₃P₂: 482.2310; Found 482.2312.

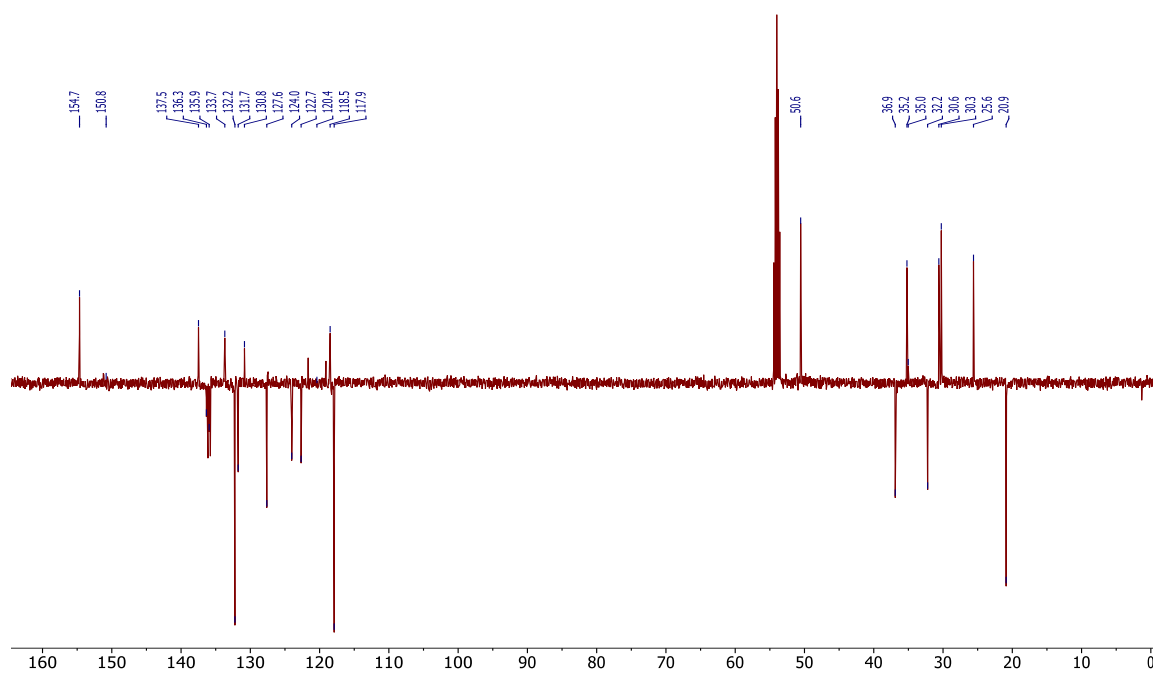
HRMS (ESI, negative ion mode) *m/z*: [M]⁻ Calcd for CF₃O₃S: 148.9520; Found: 148.9523.

mp: 177-178 °C.

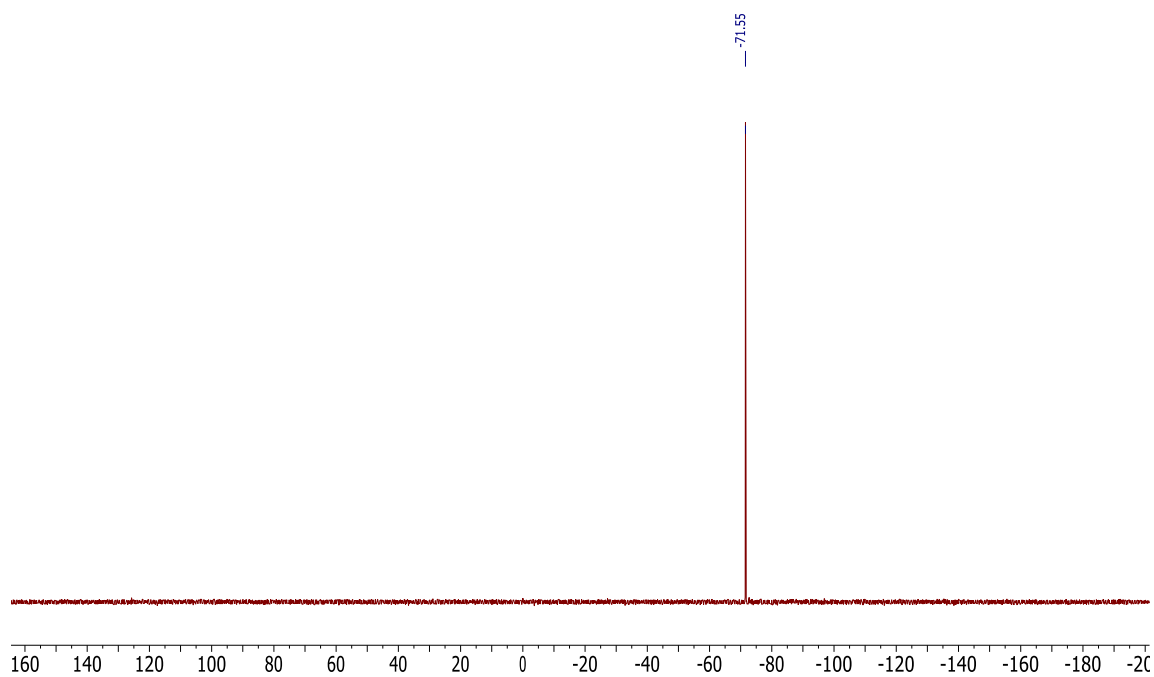
^1H NMR (500 MHz, CD_2Cl_2 , 298 K)



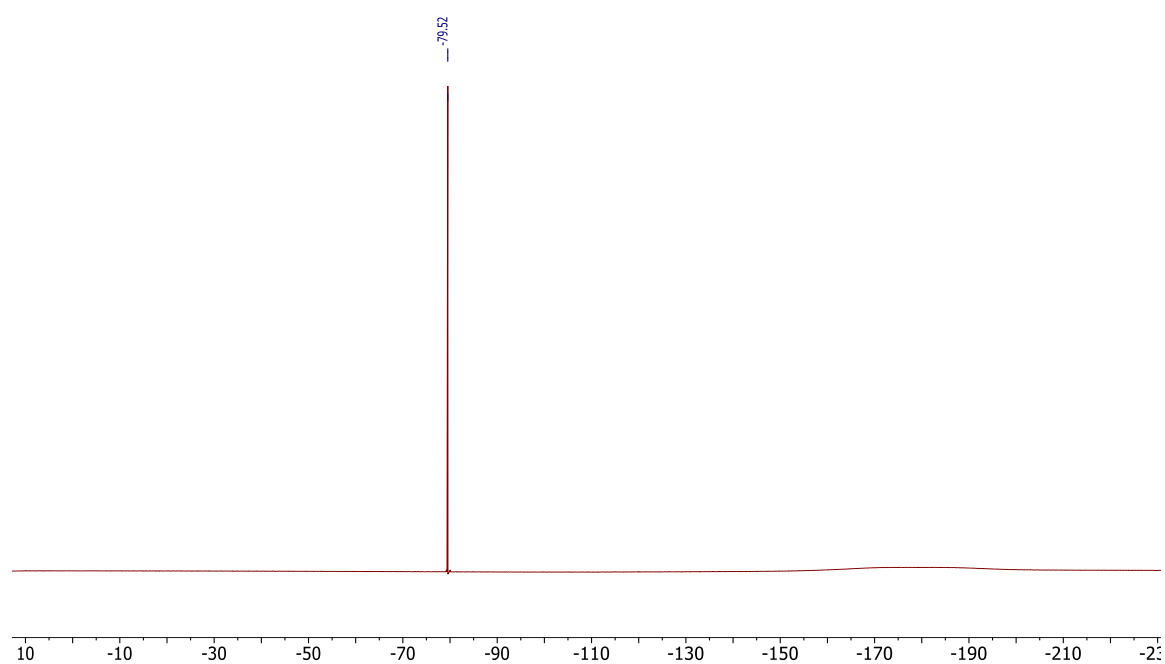
^{13}C NMR (126 MHz, CD_2Cl_2 , 298 K)



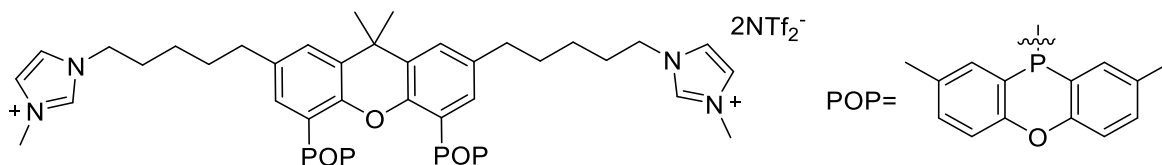
^{31}P NMR (202 MHz, CD_2Cl_2 , 298 K)



^{19}F NMR (470 MHz, CD_2Cl_2 , 298 K)



2,7-bis(5-(3-methylimidazolium)pentyl)-9,9-dimethyl-4,5-bis(2,8-dimethyl-10-phenoxa phosphino)xanthene trifluoromethanesulfonimide (46)



Sodium trifluoromethanesulfonimide (0.18 mmol, 55.77 mg, 2.1 eq.) and 2,7-bis(5-(3-methylimidazolium)pentyl)-9,9-dimethyl-4,5-di(2,8-dimethyl-10-phenoxa phosphino)xanthene bromide (0.08 mmol, 100 mg) were dissolved in MeCN (3 mL) at room temperature in a Schlenk tube equipped with a magnetic stirrer. The reaction mixture was stirred overnight. Subsequently, 12 mL of CH₂Cl₂ was added and the product was filtered through celite. The celite was washed with CH₂Cl₂/MeCN (1:3) 5 times and CH₂Cl₂/THF (3:1) once. Solvents were removed and the compound was dried under vacuum at 40 °C giving a white powder. Yield: 102 mg, 75%.

¹H NMR (500 MHz, CD₂Cl₂, 298 K): δ (ppm) = 8.94 (s, 2H, CH_{Ar}), 7.97 (d, J = 6.6 Hz, 4H, CH_{Ar}), 7.21 (dd, J = 8.4 Hz, J = 1.6 Hz, 4H, CH_{Ar}), 7.17 (bt, J = 1.6 Hz, 2H, CH_{Ar}), 7.14-7.08 (m, 8H, CH_{Ar}), 6.49 (s, 2H, CH_{Ar}), 4.07 (t, J = 7.4 Hz, 4H, CH₂), 3.86 (s, 6H, CH₃), 2.39 (t, J = 7.5 Hz, 4H, CH₂), 2.34 (s, 12H, CH₃), 1.78 (p, J = 7.6 Hz, 4H, CH₂), 1.50 (s, 12H, CH₃), 1.45 (p, J = 7.5 Hz, 4H, CH₂), 1.20 (p, J = 7.6 Hz, 4H, CH₂).

¹³C NMR (126 MHz, CD₂Cl₂, 298 K): δ (ppm) = 154.6 (s, C_q), 151.2 (t, J = 10.7 Hz, C_q), 137.5 (s, C_q), 137.3 (s, CH_{Ar}), 135.9 (t, J = 22.6 Hz, CH_{Ar}), 133.7 (t, J = 5.7 Hz, C_q), 132.2 (s, CH_{Ar}), 131.7 (s, CH_{Ar}), 130.8 (s, C_q), 127.6 (s, CH_{Ar}), 127.4 (s, C_q), 123.8 (s, CH_{Ar}), 122.4 (s, CH_{Ar}), 118.5 (t, J = 2.1 Hz, C_q), 117.9 (s, CH_{Ar}), 50.5 (s, CH₂), 36.9 (s, CH₂), 35.2 (s, CH₃), 35.0 (s, C_q), 32.3 (s, CH₂), 30.7 (s, CH₂), 30.2 (s, CH₃), 25.7 (s, CH₂), 20.9 (s, CH₃). 1 C_q missing.

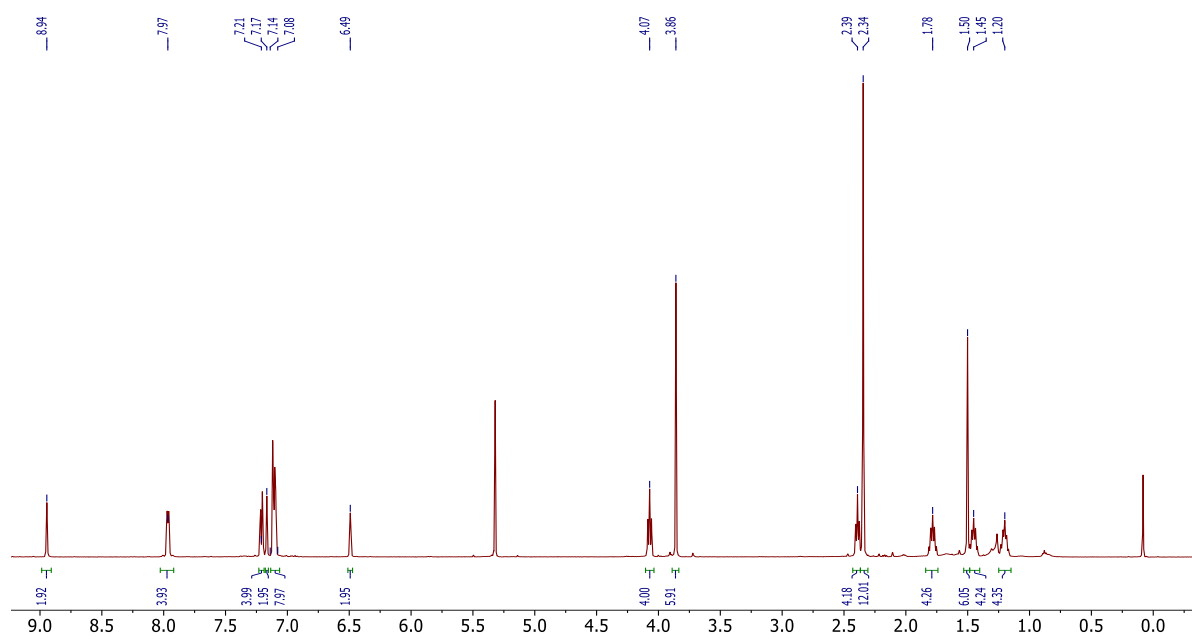
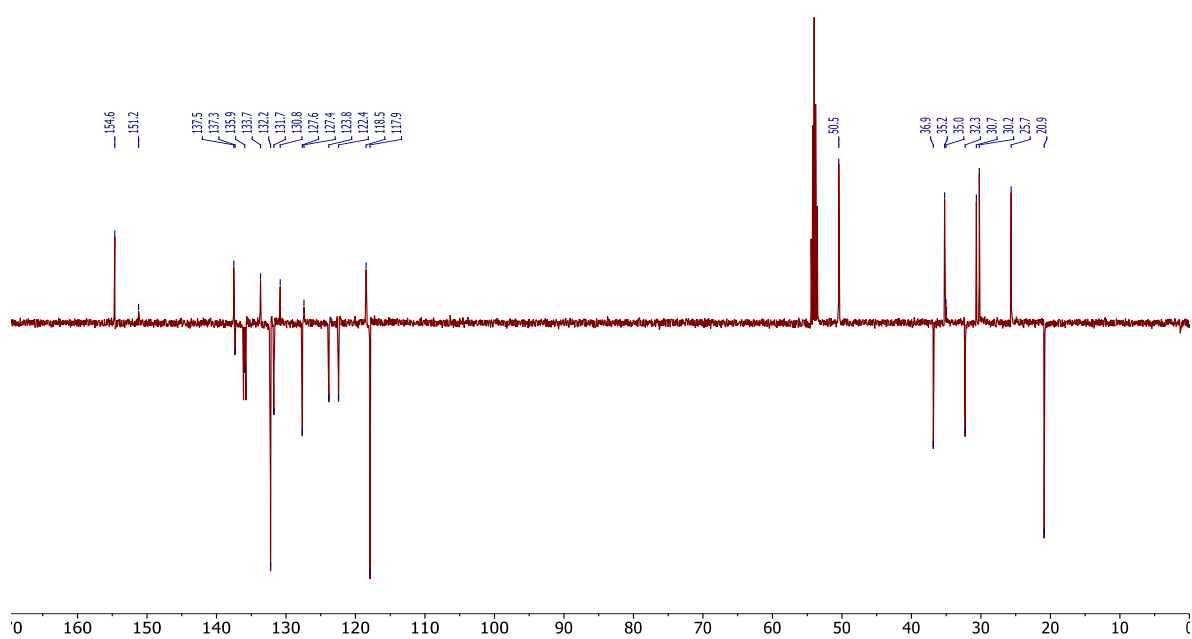
³¹P NMR (202 MHz, CD₂Cl₂, 298 K): δ (ppm) = -71.6 (s).

¹⁹F NMR (470 MHz, CD₂Cl₂, 298 K): δ (ppm) = -79.1 (s).

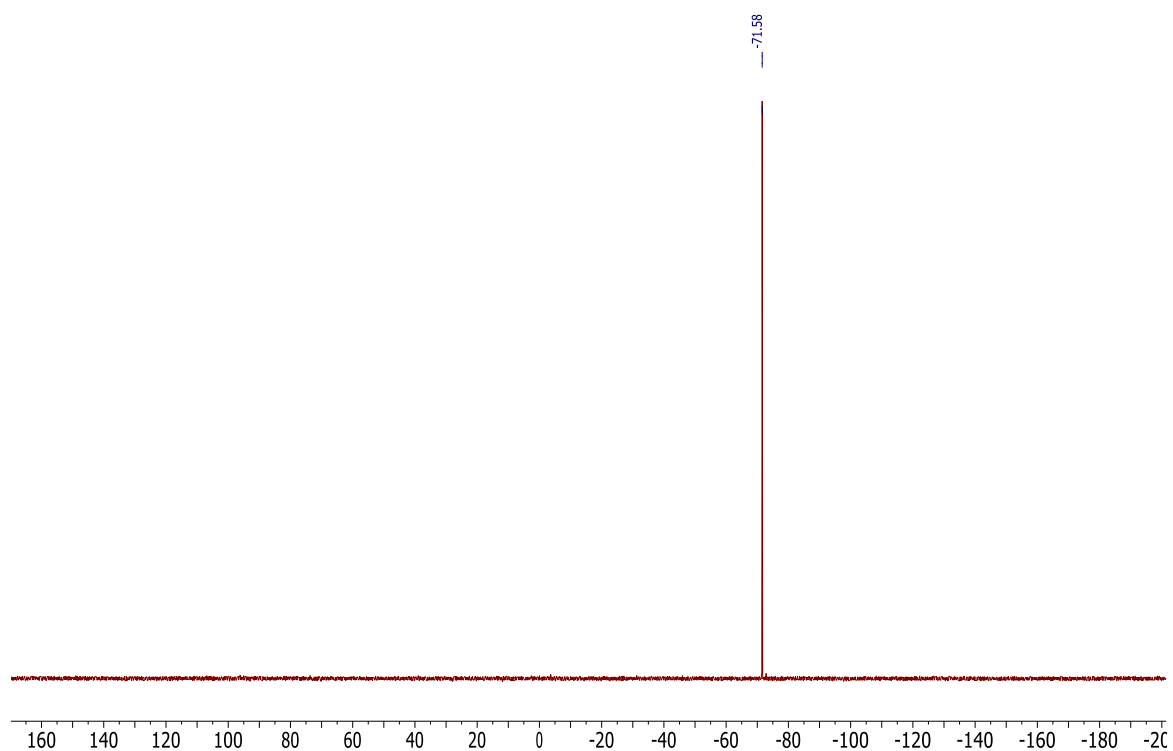
HRMS (ESI) m/z : [M-2NTf₂]²⁺ Calcd for C₆₁H₆₆N₄O₃P₂: 482.2310; Found 482.2290.

HRMS (ESI, negative ion mode) m/z : [M]⁻ Calcd for C₂F₆NO₄S₂: 279.9173; Found: 279.9284.

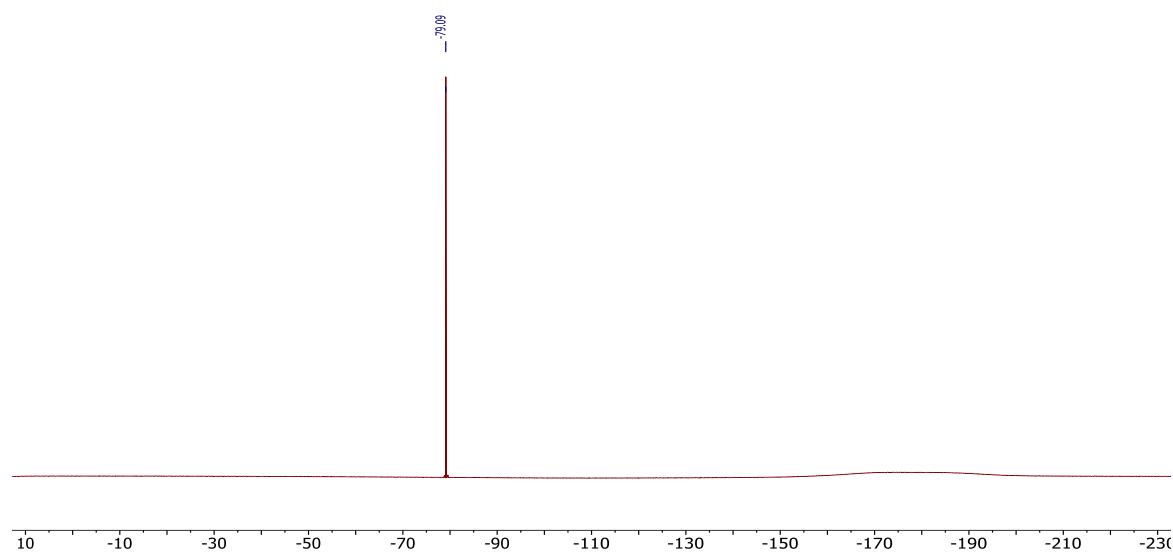
mp: >350 °C.

^1H NMR (500 MHz, CD_2Cl_2 , 298 K) ^{13}C NMR (126 MHz, CD_2Cl_2 , 298 K)

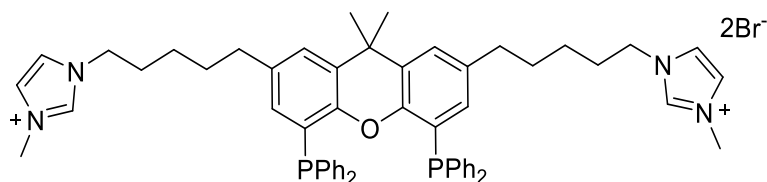
^{31}P NMR (202 MHz, CD_2Cl_2 , 298 K)



^{19}F NMR (470 MHz, CD_2Cl_2 , 298 K)



2,7-bis(5-(3-methylimidazolium)pentyl)-9,9-dimethyl-4,5-bis(diphenylphosphino)xanthene bromide (44)



2,7-bis(5-bromopentyl)-9,9-dimethyl-4,5-bis(diphenylphosphino)xanthene (0.22 mmol, 200 mg) and 4.63 mL of 1-methylimidazole (58.17 mmol, 4.7 g, 255 eq.) were dissolved in freshly distilled toluene (14 mL) in a Schlenk tube equipped with a magnetic stirrer and a condenser. The reaction mixture was then warmed to 100 °C for 8 days. Formation of an insoluble pale pink oil was observed. The reaction mixture was cooled down. The supernatant was removed by syringe and the product extensively washed with toluene, diethyl ether and *n*-pentane. The product was stirred overnight in 70 mL of diethyl ether with good stirring, washed again three times with 20 mL of this solvent. The compound was washed three times with *n*-pentane. Finally, the compound was dried under vacuum at 40 °C. The compound was washed with hexanes and dried under vacuum at 40 °C giving a white powder. Yield: 202 mg, 84%. The compound was used without further purification. *1-methylimidazole has to be previously distilled under inert conditions. If the compound is still pink extraction of impurities can be achieved with a mixture THF/Isopropanol (1:1).*

¹H NMR (300 MHz, CD₂Cl₂, 298 K): δ (ppm) = 10.63 (s, 2H, CH_{Ar}), 7.32 -7.07 (m, 26H, CH_{Ar}), 6.33 (q, *J* = 1.9 Hz, 2H, CH_{Ar}), 4.21 (t, *J* = 7.5 Hz, 4H, CH₂), 4.01 (s, 6H, CH₃), 2.43 (t, *J* = 7.5 Hz, 4H, CH₂), 1.83 (p, *J* = 7.5 Hz, 4H, CH₂), 1.62 (s, 6H, CH₃), 1.48 (p, *J* = 7.5 Hz, 4H, CH₂), 1.34-1.16 (m, 4H, CH₂).

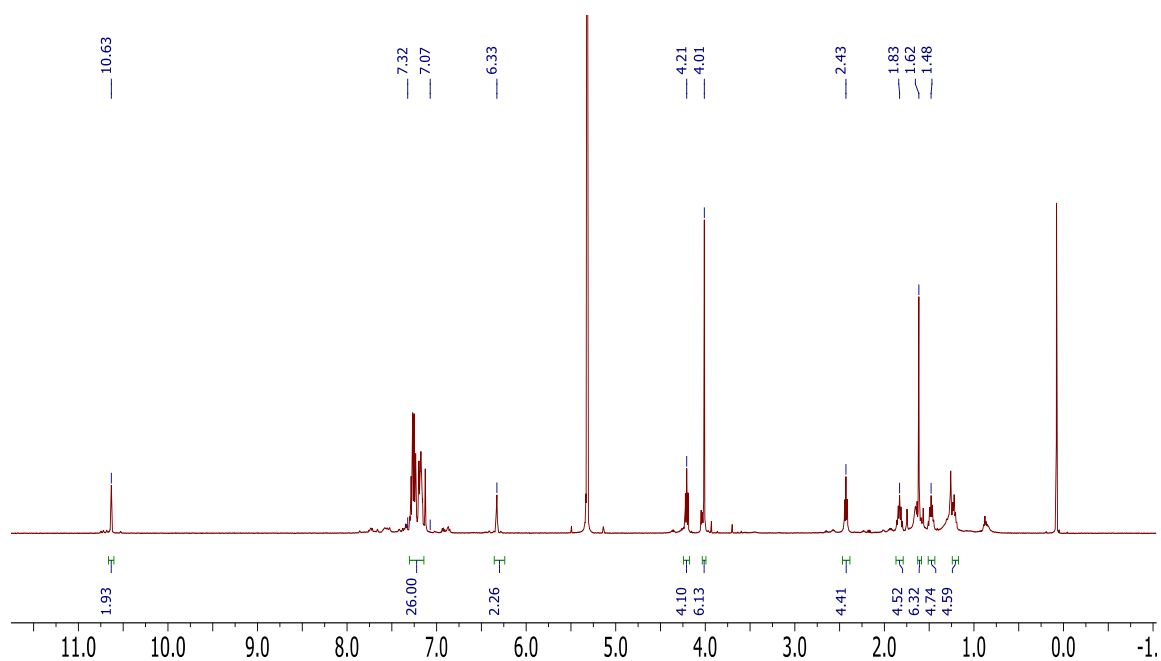
¹³C NMR (126 MHz, CD₂Cl₂, 298 K): δ (ppm) = 151.6 (t, *J* = 10.4 Hz, C_q), 138.6 (s, CH_{Ar}), 137.9 (t, *J* = 6.5 Hz, C_q), 137.3 (s, C_q), 134.4 (t, *J* = 9.1 Hz, CH_{Ar}), 132.2 (s, CH_{Ar}), 130.6 (s, C_q), 128.9 (s, CH_{Ar}), 128.7 (t, *J* = 3.4 Hz, CH_{Ar}), 127.1 (s, CH_{Ar}), 125.7 (t, *J* = 9.7 Hz, C_q), 123.4 (s, CH_{Ar}), 122.0 (s, CH_{Ar}), 50.4 (s, CH₂), 37.7 (HMBC, C_q), 37.0 (s, CH₃), 35.4 (s, CH₂), 31.9 (s, CH₃), 31.1 (s, CH₂), 30.4 (s, CH₂), 25.8 (s, CH₂).

³¹P NMR (202 MHz, CD₂Cl₂, 298 K): δ (ppm) = -18.3 (s).

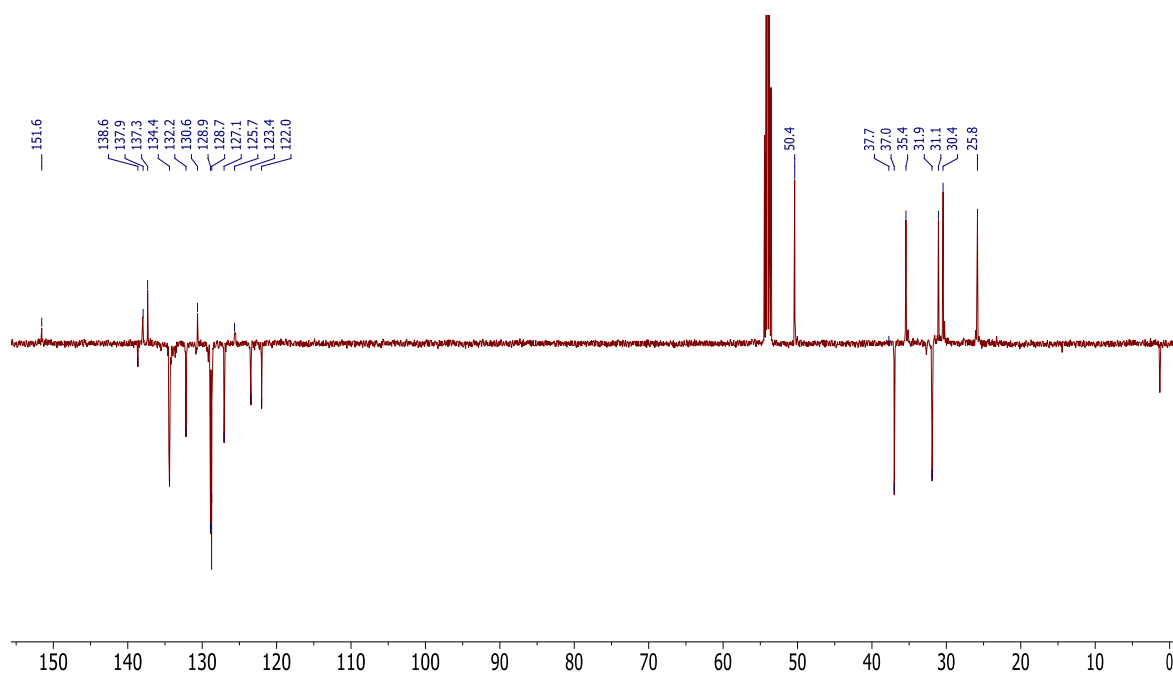
HRMS (ESI) *m/z*: [M-2Br]²⁺ Calcd for C₅₇H₆₂N₄OP₂: 440.2204; Found 440.2193.

mp: 86-87 °C.

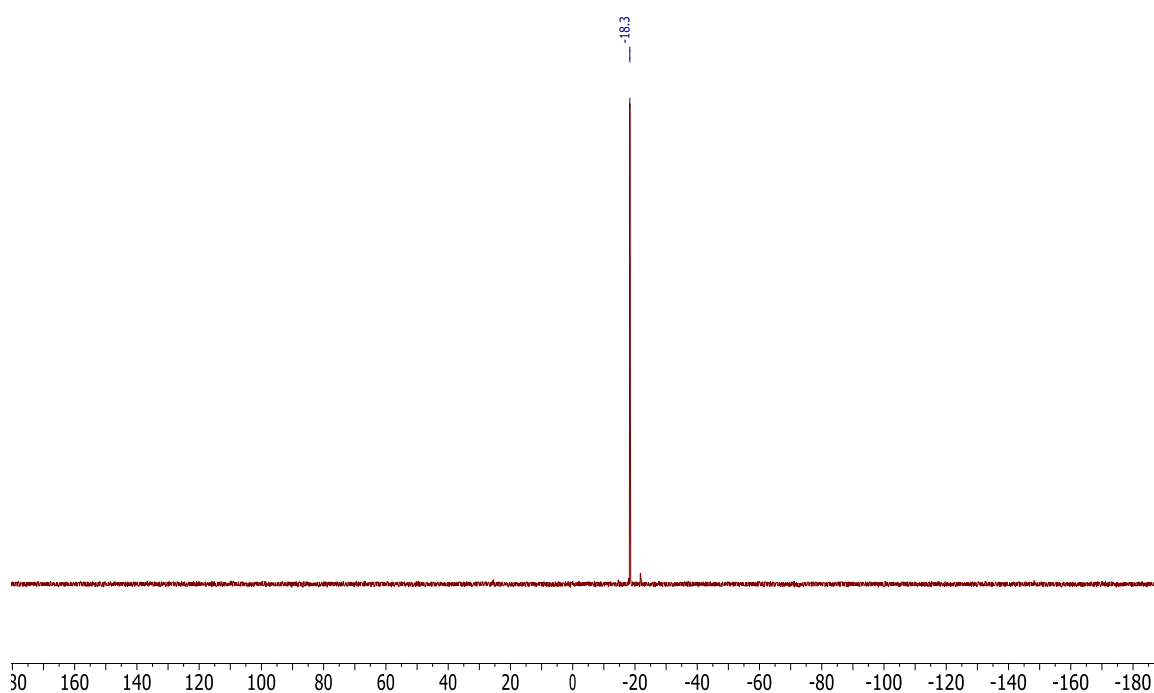
^1H NMR (300 MHz, CD_2Cl_2 , 298 K)



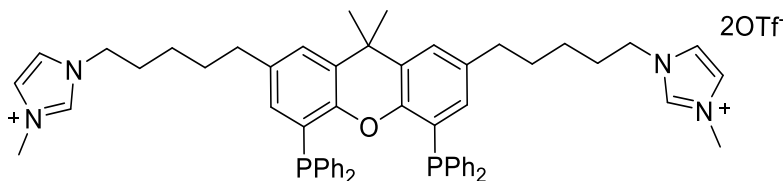
^{13}C NMR (126 MHz, CD_2Cl_2 , 298 K)



^{31}P NMR (202 MHz, CD_2Cl_2 , 298 K)



2,7-bis(5-(3-methylimidazolium)pentyl)-9,9-dimethyl-4,5-bis(2,8-dimethyl-10-phenoxa phosphino)xanthene trifluoromethanesulfonate (47)



Potassium trifluoromethanesulfonate KOTf (0.20 mmol, 37.82 mg, 2.1 eq.) and 2,7-bis(5-(3-methylimidazolium)pentyl)-9,9-dimethyl-4,5-bis(diphenylphosphino) xanthene bromide (0.09 mmol, 100 mg) were dissolved in MeCN (3 mL) at room temperature in a Schlenk tube equipped with a magnetic stirrer. The reaction mixture was stirred overnight. Subsequently, 12 mL of CH₂Cl₂ was added and the product was filtered through celite. The celite was washed with CH₂Cl₂/MeCN (1:3) 5 times and CH₂Cl₂/THF (3:1) once. Solvents were removed and the compound was dried under vacuum at 40 °C giving a white powder. Yield: 70 mg, 64%.

¹H NMR (400 MHz, CD₃OD, 298 K): δ (ppm) = 7.55 (d, *J* = 1.8 Hz, 2H, CH_{Ar}), 7.52 (d, *J* = 1.8 Hz, 2H, CH_{Ar}), 7.32-7.21 (m, 14H, CH_{Ar}), 7.15-7.09 (m, 8H, CH_{Ar}), 6.29 (q, *J* = 1.8 Hz, 2H, CH_{Ar}), 4.12 (t, *J* = 8.0 Hz, 4H, CH₂), 3.88 (s, 6H, CH₃), 2.44 (t, *J* = 6.8 Hz, 4H, CH₂), 1.80 (p, *J* = 7.6 Hz, 4H, CH₂), 1.62 (s, 6H, CH₃), 1.48 (p, *J* = 8.2 Hz, 4H, CH₂), 1.29-1.17 (m, 4H, CH₂).

¹³C NMR (101 MHz, CD₃OD, 298 K): δ (ppm) = 152.2 (t, *J* = 10.1 Hz, C_q), 138.7 (t, *J* = 6.1 Hz, C_q), 138.2 (s, C_q), 134.9 (t, *J* = 10.4 Hz, CH_{Ar}), 132.7 (s, CH_{Ar}), 131.3 (s, CH_{Ar}), 129.5 (s, C_q), 129.3 (t, *J* = 3.6 Hz, CH_{Ar}), 127.6 (s, CH_{Ar}), 126.6 (t, *J* = 10.4 Hz, C_q), 124.9 (s, CH_{Ar}), 123.4 (s, CH_{Ar}), 120.2 (s, CH_{Ar}), 50.6 (s, CH₂), 36.4 (s, CH₃), 36.0 (s, CH₂), 35.7 (s, C_q), 32.0 (s, CH₃), 31.8 (s, CH₂), 30.8 (s, CH₂), 26.5 (s, CH₂). 1 C_q missing.

³¹P NMR (162 MHz, CD₃OD, 298 K): δ (ppm) = -18.1 (s).

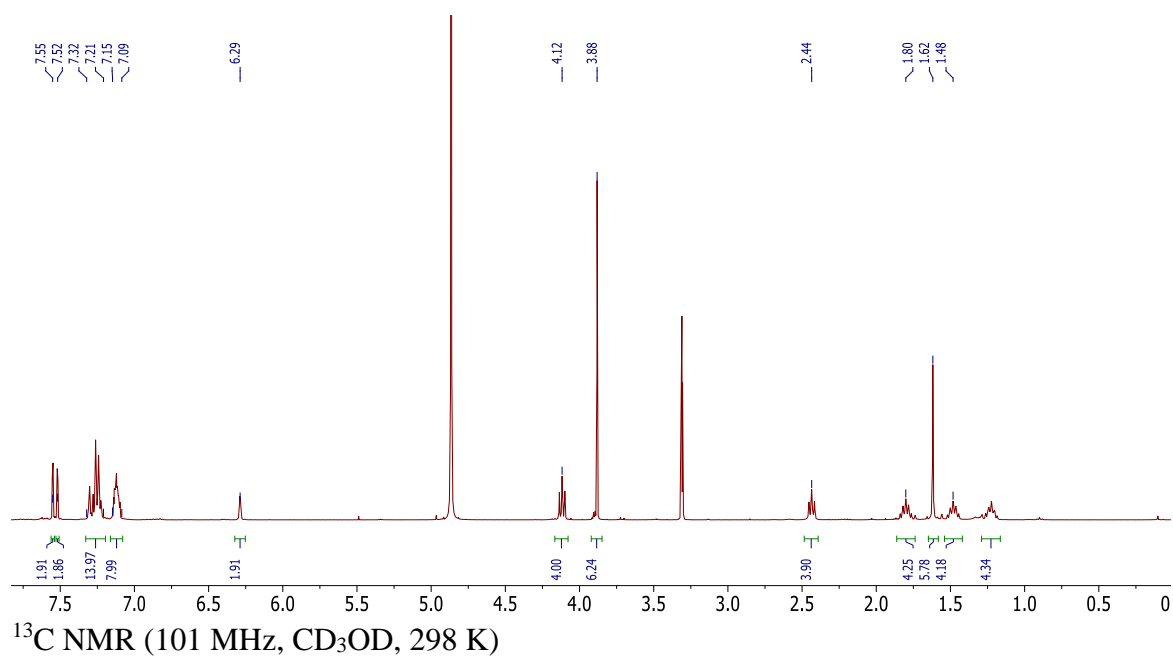
¹⁹F NMR (282 MHz, CD₃OD, 298 K): δ (ppm) = -80.1 (s).

Anal. Calcd: C, 60.09; H, 5.30; N, 4.75 **Found:** C, 60.60; H, 5.842; N, 5.038.

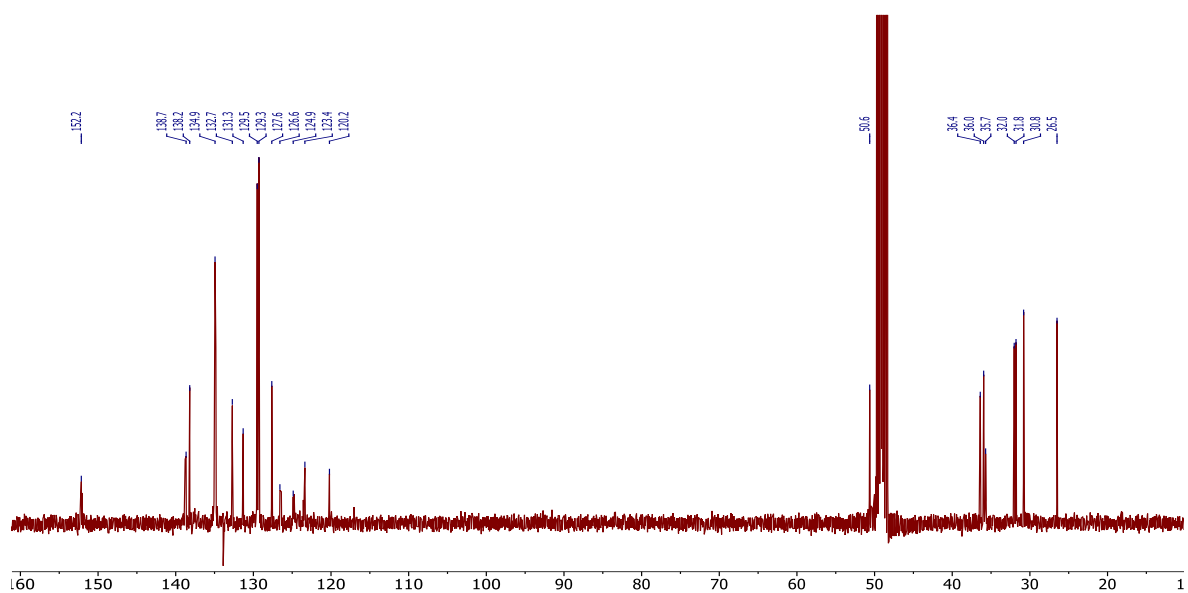
HRMS (ESI) *m/z*: [M-2OTf]²⁺ Calcd for C₅₇H₆₂N₄OP₂: 440.2204; Found 440.2198.

HRMS (ESI, negative ion mode) *m/z*: [M]⁻ Calcd for CF₃O₃S: 148.9520; Found: 148.9520.

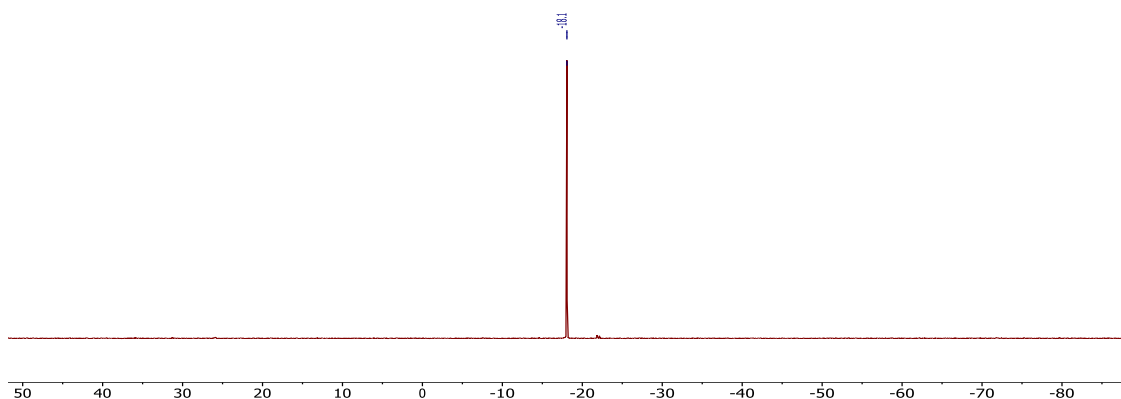
^1H NMR (400 MHz, CD_3OD , 298 K)



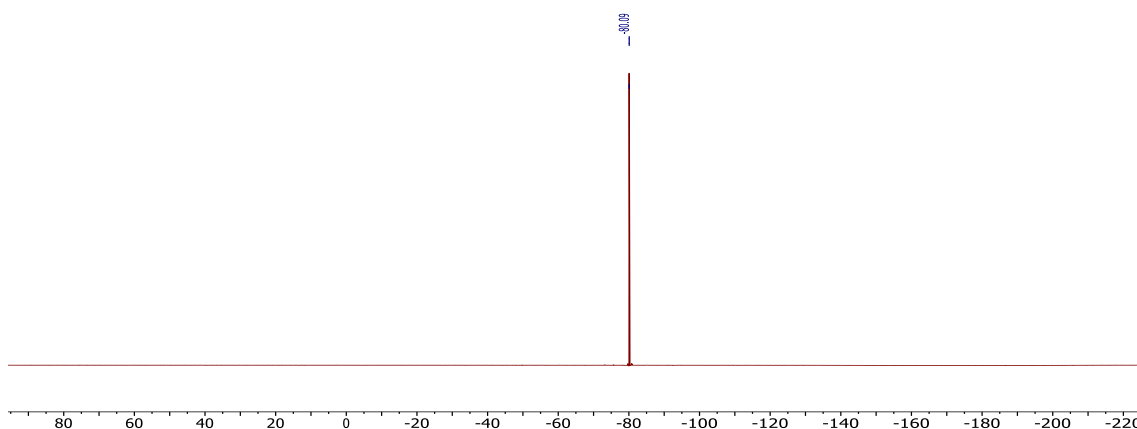
^{13}C NMR (101 MHz, CD_3OD , 298 K)



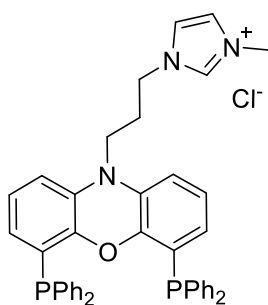
^{31}P NMR (162 MHz, CD_3OD , 298 K)



^{19}F NMR (282 MHz, CD_3OD , 298 K)



4,6-bis(diphenylphosphino)-10-propyl-methylimidazolium-phenoxazine chloride.
Imidazolium-tagged nixantphos ligand (32).

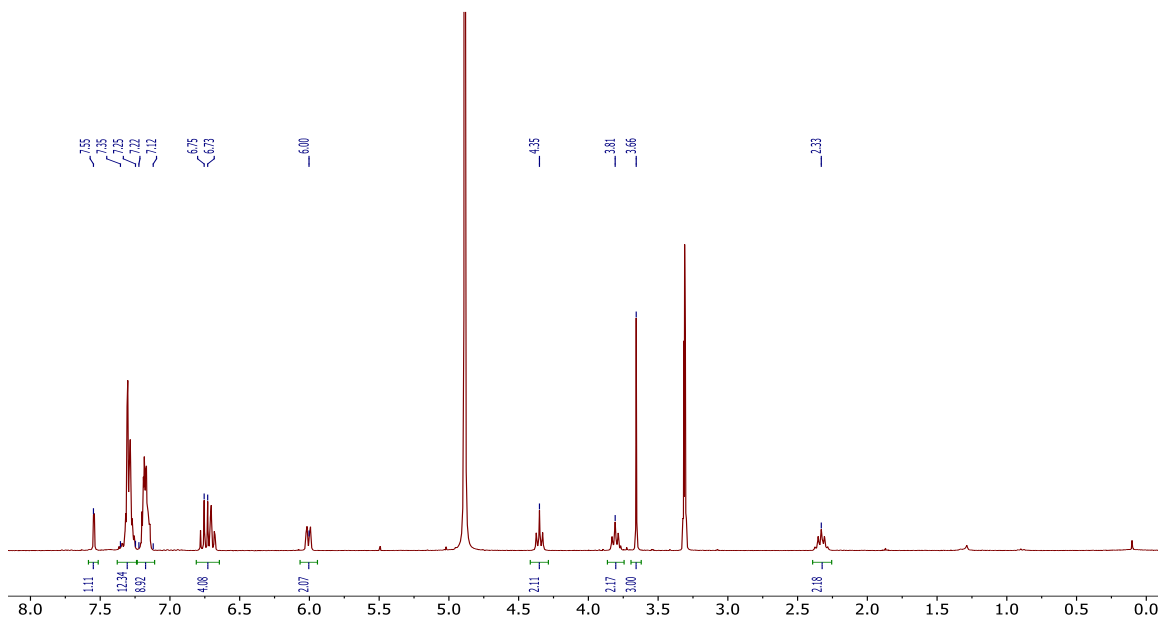


This compound was synthesized according to the procedure reported by Cole-Hamilton and co-workers. Data were found to match literature.²¹

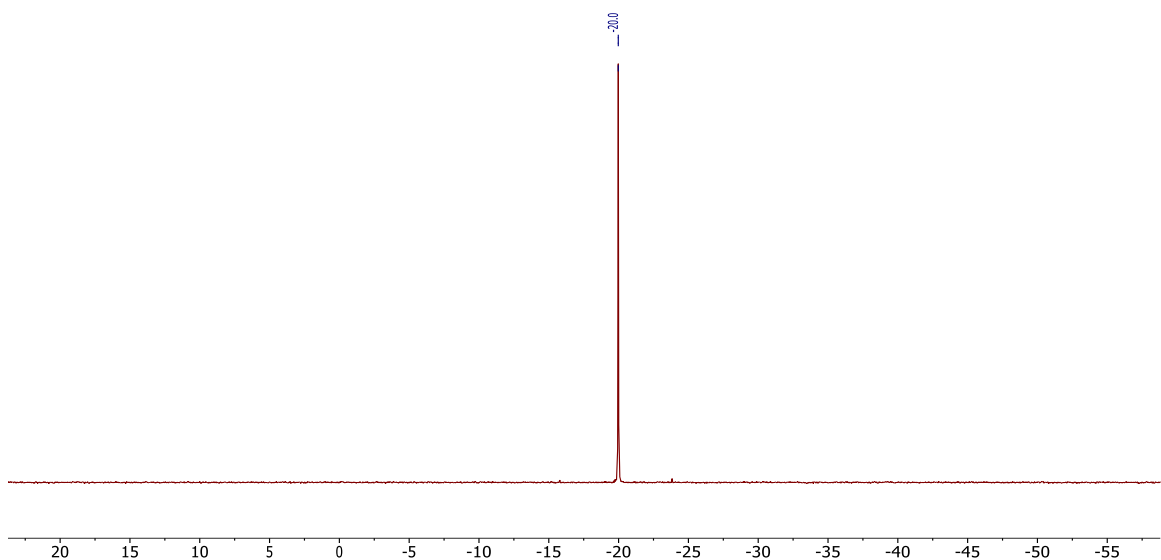
^1H NMR (300 MHz, CD_3OD , 298 K): δ (ppm) = 7.55 (d, $J = 1.8$ Hz, 1H, CH_{Ar}), 7.35-7.25 (m, 12H, CH_{Ar}), 7.22-7.12 (m, 9H, CH_{Ar}), 6.75 (t, $J = 7.8$ Hz, 2H, CH_{Ar}), 6.73 (d, $J = 7.8$ Hz, 2H, CH_{Ar}), 6.00 (dq, $J = 7.5$ Hz, $J = 1.6$ Hz, 2H, CH_{Ar}), 4.35 (t, $J = 6.6$ Hz, 2H, CH_2), 3.81 (t, $J = 6.6$ Hz, 2H, CH_2), 3.66 (s, 3H, CH_3), 2.33 (q, $J = 6.6$ Hz, 2H, CH_2).

^{31}P NMR (122 MHz, CD_3OD , 298 K): δ (ppm) = -20.0 (s).

^1H NMR (300 MHz, CD_3OD , 298 K)

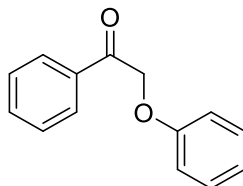


^{31}P NMR (122 MHz, CD_3OD , 298 K)



Model compound

2-phenoxy-1-phenylethan-1-one (I)



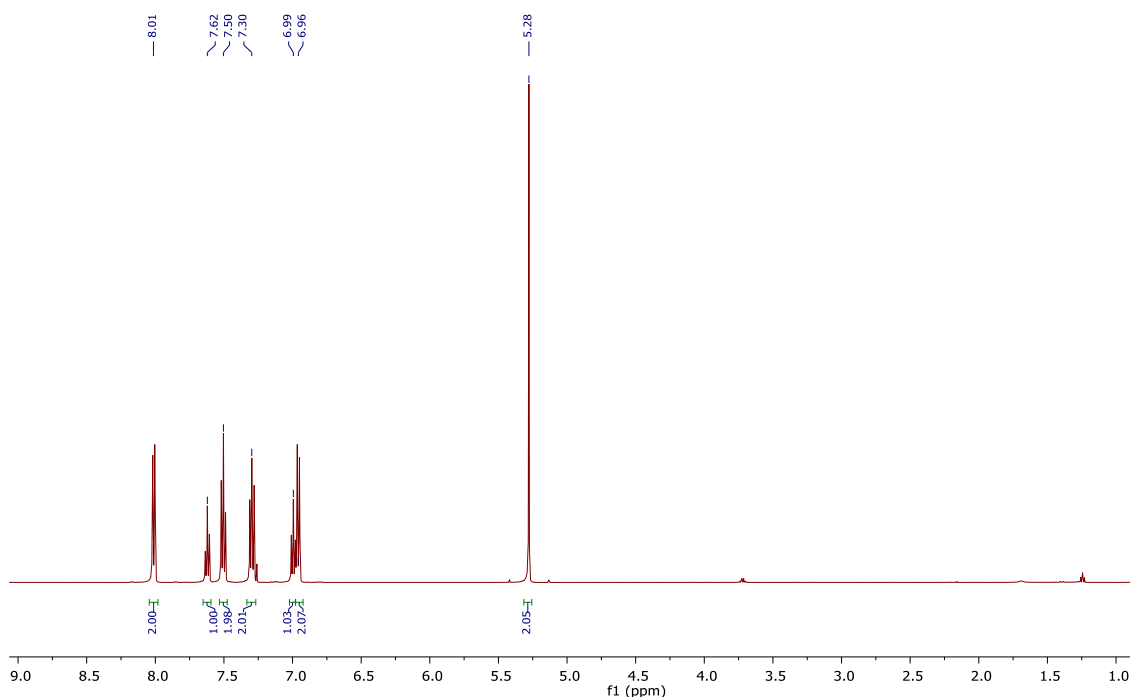
A round bottom flask equipped with a reflux condenser was charged with 2-bromoacetophenone (20.12 g, 100 mmol), potassium carbonate (20.70 g, 150 mmol),

phenol (11.80 g, 125 mmol), and acetone (45 ml, 0.6 mol). The resulting suspension was stirred and heated to reflux for four hours, after which it was filtered through celite and solvents were removed under vacuum. The resulting solid was crystallized from diethyl ether, filtered and dried under vacuum (16.54 g, 78 mmol, 78%). Data were found to match the literature.²²

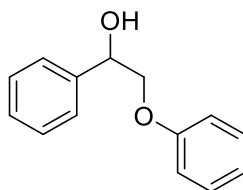
¹H NMR (500 MHz, CDCl₃, 298 K): δ (ppm) = 8.01 (d, J = 7.2 Hz, 2H, CH_{Ar}), 7.62 (t, J = 7.4 Hz, 1H, CH_{Ar}), 7.50 (t, J = 7.8 Hz, 2H, CH_{Ar}), 7.30 (t, J = 7.5 Hz, 2H, CH_{Ar}), 6.99 (t, J = 7.8 Hz, 1H, CH_{Ar}), 6.96 (d, J = 7.8 Hz, 2H, CH_{Ar}), 5.28 (s, 2H, CH₂). Data were found to match the literature.²²

mp: 71-72 °C.

¹H NMR (CDCl₃, 500 MHz, 298 K)



2-Phenoxy-1-phenylethan-1-ol (19)



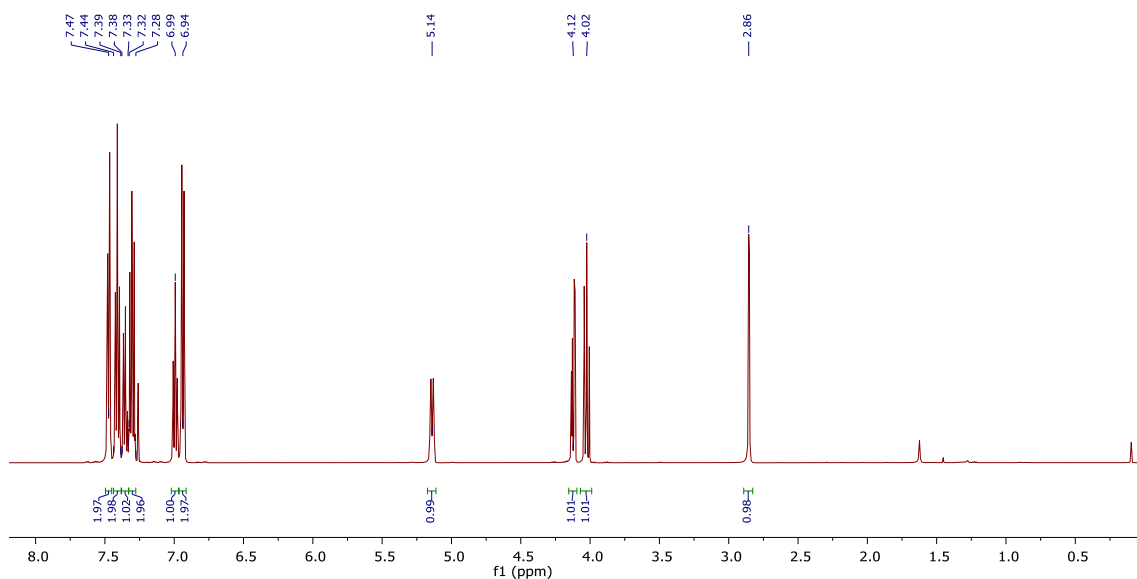
A sample of the intermediate ketone 2-phenoxy-1-phenylethan-1-one (4.50 g, 21 mmol) was dissolved in a solution with a 4:1 ratio of tetrahydrofuran (60 ml) and water (15 mL).

Sodium borohydride (1.60 g, 42 mmol) was added portion-wise with stirring. The reaction mixture was then stirred at room temperature for four hours, after which the mixture was quenched using saturated aqueous ammonium chloride (10 mL) and diluted with water (50 mL). The aqueous phase was extracted with diethyl ether (3x30 mL). The combined organic extracts were washed twice with brine (10 mL) and dried over magnesium sulfate. After removal of the drying agent by filtration the solvents were removed under vacuum providing a white crystalline product (3.91 g, 18 mmol, 87%).

^1H NMR (500 MHz, CDCl_3 , 298 K): δ (ppm) = 7.47 (d, $^3J_{\text{H-H}} = 8.5$ Hz, 2H, CH_{Ar}), 7.44-7.39 (m, 2H, CH_{Ar}), 7.38-7.33 (m, 1H, CH_{Ar}), 7.32-7.28 (m, 2H, CH_{Ar}), 6.99 (t, $J = 7.4$ Hz, 1H, CH_{Ar}), 6.94 (d, $J = 8.7$ Hz, 2H, CH_{Ar}), 5.14 (dt, $J = 8.8$ Hz, $J = 2.4$ Hz, 1H, CH), 4.12 (dd, $J = 9.6$ Hz, $J = 3.1$ Hz, 1H, CH_2), 4.02 (t, $J = 9.2$ Hz, 1H, CH_2), 2.86 (d, $J = 2.5$ Hz, 1H, OH). Data were found to match the literature.²²

mp: 60-61 °C.

^1H NMR (CDCl_3 , 500 MHz, 298 K)



Catalytic experiments

General procedure for catalytic C-O cleavage of 2-Phenoxy-1-phenylethan-1-ol

0.25 mmol of 2-phenoxy-1-phenylethan-1-ol with 10 mol% catalyst loading (0.025 mmol of $\text{RuH}_2\text{CO}(\text{PPh}_3)_3$, 0.025 mmol of xantphos ligand and 0.125 mmol of 1,2,4,5-tetramethylbenzene as the internal standard were dissolved in 2 mL of the selected ionic liquid in a closed microwave vial equipped with a magnetic stirrer. The reaction mixture was sealed and heated to 150 °C for 45 minutes after which the reaction mixture was

cooled to room temperature, washed with 5 mL of toluene, 5 mL of diethyl ether and 5 mL of ethyl acetate. The yield was determined by gas chromatography. Results presented are the averages of reactions carried out in triplicate.

5.3 Chapter IV: Photocatalytic CO₂ reduction in ionic liquid media

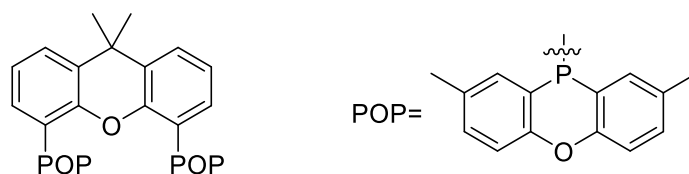
General information

For the synthesis of ligands and complexes all reactions were carried out using standard Schlenk techniques under argon atmosphere. All glassware was dried at 130 °C overnight and cooled under vacuum prior to use. ¹H, ¹³C{¹H} and ³¹P{¹H} Nuclear Magnetic Resonance (NMR) spectra were recorded at 298 K on Bruker Avance 300, Avance II 400 and Bruker Avance II 500 spectrometers using the residual solvent peak for ¹H and ¹³C{¹H} as reference. All NMR shifts are reported as δ in parts per million (ppm). A Gallenkamp melting point apparatus was used to determinate melting points. Toluene and TMEDA were distilled from sodium, THF and diethyl ether were distilled from sodium/benzophenone, hexanes from sodium/benzophenone/triglyme and dichloromethane and acetonitrile from calcium hydride. Diethylamine was dried over KOH powder. Aqueous reagents were degassed by a stream of argon before use for a minimum period of four hours. All reagents were purchased from commercial suppliers and used as received, unless otherwise noted. Mass spectrometry was carried out at National Mass Spectrometry Facility (NMSF-Swansea) and Leibniz Institute for Catalysis – LIKAT. Elemental analysis was carried out in the facilities at London Metropolitan University and Leibniz Institute for Catalysis – LIKAT. All reactions performed in this chapter require strict inert conditions.

Synthesis of ligands and complexes

4,5-bis(2,8-dimethyl-10-phenoxaphosphino)-9,9-dimethylxanthene (POP-xantphos)

(I)



Any xanthene synthetic precursor prior lithiation has been azeotropically dried three times with toluene under vacuum. 9,9-Dimethylxanthene (150 mg, 0.25 mmol) was dried azeotropically with dry toluene before being dissolved in diethyl ether (8 mL) and cooled to -78 °C. TMEDA (1 mL, 0.65 mmol) and *n*-BuLi ((2.5 M in hexanes, 0.29 mL, 0.65 mmol) were added dropwise to give a pale yellow solution. The reaction mixture was stirred overnight, allowing it to warm to room temperature. The reaction mixture was then cooled to -78 °C and a solution of 2,8-dimethyl-10-chloro-phenoxaphosphine (POP-Cl)

(170.7 mg, 0.65 mmol) in 8 mL of toluene was added dropwise. The reaction mixture was stirred overnight, while slowly warming to room temperature. Solvents were removed under vacuum and then the reaction mixture was dissolved in 30 mL of CH₂Cl₂. Subsequently, the reaction mixture was hydrolyzed with 10% HCl (aq) (10 mL). The organic layer was removed and additional CH₂Cl₂ was added to the aqueous layer (extraction repeated 4 times). The organic layers were combined and dried over Na₂SO₄. The crude mixture was then concentrated, washed with hexanes and concentrated again. The crude mixture was dissolved in a minimum amount of toluene and then isopropanol was gently layered on top (1:1). The mixture was allowed to slowly diffuse overnight to give a white solid, which was filtered and dried under vacuum (150 mg, 89%).

¹H NMR (400 MHz, CD₂Cl₂, 298 K): δ (ppm) = 7.99-7.94 (m, 4H, CH_{Ar}), 7.32 (dd, J = 7.8 Hz, J = 1.6 Hz, 2H, CH_{Ar}), 7.22 (ddd, J = 8.4 Hz, J = 2.3 Hz, J = 0.6 Hz, 4H, CH_{Ar}), 7.12 (d, J = 8.4 Hz, 4H, CH_{Ar}), 6.90 (t, J = 7.6 Hz, 2H, CH_{Ar}), 6.72 (ddd, J = 7.6 Hz, J = 2.0 Hz, J = 1.6 Hz, 2H, CH_{Ar}), 2.35 (s, 12H, CH₃), 1.54 (s, 6H, CH₃).

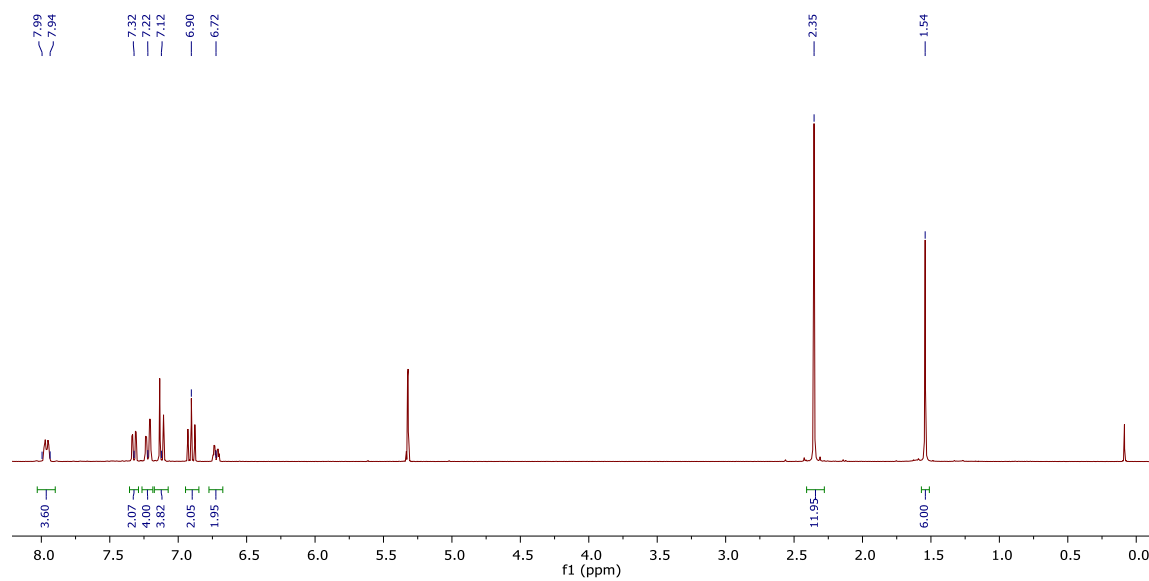
¹³C NMR (101 MHz, CD₂Cl₂, 298 K): δ (ppm) = 154.5 (s, C_q), 152.6 (HMBC, C_q), 135.9 (t, J = 21.8 Hz, CH_{Ar}), 133.6 (t, J = 6.3 Hz, C_q), 132.3 (s, CH_{Ar}), 132.2 (s, CH_{Ar}), 130.8 (s, C_q), 127.7 (s, CH_{Ar}), 124.1 (s, CH_{Ar}), 118.4 (t, J = 2.6 Hz, C_q), 117.9 (s, CH_{Ar}), 34.9 (s, C_q), 32.7 (s, CH₃), 20.9 (s, CH₃). 1 C_q missing.

³¹P NMR (162 MHz, CD₂Cl₂, 298 K): δ (ppm) = -72.2 (s). Data were found to match literature.²³

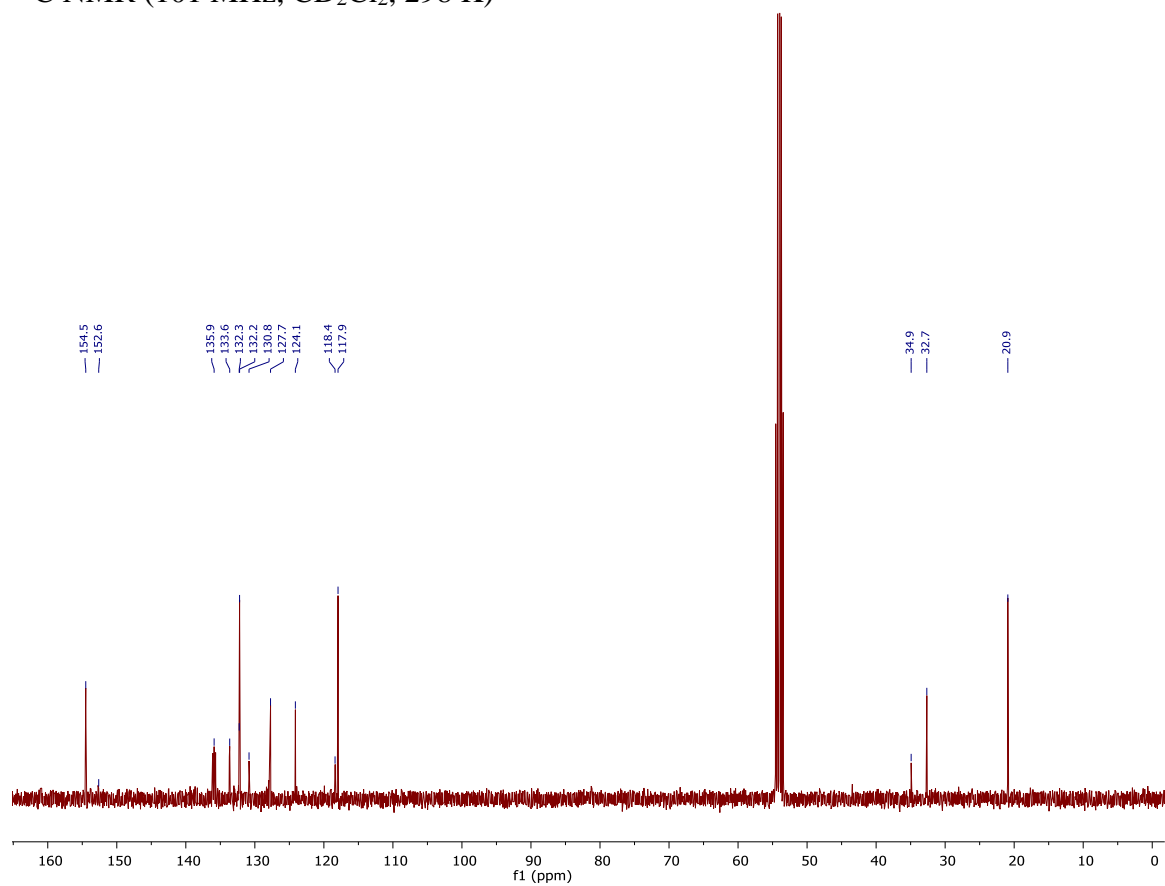
HRMS (ESI) m/z : [M+H]⁺ Calcd for C₄₃H₃₆OP₂: 663.2218; Found 663.2240.

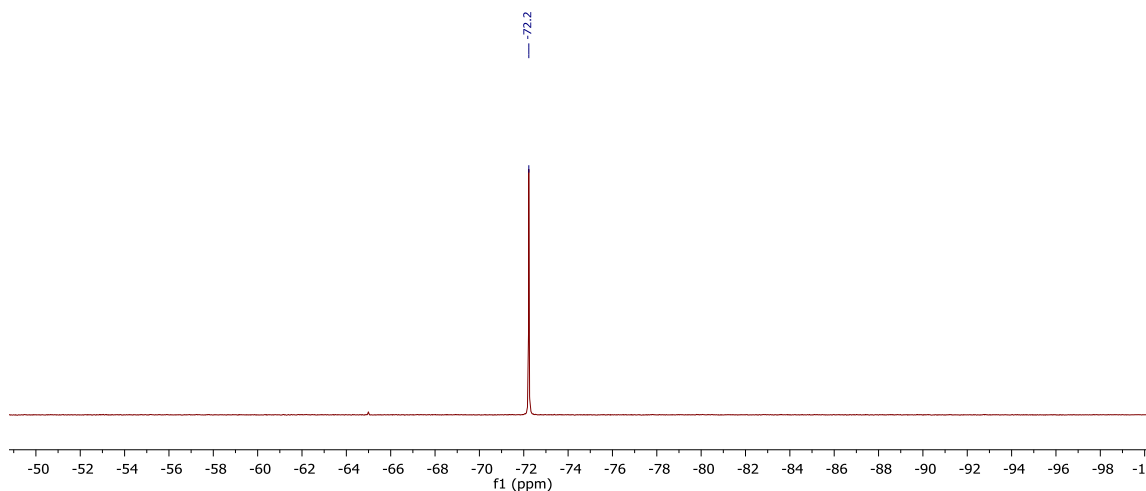
mp: 286-287 °C.

^1H NMR (400 MHz, CD_2Cl_2 , 298 K)

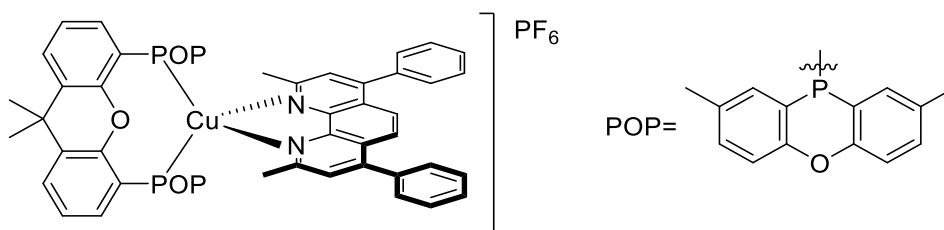


^{13}C NMR (101 MHz, CD_2Cl_2 , 298 K)



^{31}P NMR (162 MHz, CD_2Cl_2 , 298 K)

[Cu(bathocuproine)(4,5-bis((2,8-dimethyl-10-phenoxa phosphino)-9,9-dimethylxanthene)]hexafluorophosphate (2)



$[\text{Cu}(\text{MeCN})_4]\text{PF}_6$ (0.15 mmol, 56.2 mg) and POP-xantphos (0.15 mmol, 100 mg) were dissolved in CH_2Cl_2 (10 mL) at room temperature in a Schlenk flask equipped with a magnetic stirrer. The reaction mixture was refluxed overnight resulting in a colorless solution. Subsequently, the reaction mixture was cooled down to room temperature and a solution of bathocuproine (0.15 mmol, 54.3 mg) in CH_2Cl_2 (5 mL) was added dropwise. The reaction turned red and it was refluxed until the solution turned fluorescent yellow (two hours). The crude mixture was filtered through celite under inert atmosphere. The solvents were evaporated and the complex was redissolved in 2 mL of CH_2Cl_2 and precipitated by the addition of 25 mL of *n*-hexane. The fluorescent yellow precipitate was washed with *n*-hexane. The product was recrystallized by slow diffusion of *n*-hexane in a saturated solution of the complex in CH_2Cl_2 . The fluorescent yellow crystals were filtered, washed with pentane and dried under vacuum overnight obtaining a fluorescent yellow bright powder. Yield: 160 mg, 84%.

¹H NMR (400 MHz, CD₂Cl₂, 298 K): δ (ppm) = 7.79 (s, 2H, CH_{Ar}), 7.71 (dd, J = 7.8 Hz, J = 1.4 Hz, 4H, CH_{Ar}), 7.64-7.57 (m, 6H, CH_{Ar}), 7.54-7.49 (m, 6H, CH_{Ar}), 7.23 (t, J = 7.8 Hz, 4H, CH_{Ar}), 7.06 (ddd, J = 8.4 Hz, J = 2.3 Hz, J = 0.6 Hz, 4H, CH_{Ar}), 6.98-6.87 (m, 10H, CH_{Ar}), 2.25 (s, 6H, CH₃), 1.98 (s, 12H, CH₃), 1.78 (s, 6H, CH₃).

¹³C NMR (101 MHz, CD₂Cl₂, 298 K): δ (ppm) = 158.5 (s, C_q), 156.1 (HMBC, C_q), 153.7 (s, C_q), 150.9 (s, C_q), 144.2 (HMBC, C_q), 137.0 (s, C_q), 134.9 (t, J = 2.6 Hz, C_q), 134.3 (t, J = 5.3 Hz, C_q), 132.9 (s, CH_{Ar}), 132.1 (t, J = 8.0 Hz, CH_{Ar}), 131.0 (s, CH_{Ar}), 130.0 (s, CH_{Ar}), 129.9 (s, C_q), 129.5 (s, CH_{Ar}), 128.9 (s, CH_{Ar}), 126.0 (s, CH_{Ar}), 125.9 (t, J = 12.0 Hz, CH_{Ar}), 124.0 (s, CH_{Ar}), 121.4 (HMBC, C_q), 118.3 (s, CH_{Ar}), 113.8 (t, J = 17.8 Hz, C_q), 36.8 (HMBC, C_q), 29.0 (s, CH₃), 27.3 (s, CH₃), 20.9 (s, CH₃).

³¹P NMR (162 MHz, CD₂Cl₂, 298 K): δ (ppm) = -53.46 (br s), -144.53 (sept)

¹⁹F NMR (282 MHz, CD₂Cl₂, 298 K): δ (ppm) = -73.64 (d, J = 710.1 Hz)

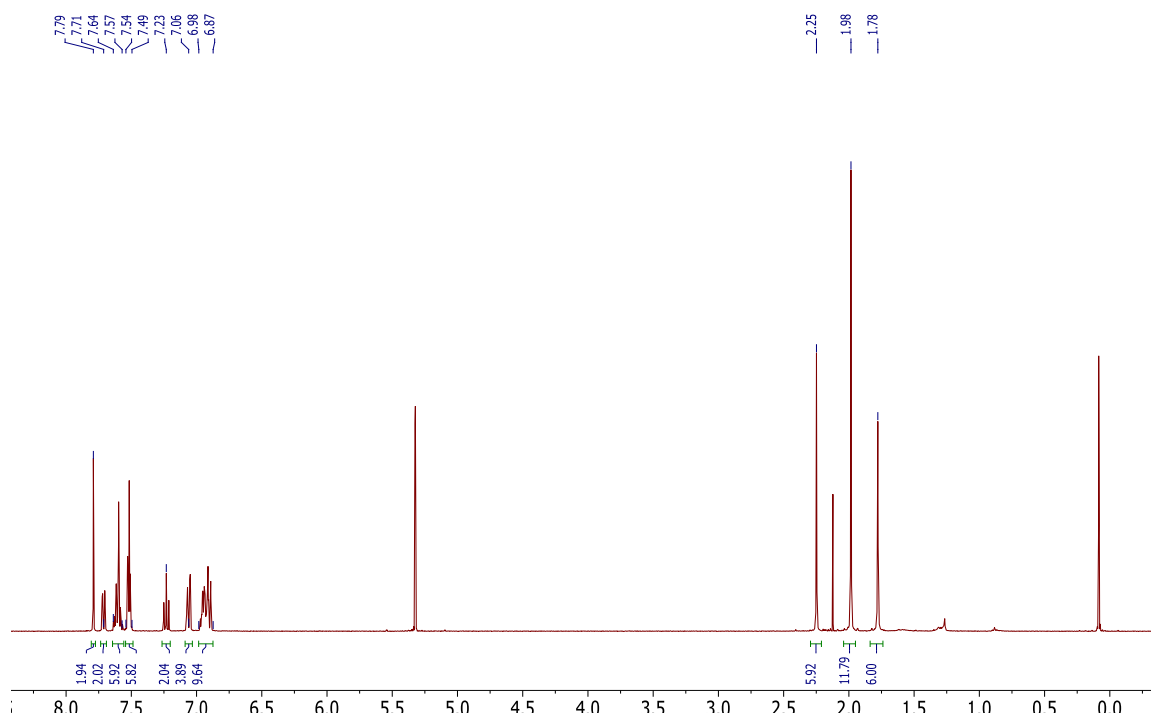
Anal. Calcd for C₆₉H₅₆O₃N₂P₂Cu: C, 67.29; H, 4.58; N, 2.27; Found: C, 67.26; H, 4.681; N, 2.049.

HRMS (ESI) m/z : [M-2PF₆]⁺ Calcd for C₆₉H₅₆O₃N₂P₂Cu: 1085.3068; Found 1085.3063.

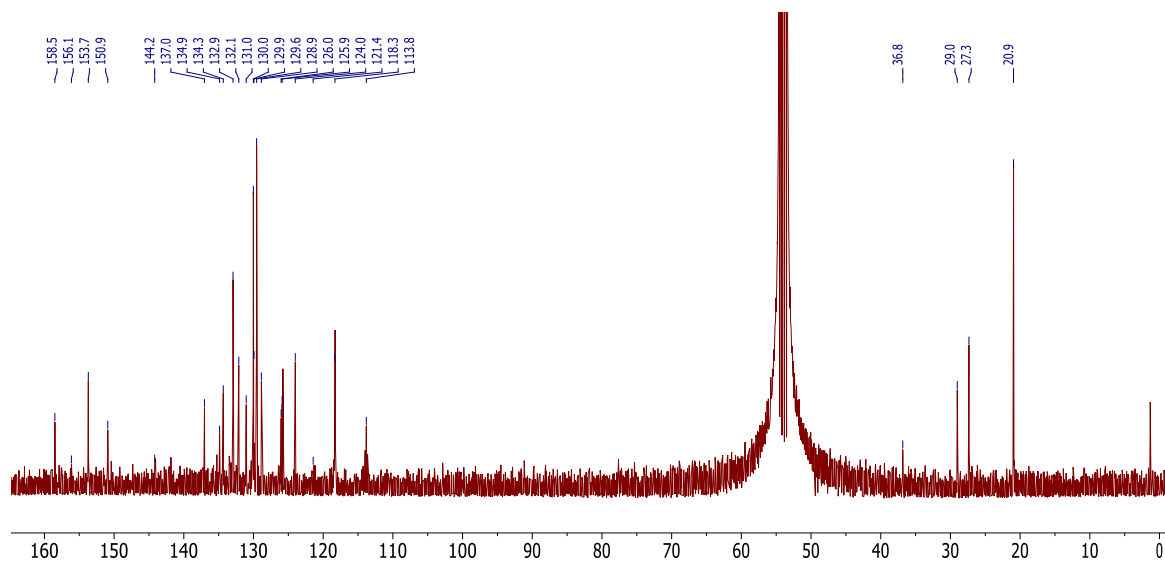
ATR-IR ν (cm⁻¹): 1617.1 (vw), 1567.8 (vw), 1488.3 (vw), 1466.5 (w), 1403.2 (m), 1308.0 (vw), 1268.6 (w), 1219.9 (w), 1139.0 (vw), 1073.7 (vw), 903.9 (vw), 874.8 (vw), 839.7 (s), 776.6 (m), 752.5 (w), 731.9 (w), 704.5 (m), 632.3 (w), 610.2 (vw), 556.5 (m), 514.3 (w), 500.2 (m), 486.7 (m), 462.5 (w), 423.5 (w).

mp: 305 °C (dec.).

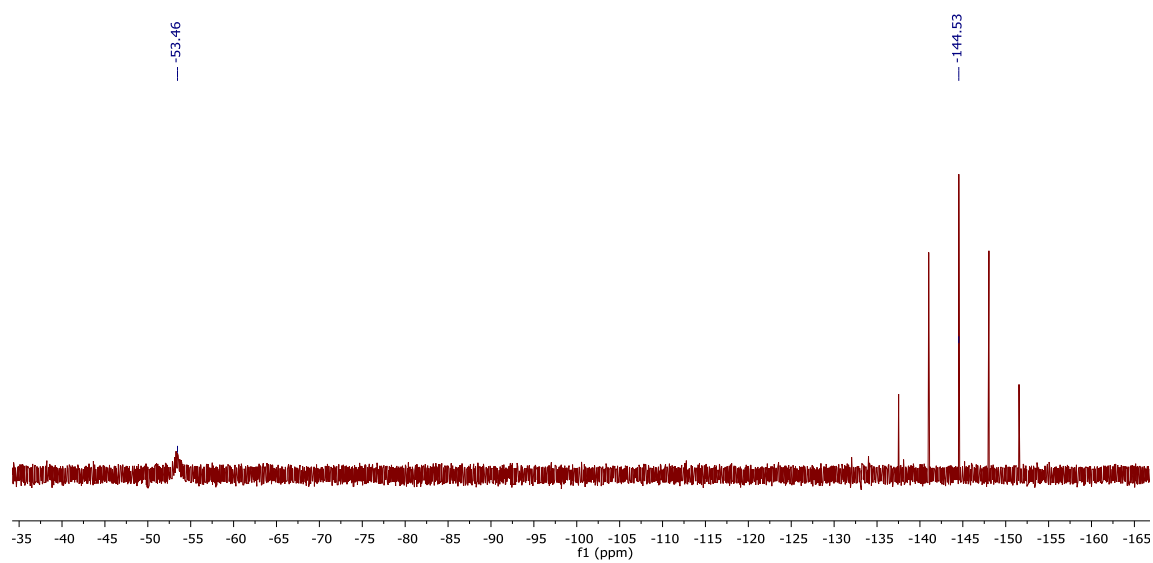
^1H NMR (400 MHz, CD_2Cl_2 , 298K)



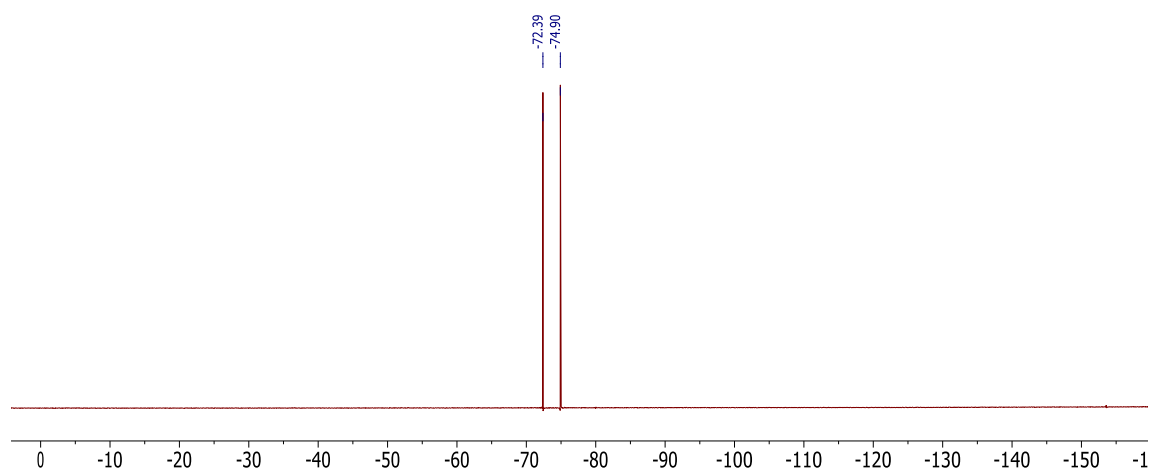
^{13}C NMR (101 MHz, CD_2Cl_2 , 298K)



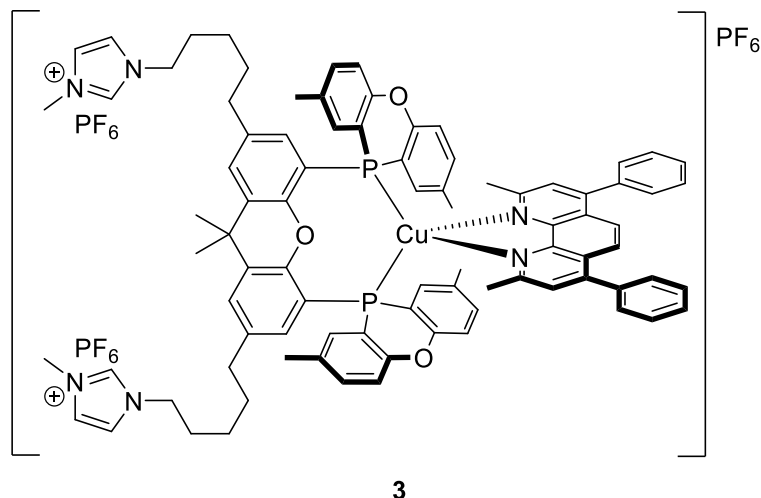
^{31}P NMR (162 MHz, CD_2Cl_2 , 298K)



^{19}F NMR (282 MHz, CD_2Cl_2 , 298K)



[Cu(bathocuproine)(2,7-bis(5-(3-methylimidazolium)pentyl)-9,9-dimethyl-4,5-bis(2,8-dimethyl-10-phenoxa phosphino)xanthene)] hexafluorophosphate (3)



[Cu(MeCN)₄]₂PF₆ (0.04 mmol, 17.7 mg) and imidazolium-tagged xantPOP (31) (Section 5.2) (0.04 mmol, 60 mg) were dissolved in CH₂Cl₂ (10 mL) at room temperature in a Schlenk flask equipped with a magnetic stirrer. The reaction mixture was refluxed overnight resulting in a colorless solution. Subsequently, the reaction mixture was cooled down to room temperature and a solution of bathocuproine (0.04 mmol, 17.2 mg) in CH₂Cl₂ (3 mL) was added dropwise. The reaction turned red and then it was refluxed until the solution turned dark yellow (two hours). The crude mixture was filtered through celite under inert atmosphere, the celite was extensively washed with CH₂Cl₂. The solvents were evaporated and the complex was dissolved in 2 mL of CH₂Cl₂ (suspension) and precipitated by the addition of 25 mL of cold *n*-pentane. The dark yellow precipitate was filtered and washed with cold *n*-pentane. The product was recrystallized by slow diffusion of *n*-hexane in a saturated solution of the complex in CH₂Cl₂. The fluorescent yellow crystals were washed with pentane, filtered and dried under vacuum overnight providing a fluorescent yellow bright powder. Yield: 50 mg, 56%.

³¹P NMR (162 MHz, CD₂Cl₂, 298 K): δ (ppm) = -52.90 (br s), -144.50 (m)

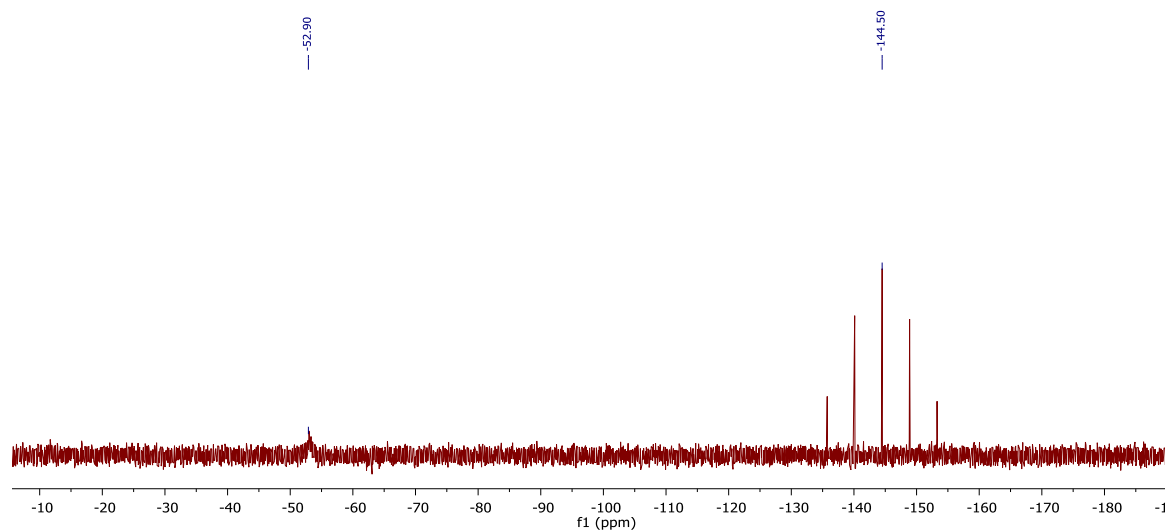
HRMS (ESI) *m/z*: [M-3PF₆]³⁺ Calcd for C₈₇H₈₃O₃N₆P₂Cu: 462.5179; Found: 462.5150.

HRMS (ESI, negative ion mode) *m/z*: [M]⁻ Calcd for F₆P: 144.9642; Found: 144.9642.

ATR-IR ν (cm⁻¹): 1569.7 (w), 1487.3 (w), 1465.4 (m), 1424.9 (m), 1387.1 (w), 1267.7 (m), 1227.4 (m), 1018.7 (m), 836.1 (s), 730.5 (s), 622.4 (m), 556.1(m), 480.2 (s).

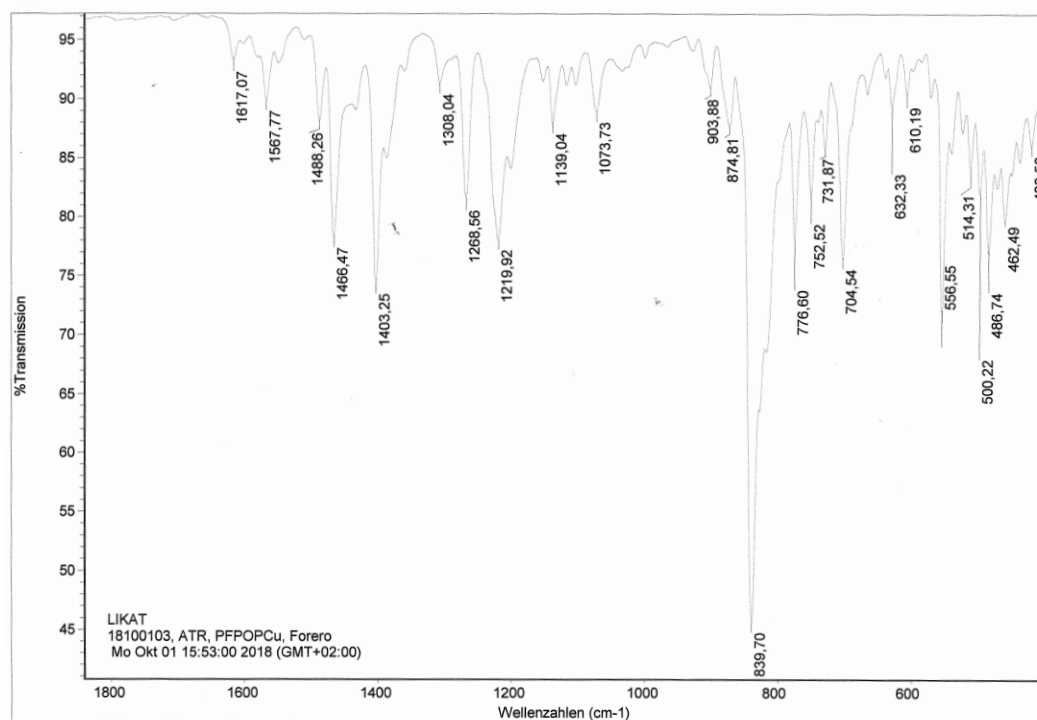
mp: 332 °C (dec.).

^{31}P NMR (162 MHz, CD_2Cl_2 , 298 K)

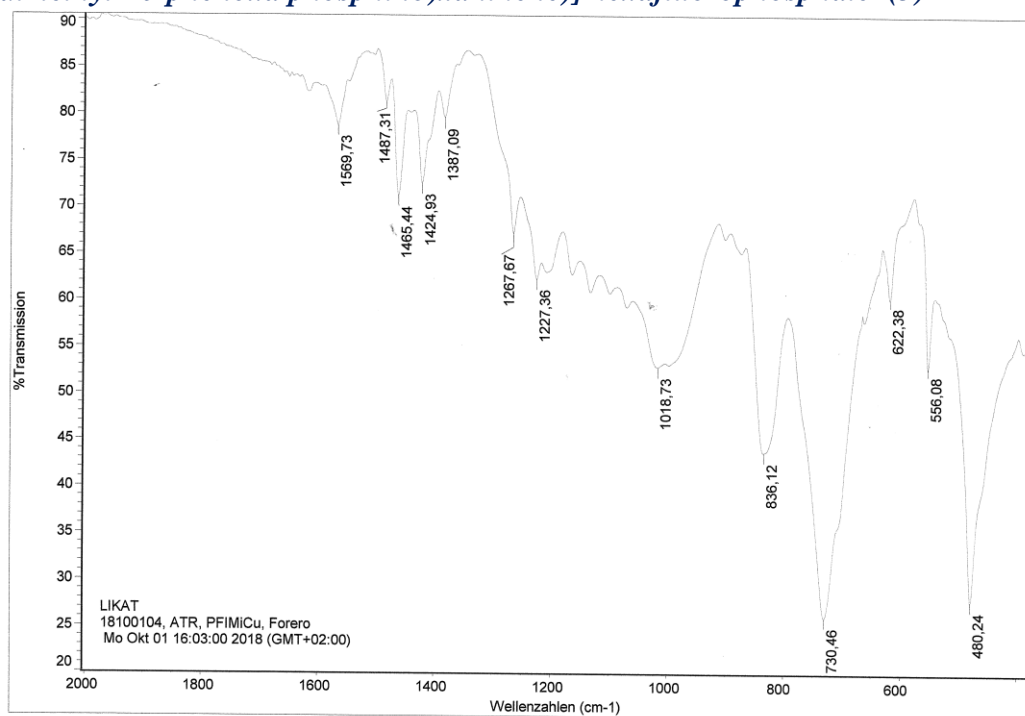


IR spectra of complexes

[Cu(bathocuproine)(4,5-bis((2,8-dimethyl-10-phenoxa phosphino)-9,9-dimethylxanthene)]hexafluorophosphate (2)



[Cu(bathocuproine)(2,7-bis(5-(3-methylimidazolium)pentyl)-9,9-dimethyl-4,5-bis(2,8-dimethyl-10-phenoxa phosphino)xanthene)] hexafluorophosphate (3)



Photocatalytic experiments

General considerations

Anhydrous 1-methylpyrrolidin-2-one (NMP) was obtained from Sigma-Aldrich or AcrosOrganics (Extra Dried by storage over Molecular Sieve 4 Å), degassed and stored over activated molecular sieves (3 or 4 Å). Triethanolamine (TEOA) was obtained from Sigma-Aldrich, degassed and stored under argon. $[\text{Cu}(\text{CH}_3\text{CN})_4]\text{PF}_6$, bathocuproine and xantphos were obtained from TCI. Carbon dioxide was obtained from Linde (4.8 grade). Ionic liquids were purchased from Iolitec and were dried for two days at 80 °C under vacuum, degassed overnight by bubbling argon steam, stored under argon. All commercially available compounds were used without further purification. Compounds Knölker complex²⁴, $[\text{Cu}(\text{bathocuproine})(\text{xantphos})]\text{PF}_6$ ²⁵ and BIH²⁶ were prepared according to literature procedures. These compounds were provided for the project by the group of Professor Matthias Beller/Henrick Junge.

Photocatalytic reactions were performed using LumatecSuperlite 400 Hg-lamps. The irradiation intensity of the lamps was adjusted prior to the reaction using a Laserpoint Plus power meter. All procedures described here require strict inert conditions.

Data analysis

The headspace of the photocatalytic reactions was analyzed *via* gas chromatography using the following GC systems:

- 1) Agilent Technologies 7890A, HP Plot Q / FID – hydrocarbons, Carboxen / TCD – Ar carrier gas.
- 2) Agilent Technologies 6890N, HP Plot Q / FID – hydrocarbons, Carboxen / TCD – He carrier gas.
- 3) Agilent Technologies 6890N, Carboxen 1000 /TCD / Methanizer / FID – He carrier gas.

For gas chromatographic analysis, 5 mL of the sample were injected under isobaric conditions.

NMR spectra were recorded on Bruker Avance 300 and Bruker Avance 400 spectrometers. ^1H NMR spectra were referenced using the solvent residual signal and converting the spectra to the TMS scale.²⁷ ^{31}P NMR shifts are given relative to 85% H_3PO_4 (external standard). Formate concentration in the reaction mixture of the photocatalytic reactions was determined by ^1H NMR, using benzene (10 μL) as an internal standard.

General procedure for photocatalytic CO_2 reduction reactions

Photocatalytic reactions in NMP/TEOA mixture were performed according to a literature procedure.⁵ Photocatalytic reactions in the presence of ionic liquid were conducted using modification of a literature procedure.²⁸

Three-necked, double-walled photoreactors (total volume of 70-80 mL) were equipped with a gas inlet tube, a Teflon-coated stirring bar, and a Teflon-coated rubber septum. The reactors were connected to a Lauda thermostat set to 25 °C. Three vacuum-argon cycles, followed by three vacuum- CO_2 cycles were performed for preparation of the CO_2 atmosphere. BIH (150 mg), TEOA (1.5 mL), the copper complex dissolved/suspended in ionic liquid (5 mL), and the Fe catalyst dissolved/suspended in ionic liquid (1 mL) were consecutively added to the reactors. It is important to clarify that all compounds were dissolved in ionic liquids by sonicating each mixture for 20 minutes prior to addition to the reactor. The mixture was stirred and purged with CO_2 for 30 min. The valve

connecting the reactor and the septum was closed and the gas inlet tube replaced by a glass stopper. The reaction mixture was illuminated through a plain borosilicate-glass wall at 400-700 nm (1.50 W) for 5 h. Gas samples were taken *via* the septum and analyzed by gas chromatography. ^1H NMR spectroscopy was applied for analysis of the liquid phase. The amount of evolved CO and H_2 was calculated *via* the van der Waals molar volume for H_2 (24.48068 mol/L) and CO (24.44323 mol/L) at 25 °C and 101325 Pa using the concentrations of the gas phase determined by GC. TONs for H_2 and CO were calculated using equation 1.

$$\text{TON}(\text{gas}) = \frac{n(\text{gas})}{n(\text{Fe complex})} \quad (1)$$

Photocatalytic CO_2 reduction using the in situ CuPS system

The reaction was performed according to a general procedure for photocatalytic CO_2 reductions.⁵ Instead of the molecular CuPS, solutions/suspensions of $\text{Cu}(\text{CH}_3\text{CN})_4\text{PF}_6$ in IL (0.62 mL), xantphos ligand in IL (2.5 mL), bathocuproine in IL (2.0 mL), and Knölker complex¹ in IL (1.0 mL) were consecutively added.

High-purity conditions

In the high-purity photocatalytic CO_2 reduction set up used for these experiments (Figures 11 and 12), stainless steel components suitable for ultra-high vacuum applications were used including the gas carrying piping system. Every connection was realized using VCR fittings to ensure a grease-free sealing of all interconnecting parts. Two mass flow controllers (MFC) were used to feed the gas to the reaction chamber. A 200 W Hg/Xe lamp (Newport Oriel) emitting UV and visible light was used as the irradiation source. A water-based filter is used for IR radiation removal from the lamp to avoid sample heating. In this work, a 420 nm cut-off filter was also used to prevent structural damage to the tested samples. The product analysis was performed using a Shimadzu Tracera GC 2010 plus gas chromatograph (GC) equipped with a barrier ionization discharge detector (BID) and a flame ionization detector (FID).

The sample (1 mL) containing Knölker complex (1 μmol), $[\text{Cu}(\text{dmp})(\text{xantPOP})]\text{PF}_6$ (5 μmol), BIH (150 mg) and TEOA was introduced in the reactor using a quartz plate under continuous argon flow (10 mL min^{-1}) to displace oxygen from the reaction chamber. The sample was irradiated (under constant stirring) using a 200 W Hg/Xe lamp. In a typical experiment, the reaction chamber is filled up to a final pressure of 1500 mbar

with the desired gas mixture (in this case argon or CO₂). The sample is irradiated and a chromatogram is collected every 45 min for a total time of six hours.

Baseline measurements

To ensure that the sample remains intact under the reaction conditions and that no products are formed without the presence of CO₂, baseline measurements took place under argon atmosphere. Under the regular irradiation conditions (200 W Hg/Xe lamp including UV and visible wavelengths) peaks were identified by the FID detector indicating that the material decomposed or changed structurally. As the UV part of the irradiation spectrum might influence the sample, a 420 nm cut-off filter was used. With use of the cut-off filter and running the experiment under argon the sample kept its original color.

CO₂ reduction to CO

The reaction chamber was flushed with CO₂ for one hour before it was filled up to final pressure of 1500 mbar. The sample was irradiated with the 200 W Hg/Xe lamp equipped with a 420 nm cut-off filter and a chromatogram was collected every 45 min for a total of six hours.



Figure 11. High-purity conditions set up. Reaction chamber and gas chromatograph (GC) equipped with a barrier ionization discharge detector (BID) and a flame ionization detector (FID).

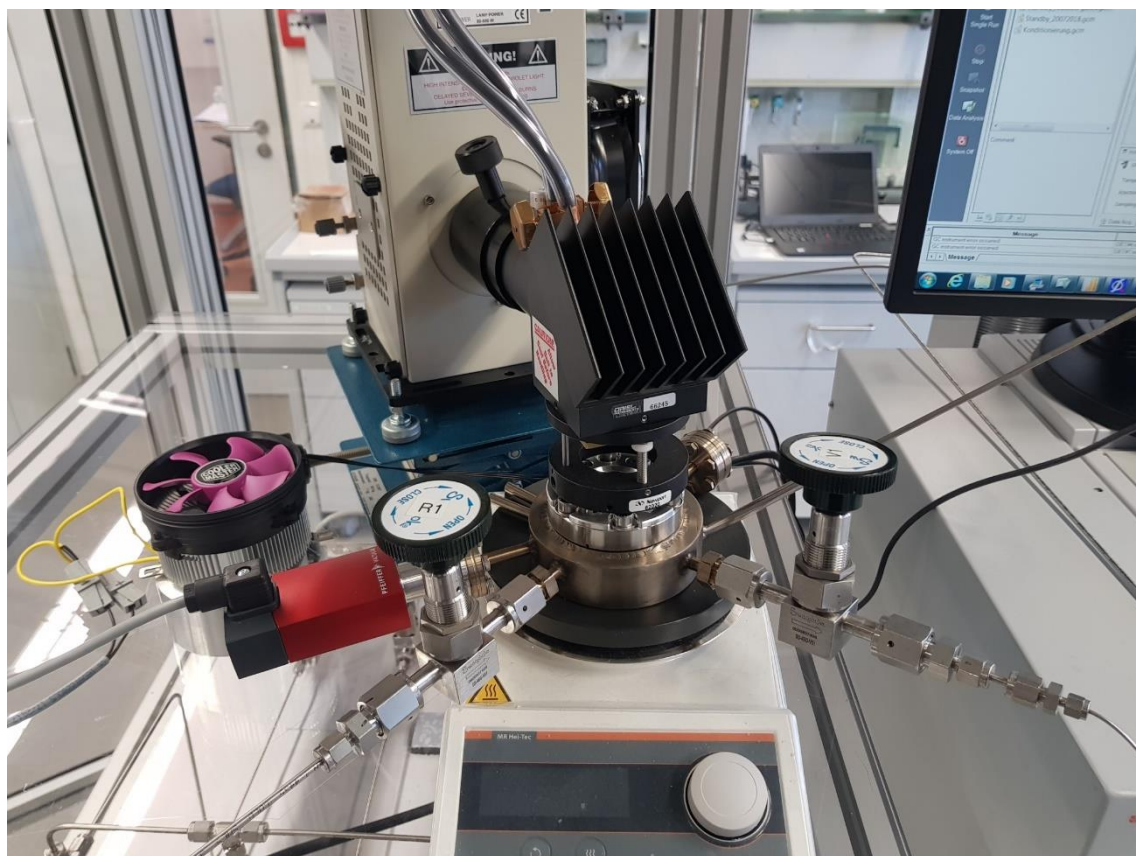


Figure 12. High-purity conditions set up. Reaction chamber.

5.4 References

1. Punji, B.; Mague, J. T.; Balakrishna, M. S. Thioether-Functionalized Ferrocenyl-bis(phosphonite), $\text{Fe}\{(\text{C}_5\text{H}_4)\text{P}(-\text{OC}_{10}\text{H}_6(\mu\text{-S})\text{C}_{10}\text{H}_6\text{O-})\}_2$: Synthesis, Coordination Behavior, and Application in Suzuki-Miyaura Cross-Coupling Reactions. *Inorg. Chem.* **2007**, *46* (24), 10268-10275.
2. Khabbass, N. D. A. H. A study of the reactions between halamines and varieties of phosphorus species. *Durham theses*. **1981**, Durham University.
3. Wolfgang, G.; Kamer, P. C. J.; van Leeuwen P. W. N. M.; Vogt, D. Asymmetric Nickel-Catalyzed Hydrocyanation of Vinylarenes by Applying Homochiral Xantphos Ligands. *Chem. Eur. J.* **2001**, *7*, 1614-1618.
4. Zhu, Y.; Rawal, V. Palladium-Catalyzed C3-Benzoylation of Indoles. *J. Am. Chem. Soc.* **2012**, *134* (1), 111-114.
5. Shaw, L.; Somisara, D. M. U. K.; How, R.C.; Westwood, N. J.; Bruijninx, P. C. A.; Weckhuysen, B. M.; Kamer, P.C. J. Electronic and bite angle effects in catalytic C–O bond cleavage of a lignin model compound using ruthenium Xantphos complexes. *Catal. Sci. Technol.* **2017**, *7*, 619-626.
6. Buhling, A.; Elgersma, J. W.; Nkrumah, S.; Kamer, P. C. J.; van Leeuwen, P.W. N. M. Novel amphiphilic diphosphines: synthesis, rhodium complexes, use in hydroformylation and rhodium recycling. *J. Chem. Soc., Dalton Trans.*, **1996**, *0*, 2143-2154.
7. *CrystalClear-SM Expert* v2.1. Rigaku Americas, The Woodlands, Texas, USA, and Rigaku Corporation, Tokyo, Japan, **2015**.
8. *CrysAlisPro* v1.171.38.46. Rigaku Oxford Diffraction, Rigaku Corporation, Oxford, U.K. **2015**.
9. Burla, M. C.; Caliendo, R.; Camalli, M.; Carrozzini, B.; Cascarano, G. L.; Giacovazzo, C.; Mallamo, M.; Mazzone, A.; Polidori, G.; Spagna, R. SIR2011: a new package for crystal structure determination and refinement. *J. Appl. Cryst.* **2012**, *45*, 357-361.
10. Burla, M. C.; Caliendo, R.; Camalli, M.; Carrozzini, B.; Cascarano, G. L. Giacovazzo, C.; Polidori, G.; Spagna, R. SIR2004: an improved tool for crystal structure determination and refinement. *J. Appl. Cryst.* **2005**, *38*, 381-388.
11. G. M. Sheldrick. Crystal structure refinement with SHELXL. *Acta Crystallogr., Sect. C* **2015**, *71*, 3-8.
12. *CrystalStructure* v4.3.0. Rigaku Americas, The Woodlands, Texas, USA, and Rigaku Corporation, Tokyo, Japan, **2018**.
13. Yang, L.; Powell, D. R.; Houser, R. P. Structural variation in copper(I) complexes with pyridylmethanamide ligands: structural analysis with a new four-coordinate geometry index, τ_4 . *Dalton Trans.* **2007**, *9*, 955-964.
14. Sheldrick, G. M. A short history of SHELX. *Acta Cryst.* **2008**, *64*, 112-122.
15. Sheldrick, G. M. Crystal structure refinement with SHELXL. *Acta Crystallogr., Sect. C* **2015**, *71*, 3-8.
16. Quaranta, M.; Murkovic, M.; Klimant, I. A new method to measure oxygen solubility in organic solvents through optical oxygen sensing. *Analyst.* **2013**, *138* (21), 6243-6245.
17. Herwig, J.; Skutta, P.; Sturm, S. Process for the production of substituted 10-chloro-phenoxaphosphines or 10-Bromo-phenoxaphosphines. United States, *Patent Application*. **2001**, US 2001/0047114A1.
18. Bronger, R. P. J.; Silva, S. M.; Kamer, P. C. J.; van Leeuwen, P. W. N. M. A novel dicationic phenoxaphosphino-modified Xantphos-type ligand: a ligand for highly active and selective, biphasic, rhodium catalyzed hydroformylation in ionic liquids. *Dalton Trans.* **2004**, *10*, 1590-1596.

19. Ono, A.; Suzuki, N.; Kamimura, J. Hydrogenolysis of diaryl and aryl alkyl ketones and carbinols by sodium borohydride and anhydrous aluminum(III) chloride. *Synthesis* **1987**, 8, 736-738.
20. Takeuchi, D.; Chiba, Y.; Takano, S.; Osakada, K. Double-Decker-Type Dinuclear Nickel Catalyst for Olefin Polymerization: Efficient Incorporation of Functional Comonomers. *Angew. Chem., Int. Ed.* **2013**, 52 (48), 12536-12540.
21. Webb, P. B.; Kunene, T. E.; Cole-Hamilton, D. J. Continuous flow homogeneous hydroformylation of alkenes using supercritical fluids. *Green Chem.* **2005**, 7 (5), 373-379.
22. Nichols, J. M.; Bishop, L. M.; Bergman, R. G.; Ellman, J. A. Catalytic C-O Bond Cleavage of 2-Aryloxy-1-arylethanol and Its Application to the Depolymerization of Lignin-Related Polymers. *J. Am. Chem. Soc.* **2010**, 132 (36), 12554-12555.
23. Bronger, R.; P. J.; Kamer, P. C. J.; Van Leeuwen, P. W. N. M. Influence of the Bite Angle on the Hydroformylation of Internal Olefins to Linear Aldehydes. *Organometallics*. **2003**, 22, 5358-5369.
24. Knoelker, H. J.; Heber, J.; Charles, H. Transition metal-diene complexes in organic synthesis. Part 14. Regioselective iron-mediated [2+2+1] cycloadditions of alkynes and carbon monoxide: synthesis of substituted cyclopentadienones. *Synlett*. **1992**, 1002-1004.
25. Lou, S.H.; Mejía, E.; Friedrich, A.; Pazidis, A.; Junge, H.; Surkus, A. E.; Jackstell, R.; Denurra, S.; Gladiali, S.; Lochbrunner, S.; Beller, M. Photocatalytic Water Reduction with Copper-Based Photosensitizers: A Noble-Metal-Free System. *Angew. Chem. Int. Ed.* **2013**, 52, 419-423.
26. Lee, I.S.H.; Jeoung, E. H.; Kreevoy, M. M. Marcus Theory of a Parallel Effect on α for Hydride Transfer Reaction between NAD⁺ Analogues. *J. Am. Chem. Soc.* **1997**, 119, 2722-2728.
27. Fulmer, G. R.; Miller, A. J. M.; Sherden, N. H.; Gottlieb, H. E.; Nudelman, A.; Stoltz, B. M.; Bercaw, J. E.; Goldberg, K. I. NMR Chemical Shifts of Trace Impurities: Common Laboratory Solvents, Organics, and Gases in Deuterated Solvents Relevant to the Organometallic Chemist. *Organometallics*. **2010**, 29, 2176-2179.
28. Rosas-Hernández, A.; Steinlechner, C.; Junge, H.; Beller, M. Earth-abundant photocatalytic systems for the visible-light-driven reduction of CO₂ to CO. *Green Chem.* **2017**, 19, 2356-2360.